

AP600 DOCUMENT COVER SHEET

Form 58202G(5/94)

AP600 CENTRAL FILE USE ONLY:

TDC: _____ IDS: 1 _____ S _____

0058.FRM

RFS#:

RFS ITEM #:

AP600 DOCUMENT NO. PXS-TZR-100	REVISION NO. 0	Page 1 of 1	ASSIGNED TO
-----------------------------------	-------------------	-------------	-------------

ALTERNATE DOCUMENT NUMBER: ~~14310~~ 14309

WORK BREAKDOWN #: 2.6.16.1

DESIGN AGENT ORGANIZATION: WESTINGHOUSE

TITLE: AP600 DESIGN CERTIFICATION PROGRAM SPES-2 TESTS FINAL DATA REPORT

ATTACHMENTS: N/A	DCP #/REV. INCORPORATED IN THIS DOCUMENT REVISION: N/A
CALCULATION/ANALYSIS REFERENCE:	

ELECTRONIC FILENAME U:\1625W.WPF U:\1625.FRM	ELECTRONIC FILE FORMAT WordPerfect 5.1 WINDOWS WordPerfect 5.1 WINDOWS	ELECTRONIC FILE DESCRIPTION DOCUMENT TEXT AND FIGURES COVER SHEET
--	--	---

(C) WESTINGHOUSE ELECTRIC CORPORATION 1995

WESTINGHOUSE PROPRIETARY CLASS 2

This document contains information proprietary to Westinghouse Electric Corporation; it is submitted in confidence and is to be used solely for the purpose for which it is furnished and returned upon request. This document and such information is not to be reproduced, transmitted, disclosed or used otherwise in whole or in part without prior written authorization of Westinghouse Electric Corporation, Energy Systems Business Unit, subject to the legends contained hereof.

WESTINGHOUSE PROPRIETARY CLASS 2C

This document is the property of and contains Proprietary Information owned by Westinghouse Electric Corporation and/or its subcontractors and suppliers. It is transmitted to you in confidence and trust, and you agree to treat this document in strict accordance with the terms and conditions of the agreement under which it was provided to you.

WESTINGHOUSE CLASS 3 (NON PROPRIETARY)

COMPLETE 1 IF WORK PERFORMED UNDER DESIGN CERTIFICATION OR COMPLETE 2 IF WORK PERFORMED UNDER FOAKE.

1 **DOE DESIGN CERTIFICATION PROGRAM - GOVERNMENT LIMITED RIGHTS STATEMENT** [See page 2]

Copyright statement: A license is reserved to the U.S. Government under contract DE-AC03-90SF18495.

DOE CONTRACT DELIVERABLES (DELIVERED DATA)

Subject to specified exceptions, disclosure of this data is restricted until September 30, 1995 or Design Certification under DOE contract DE-AC03-90SF18495, whichever is later.

EPRI CONFIDENTIAL: NOTICE: 1 2 3 4 5 CATEGORY: A B C D E F

2 **ARC FOAKE PROGRAM - ARC LIMITED RIGHTS STATEMENT** [See page 2]

Copyright statement: A license is reserved to the U.S. Government under contract DE-FC02-NE34267 and subcontract ARC-93-3-SC-001.

ARC CONTRACT DELIVERABLES (CONTRACT DATA)

Subject to specified exceptions, disclosure of this data is restricted under ARC Subcontract ARC-93-3-SC-001.

ORIGINATOR R. Hundal	SIGNATURE/DATE <i>R. Hundal</i> 4/3/95
AP600 RESPONSIBLE MANAGER E. J. Pipica	SIGNATURE/APPROVAL DATE <i>E. J. Pipica</i> 4/3/95

*Approval of the responsible manager signifies that document is complete, all required reviews are complete, electronic file is attached and document is released for use.

9504270004 950331
PDR ADOCK 05200003
A PDR

Form 58202G(5/94)

LIMITED RIGHTS STATEMENTS

DOE GOVERNMENT LIMITED RIGHTS STATEMENT

- (A) These data are submitted with limited rights under government contract No. DE-AC03-90SF18495. These data may be reproduced and used by the government with the express limitation that they will not, without written permission of the contractor, be used for purposes of manufacture nor disclosed outside the government; except that the government may disclose these data outside the government for the following purposes, if any, provided that the government makes such disclosure subject to prohibition against further use and disclosure:
- (i) This "Proprietary Data" may be disclosed for evaluation purposes under the restrictions above.
 - (ii) The "Proprietary Data" may be disclosed to the Electric Power Research Institute (EPRI), electric utility representatives and their direct consultants, excluding direct commercial competitors, and the DOE National Laboratories under the prohibitions and restrictions above.
- (B) This notice shall be marked on any reproduction of these data, in whole or in part.

ARC LIMITED RIGHTS STATEMENT:

This proprietary data, furnished under Subcontract Number ARC-93-3-SC-001 with ARC may be duplicated and used by the government and ARC, subject to the limitations of Article H-17.F. of that subcontract, with the express limitations that the proprietary data may not be disclosed outside the government or ARC, or ARC's Class 1 & 3 members or EPRI or be used for purposes of manufacture without prior permission of the Subcontractor, except that further disclosure or use may be made solely for the following purposes:

This proprietary data may be disclosed to other than commercial competitors of Subcontractor for evaluation purposes of this subcontract under the restriction that the proprietary data be retained in confidence and not be further disclosed, and subject to the terms of a non-disclosure agreement between the Subcontractor and that organization, excluding DOE and its contractors.

DEFINITIONS

CONTRACT/DELIVERED DATA — Consists of documents (e.g. specifications, drawings, reports) which are generated under the DOE or ARC contracts which contain no background proprietary data.

EPRI CONFIDENTIALITY / OBLIGATION NOTICES

NOTICE 1: The data in this document is subject to no confidentiality obligations.

NOTICE 2: The data in this document is proprietary and confidential to Westinghouse Electric Corporation and/or its Contractors. It is forwarded to recipient under an obligation of Confidence and Trust for limited purposes only. Any use, disclosure to unauthorized persons, or copying of this document or parts thereof is prohibited except as agreed to in advance by the Electric Power Research Institute (EPRI) and Westinghouse Electric Corporation. Recipient of this data has a duty to inquire of EPRI and/or Westinghouse as to the uses of the information contained herein that are permitted.

NOTICE 3: The data in this document is proprietary and confidential to Westinghouse Electric Corporation and/or its Contractors. It is forwarded to recipient under an obligation of Confidence and Trust for use only in evaluation tasks specifically authorized by the Electric Power Research Institute (EPRI). Any use, disclosure to unauthorized persons, or copying this document or parts thereof is prohibited except as agreed to in advance by EPRI and Westinghouse Electric Corporation. Recipient of this data has a duty to inquire of EPRI and/or Westinghouse as to the uses of the information contained herein that are permitted. This document and any copies or excerpts thereof that may have been generated are to be returned to Westinghouse, directly or through EPRI, when requested to do so.

NOTICE 4: The data in this document is proprietary and confidential to Westinghouse Electric Corporation and/or its Contractors. It is being revealed in confidence and trust only to Employees of EPRI and to certain contractors of EPRI for limited evaluation tasks authorized by EPRI. Any use, disclosure to unauthorized persons, or copying of this document or parts thereof is prohibited. This Document and any copies or excerpts thereof that may have been generated are to be returned to Westinghouse, directly or through EPRI, when requested to do so.

NOTICE 5: The data in this document is proprietary and confidential to Westinghouse Electric Corporation and/or its Contractors. Access to this data is given in Confidence and Trust only at Westinghouse facilities for limited evaluation tasks assigned by EPRI. Any use, disclosure to unauthorized persons, or copying of this document or parts thereof is prohibited. Neither this document nor any excerpts therefrom are to be removed from Westinghouse facilities.

EPRI CONFIDENTIALITY / OBLIGATION CATEGORIES

CATEGORY "A" — (See Delivered Data) Consists of CONTRACTOR Foreground Data that is contained in an issued report.

CATEGORY "B" — (See Delivered Data) Consists of CONTRACTOR Foreground Data that is not contained in an issued report, except for computer programs.

CATEGORY "C" — Consists of CONTRACTOR Background Data except for computer programs.

CATEGORY "D" — Consists of computer programs developed in the course of performing the Work.

CATEGORY "E" — Consists of computer programs developed prior to the Effective Date or after the Effective Date but outside the scope of the Work.

CATEGORY "F" — Consists of administrative plans and administrative reports.

WCAP-14310

AP600 DESIGN CERTIFICATION PROGRAM
SPES-2 TESTS FINAL DATA REPORT

L. Conway
R. Hundal
M. Loftus
V. Merrit
M. Ogrinsh

March 1995

LIST OF ACRONYMS

ADS	Automatic depressurization system
AICC	adiabatic isochoric complete combustion
AOV	air-operated valve
ASME	American Society of Mechanical Engineers
CHF	critical heat flux
CL	cold leg
CMT	core makeup tank
CNS	containment system
COL	combined operating license
CRDM	control rod drive mechanism
CRT	core reflood tank
CVCS	chemical and volume control system
DAS	data acquisition system
DCP	design change proposal
DEG	double-ended guillotine
DECLG	double-ended cold leg guillotine
DF	decontamination factor
DG	diesel generator
DNB	departure from nucleate boiling
DOE	United States Department of Energy
DSER	draft safety evaluation report
DVI	direct vessel injection
ECCS	emergency core cooling system
EPRI	Electric Power Research Institute
ESF	engineered safety feature
HL	hot leg
HT	heat transfer
HVAC	heating, ventilation and air conditioning
HX	heat exchanger
IASCC	irradiation-assisted stress corrosion cracking
I&C	instrumentation and control
IIS	incore instrumentation system

IRWST	in-containment refueling water storage tank
ITAAC	inspection, tests, analysis and acceptance criteria
L/D	length over diameter
LBLOCA	large-break LOCA
LOCA	loss-of-coolant accident
LTC	long-term cooling
MSILV	mainsteam line isolation valve
MSLB	mainsteam line break
MSS	main steam system
NRC	Nuclear Regulatory Commission
NRHR	normal residual heat removal system
NSSS	nuclear steam supply system
PAMS	post-accident monitoring system
P&ID	pipng and instrumentation diagram
PBL	pressure break line
PCS	passive containment cooling system
PCT	peak clad temperature
PIRT	phenomena identification rantsing table
PLS	plant control system
PMS	protection and safety monitoring system
PORV	power-operated relief valve
PRA	probabilistic risk assessment
PRHR	passive residual heat removal
PWR	pressurized water reactor
PXS	passive core cooling system
QDPS	qualified data processing system
RAI	request for additional information
RAM	reliability, availability, and maintainability
RCDT	reactor coolant drain tank
RCP	reactor coolant pump
RCS	reactor coolant system
RHR	residual heat removal
RTD	resistance temperature detector

SBLOCA	small-break LOCA
SCC	stress corrosion cracking
SFS	spent fuel cooling system
SFWS	startup feedwater system
SG	steam generator
SGS	steam generator system
SGTR	steam generator tube rupture
SI	safety injection
SMS	special monitoring system
SPS	passive containment spray system
SSAR	standard safety analysis report
STD	standard
UET	unfavorable exposure time
UPTF	upper plenum test facility
URD	utility requirements document
USC	utility steering committee
VBS	non-radioactive ventilation system
VES	passive control room ventilation system
VFS	containment air filtration system

TABLE OF CONTENTS

<u>Section</u>	<u>Title</u>	<u>Page</u>
SUMMARY		1
ACKNOWLEDGEMENTS		2
1.0	INTRODUCTION	1-1
1.1	Background	1-1
1.2	Test Objectives	1-2
1.3	Test Matrix	1-3
1.4	SPES-2 Test Runs	1-5
2.0	TEST FACILITY DESCRIPTION	2-1
2.1	Introduction	2-1
2.2	Facility Scaling Summary	2.2-1
2.2.1	General Scaling Criteria	2.2-1
2.2.2	Specific Scaling Criteria	2.2-2
2.3	Facility Description	2.3-1
2.3.1	Primary Piping	2.3-2
2.3.2	Power Channel	2.3-2
2.3.3	Rod Bundle	2.3-3
2.3.4	Power Channel Downcomer	2.3-3
2.3.5	Pressurizer	2.3-3
2.3.6	Pumps	2.3-3
2.3.7	Steam Generators	2.3-3
2.3.8	Passive Safety Systems	2.3-4
2.4	Instrumentation	2.4-1
2.4.1	Absolute and Differential Pressure Transmitters	2.4-2
2.4.2	Thermocouples and Thermoresistances	2.4-2
2.4.3	Flowmeters	2.4-2
2.4.4	Integral Mass Flowmeters	2.4-2
2.4.5	Gammadensitometers	2.4-2
2.4.6	Power Meters	2.4-3
2.5	Data Acquisition System (DAS)	2.5-1
2.5.1	Control Loops	2.5-2
2.5.2	Safety Devices	2.5-3
2.6	Facility Operation	2.6-1
2.6.1	Facility Operation for Test S00303	2.6-2
2.6.2	Facility Operation for Test S00401	2.6-7
2.6.3	Facility Operation for Test S00504	2.6-12
2.6.4	Facility Operation for Test S00605	2.6-17
2.6.5	Facility Operation for Test S00706	2.6-22
2.6.6	Facility Operation for Test S00908	2.6-28

TABLE OF CONTENTS (Cont.)

<u>Section</u>	<u>Title</u>	<u>Page</u>
	2.6.7 Facility Operation for Test S01007	2.6-34
	2.6.8 Facility Operation for Test S01110	2.6-39
	2.6.9 Facility Operation for Test S01211	2.6-44
	2.6.10 Facility Operation for Test S01309	2.6-49
	2.6.11 Facility Operation for Test S01512	2.6-55
	2.6.12 Facility Operation for Test S01613	2.6-59
	2.6.13 Facility Operation for Test S01703	2.6-64
3.0	DATA REDUCTION	3-1
3.1	Introduction	3-1
3.2	Test Validation	3-1
3.3	Pre-Operational Tests	3-2
3.4	Matrix Tests	3-3
3.5	Error Analysis	3-6
4.0	TEST RESULTS	4.1.1-1
4.1	Pre-Operational Tests	4.1.1-1
4.1.1	Cold Pre-Operational Tests	4.1.1-1
4.1.1.1	Text Matrix	4.1.1-1
4.1.1.2	Summary of Test C-02 Through C-07 Results	4.1.1-2
4.1.1.3	Summary of Test C-01 and C-09 Results	4.1.1-2
4.1.2	Hot Pre-Operational Tests	4.1.2-1
4.1.2.1	Hot Pre-Operational Test H-01	4.1.2-1
4.1.2.2	SPES-2 Hot Pre-Operational Test H-02	4.1.2-3
4.1.2.3	Hot Pre-Operational Test H-03	4.1.2-3
4.1.2.4	SPES-2 Hot Pre-Operational Test H-04	4.1.2-4
4.1.2.5	SPES-2 Pre-Operational Test H-05	4.1.2-7
4.1.2.6	SPES-2 Hot Pre-Operational Test H-06	4.1.2-8
4.2	Test Results	4.2-1
4.2.1	Test Transient Phases for Loss-of-Coolant Accident (LOCA) and Non-LOCA Tests	4.2-1
4.2.1.1	LOCAs	4.2-1
4.2.1.2	Non-LOCAs	4.2-1
4.2.2	Two-In. Cold Leg Break without Nonsafety Systems (S00303)	4.2.2-1
4.2.3	Two-In. Cold-Leg Break without Nonsafety Systems (S01703 - Repeat of S00303)	4.2.3-1
4.2.4	Two-In. Cold Leg Break with Nonsafety Systems (S00504)	4.2.4-1
4.2.5	One-In. Cold-Leg Break without Nonsafety Systems (S00401)	4.2.5-1

TABLE OF CONTENTS (Cont.)

<u>Section</u>	<u>Title</u>	<u>Page</u>
4.2.6	One-In. Cold Leg Break with Three PRHR HX Tubes, without Non-Safety Systems (S01613)	4.2.6-1
4.2.7	Two-In. Direct Vessel Injection Line Break	4.2.7-1
4.2.8	Double-Ended Guillotine DVI Line Break (S00706)	4.2.8-1
4.2.9	Two-In. Cold-Leg/Core Makeup Tank Balance Line Break without Nonsafety Systems	4.2.9-1
4.2.10	Double-Ended Guillotine Cold Leg to CMT Balance Line Break without Nonsafety Systems (S00908)	4.2.10-1
4.2.11	Steam Generator Tube Rupture with Nonsafety Systems Operational and Operator Action (S01309)	4.2.11-1
4.2.12	Steam Generator Tube Rupture without Nonsafety Systems (S01110)	4.2.12-1
4.2.13	Steam Generator Tube Rupture without Nonsafety Systems, with Inadvertent ADS (S01211)	4.2.13-1
4.2.14	Large Steam Line Break at Hot Standby Conditions without Nonsafety Systems (S01512)	4.2.14-1
5.0	TEST DATA COMPARISON	5-1
5.1	Comparison Basis for LOCAs	5.1-1
5.2	Comparison Basis for non-LOCA Events	5.2-1
5.3	Comparison of Break Locations	5.3-1
5.4	Comparison of Break Sizes	5.4-1
5.5	Effects of Nonsafety Systems	5.5-1
5.6	Other Key Test Results	5.6-1
5.6.1	Comparison of PRHR Performance	5.6-1
5.6.2	Test Repeatability	5.6-2
5.6.3	Comparison of Steam Generator Tube Rupture	5.6-2
6.0	OBSERVATIONS AND CONCLUSIONS	6-1
7.0	REFERENCES	7-1
Appendix A	Data Reduction Methods and Validation Process	A-1
Appendix B	Data Validation	B-1
Appendix C	SPES-2 Instrument List	C-1
Appendix D	SPES-2 Inoperable and Modified Instruments	D-1
Appendix E	Error Analysis	E-1
Appendix F	Full-Height Full-Power Integral Systems Test Delta-P Instrumentation Data Reduction	F-1
Appendix G	Full-Height Full-Power Integral Systems Test Delta-P Instrumentation Data Reduction	G-1

LIST OF TABLES

<u>Table No.</u>	<u>Title</u>	<u>Page</u>
1-1	SPES-2, Test Matrix	1-6
1-2	Test Rungs at SPES-2	1-8
2.2-1	Elevation Comparison	2.2-5
2.2-2	Volume Comparison	2.2-6
2.3-1	Pressure Vessel Main Characteristics	2.3-5
2.3-2	Power Channel Main Characteristics	2.3-6
2.3-3	Rod Bundle Main Characteristics	2.3-7
2.3-4	Steam Generator Main Characteristics	2.3-8
2.5-1	SPES-2 Power Decay Curve	2.5-5
2.6.1-1	SPES-2 Installed Orifices	2.6-3
2.6.1-2	Programmed Opening of ADS Valves	2.6-4
2.6.2-1	SPES-2 Installed Orifices	2.6-8
2.6.2-2	Programmed Opening of ADS Valves	2.6-9
2.6.3-1	SPES-2 Installed Orifices	2.6-13
2.6.3-2	Programmed Opening of ADS Valves	2.6-14
2.6.4-1	SPES-2 Installed Orifices	2.6-18
2.6.4-2	Programmed Opening of ADS Valves	2.6-19
2.6.5-1	SPES-2 Installed Orifices	2.6-23
2.6.5-2	Programmed Opening of ADS Valves	2.6-24
2.6.6-1	SPES-2 Installed Orifices	2.6-29
2.6.6-2	Programmed Opening of ADS Valves	2.6-30
2.6.7-1	SPES-2 Installed Orifices	2.6-35
2.6.7-2	Programmed Opening of ADS Valves	2.6-36
2.6.8-1	SPES-2 Installed Orifices	2.6-40
2.6.8-2	Programmed Opening of ADS Valves	2.6-41
2.6.9-1	SPES-2 Installed Orifices	2.6-45
2.6.9-2	Programmed Opening of ADS Valves	2.6-46
2.6.10-1	SPES-2 Installed Orifices	2.6-51
2.6.10-2	Programmed Opening of ADS Valves	2.6-52
2.6.11-1	SPES-2 Installed Orifices	2.6-56
2.6.11-2	Programmed Opening of ADS Valves	2.6-57
2.6.12-1	SPES-2 Installed Orifices	2.6-60
2.6.12-2	Programmed Opening of ADS Valves	2.6-61
2.6.13-1	SPES-2 Installed Orifices	2.6-65
2.6.13-2	Programmed Opening of ADS Valves	2.6-66

LIST OF TABLES (Cont.)

<u>Table No.</u>	<u>Title</u>	<u>Page</u>
3-1	Overall Test Acceptance Criteria	3-8
3-2	SPES-2 Critical Instruments	3-9
3-3	Typical SPES-2 Data Measurement Errors	3-11
4.1.1-1	SPES-2 Cold Pre-Operational Test Matrix	4.1.1-3
4.1.1-2	SPES-2 Cold Pre-Operational Tests vs. AP600 Comparison of SPES-2 Safety System Piping Resistances	4.1.1-4
4.1.1-3	SPES-2 Cold Pre-Operational Tests Comparison of SPES-2 vs. AP600 RCS Resistances (Both RCPs Running)	4.1.1-5
4.1.2-1	SPES-2 Hot Pre-Operational Test Summary	4.1.2-10
4.1.2-2	SPES-2 Hot Pre-Operational Test H-01 Facility Heat Losses vs. Temperature	4.1.2-11
4.1.2-3	SPES-2 Hot Pre-Operational Test H-01 Major Component Heat Losses	4.1.2-12
4.1.2-4	SPES-2 Pre-Operational Test H-01 Facility System Heat Capacities	4.1.2-13
4.1.2-5	SPES-2 Hot Pre-Operational Test H-05 Initial Conditions	4.1.2-14
4.1.2-6	SPES-2 Hot Pre-Operational Test H-05 Sequence of Events	4.1.2-15
4.1.2-7	SPES-2 Hot Pre-Operational Tests Major Event Comparison Between Tests H-05 and H-06	4.1.2-16
4.1.2-8	SPES-2 Hot Pre-Operational Test H-06 Initial Conditions	4.1.2-17
4.1.2-9	SPES-2 Hot Pre-Operational Test H-06 Sequence of Events	4.1.2-18
4.2.2-1	Sequence of Events for Test S00303	4.2.2-14
4.2.2-2	Water Inventory Before Test S00303	4.2.2-15
4.2.2-3	Water Inventory After Test S00303 Was Completed	4.2.2-16
4.2.2-4	Mass Balance for Test S00303	4.2.2-17
4.2.3-1	Sequence of Events for Test S01703	4.2.3-4
4.2.3-2	Water Inventory Before Test S01703	4.2.3-5
4.2.3-3	Water Inventory After Test S01703	4.2.3-6
4.2.3-4	Mass Balance for Test S01703	4.2.3-7
4.2.4-1	Sequence of Events for Test S00504	4.2.4-14
4.2.4-2	Water Inventory Before Test S00504	4.2.4-15
4.2.4-3	Water Inventory After Test S00504 Was Completed	4.2.4-16
4.2.4-4	Mass Balance for Test S00504	4.2.4-18
4.2.5-1	Sequence of Events for Test S00401	4.2.5-15
4.2.5.2	Water Inventory Before Test	4.2.5-16
4.2.5.3	Water Inventory After Test S00401 Was Completed	4.2.5-17
4.2.5-4	Mass Balance for Test S00401	4.2.5-18
4.2.6-1	Sequence of Events for Test S01613	4.2.6-15
4.2.6-2	Water Inventory Before Test S01613	4.2.6-16

LIST OF TABLES (Cont.)

<u>Table No.</u>	<u>Title</u>	<u>Page</u>
4.2.6-3	Water Inventory After Test S01613 Was Completed	4.2.6-17
4.2.6-4	Mass Balance for Test S01613	4.2.6-18
4.2.7-1	Sequence of Events for Test S00605	4.2.7-14
4.2.7-2	Water Inventory Before Test S00605	4.2.7-15
4.2.7-3	Water Inventory After Test S00605 Was Completed	4.2.7-16
4.2.7-4	Mass Balance for Test S00605	4.2.7-17
4.2.8-1	Sequence of Events for Test S00706	4.2.8-15
4.2.8-2	Water Inventory Before Test S00706	4.2.8-16
4.2.8-3	Water Inventory After Test S00706 Was Completed	4.2.8-17
4.2.8-4	Mass Balance for Test S00706	4.2.8-18
4.2.9-1	Sequence of Events for Test S01007	4.2.9-15
4.2.9-2	Water Inventory Before Test S01007	4.2.9-16
4.2.9-3	Water Inventory After Test S01007 Was Completed	4.2.9-17
4.2.9-4	Mass Balance for Test S01007	4.2.9-18
5.1-1	Test-To-Test Comparison	5.1-3
5.3-1	Comparison of S00605 and S00303	5.3-5

LIST OF FIGURES

<u>Figure No.</u>	<u>Title</u>	<u>Page</u>
2.2-1	SPES-2 Facility P&ID	2.2-7
2.3-1	SPES-2 Simulated Reactor Vessel	2.3-9
2.4-1	Loop A Instrumentation	2.4-5
2.4-2	Loop B Instrumentation	2.4-7
2.6.1-1	Break Line for 2-inch Cold-Leg Break	2.6-5
2.6.1-2	SPES-2 Break Orifice on CL for 2-in. Break	2.6-6
2.6.2-1	Break Line for 1-in. Cold-Leg Break	2.6-10
2.6.2-2	SPES-2 Break Orifice on CL for 1-in. Break	2.6-11
2.6.3-1	Break Line for 2-in. Cold-Leg Break	2.6-15
2.6.3-2	SPES-2 Break Orifice on CL for 2-in. Break	2.6-16
2.6.4-1	Break Line Configuration for 2-in. DVI-B Break	2.6-20
2.6.4-2	SPES-2 Break Orifice on DVI-B for 2-in. Break	2.6-21
2.6.5-1	Break Line Configuration for DEG of DVI-B	2.6-25
2.6.5-2	SPES-2 DVI-B Break Orifice Used in Position 3	2.6-26
2.6.5-3	SPES-2 DVI-B Break Orifice Used in Position 2	2.6-27
2.6.6-1	Break Line Configuration for DEG of CL-B2 to CMT-B Balance Line	2.6-31
2.6.6-2	SPES-2 DEG Break Orifice Used in Position 2	2.6-32
2.6.6-3	SPES-2 DEG Break Orifice Used in Position 3	2.6-33
2.6.7-1	Break Line Configuration for 2-in. Break in the CL-B2 to CMT-B Balance Line	2.6-37
2.6.7-2	SPES-2 Break Orifice Used in Position 1	2.6-38
2.6.8-1	Break Line Configuration for Steam Generator Tube Rupture (SGTR)	2.6-42
2.6.8-2	SPES-2 SGTR Break Orifice	2.6-43
2.6.9-1	Break Line Configuration for Steam Generator Tube Rupture (SGTR)	2.6-47
2.6.9-2	SPES-2 SGTR Break Orifice	2.6-48
2.6.10-1	Break Line Configuration for Steam Generator Tube Rupture (SGTR)	2.6-53
2.6.10-2	SPES-2 SGTR Break Orifice	2.6-54
2.6.11-1	SPES-2 Break Orifice for Main Steam Line Break	2.6-58
2.6.12-1	Break Line Configuration for 2-in. Cold-Leg Break	2.6-62
2.6.12-2	SPES-2 Break Orifice on CL for 1-in. Break	2.6-63
2.6.13-1	Break Line Configuration for 2-in. Cold Leg Break	2.6-67
2.6.13-2	SPES-2 Break Orifice on CL for 2-in. Break	2.6-68
3-1	Data Documentation Steps	3-12
3-2	Steps in SPES-2 Data Processing	3-13
4.2.2-1	Facility Response Summary for S00303	4.2.2-18
4.2.2-2	Power Channel Temperatures and Saturation Temperature for S00303	4.2.2-19
4.2.2-3	Accumulator A Pressure and Level for S00303	4.2.2-20
4.2.2-4	Accumulator B Pressure and Level for S00303	4.2.2-21

LIST OF FIGURES (Cont.)

<u>Figure No.</u>	<u>Title</u>	<u>Page</u>
4.2.3-1	Facility Response Summary for S01703	4.2.3-8
4.2.3-2	Pressurizer Pressure for S01703 and S00303	4.2.3-9
4.2.3-3	Pressurizer Pressure for S01703 and S00303	4.2.3-10
4.2.3-4	Upper Plenum Temperature for S01703 and S00303	4.2.3-11
4.2.3-5	Upper Plenum Temperature for S0170 ² and S00303	4.2.3-12
4.2.3-6	Lower Plenum Temperature for S01703 and S00303	4.2.3-13
4.2.3-7	IRWST Injection Line-A Flow Rate for S01703 and S00303	4.2.3-14
4.2.3-8	Annular Downcomer dP (Collapsed Level) for S01703 and S00303	4.2.3-15
4.2.3-9	Upper Tubular Downcomer dP (Collapsed Level) for S01703 and S00303	4.2.3-16
4.2.3-10	Rod Bundle dP (Collapsed Level) for S01703 and S00303	4.2.3-17
4.2.4-1	Facility Response Summary for S00504	4.2.4-19
4.2.4-2	Power Channel Temperatures and Saturation Temperature for S00504	4.2.4-20
4.2.5-1	Facility Response Summary for S00401	4.2.5-19
4.2.5-2	Power Channel Temperatures and Saturation Temperature for S00401	4.2.5-20
4.2.5-3	Accumulator A Pressure and Level for S00401	4.2.5-21
4.2.5-4	Accumulator B Pressure and Level for S00401	4.2.5-22
4.2.6-1	Facility Response Summary for S01613	4.2.6-19
4.2.6-2	Power Channel Temperatures and Saturation Temperature for S01613	4.6.2-20
4.2.6-3	Accumulator A Pressure and Level for S01613	4.6.2-21
4.2.6-4	Accumulator B Pressure and Level for S01613	4.6.2-22
4.2.7-1	Facility Response Summary for S00605	4.7.2-18
4.2.7-2	Power Channel Temperatures and Saturation Temperature for S00605	4.7.2-19
4.2.8-1	Facility Response Summary for S00706	4.2.8-19
4.2.8-2	Power Channel Temperatures and Saturation Temperature for S00706	4.2.8-20
4.2.8-3	dP (Collapsed Level) in Power Channel, Above Rod Bundle for S00706	4.2.8-21
4.2.9-1	Facility Response Summary for S01007	4.2.9-19
4.2.9-2	Power Channel Temperatures and Saturation Temperature for S01007	4.2.9-20
4.2.9-3	Accumulator A Pressure and Level for S01007	4.2.9-21
4.2.9-4	Accumulator B Pressure and Level for S01007	4.2.9-22
4.2.10-1	Facility Response Summary for S00908	4.2.10-18
4.2.10-2	Power Channel Temperatures and Saturation Temperature for S00908	4.2.10-19
4.2.10-3	Accumulator A Level and Pressure for S00908	4.2.10-20
4.2.10-4	Accumulator B Level and Pressure for S00908	4.2.10-21
4.2.11-1	Facility Response Summary for S01309	4.2.11-21
4.2.11-2	Primary to Secondary SGTR Flow Rate for S01309	4.2.11-22
4.2.11-3	SGTR Integrated Break Flow for S01309	4.2.11-23
4.2.11-4	SFW Flow Rate to SG-A and SG-B for S01309	4.2.11-24
4.2.12-1	Facility Response Summary for S01110	4.2.12-15

LIST OF FIGURES (Cont.)

<u>Figure No.</u>	<u>Title</u>	<u>Page</u>
4.2.12-2	Power Channel Temperatures and Saturation Temperature for S01110	4.2.12-16
4.2.12-3	Integrated SGTR Flow for S01110	4.2.12-17
4.2.12-4	SG-A and SG-B Level for S01110	4.2.12-18
4.2.12-5	Primary to Secondary SGTR Flow Rate for S01110	4.2.12-19
4.2.13-1	Facility Response Summary for S01211	4.2.13-17
4.2.13-2	Power Channel Temperatures and Saturation Temperature for S01211	4.2.13-18
4.2.13-3	Accumulator A Pressure and Level for S01211	4.2.13-19
4.2.13-4	Accumulator B Pressure and Level for S01211	4.2.13-20
4.2.13-5	Primary to Secondary SGTR Flow Rate for S01211	4.2.13-21
4.2.13-6	SGTR Integrated Break Flow for S01211	4.2.13-22
4.2.13-7	Primary System, SG-A, and SG-B Pressure for S01211	4.2.13-23
4.2.13-8	CMT A/Primary System Pressure Differential, CMT Level dP for S01211 . .	4.2.13-24
4.2.13-9	CMT B/Primary System Pressure Differential, CMT Level dP for S01211 . .	4.2.13-25
4.2.14-1	Facility Response Summary for S01512	4.2.14-17
4.2.14-2	SG-B Temperatures and U-tube Collapsed Level (dP) for S01512	4.2.14-18
4.2.14-3	PRHR HX Heat Removal Rate for S01512	4.2.14-19
4.2.14-4	CMT Heat Removal Rate for S01512	4.2.14-20
4.2.14-5	Loop-A Cold Leg Venturi dPs for S01512	4.2.14-21
4.2.14-6	Loop-B Cold Leg Temperatures for S01512	4.2.14-22
4.2.14-7	PRHR HX and CMT Natural Circulation Flow Rates	4.2.14-23
4.2.14-8	Power Channel Temperatures and Upper Head Collapsed Level (dP) for S01512	4.2.14-24
4.2.14-9	SG-A Inlet/Outlet and Primary Saturation Temperatures for S01512	4.2.14-25
4.2.14-10	SG-B Inlet/Outlet and Primary Saturation Temperatures for S01512	4.2.14-26
4.2.14-11	Integrated Primary System Mass Addition by CMTs for S01512	4.2.14-27
4.2.14-12	Integrated Steam Line Break Flow for S01512	4.2.14-28
5.1-1	Rod Bundle Fluid Steam Fraction Before ADS Actuation	5.1-5
5.1-2	Fluid Steam Fraction in Core at Minimum Coolant Inventory	5.1-6
5.3-1	Comparison of Break Locations and Total Break Flow	5.3-6
5.3-2	Comparison of Break Locations and Balance Line dP	5.3-7
5.3-3	Comparison of Break Locations and Annular Downcomer dP	5.3-8
5.3-4	Comparison of Break Locations and Tubular Downcomer dP	5.3-9
5.3-5	Comparison of Break Locations and Rod Bundle dP	5.3-10
5.3-6	System Mass In and Out for S00303	5.3-11
5.3-7	Change in System Mass Inventory for S00303	5.3-12
5.3-8	System Mass In and Out for S00605	5.3-13

LIST OF FIGURES (Cont.)

<u>Figure No.</u>	<u>Title</u>	<u>Page</u>
5.3-9	Change in System Mass Inventory for S00605	5.3-14
5.3-10	System Mass In and Out for S01007	5.3-15
5.3-11	Change in System Mass Inventory for S01007	5.3-16
5.4-1	Change in System Mass Inventory for S00303 and S00401	5.4-3
5.4-2	Change in System Mass Inventory for S00908 and S00706	5.4-4
5.4-3	Rod Temperature Relative to Saturation Temperature, S00706 and S00303	5.4-5
5.5-1	Change in System Mass Inventory for S00303 and S00504	5.5-2
5.6-1	Pressurizer Pressure for S00401 and S01613	5.6-4
5.6-2	Change in System Mass Inventory for S00401 and S01613	5.6-5
5.6-3	Change in System Mass Inventory for S00303 and S01703	5.6-6
5.6-4	Primary System Pressure for S01110 and S01309	5.6-7
5.6-5	Primary and SG-A Secondary Pressure for S01309	5.6-8
5.6-6	Rod Bundle dP (Collapsed Level) for S01110 and S01309	5.6-9
5.6-7	Pressurizer Level for S01110 and S01309	5.6-10

SUMMARY

The SPES-2 facility was a full-height, full-pressure, and 1/395th power and volume scale simulation of the AP600 nuclear steam supply system and the AP600 passive safety features. A series of twelve design basis events were simulated at SPES-2 to obtain data for verification and validation of the computer models used for the safety analysis of the AP600. This report describes the SPES-2 test program and test results.

The SPES-2 test program was performed as part of the Advanced Light Water Reactor (ALWR) program sponsored by the U.S. Department of Energy (DOE) and the Electric Power Research Institute (EPRI). Westinghouse conducted this test program in cooperation with SIET (Società Informazioni Esperienze Termoidrauliche), ENEL (Ente Nazionale per l'Energia Elettrica), ENEA (Ente per Le Nuove Tecnologie, l'Energia e l'ambiente), and Sopren-Ansaldo.

ACKNOWLEDGEMENTS

The authors wish to acknowledge Dr. Gianni Scandola, Dr. Carlo Medich, Dr. Marco Rigamonti and Dr. Oneste Viscovi of SIET for their management and technical expertise in the design, construction, and operation of the SPES-2 facility. Also, Ms. Marina Bacchiani of SIET and Mr. Mario Tarantini of ENEA are acknowledged for their tireless efforts in processing, analyzing, verifying, and transmitting test data.

The authors are indebted to Dr. Alessandro Alemberti, Cesare Frepoli and Gerardo Grazziosi of Ansaldo-Sopren for performing analyses supporting both the design of the SPES-2 facility, and the operation of the tests.

The hard work, long hours, and dedication to high quality of all the SIET personnel who constructed, operated, and maintained the SPES-2 facility are recognized. A special thank you is extended to Stephano Gandolfi and Guiseppi Visconti for their work on the instrumentation and data acquisition system, and for their delicious home-made wine.

The editing skills of Ms. Patti Todaro, Ms. Becky Jung, and Ms. Leslie McSwain; the skill and patience of the Word Processing Center operators; and Mr. Michael Mankowski's computer and graphics skills were invaluable in producing this document.

1.0 INTRODUCTION

This report describes the SPES-2 test program and test results. SPES-2 was a full-height, full-pressure integral systems simulation of the Westinghouse AP600 reactor design. This SPES-2 test was performed as part of the Advanced Light Water Reactor (ALWR) program sponsored by the U.S. Department of Energy (DOE) and the Electric Power Research Institute (EPRI). Westinghouse, in cooperation with SIET (Società Informazioni Esperienze Termoidrauliche), ENEL (Ente Nazionale per l'Energia Elettrica), ENEA (Ente per le Nuove Tecnologie, l'Energia e l'ambiente), and Sopren-Ansaldo, performed the SPES-2 tests to obtain data on the integrated behavior and performance of the AP600 passive safety systems to support validation of the computer codes used to perform the licensing safety analyses for the AP600.

1.1 Background

AP600 is a 600 MWe Westinghouse Advanced Reactor designed to increase plant safety with accident mitigation features that, once actuated, depend only on natural forces such as gravity and natural circulation to perform all required safety functions. These "passive" safety features can also result in a significant simplification in plant systems, equipment, and operation. In addition to the passive safety systems, the AP600 design incorporates many design improvements, including the following:

- a low-power density core
- a new design for primary loop arrangement that eliminates the cold-leg loop seal
- direct safety injection into the reactor-vessel downcomer

The AP600 primary system is a two-loop design. Each loop contains one hot leg, two cold legs, and one steam generator with two canned reactor coolant pumps (RCPs) attached directly to the steam generator outlet channel head. The passive safety systems are comprised of the following:

- Two full-pressure core makeup tanks (CMTs) that can provide borated makeup water to the primary system at any pressure.
- Two accumulators that provide borated water to the reactor vessel when/if primary pressure ≤ 700 psia.
- A passive residual heat removal (PRHR) heat exchanger (HX), comprised of a C-shaped tube bundle submerged inside the in-containment refueling water storage tank (IRWST), that can remove heat from the primary system at any pressure.
- The automatic depressurization system (ADS), which is comprised of a set of valves connected to the pressurizer steam space and the two hot legs. These valves are opened sequentially to provide a controlled depressurization of the primary system.
- An IRWST that provides a large source of core cooling water, which drains by gravity after the ADS has actuated.

-
- A passive containment cooling system (PCS) that utilizes the AP600 steel containment shell to transfer heat to the environment (ultimate heat sink). The PCS was not included in the SPES-2 experiments.

The SPES-2 test facility was designed to model the AP600 but made use of the existing SIET SPES facility. The original SPES test facility was constructed in 1985 as a full-height, full-pressure model of a Westinghouse three-loop pressurized water reactor (PWR).

SPES (now called SPES-2) was substantially modified to model the AP600 plant at full-scale elevation and full pressure, while simulating the full AP600 plant range of power with a volume scaling factor of 1/395. SPES-2 makes use of some major components of the previous facility such as rod bundle, pressurizer, steam generators and RCPs. However, the reactor-vessel downcomer, lower plenum, upper plenum, and upper head were all replaced to model the AP600 plant components. Also the SPES RCPs were re-oriented in order to eliminate the cold-leg loop seal that exists in standard Westinghouse PWRs. All of the main coolant loop piping and passive safety systems have been expressly designed and constructed for SPES-2 in order to model the AP600 plant. A complete description of the SPES-2 facility is provided in Reference 1.

After construction, a series of cold, low-pressure and hot, high-pressure pre-operational tests were performed to characterize the SPES-2 facility, to demonstrate proper operation of the facility, and to ensure that piping/component parameters properly matched the AP600 plant prior to the performance of matrix tests. The matrix tests discussed in Section 1.3 were developed to examine the AP600 passive safety system performance in mitigating the effects of design basis events (DBEs). Events that were simulated include loss-of-coolant accidents (LOCAs) ranging from 1-in. diameter equivalent to the double-ended guillotine (DEG) break of an 8-in. direct vessel injection (DVI) line, steam generator tube ruptures (SGTRs), and a large main steamline break (SLB).

This final data report discusses the results of the cold pre-operational tests, hot pre-operational tests, and matrix tests performed at the SPES-2 facility. This report supersedes the data and information provided in the Quick Look Reports (Reference 2).

1.2 Test Objectives

There are two primary objectives of the AP600, SPES-2 Integral Systems Test:

- To obtain data on the AP600 thermal-hydraulic phenomena and behavior of the passive safety system following specific small-break LOCAs, SGTRs, and an SLB.
- To obtain detailed experimental results for verification and validation of safety analysis computer codes.

1.3 Test Matrix

The SPES-2 test matrix was developed to examine the performance/capability of the AP600 passive safety systems to mitigate the effects of postulated DBEs and to provide useful data for computer code development and validation. These events and the individual test initial and boundary conditions were selected to challenge the passive safety systems, to provide direct comparisons between selected tests, and/or to match the limiting assumptions used in safety analysis computer codes. The resulting test matrix is shown in Table 1-1 and is discussed below.

Note that matrix test no. 2 in Table 1-1 was not performed because the AP600 actuation logic for the PRHR HX was revised to initiate PRHR operation whenever the safety systems actuation (S) signal occurs. This test was intended to simulate a LOCA recovery with steam generator startup feedwater (SFW) operating. This would have delayed PRHR HX operation until ADS was actuated, with the prior AP600 actuation logic.

Loss of Coolant Accidents

The passive safety systems are required to provide sufficient water for LOCA mitigation over a long period of time, thus CMT draindown, ADS actuation, accumulator delivery, and primary system depressurization to IRWST delivery all must occur. Therefore, eight different LOCA simulations with a wide selection of sizes and locations were required and tested to observe the integrated operation of the passive system over a wide range of conditions. All LOCA tests, with one exception, were performed without operation of the active, nonsafety pumped injection/heat removal. All tests were initiated from full-power operating conditions and used the minimum Standard Safety Analysis Report (SSAR) pressure setpoints for reactor trip and safety system actuations.

Test No. 1 A 1-in. diameter break simulation was selected as the smallest LOCA to be simulated. This was based on analyses that showed that complete heatup of the CMT water occurred prior to ADS actuation, so that any effect of CMT water flashing during depressurization could be observed.

Test No. 3 A 2-inch break simulation in the bottom of a cold-leg loop pipe (which contains a CMT balance line) was performed as the base case LOCA to which other LOCAs would be compared. Analysis showed that this break resulted in the minimum primary system water inventory during passive system mitigation of higher probability, small cold-leg breaks.

This 2-inch diameter, base case break simulation was repeated at the end of the test program to demonstrate the repeatability of the SPES-2 facility operation and passive safety system performance.

-
- Test No. 4** The 2-inch LOCA simulation with operation of the active, nonsafety systems was performed in order to observe passive safety system versus nonsafety system interactions as compared with the base case 2-inch LOCA (test no. 3).
- Test Nos. 5&7** A 2-inch break simulation in the DVI line and in the cold-leg to CMT balance line were each performed to observe the effect of break location on the passive safety system mitigation capability as compared to the base case 2-inch LOCA (test no. 3).
- Test No. 6** A DEG break simulation of one of two DVI lines was performed to minimize the amount of safety injection flow delivered to the reactor vessel (only one of two CMTs, accumulators, and IRWST injection lines deliver). Also, this was considered to be the largest break that could be reasonably simulated in the SPES-2 facility.
- Test No. 8** A DEG break simulation of one 8-inch cold-leg to CMT balance line was performed to observe the effect on the faulted CMT and to provide a comparison LOCA with the DEG DVI LOCA.
- Test No. 13** The 1-inch diameter break simulation (test no. 1) was repeated with the number of PRHR HX tubes increased from one tube to three tubes to maximize the primary system cooling and to better simulate two PRHR HXs in operation in the AP600 plant.

Steam Generator Tube Ruptures

The mitigation of an SGTR consists of reducing the pressure of the primary system to be equal to or less than the faulted steam generator pressure to terminate primary to secondary flow and to prevent overflow of the faulted generator. At the same time, heat removal from the primary system must be provided both to maintain subcooling during the primary pressure reduction and to remove core decay heat. In current PWR designs, the recovery from an SGTR typically requires operator actions to identify and isolate the faulted generator, to establish manual heat removal from the primary system, and to manually depressurize the primary system. Three SGTRs were performed at SPES-2. All these tests modeled a full rupture of a single steam generator tube, and all were initiated from full-power operating conditions and used low-low pressurizer level to initiate reactor trip and safety system actuations.

- Test No. 9** An SGTR with operator action and nonsafety systems operating in conjunction with the passive safety systems was performed to observe the combined effect of manual SGTR recovery actions (used in current plants) and passive system operation.

Test No. 10 An SGTR without operator actions and without operation of active, nonsafety, pumped injection/heat removal was simulated to observe the capability of the passive systems to terminate the event without intervention.

Test No. 11 An SGTR without operator actions or nonsafety system operation but with the inadvertent actuation of the ADS was performed to observe the effect of backflow from the faulted steam generator on ADS depressurization capability and to obtain data for determining primary system boron concentration versus time.

Steam Line Break

This test was a simulation of a large single-ended SLB. It was performed to provide a rapid primary system cooldown transient and to observe the ability of the CMT to provide primary system mass addition without requiring ADS actuation.

Test No. 12 This test was performed at AP600 hot, zero power conditions, and no core decay heat was used. Also, this test was performed with three PRHR HX tubes to maximize primary system cooling and to better simulate two PRHR HXs in operation in the AP600. The break size was scaled to simulate a 1,388 ft.² AP600 break area (full steam generator outlet area) and was performed with no operator actions or active, nonsafety system operation.

1.4 SPES-2 Test Runs

There were seventeen test runs at the SPES-2 facility—thirteen of which were successful and are reported in this final data report. Four runs were considered either unsuccessful or inappropriate to report. Table 1-2 lists all seventeen runs, the test date, a brief test description, and a comment on the test acceptance. The test numbering scheme involved six characters: the first character, S, refers to the SPES-2 facility; the second three numbers are a sequential test run number (i.e., increased by 1 each time a test was initiated); the last two characters refer to the matrix test number (from Table 1-1). For example, the eleventh test run at the facility was the performance of matrix test number 10 and was S01110.

Three of the SPES-2 matrix tests were designated as "blind" tests. The data for these three tests were reviewed only by the Westinghouse Test Engineering group. However, the initial and boundary conditions were provided to other Westinghouse personnel to allow "blind" computer code predictions of the facility responses to be performed.

**TABLE 1-1
SPES-2, TEST MATRIX**

Test No.	Test Type	Test Description (AP600 Transient Simulated)	Status Nonsafety Systems	AP600 Single Failure Simulated	Comment
1	Small Break LOCA	1-inch cold-leg break (Note 2), bottom of loop B (Note 1)	CVCS, NRHR, and SFWS Off. No operator actions (OAs).	One of two 4th-stage valves on loop B	Maximize CMT heatup prior to ADS actuation.
2	Small Break LOCA	1-inch cold-leg break, bottom of loop B	CVCS, NRHR Off; SFWS On (Note 3). No OAs.	One of two 4th-stage valves on loop B	This test deleted due to AP600 design changes.
3 (Note 4)	Small Break LOCA	2-inch cold-leg break, bottom of loop B	CVCS, NRHR, and SFWS Off. No OAs.	One of two 4th-stage valves on loop B	Reference cold-leg break.
4	Small Break LOCA	2-inch cold-leg break, bottom of loop B	CVCS, NRHR, and SFWS On (Note 3).	One of two 4th-stage valves on loop B	Nonsafety/passive system interactions.
5	Small Break LOCA	2-inch DVI break	CVCS, NRHR and SFWS Off. No OAs.	One of two 4th-stage valves on loop B	Asymmetric CMT performance.
6	Small Break LOCA	DEG break of DVI	CVCS, NRHR, and SFWS Off. No OAs.	One of two stage 1 and stage 3 valves	Complete loss of one-of-two injection flow paths.
7	Small Break LOCA	2-inch break in CL/CMTB balance line	CVCS, NRHR, and SFWS Off	One of two 4th-stage valves on loop B	Examine effect on CMT drain down.
8	Small Break LOCA	DEG break of a CL/CMTB balance line	CVCS, NRHR, and SFWS Off. No OAs.	One of two stage 1 and stage 3 ADS valves	No delivery from faulted CMT.
9	SGTR	Design basis SGTR (1 tube)	CVCS, SFWS On; Operator action to isolate SG, subcool, depressurize.	None	Recovery with operator action; show recovery margin.

**TABLE 1-1
SPES-2, TEST MATRIX (Cont.)**

Test No.	Test Type	Test Description (AP600 Transient Simulated)	Status Nonsafety Systems	Single Failure	Comment
10	SGTR	Design basis SGTR (1 tube)	No CVCS or SFWS. No OAs.	None	SGTR recovery with no operator action
11	SGTR	Design basis SGTR (1 tube) with inadvertent ADS actuation.	No CVCS or SFWS. No OAs.	One of two 4th-stage valves on loop B	ADS actuated to cause steam generator to primary flow. Observe dilution rate and effect on ADS performance.
12	SLB (with three PRHR HX tubes in service).	SL break at zero power. A 1.388 ft. ² single-ended SLB on SGA discharge.	No CVCS, NRHR, SFWS	None	Show CMTs do not drain and no ADS actuation occurs.
13	Small Break LOCA (with three PRHR HX tubes in service).	1-inch cold-leg break on bottom of loop B.	CVCS, NRHR, and SFWS off. No OAs.	One of two 4th-stage valves on loop B.	Show effect of three PRHR tubes, compare with matrix test 1.

Notes:

1. Loop B is the CMT side of plant; loop A is pressurizer and PRHR side of plant.
2. Break sizes are "a broken pipe of the indicated diameter," e.g., 2-inch break is 3.146 in.²
3. SG main feedwater isolated on S-signal and SFWS initiated, SFWS on until isolated on HI SG level or LO-Tcold.
4. Selected as repeat test to show facility repeatability.

TABLE 1-2
TEST RUNS AT SPES-2

Test Run Number	Test Date	Test Description	Comments
S00103	2/5/94	SBLOCA - 2-inch cold-leg break @ bottom of loop B	Successful, but not included in final report since AP600 ADS valve sizes and setpoints were changed.
S00203	4/9/94	SBLOCA - 2-inch cold-leg break @ bottom of loop B	Successful, but not included in final report since pressurizer to CMT balance line was subsequently deleted.
S00303	4/30/94	SBLOCA - 2-inch cold-leg break @ bottom of loop B	Successful
S00401	5/6/94	SBLOCA - 1-inch cold-leg break @ bottom of loop E	Successful
S00504	5/18/94	SBLOCA - 2-inch cold-leg break @ bottom of loop B with nonsafety systems	Successful
S00605	5/27/94	SBLOCA - 2-inch DVI break	Successful
S00706	6/10/94	SBLOCA - DEG break of DVI	Successful
S00807	6/12/94	SBLOCA - 2-inch break in CL/CMT balance line	Unsuccessful - due to valve misalignment in break piping to condenser.
S00908 (blind)	6/23/94	SBLOCA - DEG break of CL/CMT balance line	Successful
S01007	7/7/94	SBLOCA - 2-inch break in CL/CMT balance line	Successful
S01110	7/14/94	SGTR - 1 tube; passive safety systems only	Successful
S01211 (blind)	9/7/94	SGTR - 1 tube; inadvertent ADS actuation	Successful

TABLE 1-2 (Cont.)
TEST RUNS AT SPES-2

Test Run Number	Test Date	Test Description	Comments
S01309	9/22/94	SGTR - 1 tube; non-safety systems operational with operator action for mitigation	Successful
S01412	10/7/94	SLB @ hot, zero power conditions	Unsuccessful - Leak in several power channel heated rods caused unisolable water loss from facility.
S01512 (blind)	10/11/94	SLB @ hot, zero power conditions	Successful
S01613	10/15/94	SBLOCA - 1-inch cold-leg break @ bottom of loop B	Successful
S01703	11/11/94	SBLOCA - 2-inch cold-leg break @ bottom of loop B	Successful

2.0 TEST FACILITY DESCRIPTION

2.1 Introduction

The SPES facility is an experimental plant located at SIET (Societa Informazioni Esperienze Termoidrauliche) laboratories in Piacenza that was used to simulate the PWR W312 reactor with a volume scale of 1/427, full height and full pressure. To undertake a safety research program in the field of advanced reactors, ENEA (the Italian Commission for New Technologies, Energy, and Environment) proposed to SIET a study of the modifications necessary to transform the original SPES plant into a new facility, the SPES-2, which would model as closely as possible the AP600 design. The SPES facility was substantially modified to simulate the AP600 plant while maintaining full-scale elevation, full-pressure, and full-power with a volume scaling factor of 1/395. The SPES-2 facility retained some major components of the previous facility (rod bundle, pressurizer, steam generators), but had significant changes in the power channel and the primary pumps. In addition, all of the main coolant loop piping and the passive safety systems were expressly designed and constructed for SPES-2 in order to model the AP600. A complete description of the SPES-2 facility is provided in the Facility Description Report (WCAP 14073, Rev. 0, May 1994).

2.2 Facility Scaling Summary

2.2.1 General Scaling Criteria

The SPES-2 facility shall simulate the following:

- The primary sys.
- The secondary system up to the main steam line isolation valves (MSLIVs)
- The passive safety systems: accumulators, core makeup tanks (CMTs), in-containment refueling water storage tank (IRWST), passive residual heat removal (PRHR), and automatic depressurization system (ADS)
- The nonsafety systems: normal residual heat removal system (NRHR) and chemical and volume control system (CVCS)

The overall scaling factor shall be 1/395 and the main characteristics shall be:

- Process fluid water
- Loop number 2
- Pump number 2
- Primary design pressure 20 MPa
- Secondary design pressure 20 MPa
- Primary design temperature 365°C
- Secondary design temperature 310°C
- Maximum power 9 mW
- Elevation scaling 1:1

The SPES-2 scaling criteria shall preserve the following parameters:

- Fluid thermodynamic conditions
- Vertical elevations
- Power-to-volume ratio
- Power-to-flow rate ratio
- Transit time of fluid
- Heat flux

For example, the surge and passive safety system lines, where friction pressure drops are relevant to scaling of the AP600 plant, have been designed to maintain the dimensions of the reference plant, whereas the facility piping was designed with the Froude number conservatism in order to preserve the slug to stratified flow pattern transition in the horizontal piping.

The passive safety systems were designed according to the criteria described above in order to reproduce, as accurately as possible, the thermal-hydraulic phenomena in AP600 during a transient. Also, when deemed necessary, the layout of the connection lines was designed to preserve the similarity of the full-scale AP600 layout.

Elevation and volume comparisons between the SPES-2 facility and AP600 are shown in Tables 2.2-1 and 2.2-2. The facility P&ID is shown in Figure 2.2-1.

2.2.2 Specific Scaling Criteria

Power Channel

- Vertical elevations shall be preserved.
- The bundle geometry (rod pitch and diameter) shall be preserved.
- The total volume and the volumes of the single sections (lower plenum, riser, upper plenum, upper head) shall be scaled by 1/395.

The elevations of the lower plenum and upper head need not be preserved because they have no influence on the natural circulation phenomena.

Power Channel Downcomer

- The annular shape shall be maintained up to the direct vessel injection (DVI) nozzles, after which a tubular section shall connect it to the lower plenum.
- The annular and the tubular sections shall have the same friction pressure drops.
- The total volume shall be scaled by 1/395.
- Vertical elevations shall be preserved.
- The circumferential pressure drops in the annulus shall be similar to those in the AP600.

Pumps

- The nominal head shall be preserved.
- A flywheel shall be provided to better simulate the reference coastdown behavior.

Steam Generators

- While the steam generators remain the same, the number and length of the U-tubes shall not be scaled to the AP600, resulting in a lower than underestimated heat transfer surface.
- The secondary side volumes shall be scaled by 1/395 (2.5 percent difference).

The vertical elevations in the secondary side are preserved up to the top of the steam separator. The steam dome elevation, on the other hand, has no influence on the natural circulation phenomena.

Pressurizer

- The volume shall be scaled by 1/395.
- The bottom elevation shall be preserved.
- The level swelling phenomena shall be reproduced.

The level swelling phenomenon can occur in the pressurizer due to flashing of the contained liquid or because of steam inflow from the primary circuit. These phenomena have a significant influence on the quality of the fluid discharged through the ADS depressurization valves that are located on the top of the pressurizer.

The preservation of the level swelling will be accomplished by making the average void fraction in the SPES-2 pressurizer equal to that in the AP600 during similar thermal-hydraulic conditions. The diameter and the height correspond to the adoption of the Wilson (196) model.

Loop Piping

For the hot and cold legs:

- The Froude number shall be preserved.
- The horizontal part of the hot leg shall have the same length over diameter (L/D) as the AP600, and the indirect section of the hot leg shall maintain the same angle (55 degrees) as in the reference plant.
- Downstream of the surge line nozzle, the hot leg shall compensate for the volume difference between the AP600 and SPES-2 facility hot side of primary loop.
- The layout of the cold leg shall be designed to reproduce the flow path during a cold-leg break transient wherein the fluid must flow from the unbroken cold leg to the broken cold leg.

-
- The surge line friction pressure drops shall be maintained.

In the AP600, the pumps are directly attached to the steam generator outlet plena, whereas in the SPES-2 facility, the pumps are not connected to the steam generator. Therefore a section of pipe is necessary to maintain the elevation between the steam generator outlet and pump outlet. This pipe also compensates for the volume differences between the AP600 and SPES-2 facility primary loop cold side.

Passive Safety Systems

For the CMTs:

- Volume shall be scaled by 1/395.
- The metal mass shall be scaled to conserve condensation of steam along the component walls.

For the IRWST:

- The water volume shall be scaled by 1/395 and the elevation maintained.

Accumulators:

- Volume shall be scaled by 1/395
- Gas and water volume shall be scaled in the same proportion as the AP600

For the PRHR heat exchanger (HX):

- Only one of the two AP600 HXs shall be simulated. (The other one is a spare.)
- A C-shaped tube, similar to that in the AP600 design shall be used.
- The friction pressure drops shall be maintained.
- The number of tubes shall be scaled down by 1/395.

ADS:

- The four stages shall be simulated, per stage, by means of a ball valve with an ad hoc orifice.
- The flow area shall be scaled to the AP600.
- The connection of the fourth stage to the hot legs shall be located at the same L/D from the power channel as that in the AP600 reactor vessel.

**TABLE 2.2-1
ELEVATION COMPARISON**

Component	AP600 ft.	SPES-2 ft.	Difference ft.
Lower Plenum Bottom	(-7.571)	(-7.515)	(0.056)
Downcomer Bottom	(-6.168)	(-6.168)	(0)
Bottom of Active Fuel	(-5.484)	(-5.482)	(0.002)
Top of Active Fuel	(-1.827)	(-1.822)	(0.005)
Top of Upper Head	(3.819)	(2.779)	(1.04)
DVI Nozzle	(-0.508)	(-0.508)	(0)
Hot-Leg Centerline	(0)	(0)	(0)
Cold-Leg Centerline	(0.445)	(0.445)	(0)
Pressurizer Bottom	(5.856)	(5.856)	(0)
Pressurizer Top	(16.953)	(12.646)	(4.307)
Top of Steam Generator Tube Sheet	(4.107)	(4.107)	(0)
Top of U Tubes	(14.734)	(12.43)	(2.304)
CMT Bottom	(1.801)	(1.801)	(0)
CMT Top	(8.041)	(8.041)	(0)
Accumulator Bottom	(-4.026)	(-4.026)	(0)
Accumulator Top	(0.734)	(-0.982)	(1.716)
PRHR HX Bottom (average)	(2.667)	(2.667)	(0)
PRHR HX Top (average)	(8.026)	(8.026)	(0)
IRWST Bottom	(0.533)	(0.533)	(0)
IRWST Water Level	(8.53)	(8.53)	(0)

**TABLE 2.2-2
VOLUME COMPARISON**

Component	AP600 volume (ft.³)	SPES-2 ideal volume (deca meter³)	SPES-2 actual volume (deca meter³)
Hot Leg	3.542	8.967	32.6
Inlet Plenum	6.142	15.549	3.72
U-Tubes	25.366	64.218	40.65
Outlet Plenum	6.606	16.724	3.72
Pump Suctions	-	-	28.51/28.62
Pumps	5.04	12.76	4.33
Cold Legs	3.717	9.41	13.38
Total loop 1/2	50.413	127.628	126.91/127.02
Surge Line	2.878	7.286	9.63
Pressurizer	36.757	93.056	95.4
Total	39.635	100.34	105.03
Power Channel:			
Downcomer	21.479	54.377	54.38**
Lower Plenum	9.005	22.797	22.83
Riser	20.929	52.985	58.81***
Upper Plenum	17.798*	45.058	41.27
Upper Head	21.157	53.562	53.83
Total	72.57	228.779	231.12
Total primary circuit	230.819	584.37	590.08
Core Makeup Tank	56.634	143.377	143
Accumulator 56.634 143.377 143			
IRWST	2006	5.08	5.08
SG Secondary Side	157.159	398	388

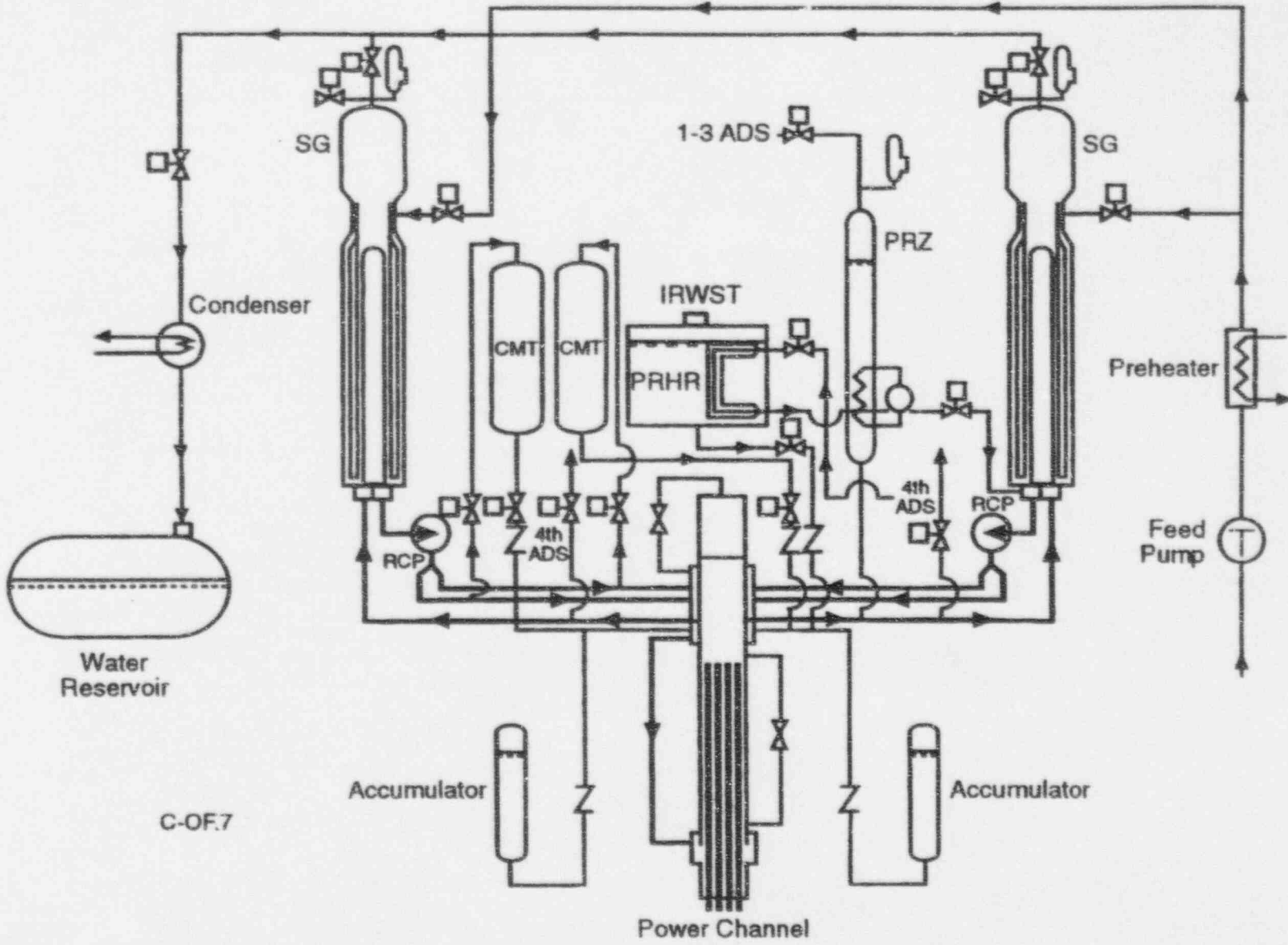


Figure 2.2-1 SPES-2 Facility P&ID

2.3 Facility Description

The SPES-2 facility consists of a full simulation of the AP600 primary and passive core cooling systems. The stainless steel test facility uses a 97-rod heated rod bundle that has a uniform axial power shape and uses skin heating of the heater rods. There are 59 heater rod thermocouples distributed over 10 elevations with most located at the top of the bundle to detect the possibility of bundle uncover. The heater rods are single ended and are connected to a ground bus at the top of the bundle at the upper core plate elevation. All but two rods are designed to have the same power. Two heater rods are hot rods that have 19 percent higher power.

The primary system, as shown in Figure 2.2-1, includes two loops—each with two cold legs, one hot leg, a steam generator and a single reactor coolant pump (RCP). The cold-leg flow splits downstream of the simulated RCP into two separate cold legs, which then flow into an annular downcomer. The pumps can deliver the scaled primary flow, and the heater rod bundle can produce the scaled full-power level such that the AP600 steady-state temperature distribution can be simulated. The steam generators have a secondary-side cooling system that removes heat from the primary loop during simulated full-power operation. Startup feedwater and power-operated relief valve (PORV) heat removal is provided following a simulated plant trip.

The upper portion of the simulated reactor vessel includes an annular downcomer region, where the hot and cold legs, as well as the safety injection lines, are connected (Figure 2.3-1). The annular downcomer is connected to a pipe downcomer below the direct vessel injection (DVI) lines; the pipe downcomer then connects to the vessel lower plenum. In this fashion, the four cold-leg, two hot-leg characteristics of AP600 can be preserved along with the downcomer injection. There are turning devices to direct the safety injection flow downwards in the annular downcomer, as in the AP600.

A full-height, PRHR HX, constructed in a C-tube design, is located in a simulated IRWST that is maintained at atmospheric pressure. The line pressure drop and elevations are preserved and the heat-transfer area is scaled such that the natural circulation behavior of the AP600 PRHR HX is simulated.

The design of the CMTs is unique and has been developed by the SIET engineers so that the CMT metal mass is scaled to the AP600 CMT. The SIET CMT design uses a thin-walled vessel inside a thicker pressure vessel, with the space between the two vessels pressurized to approximately 70 bar. In this manner, the amount of steam that condenses on the CMT walls during draindown is preserved. Since the CMTs are full height and operate at full pressure, the metal mass-volume ratio of a single pressure vessel would have been excessive, resulting in very large wall steam condensation effects.

A SPES-2 ADS combines the two sets of AP600 ADS piping off the pressurizer into a single set with the first-, second- and third-stage valves. An orifice in series with each ADS isolation valve is used to achieve the proper scaled flow area. The three ADS valves share a common discharge line to a condenser and a collection tank that has load cells to measure the mass accumulation. A similar measuring arrangement is also used for the two ADS fourth-stage lines, which are located on the hot legs of the primary system.

Small breaks are simulated using a spool piece that contains a break orifice and quick-opening valve. The break discharge is also condensed and measured by collecting the flow into a catch tank.

The specifics of the key systems/components are discussed in the following subsections.

2.3.1 Primary Piping

The primary piping consists of two loops. Each loop is made up of one hot leg and two cold legs. The hot leg, which connects the power channel to a steam generator, duplicates the AP600 up to the pressurizer surge line nozzle by maintaining the AP600 L/D in the horizontal section, and the same 55-degree angle in the inclined section.

As in the AP600 design, the SPES-2 facility has two cold legs per loop that transition from a single coolant pump vertical discharge. The split from the single pump discharge into the two cold legs is at the same elevation as the AP600 steam generator channel head in order to preserve the same flow path that the fluid must take from the unbroken cold leg to the broken one during a cold-leg break transient.

Due to the importance of the surge line during ADS depressurization, the line has been designed to preserve the friction pressure drops.

2.3.2 Power Channel

The pressure vessel consists of the following sections:

- An upper head
- An upper plenum that houses an annular downcomer and nozzles for the following lines:
 - two hot legs
 - four cold legs
 - two DVI (safety system injection lines)
 - a downcomer upper-head bypass
 - a bottom outlet going to a tubular downcomer section that connects to the lower plenum riser, with an inside octagonal cross section that houses the core bundle
- The lower plenum with the tubular downcomer inlet that contains the unheated lower portion of the rod bundle.

The volumes of the above mentioned sections are scaled by 1/395. The main features of SPES-2 pressure vessel are shown in Table 2.3-1, and the main characteristics of the power channel are shown in Table 2.3-2.

2.3.3 Rod Bundle

The rod bundle is electrically heated and consists of 97 Inconel rods that reproduce, in the active zone, the same geometry (rod pitch, rod diameter, and length) as that in the AP600 reactor core. The axial power profile is uniform for all the rods. The profile is also radially uniform with the exception of two rods that have a peaking factor of 1.19. The maximum power is 9 mW and the maximum current is 70 kA. The scaled full power used for the AP600 transients is 4.89 mW (x 1.02).

The main characteristics of the rod bundle are listed in Table 2.3-3.

2.3.4 Power Channel Downcomer

The downcomer is composed of an annular section with four cold legs and two direct vessel injection (DVI) nozzles for safety injection. Below these nozzles, a pipe connects the annular downcomer to the lower plenum. The annular and the tubular downcomer sections have the same friction pressure drops as the AP600, as well as a similar circumferential annular pressure drop. The total volume is scaled by 1/395.

2.3.5 Pressurizer

The pressurizer controls primary system pressure during normal and transient plant operation and consists of a cylindrical flanged vessel equipped with two immersible electrical heaters, each with a maximum controlled power of 16 kW. The pressurizer volume is scaled and the bottom elevation is preserved. The diameter and the height correspond to the adoption of the Wilson model for level-swelling phenomena.

2.3.6 Pumps

Two primary pumps (one per loop) drive primary coolant into the power channel downcomer to remove the generated heat. The pumps are centrifugal single-stage horizontal-shaft type. The suction line is horizontal, and the pumps' discharge is directed downwards into a 3-in. pipe common to the two cold legs. A flywheel provides an inertia closer to the AP600. The rotational speed can be controlled in the range +/-190 percent of the nominal value (with fluid in two-phase conditions) and the speed variations can be programmed by means of a motor-driven regulator.

2.3.7 Steam Generators

The SPES-2 facility has two identical generators to transfer thermal power from the primary to the secondary circuit. The steam generator primary side consists of a tube bundle and inlet/outlet plena. The steam generator bundle includes thirteen Inconel-600 U-tubes in a square array.

The secondary side volumes are scaled by 1/395, and all of the vertical elevations are preserved up to the top of the steam separator (the steam dome has no influence on the natural circulation phenomena). The main characteristics of SPES-2 steam generators are shown in Table 2.3-4.

2.3.8 Passive Safety Systems

The passive safety systems were designed to reproduce, as accurately as possible, the thermal-hydraulic phenomena that can occur in the AP600 during transients. Also, where necessary, the layout of the connections lines simulated the AP600 layout. The following safety components, associated piping, and required valves were designed following these criteria:

- Two CMTs with volume and metal mass scaled to conserve overall water temperatures and steam condensation on the CMT walls. The CMT design shall use a thin-walled vessel inside a thicker pressure vessel with the space between the two vessels pressurized with air at 70 bar.
- Two accumulators with volume scaled by 1/395.
- One passive residual heat removal (PRHR) with a full-height, C-shaped heat exchanger with friction pressure drops maintained and number of tubes scaled.
- One in-containment refueling water storage tank (IRWST) at atmospheric pressure with water volume scaled by 1/395 and elevation maintained.
- Four stages of the ADS simulated by means of ball valves (one per stage) with a series of orifices that achieve the proper scaled flow area. The two sets of piping connected to the steam space of the pressurizer in the AP600 are combined into a single set with the first, second, and third stage valves in SPES-2.

The injection capability of the AP600 nonsafety systems, such as CVCS, NRHR, and SFW, simulated any safety/nonsafety system interaction. The friction pressure drops of all the connecting lines were maintained. Small breaks were simulated using a spool piece that contained a break orifice and quick opening valve. The break, ADS, and secondary relief valve discharges were collected into different catch tanks with load cells to measure the mass accumulation.

**TABLE 2.3-1
PRESSURE VESSEL MAIN CHARACTERISTICS**

Pressure		
nominal	2250 psi	(15.5 MPa)
design	2900 psi	(20.0 MPa)
Temperature		
core inlet	529.0°F	(276.1°C)
core outlet	594.3°F	(312.4°C)
design	688.8°F	(364.9°C)
Flow rate		
hot leg	27.8 lb/sec	(12.6 kg/sec.)
core bypass	0 lb/sec	(0 kg/sec.)
downcomer upper-head bypass	0.55 lb/sec	(0.25 kg/sec.)
Overall Height	34.3 ft.	(10.45 m)
Net Volume	7.73 ft. ³	(218.75 dm ³)
Nozzle Diameter		
hot leg	2.63 in.	(66.7 mm)
cold leg	2.13 in.	(54.0 mm)
direct vessel injection	0.465 in.	(11.8 mm)
tubular downcomer	3.62 in.	(92.0 mm)
downcomer upper-head bypass	0.957 in.	(24.3 mm)
Vessel Material		AISI 316
Loose Flanges Number		
lower plenum		1
riser		1
core		21
upper plenum/head		1

**TABLE 2.3-2
POWER CHANNEL MAIN CHARACTERISTICS**

Description	Elevations (mm)		Length (mm)	D (mm)	Area (dm ²)	Flow Area (dm ²)	Volume + (dm ³)	Fluid Volume (dm ³)	Body Mass (kg)	Flange Mass (kg)	Bolting Mass (kg)
Lower Plenum	-7515	-6600	915	152	1.81	1.13	16.60	10.30	221	36	27
	-6600	-6168	432	216	3.66	2.97	15.50	12.53			
Riser	-6168	-5568	600	152	1.81	1.13	10.88	6.76	66	40	-
	-5568	-1458	4110	141*	1.65	0.97	67.94	39.68	541	794	329
Upper Plenum	-1458	683	2141	158	1.96	1.96	41.27	41.27	158	-	39
Upper Head	683	871	188	158	1.96	1.96	3.57	3.56	467	-	18
	871	2709	1838	187	2.75	2.75	50.26	50.26			
Annular Downcomer	-878	652	1530	202/168	0.99	0.99	14.87	14.87	304**	-	-
Tubular Downcomer	-800	6076	6270	87.3	0.60	0.60	37.53	37.53	346	84	23
	6020	6168	148	216/182	1.06	0.37	1.57	1.57			
Downcomer Upper-Head Bypass	600	1425	825	24.3	0.05	0.05	0.38	0.41	11	21.52	6.12
Core Bypass	-5812	-1058	8473	42.9	0.145	0.145	12.37	12.37	93	20.54	3.8
Total								231.12	2207	996.06	446

Note: The rod bundle mass, upper plate, and grids included, is 239 kg.

* Octagonal section

** The metal mass of the separation cylinder is included in the upper plenum

**TABLE 2.3-3
ROD BUNDLE MAIN CHARACTERISTICS**

Number of Rods		
total		97
standard rods		95
hot rods		2
Design Pressure, MPa/Temperature		
standard rod	2900 psi/842°F	(20/450°C)
	2321 psi/1202°F	(16/650°C)
hot rod	2900 psi/932°F	(20/500°C)
	2321 psi/1292°F	(16/700°C)
Rod External/Inner Diameter		
standard rod	0.374/0.311 in.	(9.5/7.9 mm)
hot rod	0.374/0.295 in.	(9.5/7.5 mm)
Lattice	square	square
Pitch	0.496 in.	(12.6 mm)
Minimum Rod-Wall Gap	0.110 in.	(2.8 mm)
Lengths		
total	254.61 in.	(6467 mm)
inside vessel	244.88 in.	(6220 mm)
heated	144.21 in.	(3663 mm)
Power		
nominal		4894 kW
maximum		9000 kW
Maximum Current		70 kA
Rod Material		
from 0 to 5.12 in. (0-130 mm)		copper
from 5.12 to 95.43 in. (130 mm - 2424 mm)		AISI 316
from 95.43 to 239.65 in. (2424 mm - 6087 mm)		Inconel 600
from 239.65 to 254.61 in. (6087 mm - 6467 mm)		Nickel 200

**TABLE 2.3-4
STEAM GENERATOR MAIN CHARACTERISTICS**

Design Pressure	2900 psi	(20MPa)
Design Temperature	689 °F	(365°C)
Nominal Conditions		
pressure	710.7 psi	(4.9MPa)
feedwater flowrate	2.98 lbm/sec.	(1.35 kg/sec.)
feedwater temperature	439°F	(226°C)
level	42 ft.	(12.8 m)
relief valve set pressure	1015 psi	(7.0 MPa)
safety valve set pressure	1450 psi	(10 MPa)
PORV orifice D	0.205 in.	(5.2 mm)
U Tube Number		13
U Tube Average Length	54.8 ft.	(16.7 m)
Heat Exchange Surface	127 ft. ²	(11.8 m ²)
Overall Height	51.15 ft.	(15.59 m)
Secondary Fluid Volume	13.7 ft. ³	(388 dm ³)
NOZZLE ID		
feedwater line	1.5 in.	(38.1 mm)
steam line	2.9 in.	(73.7 mm)
inlet/outlet plena	2.62 in.	(66.6 mm)
Materials		
primary plena, tube sheet		ASTM-SA 182 F 304
lower vessel		ASTM-SA 106 Gr B
intermediate vessel (sep. side)		ASTM-SA 204 Gr C
upper vessel (steam dome)		ASTM-SA Gr B
loose flanges		ASTM-SA 105
separator, dryers		AISI 304
fillers		Nickel-plated

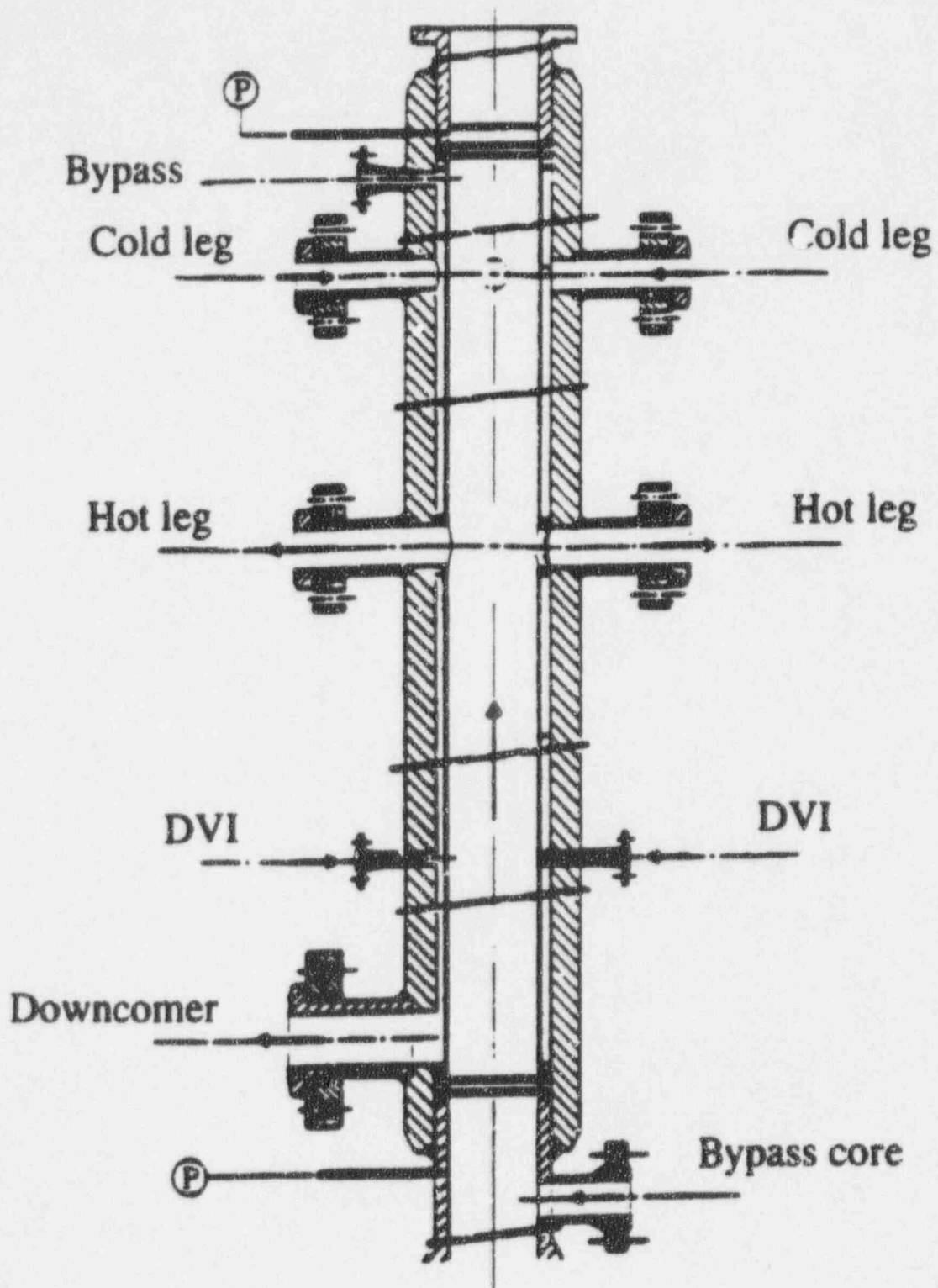


Figure 2.3-1 SPES-2 Simulated Reactor Vessel

2.4 Instrumentation

The SPES-2 facility instrumentation has been developed to provide transient mass and energy balances on the test facility. There are approximately 500 channels of instrumentation that monitor the facility and component pressure, temperature, and mass inventory.

A variety of different methods and components were used to measure the significant thermodynamic quantities that are direct (absolute and differential pressure, temperature, voltage, current, etc.) and derived quantities (mass velocity, flowrate, etc.) as shown below:

<u>Quantity</u>		<u>Method or Component</u>
Pressure	-	Pressure transmitters
Differential pressure	-	Differential pressure transmitters
Temperature	-	Thermocouples/thermoreistances
Collapsed level	-	Differential pressure transmitters
Density	-	γ -densitometers
Velocity	-	Turbines/orifices, venturi tubes
Flow rate	-	Turbines/orifices, venturi tubes
Integral flowrate	-	Catch tanks
Electrical power	-	Voltage drops and shunts

The flows into the simulated reactor system, such as the CMT discharge flow, the accumulator flow and the IRWST flow, are measured using venturi flow meters. Flows out of the test facility, such as break flow and ADS flow, are measured with a turbine meter and condenser/collection tank. The use of condensers allows accurate mass flow versus time measurements of the two-phase ADS and break flow streams. The use of collection tanks following the condensers provides redundancy for the critical measurements of the mass leaving the test system. Differential pressure measurements are arranged as level measurements on all vertical components to measure the rate of mass change in the component. There are also differential pressure measurements between components to measure the frictional pressure drop, both for single- and two-phase flow. The CMTs are instrumented with wall and fluid thermocouples to measure the CMT condensation and heatup during their operation. The PRHR HX is also instrumented with wall and fluid thermocouples so that the tube wall that flux can be calculated from the data. There are thermocouples in the simulated IRWST to measure the fluid temperature distribution and to assess the amount of mixing that occurs. The rod bundle power is measured accurately to obtain the rod heat flux and the total power input to the test facility.

The specific instrumentation for loop A is shown in Figure 2.3-1 and for loop B is shown in Figure 2.3-2. A complete listing of the SPES-2 instrumentation is provided in Appendix C. These instrumentation layouts reflect the SPES-2 facility at the end of the testing program. The modified instruments are listed in Table D2, and the failed instruments are listed in Table D1. A discussion of each instrumentation type and its applications is discussed in the following subsections.

2.4.1 Absolute and Differential Pressure Transmitters

Pressure transmitters are used to measure the following:

- Pressure drops on piping, orifices, and venturi tubes
- Absolute pressures
- Liquid and collapsed levels

The main features are the following:

- Silicon piezoresistive sensor
- Microprocessor electronics
- Compensation of temperature and static pressure changes
- Measuring ranges: 0 to 20 MPa, 0 to 700 KPa, 0 to 100 KPa
- Minimum applicable range: 20 to 400 of measuring range

2.4.2 Thermocouples and Thermoresistances

The temperatures of fluid, structures, piping, and core heater rods are measured by ungrounded sheathed type-K thermocouples. The majority of the thermocouples that measure fluid temperatures are installed in the test facility pipelines with the hot junction on the pipe axis (D/2); some of the thermocouples are installed with a different criterion (i.e., D/3).

Fluid temperatures in the IRWST are measured using a type-PT100 resistance temperature detector.

2.4.3 Flowmeters

Single-phase fluid (water or steam) flow rates are measured by using different types of flowmeters such as calibrated orifices, venturi tubes and full-flow turbine.

2.4.4 Integral Mass Flowmeters

The masses of water discharged from a break location, from ADS stages 1, 2, 3, and 4 valves, and from the steam generator relief valves are collected and measured versus time by three steam condensers and weigh tanks. The weighing system is composed of three load cells per tank with a maximum load of 3000 kg.

2.4.5 Gammadensitometers

Four gammadensitometers are provided to measure densities of single- and two-phase fluid: three Cs-137 three-beam gammadensitometers are located in the break line; and one Am-241 two-beam gammadensitometer is located in the break line.

The attenuation of γ -radiation through pipe wall and fluid is measured by using a sodium-iodine scintillation detector (accuracy = ± 5 percent of rated value) aligned in the γ -ray beam. This attenuation is proportional to fluid average (chord average density). The γ -densitometers are used both as single instruments and are coupled with a full-flow turbine to measure two-phase flows.

2.4.6 Power Meters

The dc power of the rod bundle is measured by taking the overall voltage drop across the heated rod cluster and measuring the feeding current with 6 shunts: 5 shunts for the 8-mW group and 1 shunt for the 4-mW group, with an accuracy of ± 1 percent. The power of internal/external pressurizer heaters is measured by wattmeters, with an accuracy of ± 1.7 percent power.

The following figures have been intentionally deleted
from this document due to their proprietary nature.

2.5 Data Acquisition System (DAS)

The data acquisition and elaboration system collects and handles measured signals from the plant. The large amount of operations necessary to the user are implemented in appropriate software procedures in order to avoid errors and loss of information.

SPES data acquisition basically consists of a data logger digital subsystem and the four following main components:

- DEC VAX4000-200 (main computer)
- DEC VAXSTATION 2000 (graphic workstation)
- DEC MICROVAX II (remote I/O driver)
- Device for transferring files, working in DOS environment

DEC VAX4000-200 has the following features:

- Five VUPS CPU
- DSSI 10 MIPS controller (RISC technology)
- Ten MIPS Ethernet controller (RISC technology)
- Sixty-four Megabytes of RAM
- Mass storage: 1 gigabyte RF72 DEC hard disk
 1.2 gigabytes TLZ04 DEC removable cartridge
- Peripheral equipment: 3 consoles
 4 video terminal
 DEC LA100 printer
- Interfaces: 4 serial ports
 Ethernet port

DEC VAXSTATION 2000 has the following features:

- Six megabytes of RAM
- Ethernet controller
- Mass storage: 130 megabytes of hard disk
- Peripheral equipment: 19-in. video DEC VR290 XWINDOW terminal

DEC MICROVAX II has the following features:

- ETHERNET controller
- Mass storage: 130/90 megabytes of hard disk
 70 megabytes tape streamer removable cartridge
- Peripherals: 4 serial ports
 14-in. video (with software for emulation of VT240 terminal)

The device for transferring files is a DEC VAXMATE computer AT IBM compatible with the following features:

- 80286 CPU
- One megabyte of RAM
- 5 ¼ inch, high density disk drive
- Four virtual hard disk for a total of 60 megabytes
- Ethernet controller
- Printer port

The RTVAX 300 digital data acquisition subsystem is composed of different remote data loggers linked in a star configuration to the main computer. A virtual central node is installed in the main computer. The loggers are linked by a thin ethernet cable. Each of these remote units has the following main characteristics:

- One megabyte buffer memory
- Microprocessor card with 32 bit bus, 20 MHz clock
- Ten megabytes throughput Ethernet controller
- Switch mode power box
- 100 Hz maximum value sampling rate
- Data conditioning and amplifying card

2.5.1 Control Loops

During the test, control loops manage and control the key plant parameters. Most of the control loops are electronic and are located on the control room main board. These main control loops regulate:

- Primary pressure and level
- Steam generator pressure and level
- CMT external containment air pressure
- SFW, NRHR, CVCS flow rates
- Bundle power

The basis for the SPES-2 bundle power decay is to simulate the heat flux versus time from the AP600 fuel rods, including stored energy and fission product decay heat. This power decay versus time has been determined based on AP600 LOFTRAN analyses. The fission product decay heat versus time is based on the ANS 1979 decay heat standard plus two sigma uncertainty. The SPES-2 heat loss compensation value (150 kw) is based on pre-operational testing and is added to the SPES-2 bundle power decay. Table 2.5-1 provides the SPES-2 decay heat simulation as a function of time after trip with the exception of the compensation for the SPES-2 heat losses. Because of the limitations of the SPES-2 heater rod control system, the AP600 core power versus time is simulated as follows:

- SPES-2 core power is maintained at 102 percent for 5.75 seconds after the reactor trip setpoint is reached.
- The SPES-2 power is reduced in a single step to 20 percent (maximum power of the continuous low power heated rod power control system) and maintained until 12.38 seconds after reactor trip. At this time the integrated SPES-2 heated rod power is equivalent to 1/395 of the AP600 nuclear fuel heat input.
- The SPES-2 power level is maintained at 20 percent (the maximum power level) until 14.5 seconds. At this time, the AP600 core power fraction of full power is 0.169; where $0.169 (4.89 \text{ MW}) + 150 \text{ kW} = 0.2 (4.89)$ and 150 kw is equal to the heat loss compensation.
- From 14.5 seconds until the actuation of the first stage of ADS, the SPES-2 power decay is that identified in Table 2.5-1 plus 150 kW (the heat loss compensation).
- When the first stage of ADS is actuated, the SPES-2 heat loss compensation is stopped and the power decay is as show on Table 2.5-1.

2.5.2 Safety Devices

A combination of mechanical devices, in conjunction with the DAS computer logic, were put in place to guarantee the structural integrity of the SPES-2 components and meet the safety requirements of the plant operators. The following mechanical safety devices were installed at each facility:

- Safety valve on the pressurizer top, set at 20 MPa (2900 psia)
- Safety valve on steam generator-A/-B secondary side, set at 10 MPa (1450 psia)
- Safety valve on accumulator-A/-B, set at 6.9 MPa (1000 psia)
- Safety valve on CMT-A/-B ext. containment set at 7.1 MPa (1029 psia)
- Blowout disk on CMT-A/-B, set at 110 bar differential pressure between primary and secondary side

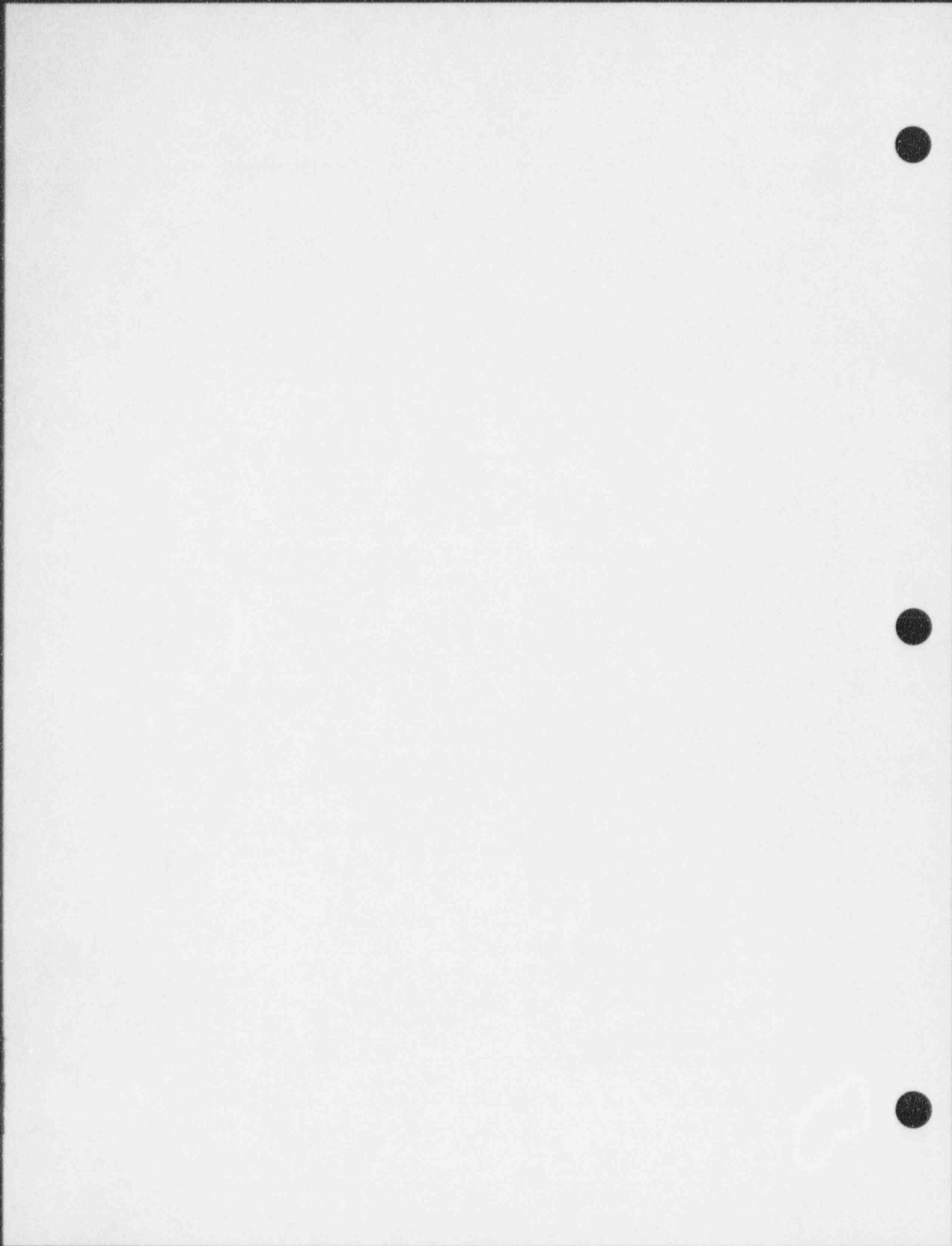
The structural integrity is also guaranteed by alarms and actions performed by a programmable logical controller (PLC). Both power groups are switched off if the power channel rod temperature greater than 590°C or the primary pressure greater than 17.2 MPa. The 8 mW group is switched off if the reactor coolant pump speed less than 600 rpm and the steam generator level is less than 2 m. Pressurizer internal heaters are switched off if the level is less than 2 m.

The pressurizer power-operated relief valve (PORV) (ADS stage 1) opens if pressure greater than 16.2 MPa and closes when pressure less than 16.2 MPa. The steam generator PORV opens if pressure greater than 7.0 MPa and closes when pressure less than 7.0 MPa. The CMT containment PORV opens if air pressure greater than 6.7 MPa and closes when pressure less than 6.7 MPa.

**TABLE 2.5-1
SPES-2 POWER DECAY CURVE**

Time From Trip (seconds)	Fractional Power
0.0	1.02
5.75	1.02
5.76	0.2
12.38	0.2
14.50	$\frac{0.169 * 4890\text{kW} + 150\text{kW}}{4890\text{kW}} = 0.2$
	(Note 1)
15.00	0.1542
17.5	0.1300
20.82	0.1121
22.5	0.0917
25.0	0.0868
27.5	0.0823
30.0	0.0782
35.0	0.0710
40.0	0.0648
45.0	0.0604
50.0	0.0573
70.0	0.0479
100.0	0.0403
200.0	0.0317
500.0	0.0259
1000.0	0.0222
2000.0	0.0183
3000.0	0.0162
4000.0	0.0148

Note 1: Heat loss compensation of 150 kW begins, but then terminates after ADS-1 actuation.



2.6 Facility Operation

The day before the test, SPES-2 personnel verify that:

- the plant is configured for the test
- all plant alarms and protection functions are operating
- the DAS test procedure can perform the required trips for the test
- all the control systems and auxiliary systems are operating
- the plant is ready for start-up

On the day of the test, several key steps are performed to bring the plant up to initial conditions.

The pressurizer internal heaters are turned on and the ADS-1 valve is opened until the primary system fluid temperature reaches 100°C, after which the level and pressure controls are set to auto mode. When primary pressure is about 3 bar, the RCPs are started up. After the rod-bundle electric resistance check (it should be ~1.9 mΩ), the 4 MW power group is turned on to give approximately 60 percent of the maximum current (equivalent to ~900 kW of generated power). The heat-up and pressurization of the facility is carried out maintaining this power until the hot leg temperature reaches 200°C, while subcooling conditions in the circuits. Steam generator levels are brought close to the nominal value and the power channel power is increased step-by-step using the 8 MW and 4 MW power groups. When nominal conditions are reached, they are maintained for about 500 seconds before starting the transient. To start the transient for all tests, a specific break valve (or valves if required) is opened to begin break flow. At this point, the transient follows a course of events that is specific to the test procedure for that particular matrix test.

However, some generalities of the sequence of events for facility operation can be made for most of the tests. Once a setpoint is reached initiating the R signal, the main feedwater (MFW) isolation valves are closed and the power decay simulation (discussed in Section 2.5.1) is begun. Upon S signal initiation, the CMT isolation valves and the PRHR isolation valves are opened, and the main steam line isolation valves are closed, all with a 2-second delay. 16.2 seconds after S signal, the RCP coastdown is initiated. ADS-1 is actuated on CMT volume of 67 percent with the other ADS stages following the delay time specified in the test procedure. Heat loss compensation is terminated with ADS stage 1 actuation. The accumulators begin injecting when the primary system pressure falls to ~700 psia. The IRWST begins injecting water when the primary system pressure is 26 psia. The test is terminated when final conditions are achieved as specified in the test procedure. The specific facility operation and configuration for each test is discussed in subsections 2.6.1 through 2.6.13.

2.6.1 Facility Operation for Test S00303

The purpose of test S00303 was to investigate the plant behavior and system response during a simulated 2 in. cold-leg break on loop B (the CMT side of the plant) with intervention of the passive safety systems only. The test was performed with the pressurizer to CMT-A/-B balance lines closed by means of blind flanges installed on both the pressurizer and CMT connections. The break was located at the bottom of loop B cold leg-B2 between the cold leg-B2 to CMT-B balance line and the power channel. The break line for the facility was configured as shown in Figure 2.6-1 with a break orifice installed as described in Figure 2.6.1-2. The orifices installed throughout the facility are listed in Table 2.6.1-1.

Once the facility was at initial conditions, the test was initiated by opening the break valve. When the reactor trip R occurred (pressurizer pressure P-027P = 12.41 MPa = 1800 psia), the heater rod bundle power was controlled to match the scaled AP600 decay heat, and the steam generator MSLIVs were closed with a 2-second delay. When the S signal occurred (pressurizer pressure P-027P = 11.72 MPa = 1700 psia), the PRHR isolation valves and the CMT injection valves were opened and the MFWIVs were closed, all with a 2-second delay, and the RCP coastdown was initiated with a 16.2-second delay.

The CVCS, NRHR, and SFW were off throughout the whole transient. The test simulated the failure of one of two 4th-stage ADS valves on loop B. The ADS valves were programmed to open versus either CMT level L-A40E or L-B40E with the delay time shown in Table 2.6.1-2. The accumulators were set to inject water via DVI when the primary pressure was lower than 4.9 MPa (710.6 psia). The IRWST was set to inject water via DVI when the primary pressure was lower than 0.18 MPa (26.1 psia). The test was terminated when the flow rates (F-A60E/F-B60E) discharged by the IRWST reached a stable flow (without significant fluctuation).

**TABLE 2.6.1-1
SPES-2 INSTALLED ORIFICES**

Location	Diameter (mm)	Thickness (mm)
ADS-1	4.37	12
ADS-2	9.35	12
ADS-3	9.35	12
ADS-4A	20.68	7
ADS-4B	14.62	7
CMT-A injection line	4.1	5.5
CMT-B injection line	5.7	5.5
CMT-A cold leg bal. line (2 orif.)	7.5	5.5
CMT-B cold leg bal. line (2 orif.)	7.5	5.5
Accumulator-A injection line	4.86	7.3
Accumulator-B injection line	4.86	7.3
Cold leg-B2 break device	2.56	3.3 *

* Rounded entrance with 2.6 mm radius

**TABLE 2.6.1-2
PROGRAMMED OPENING OF ADS VALVES**

ADS Stage	Orifice Dia. (mm/in.)	CMT Volume (%)	L-A40E or L-B40E (m/ft.)	Delay Time (sec.)
First	4.37/0.172	67	4.152/13.622	30
Second	9.35/0.368	67	4.152/13.622	125
Third	9.35/0.368	67	4.152/13.622	245
Fourth A	20.68/0.814	20	1.192/3.911	60 sec. after 20% CMT vol., but no sooner than 360 sec. after 67% CMT vol.
Fourth B	14.62/0.576	20	1.192/3.911	60 sec. after 20% CMT vol., but no sooner than 360 sec. after 67% CMT vol.

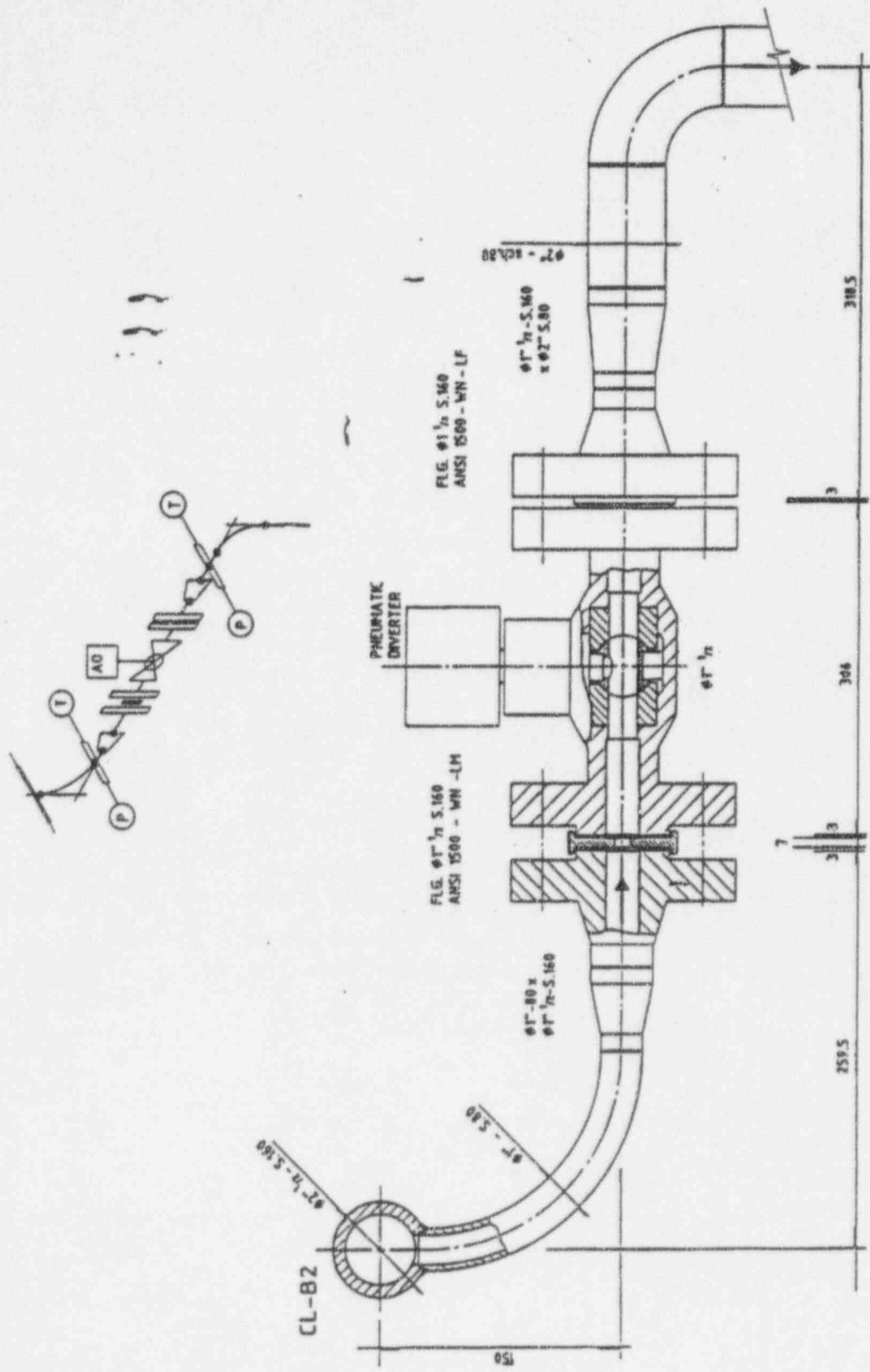


Figure 2.6.1-1 Breakline for 2-in. Cold-Leg Break

SPES2 - Break device on CL
Posizione 13 su P&ID orifizi

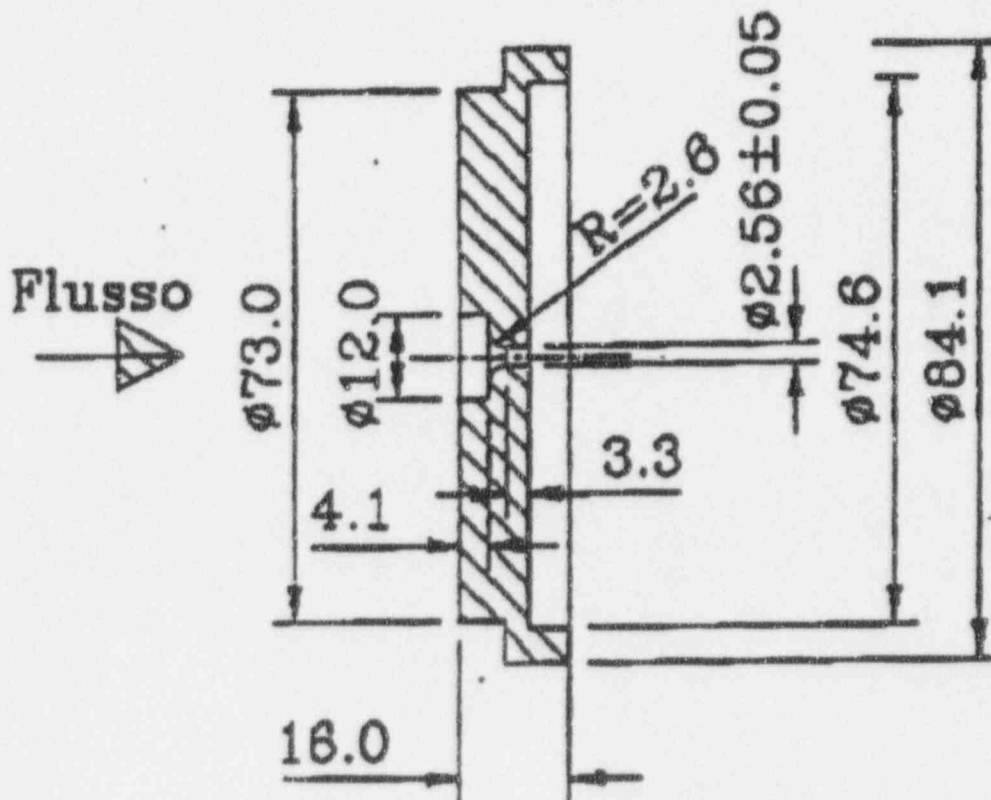


Figure 2.6.1-2 SPES-2 Break Orifice on CL for 2-in. Break

2.6.2 Facility Operation for Test S00401

The purpose of test S00401 was to investigate the CMT heatup with simultaneous operation of the PRHR during a simulated 1-in. cold-leg break on loop B (the CMT side of the plant). The test was performed with the pressurizer to CMT-A/-B balance lines closed by means of blind flanges installed on both the pressurizer and CMT connections. The break was located at the bottom of loop B cold leg B2 between the cold leg-B2 to CMT-B balance line and the power channel. The break line for the facility was configured as shown in Figure 2.6.2-1 with a break orifice installed as described in Figure 2.6.2-2. The orifices installed throughout the facility are listed in Table 2.6.2-1.

Once the facility was at initial conditions, the test was initiated by opening the break valve. When the reactor trip R signal occurred (pressurizer pressure P-027P = 12.41 MPa = 1800 psia), the heater rod bundle power was controlled to match the scaled AP600 decay heat, and the SG MSLIVs were closed with a 2 second delay. When the S signal occurred (pressurizer pressure P-027P = 11.72 MPa = 1700 psia), the PRHR isolation valves and the CMT injection valves were opened and the MFWIVs were closed, all with a 2-second delay, and the RCP coastdown was initiated with a 16.2-second delay.

The CVCS, NRHR, and SFW were off throughout the whole transient. The test simulated the failure of one of two fourth-stage ADS valves on loop B. The ADS valves were programmed to open versus either CMT level L-A40E or L-B40E with the delay time shown in Table 2.6.2-2. The accumulators were set to inject water via DVI when the primary pressure was lower than 4.9 MPa (710.6 psia). The IRWST was set to inject water via DVI when the primary pressure was lower than 0.18 MPa (26.1 psia). The test was terminated when the flowrates (F-A60E/F-B60E) discharged by the IRWST reached a stable flow (without significant fluctuation).

**TABLE 2.6.2-1
SPES-2 INSTALLED ORIFICES**

Location	Diameter (mm)	Thickness (mm)
ADS-1	4.37	12
ADS-2	9.35	12
ADS-3	9.35	12
ADS-4A	20.68	7
ADS-4B	14.62	7
CMT-A injection line	4.1	5.5
CMT-B injection line	5.7	5.5
CMT-A cold leg bal. line (2 orif.)	7.5	5.5
CMT-B cold leg bal. line (2 orif.)	7.5	5.5
Accumulator-A injection line	4.86	7.3
Accumulator-B injection line	4.86	7.3
Cold leg-B2 break device	1.28	3.3 *

* Rounded entrance with 1.3 mm radius

**TABLE 2.6.2-2
PROGRAMMED OPENING OF ADS VALVES**

ADS Stage	Orifice Dia. (mm/in.)	CMT Volume (%)	L-A40E or L-B40E (m/ft.)	Delay Time (sec.)
First	4.37/0.172	67	4.152/13.622	30
Second	9.35/0.368	67	4.152/13.622	125
Third	9.35/0.368	67	4.152/13.622	245
Fourth A	20.68/0.814	20	1.192/3.911	60 sec. after 20% CMT vol., but no sooner than 360 sec. after 67% CMT vol.
Fourth B	14.62/0.576	20	1.192/3.911	60 sec. after 20% CMT vol., but no sooner than 360 sec. after 67% CMT vol.

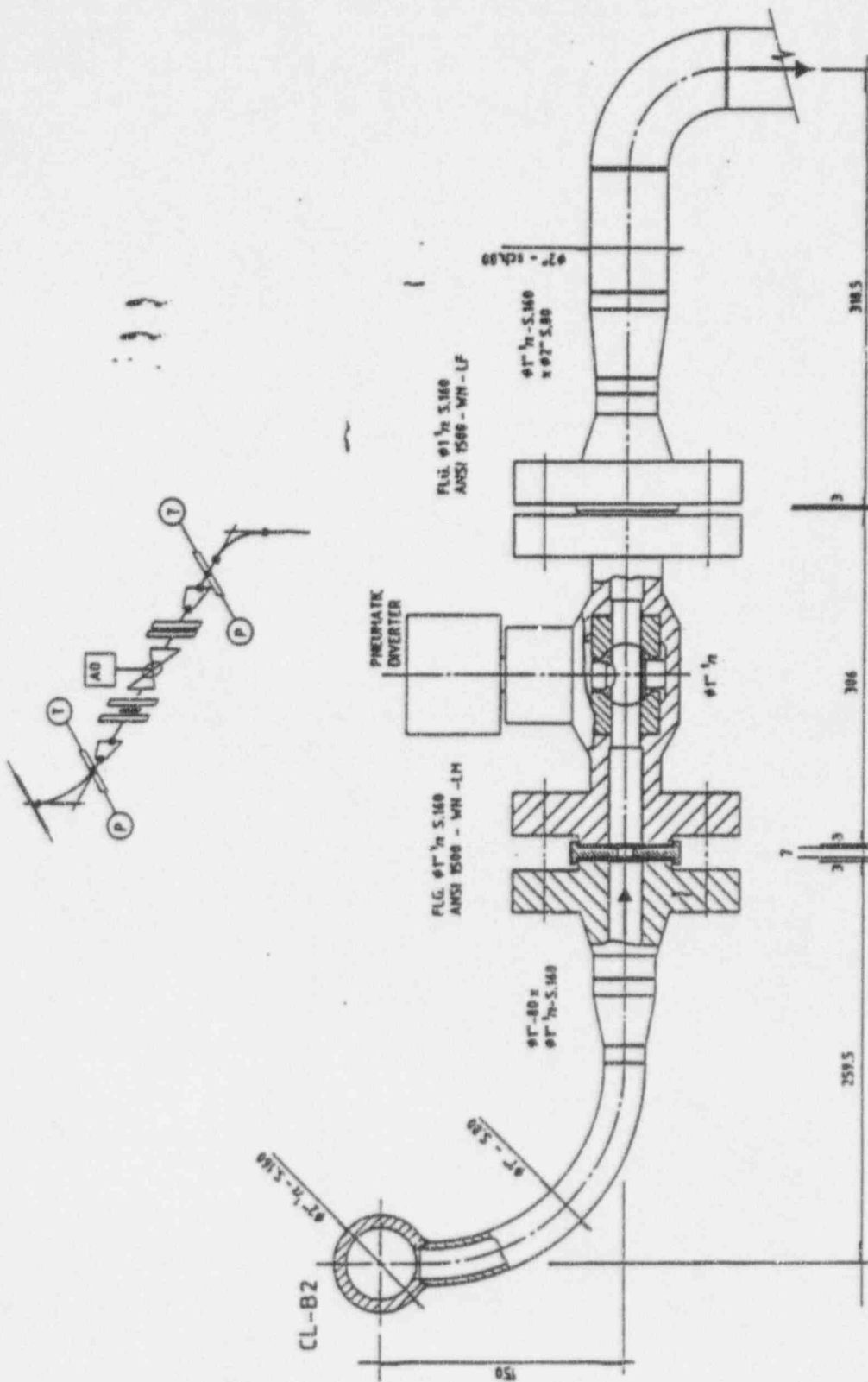
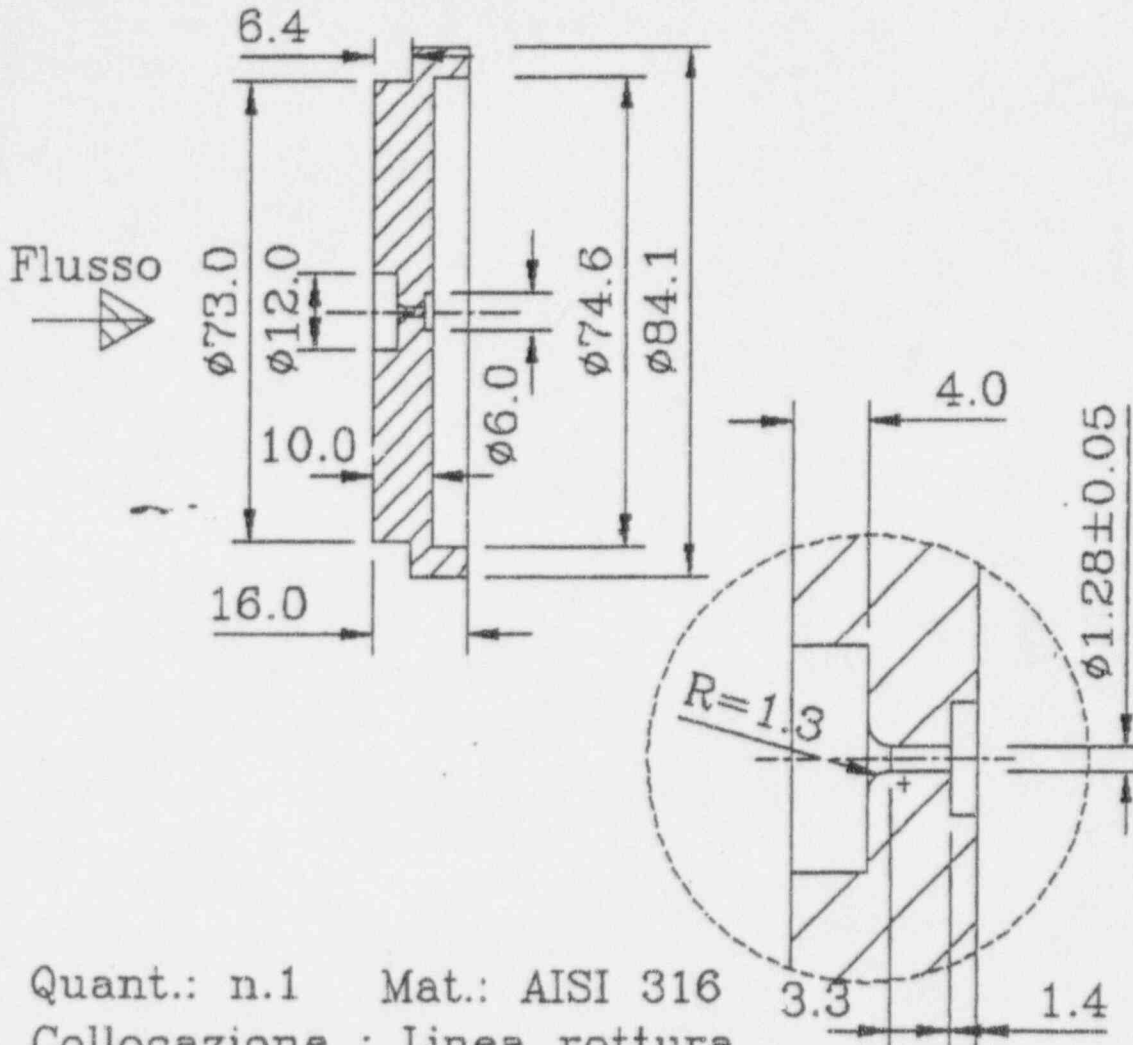


Figure 2.6.2-1 Breakline for 1-in. Cold-Leg Break

SPES2 - Break device on CL
 Posizione 13 su P&ID orifizi



Quant.: n.1 Mat.: AISI 316
 Collocazione : Linea rottura
 su CL-B2 a monte valvola BR-01
 flg. $\phi 1\frac{1}{2}$ ANSI1500 S.160 LM&LF

2	2/5/84	Geometria orifizio	Ed	mr	Kocher
Indice	Data	Modifiche	Disegn.	Controll.	Approv.
SIET Piacenza Italy		Doc. n.	Orifizi calibrati		
Scale	Disegno n.	Foglio	di		
1:1-2:1	25.03.26	15			

Figure 2.6.2-2 SPES-2 Break Orifice on CL for 1-in. Break

2.6.3 Facility Operation for Test S00504

The purpose of test S00504 was to investigate the interaction between nonsafety and safety systems during a simulated 2-in. cold-leg break on loop B (the CMT side of the plant). The break was located at the bottom of loop B cold leg-B2 between the cold leg-B2 to CMT-B balance line and the power channel. The break line for the facility was configured as shown in Figure 2.6.3-1 with a break orifice installed as described in Figure 2.6.3-2. The orifices installed throughout the facility are listed in Table 2.6.3-1.

Once the facility was at initial conditions, the test was initiated by opening the break valve. When the reactor trip R occurred (pressurizer pressure P-027P = 12.41 MPa = 1800 psia), the heater rod bundle power was controlled to match the scaled AP600 decay heat, and the SG MSLIVs were closed with a 2-second delay. When the S signal occurred (pressurizer pressure P-027P = 11.72 MPa = 1700 psia), the following actuation were performed:

- PRHR isolation valves opened with a 2-second delay.
- CMT injection valves opened with a 2-second delay.
- MFW isolation valves closed with a 2-second delay.
- SFW flow was initiated with a 2-second delay.
- CVCS flow was initiated with a 2-second delay after S signal and pressurizer level less than 10 percent (0.38 m).
- RCP coastdown was initiated with a 16.2 second delay.

The plant computer was programmed for SFW to be ON until isolated by either $T_{\text{cold}} = 268^{\circ}\text{C}$ (514°F) or high steam generator narrow-range level = 79 percent of span which corresponds to measured levels L-A20S/ L-B20S = 2.1 m (6.89 ft.). In the case of low T_{cold} , one of the four cold-leg temperatures (T-A011P, T-A012P, T-B011P, and T-B012P = $268^{\circ}\text{C} = 514^{\circ}\text{F}$) would be sufficient to completely stop SFW flow to both steam generators. However, in the case of high steam generator narrow-range level, SFW flow would be stopped only to that steam generator which has reached that setpoint. The other steam generator would continue to receive SFW flow. Additionally, SFW flow would begin again to that particular steam generator should its narrow range level fall below 79 percent.

The ADS valves were programmed to open versus either CMT level L-A40E or L-B40E with the delay time shown in Table 2.6.3-2. The accumulators were set to inject water via DVI when the primary pressure was lower than 4.9 MPa (710.6 psia). The NRHR was set to inject water via DVI when the primary system pressure was lower than 1.1 MPa (1600 psia). The IRWST was set to inject water via DVI when the primary pressure was lower than 0.18 MPa (26.1 psia). The test was terminated when the pressurizer and CMTs have refilled and their levels (L-010P, L-A40E, and L-B40E) have stabilized.

TABLE 2.6.3-1
SPES-2 INSTALLED ORIFICES

Location	Diameter (mm)	Thickness (mm)
ADS-1	4.37	12
ADS-2	9.35	12
ADS-3	9.35	12
ADS-4A	20.68	7
ADS-4B	20.68	7
CMT-A injection line	4.1	5.5
CMT-B injection line	5.7	5.5
CMT-A cold leg bal. line (2 orif.)	7.5	5.5
CMT-B cold leg bal. line (2 orif.)	7.5	5.5
Accumulator-A injection line	4.86	7.3
Accumulator-B injection line	4.86	7.3
Cold Leg-B2 break device	2.56	3.3 *
* rounded entrance with 2.6 mm radius		

**TABLE 2.6.3-2
PROGRAMMED OPENING OF ADS VALVES**

ADS Stage	Orifice Dia. (mm/in.)	CMT Volume (%)	L-A40E or L-B40E (m/ft.)	Delay Time (sec.)
First	4.37/0.172	67	4.152/13.622	30
Second	9.35/0.368	67	4.152/13.622	125
Third	9.35/0.368	67	4.152/13.622	245
Fourth A	20.68/0.814	20	1.192/3.911	60 sec. after 20% CMT vol., but no sooner than 360 sec. after 67% CMT vol.
Fourth B	20.68/0.814	20	1.192/3.911	60 sec. after 20% CMT vol., but no sooner than 360 sec. after 67% CMT vol.

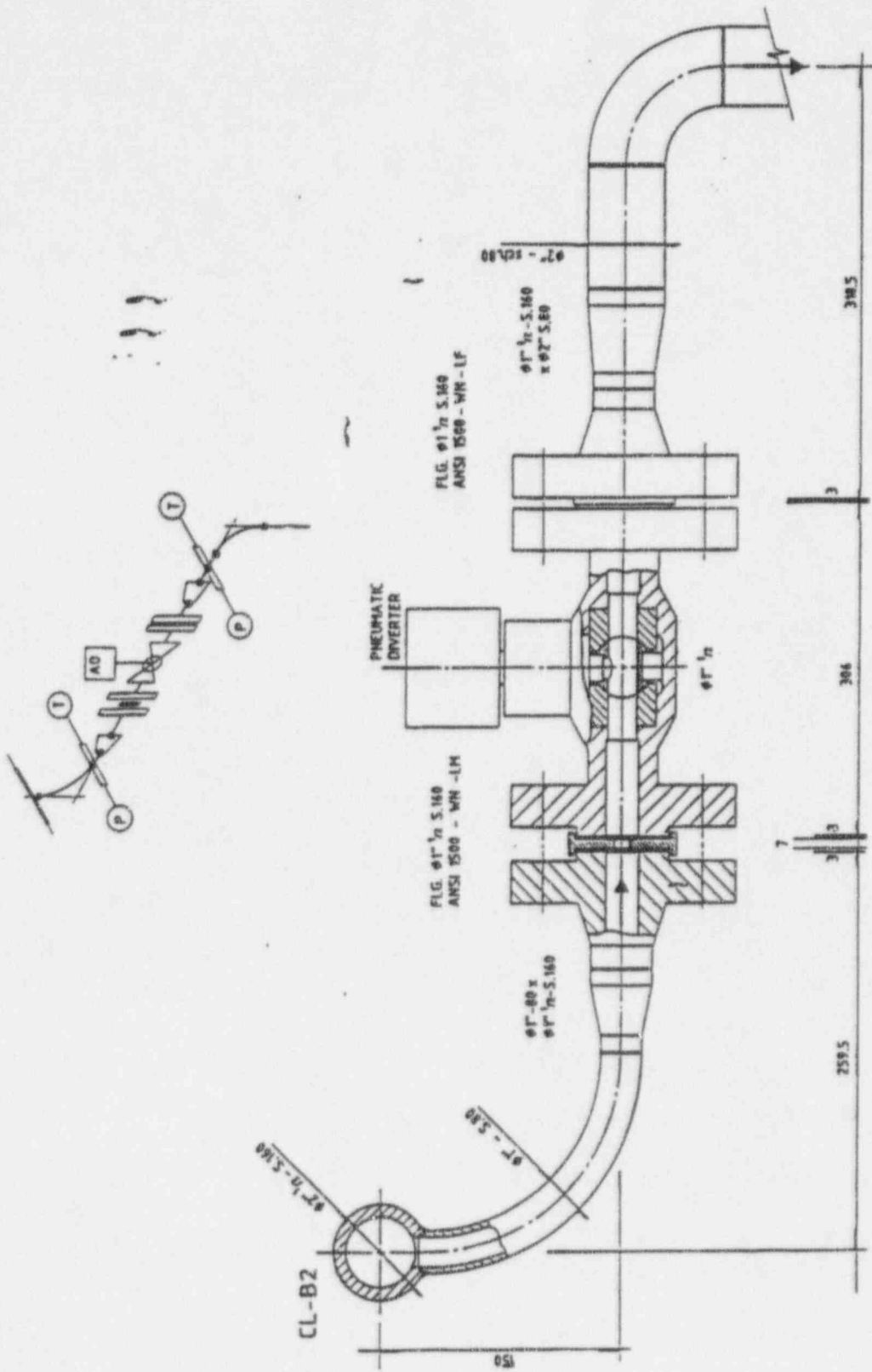
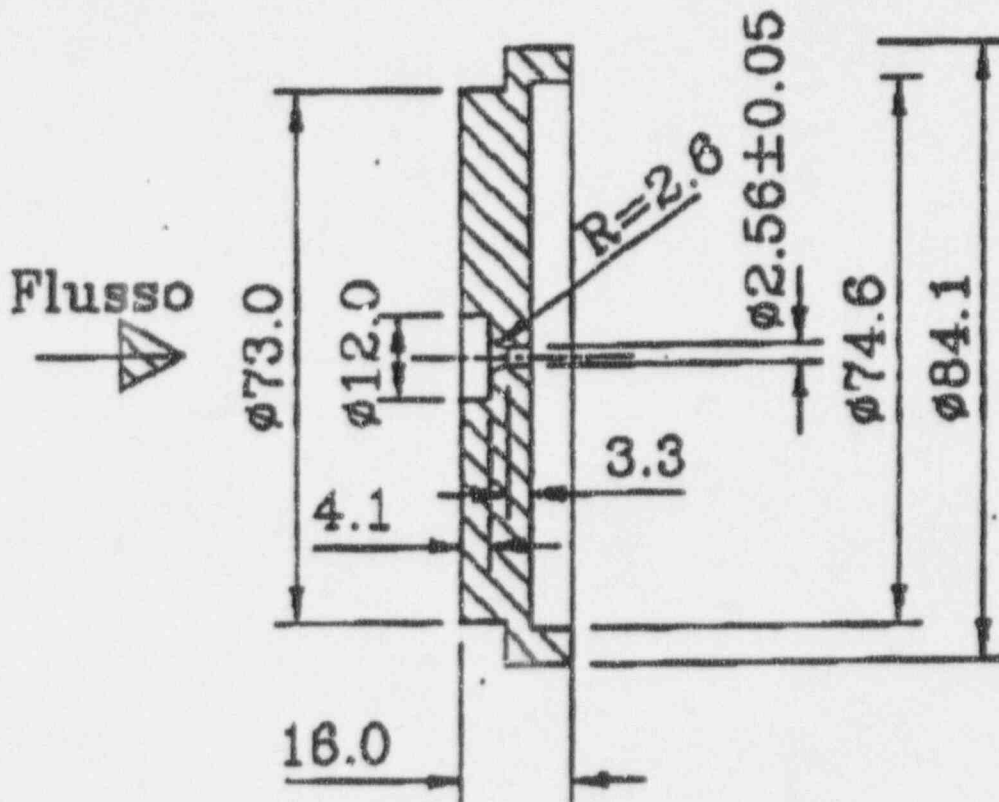


Figure 2.6.3-1 Break Line for 2-in. Cold-Leg Break

SPES2 - Break device on CL
 Posizione 13 su P&ID orifizi



Quant.: n.1 Mat.: AISI 316
 Collocazione : Linea rottura
 su CL-B2 a monte valvola RR-01
 fig. $\phi 1\frac{1}{2}$ ANSI1500 S.160 LM&LF

Figure 2.6.3-2 SPES-2 Break Orifice on CL for 2-in. Break

2.6.4 Facility Operation for Test S00605

The purpose of test S00605 was to investigate the asymmetric CMT performance with operation of the PRHR in conjunction with a simulated 2-in. DVI-B break (the CMT side of the plant) and passive safety systems only for mitigation. The break is located on DVI-B between the ECCS injection and the power channel. The test was performed with the pressurizer to CMT A/B balance lines closed by means of blind flanges installed on both the pressurizer and CMT connections. The break line for the facility was configured as shown in Figure 2.6.4-1 with a break orifice installed as described in Figure 2.6.4-2. The other orifices installed throughout the facility are listed in Table 2.6.4-1.

Once the facility was at initial conditions, the test was initiated by opening the break valve. When the reactor trip R occurred (pressurizer pressure P-027P = 12.41 MPa = 1800 psia), the heater rod bundle power was controlled to match the scaled AP600 decay heat, and the steam generator MSLIVs were closed with a 2-second delay. When the S signal occurred (pressurizer pressure P-027P = 11.72 MPa = 1700 psia), the PRHR isolation valves and the CMT injection valves were opened and the MFWIVs were closed, all with a 2-second delay, and the RCP coastdown was initiated with a 16.2-second delay.

The CVCS, NRHR, and SFW were off throughout the whole transient. The test simulated the failure of 1 of 2 fourth-stage ADS valves on loop B. The ADS valves were programmed to open versus either CMT level L-A40E or L-B40E with the delay time shown in Table 2.6.4-2. The accumulators were set to inject water via DVI when the primary pressure was lower than 4.9 MPa (710.6 psia). The IRWST was set to inject water via DVI when the primary pressure was lower than 0.18 MPa (26.1 psia). The test was terminated when the flowrates (F-A60E/F-B60E) discharged by the IRWST reached a stable flow (without significant fluctuation).

**TABLE 2.6.4-1
SPES-2 INSTALLED ORIFICES**

Location	Diameter (mm)	Thickness (mm)
ADS-1	4.37	12
ADS-2	9.35	12
ADS-3	9.35	12
ADS-4A	20.68	7
ADS-4B	14.62	7
CMT-A injection line	4.1	5.5
CMT-B injection line	5.7	5.5
CMT-A cold leg bal. line (2 orif.)	7.5	5.5
CMT-B cold leg bal. line (2 orif.)	7.5	5.5
Accumulator-A injection line	4.86	7.3
Accumulator-B injection line	4.86	7.3
Cold leg-B2 break device	2.56	3.3 *

* Rounded entrance with 2.6 mm radius

**TABLE 2.6.4-2
PROGRAMMED OPENING OF ADS VALVES**

ADS Stage	Orifice Dia. (mm/in.)	CMT Volume (%)	L-A40E or L-B40E (m/ft.)	Delay Time (sec.)
First	4.37/0.172	67	4.152/13.622	30
Second	9.35/0.368	67	4.152/13.622	125
Third	9.35/0.368	67	4.152/13.622	245
Fourth A	20.68/0.814	20	1.192/3.911	60 sec after 20% CMT vol., but no sooner than 360 sec after 67% CMT vol.
Fourth B	14.62/0.576	20	1.192/3.911	60 sec after 20% CMT vol., but no sooner than 360 sec after 67% CMT vol.

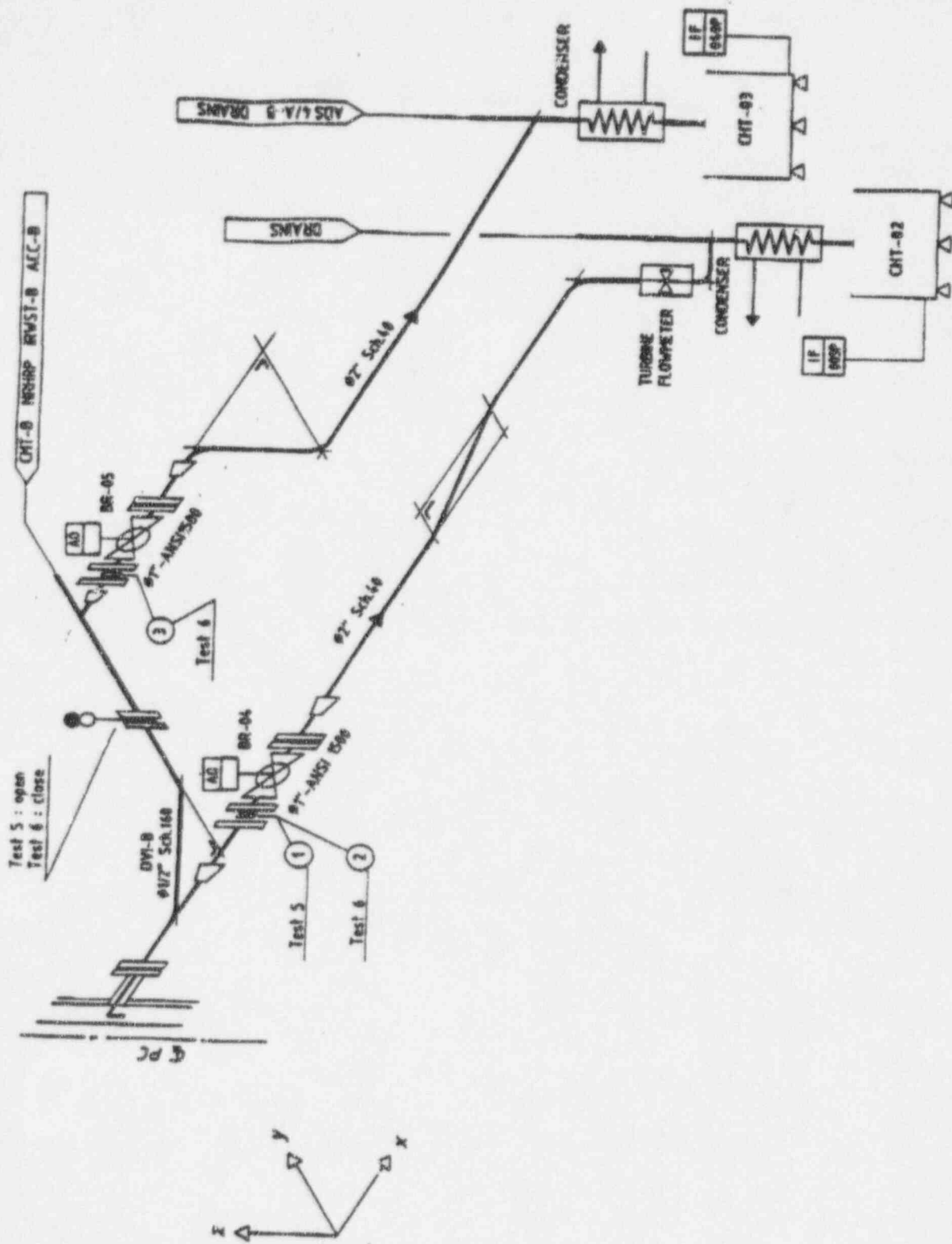
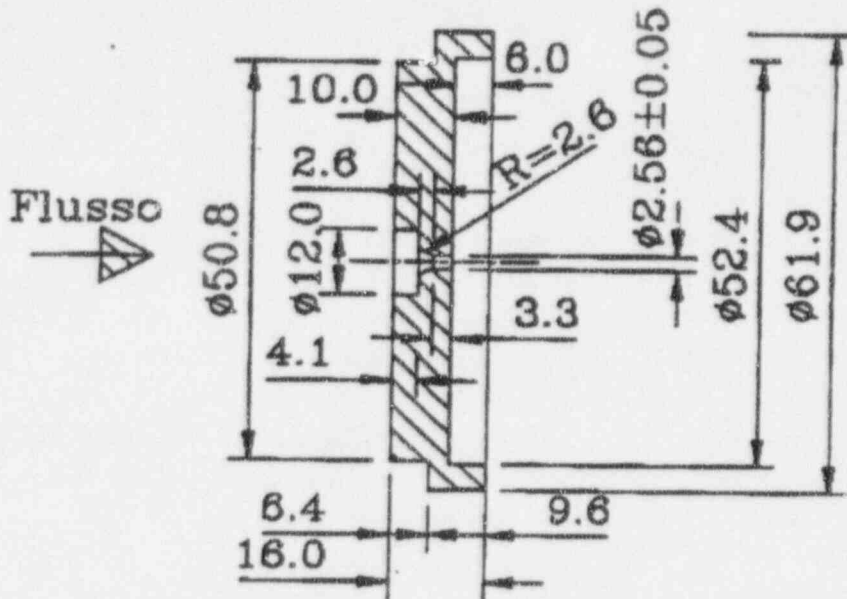


Figure 2.6.4-1 Break Line Configuration for 2-in. DVI-B Break

SPES2 - Break device on DVI-B
 Prova S00605 - Test 5



Assonometria : dis. 25.03.24 Pos.1
 Collocazione : Linea rottura su DVI-B
 a monte valvola BR-04
 flg.: $\varnothing 1''$ ANSI1500 LM & LF
 Quant.: n.1 Mat.: AISI 316

0	16/6/84	Geom.orifizio Prova S00605 Test 5			
Indice	Data	Modifiche	Disegn.	Control.	Approv.
SIET Piacenza Italy		Disegn. n.			
		SPES 2 - DVI-B - Break Device Orifizio calibrato pos. 1			
Scala	Disegno n.	Foglio	di		
1:1	25.03.26	20	22		

Figure 2.6.4-2 SPES-2 Break Orifice on DVI-B for 2-in. Break

2.6.5 Facility Operation for Test S00706

The purpose of S00706 was to investigate the plant behavior and system response during a full bore double-ended guillotine (DEG) break of DVI-B (complete loss of one of two passive injection lines) with passive safety systems only for mitigation. The break is located on DVI-B prior to entry to the power channel. The DEG is simulated by using two break valves and a spectacle flange in the open position installed between them as shown in figure 2.6.5-1. The break valve identified in Figure 2.6.5-1 as BR-05 had an orifice installed at its inlet described in Figure 2.6.5-2. The break valve identified in Figure 2.6.5-1 as BR-04 had a venturi tube installed at its inlet described in Figure 2.6.5-3 in order to simulate the flow venturi in the AP600 reactor vessel DVI nozzle. The other orifices installed in the facility are listed in Table 2.6.5-1. The test was performed with the pressurizer to CMT A/B balance lines closed by means of blind flanges installed on both the pressurizer and CMT connections.

Once the facility was at initial conditions, the test was initiated by opening the break valves. When the reactor trip (R) occurred (pressurizer pressure P-027P = 12.41 MPa = 1800 psia), the heater rod bundle power was controlled to match the scaled AP600 decay heat, and the steam generator MSLIVs were closed with a 2-second delay. When the S signal occurred (pressurizer pressure P-027P = 11.72 MPa = 1700 psia), the PRHR isolation valves and the CMT injection valves were opened and the MFWIVs were closed, all with a 2-second delay, and the RCP coastdown was initiated with a 16.2 second delay.

The CVCS, NRHR, and SFW were off throughout the whole transient. The test simulated the failure of one of two stage 1 and 3 ADS valves. The ADS valves were programmed to open versus either CMT level L-A40E or L-B40E with the delay time shown in Table 2.6.5-2. The accumulators were set to inject water via DVI when the primary pressure was lower than 4.9 MPa (696.1 psia). The IRWST was set to inject water via DVI when the primary pressure was lower than 0.18 MPa (26.1 psia). The test was terminated when the flowrates (F-A60E/F-B60E) discharged by the IRWST reached a stable flow (without significant fluctuation).

**TABLE 2.6.5-1
SPES-2 INSTALLED ORIFICES**

Location	Diameter (mm)	Thickness (mm)
ADS-1	3.09	12
ADS-2	9.35	12
ADS-3	6.61	12
ADS-4A	20.68	7
ADS-4B	20.68	7
CMT-A injection line	4.1	5.5
CMT-B injection line	5.7	5.5
CMT-A cold leg bal. line (2 orif.)	7.5	5.5
CMT-B cold leg bal. line (2 orif.)	7.5	5.5
Accumulator-A injection line	4.86	7.3
Accumulator-B injection line	4.86	7.3
DVI-B break device ECCS side	8.95	9 *
DVI-B break device vessel side	venturi	see Figure 2.6.5-3
* Rounded entrance with 9 mm radius		

**TABLE 2.6.5-2
PROGRAMMED OPENING OF ADS VALVES**

ADS Stage	Orifice Dia. (mm/in.)	CMT Volume (%)	L-A40E or L-B40E (m/ft.)	Delay Time (sec.)
First	3.09/0.122	67	4.152/13.622	30
Second	9.35/0.368	67	4.152/13.622	125
Third	6.61/0.260	67	4.152/13.622	245
Fourth A	20.68/0.814	20	1.192/3.911	60 sec after 20% CMT vol., but no sooner than 360 sec. after 67% CMT vol.
Fourth B	20.68/0.814	20	1.192/3.911	60 sec after 20% CMT vol., but no sooner than 360 sec. after 67% CMT vol.

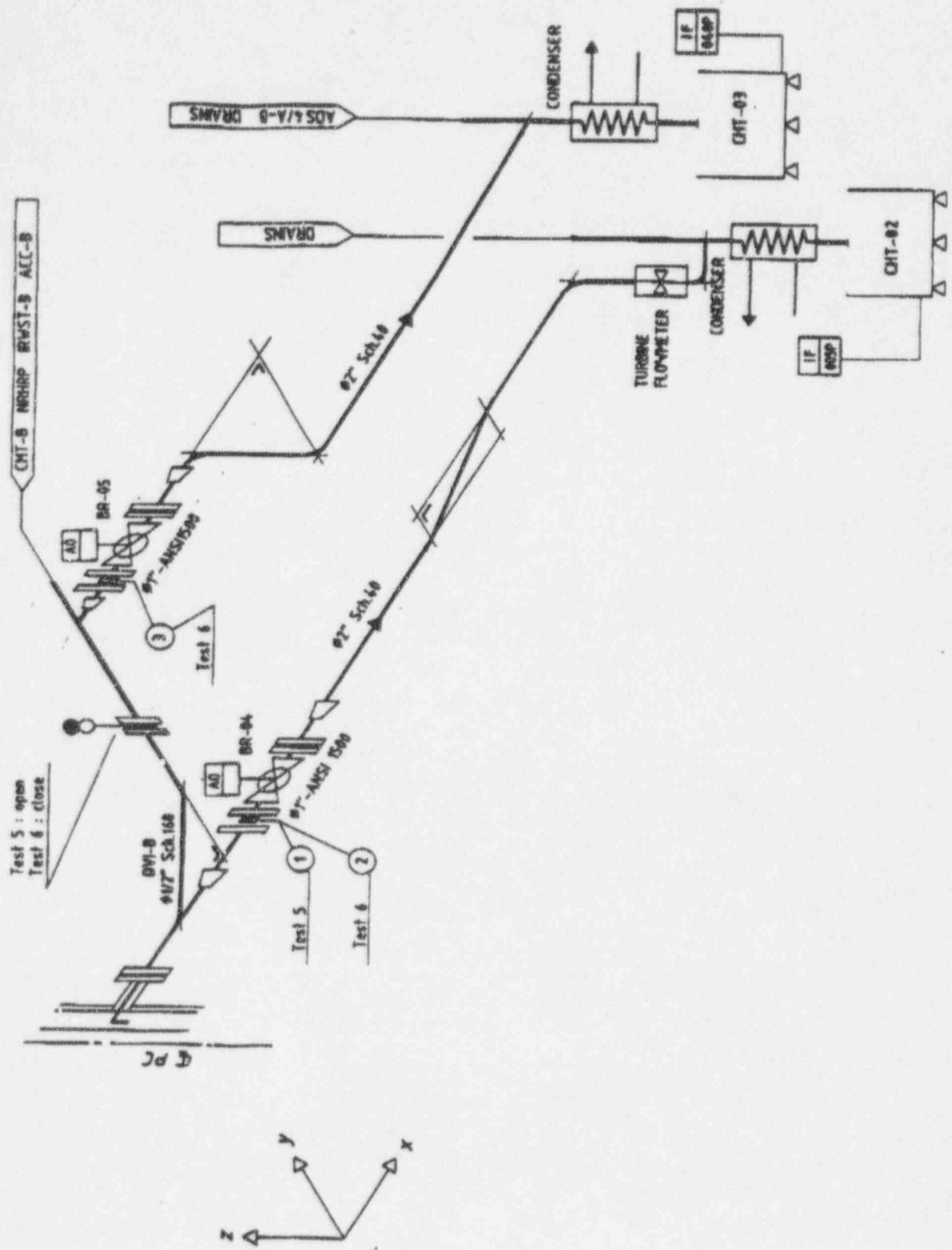
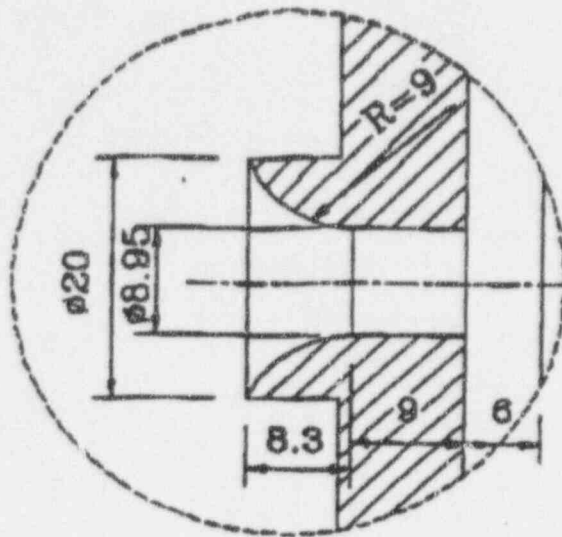
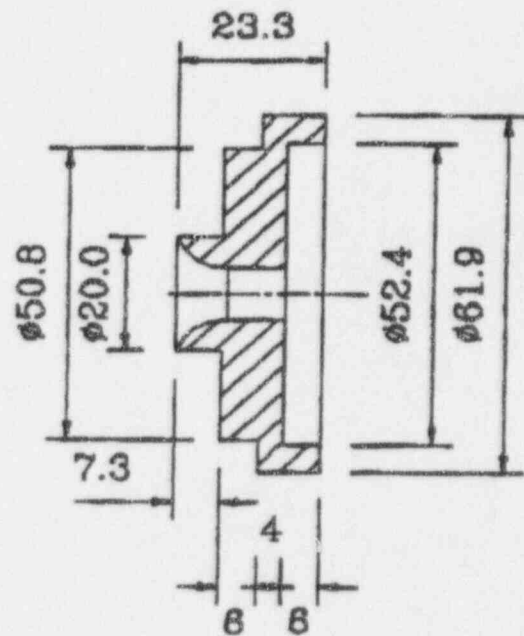
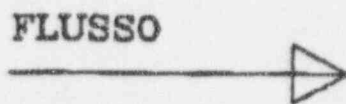


Figure 2.6.5-1 Break Line Configuration for DEG of DVI-B

Prova S00706
Test 6



Lato
valvola

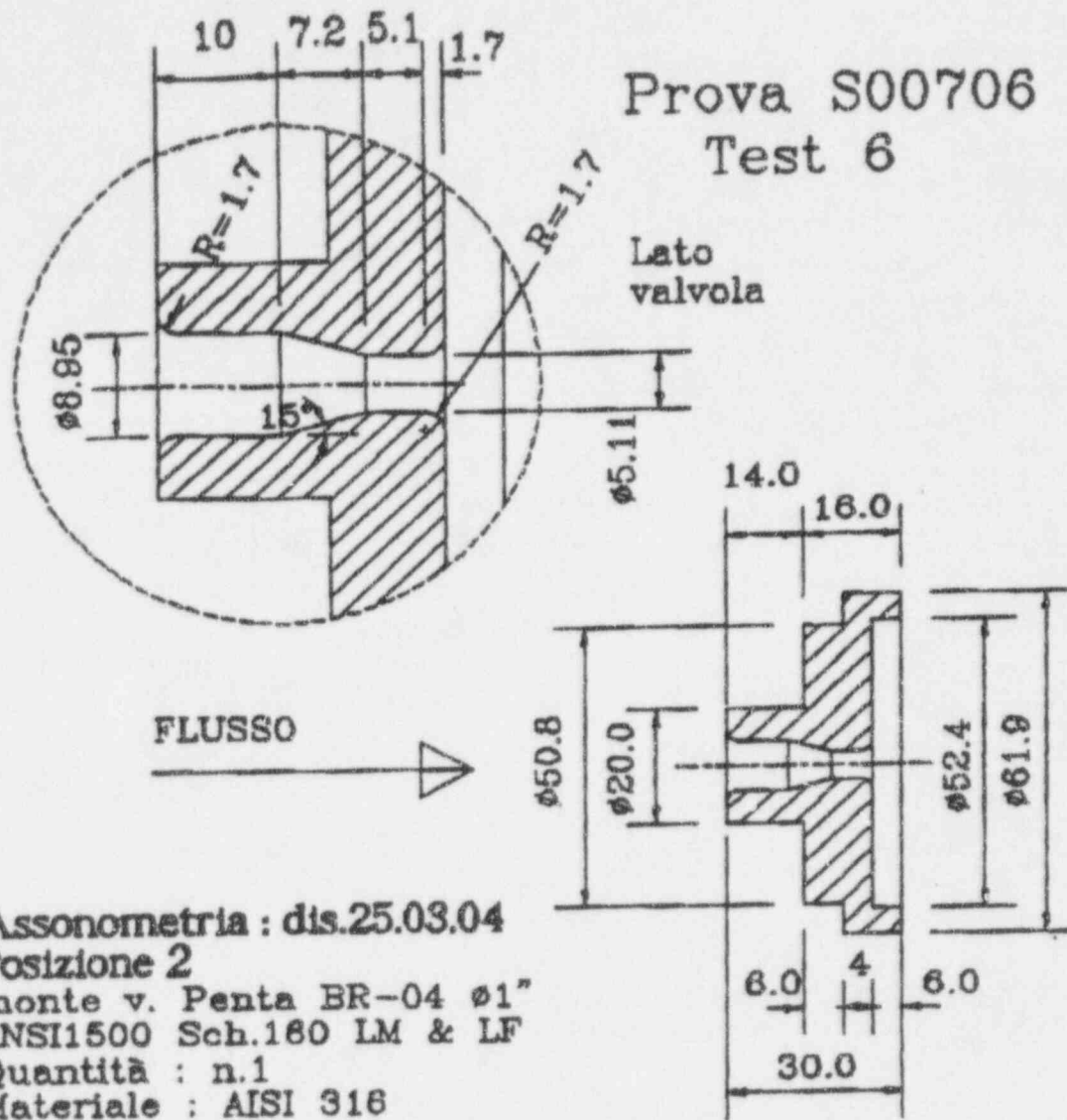


Assonometria : dis. 25.03.24
Posizione 3

monte v. Penta BR-05 $\phi 1''$
ANSI1500 Sch.160 LM & LF
Quantità : n.1
Materiale : AISI 316

0	20/6/94	Geom. orifizio Prova S00706 Test 6			
Indice	Data	Modifiche	Disegn.	Controll.	Approv.
SIET Piacenza Italy		Des. n.	SPES 2 - DVI-B - Break Device Orifizio calibrato pos.3		
		Scala	Disegno n.	Foglio di	
		25.03.26	22	22	

Figure 2.6.5-2 SPES-2 DVI-B Break Orifice Used in Position 3



0	19/5/94	Geom. orifizio Prova S00706 Test 6			
Indice	Data	Modifiche	Disegn.	Control.	Approv.
SIET Piacenza Italy		Doc. n. SPES 2 - DVI-B - Break Device Orifizio calibrato pos.2			
		Scale	Disegno n.	Foglio	di
		25.03.28	21	22	

Figure 2.6.5-3 SPES-2 DVI-B Break Orifice Used in Position 2

2.6.6 Facility Operation for Test S00908

The purpose of test S00908 was to investigate the plant behavior and system response during a full bore double-ended guillotine (DEG) break of the CL-B2 to CMT-B balance line with passive safety systems only for mitigation. The DEG break was simulated by using the two valves located on the cold leg-B2 balance line; one on each side of the CMT balance line isolation valve. The break valve identified in Figure 2.6.6-1 as BR-05 had an orifice installed at its inlet described in Figure 2.6.6-2. The break valve identified in Figure 2.6.6-1 as BR-04 had an orifice installed at its inlet described in Figure 2.6.6-3. The orifice normally in the balance line near cold leg-B2 was removed so that break flow would only be limited by the break orifice. The other orifices installed in the facility are listed in Table 2.6.6-1. The test was performed with the pressurizer to CMT-A/-B balance lines closed by means of blind flanges installed on both the pressurizer and CMT connections.

Once the facility was at initial conditions, the test was initiated by opening the break valves. When the reactor trip R occurred (pressurizer pressure P-027P = 12.41 MPa = 1800 psia), the heater rod bundle power was controlled to match the scaled AP600 decay heat, and the steam generator MSLIVs were closed with a 2 second delay. When the S signal occurred (pressurizer pressure P-027P = 11.72 MPa = 1700 psia), the PRHR isolation valves and the CMT injection valves were opened and the MFWIVs were closed, all with a 2-second delay, and the RCP coastdown was initiated with a 16.2-second delay.

The CVCS, NRHR, and SFW were off throughout the whole transient. The test simulated the failure of one of two stage 1 and 3 ADS valves. The ADS valves were programmed to open versus either CMT level L-A40E or L-B40E with the delay time shown in Table 2.6.6-2. The accumulators were set to inject water via DVI when the primary pressure was lower than 4.9 MPa (696.1 psia). The IRWST was set to inject water via DVI when the primary pressure was lower than 0.18 MPa (26.1 psia). The test was terminated when the flowrates (F-A60E/F-B60E) discharged by the IRWST reached a stable flow (without significant fluctuation).

**TABLE 2.6.6-1
SPES-2 INSTALLED ORIFICES**

Location	Diameter (mm)	Thickness (mm)
ADS-1	3.09	12
ADS-2	9.35	12
ADS-3	6.61	12
ADS-4A	20.68	7
ADS-4B	20.68	7
CMT-A injection line	4.1	5.5
CMT-B injection line	5.7	5.5
CMT-A cold leg bal. line (2 orif.)	7.5	5.5
CMT-B cold leg bal. line (2 orif.)	removed	-
Accumulator-A injection line	4.86	7.3
Accumulator-B injection line	4.86	7.3
DVI-B break device CMT side	8.95 **	9 *
DVI-B break cold leg side	8.71	9 *

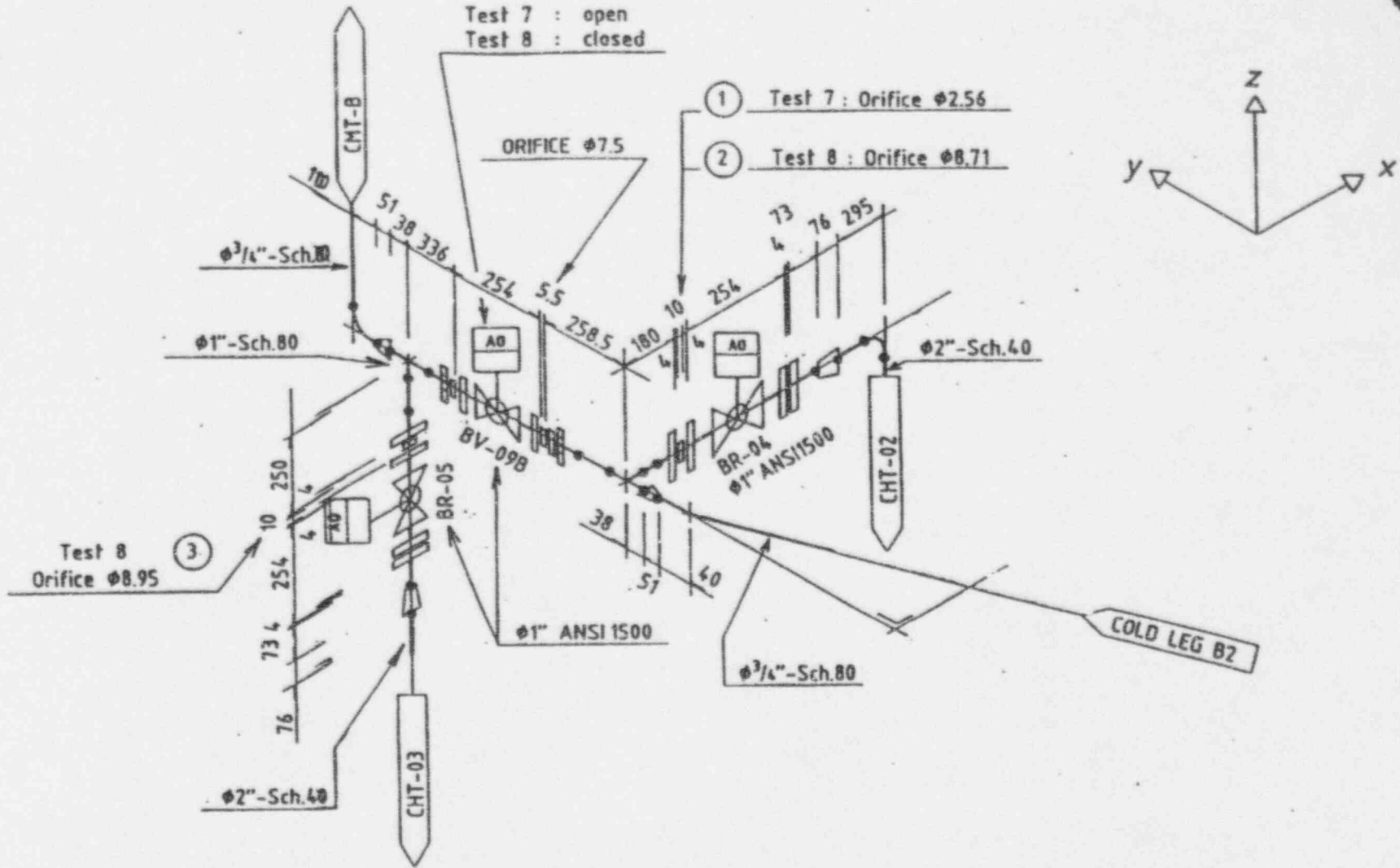
* Rounded entrance with 9 mm radius (see Figures 2.6.6-2 and 2.6.6-3)

** The actual scaled break size of the 8-inch Sch. 160 CL-BL is 8.71 mm. However, since no significant amount of break flow is discharged from this point, the 8.95 mm orifice from matrix test No. 6 was utilized (see Figure 2.6.6-3).

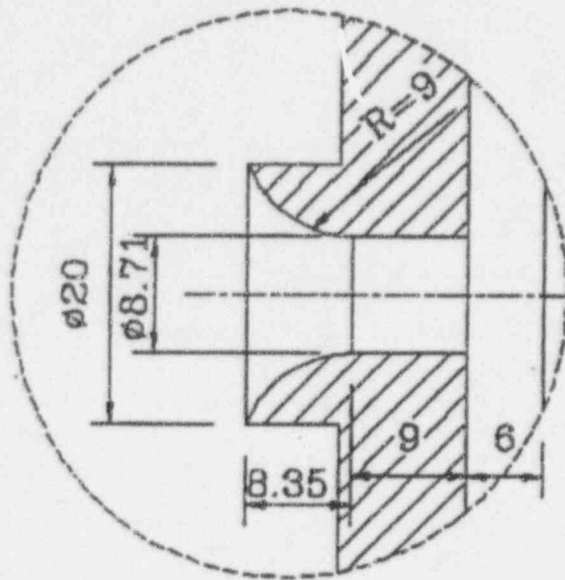
**TABLE 2.6.6-2
PROGRAMMED OPENING OF ADS VALVES**

ADS Stage	Orifice Dia. (mm/in.)	CMT Volume (%)	L-A40E or L-B40E (m/ft.)	Delay Time (sec.)
First	3.09/0.122	67	4.152/13.622	30
Second	9.35/0.368	67	4.152/13.622	125
Third	6.61/0.260	67	4.152/13.622	245
Fourth A	20.68/0.814	20	1.192/3.911	60 sec after 20% CMT vol., but no sooner than 360 sec. after 67% CMT vol.
Fourth B	20.68/0.814	20	1.192/3.911	60 sec after 20% CMT vol., but no sooner than 360 sec. after 67% CMT vol.

Figure 2.6-6-1 Break Line Configuration for DEG of CL-B2 to CMT-B Balance Line

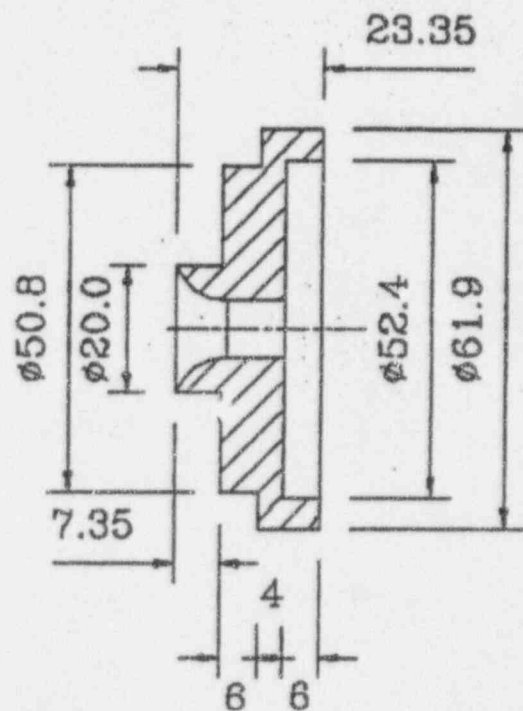


Prova S00908
Test 8



Lato
valvola

FLUSSO
→



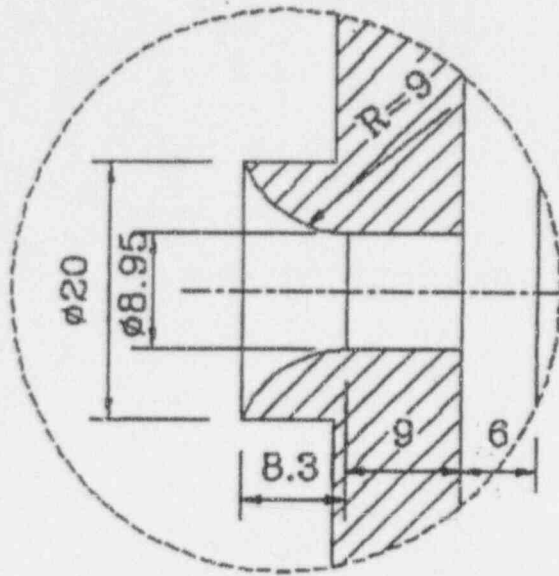
Assonometria : dis. 25.03.25
Posizione 2

monte v. Penta BR-04 $\phi 1''$
ANSI1500 Sch.160 LM & LF
Quantità : n.1
Materiale : AISI 316

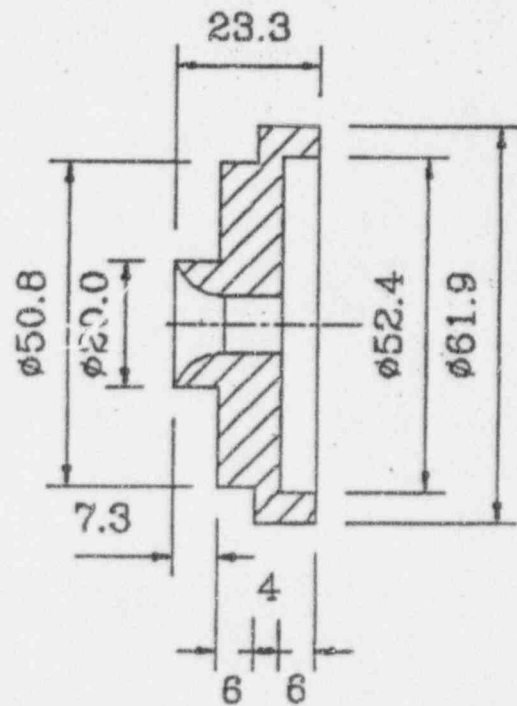
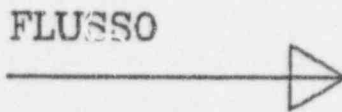
0	15/8/94	Geom. orificio Prova S00908 Test 8	El	ma	ma
Indice	Data	Modifiche	Disegn.	Controll.	Approv.
SIET Piacenza Italy		Dec. n.			
		SPES 2 - Break Device Orificio calibrato pos.2			
Scala	Disegno n.	Foglio	di		
	25.03.26	24	25		

Figure 2.6.6-2 SPES-2 DEG Break Orifice Used in Position 2

Prova S00908
Test 8



Lato
valvola



Assonometria : dis. 25.03.25
Posizione 3

monte v. Penta BR-05 $\phi 1''$
ANSI1500 Sch.160 LM & LF
Quantità : n.1
Materiale : AISI 316

0	13/08/94	Geom. orificio Prova S00908 Test 8	EG	MAR	MAR
Indice	Data	Modifiche	Disegn.	Controll.	Approv.
SIET Piacenza Italy		Dec. n.			
		SPES 2 - Break Device Orificio calibrato pos.3			
Scala	Disegno n.	Foglio	di		
	25.03.26	25	25		

Figure 2.6.6-3 SPES-2 DEG Break Orifice Used in Position 3

2.6.7 Facility Operation for Test S01007

The purpose of test S01007 was to investigate the asymmetric CMT performance following a 2-in. break in the cold leg-B2 to CMT-B balance line with passive safety systems only for mitigation. The break was located on the cold-leg side of the balance line isolation valve identified in Figure 2.6.7-1 as BV-09B. The break valve identified in Figure 2.6.7-1 as BR-04 had an orifice installed at its inlet described in Figure 2.6.7-2 in order to simulate a 2-in. break. The other orifices installed in the facility are listed in Table 2.6.7-1. The test was performed with the pressurizer to CMT-A/-B balance lines closed by means of blind flanges installed on both the pressurizer and CMT connections.

Once the facility was at initial conditions, the test was initiated by opening the break valve. When the reactor trip R occurred (pressurizer pressure P-027P = 12.41 MPa = 1800 psia), the heater rod bundle power was controlled to match the scaled AP600 decay heat, and the steam generator MSLIVs were closed with a 2-second delay. When the S signal occurred (pressurizer pressure P-027P = 11.77 MPa = 1700 psia), the PRHR isolation valves and the CMT injection valves were opened and the MSLIVs were closed, all with a 2 second delay, and the RCP coastdown was initiated with a 16.2 second delay.

The CVCS, NRHR, and SFW were off throughout the whole transient. The test simulated the failure of one of two fourth-stage ADS valves. The ADS valves were programmed to open versus either CMT level L-A40E or L-B40E with the delay time shown in Table 2.6.7-2. The accumulators were set to inject water via DVI when the primary pressure was lower than 4.9 MPa (696.1 psia). The IRWST was set to inject water via DVI when the primary pressure was lower than 0.18 MPa (26.1 psia). The test was terminated when the flowrates (F-A60E/F-B60E) discharged by the IRWST reached a stable flow (without significant fluctuation).

**TABLE 2.6.7-1
SPES-2 INSTALLED ORIFICES**

Location	Diameter (mm)	Thickness (mm)
ADS-1	4.37	12
ADS-2	9.35	12
ADS-3	9.35	12
ADS-4A	20.68	7
ADS-4B	14.62	7
CMT-A injection line	4.1	5.5
CMT-B injection line	5.7	5.5
CMT-A cold leg bal. line (2 orif.)	7.5	5.5
CMT-B cold leg bal. line (2 orif.)	7.5	-
Accumulator-A injection line	4.86	7.3
Accumulator-B injection line	4.86	7.3
Balance Line-B break device	2.56	3.3 *

* Rounded entrance with 2.6 mm radius

**TABLE 2.6.7-2
PROGRAMMED OPENING OF ADS VALVES**

ADS Stage	Orifice Dia. (mm/in.)	CMT Volume (%)	L-A40E or L-B40E (m/ft.)	Delay Time (sec.)
First	3.09/0.122	67	4.152/13.622	30
Second	9.35/0.368	67	4.152/13.622	125
Third	9.35/0.368	67	4.152/13.622	245
Fourth A	20.68/0.814	20	1.192/3.911	60 sec after 20% CMT vol., but no sooner than 360 sec after 67% CMT vol.
Fourth B	14.62/0.576	20	1.192/3.911	60 sec after 20% CMT vol., but no sooner than 360 sec after 67% CMT vol.

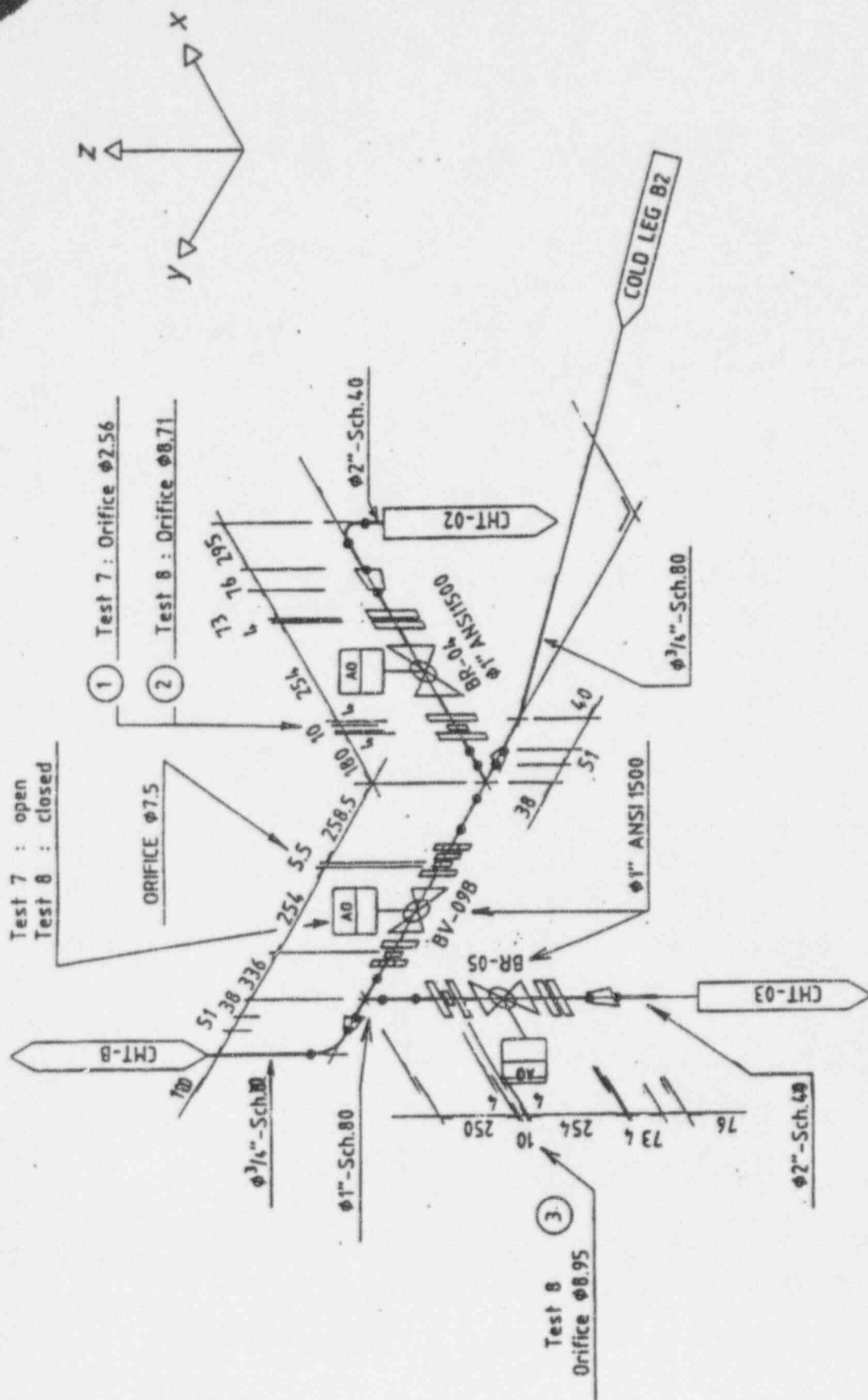
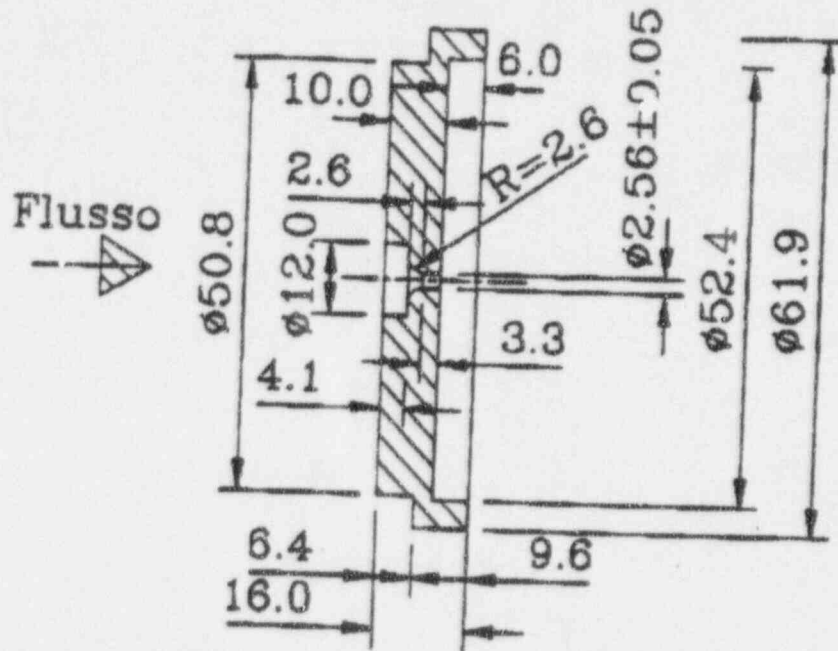


Figure 2.6.7-1 Break Line Configuration for 2-in. Break in the CL-B2 to CMT-B Balance Line

SPES2 - Break device
 CL B2 - CMT B Balance Line
 Prova S00807 - Test 7



Assonometria : dis. 25.03.25 Pos.1

Collocazione : Linea rottura CL B2-CMT B B.I
 a monte valvola BR-04

flg.: $\phi 1$ " ANSI1500 LM & LF

Quant.: n.1 Mat.: AISI 316

0	13/08/84	Geom.orifizio Prova S00807 Test 7			
Indice	Data	Modifiche	Disegn.	Control.	Approv.
SIET		Des. n.			
Placenza		SPES 2 - Break Device			
Italy		Orifizio calibrato pos. 1			
Scale	Disegno n.	Foglio	di		
1:1	25.03.26	23	25		

Figure 2.6.7-2 SPES-2 Break Orifice Used in Position 1

2.6.8 Facility Operation for Test S01110

The purpose of test S01110 was to investigate the plant behavior and system response during a single steam generator tube rupture (SGTR) using only the passive safety systems for mitigation. The test was performed with the pressurizer to CMT-A/-B balance lines closed by means of blind flanges installed on both the pressurizer and CMT connections. The tube rupture was simulated via a line connected from the primary side (RCP B suction piping) to the secondary side of steam generator-B. Two venturi flowmeters were installed in the line; one to measure fluid flow from the primary side to the secondary side, and the other to measure flow from the secondary side to the primary side. A detailed drawing of this arrangement is given in Figure 2.6.8-1. A break orifice, scaled to the size of a single AP600 steam generator tube inner diameter of 0.6075 inches, was installed at the inlet of the break valve (BR-04). A detailed drawing of the orifice is shown in Figure 2.6.8-2. The other orifices installed throughout the facility are listed in Table 2.6.8-1.

Once the facility was at initial conditions, the test was initiated by opening the break valve. When the reactor trip R and safety injection signal S occurred due to low pressurizer level (pressurizer level L-010P = 0.378m = 1.24 ft.), the heater rod bundle power was controlled to match the scaled AP600 decay heat, and the steam generator MSLIVs were closed with a 2-second delay. Additionally, the PRHR isolation valves and the CMT injection valves were opened and the MFWIVs were closed, all with a 2-second delay, and the RCP coastdown was initiated with a 16.2 second delay.

The CVCS, NRHR, and SFW were off throughout the whole transient. The test simulated the failure of one of two fourth-stage ADS valves on loop B. Although ADS actuation did not occur, the ADS valves were programmed anyway to open versus either CMT level L-A40E or L-B40E with the delay time shown in Table 2.6.8-2. The accumulators were set to inject water via DVI when the primary pressure was lower than 4.9 MPa (696.1 psia). The IRWST was set to inject water via DVI when the primary pressure was lower than 0.18 MPa (26.4 psia). The test was terminated when the primary and secondary system pressures equalized so that the average break flow for 10 minutes was essentially zero and the CMT levels were not decreasing.

TABLE 2.6.8-1
SPES-2 INSTALLED ORIFICES

Location	Diameter (mm)	Thickness (mm)
ADS-1	4.37	12
ADS-2	9.35	12
ADS-3	9.35	12
ADS-4A	20.68	7
ADS-4B	14.62	7
CMT-A injection line	4.1	5.5
CMT-B injection line	5.7	5.5
CMT-A cold leg bal. line (2 orif.)	7.5	5.5
CMT-B cold leg bal. line (2 orif.)	7.5	5.5
Accumulator-A injection line	4.86	7.3
Accumulator-B injection line	4.86	7.3
Cold leg-B2 break device	0.85	5 *
* Rounded entrance with 0.9 mm radius		

**TABLE 2.6.8-2
PROGRAMMED OPENING OF ADS VALVES**

ADS Stage	Orifice Dia. (mm/in.)	CMT Volume (%)	L-A40E or L-B40E (m/ft.)	Delay Time (sec.)
First	4.37/0.172	67	4.152/13.622	30
Second	9.35/0.368	67	4.152/13.622	125
Third	9.35/0.368	67	4.152/13.622	245
Fourth A	20.68/0.814	20	1.192/3.911	60 sec after 20% CMT vol., but no sooner than 360 sec after 67% CMT vol.
Fourth B	14.62/0.576	20	1.192/3.911	60 sec after 20% CMT vol., but no sooner than 360 sec after 67% CMT vol.

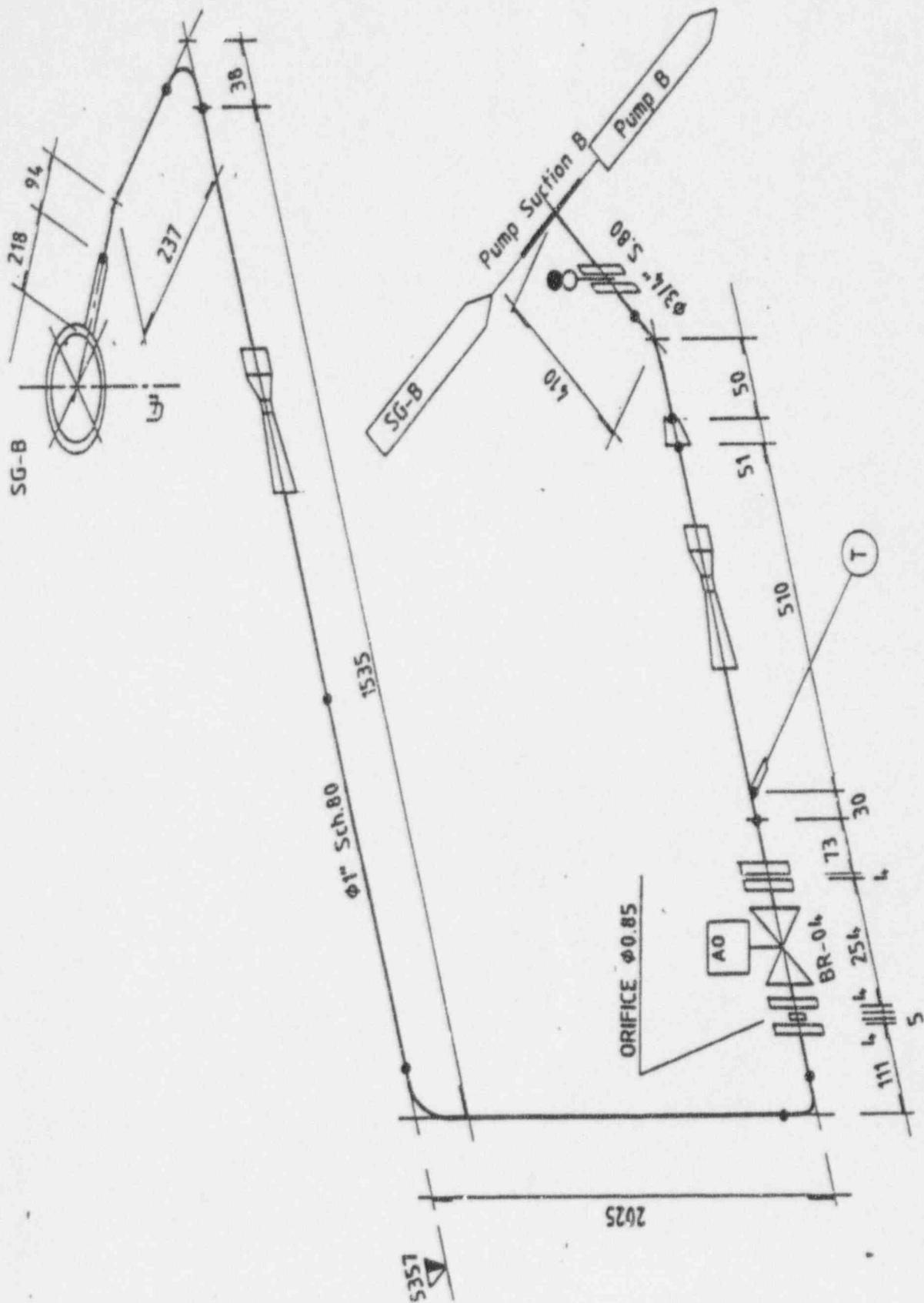


Figure 2.6.8-1 Break Line Configuration for Steam Generator Tube Rupture (SGTR)

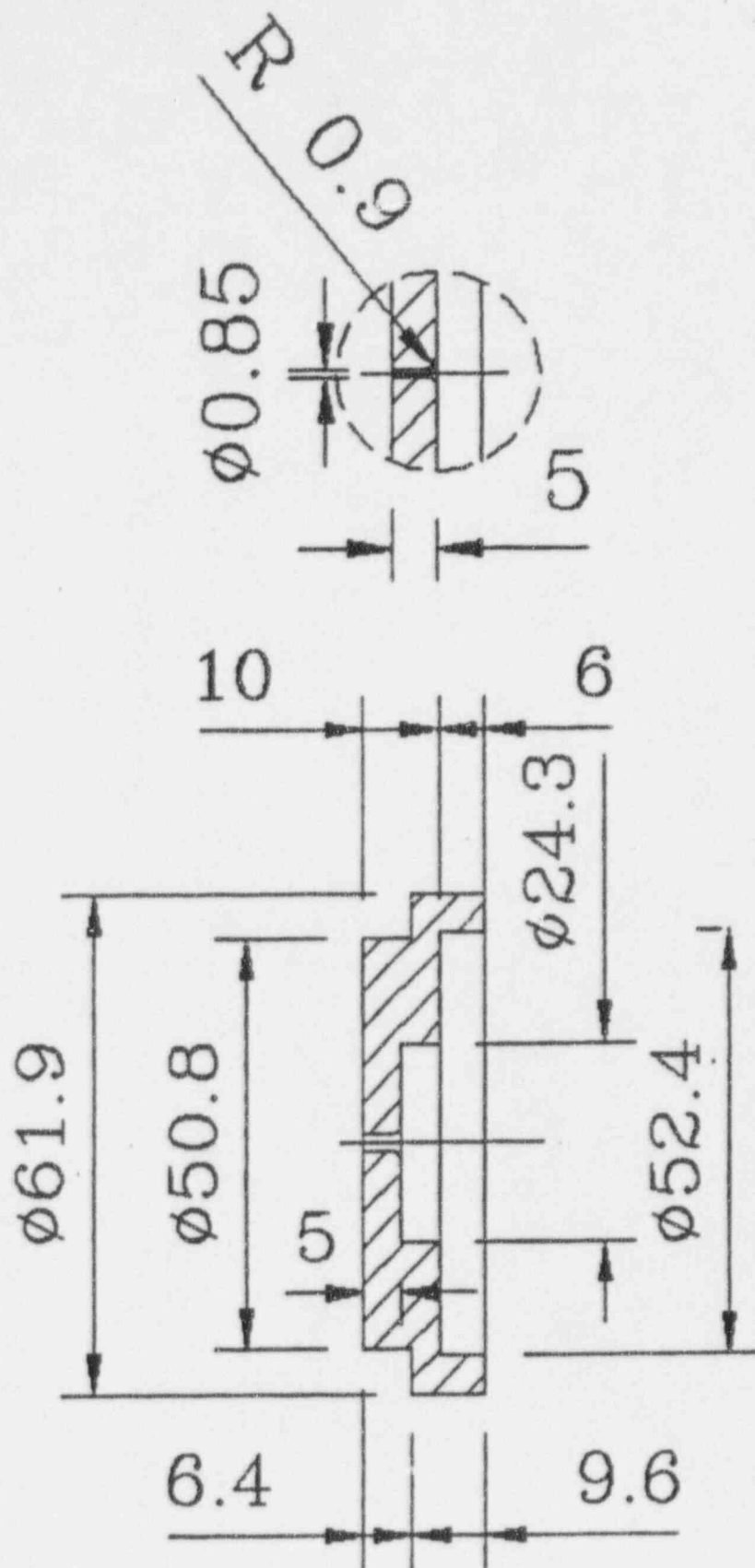


Figure 2.6.8-2 SPES-2 SGTR Break Orifice

2.6.9 Facility Operation for Test S01211

The purpose of test S012011 was to investigate the plant behavior and system response during a single steam generator tube rupture (steam generator-TR) and an inadvertent ADS actuation 2 minutes + 30 seconds after S signal using only the passive safety systems for mitigation. The test was performed with the pressurizer to CMT-A/B balance lines closed by means of blind flanges installed on both the pressurizer and CMT connections. The tube rupture was simulated via a line connected from the primary side (RCP B suction piping) to the secondary side of steam generator-B. Two venturi flowmeters were installed in the line; one to measure fluid flow from the primary side to the secondary side, and the other to measure flow from the secondary side to the primary side. A detailed drawing of this arrangement is given in Figure 2.6.9-1. A break orifice, scaled to the size of a single AP600 steam generator tube inner diameter of 0.6075 in., was installed at the inlet of the break valve (BR-04). A detailed drawing of the orifice is shown in Figure 2.6.9-2. The other orifices installed throughout the facility are listed in Table 2.6.9-1.

Once the facility was at initial conditions, the test was initiated by opening the break valve. When the reactor trip R and safety systems actuation signal (S) occurred due to low pressurizer level (pressurizer level L-010P = 0.676m = 2.22 ft.), the heater rod bundle power was controlled to match the scaled AP600 decay heat, and the steam generator MSLIVs were closed with a 2-second delay. Additionally, the PRHR isolation valves and the CMT injection valves were opened and the MFWIVs were closed, all with a 2-second delay, and the RCP coastdown was initiated with a 16.2-second delay.

The CVCS, NRHR, and SFW were off throughout the whole transient. The test simulated the failure of one of two fourth-stage ADS valves on loop B. The ADS valves were programmed to open with the delay times shown in Table 2.6.9-2. Additionally, heat loss compensation of 150 kW was terminated after ADS stage 2 actuation, instead of the typical ADS stage 1. The accumulators were pressurized to inject water via DVI when the primary pressure was lower than 4.9 MPa (696.1 psia). The test was terminated when the secondary side of the faulted steam generator was nearly empty.

**TABLE 2.6.9-1
SPES-2 INSTALLED ORIFICES**

Location	Diameter (mm)	Thickness (mm)
ADS-1	4.37	12
ADS-2	9.35	12
ADS-3	9.35	12
ADS-4A	20.68	7
ADS-4B	14.62	7
CMT-A injection line	4.1	5.5
CMT-B injection line	5.7	5.5
CMT-A CL bal. line (2 orif.)	7.5	5.5
CMT-B CL bal. line (2 orif.)	7.5	5.5
Accumulator-A injection line	4.86	7.3
Accumulator-B injection line	4.86	7.3
Cold leg-B2 break device	0.85	5 *

* Rounded entrance with 0.9 mm radius

**TABLE 2.6.9-2
PROGRAMMED OPENING OF ADS VALVES**

ADS Stage	Orifice Dia. (mm/in.)	CMT Volume (%)	L-A40E or L-B40E (m/ft.)	Delay Time (sec.)
First	4.37/0.172	-	-	2 min + 30 sec after "S"
Second	9.35/0.368	-	-	2 min + 125 sec after "S"
Third	9.35/0.368	-	-	2 min + 245 sec after "S"
Fourth A	20.68/0.814	20	1.192/3.911	0 sec after 20% CMT vol., but no sooner than 360 sec after 67%
Fourth B	14.62/0.576	20	1.192/3.911	60 sec after 20% CMT vol., but no sooner than 360 sec after 67%

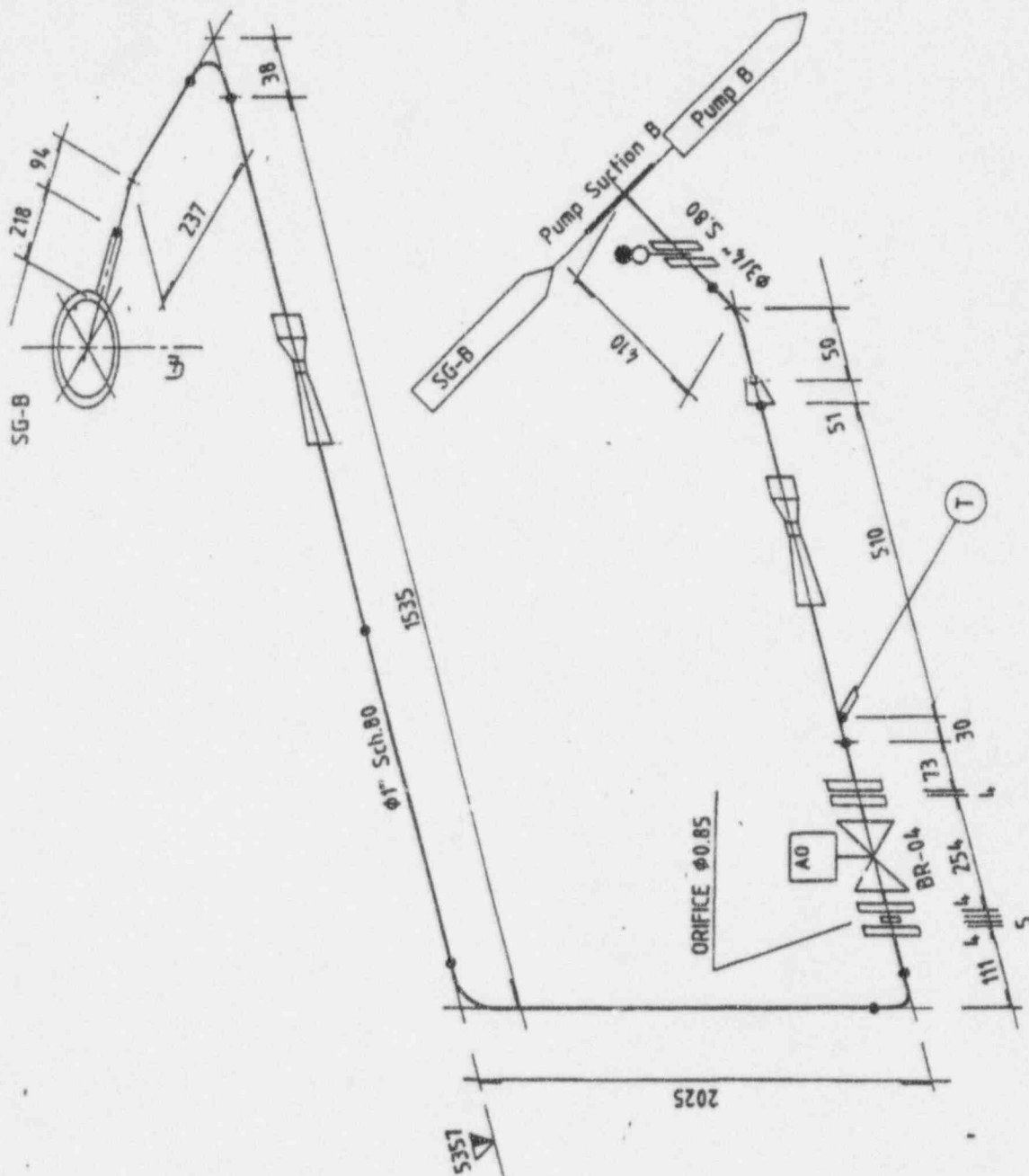
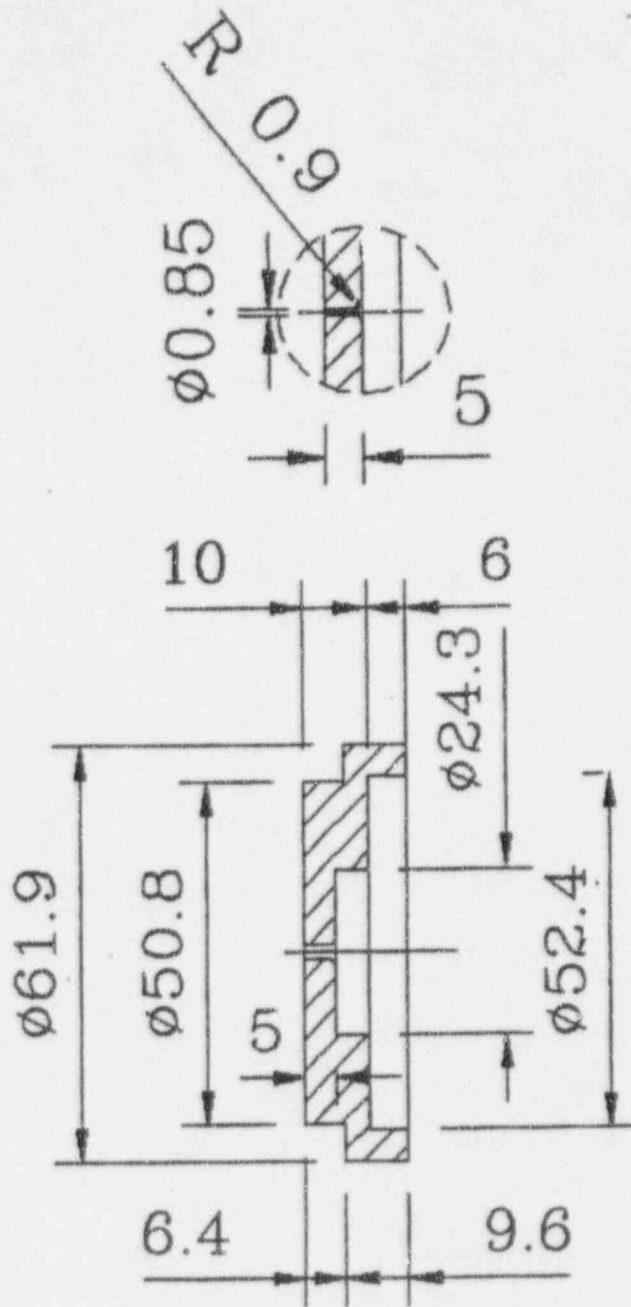


Figure 2.6.9-1 Break Line Configuration for Single Steam Generator Tube Rupture (SGTR)



0	01/07/94	EMISSIONE			
Indice	Data	Modifiche	Disegn.	Controllo	Approv.
SIET Piacenza Italy		Doc. n.			
		SPES 2 - SGTR matrix test 10 Orifice particulars			
Scale	Disegno n.	Foglio	di		
1:1	025.03.26	26	26		

Figure 2.6.9-2 SPES-2 SGTR Break Orifice

2.6.10 Facility Operation for Test S01309

The purpose of test S01309 was to investigate the plant behavior and system response during a single steam generator tube rupture (SGTR) using nonsafety and safety systems along with operator action to isolate the faulted steam generator, subcool and depressurize the primary system. The test was performed with the pressurizer to CMT-A/B balance lines closed by means of blind flanges installed on both the pressurizer and CMT connections. The tube rupture was simulated via a line connected from the primary side (RCP-B suction piping) to the secondary side of steam generator-B. Two venturi flowmeters were installed in the line; one to measure fluid flow from the primary side to the secondary side, and the other to measure flow from the secondary side to the primary side. A detailed drawing of this arrangement is given in Figure 2.6.10-1. A break orifice, scaled to the size of a single AP600 steam generator tube inner diameter of 0.6075 inches, was installed at the inlet of the break valve (BR-04). A detailed drawing of the orifice is shown in Figure 2.6.10-2. The other orifices installed throughout the facility are listed in Table 2.6.10-1.

Once the facility was at initial conditions, the test was initiated by opening the break valve. When the reactor trip (R) and safety systems actuation signal (S) occurred due to low pressurizer level (pressurizer level L-010P = 0.378m = 1.24 ft.), the heater rod bundle power was controlled to match the scaled AP600 decay heat, and the steam generator MSLIVs were closed with a 2-second delay. Additionally, the PRHR isolation valves and the CMT injection valves were opened and the MFWIVs were closed, all with a 2-second delay, and the RCP coastdown was initiated with a 16.2-second delay.

The CVCS was programmed to start when pressurizer level (L-010P) = 3.1 m = 10.17 ft. and deliver a scaled flow rate (F-001A) = 0.016 kg/sec. = 0.0353 lbm/sec. After the S signal, the CVCS setpoints were automatically reset to be ON at pressurizer level ≤ 10 percent (L-010P ≤ 0.676 m) and OFF at pressurizer level ≥ 20 percent (L-010P ≥ 1.352 m). The SFW was automatically initiated after the S signal at its nominal flowrate to try to restore the steam generator narrow range level (L-A20S/L-B20S) at the nominal value of 1.48m (4.86 ft.).

It was determined that an operator would be able to identify the faulted steam generator approximately 5 minutes after an S signal. Therefore, for this test the operator isolated the faulted steam generator 5 minutes after the S signal by closing the SFW isolation valve (CV-06B), but still continued to feed SFW to the intact steam generator (steam generator-A). The operator actions to subcool and depressurize were originally programmed into the plant control computer to perform. However, during the performance of the test, it was apparent that a higher cooldown rate was required at the SPES-2 facility in order for the logic programmed into the computer to perform the operator actions as specified. Therefore, the actions to open the ADS-1 valve and steam generator-A PORV to subcool and depressurize were performed manually by plant personnel.

The pressurizer internal heaters remained on until low pressurizer level = 2m = 6.56 ft., but the two bottom external pressurizer heaters remained on throughout the transient to compensate for pressurizer heat loss and to maintain pressurizer pressure. The test simulated the failure of one of two fourth-stage ADS valves on loop B. Additionally, the ADS-1 and ADS-3 had smaller orifices installed equivalent to one-half the AP600 ADS-1 and -3 valves in order to have better control of the primary

system depressurization. Although ADS actuation did not occur during the test, the ADS valves were programmed to open versus either CMT level L-A40E or L-B40E with the delay time shown in Table 2.6.10-2. The accumulators were set to inject water via DVI when the primary pressure was lower than 4.9 MPa (696.1 psia). The IRWST was set to inject water via DVI when the primary pressure was lower than 0.18 MPa (26.1 psia). The test was terminated when the primary and secondary system pressures equalized so that the average break flow for 10 minutes was essentially zero and the CMT levels were not decreasing.

**TABLE 2.6.10-1
SPES-2 INSTALLED ORIFICES**

Location	Diameter (mm)	Thickness (mm)
ADS-1	2.2	12
ADS-2	9.35	12
ADS-3	2.2	12
ADS-4A	20.68	7
ADS-4B	14.62	7
CMT-A injection line	4.1	5.5
CMT-B injection line	5.7	5.5
CMT-A cold leg bal. line (2 orif.)	7.5	5.5
CMT-B cold leg bal. line (2 orif.)	7.5	5.5
Accumulator-A injection line	4.86	7.3
Accumulator-B injection line	4.86	7.3
Cold leg-B2 break device	0.85	5 *

* Rounded entrance with 0.9 mm radius

**TABLE 2.6.10-2
PROGRAMMED OPENING OF ADS VALVES**

ADS Stage	Orifice Dia. (mm/in.)	CMT Volume (%)	L-A40E or L-B40E (m/ft.)	Delay Time (sec.)
First	2.2/0.072	67	4.152/13.622	30
Second	9.35/0.368	67	4.152/13.622	125
Third	2.2/0.072	67	4.152/13.622	245
Fourth A	20.68/0.814	20	1.192/3.911	60 sec after 20% CMT vol., but no sooner than 360 sec. after 67% CMT vol.
Fourth B	14.62/0.576	20	1.192/3.911	60 sec after 20% CMT vol., but no sooner than 360 sec. after 67% CMT vol.

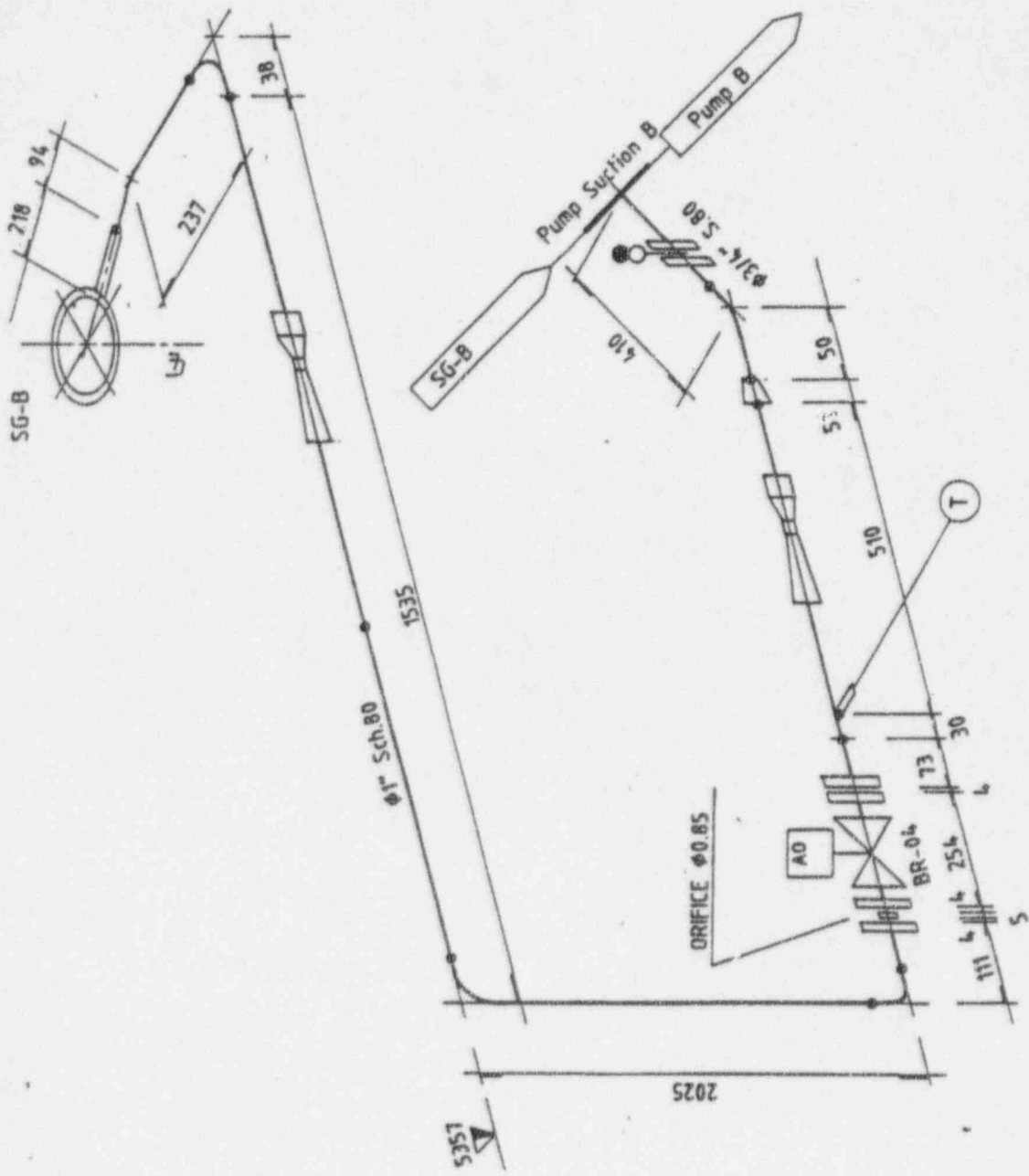
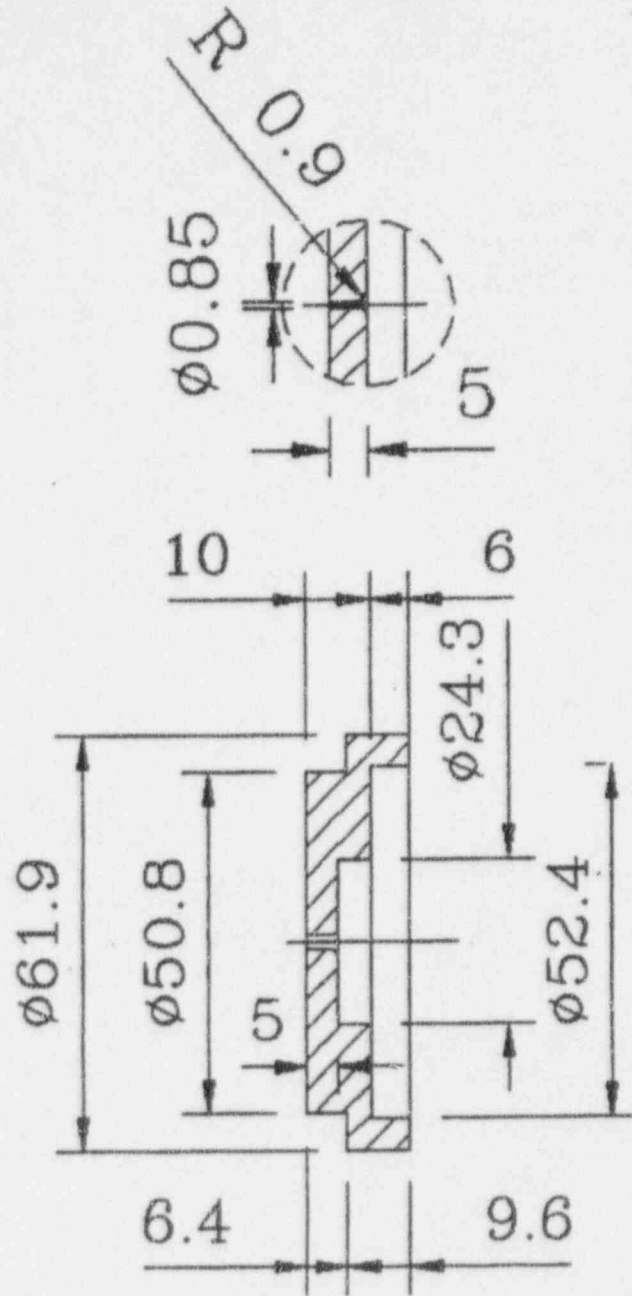


Figure 2.6.10-1 Break Line Configuration for Steam Generator Tube Rupture (SGTR)



0	01/07/94	EMISSTONK			
Indice	Data	Modifiche	Disegn.	Control.	Approv.
SIET Piacenza Italy		Dec. n.			
		SPES 2 - SGTR matrix test 10 Orifice particulars			
Scala	Disegno n.	Foglio	di		
1:1	025.03.26	26	26		

Figure 2.6.10-2 SPES-2 SGTR Break Orifice

2.6.11 Facility Operation for Test S01512

Test S01512, a large steam line break with passive safety systems only, was simulated using the steam generator-A PORV as the break opening. The steam generator-A PORV had an orifice installed with a diameter of 20.4 mm (shown in Figure 2.6.11-1) which corresponds to an AP600 break area of 1.388 ft². (This area corresponds to the steam generator outlet nozzle orifice area.) The other orifices installed at the facility are listed in Table 2.6.11-1.

Test S01512 was performed with the facility operating at full pressure and flow, but at "hot standby" conditions. The power channel was at zero power (i.e., no decay heat was simulated) but with heater rod power at 150 kW for facility heat loss compensation. Additionally, the following initial conditions existed:

- RCPs were running at normal flow (cold leg flow = 12.92 lb/sec.)
- pressurizer pressure was at 2250 psia
- core ΔT was $\sim 1^\circ\text{F}$ ($t_{\text{avg}} = 545^\circ\text{F}$)
- pressurizer level was between 6.56 ft. and 8.2 ft.
- steam generators pressure was approximately 1000 psi
- steam generators narrow range level was approximately 4.9 ft.
- main feedwater isolation valves were closed
- common steam line isolation valve (BV-07) was closed
- main steam isolation valves (BV-05A/BV-05B) were opened
- CVCS, NRHR, and SFW were not operational.

The test was initiated by opening the steam generator-A PORV (BV-06A) at time zero. All heat loss compensation was terminated when the steam generator-A PORV was opened. Based on pretest predictions using a lead/lag function of 50/5, the S signal was manually generated by the SPES plant computer one second after the break opening. The pressurizer internal heaters were shut off by the S signal. Also, at S signal, the CMT and PRHR isolation valves were opened with a two-second delay, the main steam line isolation valves were closed with a 4-second delay, and the RCPs were shutdown with a 16.2-second delay.

The ADS was not expected to actuate for this test, but was programmed to open versus CMT level with the appropriate time delays as listed in Table 2.6.11-2. The accumulators were pressurized to inject when the primary pressure was reduced to less than 696 psia. The IRWST was at full normal level such that it would inject water when the primary pressure was lower than 26.1 psia. The test was terminated when the primary system temperatures and pressures had stabilized and the CMT level was not decreasing.

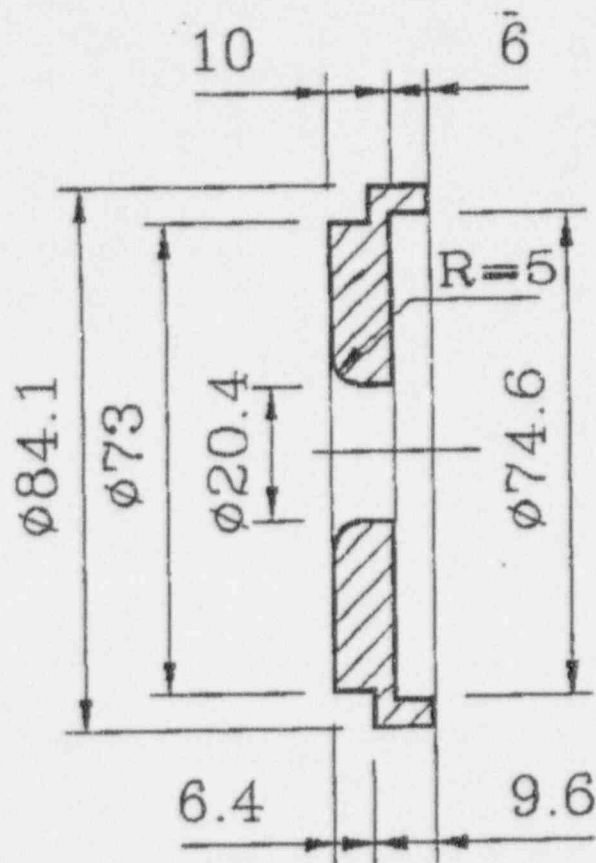
**TABLE 2.6.11-1
SPES-2 INSTALLED ORIFICES**

Location	Diameter (mm)	Thickness (mm)
ADS-1	4.37	12
ADS-2	9.35	12
ADS-3	9.35	12
ADS-4A	20.68	7
ADS-4B	20.68	7
CMT-A injection line	4.1	5.5
CMT-B injection line	5.7	5.5
CMT-A CL bal. line (2 orif.)	7.5	5.5
CMT-B CL bal. line (2 orif.)	7.5	5.5
Accumulator-A injection line	4.86	7.3
Accumulator-B injection line	4.86	7.3
Cold leg-B2 break device	20.4	10 *

* Rounded entrance with 5 mm radius

**TABLE 2.6.11-2
PROGRAMMED OPENING OF ADS VALVES**

ADS Stage	Orifice Dia. (mm/in.)	CMT Volume (%)	L-A40E or L-B40E (m/ft.)	Delay Time (sec.)
First	4.37/0.172	67	4.152/13.622	30
Second	9.35/0.368	67	4.152/13.622	125
Third	9.35/0.368	67	4.152/13.622	245
Fourth A	20.68/0.814	20	1.192/3.911	60 sec after 20% CMT vol., but no sooner than 360 sec. after 67% CMT vol.
Fourth B	20.68/0.814	20	1.192/3.911	60 sec after 20% CMT vol., but no sooner than 360 sec. after 67% CMT vol.



1	27/9/94	EMISSIONE			
Indice	Data	Modifiche	Doc. n.	Disegn.	Controll. Approv.
SIET Piacenza Italy			SPES 2 - SG-A orifizio valvola PORV BV06A		
Scala	Disegno n.	Foglio	di		
1:1	025.03.26	18	27		

Figure 2.6.11-1 SPES-2 Break Orifice for Main Steam Line Break

2.6.12 Facility Operation for Test S01613

The purpose of test S01613 was to investigate the CMT heatup with simultaneous operation of the PRHR with 3 heat exchanger tubes in operation during a simulated 1-in. cold leg break on loop B (the CMT side of the plant). The test was performed with the pressurizer to CMT-A/B balance lines closed by means of blind flanges installed on both the pressurizer and CMT connections. The break was located at the bottom of loop B cold leg-B2 between the cold leg-B2 to CMT-B balance line and the power channel. The break line for the facility was configured as shown in Figure 2.6.12-1 with a break orifice installed as described in Figure 2.6.12-2. The orifices installed throughout the facility are listed in Table 2.6.12-1.

Once the facility was at initial conditions, the test was initiated by opening the break valve. When the reactor trip (R) occurred (pressurizer pressure P-027P = 12.41 MPa = 1800 psia), the heater rod bundle power was controlled to match the scaled AP600 decay heat, and the steam generator MSLIVs were closed with a 2-second delay. When the S signal occurred (pressurizer pressure P-027P = 11.72 MPa = 1700 psia), the PRHR isolation valves and the CMT injection valves were opened and the MFWIVs were closed, all with a 2-second delay, and the RCP coastdown was initiated with a 16.2-second delay.

The CVCS, NRHR, and SFW were off throughout the whole transient. The test simulated the failure of one of two fourth-stage ADS valves on loop B. The ADS valves were programmed to open versus either CMT level L-A40E or L-B40E with the delay time shown in Table 2.6.12-2. The accumulators were set to inject water via DVI when the primary pressure was lower than 4.9 MPa (710.6 psia). The IRWST was set to inject water via DVI when the primary pressure was lower than 0.18 MPa (26.1 psia). The test was terminated when the flowrates (F-A60E/F-B60E) discharged by the IRWST reached a stable flow (without significant fluctuation).

**TABLE 2.6.12-1
SPES-2 INSTALLED ORIFICES**

Location	Diameter (mm)	Thickness (mm)
ADS-1	4.37	12
ADS-2	9.35	12
ADS-3	9.35	12
ADS-4A	20.68	7
ADS-4B	14.62	7
CMT-A injection line	4.1	5.5
CMT-B injection line	5.7	5.5
CMT-A cold leg bal. line (2 orif.)	7.5	5.5
CMT-B cold leg bal. line (2 orif.)	7.5	5.5
Accumulator-A injection line	4.86	7.3
Accumulator-B injection line	4.86	7.3
Cold leg-B2 break device	1.28	3.3 *

* Rounded entrance with 1.3 mm radius

**TABLE 2.6.12-2
PROGRAMMED OPENING OF ADS VALVES**

ADS Stage	Orifice Dia. (mm/in.)	CMT Volume (%)	L-A40E or L-B40E (m/ft.)	Delay Time (sec.)
First	4.37/0.172	67	4.152/13.622	30
Second	9.35/0.368	67	4.152/13.622	125
Third	9.35/0.368	67	4.152/13.622	245
Fourth A	20.68/0.814	20	1.192/3.911	60 sec. after 20% CMT vol., but no sooner than 360 sec. after 67% CMT vol.
Fourth B	14.62/0.576	20	1.192/3.911	60 sec. after 20% CMT vol., but no sooner than 360 sec. after 67% CMT vol.

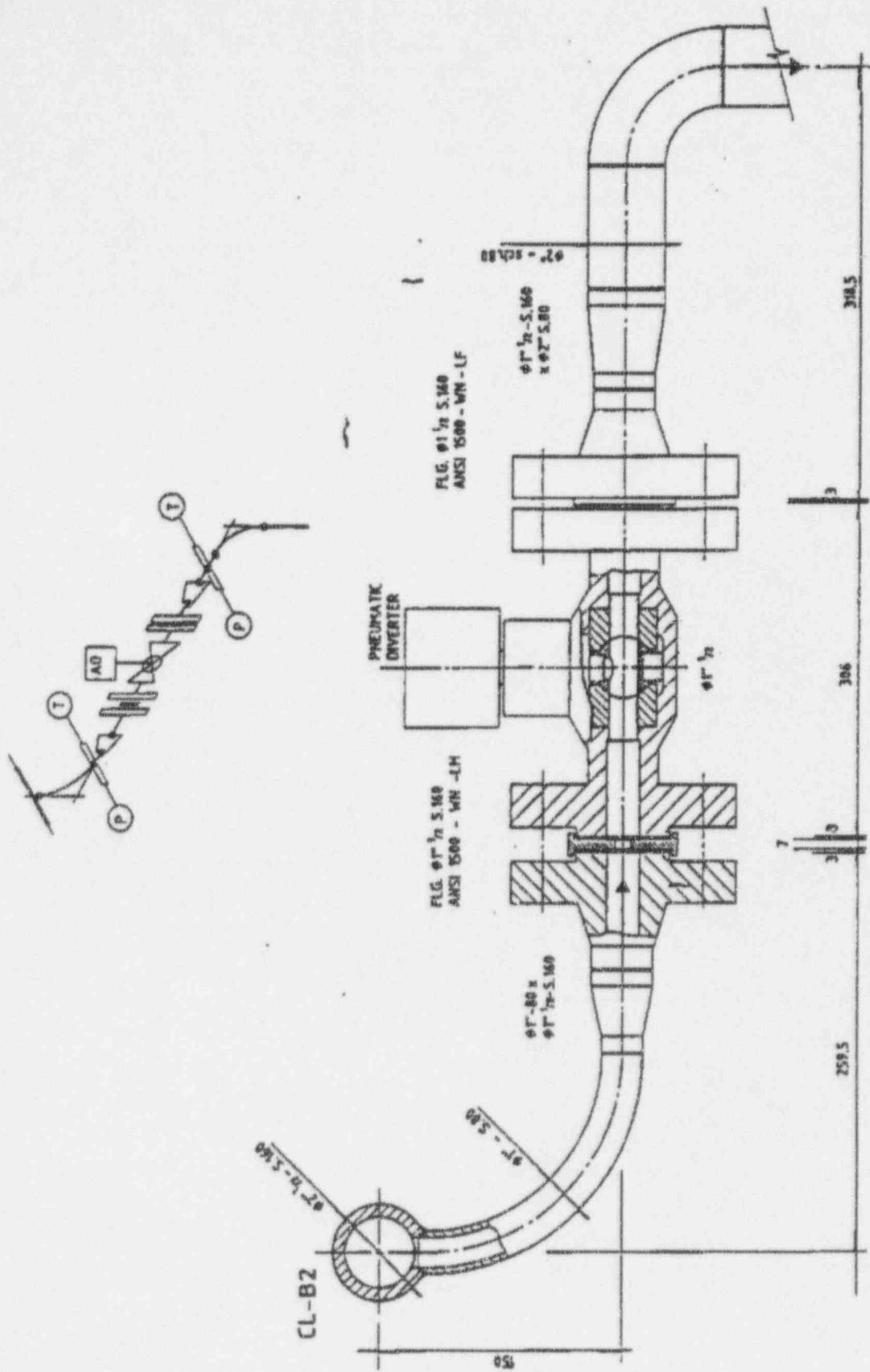
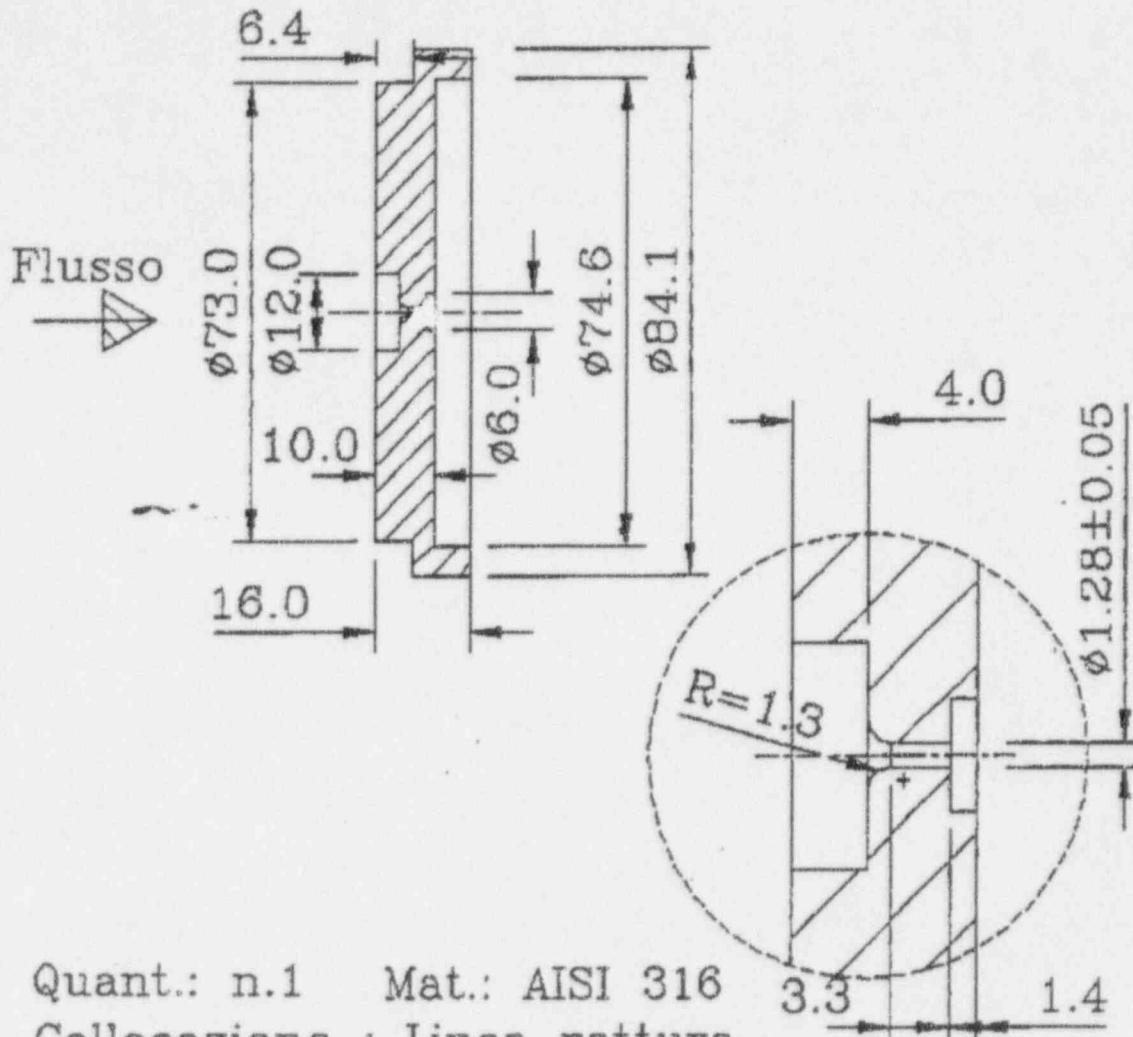


Figure 2.6.12-1 Break Line Configuration for 1-in. Cold Leg Break

SPES2 - Break device on CL
 Posizione 13 su P&ID orifizi



Quant.: n.1 Mat.: AISI 316
 Collocazione : Linea rottura
 su CL-B2 a monte valvola BR-01
 fig. $\phi 1\frac{1}{2}$ ANSI1500 S.160 LM&LF

2	2/5/94	Geometria orifizio	Ed.	Mr	Verif.
Indice	Data	Modifiche	Disegn.	Controll.	Approv.
SIET		Doc. n.	Orifizi calibrati		
Piacenza					
Italy					
Scala	Disegno n.	Foglio	di		
1:1-2:1	25.03.26	15			

Figure 2.6.12-2 SPES-2 Break Orifice on CL for 1-in. Break

2.6.13 Facility Operation for Test S01703

The purpose of this test run was to repeat test S00303 in order to investigate the repeatability of the plant behavior and system response during a simulated 2-in. cold leg break on loop B (the CMT side of the plant) with intervention of the passive safety systems only. The test was performed with the pressurizer to CMT-A/-B balance lines closed by means of blind flanges installed on both the pressurizer and CMT connections. The break was located at the bottom of loop B cold leg-B2 between the cold leg-B2 to CMT-B balance line and the power channel. The break line for the facility was configured as shown in Figure 2.6.13-1 with a break orifice installed as described in Figure 2.6.13-2. The orifices installed throughout the facility are listed in Table 2.6.13-1.

Once the facility was at initial conditions, the test was initiated by opening the break valve. When the reactor trip (R) occurred (pressurizer pressure P-027P = 12.41 MPa = 1800 psia), the heater rod bundle power was controlled to match the scaled AP600 decay heat, and the steam generator MSLIVs were closed with a 2-second delay. When the S signal occurred (pressurizer pressure P-027P = 11.72 MPa = 1700 psia), the PRHR isolation valves and the CMT injection valves were opened and the MFWIVs were closed, all with a 2-second delay, and the RCP coastdown was initiated with a 16.2-second delay.

The CVCS, NRHR, and SFW were off throughout the whole transient. The test simulated the failure of one of two fourth-stage ADS valves on loop B. The ADS valves were programmed to open versus either CMT level L-A40E or L-B40E with the delay time shown in Table 2.6.13-2. The accumulators were set to inject water via DVI when the primary pressure was lower than 4.9 MPa (710.6 psia). The IRWST was set to inject water via DVI when the primary pressure was lower than 0.18 MPa (26.1 psia). The test was terminated when the flowrates (F-A60E/F-B60E) discharged by the IRWST reached a stable flow (without significant fluctuation).

**TABLE 2.6.13-1
SPES-2 INSTALLED ORIFICES**

Location	Diameter (mm)	Thickness (mm)
ADS-1	4.37	12
ADS-2	9.35	12
ADS-3	9.35	12
ADS-4A	20.68	7
ADS-4B	14.62	7
CMT-A injection line	4.1	5.5
CMT-B injection line	5.7	5.5
CMT-A cold leg bal. line (2 orif.)	7.5	5.5
CMT-B cold leg bal. line (2 orif.)	7.5	5.5
Accumulator-A injection line	4.86	7.3
Accumulator-B injection line	4.86	7.3
Cold leg-B2 break device	2.56	3.3 *

* Rounded entrance with 2.6 mm radius

**TABLE 2.6.13-2
PROGRAMMED OPENING OF ADS VALVES**

ADS Stage	Orifice Dia. (mm/in.)	CMT Volume (%)	L-A40E or L-B40E (m/ft.)	Delay Time (sec.)
First	4.37/0.172	67	4.152/13.622	30
Second	9.35/0.368	67	4.152/13.622	125
Third	9.35/0.368	67	4.152/13.622	245
Fourth A	20.68/0.814	20	1.192/3.911	60 sec. after 20% CMT vol., but no sooner than 360 sec. after 67% CMT vol.
Fourth B	14.62/0.576	20	1.192/3.911	60 sec. after 20% CMT vol., but no sooner than 360 sec. after 67% CMT vol.

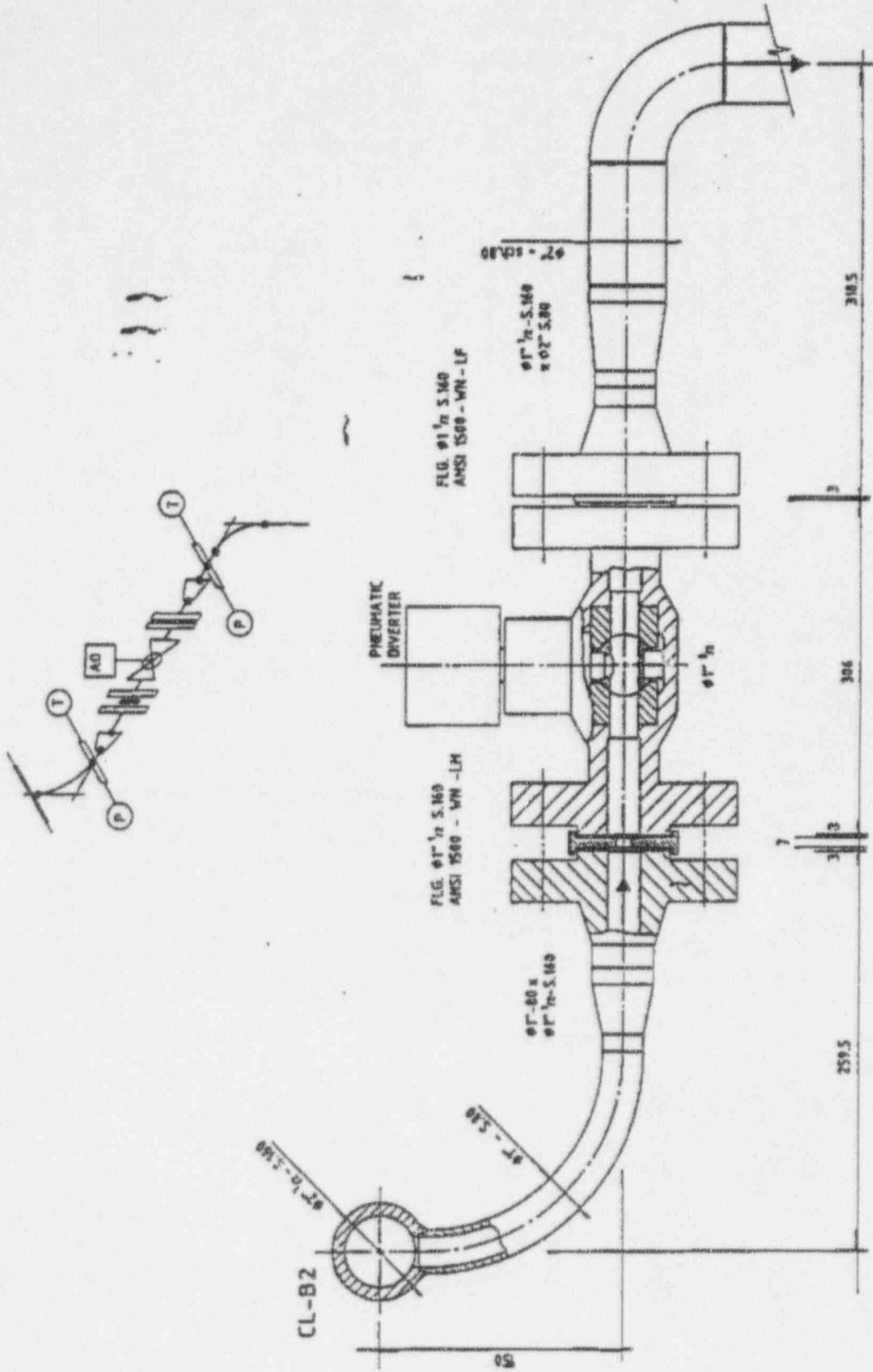
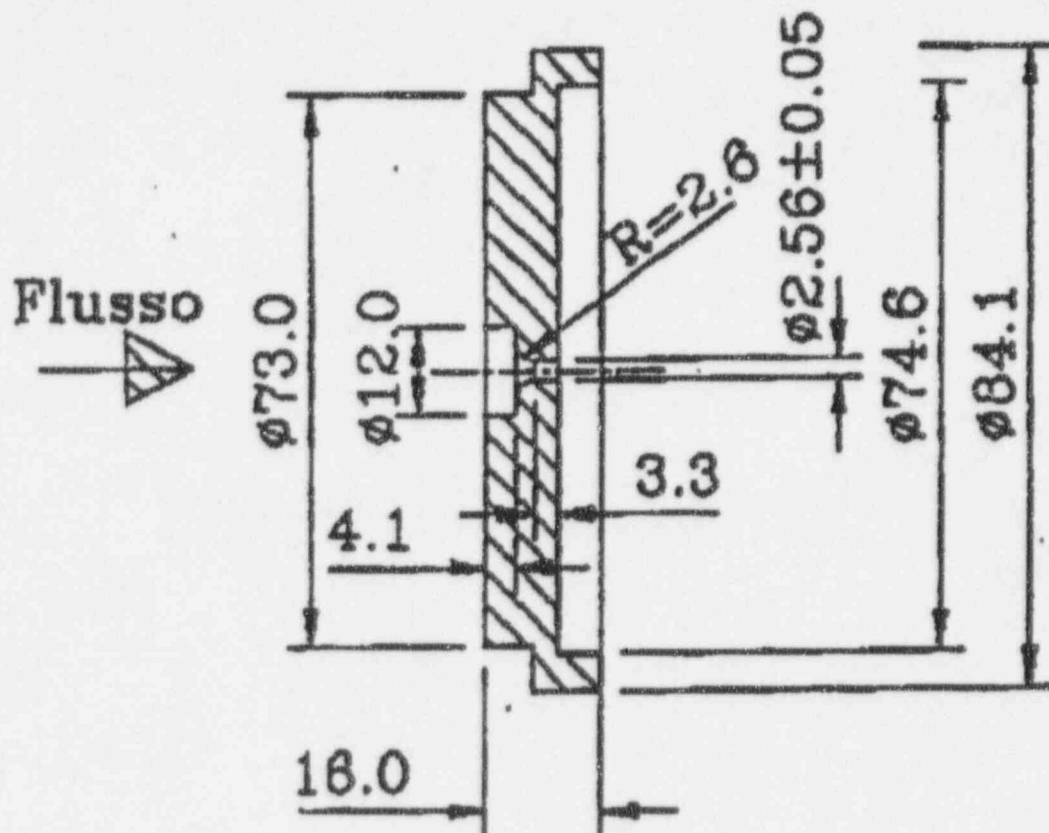


Figure 2.6.13-1 Break Line Configuration for 2-in. Cold Leg Break

SPES2 - Break device on CL
 Posizione 13 su P&ID orifizi



Quant.: n.1 Mat.: AISI 316
 Collocazione : Linea rottura
 su CL-B2 a monte valvola RR-01
 flg. $\phi 1^{\prime\prime} 1/2$ ANSI1500 S.160 LM&LF

Figure 2.6.13-2 SPES-2 Break Orifice on CL for 2-in. Break

3.0 DATA REDUCTION

3.1 Introduction

The following sections describe the data reduction and validation processes used for the SPES-2 tests. In general, the data were transmitted from the test site by SIET to Westinghouse on DEC TK-50 tape cartridges; however, the cold pre-operational tests were provided on 3.5-in. diskettes. The SIET data files were run through several software programs at Westinghouse as part of the validation process in order to convert the data to English engineering units and to create useable data files and plots. Various ways of plotting the data were used in order to review, validate, and present the data.

Information regarding acquiring and recording data at the test site can be found in Section 2.5. Section 2.5 describes the data acquisition systems (DAS) for the SPES-2 facility.

3.2 Test Validation

The SPES-2 test data were reviewed and validated using a three-step process.

The first step was performed at the test site immediately following the test and documented in the Day-of-Test Report by SIET personnel. The Day-of-Test Report and the TK-50 tape cartridge were sent to Westinghouse generally within a few of days after the test. Depending upon the length of the test, the data fit onto one or two tape cartridges. The Day-of-Test Report evaluated the operability of key instruments and deviations from specified initial conditions (for example, did the test meet the minimum acceptance criteria?). The Day-of-Test Report also documented any facility modifications or onsite test observations. Specifically, the Day-of-Test Report assessed whether the test needed to be rerun due to some significant problem observed during the performance of the test. See Appendix A for a sample of the Day-of-Test Report format.

The overall test acceptance criteria established prior to the SPES-2 tests is shown in Table 3-1. Although not an explicit part of this pre-test acceptance criteria, an overall facility mass balance objective of 10 percent was established. The critical instruments identified in the acceptance criteria were the minimum set of instruments identified by the safety analysis personnel to perform a transient, component-by-component mass and energy balance. The critical instruments for the SPES-2 facility are identified in Table 3-2.

The second step in the data validation process was performed at the Westinghouse Energy Center by Test Engineering personnel. This step was performed after receiving the Day-of-Test Report and processing the data tape. This data validation was documented in the Quick Look Report (QLR). The QLR provided a preliminary validation of all test data (for example, did the data meet all acceptance criteria?). A standard outline was issued to and accepted by the Nuclear Regulatory Commission (NRC) prior to writing the QLRs. The key purpose of the QLR was to issue some pedigree of the data (reviewed but not validated data) to the NRC shortly after the test was performed without specifically evaluating the data for code validation purposes.

The QLR examined the test in more detail than the Day-of-Test Report and included items such as calculation of an overall facility mass balance; deviations from specified initial and boundary conditions, such as heater rod power decay; and identification of any out-of-range, suspicious, or failed instruments. As part of the QLR process, different types of instruments were compared to verify their response (for example, tank levels were compared flow instrumentation).

The safety analysis personnel reviewed and signed-off on the QLRs prior to issuance to ensure understanding of the test performance and to determine if any unusual facility responses occurred. A preliminary data file on digital audio tape (DAT), including the identification of the failed instrumentation channels, was transmitted with the QLR to the NRC. A QLR was issued for each accepted test. Several tests were judged to be unacceptable, and therefore, a QLR was not issued. For those tests deemed unacceptable at test site, the test was rerun until an acceptable run was accomplished.

The third and final step in validating the data was performed for the Final Data Report. This included a detailed review of the transient progression, evaluation of facility and component performance, and cross-test comparisons as included herein. The Final Data Report provides the final assessment as to whether the respective data were acceptable for code validation purposes.

Figure 3-1 illustrates the progression of the data validation process from the SPES-2 test site to the Westinghouse Energy Center. This figure shows the building-block approach followed in reviewing, evaluating, validating, and documenting the data. Each step in the process was based upon the information/knowledge gained from the previous step, but was generally performed by a different set of personnel. As the process progressed from left to right, the steps evolved from *problem identification* to *problem resolution*. This three-step process allowed various personnel from different disciplines to review the data prior to final publication. These steps were followed in order to provide a high level of data quality assurance.

3.3 Pre-Operational Tests

The pre-operational tests were segregated into cold and hot tests. The cold pre-operational tests were used to determine facility characteristics (such as component flow resistances) using cold water. The cold pre-operational test data were provided to Westinghouse by SIET on 3.5-in. disks. Although the raw data were provided to Westinghouse by SIET, the cold pre-operational tests were evaluated and reported by SIET. The SIET report was reviewed independently by Westinghouse and issued to the NRC as a preliminary document, which was similar to a QLR but not in the same format. However, the associated data files were not issued with the SIET report, since this data was not used directly for code validation. The flow resistances for the various facility components were calculated based upon the measured pressure drop and flow rate over a range of flow rates. Section 4.1.1 describes the results of the cold pre-operational tests.

The hot pre-operational tests were used to determine the facility characteristics (such as facility heat losses and operation) at hot pressurized hot pressurized operating conditions. The hot pre-operational

test data were provided on DEC TK-50 tapes. The hot pre-operational test data were reduced and reviewed by Westinghouse. The hot pre-operational tests were evaluated and reported by SIET. The SIET report was reviewed independently by Westinghouse and issued to the NRC as a preliminary document (similar to a QLR but not in the same format); however, the associated data files were not issued with the SIET report, since this data was not used directly for code validation. Section 4.1.2 describes the results of the hot pre-operational tests.

3.4 Matrix Tests

The data for the SPES-2 matrix tests were provided by SIET on DEC TK-50 tapes in approximately 15 to 18 ASCII files depending upon the test. These ASCII files segregated the data into differential pressure (dP) cells, thermocouples, flows, catch tank masses, power, fluid levels, etc. The data provided by SIET was in metric units with a nonzero test start time, since the data acquisition system (DAS) was started well in advance of the test initiation. The typical starting time of the test was around the 20,000-second time mark.

A series of software programs was written to reduce this data. Prior to using these programs, these 15 to 18 ASCII files were manually combined into one file. A summary of the data processing steps is provided in Figure 3-2.

The data provided by SIET included the measured data (such as dPs and temperatures) and the derived quantities (such as flow rates and fluid levels). For the most part, the derived quantities were used in the SPES-2 data review and validation process. The derived quantities are designated with an underscore (_) in the channel number (for example, F_A20E); and the measured quantities have a dash (-) in the channel number (for example, F-A20E).

A software program called SPES_REDUCE was written to convert the metric units to English units and to set the test start time (break opening time) as zero time. SIET provided the actual test start time to Westinghouse, which was subsequently subtracted from the recorded times using SPES_REDUCE. Generally, there was about 5 minutes of pre-test data recorded to establish the facility steady-state condition prior to performing the test. This pre-test data was represented as negative time data in the data files and plots.

After running the SPES_REDUCE program, a single output file was created in the same format as the SIET files—except for conversion of the data units, setting the zero time, and removing extraneous data file headers. The data was then plotted by using a program called SPES_CREATE. The SPES_CREATE program generated a set of plots using the Westinghouse NSA plot program. The NSA plot program then plotted the data in a variety of ways. A set of single channel plots and multiple channel plots were produced and issued for internal Westinghouse review. The multiple channel plots generally included data from loop A and loop B instruments, or a family of instruments from a key component such as the CMT. The plots also contained 20-character instrument descriptions/locations. The processed data file also was made available for use (read-only) to analysts

within Westinghouse. However, the data (both the hard copy plots and the electronic file) for the three blind tests were secured from the safety analysis personnel.

After running the SPES_CREATE program, the SPES_CHECK program was run to identify missing, extraneous, or duplicate instrumentation channels on the data file. The channels on the data file were compared to a standard list of instrumentation channels. Due to the large number of SPES-2 instrumentation channels, it was possible that some channels were missing on the data tape (from SIET) or that a duplicate record was inadvertently provided (by SIET). Those channels deemed failed by SIET were generally not provided on the tape; and after running the SPES_CHECK program, those channels were labeled as missing. Also, during the course of the test program, several instrumentation channels were added to the facility; and after running the SPES_CHECK program, those channels were labeled as extraneous. Therefore, there were logical justifications for having missing and/or extraneous channels. After the QLR was issued, several additional categories of instruments were added manually to the SPES_CHECK program output file. These categories included those channels that were considered failed and those channels that were considered out-of-range. This file, called an error file, was used by safety analysts to determine which channels were not available for code development and code validation purposes.

In rare instances, it was necessary to modify some of the test data; therefore a program called SPES_CORRECT was developed. This program provided the capability to modify or correct existing data using the following general equation:

$$\text{NEW} = a * (\text{OLD} + b)^d + c$$

where:

NEW = newly created data
OLD = data to be modified or corrected
a, b, c, d = constants

The newly created data was appended to the end of the data file, and the old data was left in the preliminary file. By leaving the old data in the preliminary file, it was easier for Test Engineering to track the various data modifications. The newly created data was usually labeled with a new channel number to distinguish it from the old data. For the final file contained in this report, only valid data was provided (for example, the old data from the operation described above was removed).

As an example, for test S00303, it was determined that a dP cell in the in-containment refueling water storage tank (IRWST) line could be substituted for an overranged IRWST flow meter dP cell. Since a dP cell in the IRWST flow line was calibrated during the cold pre-operational tests, the data from this dP cell could be converted to a flow rate using the above equation if the appropriate calibration coefficients are known. See Appendix A for detailed description of the data reduction for these specific IRWST channels and for other the instrumentation channels affected.

After the plots of all data channels were distributed for internal Westinghouse review, two additional sets of plots were produced. The first set consisted of the initial condition validation plots for those channels important to establishing facility steady-state conditions, such as rod power, cold-leg flows, and hot-leg temperatures. These plots presented the data for the steady-state period prior to test initiation (that is, negative time period) in conjunction with the average of the respective data. The average was calculated via the NSA plot program. Comparisons to the specified initial condition and allowable tolerances were performed and reported in the QLR. Any deviations outside the allowable tolerance were generally quite small and accepted. The deviations outside the established tolerances were accepted since tight tolerances were imposed on the personnel performing the tests. These tight tolerances were established in order to achieve test conditions repeatable from test to test. See Appendix B for comparison of the test conditions.

In addition to the plots of initial test conditions, a normalized power decay plot was generated. This plot compared the actual heater rod power decay curve with the specified power decay curve. The actual power decay curve was normalized by dividing the measured power after test initiation by the calculated average power prior to test initiation.

The second set of plots consisted of multi-channel plots for inclusion into the QLR. This set of plots, which presented a concise, yet overall view of the test, were standard for each test—except for some additional plots needed for the steam generator tube rupture (SGTR) and steam line break tests.

As part of the QLR data review process, an overall facility mass balance was performed. This mass balance consisted of calculating the water masses in each of the major components prior to the test, calculating the water masses in each of the same components after the test, and calculating the percent difference between masses from the two time periods. This facility mass balance provided a measure of confidence in the response of the component dP cells and catch tanks, and overall facility performance during the test. If the overall mass balance had been significantly affected (for example, greater than 10 percent), the test may have been repeated. The overall mass balance results are reported in this Final Data Report. The results of a transient mass and energy balance will be reported in the Test Analysis Report.

As the final part of the QLR data review process, the fluid levels and void fractions in the heater rod bundle, upper plenum, upper head, and hot legs were calculated based upon the differential pressure and fluid temperature readings. These fluid levels and void fractions were then evaluated with respect to the actuation of the safety systems (accumulators, CMTs, IRWST) to determine their effect on the condition of the heater rod bundle (for example, was there any impact of the accumulator injection on the fluid level and void fraction in the heater rod bundle?). A more detailed evaluation of the fluid levels and void fractions in the heater rod bundle is contained in this Final Data Report.

Wherever appropriate, the saturation temperature corresponding to the component pressure (or pressurizer pressure) was plotted on temperature graphs to aid in understanding the response of the respective component thermocouples. For example, the system saturation temperature was plotted on the family of CMT thermocouple responses. This activity helped to identify a problem with the

CMT-B thermocouples for tests S00504 and S00605, which was subsequently diagnosed as an acquisition card fault.

For the Final Data Report, several additional steps were performed to validate the data. These included a detailed review of the transient progression; a review of the performance of each of the major components; a detailed comparison of the different tests to ascertain effects of break size, break location, and nonsafety system operation; and an instrument error analysis.

3.5 Error Analysis

The error associated with the measured data from the SPES-2 test facility was derived from equipment manufacturer's specifications. Component calibrations were performed to verify that the manufacturer's specifications were met.

The absolute maximum error of the directly measured physical quantities (such as absolute and differential pressures, temperatures, etc.) is defined as follows:

$$\Delta = \pm (\Delta_I + \Delta_K + \Delta_{BV} + \Delta_{RJ})$$

where:

- Δ = absolute maximum error of the directly measured physical quantities
- Δ_I = $\pm (\Delta_C + \Delta_{PS} + \Delta_{LCH})$ = SIET assigned instrument error
- Δ_K = maximum error of the instrument hydraulic head
- Δ_{BV} = acquisition card A/D converter bit value (acquisition card error)
- Δ_{RJ} = maximum error of the cold junction (only for thermocouples)

and where:

- Δ_C = maximum value between the manufacturer error and the maximum error of the performed calibrations for absolute and differential transmitters; maximum value between the ANSI special error and the maximum error of the performed calibrations for thermocouples; maximum value between the UNI-7937 error and the maximum error of the performed calibrations for thermoresistances.
- Δ_{PS} = error of the reference primary standard (pressure gauge, reference thermocouple, reference thermoresistance) used in calibration.
- Δ_{LCH} = error of the voltmeter used to acquire the instrument output signal during the calibration.

The standard deviation of the directly measured physical quantities (such as absolute and differential pressures, temperatures, etc.) is defined as follows:

$$\sigma = \pm (\Delta_I^2 + \Delta^2 K + \Delta_{BV}^2 + \Delta_{RI}^2)^{0.5}$$

where:

σ = standard deviation of the directly measured physical quantities

The absolute maximum error and the standard deviation of the derived quantities (flow rate, levels, etc.) are calculated using the following error propagation formulas:

$$\Delta Y = \pm \sum_{i=1}^n \left| \frac{\delta Y}{\delta X_i} * \Delta X_i \right|$$

$$Y = Y(X_i) \quad \text{with } i = 1 \dots n$$

$$\sigma Y = \pm \left[\sum_{i=1}^n \left(\frac{\delta Y}{\delta X_i} \right)^2 * \sigma^2 X_i \right]^{0.5}$$

where:

ΔX_i = maximum error of the quantities X_i
 σX_i = standard deviation of the quantities X_i

The error calculations were carried out using, in a conservative way, the upper value range of the instrument. All of the derivations for the different types of instruments and the corresponding results for each channel are provided in Appendix E. A sample of the results is presented in Table 3-3 for each type of instrument (load cells, pressure transmitters, dP cells, etc.).

TABLE 3-1
OVERALL TEST ACCEPTANCE CRITERIA

- Test initial conditions shall be within a specified tolerance.
- Component actuations shall occur within an acceptable tolerance band of the ideal actuation setpoint.
- Instrumentation shall be operational before the test. Exceptions shall be identified to Westinghouse.
- Any critical instruments not operating shall be identified to the Westinghouse test engineer before the tests. These instruments must be operational before and during the test unless specifically exempted by the Westinghouse test engineer.
- The zero points for pressure and differential pressure transmitters shall be checked before the start of the test.

**TABLE 3-2
SPES-2 CRITICAL INSTRUMENTS**

Channel	Description
DP-000P	Vessel level
DP-027P/DP-026P	Pressurizer pressure drop
DP-A05P/DP-A06P DP-B05P/DP-B06P	Steam generator tube hot side dP
DP-A07P/DP-A08P DP-B07P/DP-B08P	Steam generator tube cold side dP
DP-A82E	PRHR pressure drop
F-A60E/F-B60E	IRWST flow rates
F-A80E	PRHR flow
I-01P/02P/03P/04P/05P/06P	Power channel power busbar
IF-005P/IF-030P/IF-040P	Catch tank masses
L-010P	Pressurizer level
L-060E	IRWST level
L-A10S/L-B10S	Steam generator levels
L-A20E/L-B20E or F-A20E/F-B20E	Accumulator levels or flows
L-A40E/L-B40E	CMT levels
P-017P	Vessel pressure
P-027P	Pressurizer pressure
P-A04P/P-B04P	Hot-leg pressure
P-A04S/P-B04S	Surge line secondary-side pressure
P-A20E/P-B20E	Accumulator pressures
P-A40E/P-B40E	CMT pressure
T-003P or T-004P	Bundle inlet fluid temperature
T-021P/T-026P	Pressurizer fluid temperatures
T-043P/44P/45P/46P	Annular downcomer fluid temperatures
T-061E/T-065E	IRWST temperatures

TABLE 3-2
SPES-2 CRITICAL INSTRUMENTS (Cont.)

Channel	Description
T-A04P or T-A05P T-B04P or T-B05P	Steam generator inlet temperature
T-A05S or T-A09S T-B05S or T-B09S T-A06S or T-A08S T-B06S or T-B08S T-A07S/T-B07S	SG secondary-side fluid temperatures
T-A10P or T-A09P T-B10P or T-B09P	SG outlet temperature
T-A21E/T-B21E	Accumulator gas temperature
T-A22E/T-B22E or T-A23E/T-B23E	Accumulator fluid temperature
T-A401E-20E/T-B401E-9E (any 3)	CMT temperatures
T-A41A or T-A42A T-B41A or T-B42A	CMT containment air temperature
T-A82E/T-A83E	PRHR supply and return line temperatures
TW-020PXY	Rod temperatures (any 2)
TW-A41E/A43E/A45E/B41E/B44E TW-A411/TW-A421/B411/B421	CMT wall temperature
V-01P	Power channel voltmeter
W-000P	Rod bundle power
W-027PE1/PE2/PE3/PI	Wattmeter

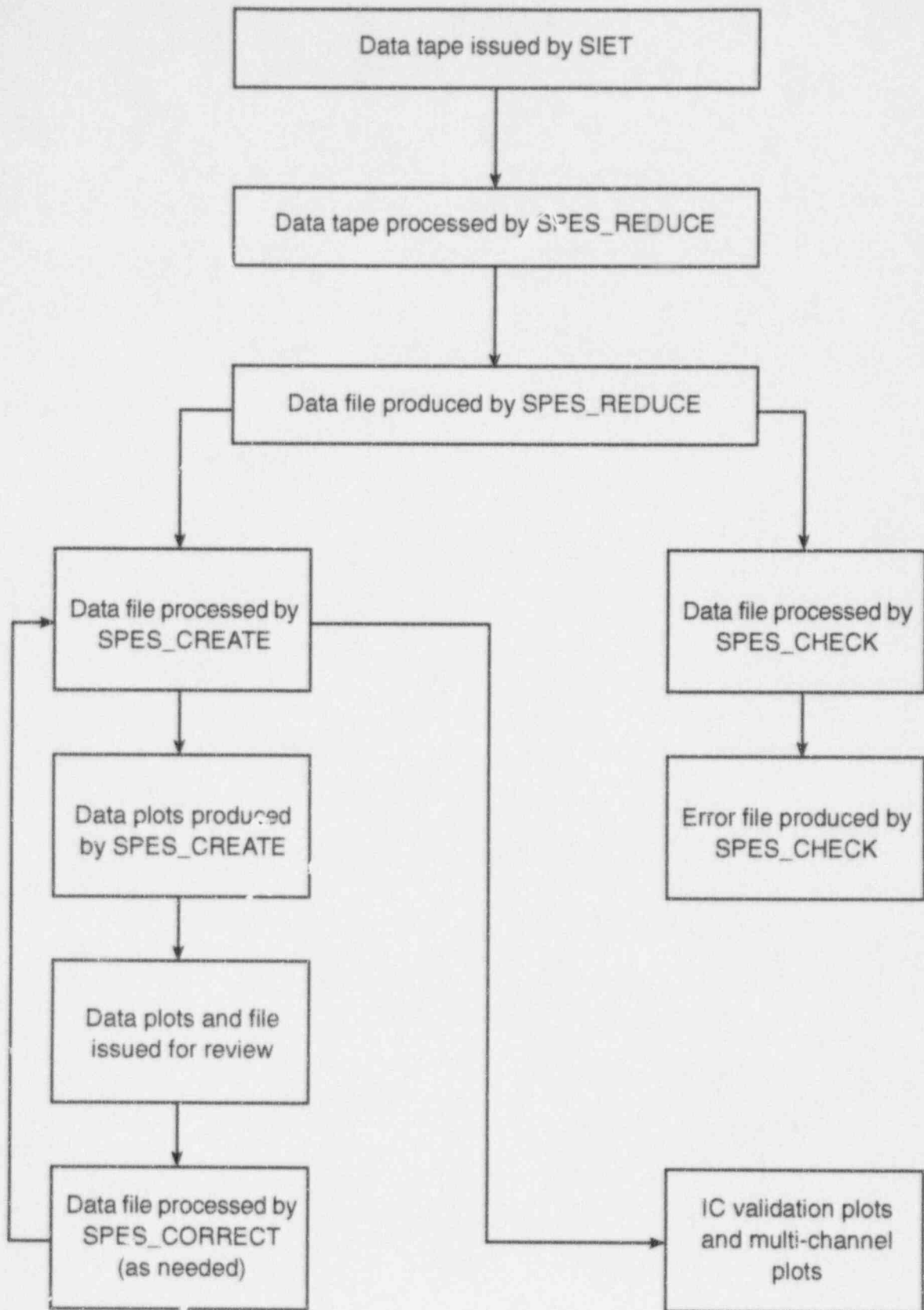
**TABLE 3-3
TYPICAL SPES-2 DATA MEASUREMENT ERRORS**

Channel	Description	Maximum Error	Standard Deviation
IF005P	Break line catch tank		(a,b,c)
W-00P	Rod bundle power (at full power and 4991.6 kW)		
P-027P	Pressurizer pressure		
L-010P	Pressurizer level		
L_010P*	Pressurizer level		
F-A20E	Accumulator-A flow		
F_A20E*	Accumulator-A flow		
T-024P	Pressurizer temperature		
TWO18P20	Heater rod temperature		
DP-000P	Heater rod bundle differential pressure		

*Calculated values.

		STEP 3
		Perform evaluation of parametric effects; i.e., break sizes, etc.
		Provide and review cross-plots of data between tests.
		Perform data uncertainty analysis.
		Perform transient and component evaluation.
STEP 2		
Perform simple benchmark evaluation on rod bundle.		Perform system-wide transient evaluation.
Perform overall mass balance.		Confirm overall mass balance.
Provide minimum facility design information.		Provide adequate facility design information.
STEP 1		
Determine if test met minimum acceptance criteria.	Determine if test met all acceptance criteria.	Identify all tests performed as valid and invalid and why.
Provide unqualified data files for all tests.	Provide unqualified data files for acceptable tests only.	Provide qualified data files with 0 time shift (valid data only).
Provide key data plots.	Provide key multi-channel plots; e.g., loop A vs. loop B.	Provide key multi-channel plots; e.g., loop A vs. loop B.
Identify anomalous data.	Identify/resolve anomalous data.	Identify/resolve anomalous data.
Provide test observations.	Provide test observations.	Provide and discuss test observations and resolve problems.
Provide sequence of events.	Compare actual and specified sequence of events.	Resolve differences in actual and specified sequence of events.
Identify procedure deviations.	Identify procedure deviations, and briefly describe procedure.	Resolve procedure deviations, and describe test procedure.
Identify facility configuration/modifications.	Identify facility configuration/modifications.	Identify facility configuration/modifications.
Check key initial conditions.	Check all initial conditions (IC) and boundary conditions (BC).	Resolve deviations in ICs and BCs.
Identify inoperable instruments.	Identify inoperable and erratic instruments.	Develop integrated inoperable instrument list.
Check critical instruments.	Check all instruments.	Verify all instruments.
Perform Day-of-Test Report at SPES-2 test site.	Document data in a Quick Look Report at Westinghouse Energy Center.	Develop a Final Data Report at Westinghouse Energy Center.

Figure 3-1 Data Documentation Steps



51491C.1

Figure 3-2 Steps in SPES-2 Data Processing

4.0 TEST RESULTS

4.1 Pre-Operational Tests

Tests were performed on the SPES-2 facility prior to performing the matrix tests. These pre-operational tests included: cold pre-operational tests that were performed with cold water and with the facility at atmospheric pressure (with the exception of accumulator gas pressure); and hot pre-operational tests that were performed with the facility heated and pressurized.

The cold pre-operational tests were primarily performed to determine/establish the proper resistances of the primary system loop piping and the piping which connects passive safety features to the primary system. Table 4.1.1-1 provides a summary of the SPES-2 cold pre-operational tests.

The hot pre-operational tests were performed to verify the operation of the many facility controls needed to simulate both full-power operation, and actions simulating the AP600 plant actuations that occur in response to the transients to be simulated in the matrix tests. The hot pre-operational tests also included tests to further characterize the facility and to directly test safety feature performance that occurs due to natural circulation. Table 4.1.2-1 provides a summary of the SPES-2 hot pre-operational tests.

4.1.1 Cold Pre-Operational Tests

A series of cold (no power to the heater rods) pre-operational tests were performed on the SPES-2 test facility. The purpose of these tests was to characterize the facility; that is:

- To determine the resistance of the primary loop components and of the safety system piping.
- To establish and verify the size of orifices in the passive system and primary loop piping runs.
- To quantify the volume of the entire facility.
- To demonstrate the reactor coolant pumps' (RCPs') coastdown speed at low pressure.
- To verify the injection characteristics of the chemical and volume control system (CVCS), normal residual heat removal (NRHR), and startup feed water system (SFWS) pump.

4.1.1.1 Test Matrix

The data obtained were utilized to set-up the computer model used to perform pre-test analyses and to maximize the correspondence between the facility and the AP600 reactor.

Table 4.1.1-1 shows the cold pre-operational test matrix and summarizes the purpose of each test. As indicated, tests were performed with pumped flow and/or gravity flow where feasible. All tests were performed with cold water and, with the exception of the accumulators, at atmospheric pressure. The passive safety components were tested over a range of flow rates that included the expected range of scaled AP600 flow rates.

4.1.1.2 Summary of Test C-02 Through C-07 Results

Table 4.1.1-2 provides a summary of the SPES-2 observed piping resistances for each of the passive safety system piping runs. These resistances are also shown multiplied by $(1/395)^2$ in the table and compared with the nominal piping resistances specified for the AP600. With the exception of the accumulator discharge piping, the SPES-2 scaled resistances are within []^{±c} percent of the AP600 specified resistances and all are within the AP600 specified tolerances. The SPES-2 accumulator discharge lines were later orificed, retested, and re-orificed. The accumulator performance was then compared and found to agree with the accumulator flow rates predicted in the pre-test analyses.

4.1.1.3 Summary of Test C-01 and C-09 Results

Table 4.1.1-3 provides a summary of the SPES-2 observed resistances for all the reactor coolant system (RCS) components. These resistances are also multiplied by $(1/395)^2$ and compared with the resistances specified for the AP600. As shown, the SPES-2 overall RCS and power-channel (with downcomers) resistances are []^{±c} and []^{±c} times the expected AP600 resistances; and the SPES-2 steam generator resistances are approximately []^{±c} percent higher than the AP600. Other items to note include: the SPES-2 surge line resistance is only []^{±c} percent of the AP600, and the SPES-2 power channel tubular downcomer has approximately []^{±c} times more resistance than the AP600 reactor-vessel downcomer.

**TABLE 4.1.1-1
SPES-2 COLD PRE-OPERATIONAL TEST MATRIX**

Test	Test Description	Purpose of Test	Comments
C-01	Single-phase flow through pressurizer surge line.	Determine the resistance of pressurizer surge line. Calibrate core makeup tank (CMT) discharge flowmeter.	Pumped cold water used.
C-02A,B	Single-phase flow through the pressurizer to CMT balance line.	Determine the resistance of the balance lines. Provide basis for sizing the CMT line orifices.	Pumped cold water used.
C-03A,B	Single-phase flow through the cold leg to CMT balance line and from CMT to reactor vessel.	Verify CMT discharge flowmeter calibration.	CMT discharge line resistance measured during the test (See C-04A,B).
C-04A,B	CMT gravity draindown by using cold leg to CMT balance line.	Verify CMT discharge line orifice sizing and overall line resistance.	This test was not performed. C-03 test results used.
C-05A,B	CMT gravity draindown using pressurizer to CMT balance line.	Characterize CMT draindown with no condensation effects.	Pressurizer to CMT balance line used as a vent path.
C-06A,B	Accumulator blowdown.	Determine the resistance of accumulator discharge line. Verify the venturi flowmeter.	A high pressure blowdown from 700 psig performed.
C-07A,B	In-containment refueling water storage tank (IRWST) gravity draindown.	Determine the IRWST injection lines resistance. Establish and verify orifice size. Verify flowmeter calibration.	IRWST draindown starting from 8.5 m, 3 m, 1 m.
C-08	CVCS, NRHR, and SFWS pump flow rate verification.	Verify AP600 pump flow/head curves can be reproduced.	SPES-2 pump parameters required to model CVCS, NRHR and SFWS pumps determined.
C-09	Primary system operation with two RCPs running.	Establish primary circuit dPs. Calibrate hot leg turbine flowmeter. Verify RCP operating speed. Determine PRHR dPs. Equalize flow rate in cold legs. Determine RCP coastdown time.	

Notes:

1. Cold pre-operational tests are all performed at ambient temperature.
2. Each specified test for the CMTs, accumulators, and IRWST are designated A or B to correspond to the component tested; for example, CMT-A or CMT-B.

**TABLE 4.1.1-2
SPES-2 COLD PRE-OPERATIONAL TESTS
VS. AP600
COMPARISON OF SPES-2 SAFETY SYSTEM PIPING RESISTANCES**

Component	SPES-2 Observed ⁽¹⁾ Resistance (ft./gpm ²)	SPES-2 Scaled Resistance (x(1/395) ²)	AP600 Specified ⁽²⁾ Resistance (ft./gpm ²)	Ratio of SPES-2 Scaled/To AP600 Specified Resist.
Accumulator to DVI nozzle	[] ^(a,b,c)	[] ^(a,b,c)	[] ^(a,b,c)	[] ^(a,b,c)
CMT, pressurizer to CMT balance line	[]	[]	[]	[]
CMT, cold leg to CMT balance line	[]	[]	[]	[]
CMT, discharge to DVI	[]	[]	[]	[]
IRWST, discharge to DVI	[]	[]	[]	[]
PRHR HX and Supply/Return	[]	[]	[]	[]

Notes:

1. The SPES-2 resistances listed were observed at the expected nominal flow rates.
2. Nominal AP600 values listed. []^{sc} is typically specified for plant acceptance criteria.
3. Accumulator discharge lines were unorificed. Orifices were added prior to matrix testing.
4. Shown to be identical to line A by calculation.

**TABLE 4.1.1-3
SPES-2 COLD PRE-OPERATIONAL TESTS
COMPARISON OF SPES-2 VS. AP600 RCS RESISTANCES (BOTH RCPS RUNNING)**

System/Component	SPES-2 Observed Resistance (ft./gpm ²) <small>(a,b,c)</small>	SPES-2 Scaled Resistance (x(1/395) ²) <small>(a,b,c)</small>	AP600 Specified ⁽¹⁾ Resistance (ft./gpm ²) <small>(a,b,c)</small>	Ratio of SPES-2 Scaled to AP600 Specified Resist. <small>(a,b,c)</small>
RCS ⁽²⁾ (overall)				
Hot leg-A				
Hot leg-B				
Cold leg-1A				
Cold leg-2A				
Cold leg-1B				
Cold leg-2B				
Surge line (hot leg to pressurizer)				
Steam generator A				
Steam generator B				
Reactor vessel (overall)				
Reactor vessel inlet				
Reactor vessel downcomer barrel				
Lower plenum				
Core				
Upper plenum and outlet nozzles				

Notes:

1. Based on total RV flow (B.E. flow 204,000 gpm) and overall DP.
2. SPES-2 loop and component ID's used.
3. AD is annular downcomer; TD is tubular downcomer

4.1.2 Hot Pre-Operational Tests

A series of hot pre-operational tests were performed with the SPES-2 facility prior to the initiation of the actual matrix tests. The purpose of these tests was to obtain data for the computer model of the SPES-2 facility used for pre-test predictions, and to verify the proper operation of the facility control system, components, and instrumentation at power, pressure and temperature conditions to be simulated. Specific hot pre-operational test objectives include the following:

- To determine the heat losses versus temperature of the entire facility and main components.
- To quantify the metal and water heat capacity of the facility and main components.
- To demonstrate the natural circulation flow rate and heat removal rate of the passive residual heat removal (PRHR) heat exchanger (HX).
- To demonstrate the natural circulation flow rate and heat-up of the core makeup tanks (CMTs).
- To verify the sizing of the ADS-1, -2, and -3 flow path orifices (that is, facility depressurization rate is similar to calculated AP600 depressurization rate).

Table 4.1.2-1 provides a summary of the hot pre-operational tests performed on the SPES-2 facility. These tests are identified as test numbers H-01 to H-06.

4.1.2.1 Hot Pre-Operational Test H-01

The purpose of test H-01 was to measure the heat losses versus temperature for the entire SPES-2 facility and for each of the main components.

Test H-01 Description

Test H-01 was performed with the facility primary system filled with water and heated up to four essentially steady-state temperatures. Heat was added to the primary system by the power channel heater rods and by the two primary system pumps. The pressurizer internal heaters (used for pressure control) were not operated during heat loss measurement times. The test was performed with the following additional conditions:

- The primary system flow through the power channel was maintained at approximately []^(a,b,c) lbm/sec. (approximately 50 percent of the nominal simulated full-power flow rate).
- The pressurizer water level was maintained at approximately []^(a,b,c) ft. (approximately 65 percent) using makeup/letdown to adjust for primary system water density changes between data collection periods.

-
- The steam generators were initially filled to ≤ 10 percent of the wide-range level and kept in thermal equilibrium with the primary system (no heat removal via the steam system and no feedwater injection).
 - The pressurizer internal heaters were used to maintain the primary system pressure above saturation pressure throughout the test.
 - The CMTs, PRHR HX, and accumulators were isolated throughout this test.

The test was conducted by setting the heater rod power to obtain a constant primary system temperature, where the total facility heat loss would be the heater rod power plus the power input from the two reactor coolant pumps (RCPs). Four primary system temperatures were selected between approximately 310°F and 590°F. A truly constant temperature could not be achieved for two reasons: (1) the primary temperature asymptotically approached a constant temperature when the heat input was fixed; and (2) the continuous adjustment heater rod power control was not operable. Data were therefore obtained from a series of power plateaus, by choosing the power that gave the smallest achievable temperature change versus time.

After the facility heat loss at 590°F (310°C) was measured, the speed of the RCPs was reduced to 500 rpm. The reduced flow rate increased the temperature difference measured across each of the primary system components. This condition was maintained long enough to obtain steady-state conditions, so that the measured ΔT across the component versus the total primary system ΔT represented the proportion of the component heat loss versus the total facility heat loss.

Test H-01 Heat Loss Calculations and Results

For the measurements of the facility heat losses, time intervals when the primary system was at almost steady-state temperature were utilized. The facility heat losses were established at four different steady-state temperature conditions and are presented in Table 4.1.2-2. Also presented in this table is a best-fit quadratic equation based on the measured data.

Since it was not possible to measure the heat losses for every component in the primary system, the system was divided into parts: the power channel and hot legs; each RCP and its two associated cold legs; and each steam generator. For these calculations, the data recorded after the pump speed was reduced were utilized. Since steady-state temperature conditions were not completely reached for these tests, time intervals with the minimum temperature change were used. For the heat loss analysis, the temperatures were averaged over the time interval to eliminate the effect of the temperature change. For the hot-leg and RCP/cold-leg heat losses, this effect was compensated by subtracting a calculated value of the corresponding metal mass heat capacity. This was not necessary for the steam generators, where the temperature of the secondary side was essentially constant due to the fact that the steam generators were filled with saturated steam during the test. For each loop section considered, the difference in fluid enthalpy was determined, corresponding to the average temperature of the subcooled fluid at the inlet and outlet of the sections. The component heat loss was calculated by multiplying the enthalpic change by the actual flow rate through the section and was corrected for the metal heat

capacity. For the power channel, the heat loss was measured as the difference between the measured electrical power input and the power calculated from the enthalpy increase and flow through the power channel. The component heat losses are provided in Table 4.1.2-3.

4.1.2.2 SPES-2 Hot Pre-Operational Test H-02

The purpose of test H-02 was to quantify the heat capacity of the SPES-2 facility.

Test H-02 Description

This test was performed in conjunction with test H-01, utilizing times during the test when the SPES-2 facility temperature was linearly increasing. The data were then used in conjunction with the measured facility heat loss versus temperature from test H-01 to quantify the facility heat capacity. The facility loop conditions were as stated for test H-01 with the RCPs operating at 2500 rpm. The pressurizer water level, temperature, and pressure remained constant throughout the data collection; thus the heat capacity results do not include the pressurizer and surge line water and metal mass. Also, the steam generators did not contain the water mass corresponding to full-power operation.

Test H-02 Heat Capacity Calculation and Results

Table 4.1.2-4 provides the facility heat capacity results at three different temperatures. It includes the total input powers, the calculated heat losses, and the calculated heat capacities from the test measurements. The measured electrical power (the power input from the power channel plus the pump work) is the sum of the heat losses for the average temperature conditions being evaluated, plus the energy required to raise the system temperature due to its thermal mass (heat capacity).

4.1.2.3 Hot Pre-Operational Test H-03

The purpose of this test was to verify proper operation of the SPES-2 facility at simulated full-power operating conditions.

Test H-03 Description

The SPES-2 facility was operated at simulated full-power conditions prior to performing hot pre-operational test H-06 and prior to the first matrix test S00103. The purposes of the test included the following:

- To establish the RCP rpm to obtain the proper loop flow rate at hot conditions.
- To verify proper operation of the RCP seal injection system.
- To verify proper operation of the steam generator heat removal system (main feedwater pumps, steam generator level control, steam generator pressure control, steam condenser).

-
- To verify proper operation of the power channel heater rod bundle and rod instrumentation at full-power conditions.
 - To verify proper operation of the pressurizer pressure and level control systems.

Test H-03 Results

Proper operation of the plant components and control systems required for normal operation were confirmed. Key observations/results included the following:

- The RCP rpm required to obtain the proper scaled primary loop flow rate was 2710 rpm (average cold-leg flow was []^(a,b,c) lbs/sec.).
- The power channel upper-head temperature achieved ([]^(a,b,c)°F) was slightly less than the cold-leg temperature ([]^(a,b,c)°F).
- During the heatup of the facility and ascension in power of the heater rod bundle, some thermocouples in the bundle failed at high temperature or exhibited a large rise in temperature when power was increased. This is apparently due to failed or failing insulation in the thermocouple leads.

Thermocouples that exhibited this anomaly were disconnected, since the false high temperature readings will result in a trip of the heated rod power supply.

- All major component control functions were demonstrated.

4.1.2.4 SPES-2 Hot Pre-Operational Test H-04

The purpose of this test was threefold:

- To simulate a plant trip and the transition from full-power operation (test H-03) to a hot shutdown/natural circulation mode of operation, with the heater rod bundle powered to match the post-trip AP600 core heat.
- To demonstrate the heat removal capability and natural circulation flow rate of the PRHR HX (1 tube).
- To demonstrate the natural circulation and flow through the CMTs.

The test was therefore performed in three separate operations.

Test H-04 Description

Decay Power Simulation

This test was to include a reactor trip from full-power operation; however, failure of the steam generator main feedwater system limited the rod bundle power to the capacity of the startup feedwater system (SFWS). Therefore, the rod bundle power was limited to []^(a,b,c) Mw (approximately []^(a,b,c) percent of full power).

The verification of the heater rod decay power control was initiated from 1.03 MW power, with simultaneous trip of the RCPs and isolation of the steam generator main steam isolation valves. Plant heat removal was maintained by steam relief via the steam generator power-operated relief valves (PORV relief setpoint 1015 psia) and startup feedwater (SFW) was used to maintain steam generator secondary-side level.

PRHR HX Flow and Heat Removal

The PRHR HX natural circulation flow rate and heat removal capability was demonstrated by opening the PRHR HX outlet isolation valves with the heater rod power at []^(a,b,c) kW, and the hot-leg temperature at 580°F. The primary system temperature response, PRHR inlet and outlet temperatures, PRHR flow rate, and the steam generator PORV operation was observed until steady-state conditions were achieved. Core power was increased to []^(a,b,c) kW and then to []^(a,b,c) kW to observe the effect on PRHR HX, primary system, and secondary system operation.

CMT Recirculation

The cold (ambient temperature) CMTs were actuated by simultaneously opening the cold leg to CMT balance line isolation valves and CMT discharge line isolation valves, with the primary system at steady-state natural circulation conditions (T_H at []^(a,b,c)°F and T_C at []^(a,b,c)°F) and core power at []^(a,b,c) kW. CMT inlet temperature, CMT heatup, CMT flow rates, and primary system and steam generator responses were observed.

Hot Pre-Operational Test H-04 Calculations and Results

Decay Power Simulation

The results of the bundle power decay heat versus time as controlled by the facility computer agreed well with the specified power decay from the initial power (approximately []^(a,b,c) kW plus 110 kW of heat loss compensation) at time 0 to approximately []^(a,b,c) kW plus 110 kW of heat loss compensation at 2000 sec.

The coastdown time of the RCPs was approximately []^(a,b,c) seconds for pump A (from []^(a,b,c) seconds) and approximately []^(a,b,c) seconds for pump B (from []^(a,b,c) seconds). Note

CMT Recirculation

When the CMTs were actuated with the primary system at steady-state conditions (T_H at []^(a,b,c)°F and T_C at []^(a,b,c)°F, natural circulation flow, and bundle power at []^(a,b,c) kW), natural circulation flow through the CMTs began as expected.

The CMT natural circulation flow rate observed was initially []^(a,b,c) lbm/sec. in CMT-A and []^(a,b,c) lbm/sec. in CMT-B. The CMT-B flow rate decreased to []^(a,b,c) lbm/sec. after approximately []^(a,b,c) seconds as the CMT heated. This corresponds to an AP600 flow rate of []^(a,b,c) lbm/sec. to []^(a,b,c) lbm/sec. for CMT-B, which agrees well with expected performance. The CMT heatup versus time observed with thermocouples placed internally down the length of the CMTs, showed that the hot water entering the top of the CMTs remained thermally stratified. Also, the water temperature decreased as it moved down the CMT, apparently due to initially heating the CMT walls and due to heat losses from the CMT surface.

As the CMTs heated and approached steady-state, the primary system temperature increased toward the initial condition before CMT actuation and heat removal via the steam generator PORVs reinitiated approximately []^(a,b,c) seconds after the actuation. The CMT levels during the recirculation heatup were observed to decrease from approximately []^(a,b,c) ft. to approximately []^(a,b,c) ft. This was due to the decrease in CMT water density as hot water replaced cold water increasing the CMT average temperature to approximately []^(a,b,c)°F.

The CMT-A flow rate was initially less than CMT-B, and it did not decrease smoothly as the CMT heated up. This was apparently due to the check valve in the CMT-A discharge line, which does not work as smoothly as the check valve in CMT-B discharge line. This valve was replaced prior to the start of matrix testing.

Also as expected, the natural circulation of the CMTs resulted in an increase in pressurizer level as cold CMT water was heated up in the primary system, requiring that the letdown flow path be utilized.

4.1.2.5 SPES-2 Pre-Operational Test H-05

The purpose of this test was to verify that the passive safety system actuations occur properly and that these systems perform as expected. The test was conducted at a low initial primary system pressure, since this would be the first time the plant safety systems were actuated. Note that the test initial conditions were selected to be similar to the expected Oregon State University (OSU) test facility.

Test H-05 Description

This test was a simulation of an inadvertent opening of the first stage of ADS but was performed from a low initial pressure and temperature. In order to more closely simulate the plant and safety system response times that would be expected to occur in a full-pressure and temperature transient, the test boundary and initial conditions used were similar to those anticipated for the test facility at Oregon

State University. In addition, the size of the ADS-1, -2, and -3 flow path orifices was increased from 1/395th area scale (AP600/SPES-2 scale factor) to approximately 1/100th area scale. The ADS-4 flow path area was maintained at the SPES-2 scaled area (however, the fourth-stage valve failed to open in the actual test).

The facility initial conditions are provided in Table 4.1.2-5.

Test H-05 Results

As shown in Table 4.1.2-6, all control system actuations occurred during the test. However, some actuation times were delayed and two valve operators did not actuate. The valve operators and logic control for the actuations were inspected and revised.

Pre-operational Test H-06, discussed in Section 4.1.2-6, was the same inadvertent ADS event as H-05 but was performed from simulated full AP600 power, and full pressure and temperature. Table 4.1.2-7 provides a comparison of major events timing for these two tests.

All major events occur at similar times and the primary system depressurization curves are very similar, with the exception of the initiation of IRWST injection flow. This exception is expected since the SPES-2 IRWST was filled to the full height AP600 level while OSU plans to utilize a 1/4 height IRWST. CMT flow versus time, accumulator flow versus time, and PRHR HX performance all exhibit similar behavior in both tests.

4.1.2.6 SPES-2 Hot Pre-Operational Test H-06

This test was a simulation of an inadvertent actuation of the ADS-1 from a simulated full-power operating condition. The purpose of this test was to verify that all actuations occur properly and that the ADS flow paths were properly sized.

The results of this test can be compared with the computer models of both the SPES-2 facility and the AP600.

Test H-06 Description

This test was initiated with the facility at full-power conditions, by opening the first-stage isolation valve of ADS (simulates both AP600 first-stage flow path flow areas). This results in a rapid depressurization of the primary system, reactor trip and safety injection signal actuations, and resulting mitigation of the event by the passive safety systems.

Test H-06 Results

As indicated in Table 4.1.2-8, test H-06 initial conditions closely matched the specified initial conditions. Also, as shown the sequence of events in Table 4.1.2-9, all required actuations were

Test H-04 Description

Decay Power Simulation

This test was to include a reactor trip from full-power operation; however, failure of the steam generator main feedwater system limited the rod bundle power to the capacity of the startup feedwater system (SFWS). Therefore, the rod bundle power was limited to []^(a,b,c) Mw (approximately []^(a,b,c) percent of full power).

The verification of the heater rod decay power control was initiated from 1.03 MW power, with simultaneous trip of the RCPs and isolation of the steam generator main steam isolation valves. Plant heat removal was maintained by steam relief via the steam generator power-operated relief valves (PORV relief setpoint 1015 psia) and startup feedwater (SFW) was used to maintain steam generator secondary-side level.

PRHR HX Flow and Heat Removal

The PRHR HX natural circulation flow rate and heat removal capability was demonstrated by opening the PRHR HX outlet isolation valves with the heater rod power at []^(a,b,c) kW, and the hot-leg temperature at 580°F. The primary system temperature response, PRHR inlet and outlet temperatures, PRHR flow rate, and the steam generator PORV operation was observed until steady-state conditions were achieved. Core power was increased to []^(a,b,c) kW and then to []^(a,b,c) kW to observe the effect on PRHR HX, primary system, and secondary system operation.

CMT Recirculation

The cold (ambient temperature) CMTs were actuated by simultaneously opening the cold leg to CMT balance line isolation valves and CMT discharge line isolation valves, with the primary system at steady-state natural circulation conditions (T_H at []^(a,b,c)°F and T_C at []^(a,b,c)°F) and core power at []^(a,b,c) kW. CMT inlet temperature, CMT heatup, CMT flow rates, and primary system and steam generator responses were observed.

Hot Pre-Operational Test H-04 Calculations and Results

Decay Power Simulation

The results of the bundle power decay heat versus time as controlled by the facility computer agreed well with the specified power decay from the initial power (approximately []^(a,b,c) kW plus 110 kW of heat loss compensation) at time 0 to approximately []^(a,b,c) kW plus 110 kW of heat loss compensation at 2000 sec.

The coastdown time of the RCPs was approximately []^(a,b,c) seconds for pump A (from []^(a,b,c) seconds) and approximately []^(a,b,c) seconds for pump B (from []^(a,b,c) seconds). Note

that the primary pressure at the time of the RCP trip was approximately []^(a,b,c) psia. Slightly longer coastdown times occurred during the planned matrix tests, when the RCPs were tripped after the safety systems actuation (S) signal generated at 1700 psia, due to the reduced forces on the RCP thrust bearings at lower pressure.

The cold-leg flow rates following the trip of the RCPs quickly stabilized at approximately []^(a,b,c) lbm/sec. ([]^(a,b,c) kg/sec.) per cold leg, which is approximately []^(a,b,c) percent of the nominal full flow, indicating that natural circulation heat removal was established. The hot-leg temperature quickly responded to the RCP trip, increasing from []^(a,b,c)°F to a peak of []^(a,b,c)°F. The hot-leg temperature then decreased to []^(a,b,c)°F as natural circulation flow was established and stabilized. Hot-leg temperatures then responded as expected to steam generator pressure increasing to the steam generator PORV setpoint and operation.

PRHR HX Flow and Heat Removal

Upon initiation of the PRHR HX at 4500 seconds with power at []^(a,b,c) kW, []^(a,b,c) percent decay power plus 110 kW of heat loss compensation, the hot-leg temperature was reduced from []^(a,b,c)°F to []^(a,b,c)°F where it stabilized. Also, during this time no actuation of the steam generator PORVs occurred, indicating that all core heat was being dissipated by the PRHR and heat losses. The estimated heat loss from the primary system at this time was approximately 120 kW, which indicates that the PRHR was removing approximately []^(a,b,c) kW of heat with a hot-leg temperature of []^(a,b,c)°F ([]^(a,b,c) percent of full power).

During this time, the PRHR HX natural circulation flow rate was []^(a,b,c) lbm/second, the measured T_{in} was 533°F, and the measured T_{out} was []^(a,b,c)°F. The calculated heat removal from these parameters is []^(a,b,c) kW, which agrees well with the above overall core power and estimated heat losses. In comparison to expected decay heat, the PRHR will match decay heat at less than or equal to 30 minutes, which agrees well with the AP600 PRHR design basis.

It is also noted that the SPES-2 PRHR HX flow rate of []^(a,b,c) lbm/sec. corresponds to an AP600 flow rate of []^(a,b,c) lbs/sec. or approximately []^(a,b,c) gpm, which also agrees well with the AP600 design.

Bundle power was increased to []^(a,b,c) kW and []^(a,b,c) kW to observe the effect on PRHR HX operation. At []^(a,b,c) kW, the hot leg temperature increased from []^(a,b,c)°C to []^(a,b,c)°C and the PRHR HX inlet temperature increased from []^(a,b,c)°F to []^(a,b,c)°F. In these conditions, the PRHR HX heat removal was []^(a,b,c) kW. At []^(a,b,c) kW, the steam generator PORVs were actuating; therefore, the PRHR could not match core power minus heat losses.

CMT Recirculation

When the CMTs were actuated with the primary system at steady-state conditions (T_H at []^(a,b,c)°F and T_C at []^(a,b,c)°F, natural circulation flow, and bundle power at []^(a,b,c) kW), natural circulation flow through the CMTs began as expected.

The CMT natural circulation flow rate observed was initially []^(a,b,c) lbm/sec. in CMT-A and []^(a,b,c) lbm/sec. in CMT-B. The CMT-B flow rate decreased to []^(a,b,c) lbm/sec. after approximately []^(a,b,c) seconds as the CMT heated. This corresponds to an AP600 flow rate of []^(a,b,c) lbm/sec. to []^(a,b,c) lbm/sec. for CMT-B, which agrees well with expected performance. The CMT heatup versus time observed with thermocouples placed internally down the length of the CMTs, showed that the hot water entering the top of the CMTs remained thermally stratified. Also, the water temperature decreased as it moved down the CMT, apparently due to initially heating the CMT walls and due to heat losses from the CMT surface.

As the CMTs heated and approached steady-state, the primary system temperature increased toward the initial condition before CMT actuation and heat removal via the steam generator PORVs reinitiated approximately []^(a,b,c) seconds after the actuation. The CMT levels during the recirculation heatup were observed to decrease from approximately []^(a,b,c) ft. to approximately []^(a,b,c) ft. This was due to the decrease in CMT water density as hot water replaced cold water increasing the CMT average temperature to approximately []^(a,b,c)°F.

The CMT-A flow rate was initially less than CMT-B, and it did not decrease smoothly as the CMT heated up. This was apparently due to the check valve in the CMT-A discharge line, which does not work as smoothly as the check valve in CMT-B discharge line. This valve was replaced prior to the start of matrix testing.

Also as expected, the natural circulation of the CMTs resulted in an increase in pressurizer level as cold CMT water was heated up in the primary system, requiring that the letdown flow path be utilized.

4.1.2.5 SPES-2 Pre-Operational Test H-05

The purpose of this test was to verify that the passive safety system actuations occur properly and that these systems perform as expected. The test was conducted at a low initial primary system pressure, since this would be the first time the plant safety systems were actuated. Note that the test initial conditions were selected to be similar to the expected Oregon State University (OSU) test facility.

Test H-05 Description

This test was a simulation of an inadvertent opening of the first stage of ADS but was performed from a low initial pressure and temperature. In order to more closely simulate the plant and safety system response times that would be expected to occur in a full-pressure and temperature transient, the test boundary and initial conditions used were similar to those anticipated for the test facility at Oregon

State University. In addition, the size of the ADS-1, -2, and -3 flow path orifices was increased from 1/395th area scale (AP600/SPES-2 scale factor) to approximately 1/100th area scale. The ADS-4 flow path area was maintained at the SPES-2 scaled area (however, the fourth-stage valve failed to open in the actual test).

The facility initial conditions are provided in Table 4.1.2-5.

Test H-05 Results

As shown in Table 4.1.2-6, all control system actuations occurred during the test. However, some actuation times were delayed and two valve operators did not actuate. The valve operators and logic control for the actuations were inspected and revised.

Pre-operational Test H-06, discussed in Section 4.1.2-6, was the same inadvertent ADS event as H-05 but was performed from simulated full AP600 power, and full pressure and temperature. Table 4.1.2-7 provides a comparison of major events timing for these two tests.

All major events occur at similar times and the primary system depressurization curves are very similar, with the exception of the initiation of IRWST injection flow. This exception is expected since the SPES-2 IRWST was filled to the full height AP600 level while OSU plans to utilize a 1/4 height IRWST. CMT flow versus time, accumulator flow versus time, and PRHR HX performance all exhibit similar behavior in both tests.

4.1.2.6 SPES-2 Hot Pre-Operational Test H-06

This test was a simulation of an inadvertent actuation of the ADS-1 from a simulated full-power operating condition. The purpose of this test was to verify that all actuations occur properly and that the ADS flow paths were properly sized.

The results of this test can be compared with the computer models of both the SPES-2 facility and the AP600.

Test H-06 Description

This test was initiated with the facility at full-power conditions, by opening the first-stage isolation valve of ADS (simulates both AP600 first-stage flow path flow areas). This results in a rapid depressurization of the primary system, reactor trip and safety injection signal actuations, and resulting mitigation of the event by the passive safety systems.

Test H-06 Results

As indicated in Table 4.1.2-8, test H-06 initial conditions closely matched the specified initial conditions. Also, as shown the sequence of events in Table 4.1.2-9, all required actuations were

performed; however, closer adjustments of actuation delay times are needed to better match the specified values.

Other items to note include the following:

- The ADS-4 valve did not open, in spite of receiving the actuation signal from the facility control system.
- Flow from the IRWST began prior to termination of flow from either CMT-A or -B, even with no venting from the ADS-4. However, it should be kept in mind that SPES-2 ADS-1, -2, and -3 discharge to a condenser at atmospheric pressure and no back pressure due to the ADS sparger or overpressure due to sparger submergence is present.
- The pressure balance between the IRWST and primary system is very delicate (with no 4th stage venting). This is evidenced by the stoppage of IRWST delivery when the pressurizer water level is high and by the sensitivity of IRWST injection flow rate to the pressurizer water level.
- Only CMT fluid thermocouples T-A/B401E through T-A/B403E were heated prior to the transition of the CMTs from natural circulation to draindown mode, which occurred at []^(a,b,c) seconds. This means that only the top approximately []^(a,b,c) feet of CMT water was heated. Subsequent heatup of the CMT fluid thermocouples lower in the tank was due to this heated, top layer of water moving down through the tank as the CMT drained; and then exposure of the thermocouples to the steam above the CMT water level. The CMT fluid thermocouples generally follow the saturation temperature corresponding to the primary pressure with the following two exceptions:
 - From approximately []^(a,b,c) seconds the topmost CMT fluid thermocouples indicate slightly superheated steam, apparently due to steam flow from the hot legs through steam generators.
 - The lowest six CMT fluid thermocouples indicate temperatures below saturation starting at approximately []^(a,b,c) seconds, which is after the accumulators empty. This may be due to accumulator air injected into the primary system. If air enters the CMTs, it would collect in the lower portion of the empty (or emptying) CMT gas space.
- CMTs empty and then slightly refill ([]^(a,b,c) seconds). The refills occur just after pressurizer level increases and are probably due to water flow through the pressurizer to CMT balance lines since DP-A45P and DP-B45P, the cold leg to CMT balance line differential pressures (dPs), do not indicate that these balance lines refill.
- The heated rod temperatures follow the saturation temperature corresponding to primary pressure. No elevated rod temperatures occur at anytime in the transient.

**TABLE 4.1.2-1
SPES-2 HOT PRE-OPERATIONAL TEST SUMMARY**

Test	Test Description	Test Purpose	Comments
H-01	The facility was heated and held at four "constant" temperatures.	Determine the facility and major component heat losses vs. temperature.	
H-02	This test was performed concurrent with H-01 test.	Quantify the water and metal heat capacity of the facility.	
H-03	The facility was operated at normal full pressure, temperature, and power.	Verified the proper operation of all components and instrumentation.	Performed as part of first matrix test pre-test initial conditions.
H-04	The facility was transitioned from ~1 MW power operating conditions to a hot shutdown/natural circulation mode of operation.	Verified computer controlled heater rod power decay and SFW flow control on SG level. Characterized the loop, PRHR heat exchanger and CMT natural circulation flows; confirmed PRHR heat removal rate.	
H-05	Simulated an inadvertent ADS actuation from low pressure (335 psig) with subsequent safety actuations.	Verified the proper safety system actuation at low pressure; the initial conditions used were similar to OSU.	Provided full height vs. 1/4 height comparison to OSU. No intervention of ADS-4 and of nonsafety systems.
H-06	The test was performed from full-power conditions and initiated by opening the ADS-1	Verified the actuation and performance of the safety systems.	No ADS-4 or nonsafety system operation.

**TABLE 4.1.2-3
SPES-2 HOT PRE-OPERATIONAL TEST H-01 MAJOR COMPONENT HEAT LOSSES**

Flow rate in each cold leg = 0.619 kg/sec.
Total power = 142.6 kW

Component	Component Metal Mass lbm ⁽¹⁾	Component Heat Capty. (Btu/°F)	Inlet Average Temperature (°F)	Outlet Average Temperature (°C)	Heat Losses (kW)	Heat Loss Percentage due to the Component (%)
PC/HL (A&B)						
RCP-A/ CL-A1,A2						
RCP-B/ CL-B1,B2						
SG-A						
SG-B						
Total Heat Losses =					[]	(kW)

Notes:

- (1) The weight of these components does not include flange and bolting metal masses.
- (2) These data are not relevant for the calculation of steam generator heat losses, as their metal heat capacity contribution can be neglected.
- (3) Pump power released to the fluid at low flow can be neglected.
- (4) The difference between total power and total heat losses is due to the heat capacity of the system.

**TABLE 4.1.2-4
SPES2 PRE-OPERATIONAL TEST H-01 FACILITY SYSTEM HEAT CAPACITIES**

Source File	Time Interval ⁽¹⁾ (sec.)	Temperature Linear Increase (°C)	Total Power Input Rate ⁽²⁾ (kW)	Calculate d Heat Losses (kW)	Calculate d Heat Capacity (kJ/°C)
acqdat_spes.dat;242					
acqdat_spes.dat;242					
acqdat_spes.dat;244					
Average Heat Capacity =					8480

(a,b,c)

Notes:

- (1) This time interval is considered valid for the value of data recorded.
- (2) The total power includes pump heat power released to fluid:

Pump A = kW
 Pump B = kW

**TABLE 4.1.2-5
SPES-2 HOT PRE-OPERATIONAL TEST H-05
INITIAL CONDITIONS**

Condition	Specified	Actual
Pressurizer pressure	360.5 psig (24.9 bar)	
Pressurizer level	12.4 ft. (3.78 m)	
Hot-leg temperature	415.6°F (213.1°C)	
Cold-leg temperature	---	
Power (kW)	192.3	
Upper-head flow rate	0.40 lb/sec. (0.18 kg/sec.)	
Steam generator pressure	270.6 psig (18.66 bar)	
Steam generator level	>36.2 ft. (>11.02 m)	
Accumulator pressure	197 psig (13.59 bar)	
Accumulator level	6.86 ft. (2.09 m)	
IRWST level	28 ft. (8.53 m)	
Cold-leg/CMT balance line temperature	Cold-leg temperature	
CMT external vessel	not pressurized	
PRHR supply line temperature	302°F (150°C)	
Pressurizer Cold-leg balance line	>437.9°F (>225.5°C)	

(a,b,c)

**TABLE 4.1.2-6
SPES-2 HOT PRE-OPERATIONAL TEST H-05
SEQUENCE OF EVENTS**

Event	Specified Actuation Signal	Actual Time(s)
ADS-1 opening	---	
Main steamline isolation valve (MSLIV) start closing	ADS-1 opening	
Main feedwater isolation valve (MFWIV) start closing	ADS-1 opening	
CMT balance line start opening	ADS-1 opening	
CMT injection line start opening	ADS-1 opening	
SFW closed	ADS-1 opening	
RCP trip	ADS-1 + 15 sec.	
PRHR HX on	ADS-1 + 45 sec.	
Heated rod power	ADS-1 opening +200 sec.	
Accumulator injection start	---	
ADS-2 opening	CMT level = 60%	
ADS-3 opening	CMT level = 50%	
Heat loss compensation off	ADS-2 opening	
ADS-4 opening	CMT level = 20%	
Accumulator empty	---	
IRWST injection	---	

**TABLE 4.1.2-7
SPES-2 HOT PRE-OPERATIONAL TESTS
MAJOR EVENT COMPARISON BETWEEN
TESTS H-05 AND H-06**

Event	Time (sec.)	
	Test H-05	Test H-06
ADS-1 opening		
CMT recirculation to draindown transition		
Accumulator injection start		
ADS-2 opening		
ADS-3 opening		
Accumulators empty		
ADS-4		
IRWST injection		
Pressurizer pressure decay		

(a,b,c)

- (1) Longer accumulator draindown expected; orifices were installed in the accumulator discharge lines (0.375-in. diameter) prior to H-06 to better match the scaled AP600 line resistance.

**TABLE 4.1.2-8
SPES-2 HOT PRE-OPERATIONAL TEST H-06
INITIAL CONDITIONS**

Condition	Specified	Actual
Pressurizer pressure (bar)	2248 psig (155 bar)	
Pressurizer level (m)	12.4 ft. (3.78 m)	
Hot-leg temperature (°C)	600°F (316°C)	
Core inlet temperature (°C)	530°F (276.4°C)	
Power (MW)	(4.99 MW)	
Downcomer flow rate (kg/sec.)	51.3 lbs/sec. (23.25 kg/sec.)	
Steam generator pressure (bar)	710 psig (49 bar)	
Steam generator level (m)	>36.1 ft. (>11.02 m)	
Steam generator MFW flow rate (kg/sec.)	2.65 lbs/sec. (1.2 kg/sec.)	
Steam generator MFW temperature (°C)	439°F (226°C)	
Accumulator pressure (bar)	700 psig (48.3 bar)	
Accumulator level (m)	8.5 ft (2.6 m)	
IRWST level (m)	28.0 ft. (8.53 m)	
Cold-leg to CMT balance line temperature (°C)	>529, <563°F (>276, <295°C)	
Cold-leg to pressurizer balance line temperature (°C)	>669, <698°F (>354, <370°C)	

(a,b,c)

TABLE 4.1.2-9
SPES-2 HOT PRE-OPERATIONAL TEST H-06
SEQUENCE OF EVENTS

Event	Actuation Signal Setpoints ⁽¹⁾	Time (sec.)
ADS-1 opening	---	
R signal	Pressurizer pressure = 123.1 bar	
Core decay heat reduction	R signal + delay time (7 sec.)	
MSLIV closed	R signal	
S signal	Pressurizer pressure = 116.2 bar	
MFWIV closed	S signal	
CMT balance line opened	S signal + 2 sec.	
CMT injection line opened	S signal + 8 sec.	
RCP trip	S signal + 16.2 sec.	
PRHR HX on	S signal + 45 sec.	
ACC injection start	---	
ADS-2 opening	CMT level = 60%	
Heat loss compensation off	ADS-2 opening	
ADS-3 opening	CMT level = 50%	
ADS-4 opening	CMT level 20%	
Accumulator empty	---	
IRWST injection start	---	

Notes:

- (1) Specified by test procedure.
- (2) One of two ADS 4-stage valves (A loop) was actuated but the discharge flow path was blocked; i.e., no 4th-stage flow was permitted.

4.2 Test Results

4.2.1 Test Transient Phases for Loss-of-Coolant Accident (LOCA) and Non-LOCA Tests

All of the matrix tests at SPES-2 can be divided into phases which are characterized by the rate at which the RCS (primary system) pressure decreases and/or by actuations of the passive safety system features. These phases conveniently subdivide the test with similar thermal-hydraulic phenomena and passive safety system responses

For the discussion of the tests in Section 4.2, each test was subdivided into the following phases.

4.2.1.1 LOCAs

The LOCA tests consisted of four definable phases:

- initial depressurization phase (IDP)
- pressure decay phase (PDP)
- automatic depressurization system (ADS) phase
- post-automatic depressurization system (post-ADS) phase

The IDP is the time of rapid primary system pressure decrease, resulting from the inventory loss through the break and/or rapid cooldown after rod power was decreased. The PDP follows the IDP and is characterized by a much slower rate of pressure decrease in primary system that corresponds to the saturation pressure of the hottest portion of the primary system.

The ADS phase is the time from the initiation of ADS-1 until ADS-4; and the post-ADS phase is the time from ADS-4 until the end of the test. The ADS phase therefore includes the accumulator delivery (for most LOCA events); and the post-ADS phase includes the in-containment refueling water storage tank (IRWST) injection.

4.2.1.2 Non-LOCAs

The non-LOCA tests in SPES-2 did not proceed through all the phases experienced in LOCA tests and normally consisted of two definable phases:

- IDP
- PDP

In one test (S01211), a single tube steam generator tube rupture (SGTR), an inadvertent ADS actuation was simulated, thereby adding the ADS and post-ADS phase to that test.

4.2.2 Two-In. Cold Leg Break without Nonsafety Systems (S00303)

This matrix test simulated a 2-in. break in the bottom of cold leg-B2. The test began with the initiation of the break in cold leg-B2, which was the cold leg with the CMT-B pressure balance line connection. The break location was just downstream from the cold leg to the core makeup tank (CMT) balance line connection. This test was performed without any nonsafety systems (chemical and volume control system [CVCS] makeup pumps, steam generator startup feedwater [SFW] pumps, and normal residual heat removal system [NRHR] pumps) operating.

Results are provided in the data plot package at the end of this section. The sequence of events for S00303 is listed in Table 4.2.2-1.

The SPES-2 tests were marked by distinctly different phases. These phases were characterized by the rate at which the primary system pressure decreased and the thermal-hydraulic phenomena occurring within the primary and safety systems. The different phases selected for the purpose of detailed evaluation of this LOCA are shown in Figure 4.2.2-1 and are as follows:

- Initial depressurization phase (IDP)—Point 1 to 2
- Pressure decay phase (PDP)—Point 2 to 3
- Automatic depressurization system (ADS) phase—Point 3 to 4
- Post-automatic depressurization system (post-ADS) phase—Point 4 to 5

Overall Test Observations

Figure 4.2.2-1 shows the plant primary system pressure during test S00303 (as measured at the top of the pressurizer), with selected component actuations and plant responses shown in relation to pressure.

The IDP began with the initiation of the break, which resulted in a rapid reduction in pressure. The reactor trip (R) signal initiated at []^(a,b,c) psia, and the safety systems actuation (S) signal initiated at []^(a,b,c) psia. The R and the S signals initiated the following actions:

- Decay power simulation (with heat loss compensation).
- Main steamline isolation valves (MSLIVs) closed.
- Main feedwater isolation valves (MFWIVs) closed.
- CMT injection line isolation valves opened.
- Passive residual heat removal (PRHR) return line isolation valve opened.
- Reactor coolant pumps (RCPs) turned off.

Recirculation flow through the CMTs and the flow through the PRHR began immediately after their isolation valves opened. Flashing occurred in the rod bundle and upper-upper plenum of the power channel due to the rapid decrease in primary pressure. The measured fluid level in the upper-upper plenum dropped to the hot-leg elevation. The flashing on the hot-leg side of the primary system stopped the rapid drop in primary system pressure. When the RCPs were shut off (at

[]^(a,b,c) seconds), the flow through the rod bundle began to oscillate (period approximately []^(a,b,c) seconds). This resulted in oscillations in the power channel and the lower-upper plenum steam fractions and temperatures, and system pressure.

During the initial stages of the PDP, the rod bundle steam fraction increased. This resulted in an increasing steam fraction in the lower-upper plenum and the hot legs. The hot leg-B fluid had a steam fraction very close to that observed in the lower-upper plenum. The steam fraction in hot leg-A was much lower due to the selective removal of steam from the hot leg into the PRHR HX inlet line.

The two-phase flow in the hot legs initiated draining of the steam generator U-tubes, as steam collected in the top of the U-tubes. This stopped the primary system flow through the SGs so that the power channel flow was composed predominantly of the flow through the PRHR HX. The level oscillations observed in the rod bundle and in the upper plenum stopped when the flow through the steam generators ended. Approximately []^(a,b,c) seconds into the test, the steam generator-B U-tubes began to drain. The steam generator-A U-tubes began to drain approximately []^(a,b,c) seconds later, due to the lower steam fraction in hot leg-A.

Two-phase flow from the rod bundle entered the hot leg and flowed to the PRHR HX. The flow through the PRHR HX consisted of alternating slugs of steam and saturated water, which had an average steam fraction significantly greater than in the upper plenum. The average steam fraction at the PRHR HX inlet was as high as []^(a,b,c) percent, which enhanced the PRHR HX heat removal from the primary system as compared to its heat removal capability with single-phase saturated or subcooled water. When the primary system flow stabilized after the initial flow oscillations, a PRHR HX heat removal rate of []^(a,b,c) kW was calculated. This calculation was based on the average steam fraction at the PRHR HX inlet as calculated from the dP instrument readings in data plot 29, the average return flow rate, the inlet and outlet temperature, and the pressure. This calculation assumed a slip coefficient of 1 between steam and water, and may be slightly lower than the actual PRHR HX heat transfer. It should, therefore, be used for test-to-test comparison only.

When the loop-B cold legs had partially emptied, the CMTs transitioned from their recirculation mode to a draindown mode of operation. This increased the CMT injection flow and the rate of system pressure decay. This occurred at approximately []^(a,b,c) seconds for CMT-B and []^(a,b,c) seconds for CMT-A. When system pressure dropped to the saturation pressure for the upper head, the upper head began to drain at []^(a,b,c) seconds.

During the first []^(a,b,c) seconds of this LOCA, []^(a,b,c) lbm of steam and water were expelled through the break while draining the pressurizer, the steam generator U-tubes, the upper head, the upper-upper plenum, most of the cold legs, and approximately []^(a,b,c) percent of the CMTs. The heated rods had decreased in power to approximately 240 kW at 900 seconds. This value consisted of 90-kW decay heat and 150-kW heat loss compensation. The break flow was decreasing slowly with primary pressure and indicated that cold leg-B2 was not empty.

The ADS phase began with the actuation of ADS-1 (at approximately []^(a,b,c) seconds into the event). ADS-2 and -3 occurred within the next []^(a,b,c) seconds. The heat loss compensation portion of the rod bundle power was terminated when ADS-1 occurred, and power was reduced to approximately 90 kW.

The ADS actuation increased the rate of primary system depressurization and resulted in high injection flow from the accumulators. The rapid injection of cold fluid from the accumulators (at []^(a,b,c) seconds into the event), temporarily refilled the rod bundle, lower-upper plenum, hot legs, and the pressurizer. When the accumulator discharge ended, the flow through the rod bundle was reduced to the injection rate of the CMTs and the PRHR HX flow, and two-phase fluid flow occurred again through the rod bundle, lower-upper plenum, hot leg-A, the PRHR HX, and to the pressurizer.

The discharge of liquid through the break was replaced by steam at approximately []^(a,b,c) seconds. During this ADS phase, approximately []^(a,b,c) lbm of steam and water were discharged from ADS-1, -2, and -3. This water was primarily supplied by the accumulators. After the accumulators drained the collapsed liquid level in the rod bundle decreased (steam fraction increased) since only the CMTs were providing injection flow.

The post-ADS phase began when ADS-4 actuated and fluid was discharged through ADS-4. The fluid discharge through ADS-1, -2, and -3 stopped, and the pressurizer water level decreased. A small amount of CMT flow was still being provided via the DVI line to the annular downcomer. When system pressure had been reduced below the pressure corresponding to the water elevation head of the IRWST, flow from the IRWST began. Shortly thereafter, the CMT flow ended. The flow from the IRWST refilled and subcooled the power channel and hot legs, and the upper-upper plenum partially refilled. The PRHR HX supply line emptied approximately []^(a,b,c) seconds into the test and was no longer effective. A steady flow of subcooled water was then flowing from the IRWST into the annular downcomer, through the power channel, and left the primary system through the ADS-4 flow paths.

The heater bundle remained fully cooled by single-phase water or two-phase mixture flow at all times during this test (data plots 30 and 31). There was no indication of an increase in heater rod temperatures due to lack of cooling (data plot 3).

Discussion of Test Transient Phases

- **Initial Depressurization Phase (0 to []^(a,b,c) Seconds)**

The initial depressurization phase (IDP) began with the initiation of the break (at time 0) and continued until primary system pressure reached the saturation pressure of the fluid in the upper plenum and the hot legs (Figure 4.2.2-1). This phase included the following events: R signal at 1800 psia (decay power simulation initiated and the MSIV closed), and S signal at 1700 psia (the MFWIV closed, the CMT injection line isolation valves opened, and the PRHR heat exchanger

return line isolation valve opened—all with a []^(a,b,c)-second delay, and RCP coastdown started after a []^(a,b,c)-second delay). See Table 4.2.2-1.

Facility Response during the IDP:

From time 0 until the R signal occurred, the system depressurized due to the fluid loss through the break resulting from the expansion of the pressurizer steam volume. The pressurizer partially compensated for the loss of pressure by flashing, however it was drained after []^(a,b,c) seconds (data plot 32). The R (at []^(a,b,c) seconds) and the S (at []^(a,b,c) seconds) signals were based on pressurizer pressure only. When the R signal occurred, the MSLIV was closed, and power was reduced to 20 percent after a 5.75 second delay and began to decay after a 14.5 second delay.

As a result of the power reduction without flow reduction, the core ΔT decreased due to the low power/flow ratio, and the upper plenum temperature dropped toward the cold-leg temperature. Since system pressure was controlled by the saturation pressure at the hot-leg/upper-plenum temperature, system pressure dropped to the saturation pressure at []^(a,b,c) (approximately []^(a,b,c) psia at approximately []^(a,b,c) seconds). See Figure 4.2.2-2. When the RCPs tripped (at []^(a,b,c) seconds), the rod bundle and the lower-upper plenum temperatures increased due to the increased rod bundle power/flow ratio at the lower flow. System pressure increased temporarily until the decreasing decay power and the decreasing lower-plenum temperature (due to CMT injecting cold fluid into the downcomer) started to reduce the upper-plenum temperature. The primary system pressure decrease resulted from the balance between the steam generation rate (from flashing primary fluid), the volumetric flow of liquid out the break, and the steam condensation rate by the PRHR HX. Steam was continually generated by boiling due to the rod bundle power. As system pressure continued to fall, more and more water reached its saturation pressure and began to flash. PRHR flow started before the RCPs were tripped and continued by natural circulation afterward (data plot 37). Primary system pressure stabilized at the saturation pressure for the bulk hot fluid in the system (approximately []^(a,b,c)). This ended the IDP.

- **Pressure Decay Phase ([170 to 900])^(a,b,c) Seconds**

The pressure decay phase (PDP) began when system pressure (Figure 4.2.2-2) reached saturation pressure corresponding to the fluid temperature on the hot-leg side of the power channel. The phase ended when ADS-1 was opened on low CMT level and augmented the system depressurization. This phase was characterized by a slow decrease in overall system pressure and temperature. The rod bundle power was reduced from 340 kW to 240 kW (data plot 1). The PRHR HX heat removal rate was approximately []^(a,b,c) kW. The recirculating CMTs provided approximately []^(a,b,c) kW of heat removal from the primary system due to the removal of hot water from the primary system, which was replaced with cold CMT water.

The initial CMT natural circulation operating mode was followed by draindown injection when the loop B cold legs drained (data plot 38). The U-tubes of the steam generators were completely drained at this time (data plots 20 to 23). The steam generators did not affect the rest of the

event. The accumulator injection was initiated when the primary system pressure dropped below 711 psia prior to ADS-1 actuation. However, the injection rate was low (less than []^(a,b,c) lbm/sec.) due to the small difference between primary system pressure and accumulator gas pressure (data plot 39).

Facility Response during the PDP:

Following reactor coolant pump shutdown, the oscillating flow in the tubular downcomer and in the rod bundle region continued into the PDP. The flow oscillations resulted in large oscillations of the steam fraction of the mixture exiting the core and flowing into the hot legs (data plots 30 and 31). These oscillations in steam fraction had a significant effect on the thermal buoyancy head that drove the flow through the primary system at this time, since it affected the mixture density. The steam fraction oscillations were observed through the hot leg and the steam generators (data plots 20 and 21). The steam fraction oscillations were converted to flow oscillations in the cold legs, since the two-phase mixture entering the steam generators left the steam generators as saturated water (data plots 24 through 27). It is postulated that some of the steam was condensed in the U-tubes since the primary-side pressure was higher than the secondary-side pressure at this time, allowing some heat to be transferred to the secondary-side fluid. The remaining steam was separated from the two-phase mixture in the high point of the U-tubes (due to the low velocity), which eventually stopped natural circulation in the U-tubes. For steam generator-A, the flow continued until []^(a,b,c) seconds into the transient. From []^(a,b,c) seconds until []^(a,b,c) seconds, intermittent flow was observed through steam generator-A (plots 20 and 22). A free-water surface occurred at the top of the U-tubes. However, the buoyancy head in the hot leg was high enough to spill over the top of the U-tubes at the peaks of the oscillating buoyancy head. At []^(a,b,c) seconds, all flow stopped in steam generator-A, since the free-water surface had fallen too low to be overcome by the buoyancy head oscillations. Oscillations were measured in temperatures and pressures throughout the primary system. When the steam generator U-tubes were drained (approximately []^(a,b,c) seconds), the oscillations stopped. For steam generator-B, flow stopped earlier than for steam generator-A due to the higher steam fraction in the fluid from hot leg-B.

The primary system pressure decay during the PDP started at a slow rate of []^(a,b,c) psi/sec. At approximately []^(a,b,c) seconds into the event, the primary system pressure decay rate increased to []^(a,b,c) psi/sec. This happened when the transition of the CMTs from their recirculation mode of operation to their draindown mode occurred. The increased rate of pressure decay was due to the increased injection rate of the cold liquid from the CMTs, which occurred at different times for the two CMTs, and steam flow from the cold legs to the top of the CMTs.

The CMTs began injecting cold fluid into the annular downcomer via the DVI line when the S signal occurred. Initially this injection was by natural circulation (at approximately []^(a,b,c) lbm/sec. from each CMT), with hot water flowing from the cold leg through the cold-leg balance line (CLBL) into the top of the CMT and cold water flowing from the bottom of the CMT into the downcomer. In the time period from []^(a,b,c) seconds to []^(a,b,c) seconds (data

plot 38), CMT-A transitioned to draindown when the cold leg balance line (CLBL) for CMT-A drained, and a free-water surface developed in the top of CMT-A as the level began to drop (data plot 33). The injection flow, when draindown started, increased to approximately []^(a,b,c) lbm/sec. and gradually decreased as the CMT level decreased (reducing the driving head). Steam from the cold legs flowed to the CMTs after the cold legs drained and condensed on the cold CMT and water surfaces, heating them to saturation temperature.

For CMT-B, the break of the recirculation in the CLBL occurred at approximately []^(a,b,c) seconds (earlier than for CMT-A), and the transformation from natural circulation to CMT draindown occurred between []^(a,b,c) seconds and []^(a,b,c) seconds. The draindown injection flow began at approximately []^(a,b,c) lbm/sec. and gradually decreased.

The free-liquid surfaces in the CMTs were established after recirculation through the CLBLs ended (the end of recirculation was caused by steam flowing from the cold legs to the CMTs). However, flashing in the CMTs seemed to occur after this time due to the high temperature of the fluid in the top of the CMTs (data plots 15 and 16) and the decreasing primary system pressure. The steam above the liquid surface in the CMTs was superheated after []^(a,b,c) in CMT-B. Flashing occurred in order to keep the water temperature at saturation temperature as the pressure decreased.

The accumulators began to inject into the annular downcomer via the DVI lines when system pressure dropped below 711 psia (at approximately []^(a,b,c) seconds). However, the injection rate was very low prior to ADS-1 (data plot 39).

Throughout the PDP, the PRHR removed energy from the primary system. The combined effect of the PRHR cooling the primary fluid and the injection flow from the CMTs was sufficient to limit the steam fraction of the fluid in the rod bundle to []^(a,b,c) percent (steam fraction was actually decreasing), and to maintain adequate cooling of the rod bundle during this phase (data plots 30 and 31).

• **Automatic Depressurization System Phase ([]^(a,b,c) Seconds)**

The automatic depressurization system (ADS) phase began with the actuation of ADS-1 and ended with the actuation of ADS-4 (Figure 4.2.2-1).

Facility Response during the ADS Phase:

With the actuation of ADS-1, followed by ADS-2 and ADS-3 within approximately []^(a,b,c) seconds, the rate of system depressurization increased from []^(a,b,c) psi/sec. (at the end of the PDP) to []^(a,b,c) psi/sec. (at the start of the ADS phase). This rate gradually decreased as system pressure decreased.

After ADS actuation, the rate of water injection from accumulators-A and -B increased sharply (data plot 39). The accumulators and injected cold water into the primary system for approximately []^(a,b,c) seconds (from []^(a,b,c) seconds to []^(a,b,c) seconds) and then were drained. The accumulator and CMT injection refilled the rod bundle, lower-upper plenum, and hot legs with water.

The pressurizer immediately began to refill when ADS-1 occurred, reached a collapsed liquid level of approximately []^(a,b,c) ft., and steam and water were vented from the pressurizer through the ADS (data plot 32). When ADS-4 occurred, the pressurizer drained and only a small amount of saturated steam was vented through ADS-1, -2, and -3.

Prior to the ADS period, liquid left the primary system through the break in the cold leg. With the actuation of the ADS, fluid left the system through the ADS from the top of the pressurizer. The mass flow through the cold-leg break decreased and converted from liquid to mostly saturated steam as the cold leg completely drained (data plot 43).

- **Post-Automatic Depressurization System Phase ([]^(a,b,c) Seconds to End-of-Test)**

The post-automatic depressurization system (post-ADS) phase began when ADS-4 occurred (Figure 4.2.2-1) and continued to the end of the test.

Facility Response during the Post-ADS Phase:

The water level in the downcomer decreased into the tubular downcomer due to ADS-4 flow and the fact that the CMT injection was less than the mass discharged by the ADS (data plot 25). This net loss in primary system mass resulted in a decrease in the collapsed liquid level measurement in the rod bundle region and a significant increase in the steam fraction of the flow through the rod bundle and upper plenum. The liquid level measured in the upper plenum indicated the presence of two-phase mixture throughout the rod bundle region (data plots 30 and 31).

The system responded to ADS-4 by rapidly decreasing the system pressure to near ambient, and gravity flow from the IRWST through the direct vessel injection (DVI) line began to occur (data plot 40). The cold water from the IRWST gradually suppressed boiling in the rod bundle and refilled the power channel and hot legs with subcooled water. The water levels in the power channel stabilized, and the upper-upper plenum became subcooled and partially refilled. This steady-state condition was considered to be the end of the test.

At this time the system pressure was very low, and steam flow through ADS-4 ended flow through ADS-1, -2, and -3.

The PRHR HX stopped flowing at approximately []^(a,b,c) seconds as the HX and supply line partially drained (data plot 37).

Component Responses

• Power Channel

The power channel consisted of five volumes: the lower plenum, the heater rod bundle, the lower-upper plenum (below the hot leg), the upper-upper plenum (above the hot leg), and the upper head. When the break occurred, the system pressure decreased to the R trip point (1800 psia) and the S trip point (1700 psia). However, since the coolant in the power channel was subcooled relative to the saturation temperature for system pressure, no boiling or flashing occurred up to this point. Nothing significant happened in the power channel until []^(a,b,c) seconds after the R signal when the core power was reduced to []^(a,b,c) percent. At this time, the temperature gradient across the rod bundle quickly decreased due to the reduced power/flow ratio (still full flow), and the power channel outlet temperature dropped toward the lower-plenum inlet temperature (Figure 4.2.2-2). The upper-upper plenum still contained []^(a,b,c)°F liquid, and the liquid in the upper plenum began to flash when system pressure dropped below []^(a,b,c) psia. When the RCPs were stopped ([]^(a,b,c) seconds after the S signal), the power/flow ratio increased and the power channel outlet temperature increased again, resulting in boiling in the rod bundle and flashing in the upper plenum. This produced sufficient steam to temporarily stop the system pressure decrease. Both the primary system temperature and pressure increased momentarily until the upper-upper plenum was empty down to the hot-leg elevation (data plots 30 and 31). The lower-upper plenum temperature reached a peak and began to decrease (responding to the increased primary system flow caused by the increasing buoyancy head) and stabilized at lower-upper plenum and hot-leg temperature of approximately []^(a,b,c)°F. The pressure stabilized at the hot-leg saturation pressure (approximately []^(a,b,c) psia) at the end of the IDP.

The temperature of the liquid in the lower-upper plenum controlled system pressure during the PDP (data plot 4). Oscillations with a period of []^(a,b,c) seconds in the flow in the tubular downcomer and differential pressure across the rod bundle were observed after the RCPs coasted down and continued until approximately []^(a,b,c) seconds into the event. These flow oscillations led to oscillations in the apparent density of the fluid in the rod bundle, lower-upper plenum, and hot leg (data plots 30 and 31). When the flow decreased, steam fractions increased, causing an increase of the overall system pressure and in the lower-upper plenum temperature (Figure 4.2.2-2). The overall system pressure oscillations were therefore out of phase with the tubular downcomer flow oscillations.

Data plots 30 and 31 show the collapsed liquid levels at various sections of the power channel during the S00303 event.

The upper head began to drain when primary system pressure decreased to the saturation pressure of the fluid in the upper head at about []^(a,b,c) seconds. Initially, the upper-head fluid temperature was []^(a,b,c)°F and was therefore considerably cooler than the upper-head fluid temperature. Flashing of the fluid in the upper head began at []^(a,b,c) seconds, and the upper head drained completely when ADS-1 occurred at approximately []^(a,b,c) seconds (see data plot 4).

The fluid in the upper-upper plenum flashed when the RCPs were shut off and coasted down, and the measured water level dropped to the hot-leg elevation. This level remained at the hot-leg elevation until the end of the accumulator injection, when the upper-upper plenum became sufficiently subcooled to temporarily condense the steam bubble in the top of the upper plenum (see temperatures in data plot 4). However, when the accumulator injection ended, the level again decreased to the hot-leg elevation or below. At []^(a,b,c) seconds, the upper plenum was subcooled again and filled with water injected from the IRWST.

The presence of liquid level in the lower-upper plenum indicates that the rod bundle was covered with two-phase fluid throughout the entire event. The maximum steam fraction of fluid in the lower-upper plenum was estimated to be []^(a,b,c) percent during the PDP from about []^(a,b,c) seconds to []^(a,b,c) seconds.

Data plot 30 shows the collapsed levels in the rod bundle oscillating after the pump coastdown (period approximately []^(a,b,c) seconds). This indicates apparent steam fractions in the rod bundle region ranging from []^(a,b,c) percent to []^(a,b,c) percent in this period. When the oscillations ended at []^(a,b,c) seconds, the maximum steam fraction in the rod bundle was [44]^(a,b,c) percent. The accumulator injection completely suppressed boiling in the rod bundle. However, when the accumulation injection ended, the boiling again started and the steam fraction increased and reached a maximum of []^(a,b,c) percent, just before the IRWST injection started during the post-ADS period. The lower-upper plenum showed an apparent higher steam fraction of []^(a,b,c) percent prior to ADS-4, which was due to the fact that the two-phase mixture level in the upper plenum temporarily dropped below the hot leg elevation.

The collapsed level measured just above the top of the heated portion of the rod bundle (TAF, data plot 31) gives steam fractions that correlate well with those measured for the rod bundle during this test.

- **Pressurizer**

The pressurizer began to drain when the break occurred and was completely drained in approximately []^(a,b,c) seconds (data plot 32). The water in the pressurizer flashed due to the loss of system pressure, and the temperature of the water dropped from []^(a,b,c)°F during this initial depressurization (data plot 18). The hot water leaving the pressurizer surge line into hot leg-A caused a slight increase in the hot-leg temperature during this period, since it mixed with the flow from the power channel/upper plenum. The pressurizer stayed drained until after ADS-1 occurred, at which time it partially refilled and discharged steam and water via the ADS-1, -2 and -3. The pressurizer level temporarily decreased at about []^(a,b,c) seconds when the upper-upper plenum partially refilled. The level slowly decreased as the steam fraction of fluid from the power channel increased prior to ADS-4. This continued until ADS-4, when the pressurizer again drained and its water level reached manometric agreement with the water level pressure in the primary system.

- **Steam Generator**

The steam generators acted as the heat sink until the MSLIV closed and prevented further energy removal from the secondary side. This caused the temperature of the secondary side to increase toward the primary system hot-leg temperature, which at the same time was dropping due to the reduced power/flow ratio. When the RCPs coasted down, a temporary temperature increase occurred due to the increased power/flow ratio with natural circulation flow in the primary system (Figure 4.2.2-2). The steam generator temperatures stabilized at approximately []^(a,b,c)°F at the end of the IDP.

For the first part of the PDP, the pressure on the primary side of the steam generator U-tubes was higher than the secondary side (data plot 2). This indicated that some heat transfer from the primary to secondary side was occurring and caused some condensation of the steam in the two-phase fluid coming from the hot leg. The primary system pressure did not drop below the secondary side pressure until approximately []^(a,b,c) seconds into the test, at which time the U-tubes were nearly drained.

At the end of the pump coastdown, flow oscillations began to occur in the tubular downcomer and through the power channel. This caused significant oscillations in the collapsed liquid levels in the power channel and, consequently, in the density of the two-phase mixture flowing from the power channel into the hot leg and to the steam generators (data plots 20 and 21). Since the driving force for the natural circulation flow was the density difference between the single-phase fluid in the cold legs and downcomer entering the power channel and the two-phase mixture in the tube bundle, upper plenum, and the hot legs, the flow oscillations were sustained as long as there was flow through the steam generators (primary system natural circulation).

The level in the hot leg side of the steam generator U-tubes gradually decreased to about []^(a,b,c) of the tube height at []^(a,b,c) seconds and they drained completely when ADS-1 was actuated. The level in the cold leg side of the steam generator U-tubes exhibited significant level oscillations from about []^(a,b,c) seconds until they drained completely at about []^(a,b,c) seconds (data plots 22 and 23).

- **Hot Legs**

Hot legs-A and -B contained two-phase mixture when ADS-1 was actuated (data plots 20 and 21). After ADS-1, the collapsed level began to decrease. The hot legs were nearly drained by ADS-4 ([]^(a,b,c) seconds) and partially refilled later after IRWST injection began. The principal difference between hot legs-A and -B was the influence of the PRHR HX on the steam fraction of the fluid in the hot legs. The mixture discharged from the upper plenum into the hot legs had the same steam fraction as in the upper plenum fluid. However, the PRHR HX preferentially removed steam from hot leg-A (as seen in the very high steam fraction in the PRHR inlet fluid), thereby reducing the steam fraction of the mixture in hot leg-A to less than the steam fraction in hot leg-B.

The hot leg steam fraction affected the end of natural circulation flow through the steam generators, resulting in earlier U-tube draining in steam generator-B than in steam generator-A.

- **Cold Legs**

Cold legs-A1 and -A2 remained full until []^(a,b,c) seconds into the test (data plots 22 through 27). Then flashing occurred and the measured water level started to decrease. When ADS-1 occurred, the level decreased further until even the horizontal pipes were drained at about []^(a,b,c) seconds. Flashing continued throughout this period. When ADS-4 occurred, the liquid level decreased into the annular downcomer and dropped below the top of the tubular downcomer (data plot 24). When IRWST injection began at []^(a,b,c) seconds into the event, the annular downcomer level was restored and cold legs-A1 and -A2 were partially refilled after []^(a,b,c) seconds.

Cold legs-B1 and -B2 remained full until []^(a,b,c) seconds into the event. At this time both cold legs-B1 and -B2 drained, and CMT draindown started. Cold leg-B2 (where the simulated break was located) drained prior to cold leg-B1, as shown by CMT-B switching to draindown mode before CMT-A. Cold legs-B1 and -B2 were refilled rapidly after []^(a,b,c) seconds into the event, and a small amount of liquid flow started through the break. At this time, CMT balance lines were partially filled.

- **PRHR and IRWST**

At the initiation of the event, the PRHR HX was filled with subcooled liquid. When the S signal occurred, the PRHR HX return line isolation valve opened and flow at a high flow rate started through the HX because the RCP was still operating. When the RCPs were shut off and the power channel upper plenum and the hot legs filled with two-phase mixture, a large portion of the steam in hot leg-A flowed to the PRHR HX (the steam fraction was []^(a,b,c) percent based on data plot 29) in the form of intermittent slugs of steam and water. The two-phase mixture was condensed and subcooled in the PRHR HX (data plot 28). During the PDP (prior to ADS-1), significant variations in the flow rate through the PRHR were caused by the variation in the average steam fraction in hot leg-A. After the flow oscillations in the primary system ended, condensation occurring in the PRHR HX caused the rapid and wide variations in dP measurements shown in data plots 28, 29, and 37.

After the ADS was initiated, the power channel and the hot leg were refilled with subcooled liquid by the accumulator and CMT injection flow and the driving head for the flow in the PRHR HX decreased. The flow decreased and stopped, and it actually had a short period of reverse flow at the end of the accumulator discharge. The subcooled fluid in the hot leg never filled the PRHR supply line, and hot fluid in this line flashed as the system pressure decreased. The simultaneous flashing in the supply line and steam condensation in the HX resulted in wide variations in the measured flow in the PRHR return line.

After the accumulator injection ended, the fluid in the rod bundle again reached saturation temperature, and a two-phase mixture again occurred in the hot legs. Flow restarted in the PRHR HX, and the flow rate varied in response to the steam fraction existing in the hot leg. When ADS-4 depressurized the primary system and the IRWST flow again subcooled the power channel and the hot leg, the flow in the PRHR HX stopped for the remainder of the test. The heatup of the water within the IRWST due to PRHR HX operation is shown in data plot 17.

Following ADS-4, the primary system pressure decreased to near ambient flow due to the water elevation head in the IRWST began to inject water into the annular downcomer via the DVI lines (data plots 32 and 40).

- **Core Makeup Tanks (CMTs)**

The CMT injection was initiated two seconds after the S signal by opening the CMT injection line isolation valves. Initially, the flow from the CMT occurred by natural circulation; hot water from the B loop cold legs flowed through the CLBLs to the top of the CMTs; and cold water from the CMTs drained into the downcomer and into the power channel.

When cold legs-B1 and -B2 voided, steam flowed through the CLBLs to the top of the CMTs. This resulted in a free-water surface in the CMTs ending CMT recirculation. This increased the driving head and increased the CMT injection flow rate. For this cold-leg break simulation, the break was located in cold leg-B2, and resulted in cold leg-B2 draining before cold leg-B1. Since the CMT-B balance line was connected to cold leg-B2, the transition to draindown injection flow occurred earlier for CMT-B than for CMT-A (data plot 38).

The CMTs were heated first by the hot liquid from the cold legs that replaced the cold water being injected from the bottom of the CMTs. A stratified temperature gradient was established in the CMTs (data plots 15 and 16). Later, steam from the cold legs condensed on the free-water and metal surfaces in the upper part of the CMTs, raising the free-water surface temperature to near saturation temperature.

The recirculation injection for the CMTs started at approximately 0.13 lbm/sec. and was steady until the CMTs transitioned to draindown injection. The draindown injection flow rate started at []^(a,b,c) lbm/sec. and gradually decreased with time. During the accumulator injection at high flow rate, the CMT draindown rate was reduced. The CMTs injection flow ended at approximately []^(a,b,c) seconds, at which time there was still some water left in both CMTs (data plot 33).

- **Accumulators**

The accumulators provided injection by a polytropic expansion of a compressed air volume stored within the accumulator. Water from the accumulators was injected when the primary system pressure dropped below 711 psia. The accumulator injection started before ADS-1 at a very low

flow rate. However, when ADS-1 occurred, the injection rate increased (data plot 39). The accumulator injection for the S00303 test lasted approximately []^(a,b,c) seconds, and the accumulators were completely drained when the injection ended (data plot 34).

The effective polytropic coefficient of expansion was calculated to be []^(a,b,c) for accumulator-A and []^(a,b,c) for accumulator-B (Figures 4.2.2-3 and 4.2.2-4). This is near the []^(a,b,c) between isothermal expansion (n=1) and adiabatic expansion (n=1.4) and shows that some heat is picked up by the air from the internal metal surfaces of the accumulator during the expansion.

Mass Discharge and Mass Balance

The catch tank weight measurements are shown in data plot 43 for the break flow; for the ADS-1, -2, and -3 flows; and for ADS-4 flow. The break flow as shown in plot 44, which started when the event was initiated, decreased as the system pressure dropped during the IDP and the PDP. When the ADS phase occurred, the cold leg drained and the break flow transitioned to primarily steam until the IRWST injection refilled the cold legs after ADS-4.

The discharge from ADS-1, -2, and -3 was stable throughout the accumulator injection and increased temporarily when accumulator injection ended. When ADS-4 occurred, the discharge of fluid from the top of the pressurizer ended, and fluid discharge from ADS-4 began. The ADS-4 fluid discharge flow rate was relatively stable but decreased temporarily when the upper-upper plenum refilled. ADS-4 flow continued until the test was terminated. The discharged masses are shown in Table 4.2.2-3.

The mass balance results for test S00303 were calculated based on the water inventory before and after the event. Table 4.2.2-2 gives a detailed listing of the inventories of water in the various components before the test. Table 4.2.2-3 lists the inventories after the test and the amount of water injected into the power channel from the IRWST. The water level in the vessel was determined by the DP-B16P measurement to be []^(a,b,c) in. above the hot-leg centerline at the end of the test. Table 4.2.2-4 compares the mass balance before and after the test and shows excellent agreement (within 1 percent) between the measurements.

**TABLE 4.2.2-1
SEQUENCE OF EVENTS FOR TEST S00303**

Event	Specified	Instrument Channel	Actual Time (sec.)
Break Opens	0		(a,b,c)
R Signal	P = 1800 psia	P-027P	
MSLIV	R signal + 2 sec.	Z_A04S0, F_A04S	
		Z_B04S0, F_B04S	
S Signal	P = 1700 psia	P-027P	
MFW IV Closure	S signal + 2 sec.	Z_B02S0, F_B01S	
		Z_A02S0, F_A01S	
CMT IV Opening	S signal + 2 sec.	Z_A040EC, F-A40E	
		Z_B040EC, F-B40E	
RCPs Tripped	S signal + 16.2 sec.	I-A1P, S-A1P	
		I-B1P, S-B1P	
PRHR HX Actuation	S signal + 2 sec.	Z_A81EC, F_A80E	
ADS-1	CMT level 67%	L_B40E	
	+30 sec.	Z_001PC	
Accumulators	P-027P = 710 psia	F_A20E	
		F_B20E	
ADS-2	CMT level 67%	L_B40E	
	+125 sec.	Z_002PC	
ADS-3	CMT level 67%	L_B40E	
	+245 sec.	Z_003PC	
ADS-4	CMT level 20%	L_B40E	
	+60 sec.	Z_004PC, F-040P	
IRWST Injection	P-027P = 26 psia	F_A60E	
		F_B60E	

**TABLE 4.2.2-2
WATER INVENTORY BEFORE TEST S00303**

Component	Volume (ft. ³)/(l)	Net Vol (ft. ³)/(l)	Temp (°F)	Relative Density	Mass (lbm)
Loops	8.97 (254.0)	8.91 (254.0)		(a,b,c)	(a,b,c)
Pressurizer	3.37 (95.4)	1.90 (54)			
Surge Line	0.34 (9.6)	0.34 (9.6)			
Tubular Downcomer	1.38 (39.1)	1.38 (39.1)			
Annular Downcomer + High-Pressure Bypass	0.54 (15.3)	0.54 (15.3)			
Core Bypass	0.44 (12.4)	0.44 (12.4)			
Lower Plenum	0.81 (22.8)	0.81 (22.8)			
Riser	1.64 (46.4)	1.64 (46.4)			
Upper Plenum	1.46 (41.3)	1.46 (41.3)			
Upper Head	1.90 (53.8)	1.90 (53.8)			
CMTs	10.1 (286)	10.1 (286)			
Accumulator	10.1 (286)	7.64 (216.2)			
IRWST Injection Line	0.18 (5.1)	0.18 (5.1)			
TOTAL INVENTORY					[] (a,b,c)

TABLE 4.2.2-3
WATER INVENTORY AFTER TEST S00303 WAS COMPLETED
 Water level as measured by DP-B16P (-0.55 psi) is 15.48 in. (387 mm) above Hot Leg

Component	Volume (ft. ³)/(l)	Net Vol (ft. ³)/(l)	Temp (°F)	Relative Density	Mass (lbm)
Loops	8.97 (254.0)	0.0 (0.0)			(a,b,c)
Pressurizer	3.37 (95.4)	0.0 (0.0)			
Surge Line	0.34 (9.6)	0.0 (0.0)			
Tubular Downcomer	1.38 (39.1)	1.38 (39.1)			
Annular Downcomer + High-Pressure Bypass	0.54 (15.3)	0.45 (12.7)			
Core Bypass	0.44 (12.4)	0.44 (12.4)			
Lower Plenum	0.81 (22.8)	0.81 (22.8)			
Riser	1.64 (46.4)	1.64 (46.4)			
Upper Plenum	1.46 (41.3)	1.26 (35.6)			
Upper Head	1.90 (53.8)	0.0 (0.0)			
CMTs	10.1 (286)	0.65 (18.3)			
Accumulator	10.1 (286)	0.0 (0.0)			
IRWST Injection Line	0.18 (5.1)	0.18 (5.1)			
TOTAL INVENTORY					[] (a,b,c)
Water Injected from One IRWST During Test					
IRWST Injection	DP (psi)	Area (in. ²)		Mass (lbm)	
	[] (a,b,c)	1007.5		[] (a,b,c)	

**TABLE 4.2.2-4
MASS BALANCE FOR TEST S00303**

	Starting Inventory (lbm)	Ending Inventory (lbm)
Total Primary System	[]] (a,b,c)
IRWST Injection		
Break		
ADS-1, -2, -3		
ADS-4		
TOTAL	[]] (a,b,c)
Ending Inventory/Starting Inventory (lbm)		[] (a,b,c)
Ending Inventory/Starting Inventory (%)		100.3

The following figures have been intentionally deleted
from this document due to their proprietary nature.

**TEST S00303 PLOT PACKAGE
CHANNEL LIST BY COMPONENT**

COMPONENT	CHANNEL	UNITS	PLOT	COMMENT
ACCA	F_A20E	lbm/sec.	39	
ACCA	L_A20E	ft.	34	
ACCB	F_B20E	lbm/sec.	39	
ACCB	L_B20E	ft.	34	
ADS 1, 2, & 3	IF30FLW	lbm/sec.	44	Flow rate derived from 1F030P
ADS 1, 2, & 3	IF030P	lbm	43	Catch tank
ADS 4 & SG	IF40FLW	lbm/sec.	44	Flow rate derived from 1F040P
ADS 4 & SG	IF040P	lbm	43	Catch tank
ANNDC	DP-A021P	psi	24	To cold leg-A1
ANNDC	DP-A022P	psi	25	To cold leg-A2
ANNDC	DP-B021P	psi	26	To cold leg-B1
ANNDC	DP-B022P	psi	27	To cold leg-B2
BREAK LINE	IF05FLW	lbm/sec.	44	Flow rate derived from 1F005P
BREAK LINE	IF005P	lbm	43	Catch tank
CLA	DP-A001P	psi	24	To cold leg-A1
CLA	DP-A002P	psi	25	To cold leg-A2
CLA	DP-A09P	psi	22	Pump suction
CLA	T-A10P	°F	11	Steam generator outlet
CLA1	F_A01P	lbm/sec.	36	
CLA1	T-A021PL	°F	13	Downcomer inlet
CLA1	T-A11P	°F	11	Pump outlet
CLA2	F_A02P	lbm/sec.	36	
CLA2	T-A022PL	°F	13	Downcomer inlet
CLB	DP-B001P	psi	26	To cold leg-B1

TEST DATA PLOT PACKAGE
CHANNEL LIST BY COMPONENT (Cont.)

COMPONENT	CHANNEL	UNITS	PLOT	COMMENT
CLB	DP-B002P	psi	27	To cold leg-B2
CLB	DP-B09P	psi	23	Pump suction
CLB	T-B10P	°F	12	Steam generator outlet
CLB1	F_B01P	lbm/sec.	36	
CLB1	T-B021PL	°F	14	Downcomer inlet
CLB1	T-B11P	°F	12	Pump outlet
CLB2	F_B02P	lbm/sec.	36	
CLB2	T-B022PL	°F	14	Downcomer inlet
CMTA	F_A40E	lbm/sec.	38	
CMTA	L_A40E	ft.	33	
CMTA	T-A401E	°F	15	Top (242.25 in.)
CMTA	T-A403E	°F	15	216.75 in.
CMTA	T-A405E	°F	15	191.25 in.
CMTA	T-A407E	°F	15	165.75 in.
CMTA	T-A409E	°F	15	140.25 in.
CMTA	T-A411E	°F	15	114.75 in.
CMTA	T-A413E	°F	15	89.25 in.
CMTA	T-A415E	°F	15	63.75 in.
CMTA	T-A417E	°F	15	38.25 in.
CMTA	T-A420E	°F	15	Bottom (0 in.)
CMTB	F_B40E	lbm/sec.	38	
CMTB	L_B40E	ft.	33	
CMTB	T-B401E	°F	16	Top (242.25 in.)
CMTB	T-B403E	°F	16	216.75 in.
CMTB	T-B405E	°F	16	191.25 in.
CMTB	T-B407E	°F	16	165.75 in.
CMTB	T-B409E	°F	16	140.25 in.
CMTB	T-B411E	°F	16	114.75 in.
CMTB	T-B413E	°F	16	89.25 in.

**TEST DATA PLOT PACKAGE
CHANNEL LIST BY COMPONENT (Cont.)**

COMPONENT	CHANNEL	UNITS	PLOT	COMMENT
CMTB	T-B415E	°F	16	63.75 in.
CMTB	T-B417E	°F	16	38.25 in.
CMTB	T-B420E	°F	16	Bottom (0 in.)
CVCS	F-001A	psi	42	
DVIA	T-A00E	°F	13	
DVIB	T-B00E	°F	14	
HLA	DP-A04P	psi	20	
HLA	T-A03PL	°F	5	Vertical, near power channel
HLA	T-A03PO	°F	5	Horizontal, near power channel
HLA	T-A04P	°F	5	Near steam generator inlet
HLB	DP-B04P	psi	21	
HLB	T-B03PL	°F	6	Vertical, near power channel
HLB	T-B03PO	°F	6	Horizontal, near power channel
HLB	T-B04P	°F	6	Near steam generator inlet
IRWST	F_A60E	lbm/sec.	40	F_A61E for S00303
IRWST	F_B60E	lbm/sec.	40	F_B61E for S00303
IRWST	L_060E	ft	32	
IRWST	T-061E	°F	17	Bottom
IRWST	T-062E	°F	17	Below middle
IRWST	T-063E	°F	17	Middle
IRWST	T-064E	°F	17	Above middle
IRWST	T-065E	°F	17	Top
PC	W_00P	kW	1	
PC-HB	L_000P	ft	30	Heater bundle
PC-HR	TW018P20	°F	3	Heater rod
PC-HR	TW018P48	°F	3	Heater rod
PC-HR	TW019P82	°F	3	Heater rod
PC-HR	TW020P24	°F	3	Heater rod
PC-HR	TW020P87	°F	3	Heater rod

TEST DATA PLOT PACKAGE
CHANNEL LIST BY COMPONENT (Cont.)

COMPONENT	CHANNEL	UNITS	PLOT	COMMENT
PC-UH	T-016P	°F	4	Upper head
PC-UP	L_A15P	ft.	30	Lower-upper plenum
PC-UP	L_A16P	ft.	31	Upper-upper plenum
PC-UP	T-015P	°F	4	Upper plenum
PC-UH	L_017P	ft.	31	Upper head
PC-UP	L_A14P	ft.	31	Above top of the active fuel
PRHR	DP-A81AE	psi	29	Supply line inverted U-tube
PRHR	DP-A81BE	psi	29	Supply line inverted U-tube
PRHR	DP-A81E	psi	28	Supply line
PRHR	DP-A82E	psi	28	Heat exchanger
PRHR	DP-A83E	psi	28	Return line
PRHR	F_A80E	lbm/sec.	37	Return line
PRHR	T-A82E	°F	19	Inlet
PRHR	T-A83E	°F	19	Exit
PRZ	L_010P	ft.	32	
PRZ	P-027P	psia	2	
PRZ	T-026P	°F	18	487 in.
SGA	DP-A05P	psi	20	Hot side
SGA	DP-A06P	psi	20	Hot side
SGA	DP-A07P	psi	22	Cold side
SGA	DP-A08P	psi	22	Cold side
SGA	F_A01S	lbm/sec.	41	Main feed
SGA	F_A20A	lbm/sec.	41	Secondary feed
SGA	L_A10S	ft.	35	Overall level
SGA	P-A04S	psia	2	Secondary system
SGA	T-A01S	°F	10	MFW-A
SGA	T-A05P	°F	7	Hot side
SGA	T-A05S	°F	9	Hot side - riser
SGA	T-A06P	°F	7	Hot side

**TEST DATA PLOT PACKAGE
CHANNEL LIST BY COMPONENT (Cont.)**

COMPONENT	CHANNEL	UNITS	PLOT	COMMENT
SGA	T-A08P	°F	11	Cold side
SGA	TW-A06S	°F	7	Hot side
SGB	DP-B05P	psi	21	Hot side
SGB	DP-B06P	psi	21	Hot side
SGB	DP-B07P	psi	23	Cold side
SGB	DP-B08P	psi	23	Cold side
SGB	F_B01S	lbm/sec.	41	Main feed
SGB	F_B20A	lbm/sec.	41	Secondary feed
SGB	L_B10S	ft.	35	Overall level
SGB	P-B04S	psia	2	Secondary system
SGB	T-B01S	°F	10	MFW-B
SGB	T-B05P	°F	8	Hot side
SGB	T-B05S	°F	9	Hot side - riser
SGB	T-B06P	°F	8	Hot side
SGB	T-B07P	°F	8	U-tube top
SGB	T-B08P	°F	12	Cold side
SGB	TW-B06S	°F	8	Hot side
SL	T-020P	°F	18	Surge line near pressurizer
TDC	DP-001P	psi	25,26	Top
TDC	DP-002P	psi	24,25,26,27	Bottom
TDC	T-001PL	°F	13,14	Top
TDC	T-003P	°F	4,13,14	Bottom
TSAT-PRZ	n/a	°F	18,19	Based on P-027P
TSAT-UH	n/a	°F	4	Based on P-017P

The data plots are found in the proprietary version of this document.

4.2.3 Two-In. Cold-Leg Break without Nonsafety Systems (S01703)—Repeat of S00303

Matrix test S01703 was a repeat of test S00303 and was performed to determine the repeatability of the SPES-2 facility response. Test S00303 was the first matrix test to be performed, and test S01703 was performed at the end of the matrix tests.

Matrix test S01703 simulated a 2-in. break in the bottom of cold leg-B2. The test began with the initiation of the break in cold leg-B2, which was the cold leg with the CMT-B pressure balance line connection. The break location just downstream from the cold leg to core makeup tank (CMT) balance line connection. This test was performed without any nonsafety systems (chemical and volume control system [CVCS] makeup pumps, steam generator startup feedwater [SFW] pumps and normal residual heat removal system [NRHR] pumps) operating.

Results are provided in the data plot package at the end of this section. The sequence of events for S01703 is listed in Table 4.2.3-1.

The AP600 SPES-2 test were marked by distinctly different phases. These phases were characterized by the rate at which the primary system pressure decreased and the thermal-hydraulic phenomena occurring within the primary and safety systems. The different phases selected for purpose of detailed evaluation of this LOCA are shown in Figure 4.2.3-1 and are as follows: 4.

- Initial depressurization phase (IDP)—Point 1 to 2
- Pressure decay phase (PDP)—Point 2 to 3
- Automatic depressurization system (ADS) phase—Point 3 to 4
- Post-automatic depressurization system (post-ADS) phase—Point 4 to 5

Overall Event Observations

Since this is a repeat of test S00303 that has already been evaluated in detail (in Section 4.2.2), only notable differences in the system response and behavior are discussed for test S01703. Most of those which are apparent can be explained as minor differences in initial conditions for the test and as a difference in the amount of mass discharged from the break.

Figure 4.2.3-1 shows the primary system pressure during test S01703 (as measured at the top of the pressurizer), with selected component actuations and plant responses shown in relation to the primary system pressure. A detailed comparison of the system pressures for these two tests is shown in Figures 4.2.3-2 and 4.2.3-3. In the first figure, the initial depressurization phase (IDP) and the beginning of the pressure decay phase (PDP) are compared for the two tests. The two tests are almost identical in terms of absolute pressure and timing of the system responses. A slightly earlier reactor coolant pump (RCP) trip for S01703 caused a slight time shift in the pressure increase that follows the trip and resulting decrease in flow rate through the power channel. At the start of the PDP, both the overall pressure and the small pressure oscillations were essentially identical for the two.

Figure 4.2.3-3 compares the end of the PDP, the ADS phase in its entirety, and the start of the post-ADS phase. The PDPs ended at identical pressures and times in both tests. There was a slight difference in the pressure decay following ADS—test S01703 followed a slightly higher curve for most of the ADS phase. Also, the pressure increase associated with the end of the accumulator discharge (water splashed into the steam generator U-tubes and flashed, causing a system pressure increase) occurred approximately []^(a,b,c) seconds earlier for test S01703. For the rest of the ADS and post-ADS phases, the pressures were identical.

Figure 4.2.3-4 compares the power channel upper plenum temperature for both tests to the end of accumulator discharge. There was no notable temperature difference during the IDP and PDP. During the ADS phase—the upper plenum in test S01703 was at a slightly higher temperature during the accumulator discharge (which agrees with the higher system pressure observed for S01703 in Figure 4.2.3-3). Figure 4.2.3-5 shows that in both tests, the upper plenum temperature rose to the saturation temperature after the accumulators emptied at identical times. Since ADS-4 occurred approximately []^(a,b,c) seconds later for the S01703 test, the effect of the IRWST injection flow began decreasing the upper plenum temperature 50 seconds later than for test S00303.

Figure 4.2.3-6 shows the power channel lower plenum temperature was approximately 10°F cooler for test S01703 during and after the accumulator injection. This was due to the fact that the accumulator and IRWST initial water temperatures were []^(a,b,c)°F cooler for test S01703. This is attributed to the difference in ambient conditions. Figure 4.2.3-7 shows that the IRWST injection occurred later for test S01703, but that the magnitude of the flows were similar.

Figure 4.2.3-8 shows that the annular downcomer drained earlier in the post-ADS phase for test S00303, but that the refill was initiated at identical times. Figure 4.2.3-9 shows that the levels dropped to nearly the same elevation in the tubular downcomer during the post-ADS phase. Test S01703 reached a minimum level of []^(a,b,c) ft. at []^(a,b,c) seconds, and test S00303 reached -6.2 ft. at 2050 seconds. In both tests, the tubular downcomer was completely refilled at identical times. Figure 4.2.3-10 shows that the minimum collapsed levels in the rod bundle after the accumulator injection, were essentially identical (bundle void fraction calculated to be []^(a,b,c) for test S00303 and 28 percent for test S01703). Similarly, the level change versus time and the minimum water levels in the tubular downcomer were essentially identical in both tests.

These figures show that the two tests were similar, especially considering the complexity of this test facility and the differences in the initial conditions. This comparison shows that the test facility and instrumentation had a high level of repeatability and that no noticeable change in response could be attributed to changes in the test facility from the first test (S00303) to the last test (S01703).

Table 5.1-1 in Section 5.0 provides comparison of key parameters for the two tests.

Discussion of Event Phases

Since test S01703 is a repeat of test S00303 and is essentially identical in system response to that event, further discussion of event phases is unnecessary. For a detailed discussion of the system responses during the 2-in. cold-leg break event, please refer to Section 4.2.2 of this report.

Component Responses

Since test S01703 is a repeat of test S00303 and the component responses are essentially identical, further discussion of these responses is unnecessary. For a detailed discussion of the component responses during the 2-in. cold-leg break event, please refer to Section 4.2.2 of this report.

Mass Discharge and Mass Balance

As shown in Table 5.1-1 in Section 5.0, there were differences in mass discharge between test S01703 and test S00303. Part of the difference was because test S01703 extended beyond the time when test S00303 ended. For this reason, numbers for test S01703 comparable to the end of test S00303 are given (bracket) in the table.

The catch tank weight measurements for the break flow for the ADS-1, -2, and -3 flows and for the ADS-4 flow are shown in data plot 43. The break flow, which started when the LOCA was initiated, decreased as the system pressure dropped during the IDP and the PDP. When ADS occurred, the cold legs emptied so that subsequent discharge from the break was primarily saturated steam until the IRWST injection refilled the cold leg after ADS-4. The total measured mass discharge from the break was approximately 10 percent less for test S01703 than for test S00303. The discharge from ADS-1, -2, and -3 was stable throughout the accumulator injection and increased temporarily when the injection ended. When ADS-4 occurred, the fluid discharge from the top of the pressurizer ended, and the fluid discharge from ADS-4 began. The ADS-4 fluid discharge was relatively stable and continued until the end of the test. For ADS-1, -2, and -3 and for ADS-4, the discharged mass for test S01703 was similar to test S00303.

The mass balance results for test S01703 were calculated based on the water inventory before and after the test. Table 4.2.3-2 gives a detailed listing of the inventories of water in the various components before the test. Table 4.2.3-3 lists the inventories after the test and the amount of water injected into the vessel from the IRWST. The water level in the vessel was determined by the DP-B16P measurement to be []^(a,b,c) above the hot leg centerline at the end of the test. Table 4.2.3-4 compares the mass balance for the system before and after the test and shows good agreement between the measurements (1.5 percent difference).

**TABLE 4.2.3-1
SEQUENCE OF EVENTS FOR TEST S01703**

Event	Specified	Instrument Channel	Actual Time (Sec.)
Break Opens	0	Z_001BC	
Reactor Trip Signal "R"	P = 1800 psia	P-027P	
MSL IV Closure	R Signal + 2s	Z_A04SO, F_A04S	
		Z_B04SO, F_B04S	
SCRAM	R signal + 5.7s		
S Signal	P = 1700 psia	P-027P	
CMT IV Opening	S Signal + 2s	Z_A040EC, F-A40E	
		Z_B040EC, F-B40E	
PRHR HX Actuation	S Signal + 2s	Z_A81EC, F_A80E	
MFWIV Closure	S signal + 2S	Z_B02S0, F_B01S	
		Z_A02S0, F_A01S	
Reactor Coolant Pumps Tripped	S signal + 16.2s	DP-A00P	
		DP-B00P	
Accumulators	P-027P = 710 psia	F_A20E	
		F_B20E	
ADS 1	CMT Level 67%	L_B40E	
		+30s	Z_001PC
ADS 2	CMT Level 67%	L_B40E	
		+125s	Z_002PC
ADS 3	CMT Level 67%	L_B40E	
		+245s	Z_003PC
ADS 4 A/B	CMT Level 20%	L_B40E	
		+60s	Z_004PC, F-040P
IRWST Injection	P-027P = 26 psia	F_A60E	
		F_B60E	

(a,b,c)

**TABLE 4.2.3-2
WATER INVENTORY BEFORE TEST S01703**

Component	Volume (ft.³)/(l)	Net Vol (ft.³)/(l)	Temp (°F)	Relative Density	Mass (lbm) (a,b,c)
Loops	8.97 ft. ³ (254.0 l)	8.97 ft. ³ (254.0 l)			
Pressurizer	3.37 ft. ³ (95.4 l)	1.87 ft. ³ (53.0 l)			
Surge Line	0.34 ft. ³ (9.6 l)	0.34 ft. ³ (9.6 l)			
Tubular Downcomer	1.38 ft. ³ (39.1 l)	1.38 ft. ³ (39.1 l)			
Annular Downcomer + High-Pressure Bypass	0.54 ft. ³ (15.3 l)	0.54 ft. ³ (15.3 l)			
Core Bypass	0.44 ft. ³ (12.4 l)	0.44 ft. ³ (12.4 l)			
Lower Plenum	0.81 ft. ³ (22.8 l)	0.81 ft. ³ (22.8 l)			
Riser	1.64 ft. ³ (46.4 l)	1.64 ft. ³ (46.4 l)			
Upper Plenum	1.46 ft. ³ (41.3 l)	1.46 ft. ³ (41.3 l)			
Upper Head	1.90 ft. ³ (53.8 l)	1.90 ft. ³ (53.8 l)			
CMT-A	5.05 ft. ³ (143.0 l)	5.05 ft. ³ (143.0 l)			
CMT-B	5.05 ft. ³ (143.0 l)	5.05 ft. ³ (143.0 l)			
Accumulator-A	5.05 ft. ³ (143.0 l)	3.93 ft. ³ (111.2 l)			
Accumulator-B	5.05 ft. ³ (143.0 l)	3.90 ft. ³ (110.4 l)			
IRWST Injection Line	0.18 ft. ³ (5.1 l)	0.18 ft. ³ (5.1 l)			
TOTAL INVENTORY					

**TABLE 4.2.3-3
WATER INVENTORY AFTER S01703**

Water level as measured by DP-B16P (-0.68 psi) was 19.2 in. (478 mm) above hot leg

Component	Volume (ft. ³)/(l)	Net Vol (ft. ³)/(l)	Temp (°F)	Relative Density	Mass (lbm)
Loops	8.97 ft. ³ (254.0 l)	1.33 ft. ³ (37.6 l)			
Pressurizer	3.37 ft. ³ (95.4 l)	0.05 ft. ³ (1.4 l)			
Surge Line	0.34 ft. ³ (9.6 l)	0.34 ft. ³ (9.6 l)			
Tubular Downcomer	1.38 ft. ³ (39.1 l)	1.38 ft. ³ (39.1 l)			
Annular Downcomer + High-Pressure Bypass	0.54 ft. ³ (15.3 l)	0.54 ft. ³ (15.3 l)			
Core Bypass	0.44 ft. ³ (12.4 l)	0.44 ft. ³ (12.4 l)			
Lower Plenum	0.81 ft. ³ (22.8 l)	0.81 ft. ³ (22.8 l)			
Riser	1.64 ft. ³ (46.4 l)	1.64 ft. ³ (46.4 l)			
Upper Plenum	1.46 ft. ³ (41.3 l)	1.34 ft. ³ (37.9 l)			
Upper Head	1.90 ft. ³ (53.8 l)	0.0 ft. ³ (0.0 l)			
CMT-A	5.05 ft. ³ (143.0 l)	0.44 ft. ³ (12.6 l)			
CMT-B	5.05 ft. ³ (143.0 l)	0.25 ft. ³ (7.0 l)			
Accumulator-A	5.05 ft. ³ (143.0 l)	0.0 ft. ³ (0.0 l)			
Accumulator-B	5.05 ft. ³ (143.0 l)	0.0 ft. ³ (0.0 l)			
IRWST Injection Line	0.18 ft. ³ (5.1 l)	0.18 ft. ³ (5.1 l)			
TOTAL INVENTORY					

(a,b,c)

WATER INJECTED FROM THE IRWST DURING EVENT

IRWST Injection	dP (psi)	Area (in ²)	Mass (lbm)
Note 1	1.15	1007.5	[] (a,b,c)

**TABLE 4.2.3-4
MASS BALANCE FOR TEST S01703**

PRIMARY SYSTEM		
	Starting Inventory (lbm)	Ending Inventory (lbm)
Total Primary System		
IRWST Injection During Transient		
Break Catch Tank		
ADS-1,-2,-3 Catch Tank		
ADS-4/Steam Generator Catch Tank		
TOTAL		
Ending Inventory/Starting Inventory (lbm)		
Ending Inventory/Starting Inventory (%)		

(a,b,c)

The following figures have been intentionally deleted
from this document due to their proprietary nature.

**TEST S01703 PLOT PACKAGE
CHANNEL LIST BY COMPONENT**

COMPONENT	CHANNEL	UNITS	PLOT	COMMENT
ACCA	F_A20E	lbm/sec.	39	
ACCA	L_A20E	ft.	34	
ACCB	F_B20E	lbm/sec.	39	
ACCB	L_B20E	ft.	34	
ADS 1, 2, & 3	IF30f1w	lbm/sec.	44	Flow rate derived from 1F030P
ADS 1, 2, & 3	IF030P	lbm	43	Catch tank
ADS 4 & SG	IF40f1w	lbm/sec.	44	Flow rate derived from 1F040P
ADS 4 & SG	IF040P	lbm	43	Catch tank
ANNDNC	DP-A021P	psi	24	To cold leg-A1
ANNDNC	DP-A022P	psi	25	To cold leg-A2
ANNDNC	DP-B021P	psi	26	To cold leg-B1
ANNDNC	DP-B022P	psi	27	To cold leg-B2
BREAK LINE	IF05f1w	lbm/sec.	44	Flow rate derived from 1F005P
BREAK LINE	IF005P	lbm	43	Catch tank
CLA	DP-A001P	psi	24	To cold leg-A1
CLA	DP-A002P	psi	25	To cold leg-A2
CLA	DP-A09P	psi	22	Pump suction
CLA	T-A10P	°F	11	Steam generator outlet
CLA1	F-A01P	lbm/sec.	36	
CLA1	T-A021PL	°F	13	Downcomer inlet
CLA1	T-A11P	°F	11	Pump outlet
CLA2	F_A02P	lbm/sec.	36	
CLA2	T-A022PL	°F	13	Downcomer inlet
CLB	DP-B001P	psi	26	To cold leg-B1
CLB	DP-B002P	psi	27	To cold leg-B2
CLB	DP-B09P	psi	23	Pump suction
CLB	T-B10P	°F	12	Steam generator outlet
CLB1	F_B01P	lbm/sec.	36	
CLB1	T-B021PL	°F	14	Downcomer inlet
CLB1	T-B11P	°F	12	Pump outlet

TEST S01703 PLOT PACKAGE
CHANNEL LIST BY COMPONENT (Cont.)

COMPONENT	CHANNEL	UNITS	PLOT	COMMENT
CLB2	F-B02P	lbm/sec.	36	
CLB2	T-B022PL	°F	14	Downcomer inlet
CMTA	F_A40E	lbm/sec.	38	
CMTA	L_A40E	ft.	33	
CMTA	T-A401E	°F	15	Top (242.25 in.)
CMTA	T-A403E	°F	15	216.75 in.
CMTA	T-A405E	°F	15	191.25 in.
CMTA	T-A407E	°F	15	165.75 in.
CMTA	T-A409E	°F	15	140.25 in.
CMTA	T-A411E	°F	15	114.75 in.
CMTA	T-A413E	°F	15	89.25 in.
CMTA	T-A415E	°F	15	63.75 in.
CMTA	T-A417E	°F	15	38.25 in.
CMTA	T-A420E	°F	15	Bottom (0 in.)
CMTB	F_B40E	lbm/sec.	38	
CMTB	L_B40E	ft.	33	
CMTB	T-B401E	°F	16	Top (242.25 in.)
CMTB	T-B403E	°F	16	216.75 in.
CMTB	T-B405E	°F	16	191.25 in.
CMTB	T-B407E	°F	16	165.75 in.
CMTB	T-B409E	°F	16	140.25 in.
CMTB	T-B411E	°F	16	114.75 in.
CMTB	T-B413E	°F	16	89.25 in.
CMTB	T-B415E	°F	16	63.75 in.
CMTB	T-B417E	°F	16	38.25 in.
CMTB	T-B420E	°F	16	Bottom (0 in.)
CVCS	F-001A	psi	42	
DVIA	T-A00E	°F	13	
DVIB	T-B00E	°F	14	
HLA	DP-A04P	psi	20	

**TEST S01703 PLOT PACKAGE
CHANNEL LIST BY COMPONENT (Cont.)**

COMPONENT	CHANNEL	UNITS	PLOT	COMMENT
HLA	T-A03PL	°F	5	Vertical, near power channel
HLA	T-A03PO	°F	5	Horizontal, near power channel
HLA	T-A04P	°F	5	Near steam generator inlet
HLB	DP-B04P	psi	21	
HLB	T-B03PL	°F	6	Vertical, near power channel
HLB	T-B03PO	°F	6	Horizontal, near power channel
HLB	T-B04P	°F	6	Near steam generator inlet
IRWST	F_A60E	lbm/sec.	40	
IRWST	F_B60E	lbm/sec.	40	
IRWST	L_060E	ft.	32	
IRWST	T_061E	°F	17	Bottom Tank
IRWST	T_062E	°F	17	Bottom Tube
IRWST	T_062EA	°F	17	Bottom Tube
IRWST	T_063E	°F	17	Middle Tube
IRWST	T_063EA	°F	17	Middle Tube
IRWST	T_064E	°F	17	Top Tube
IRWST	T_064E(-3)	°F	17	Top Tube (average of 3)
IRWST	T-065E(-4)	°F	17	Top Tank (average of 4)
NRHRA	F-A00E	psi	42	
NRHRB	F-B00E	psi	42	
PC	W_00P	kW	1	
PC-HB	L_000P	ft.	30	Heater bundle
PC-HR	TW018P20	F	3	Heater rod
PC-HR	TW018P48	F	3	Heater rod
PC-HR	TW020P87	°F	3	Heater rod
PC-UH	T-016P	°F	4	Upper head
PC-UP	L_A15P	ft.	30	Bottom of upper plenum
PC-UP	L_A16P	ft.	31	Top of upper plenum
PC-UP	T-015P	°F	4	Upper plenum
PC_UH	L_017P	ft.	31	Upper head
PC_UP	L_A14P	ft.	31	Above top of the active fuel

**TEST S01703 PLOT PACKAGE
CHANNEL LIST BY COMPONENT (Cont.)**

COMPONENT	CHANNEL	UNITS	PLOT	COMMENT
PRHR	DP-A81AE	psi	29	Supply line inverted U-tube
PRHR	DP-A81BE	psi	29	Supply line inverted U-tube
PRHR	DP-A81E	psi	28	Supply line
PRHR	DP-A82E	psi	28	Heat exchanger
PRHR	DP-A83E	psi	28	Return line
PRHR	F_A80E	lbm/sec.	37	Return line
PRHR	T-A82E	°F	19	Inlet
PRHR	T-A83E	°F	19	Exit
PRZ	L_010P	ft.	32	
PRZ	P-027P	psia	2	
PRZ	T-026P	°F	18	487 in.
SGA	DP-A05P	psi	20	Hot side
SGA	DP-A06P	psi	20	Hot side
SGA	DP-A07P	psi	22	Cold side
SGA	DP-A08P	psi	22	Cold side
SGA	F_A01S	lbm/sec.	41	Main SLA feed
SGA	F_A20A	lbm/sec.	41	Secondary SLA feed
SGA	L_A10S	ft.	35	Overall level
SGA	P-A04S	psia	2	Secondary system
SGA	T-A01S	°F	10	MFW-A
SGA	T-A05P	°F	7	Hot side
SGA	T-A05S	°F	9	Hot side - riser
SGA	T-A06P	°F	7	Hot side
SGA	T-A08P	°F	11	Cold side
SGA	TW-A06S	°F	7	Hot side
SGB	DP-B05P	psi	21	Hot side
SGB	DP-B06P	psi	21	Hot side
SGB	DP-B07P	psi	23	Cold side
SGB	DP-B08P	psi	23	Cold side
SGB	F_B01S	lbm/sec.	41	Main SLB feed

**TEST S01703 PLOT PACKAGE
CHANNEL LIST BY COMPONENT (Cont.)**

COMPONENT	CHANNEL	UNITS	PLOT	COMMENT
SGB	F_B20A	lbm/sec.	41	Secondary SLB feed
SGB	L_B10S	ft.	35	Overall level
SGB	P-B04S	psia	2	Secondary system
SGB	T-B01S	°F	10	MFW-B
SGB	T-B05P	°F	8	Hot side
SGB	T-B05S	°F	9	Hot side - riser
SGB	T-B06P	°F	8	Hot side
SGB	T-B07P	°F	8	U-tube top
SGB	T-B08P	°F	12	Cold side
SGB	TW-B06S	°F	8	Hot side
SL	T-020P	°F	18	Surge line near pressurizer
TDC	DP-001P	psi	25,26	Top
TDC	DP-002P	psi	24,25,26,27	Bottom
TDC	T-001PL	°F	13,14	Top
TDC	T-003P	°F	13,14	Bottom
TSAT-PRZ		°F	18	Based on P-027P
UH-TSAT		°F	4	Based on P-017P

The data plots are found in the proprietary version of this document.

4.2.4 Two-In. Cold Leg Break with Nonsafety Systems (S00504)

This matrix test simulated a 2-in. break in the bottom of cold leg-B2. The test began with the initiation of the break in cold leg-B2, which is the cold leg with the CMT-B pressure balance line connection. The break location was just downstream from the cold leg to the core makeup tank (CMT) balance line connection. This test was performed with nonsafety systems, chemical and volume control system (CVCS) makeup pumps, steam generator startup feedwater (SFW) pumps, and normal residual heat removal system (NRHR) pumps operating.

Results are provided in the data plot package at the end of this section. The sequence of events for S00504 is listed in Table 4.2.4-1.

The following phases were selected for detailed evaluation of this LOCA and are shown in Figure 4.2.4-1:

- Initial depressurization phase (IDP)—Point 1 to 2
- Pressure decay phase (PDP)—Point 2 to 3
- Automatic depressurization system (ADS) phase—Point 3 to 4

Overall Test Observations

Figure 4.2.4-1 shows facility primary system pressure during test S00504 (as measured at the top of the pressurizer) with selected component actuations and plant responses shown in relation to primary system pressure.

The IDP began with the initiation of the break, which resulted in a rapid reduction in pressure. The reactor trip (R) signal initiated at 1800 psia, and the safety systems actuation (S) signal initiated at 1700 psia. The R and the S signals initiated the following actions:

- Decay power simulation (with heat loss compensation).
- Main steamline isolation valves (MSLIVs) closed.
- Main feedwater isolation valve (MFWIV) closed.
- CMT injection line isolation valves opened.
- Passive residual heat removal (PRHR) return line isolation valve opened.
- Reactor coolant pumps (RCPs) turned off.

Recirculation flow through the CMTs and PRHR HX flow began immediately after their isolation valves opened. Flashing occurred in the rod bundle and upper-upper plenum regions of the power channel due to the rapid decrease in primary pressure to the fluid saturation pressure. The measured fluid level dropped to the hot-leg elevation. This flashing on the hot-leg side of the primary system stopped the rapid drop in primary system pressure. When the RCPs were shut off (at []^(a,b,c) seconds), the flow through the rod bundle began to oscillate (with an approximately []^(a,b,c) second

period). This was observed as oscillations in the rod bundle and upper-plenum collapsed liquid level, upper-plenum fluid temperature, and system pressure.

During the initial stages of the PDP, the rod bundle steam fraction increased, as evidenced by decreasing water levels in the lower-upper plenum and the hot legs. Hot leg-B had a steam fraction very close to that observed at the outlet of the rod bundle. The steam fraction in hot leg-A was much lower due to the selective removal of steam from the hot leg into the PRHR HX inlet line.

Two-phase flow in the hot legs initiated draining of the steam generator U-tubes, as steam from the two-phase mixture collected in the top of the U-tubes. This stopped the primary system flow through the steam generators so that the power channel flow was composed predominantly of the flow through the PRHR HX. The level oscillations in the rod bundle and in the upper plenum stopped when the flow through the steam generators stopped. The steam generator U-tubes began to drain at approximately []^(a,b,c) seconds after break initiation.

The two-phase flow through the rod bundle (data plots 30 and 31) entered the hot leg from the lower-upper plenum and flowed through the PRHR heat exchanger (HX). The two-phase flow through the PRHR HX, consisting of alternating slugs of steam and water, had an average integrated steam fraction significantly greater than the mixture in the upper plenum. The average steam fraction at the PRHR HX inlet was as high as []^(a,b,c) percent, which enhanced the PRHR HX heat removal from the primary system, as compared to its heat removal capability with single-phase saturated or subcooled water. When the primary system flow stabilized after the initial flow oscillations, a PRHR HX heat removal rate of 142 kW was calculated. This calculation was based on the average steam fraction at the PRHR HX inlet (as calculated from the dP instrument readings in data plot 29), the average return flow rate, the inlet and outlet temperatures, and the pressure. This calculation assumes a slip coefficient of 1 between steam and water and may therefore give slightly lower values than the actual heat transfer. It should be used only for test-to-test comparison.

When the loop-B cold legs had partially emptied, the CMTs transitioned from the recirculation mode to draindown mode of operation. This increased their injection flow rate and the rate of system pressure decay. This occurred at approximately []^(a,b,c) seconds for CMT-B and []^(a,b,c) seconds for CMT-A. When system pressure dropped to the saturation pressure for the upper head fluid, the upper head began to drain (at 400 seconds).

During the first []^(a,b,c) seconds of this LOCA (until ADS-1), []^(a,b,c) lbm of water were expelled through the break. This drained the pressurizer, the steam generator U-tubes, the power channel upper-upper head, most of the cold legs, and approximately []^(a,b,c) percent of the CMTs. The heater rod power had decreased to approximately 240 kW. This rod bundle power consisted of 90 kW of decay power and 150 kW for facility heat loss compensation. The break flow was decreasing, indicating that cold leg-B2 was almost empty.

The ADS phase began with the actuation of ADS-1 at []^(a,b,c) seconds. ADS-2 and -3 occurred within the next []^(a,b,c) seconds. The heat loss compensation was terminated when ADS-1 occurred and the rod bundle power was reduced to approximately 90 kW.

The ADS actuation increased the rate of primary system depressurization and resulted in high injection flow rate from the accumulators. The rapid injection of cold fluid from the accumulators ([]^(a,b,c) seconds) refilled the rod bundle region, upper-upper plenum, hot legs, and the pressurizer with subcooled water. When the accumulator discharge ended, the flow through the rod bundle decreased but included the injection flow from the CMTs, the PRHR HX return flow, and pumped flow from the CVCS and NRHR. Significant boiling was not detected in the rod bundle for the rest of the test. The water temperature in the upper-upper plenum did reach saturation temperature and its water level again decreased to the hot-leg elevation. When the NRHR flow subcooled the rod bundle and lower-upper plenum, the steam in the upper-upper plenum was condensed and it refilled again.

The mass flow rate through the break decreased after ADS actuation as primary pressure decreased and cold leg-B2 emptied. Break flow then increased at []^(a,b,c) seconds when injection flow supplied by the CVCS and NRHR refilled the loop-B cold legs. The PRHR HX flow stopped at approximately 1700 seconds. During the ADS phase, approximately 2070 lbm of subcooled water were discharged from ADS-1, -2, and -3. This water was supplied primarily by the accumulator discharge and the continuing CVCS and NRHR flow since the CMT draindown stopped at approximately []^(a,b,c) seconds.

Subcooled water was then flowing steadily from the CVCS and NRHR into the downcomer and left the primary system through ADS-1, -2, -3 and the break. Because the CMTs never drained below 50 percent level, no ADS-4 actuation occurred in S00504.

This test demonstrated that the rod bundle was fully covered by two-phase mixture until ADS-1 actuation and by single-phase liquid during the rest of the test (data plots 30 and 31). There was no indication of an increase in heater rod temperatures due to lack of cooling (data plot 3). The operation of the CVCS and NRHR complimented the capability of the passive safety systems and terminated draindown of the CMTs preventing ADS-4 actuation.

Key parameters comparing the S00504 test with other tests are listed in Table 5-1 in Section 5.0.

Discussion of Test Transient Phases

- **Initial Depressurization Phase (0 to 170 Seconds)**

The initial depressurization phase (IDP) began with the initiation of the break (at time 0) and continued until primary system pressure reached saturation pressure of the fluid the lower-upper plenum and the hot legs (Figure 4.2.4-1). This phase included the following events: R signal at 1800 psia (decay power simulation initiated and the MSLIV closed), and S signal at 1700 psia (the MFWIV closed, the CMT injection line isolation valves opened, and the PRHR heat exchanger

return line isolation valve opened—all with a 2-second delay; and RCP coastdown started after a 16.2-second delay). See Table 4.2.4-1.

Facility Response During the IDP:

A comparison of the timing of the responses in test S00504 to the base case LOCA test S00303 shows that the R and the S signals occurred 1 second later and the RCP trip occurred 2 seconds later in S00504. From time 0 until the R signal, the primary system pressure decreased due to the expansion of the pressurizer steam volume caused by fluid loss through the break. The pressurizer partially compensated for the loss of pressure by flashing; however, it was drained at []^(a,b,c) seconds (data plot 32). The R (at 57 seconds) and the S (at 67 seconds) signals were based on pressurizer pressure only. When the R signal occurred, the MSLIV was closed, and the power was reduced to 20 percent of full power after a 5.75-second delay and began to simulate decay power after a 14.5-second delay (Table 4.2.4-1).

As a result of the reduction in the power to flow ratio, the rod bundle ΔT decreased and the upper-plenum temperature dropped toward the cold-leg temperature of ([]^(a,b,c)). System pressure was controlled at the hot-leg/upper-plenum fluid saturation pressure and decreased to []^(a,b,c) psia at approximately []^(a,b,c) seconds (Figure 4.2.4-2). When the RCPs were shut off (at []^(a,b,c) seconds), the rod bundle and the upper-plenum fluid temperatures increased due to the increased rod bundle power/flow ratio. System pressure increased temporarily until the decreasing decay power and the decreasing lower-plenum temperature (due to CMT injecting cold fluid into the downcomer) started reducing the upper-plenum temperature. The primary system pressure decrease resulted from the balance between the steam generation rate (from flashing primary fluid), the volumetric flow of liquid out of the break, and the steam condensation rate of the PRHR HX. Steam was continually being generated by boiling due to the heater power. As system pressure continued to decrease, more fluid reached its saturation pressure and began to flash. The PRHR HX flow began before the RCPs were shut off and continued by natural circulation after they were turned off (data plot 37). Primary system pressure stabilized at the saturation pressure for the bulk hot fluid in the system (approximately []^(a,b,c)). This ended the IDP.

• Pressure Decay Phase (170 to 956 Seconds)

The pressure decay phase (PDP) began when system pressure (Figure 4.2.4-1) reached saturation pressure for the bulk hot fluid in the system. The phase ended when ADS-1 was opened on low CMT level and augmented the system depressurization. This phase was characterized by a slow decrease in overall system pressure and temperature. The rod bundle power was reduced from 340 kW to 240 kW (data plot 1) during this phase. The PRHR HX provided heat removal at a rate of approximately 142 kW, and the recirculating CMTs provided an approximately 100-kW effective heat removal rate from the primary system.

The initial CMT natural circulation operating mode was followed by draindown injection when the B-loop cold legs drained (data plot 38). The U-tubes of the steam generators were completely

drained at this time (data plots 20 through 23) and did not affect the rest of the test. The accumulator injection was initiated when the primary system pressure dropped below []^(a,b,c) psia prior to ADS-1 actuation. However, the injection rate was low (less than []^(a,b,c) lbm/sec.) due to the small difference between the primary system and accumulator pressures (data plot 39).

Facility Response During the PDP:

The system response during the PDP was almost identical to that of test S00303, with the exception that ADS-1 occurred []^(a,b,c) seconds later in this test S00504.

The oscillating flow that was observed in the tubular downcomer and in the rod bundle following the RCP coastdown continued into the PDP. The flow oscillations resulted in large oscillations of the steam fraction of the two-phase mixture exiting the rod bundle and flowing into the hot legs (data plots 30 and 31). These oscillations in steam fraction had a significant effect on the thermal buoyancy head that drove the flow through the primary system at this time. The fluid steam fraction oscillations were observed through the hot leg and the steam generators (data plots 20 and 21). However, the two-phase mixture entering the steam generators left the steam generators as saturated water (data plots 24 through 27). Some of the steam was condensed in the U-tubes (the primary-side pressure was higher than the secondary-side pressure at this time, allowing some heat to be transferred to the secondary-side fluid). The remaining steam was separated from the two-phase mixture in the high point of the U-tubes due to the low velocity, which eventually caused the U-tubes to begin to drain. For steam generator-A, primary system flow continued until 210 seconds into the transient, then intermittent flow was observed through steam generator-A (plots 20 and 22). This was caused by the oscillations in the steam fraction where the buoyancy head in the hot leg was high enough to spill over the top of the U-tubes at the peaks of the oscillating buoyancy head. At approximately []^(a,b,c) seconds ([]^(a,b,c) seconds), all flow through the steam generators ended since the free-water surface in the U-tubes had fallen too low to be overcome by the buoyancy head oscillations. These oscillations were seen in temperatures and pressures throughout the primary system. When the cold-leg side of the steam generator U-tubes were completely drained (about []^(a,b,c) seconds), these oscillations stopped.

The primary system pressure decrease during the PDP began at a slow rate of []^(a,b,c) psi/sec. At approximately []^(a,b,c) seconds into the event, the primary system pressure decay rate increased to []^(a,b,c) psi/sec. This happened when the CMTs transitioned from their recirculation mode of operation to their draindown mode. This transition occurred when the B-loop cold legs partially drained and the CMT balance lines drained. This resulted in a higher CMT injection rate (Figure 4.2.4-1). The increased rate of pressure decay in the primary system was due to the increased injection rate of the cold liquid from the CMTs (occurred at different times for the two CMTs).

The CMTs began injecting cold fluid into the annular downcomer []^(a,b,c) seconds after the S signal occurred. Initially, this injection was by natural circulation at approximately 0.12 lbm/sec. through each CMT, with hot fluid flowing from the cold leg through the cold-leg balance line

(CLBL) into the top of the CMT, and cold fluid flowing from the bottom of CMT. Between []^(a,b,c) seconds (data plot 38), CMT-A transitioned to draindown mode when cold leg-B2 partially drained and subsequently the cold-leg balance line (CLBL) for CMT-A drained, and a free-water surface developed in the top of the CMT-A as the level started to drop (data plot 33). The CMT injection flow, when draindown began, increased to approximately 0.28 lbm/sec. and gradually decreased as the CMT level decreased (reducing the driving head). See data plot 38.

For CMT-B the transition from recirculation to draindown occurred at approximately []^(a,b,c) seconds (earlier than for CMT-A), and its injection flow increased to approximately []^(a,b,c) lbm/sec. and gradually decreased.

The free-liquid surfaces in the CMTs were established by steam flowing from the cold legs to the CMTs through the CLBLs. The steam flow from the cold legs condensed in the CMTs and heated the free-water surface. For CMT-A, the CMT water surface was heated by the steam to saturation temperature (data plot 15) and flashing could occur as the pressure decreased in the system.

Both the recirculation and draindown modes of CMT operation established a stable thermal gradient in the CMT water. The CMT water maintained a stable thermal stratification throughout its operation.

The accumulators began to inject fluid into annular downcomer via the DVI lines when system pressure dropped below []^(a,b,c) psia (at approximately []^(a,b,c) seconds). However, the injection rate was very low prior to ADS-1 (data plot 39).

Throughout the PDP, the PRHR removed energy from the primary system. However, the combined effect of the PRHR cooling the primary fluid and the cold injection flow from the CVCS and CMTs was sufficient to limit the steam fraction of the two-phase fluid flowing through the rod bundle and rod bundle cooling was maintained during this phase (data plots 30 and 31).

- **Automatic Depressurization System Phase ([]^(a,b,c) Seconds to End Of Test)**

The automatic depressurization system (ADS) phase began with the actuation of ADS-1 and continued until the end of the transient (Figure 4.2.4-1).

Facility Response During the ADS Phase:

With the actuation of ADS-1, followed by ADS-2 and ADS-3 within approximately []^(a,b,c) seconds, the rate of system depressurization increased from []^(a,b,c) psi/sec. at the end of the PDP to []^(a,b,c) psi/sec. at the start of the ADS phase. This rate gradually decreased as system pressure decreased.

The primary system depressurization after ADS actuation resulted in a high rate of water injection from accumulators-A and -B (data plot 39). The accumulators injected cold water into the primary system for approximately 500 seconds (from []^(a,b,c) seconds) and were then drained. The accumulator injection refilled and subcooled the rod bundle, lower-upper plenum, hot-legs, and upper-upper plenum.

When the accumulator delivery was completed, the water level in the annular downcomer only decreased to approximately []^(a,b,c) in. below the hot-leg elevation. This level then recovered due to the NRHR (and CVCS) injection flow (data plot 25). The rod bundle was essentially free from boiling after the accumulator injection (data plots 30 and 31). However, the upper-upper plenum reached saturation temperature and its water level dropped temporarily down to the hot-leg nozzle elevation until subcooled flow through the rod bundle was established and the upper-upper plenum steam volume was condensed.

The pressurizer immediately began to refill when ADS-1 was actuated and steam and water were vented from the pressurizer through the ADS (data plot 32). The pressurizer was completely filled by NRHR (and CVCS) injection. This flow was directed back to the IRWST via the ADS flow path.

Prior to the ADS phase, liquid left the primary system through the break in the cold leg. With the actuation of the ADS, liquid also left the system through the ADS from the top of the pressurizer. The mass flow through the cold-leg break slowed to a lower steady rate when the NRHR (and CVCS) flow refilled the cold legs (data plot 43) and continued to the end of the test.

- **Post-Automatic Depressurization System Phase**

Since the NRHR flow stopped CMT draindown at approximately 50 percent level and partially refilled the CMTs, no ADS-4 occurred in test S00504. Therefore the post-automatic depressurization system (post-ADS) phase did not occur, and there was no IRWST injection into the primary system.

Component Responses

- **Power Channel**

The response in the power channel during test S00504 was essentially identical to the reference test S00303 from the break initiation until the end of the accumulator discharge at approximately []^(a,b,c) seconds.

The power channel consisted of five volumes: the lower plenum, the heated rod bundle, the lower-upper plenum below the hot leg, the upper-upper plenum above the hot leg, and the upper head. When the break occurred, system pressure decreased to the R signal (1800 psia) and the S signal (1700 psia) actuation pressures. However, since the coolant in the power channel was

subcooled relative to system pressure, no boiling or flashing occurred up to this point. When the rod bundle power was reduced to 20 percent 5.75 seconds after the R signal, the temperature gradient across the rod bundle rapidly decreased due to the reduced power/flow ratio (still full flow), and the power channel outlet temperature dropped toward the lower-plenum inlet temperature (Figure 4.2.4-2). The upper-upper plenum still contained []^(a,b,c) water and began to flash when system pressure dropped below []^(a,b,c) psia. When the RCPs were shutoff (16.2 seconds after the S signal), the power/flow ratio increased, and the power channel outlet temperature again increased. The boiling in the rod bundle and the flashing in the upper plenum produced sufficient steam to dictate system pressure, and both temperature and pressure increased momentarily until the upper-upper plenum was drained down to the hot-leg elevation (data plots 30 and 31). The fluid temperature in the lower-upper plenum reached a peak and then decreased, responding to the increased primary system flow through the power channel caused by the increasing buoyancy head. The hot-leg side of the power channel stabilized at a temperature of approximately []^(a,b,c). The pressure was stabilized at the corresponding saturation pressure (approximately []^(a,b,c) psia) at the end of the IDP.

The temperature of the liquid in the lower-upper plenum controlled system pressure during the PDP (data plot 4). Oscillations with a period of []^(a,b,c) seconds in the tubular downcomer flow and differential pressure across the rod bundle were observed after the RCPs coasted down. These oscillations continued until approximately []^(a,b,c) seconds into the transient. These flow oscillations led to oscillations in the rod bundle steam fraction and, therefore, in the apparent density of the fluid in the heater bundle, upper plenum, and hot leg. When the flow decreased, steam fractions increased, causing an increase of the overall system pressure and in the lower-upper plenum temperature (Figure 4.2.4-2). The overall system pressure oscillations therefore were out of phase with the tubular downcomer flow oscillations. Data plots 30 and 31 show the collapsed liquid levels at various sections of the power channel during test S00504.

The upper head began to drain when system pressure decreased to the saturation pressure for the water in the upper head. Initially, the upper-head fluid temperature was []^(a,b,c). Flashing of the fluid in the upper head began at approximately []^(a,b,c) seconds, and the upper head drained completely when ADS-1 occurred at 956 seconds.

The upper-upper plenum (above the hot-leg elevation) flashed when the RCPs were shutoff and coasted down, and the measured water level dropped to the hot-leg elevation. This level stayed at the hot-leg elevation until the latter part of the accumulator injection, when the lower-upper plenum fluid became sufficiently subcooled to temporarily condense the steam bubble in the upper-upper plenum (see temperatures in data plot 4). When accumulator injection ended, this level again decreased temporarily to the hot-leg elevation. At []^(a,b,c) seconds, the upper-upper plenum was again subcooled and filled with water injected from NRHR until the test was terminated.

Data plots 30 and 31 show the collapsed levels in the rod bundle section of the power channel oscillated following the pump coastdown and indicate apparent steam fractions in the bundle

ranging from 4 percent to 50 percent. The oscillations ended at a maximum rod bundle steam fraction of 45 percent at approximately 600 seconds. From about []^(a,b,c) seconds, the steam fraction at the top of the rod bundle was approximately []^(a,b,c) percent. After ADS actuation, the accumulator injection completely filled the rod bundle. The amount of subcooling of the lower-upper plenum during the accumulator discharge was greater in test S00504 than in S00303. When the injection ended, single-phase water flow was maintained through the rod bundle for the rest of the test.

- **Pressurizer**

The pressurizer began to drain when the break occurred and was completely drained in approximately 100 seconds (data plot 32). The water in the pressurizer flashed due to the loss of system pressure, and the temperature of the water dropped below []^(a,b,c) during this initial depressurization (data plot 18). The hot water exiting the pressurizer surge line into hot leg-A caused a slight increase in the hot-leg temperature during this period, since it mixed with the flow from the power channel/upper plenum. The pressurizer stayed drained until ADS occurred. At this time, it refilled completely and discharged water through the ADS. After accumulator injection ended, the collapsed liquid level decreased to approximately []^(a,b,c) ft. NRHR (and CVCS) injection flow gradually refilled the pressurizer with water.

- **Steam Generator**

The behavior of the steam generators in test S00504 was essentially identical to test S00303 from break initiation until the steam generator U-tubes were drained.

The steam generators acted as the heat sink until the MSLIV closed and prevented further energy removal from the secondary side. This caused the temperature (and pressure) of the steam generator secondary side to increase toward the primary system hot-leg temperature (Figure 4.2.4-2). However, through the IDP and for the first part of the PDP, the pressure on the primary side of the steam generators U-tubes was higher than the secondary side (data plot 2). This indicated that some heat transfer from the primary to secondary side was occurring and causing some condensation of the steam in the two-phase fluid coming from the hot leg. The primary system pressure did not drop below the steam generator secondary-side pressure until approximately []^(a,b,c) seconds into the test, at which time the U-tubes had mostly drained.

At the end of the RCP coastdown, flow oscillations began to occur in the tubular downcomer and through the power channel. This caused significant oscillations in the measured collapsed liquid level in the rod bundle and, consequently, in the density of the two-phase flow from the rod bundle into the hot legs and to the steam generators (data plots 20 and 21). Since the driving force for the natural circulation flow was the density difference between the single-phase fluid in the cold legs and downcomer entering the power channel and the two-phase mixture in the rod bundle, upper plenum and the hot legs the flow oscillations were sustained as long as there was flow through the steam generators.

The level in the hot-leg side of the steam generator U-tubes gradually dropped to about 1/3 of the tube height at approximately 500 seconds, and they drained completely when ADS-1 was actuated. The level in the cold-leg side of the steam generator U-tubes exhibited significant level oscillations from about 200 seconds until they drained completely at approximately []^(a,b,c) seconds (data plots 22 and 23).

Primary system flow through the steam generators stopped at about the same times in this test as in test S00303, and the hot-leg side of the U-tubes drained at ADS-1 actuation in both tests. Once the steam generator U-tubes were drained, they remained drained for the rest of the test.

- **Hot Legs**

Hot legs-A and -B were full of two-phase mixture until ADS-1 was actuated (data plots 20 and 21). After ADS-1, hot leg-A partially drained and remained partially drained for the rest of the test. Hot leg-B drained completely when the accumulator injection ended and then partially refilled as the NRHR injection refilled the primary system.

The principal difference between hot legs-A and -B was the influence of the PRHR HX on the steam fraction in the hot legs. The PRHR HX preferentially removed steam from hot leg-A (as seen in the very high steam fraction of the PRHR HX inlet fluid), thereby reducing the steam fraction in hot leg-A to less than that in hot leg-B. The hot-leg steam fraction affected the draindown of the steam generator U-tubes, with steam generator-B draining earlier than steam generator-A.

- **Cold Legs**

Cold legs-A1 and -A2 remained full until ADS-1 (data plots 22 through 27), when flashing occurred and their level started to decrease. Accumulator injection refilled the cold legs into the vertical pipe section at the RCP discharge. After accumulator delivery ended, the level decreased until the horizontal pipe sections were drained at approximately 1720 seconds and the liquid level decreased into the annular downcomer (approximately []^(a,b,c) below the hot-leg elevation [data plot 24]). When the NRHR (and CVCS) injection refilled the annular downcomer, cold legs-A1 and -A2 horizontal sections were refilled beginning at []^(a,b,c) seconds.

Cold legs-B1 and -B2 remained full until []^(a,b,c) seconds into the event. At this time, both cold legs-B1 and -B2 drained and CMT gravity injection started. Cold leg-B2 (where the simulated break was located) drained prior to cold leg-B1, as evidenced by CMT-B switching to draindown mode before CMT-A1A. Cold legs-B1 and -B2 started to refill at []^(a,b,c) seconds and steady liquid flow out the break was restored. After []^(a,b,c) seconds, the cold leg to CMT balance lines were partially filled.

- **PRHR**

The initial PRHR operation in test S00504 was similar to S00303. Also, as was observed in S00303, the PRHR HX flow decreased after the accumulation injection refilled the power channel and hot leg with subcooled water. However, due to the continued subcooled flow through the power channel provided by NRHR (and CVCS) injection and the resulting lack of thermal buoyancy or two-phase flow driving head, PRHR HX flow did not resume.

At the initiation of the test, the PRHR HX was filled with subcooled liquid. When the S signal occurred, the PRHR return line isolation valve opened, and a high rate of flow started through the PRHR HX due to the still operating RCPs. When the RCPs were shut off and the upper plenum and the hot leg filled with two-phase fluid, a large portion of the steam in hot leg-A flowed to the PRHR HX (void fraction is 80 to 95 percent based on data plot 29). The two-phase mixture, consisting of alternating slugs of steam and water, was condensed and subcooled in the PRHR HX (data plot 28). During the PDP (prior to ADS-1), a significant variation in the flow through the PRHR was caused by the variation in the steam fraction of the fluid in hot leg-A. The condensation process observed in the PRHR HX resulted in the rapid and wide variations in differential pressure (dP) measurements shown in data plots 28, 29, and 37.

After ADS was initiated, the power channel and the hot leg were refilled with subcooled liquid by the cold accumulators injection flow. The driving head for the flow in the PRHR HX decreased (caused by the loss of density difference between the fluid in the PRHR supply line and the return line). The flow decreased and stopped at approximately []^(a,b,c) seconds, and no flow through the PRHR HX occurred for the rest of the test.

The PRHR heat exchanger was submerged in the IRWST and a heatup of the water within the IRWST is shown in data plot 17. Since ADS-4 never occurred in S00504, there was no injection of water from the IRWST into the primary system.

- **Core Makeup Tanks (CMTs)**

The CMT injection was initiated two seconds after the S signal by opening the CMT injection line isolation valves. Initially, the flow from the CMT was by natural circulation, with hot water from the cold leg-B flowing through the CLBL to the top of the CMTs and cold water from the CMTs flowing into the downcomer and into the power channel.

When cold legs-B1 and -B2 voided, steam flowed through the CLBL to the top of the CMTs. This resulted in a free-water surface in the CMTs (ending CMT recirculation). The presence of steam in the CLBL increased the driving head for CMT injection. Therefore, the transition of the CMTs from their recirculation mode to their draindown mode was accompanied by an increase in CMT injection flow rate. For this test, the break was located in cold leg-B2 and resulted in cold leg-B2 draining before -B1. Since the CMT-B balance line was connected to cold leg-B2, the transition to draindown injection flow occurred earlier for CMT-B than for CMT-A (data plot 38).

The CMTs were heated first by the hot liquid from the cold legs, which replaced the cold water being injected from the bottom of the CMT CLBL. A stratified temperature gradient was established in the CMTs (data plots 15 and 16), where the water at the top of the CMT was hot while lower water remained cold. As the CMT recirculation continued, the depth of the hot water provided from the cold legs increased. The temperature stratification appeared stable; however, the temperature of the leading, lower layer of heated water decreased since it must heat the cold CMT surfaces it contacts. Later steam from the cold legs condensed on the free-water and metal surfaces in the upper part of the CMTs. The free-water surface increased to or near the saturation temperature.

The recirculation flow through the CMTs started at approximately []^(a,b,c) for CMT-A and []^(a,b,c) lbm/sec. for CMT-B. The draindown injection started at []^(a,b,c) lbm/sec. and gradually decreased with time. During the last half of the accumulator injection, CMT draindown stopped. The CMTs started to refill at approximately []^(a,b,c) seconds (data plot 33).

- **Accumulators**

The accumulators provided water injection by a polytropic expansion of a compressed air volume stored within the accumulator. Water from the accumulators was injected when the primary system pressure drops below []^(a,b,c) psia. The accumulator injection started before ADS-1 at a very low flow rate. However, when ADS-1 occurred and primary system pressure was reduced, the injection rate increased (data plot 39). The accumulator injection for the S00504 test continued approximately []^(a,b,c) seconds, and the accumulators were completely drained when their injection ended (data plot 34).

Mass Discharge and Mass Balance

The catch tank weight measurements are shown in data plot 43 for the break flow and for ADS-1, -2, and -3 flows.

The break flow decreased as system pressure dropped during the IDP and the PDP. When ADS occurred, cold leg-B2 temporarily drained and steam was discharged from the break until the NRHR (and CVCS) injection flow refilled the cold leg.

The discharge from ADS-1, -2, and -3 was high throughout the accumulator injection and decreased when accumulator injection ended to a lower but steady flow dictated by CVCS and NRHR injection flow.

The mass balance results for test S00504 were calculated based on water inventory before and after the test. Table 4.2.4-2 gives a detailed listing of the inventories of water in the various components before the test. Table 4.2.4-3 lists the inventories after the event and the amount of water injected into the vessel from the CVCS and the NRHR. The water level in the vessel was determined by the DP-B16P measurement to be []^(a,b,c) above the hot-leg centerline at the end of the test.

Table 4.2.4-4 compares the mass balance for the system before and after the test. The results indicate 5.9 percent more water after the event than can be accounted for. This was most likely due to the uncertainty of integrating the flow rate from CVCS and NRHR.

**TABLE 4.2.4-1
SEQUENCE OF EVENTS FOR TEST S00504**

Event	Specified	Instrument Channel	Actual Time
Break Opens	0		(a,b,c)
R Signal	P = 1800 psia	P-027P	
MSLIV	R signal + 2 sec.	Z_A04SC, F_A04S	
		Z_B04SC, F_B04S	
S Signal	P = 1700 psia	P-027P	
MFW-IV Closure	S signal + 2 sec.	Z_B02SC, F_B01S	
		Z_A02SC, F_A01S	
CMT-IV Opening	S signal + 2 sec.	Z_A040EC, F-A40E	
		Z_B040EC, F-B40E	
RCPs Tripped	S signal + 16.2 sec.	I-A1P, S-A1P	
		I-B1P, S-B1P	
PRHR Heat Exchanger Actuation	S signal + 2 sec.	Z_A81EC, F_A80EG	
Accumulators	P-027P = 700 psia	F_A20EG	
		F_B20EG	
ADS-1	CMT level 67% +30 sec.	L_B40E	
		Z_001PC	
ADS-2	CMT level 67% +125 sec.	L_B40E	
		Z_002PC	
ADS-3	CMT level 67% +245 sec.	L_B40E	
		Z_003PC	
ADS-4	CMT level 20% +600 sec.	L_B40E	
		Z_004PC, F-040P	
IRWST Injection	P-027P = 26 psia	F_A60EG	
		F_B60EG	
CVCS On	S signal + PR level 10%	L-010P	
NRHR On	P = 160 psia	P-027P	
SFW Stop	TCL = 547°F or SG level = 6.9 ft.	L-A20S/L-B20S	
SFW Injection	S	F-A20A/F-B20A	

TABLE 4.2.4-2

WATER INVENTORY BEFCRKE TEST S90504

Component	Volume (ft. ³)/(l)	Net Vol (ft. ³)/(l)	Temp (°F)	Relative Density	Mass (lbm)
Loops	8.97 ft. ³ (254.0 l)	8.97 ft. ³ (254.0 l)			
Pressurizer	3.37 ft. ³ (95.4 l)	1.96 ft. ³ (55.6 l)			
Surge Line	0.34 ft. ³ (9.6 l)	0.34 ft. ³ (9.6 l)			
Tubular Downcomer	1.38 ft. ³ (39.1 l)	1.38 ft. ³ (39.1 l)			
Annular Downcomer + High-Pressure Bypass	0.54 ft. ³ (15.3 l)	0.54 ft. ³ (15.3 l)			
Core Bypass	0.44 ft. ³ (12.4 l)	0.44 ft. ³ (12.4 l)			
Lower Plenum	0.81 ft. ³ (22.8 l)	0.81 ft. ³ (22.8 l)			
Riser	1.64 ft. ³ (46.4 l)	1.64 ft. ³ (46.4 l)			
Upper Plenum	1.46 ft. ³ (41.3 l)	1.46 ft. ³ (41.3 l)			
Upper Head	1.90 ft. ³ (53.8 l)	1.90 ft. ³ (53.8 l)			
CMTs	10.1 ft. ³ (286.0 l)	10.1 ft. ³ (286.0 l)			
Accumulator	10.1 ft. ³ (286.0 l)	7.73 ft. ³ (219.9 l)			
IRWST Injection Line	0.18 ft. ³ (5.1 l)	0.18 ft. ³ (5.1 l)			
TOTAL INVENTORY					

(a,b,c)

TABLE 4.2.4-3

WATER INVENTORY AFTER TEST S00504 WAS COMPLETED
 Water level as measured by DP-B16P (-0.67 psi) was 19.04 in. (476 mm) above Hot Leg

Component	Volume (ft. ³)/(l)	Net Vol (ft. ³)/(l)	Temp (°F)	Relative Density	Mass (lbm)
Loops	8.97 ft. ³ (254.0 l)	7.53 ft. ³ (213.3 l)			
Pressurizer	3.37 ft. ³ (95.4 l)	3.37 ft. ³ (95.4 l)			
Surge Line	0.34 ft. ³ (9.6 l)	0.34 ft. ³ (9.6 l)			
Tubular Downcomer	1.38 ft. ³ (39.1 l)	1.38 ft. ³ (39.1 l)			
Annular Downcomer + High-Pressure Bypass	0.54 ft. ³ (15.3 l)	0.54 ft. ³ (15.3 l)			
Core Bypass	0.44 ft. ³ (12.4 l)	0.44 ft. ³ (12.4 l)			
Lower Plenum	0.81 ft. ³ (22.8 l)	0.81 ft. ³ (22.8 l)			
Riser	1.64 ft. ³ (46.4 l)	1.64 ft. ³ (46.4 l)			
Upper Plenum	1.46 ft. ³ (41.3 l)	1.32 ft. ³ (37.3 l)			
Upper Head	1.90 ft. ³ (53.8 l)	0.0 ft. ³ (0.0 l)			
CMT-A	5.05 ft. ³ (143.0 l)	3.99 ft. ³ (113.1 l)			
CMT-B	5.05 ft. ³ (143.0 l)	3.89 ft. ³ (110.1 l)			
Accumulator	10.1 ft. ³ (286.0 l)	0.0 ft. ³ (0.0 l)			
IRWST Injection Line	0.18 ft. ³ (5.1 l)	0.18 ft. ³ (5.1 l)			
TOTAL INVENTORY					

(a,b,c)

TABLE 4.2.4-3 (Cont.)

WATER INVENTORY AFTER TEST 500504 WAS COMPLETED
Water level as measured by DP-B16P (-0.67 psi) was 19.04 in. (475 mm) above Hot Leg

WATER INJECTED DURING EVENT

	Mass (lbm)
CVCS Injection	
NRHR Injection - A	
NRHR Injection - B	
NRHR Total	

(a,b,c)

TABLE 4.2.4-4
MASS BALANCE FOR TEST S00504

	Starting Inventory (lbm)	Ending Inventory (lbm)	
Total Primary System			(a,b,c)
CVCS Injection			
RNRHR Injection			
BREAK			
ADS-1, -2, -3			
ADS-4			
TOTAL			
Ending Inventory/Starting Inventory (lbm)			
Ending Inventory/Starting Inventory (%)			

The following figures have been intentionally deleted
from this document due to their proprietary nature.

**TEST S00504 PLOT PACKAGE
CHANNEL LIST BY COMPONENT**

COMPONENT	CHANNEL	UNITS	PLOT	COMMENT
ACCA	F_A20E	lbm/sec.	39	
ACCA	L_A20E	ft.	34	
ACCB	F_B20E	lbm/sec.	39	
ACCB	L_B20E	ft.	34	
ADS 1, 2, & 3	IF30flw	lbm/sec.	44	Flow rate derived from IF030P
ADS 1, 2, & 3	IF030P	lbm	43	Catch tank
ADS 4 & SG	IF40flw	lbm/sec.	44	Flow rate derived from IF040P
ADS 4 & SG	IF040P	lbm	43	Catch tank
ANN DC	DP-A021P	psi	24	To cold leg-A1
ANN DC	DP-A022P	psi	25	To cold leg-A2
ANN DC	DP-B021P	psi	26	To cold leg-B1
ANN DC	DP-B022P	psi	27	To cold leg-B2
BREAK LINE	IF05flw	lbm/sec.	44	Flow rate derived from IF005P
BREAK LINE	IF005P	lbm	43	Catch tank
CLA	DP-A001P	psi	24	To cold leg-A1
CLA	DP-A002P	psi	25	To cold leg-A2
CLA	DP-A09P	psi	22	Pump suction
CLA	T-A10P	°F	11	Steam generator outlet
CLA1	F_A01P	lbm/sec.	36	
CLA1	T-A021PL	°F	13	Downcomer inlet
CLA1	T-A11P	°F	11	Pump outlet
CLA2	F_A02P	lbm/sec.	36	
CLA2	T-A022PL	°F	13	Downcomer inlet
CLB	DP-B001P	psi	26	To cold leg-B1

**TEST S00504 PLOT PACKAGE
CHANNEL LIST BY COMPONENT (Cont.)**

COMPONENT	CHANNEL	UNITS	PLOT	COMMENT
CLB	DP-B002P	psi	27	To cold leg-B2
CLB	DP-B09P	psi	23	Pump suction
CLB	T-B10P	°F	12	Steam generator outlet
CLB1	F_B01P	lbm/sec.	36	
CLB1	T-B021PL	°F	14	Downcomer inlet
CLB1	T-B11P	°F	12	Pump outlet
CLB2	F_B02P	lbm/sec.	36	
CLB2	T_B022PL	°F	14	Downcomer inlet
CMTA	F_A40E	lbm/sec.	38	
CMTA	L_A40E	ft.	33	
CMTA	T-A401E	°F	15	Top (242.25 in.)
CMTA	T-A403E	°F	15	216.75 in.
CMTA	T-A405E	°F	15	191.25 in.
CMTA	T-A407E	°F	15	165.75 in.
CMTA	T-A409E	°F	15	140.25 in.
CMTA	T-A411E	°F	15	114.75 in.
CMTA	T-A413E	°F	15	89.25 in.
CMTA	T-A415E	°F	15	63.75 in.
CMTA	T-A417E	°F	15	38.25 in.
CMTA	T-A420E	°F	15	Bottom (0 in.)
CMTB	F_B40E	lbm/sec.	38	
CMTB	L_B40E	ft.	33	
CMTB	T-B401E*	°F	16	Top (242.25 in.)
CMTB	T-B403E*	°F	16	216.75 in.
CMTB	T-B405E*	°F	16	191.25 in.
CMTB	T-B407E*	°F	16	165.75 in.
CMTB	T-B409E*	°F	16	140.25 in.
CMTB	T-B411E*	°F	16	114.75 in.

**TEST S00504 PLOT PACKAGE
CHANNEL LIST BY COMPONENT (Cont.)**

COMPONENT	CHANNEL	UNITS	PLOT	COMMENT
CMTB	T-B413E*	°F	16	89.25 in.
CMTB	T-B415E*	°F	16	63.75 in.
CMTB	T-B417E*	°F	16	38.25 in.
CMTB	T-B420E*	°F	16	Bottom (0 in.)
CVCS	F_001AG	lbm/sec	42	
DVIA	T-A00E	°F	13	
DVIB	T-B00E	°F	14	
HLA	DP-A04P	psi	20	
HLA	T-A03PL	°F	5	Vertical, near power channel
HLA	T-A03PO	°F	5	Horizontal, near power channel
HLA	T-A04P	°F	5	Near steam generator inlet
HLB	DP-B04P	psi	21	
HLB	T-B03PL	°F	6	Vertical, near power channel
HLB	T-B03PO	°F	6	Horizontal, near power channel
HLB	T-B04P	°F	6	Near steam generator inlet
IRWST	F_A60E	lbm/sec.	40	
IRWST	F_B60E	lbm/sec.	40	
IRWST	L_060E	ft	32	
IRWST	T-061E	°F	17	Bottom
IRWST	T-062E	°F	17	Below middle
IRWST	T-063E	°F	17	Middle
IRWST	T-064E	°F	17	Above middle
IRWST	T-065E	°F	17	Top
NRHRA	F_A00E	lbm/sec	42	
NRHRB	F_B00E	lbm/sec	42	
PC	W_00P	kW	1	
PC-HB	L_000P	ft	30	Heater bundle
PC-HR	TW018P20	°F	3	Heater rod

**TEST S00504 PLOT PACKAGE
CHANNEL LIST BY COMPONENT (Cont.)**

COMPONENT	CHANNEL	UNITS	PLOT	COMMENT
PC-HR	TW018P48	°F	3	Heater rod
PC-HR	TW020P87	°F	3	Heater rod
PC-UH	T-016P	°F	4	Upper head
PC-UP	L_A15P	ft.	30	Bottom of the upper plenum
PC-UP	L_A16P	ft.	31	Top of the upper plenum
PC-UP	T-015P	°F	4	Upper plenum
PC-UH	L_017P	ft.	31	Upper head
PC-UP	L_A14P	ft.	31	Above top of the heated length
PRHR	DP-A81AE	psi	29	Supply line inverted U-tube
PRHR	DP-A81BE	psi	29	Supply line inverted U-tube
PRHR	DP-A81E	psi	28	Supply line
PRHR	DP-A82E	psi	28	Heat exchanger
PRHR	DP-A83E	psi	28	Return line
PRHR	F_A80E	lbm/sec.	37	Return line
PRHR	T-A82E	°F	19	Inlet
PRHR	T-A83E	°F	19	Exit
PRZ	L_010P	ft.	32	
PRZ	P-027P	psia	2	
PRZ	T-026P	°F	18	At top
SGA	DP-A05P	psi	20	Hot side
SGA	DP-A06P	psi	20	Hot side
SGA	DP-A07P	psi	22	Cold side
SGA	DP-A08P	psi	22	Cold side
SGA	F_A01S	lbm/sec.	41	
SGA	F_A20A	lbm/sec.	41	
SGA	L_A10S	ft.	35	Overall level
SGA	P-A04S	psia	2	Secondary system
SGA	T-A01S	°F	10	MFW-A

**TEST S00504 PLOT PACKAGE
CHANNEL LIST BY COMPONENT (Cont.)**

COMPONENT	CHANNEL	UNITS	PLOT	COMMENT
SGA	T-A05P	°F	7	Hot side
SGA	T-A05S	°F	9	Hot side - riser
SGA	T-A06P	°F	7	Hot side
SGA	T-A08P	°F	11	Cold side
SGA	TW-A06S	°F	7	Hot side
SGB	DP-B05P	psi	21	Hot side
SGB	DP-B06P	psi	21	Hot side
SGB	DP-B07P	psi	23	Cold side
SGB	DP-B08P	psi	23	Cold side
SGB	F_B01S	lbm/sec.	41	
SGB	F_B20A	lbm/sec.	41	
SGB	L_B10S	ft.	35	Overall level
SGB	P-B04S	psia	2	Secondary system
SGB	T-B01S	°F	10	MFW-B
SGB	T-B05P	°F	8	Hot side
SGB	T-B05S	°F	9	Hot side - riser
SGB	T-B06P	°F	8	Hot side
SGB	T-B07P	°F	8	U-tube top
SGB	T-B08P	°F	12	Cold side
SGB	TW-B06S	°F	8	Hot side
SL	T-020P	°F	18	Surge line near pressurizer
TDC	DP-001P	psi	25,26	Top
TDC	DP-002P	psi	24,25,26,27	Bottom
TDC	T-001PL	°F	13,14	Top
TDC	T-003P	°F	13,14	Bottom
TSAT-PRZ		°F	18	Based on P-027P
UH-TSAT		°F	4	Based on P-017P

*All CMT-B temperature channels were failed.

The data plots are found in the proprietary version of this document.

4.2.5 One-In. Cold-Leg Break without Nonsafety Systems (S00401)

This matrix test simulated a 1-in. break in the bottom of cold leg-B2. The test began with the initiation of the break in cold leg-B2, which was the cold leg with the CMT-B pressure balance line connection. The break location was just downstream from the cold leg to the core makeup tank (CMT) balance line connection. This test was performed without any nonsafety systems (chemical and volume control system [CVCS] makeup pumps, steam generator startup feedwater [SFW] pumps, and normal residual heat removal system [NRHR] pumps) operating. Results are provided in the data plot package at the end of this section. The sequence of events for S00401 is listed in Table 4.2.5-1.

Loss-of-coolant accident (LOCA) events in the AP600 SPES-2 tests were marked by distinctly different phases. These phases were characterized by the rate at which the primary system pressure decreased and the thermal-hydraulic phenomena occurring within the primary and safety systems. The different phases selected for the purpose of detailed evaluation of this LOCA are shown in Figure 4.2.5-1 and are as follows:

- Initial depressurization phase (IDP)—Point 1 to 2
- Pressure decay phase (PDP)—Point 2 to 3
- Automatic depressurization system (ADS) phase—Point 3 to 4
- Post-automatic depressurization system (post-ADS) phase—Point 4 to 5

Overall Test Observations

Figure 4.2.5-1 shows the plant primary system pressure during test S00401 (as measured at the top of the pressurizer), with selected component actuations and plant responses shown in relation to primary system pressure.

The IDP began with the initiation of the break, which resulted in a rapid reduction in pressure. The reactor trip (R) signal initiated at 1800 psia. The safety systems actuation (S) signal initiated at 1700 psia. The R and the S signals initiated the following actions:

- Decay power simulation (with heat loss compensation) initiated.
- Main steamline isolation valves (MSLIVs) closed.
- Main feedwater isolation valves (MFWIVs) closed.
- CMT injection line isolation valves opened.
- Passive residual heat removal (PRHR) return line isolation valve opened.
- Reactor coolant pumps (RCPs) topped running.

Recirculation flow through the CMTs and flow through the PRHR heat exchanger (HX) began immediately after their isolation valves opened. Flashing/boiling occurred in the rod bundle and upper-plenum regions of the power channel due to the rapid decrease in primary pressure to the fluid saturation pressure. The measured fluid level in the upper-upper plenum decreased to the hot-leg elevation. The flashing on the hot-leg side of the primary system stopped the rapid drop in primary

system pressure. When the RCPs were shut off (at []^(a,b,c) seconds), the flow through the rod bundle began to oscillate (with a []^(a,b,c)-second period). This resulted in oscillations in the rod bundle and lower-upper plenum collapsed liquid level and fluid temperature, and system pressure.

During the initial stages of the PDP, the rod bundle collapsed liquid level decreased (fluid steam fraction increased). This caused an increasing steam fraction in the upper plenum and the hot legs. The hot leg-B fluid had a steam fraction close to that observed in the upper plenum. The steam fraction in hot leg-A was lower due to the selective removal of vapor from the hot leg into the PRHR HX inlet line.

Two-phase flow in the hot legs initiated draining of the steam generator U-tubes, as steam from the two-phase mixture collected in the top of the U-tubes. This stopped the primary system flow through the steam generators so that the power channel flow was composed predominantly of the flow through the PRHR HX. The steam fraction oscillations observed in the rod bundle and in the upper plenum ended when the steam generator U-tubes drained. Approximately []^(a,b,c) seconds into the test, the steam generator-B U-tubes began to drain. The steam generator-A U-tubes began to drain, approximately []^(a,b,c) seconds later due to the lower fluid steam fraction in hot leg-A.

Due to boiling in the rod bundle (data plots 30 and 31), two-phase flow entered the hot leg from the upper plenum and flowed through the PRHR HX. The flow into the PRHR HX consisted of intermittent periods of saturated water and steam which had an average steam fraction significantly greater than the fluid in the upper plenum. The average steam fraction at the PRHR HX inlet was as high as []^(a,b,c) percent, which enhanced the PRHR HX heat transfer from the primary system, as compared to its heat removal capability with single-phase saturated or subcooled water. When the primary system flow stabilized after the initial flow oscillations, a PRHR HX heat removal rate of []^(a,b,c) kW was calculated. This calculation was based on the steam fraction at the PRHR HX inlet (as calculated from the dP instrument readings in data plot 29), the averaged return flow rate, the HX inlet and outlet temperatures, and the pressure. This calculation, which assumes a slip coefficient of 1 between water and steam, may be lower than the actual heat transfer and should only be used for test-to-test comparison.

When the primary system pressure decreased to the saturation pressure for the fluid in the upper head, it began to drain (at []^(a,b,c) seconds).

When the loop-B cold legs had partially emptied, the CMTs transitioned from their recirculation mode of operation to an intermittent draindown mode of operation. This began at approximately []^(a,b,c) seconds for CMT-B and []^(a,b,c) seconds for CMT-A.

During the first []^(a,b,c) seconds of this test (until ADS-1), []^(a,b,c) lbm of water were expelled through the break draining the: the pressurizer, the steam generator U-tubes, the power channel upper head, the power channel upper plenum above the hot leg, most of the cold legs, and approximately []^(a,b,c) percent of the CMTs. The heat source that simulate the AP600 core decay heat reduced power to approximately 240 kW at []^(a,b,c) seconds. This value consisted of 90-kW of decay heat

and 150-kW of heat loss compensation. The mass flow rate out of the break was decreasing, indicating that cold leg-B2 was almost empty.

The ADS phase began with the actuation of ADS-1 (at approximately []^(a,b,c) seconds). ADS-2 and -3 occurred within the next []^(a,b,c) seconds. The heat loss compensation was removed from the rod bundle power decay simulation when ADS-1 occurred, reducing the rod bundle power to approximately 90 kW.

The ADS actuation increased the rate of primary system depressurization and resulted in high injection flow from the accumulators. The rapid injection of cold water from the accumulators (from []^(a,b,c) seconds) and the CMT injection flow refilled the power channel/upper plenum, the horizontal portion of the hot legs, and the pressurizer. When the accumulator discharge ended, the flow through the heater bundle decreased to the injection rate of the CMTs and the PRHR HX flow, and two-phase flow occurred again the heater bundle, hot leg-A, the PRHR HX, and into the pressurizer. The rod bundle steam fraction continued to increase (collapsed liquid level decreased) until after ADS-4 was actuated.

The mass flow rate through the break decreased sharply at approximately []^(a,b,c) seconds, indicating that cold leg-B2 emptied and that the break flow was steam. During the ADS phase, approximately []^(a,b,c) lbm of subcooled water were discharged from ADS-1, -2, and -3.

The post-ADS period began when ADS-4 actuated. ADS-4 occurred at []^(a,b,c) seconds, the fluid discharge through ADS-1, -2, and -3 stopped, and the pressurizer water drained back into hot leg-A. A small amount of CMT flow continued into the downcomer via the direct vessel injection (DVI) line. When the primary system pressure decreased below the pressure corresponding to the water elevation head of the IRWST, flow from the IRWST began. Shortly thereafter, the CMT flow ended. The flow from the IRWST gradually refilled and subcooled the power channel, restored single-phase water flow through the rod bundle, and partially refilled the upper-upper plenum. The PRHR HX supply line partially emptied at approximately []^(a,b,c) seconds and the PRHR HX was no longer effective. A steady flow of subcooled water was established from the IRWST into the downcomer, through the power channel, and left the primary system through the ADS-4 flow paths.

This test demonstrated that the heater bundle was fully covered by a single- or two-phase fluid at all times (data plots 30 and 31). There was no indication of heater rod temperature increase due to lack of cooling (data plot 3). Key parameters comparing the S00401 test with other tests are listed in Table 5-1 in Section 5.0.

Discussion of Test Transient Phases

- **Initial Depressurization Phase (0 to []^(a,b,c) Seconds)**

The initial depressurization phase (IDP) began with the initiation of the break (at time 0) and ended when the primary system pressure reached the saturation pressure of the fluid in the

lower-upper plenum and the hot legs (Figure 4.2.5-1). This phase included the following events: R signal at 1800 psia (decay power simulation initiated and the MSIV closed), and S signal at 1700 psia (the MFWIV closed, the CMT injection line isolation valves opened, and the PRHR heat exchanger return line isolation valve opened—all with a 2-second delay; and RCP coastdown started after a 16.2-second delay). See Table 4.2.5-1.

Facility Response during the IDP:

From time 0 until the R signal occurred, the primary system pressure decreased due to the expansion of the pressurizer steam volume caused by fluid loss through the break. The pressurizer partially compensated for the loss of pressure by flashing; however, it was drained after []^(a,b,c) seconds (data plot 32). The R (at []^(a,b,c) seconds) and the S (at []^(a,b,c) seconds) signals were based on pressurizer pressure only. When the R signal occurred, the MSLIV closed and the power was reduced to 20 percent of full power after a 5.75-second delay and began to decay after a 14.5-second delay.

As a result of the power reduction without flow reduction, the rod bundle ΔT decreased due to the low power/flow ratio and the lower-upper plenum temperature dropped toward the cold-leg temperature. At the same time, the primary system pressure had decreased to []^(a,b,c) psia (the saturation pressure of the []^(a,b,c) water in the upper-upper plenum), and the upper-upper plenum began to flash and rapidly drain. System pressure decreased to approximately []^(a,b,c) psia at []^(a,b,c) seconds. At this time, the pressurizer was drained, but primary system pressure was still dictated by the temperature of the saturated vapor in the pressurizer (about []^(a,b,c)°F) and the fluid in the surge line. When the RCPs tripped (at []^(a,b,c) seconds), the rod bundle and upper-plenum fluid temperatures increased due to the increased power/flow ratio at the lower flow. System pressure increased temporarily until the decreasing rod bundle decay power and the decreasing lower-plenum temperature (due to the CMTs injecting cold water into the downcomer) began to reduce the lower-upper plenum fluid temperature. The decrease in primary system pressure resulted from the balance between the steam generation rate (from flashing primary fluid), the volumetric flow of liquid out of the break, and the steam condensation occurring in the PRHR HX. Steam was continually generated by boiling due to the heater power. As system pressure continued to decrease, more fluid reached its saturation pressure and flashed. The PRHR HX flow started before the RCPs were tripped and then continued by natural circulation (data plot 37). Primary system pressure stabilized at saturation pressure for the bulk hot fluid in the primary system (approximately []^(a,b,c)°F), as shown in Figure 4.2.5-1. This ended the IDP.

- **Pressure Decay Phase (400 to 4600 Seconds)**

The pressure decay phase (PDP) began when system pressure (Figure 4.2.5-2) reached saturation pressure for the bulk hot fluid in the primary system. This phase ended when ADS-1 opened on low CMT level (at approximately []^(a,b,c) seconds) and augmented the system depressurization. This phase was characterized by a slow decrease in overall system pressure and temperature. The

rod bundle power (decay power plus heat loss compensation) was reduced from 330 kW to 240 kW (data plot 1). At []^(a,b,c) seconds (rod bundle power was about 250 kW), the PRHR HX heat removal rate was approximately []^(a,b,c) kW. The recirculating CMTs provided approximately []^(a,b,c)-kW effective heat removal from the primary system at this time. This heat removal plus energy lost through the break and the facility heat losses exceeded the rod bundle heat input to the primary system.

The initial CMT natural circulation operating mode was followed by draindown injection when the loop-B cold legs drained (data plot 38). The U-tubes of the steam generators had completely drained at this time (data plots 20 through 23) and had no effect on the rest of the test.

Accumulator injection was initiated when the primary system pressure dropped below 711 psia (at approximately []^(a,b,c) seconds) prior to ADS-1 actuation; however, the injection rate was low (less than []^(a,b,c) lbm/sec.) due to the small difference between system pressure and accumulator gas pressure (data plot 39).

Facility Response during the PDP:

The oscillating flow in the primary system that began after the RCPs were shutoff continued into the PDP. These flow oscillations resulted in wide variations in the steam fraction of the two-phase mixture exiting the rod bundle and flowing into the hot legs (data plots 30 and 31). These oscillations in steam fraction had a significant effect on the thermal buoyancy head that drove the flow in the primary system at this time, since it affected the two-phase flow density. These steam fraction oscillations were observed through the hot leg and the steam generators (data plots 20 and 21). However, the steam fraction oscillations were converted to flow oscillations in the cold legs since the two-phase mixture entering the steam generators left the steam generators as saturated water (data plots 24 through 27). Some of the steam was condensed in the steam generator U-tubes (the primary-side pressure was higher than the secondary-side pressure at this time, allowing some heat to be transferred to the secondary-side fluid). The remaining steam was separated from the two-phase mixture in the high point of the U-tubes (due to low velocity), eventually causing the U-tubes to begin to drain, and a free-water surface appeared at the top of the U-tubes (plots 20 and 22). At []^(a,b,c) seconds, all flow through steam generator-A stopped, since the free-water surface in the U-tubes had fallen too low to be overcome by the buoyancy head steam fraction oscillations. The oscillations were seen in temperatures and pressures throughout the primary system. When the steam generator U-tubes drained, these oscillations stopped. The steam generator-B U-tubes drained earlier than for steam generator-A due to the higher steam fraction in the fluid from hot leg-B.

The primary system pressure decay during the PDP began at a slow rate ([]^(a,b,c) psi/sec.). At approximately []^(a,b,c) seconds, the primary system pressure decay rate increased to []^(a,b,c) psi/sec., (Figure 4.2.5-1). This happened when the CMTs transitioned from their recirculation mode to their draindown mode of operation. This transition occurred when the steam generator U-tubes on the cold-leg side drained and the B-loop cold legs partially drained, allowing the cold leg

to CMT balance lines to drain. The increased rate of pressure decay was due to the increased injection rate of the cold liquid from the CMTs.

The CMTs began injecting cold fluid into the annular downcomer via the DVI lines when the S signal occurred. Initially, this injection from each CMT was driven by natural circulation (at approximately []^(a,b,c) lbm/sec.), with hot fluid flowing from the cold leg through the cold-leg balance line (CLBL) into the top of the CMT, replacing the cold fluid flowing from the bottom of the CMT. The CMT natural circulation flow rate slowed to []^(a,b,c) lbm/sec. at []^(a,b,c) seconds as the CMT filled with hot water and the cold-leg fluid temperature decreased, reducing the natural circulation driving head. When the loop-B cold legs were partially drained at about []^(a,b,c) seconds, the CLBLs of both CMTs drained, and the CMTs transitioned to their draindown mode. For this 1-in. LOCA, the break flow at this time was less than the nominal CMT draindown injection flow rate from the two CMTs. Therefore, when a free-water surface developed in the top of each CMT and the injection flow rate increased significantly, the cold-leg water level apparently increased. This blocked the path for steam to enter the balance lines and they refilled with water. This caused the CMT injection to consist of intermittent short periods of draindown, alternating with short periods of refill with water from the cold legs (data plot 38). This resulted in a slow net drop of the CMT level. Complete transition to draindown occurred earlier in CMT-B than in CMT-A. The free-liquid surfaces in the CMTs were apparently established by both flashing of the water in the CLBLs and steam flowing to the CMTs from the cold legs.

The steam flow from the cold legs into the top of the CMTs heated/maintained the upper CMT surfaces and water surface at saturation temperature. However, flashing also occurred in the CMTs due to the high temperature of the fluid in the top of the CMTs (data plots 15 and 16) and the decreasing system pressure. The steam above the liquid surface in the CMTs and in the balance lines was superheated after ADS-1. Flashing kept the water temperature at saturation temperature while system pressure decayed.

The accumulators began to inject fluid when the primary system pressure dropped below 711 psia (at approximately []^(a,b,c) seconds); however, the injection rate was low prior to ADS-1 (data plot 39). However, this small accumulator flow contributed to maintaining sufficient water level in the loop-B cold legs to cause the observed intermittent CMT draindown/refill.

Throughout the PDP, the PRHR HX removed energy from the primary system. The combined effect of the PRHR HX heat removal and CMT heat removal and injection of cold water were sufficient to limit the steam fraction of the two-phase mixture exiting the rod bundle to approximately []^(a,b,c) percent during this phase (data plots 30 and 31).

• **Automatic Depressurization System Phase ([]^(a,b,c) Seconds)**

The automatic depressurization system (ADS) phase began with the actuation of ADS-1 and ended with the actuation of ADS-4 (Figure 4.2.5-1).

Facility Response during the ADS Phase:

With the actuation of ADS-1, followed by ADS-2 and ADS-3 within approximately []^(a,b,c) seconds, the rate of primary system depressurization increased from []^(a,b,c) psi/sec. (at the end of PDP) to []^(a,b,c) psi/sec. (at the start of the ADS phase). This rate gradually decreased as system pressure decreased.

The primary system depressurization after ADS actuation resulted in a high rate of water injection from accumulators-A and -B (data plot 39). The CMTs' injection flow increased to approximately []^(a,b,c) lbm/sec. after ADS-1 and gradually decreased as CMT level decreased (data plot 38). The accumulators injected cold water into the primary system for approximately []^(a,b,c) seconds (from []^(a,b,c) seconds) and then were empty. The accumulator and CMTs' injection refilled the power channel rod bundle region and upper plenum with subcooled water.

The pressurizer immediately began to refill when ADS-1 occurred (data plot 32). The pressurizer never filled completely with liquid, as two-phase fluid was discharged out of the primary system through the ADS-1, -2, and -3 flow paths. When ADS-4 occurred, the pressurizer drained and only a small amount of steam was vented through ADS-1, -2, and -3.

Prior to the ADS period, liquid left the primary system only through the break in the cold leg. With the actuation of the ADS, fluid left the system through the ADS from the top of the pressurizer. The mass flow through the cold-leg break decreased as break flow converted from liquid to predominately saturated steam as the cold leg voided and primary system pressure decreased (data plot 43).

The PRHR HX stopped flowing (at approximately []^(a,b,c) seconds) after the accumulators had emptied and the power channel/hot leg-A contained subcooled water. PRHR HX flow did not restart in spite of the subsequent increase in the steam fraction of fluid from the power channel.

• Post-Automatic Depressurization System Phase ([]^(a,b,c) Seconds to End-of-Test)

The post-automatic depressurization system (post-ADS) phase began when ADS-4 occurred (Figure 4.2.5-1) and continued to the end of the test.

Facility Response during the Post-ADS Phase:

The primary system pressure rapidly decreased to near ambient after ADS-4 actuated. This caused the water level on the cold-leg side of the primary system to suddenly drop below the annular downcomer into the tubular downcomer (data plot 25). This resulted in a significant increase in the steam fraction in the rod bundle and upper plenum; however, there was sufficient two-phase flow to keep the bundle fully cooled (data plots 30 and 31). Gravity flow from the IRWST began at approximately []^(a,b,c) seconds and quickly refilled the tubular and annular portions of the downcomer (data plot 40). The steam fraction of flow through the power channel immediately

began to decrease and subcooled flow through the power channel and hot leg-A and out through ADS-4 was established by []^(a,b,c) seconds. Also, the upper plenum became subcooled and partially refilled. This steady-state condition was the end of the test.

When ADS-4 occurred, liquid again left the system while only a small amount of steam left the system from ADS-1, -2 and -3.

Component Responses

• Power Channel

The power channel consisted of five volumes: the lower plenum, the riser with the heater rod bundle, the lower portion of the upper plenum below the hot leg, the upper portion of the upper plenum above the hot leg, and the upper head. When the break occurred, primary system pressure decreased to the R trip point (1800 psia) and the S trip point (1700 psia). However, since the water everywhere in the power channel was subcooled relative to system pressure, no boiling or flashing occurred up to this point. Nothing significant happened in the power channel until the rod bundle power was reduced to []^(a,b,c) percent, []^(a,b,c) seconds after the R signal. At this time, the temperature gradient across the rod bundle quickly decreased due to the reduced power/flow ratio (still full flow), and the power channel outlet temperature dropped toward the lower-plenum inlet temperature (Figure 4.2.5-2). However, the water in the upper portion of the upper plenum remained at []^(a,b,c)°F and it began to flash when system pressure dropped below the saturation pressure of []^(a,b,c). When the RCPs were turned off (16.2 seconds after the S signal), the power/flow ratio increased and the power channel outlet temperature increased resulting in boiling in the rod bundle and flashing in the upper plenum. This produced sufficient steam to control system pressure, and both temperature and pressure increased momentarily (data plots 30 and 31). The water temperature in the lower portion of the upper-plenum reached a peak and started to drop in response to increasing primary system natural circulation flow caused by the increasing steam fraction of fluid on the hot-leg side of the power channel, PRHR HX flow, and CMT flow. The upper-plenum and hot-leg temperatures stabilized at approximately []^(a,b,c)°F, and the primary pressure stabilized at the corresponding saturation pressure (approximately 960 psia) at the end of the IDP.

The temperature of the liquid in the upper plenum and hot legs controlled system pressure during the PDP (data plot 4). Flow oscillations were observed in the tubular downcomer and dP across the rod bundle (period []^(a,b,c) seconds) when the RCPs had coasted down, and these oscillations continued until about []^(a,b,c) seconds into the test. The flow oscillations led to oscillations in the rod bundle steam fraction as measured by the collapsed liquid levels in the heater bundle, upper plenum, and hot leg (data plots 30 and 31). When the flow decreased, the steam fraction increased and resulted in an increase of the overall system pressure and the lower-upper plenum temperature (Figure 4.2.5-2). The overall system pressure oscillations were therefore out of phase with the tubular downcomer flow oscillations.

Data plots 30 and 31 show the collapsed liquid levels at various sections of the power channel during the S00401 test.

The liquid level in upper head started to decrease when system pressure decreased to the saturation pressure of the fluid temperature in the upper head (at about []^(a,b,c) seconds). Initially, the upper-head fluid temperature was only []^(a,b,c)°F and was therefore considerably cooler than the upper-plenum fluid temperature. Flashing of the fluid in the upper head began at []^(a,b,c) seconds, and the upper head was completely drained at approximately []^(a,b,c) seconds (data plot 4).

The upper-upper plenum began to flash when the primary system pressure decreased below []^(a,b,c) psia, and its level decreased reaching the hot-leg elevation at about []^(a,b,c) seconds. The top of the upper-upper plenum remained filled with steam until the end of the accumulator injection, when subcooled water in the lower portion of the upper plenum condensed the steam bubble in the upper-upper plenum (data plot 4). However, when accumulator injection ended, the upper-upper plenum again filled with steam. At []^(a,b,c) seconds, the upper-upper plenum again filled when water injected from the IRWST restored subcooled flow through the power channel.

The collapsed liquid level measurement in the lower-upper plenum provided a measurement of the steam fraction of flow exiting the rod bundle. During the PDP, this two-phase flow had a maximum steam fraction of []^(a,b,c) percent.

Data plot 30 shows the collapsed water level in the rod bundle oscillating following pump coastdown up until []^(a,b,c) seconds. This indicates apparent steam fractions in the rod bundle varying from []^(a,b,c) percent (with an approximately []^(a,b,c)-second period). After the oscillations ended, the steam fraction of the rod bundle region increased from []^(a,b,c) percent to []^(a,b,c) percent, just before accumulator injection. The accumulator injection completely subcooled the rod bundle. However, when the injection ended, the two-phase flow was again produced, and the steam fraction of fluid in the rod bundle region reached a maximum ([]^(a,b,c) percent) just before IRWST injection during the post-ADS phase. The lower-upper plenum steam fraction increased to []^(a,b,c) percent at this time, but this high steam fraction was due to the fact that the level of the two-phase mixture temporarily dropped below the hot-leg elevation.

The collapsed level measured just above the heated portion of the rod bundle (data plot 31) provided steam fractions that correlated well with those measured for the rod bundle and provided evidence of the steam/water fraction of the two-phase flow exiting the top of the rod bundle.

- **Pressurizer**

The pressurizer began to drain when the break occurred and was completely drained in approximately []^(a,b,c) seconds (data plot 32). The water in the pressurizer flashed due to the loss of system pressure, and the temperature of the water dropped from []^(a,b,c)°F during this initial depressurization (data plot 18). The hot water flowing from the pressurizer surge line into

hot leg-A caused a slight increase in the hot-leg temperature during this period, since it mixed with the flow from the power channel/upper plenum. The pressurizer remained drained until about []^(a,b,c) seconds, at which time it was slightly refilled by alternating and pulsed flow in the pressurizer surge line which occurred until about []^(a,b,c) seconds, and then by a steady flow until []^(a,b,c) seconds. The pressurizer drained again at []^(a,b,c) seconds and remained drained until ADS-1 occurred, at approximately []^(a,b,c) seconds, when it refilled and reached a collapsed liquid level of approximately []^(a,b,c) feet and a two-phase mixture was discharged from the top of the pressurizer via the ADS-1, -2 and -3 flow paths. The collapsed liquid level decreased as the steam fraction of the two-phase flow through the rod bundle increased. A sharp decrease in level occurred at approximately []^(a,b,c) seconds when the upper-upper plenum partially refilled with water. This continued after ADS-4, the pressurizer drained again at []^(a,b,c) seconds, and its level then reached manometric agreement with the water level/pressure in the primary system.

- **Steam Generator**

The steam generators acted as the heat sink until the MSLIV closed and prevented further energy removal from the secondary side. This caused the temperature of the secondary side to increase toward the primary system hot-leg temperature, which at the same time was dropping due to the reduced power/flow ratio. When the RCPs coasted down, there was a temporary temperature increase due to the increased power/flow ratio with natural circulation flow in the primary system (Figure 4.2.5-2). The steam generator secondary-side water temperature then stabilized at approximately []^(a,b,c)°F at the end of the IDP.

For the first part of the PDP, the pressure on the primary side of the steam generator U-tubes was higher than the secondary side (data plot 2). This indicated that some heat transfer from the primary to secondary side occurred and caused some condensation of the steam in the two-phase fluid coming from the hot leg. Primary system pressure did not drop below the steam generator secondary-side pressure until approximately []^(a,b,c) seconds into the event, at which time the steam generator U-tubes were nearly drained.

At the end of the pump coastdown, flow oscillations began in the tubular downcomer and through the power channel. This caused significant oscillations in the collapsed liquid level in the rod bundle and, consequently, in the density of the two-phase flow from the rod bundle into the lower-upper plenum, the hot legs, and to the steam generators (data plots 20 and 21). Since the driving force for the natural circulation flow was the density difference between the single-phase fluid in the cold legs and downcomer entering the power channel and the two-phase mixture leaving the rod bundle in the lower-upper plenum and the hot legs; the flow oscillations were sustained as long as there was flow through the steam generators.

The flow oscillations in the hot legs reached the steam generators. In steam generator-A, the U-tubes were full until approximately []^(a,b,c) seconds into the transient. At this time, a free-water surface began to develop in the top of the U-tubes, primarily due to the separation of

steam from the two-phase mixture from the hot leg at the low-flow velocities existing at natural circulation flow conditions. The fluid level on the hot-leg side of the U-tubes oscillated as it decreased. This condition continued until approximately []^(a,b,c) seconds into the transient, at which time the top of the U-tubes remained filled with saturated vapor and the U-tube water level decreased smoothly.

The fluid level on the cold-leg side of the steam generator-A U-tubes exhibited significant level oscillations from about []^(a,b,c) seconds and it appeared that intermittent flow over the top of the U-tubes occurred. At []^(a,b,c) seconds, the U-tube water level decreased smoothly and was drained at about []^(a,b,c) seconds.

Because of the higher steam fraction of the fluid in hot leg-B and steam generator-B, the time over which oscillations occurred was reduced and the U-tubes filled with saturated vapor sooner. As a result, the steam generator-B U-tubes began to drain at about []^(a,b,c) seconds.

The level in the steam generator-B hot-leg side U-tubes dropped to near zero at about []^(a,b,c) seconds. The cold-leg side U-tubes exhibited significant level oscillations from about []^(a,b,c) seconds which continued until the U-tubes were drained at []^(a,b,c) seconds (data plots 22 and 23).

- **Hot Legs**

Hot legs-A and -B were full of two-phase fluid until ADS-1 was actuated, when the measured level decreased (data plots 20 and 21). The hot legs were nearly drained at ADS-4 ([]^(a,b,c) seconds) and partially refilled after IRWST injection began. The principal difference between hot legs-A and -B was the influence of the PRHR HX on the void fraction in the hot legs during the PDP. Assuming that the fluid in the hot legs initially had the same steam fractions at the outlet of the power channel lower-upper plenum, the PRHR appeared to have preferentially removed steam from hot leg-A (as seen in the very high steam fraction for the PRHR inlet flow)—thereby reducing the steam fraction of the fluid in hot leg-A to less than the fluid steam fraction in hot leg-B. The apparent steam fraction in hot leg-A was []^(a,b,c) percent at []^(a,b,c) seconds; while in hot leg-B it was []^(a,b,c) percent. The hot-leg steam fraction affected the draining of the steam generators U-tubes, with steam generator-B draining earlier than steam generator-A.

- **Cold Legs**

Cold legs-A1 and -A2 remained full until []^(a,b,c) seconds (data plots 22 through 27), at which time the level decreased to the horizontal section of the pipes and drained at about []^(a,b,c) seconds. When ADS-4 occurred, the water level in the tubular downcomer temporarily dropped reaching []^(a,b,c) ft. below the hot-leg elevation at []^(a,b,c) seconds (data plot 24). The rod bundle steam fraction fluid increased. After IRWST injection began at []^(a,b,c) seconds, the annular downcomer refilled and the cold and hot legs were partially refilled after []^(a,b,c) seconds to the level of []^(a,b,c) ft. above the hot leg.

Cold legs-B1 and -B2 remained full until []^(a,b,c) seconds into the event, at which time both cold legs-B1 and -B2 drained rapidly to the level of the horizontal section of the pipes. This reduced water level in cold leg-B1 and cold leg B-2 initiated the transition of the CMTs from their recirculation to draindown mode of operation. Cold legs-B1 and -B2 were refilled at []^(a,b,c) seconds to the level of []^(a,b,c) ft. above the hot leg. At this time, the cold leg to CMT balance lines were partially filled.

• **PRHR and IRWST**

At the initiation of the test, the PRHR HX was filled with subcooled liquid. When the S signal occurred, the PRHR HX isolation valve opened and flow started through the HX at a high flow rate due to the still operating RCPs. When the RCPs were shutoff and the power channel upper plenum and the hot legs filled with two-phase fluid, a large portion of the steam in hot leg-A flowed to the PRHR HX (data plot 29). The two-phase mixture, consisting of alternating slugs of steam and water, was condensed and subcooled in the PRHR HX (data plot 28) from []^(a,b,c)°F to below []^(a,b,c)°F. During the PDP (prior to ADS-1), there was a significant variation in the flow through the PRHR HX, caused by the variation in the steam fraction in hot leg-A. Steam condensation was apparently occurring in the PRHR HX as evidenced by the rapid and wide variations in dP measurements (data plots 28, 29, and 37).

When ADS-1 began, the power channel and the hot leg were refilled with subcooled water by accumulator injection. The driving head for the flow in the PRHR HX decreased (caused by the density difference between the fluid in the PRHR supply line and the return line) and the flow decreased and stopped. There was a short period of reverse flow at the end of the accumulator discharge. The subcooled fluid in the hot leg never filled the PRHR supply line, and hot fluid in this line flashed as system pressure decreased. Simultaneous flashing in the supply line and condensation in the PRHR HX resulted in a wide variations in the measured flow in the PRHR HX return line.

After the accumulator injection had ended, the rod bundle upper plenum again reached saturation temperature, and a two-phase mixture again occurred in the hot legs. Flow restarted in the PRHR HX, and the flow rate varied in response to the steam fraction in the hot leg. When ADS-4 fully depressurized the primary system and the IRWST flow began and refilled the power channel and the hot leg with subcooled water again, the flow through the PRHR HX stopped for the remainder of the transient. The subcooled fluid in the hot leg filled the PRHR supply line at []^(a,b,c) seconds.

Following ADS-4, primary system pressure decreased to near ambient, and gravity flow due to the water elevation head in the IRWST began injecting water into the annular downcomer via the DVI lines. The flow from the IRWST was sufficient to refill the power channel, downcomer, and loop piping and to establish subcooled fluid flow through the tube bundle and out through the ADS-4 flow paths (data plots 32 and 40).

- **Core Makeup Tanks**

The CMT injection was initiated two seconds after the S signal when the CMT injection line isolation valves were opened. Initially, the flow from the CMTs occurred by natural circulation; hot water from cold legs flowed to the top of the CMTs and cold water from the bottom of the CMTs flowed to the downcomer, via the DVI lines, into the power channel.

Initially, this recirculation rate was approximately 0.13 lbm/sec. from each CMT. The flow rate slowed down to []^(a,b,c) lbm/sec. at []^(a,b,c) seconds due to the decreased buoyant head driving force that occurred as the CMT water was replaced with hot water from the cold legs, and as the cold-leg water temperature decreased.

After cold legs-B1 and -B2 drained to the level of horizontal pipes at []^(a,b,c) seconds, flashing/drainage began in the cold-leg balance line. When the temperature at the top of the CMT reached the saturation temperature for primary system pressure, a free-water surface was established in the CMTs. This increased the driving head for the injection flow and resulted in a higher drandown flow rate. For the 1-inch LOCA, the break flow at this time was less than full CMT drandown flow rate. This caused the CMT injection to consist intermittent short periods of drandown, which increased the cold-leg water level and short periods of refill with water from the cold legs. This resulted in a slow decrease in CMT levels and the ADS-1 actuation was therefore delayed and occurred at a system pressure of approximately []^(a,b,c) psia, considerably below 711 psia accumulator gas pressure. Part of the accumulator coolant inventory was therefore injected into the primary system prior to ADS-1. This accumulator injection helped maintain the primary system coolant inventory at cold-leg elevation and thus contributed to intermittent CMT drandown/refill. For test S00401, the break was located in cold leg-B2, resulting in cold leg-B2 draining before cold leg-B1. Since the CMT-B balance line was connected to cold leg-B2, the drandown began earlier for CMT-B (at 2300 seconds) than for CMT-A (at []^(a,b,c) seconds), as shown in data plot 38. The CMT balance lines finally completely drained at []^(a,b,c) seconds (ADS-1), resulting in an increase in CMT injection flow rate. The steam in the CMT balance lines and at top of the CMTs was slightly superheated as the primary system pressure was rapidly reduced by ADS operation.

The CMTs were heated first by the hot liquid which replaced the cold water draining from the bottom of the CMTs. A stable, stratified thermal gradient was established in the CMTs (data plots 15 and 16). Later steam from the cold legs maintained the exposed metal and free-water surface temperatures at or near saturation temperature.

The CMT recirculation mode flow rate was initially approximately []^(a,b,c) lbm/sec. and steadily decreased to approximately []^(a,b,c) lbm/sec. when the transition to drandown began. The CMT average injection flow rate increased to approximately []^(a,b,c) lbm/sec. during the transition period. After ADS-1 actuated, CMT injection increased again to []^(a,b,c) lbm/sec. and then gradually decreased with time. During the accumulator injection (ADS-1), the CMTs' drandown rate remained high. CMT-A was drained at about ADS-4 ([]^(a,b,c) seconds). The CMT-B

injection flow rate decreased when the IRWST started at about []^(a,b,c) seconds, and CMT-B drained at []^(a,b,c) seconds (data plot 33).

- **Accumulators**

The accumulators provided water injection by a polytropic expansion of a compressed air volume stored within the accumulator. Accumulator injection started when the primary system pressure dropped below 711 psia at []^(a,b,c) seconds. The accumulator injection flow rate was low until ADS-1 was actuated at approximately []^(a,b,c) seconds when the flow rate increased to approximately []^(a,b,c) lbm/sec. The accumulator injection after ADS actuation lasted approximately []^(a,b,c) seconds, and the accumulators were completely drained (data plot 34).

The effective polytropic coefficient of expansion was calculated for the accumulators (Figures 4.2.5-3 and 4.2.5-4) to be []^(a,b,c) for accumulator-A and [1.21]^(a,b,c) for accumulator-B. This was near the mid-point between isothermal expansion ($k = 1$) and adiabatic expansion ($k = 1.4$) and showed that some heat was picked up by the compressed air from the internal metal surfaces of the accumulator during the expansion.

Mass Discharge and Mass Balance

The catch tank weight measurements are shown in data plot 43 for the break flow, for the ADS-1, -2, and -3 flows, and for the ADS-4 flow. The break flow as shown in plot 44, which began when the test was initiated, decreases as system pressure drops during the IDP and the PDP. When the ADS was actuated, the break location voided, and further discharge from the break was primarily saturated steam until IRWST injection refilled the cold leg after ADS-4.

The discharge from ADS-1, -2, and -3 was stable throughout the accumulator injection and increased temporarily when the injection ended. When ADS-4 occurred, the discharge of fluid from the top of the pressurizer essentially ended, and the fluid discharge from ADS-4 began. The ADS-4 fluid discharge rate was relatively stable and continued until the end of the test. The discharged masses are shown in Table 4.2.5-4.

The mass balance results for test S00401 were calculated based on water inventory before and after the test. Table 4.2.5-2 gives a detailed listing of the inventories of water in the various components before the test. Table 4.2.5-3 lists the inventories after the test and the amount of water injected into the vessel from the IRWST. The water level in the vessel was determined by the DP-B16P measurement to be []^(a,b,c) in. []^(a,b,c) above the hot-leg centerline at the end of the test. Table 4.2.5-4 compares the mass balance for the system before and after the test and shows 98.5% agreement of the measurements.

**TABLE 4.2.5-1
SEQUENCE OF EVENTS FOR TEST S00401**

Event	Specified	Instrument Channel	Actual Time(s)
Break Opens	0		(a,b,c)
R Signal	P = 1800 psia	P-027P	
MSLIV	R signal + 2 sec.	Z_A04S0, F_A04S	
		Z_B04S0, F_B04S	
S Signal	P = 1700 psia	P-027P	
MFW IV Closure	S signal + 2 sec.	Z_B02S0, F_B01S	
		Z_A02S0, F_A01S	
CMT IV Opening	S signal + 2 sec.	Z_A040EC, F-A40E	
		Z_B040EC, F-B40E	
RCPs Tripped	S signal +16.2 sec.	I-A1P, S-A1P	
		I-B1P, S-B1P	
PRHR Heat Exchanger Actuation	S signal +2 sec.	Z_A81EC, F_A80E	
ADS-1	CMT level 67% +30 sec.	L_B40E	
		Z_001PC	
Accumulators	P-027P = 710 psia	F_A20E	
		F_B20E	
ADS-2	CMT level 67% + 125 sec.	L_B40E	
		Z_002PC	
ADS-3	CMT level 67% + 245 sec.	L_B40E	
		Z_003PC	
ADS-4	CMT level 20% +60 sec.	L_B40E	
		Z_004PC A/B	
IRWST Injection	P-027P = 26 psia	F_A60E	
		F_B60E	

*Manually opened

**TABLE 4.2.5-2
WATER INVENTORY BEFORE TEST**

Component	Volume (ft.³)/(l)	Net Vol (ft.³)/(l)	Temp (°F)	Relative Density	Mass (lbm)
Loops	8.97 ft. ³ (254.0 l)	8.97 ft. ³ (254.0 l)			(a,b,c)
Pressurizer	3.37 ft. ³ (95.4 l)	1.85 ft. ³ (52.4 l)			
Surge Line	0.34 ft. ³ (9.6 l)	0.34 ft. ³ (9.6 l)			
Tubular Downcomer	1.38 ft. ³ (39.1 l)	1.38 ft. ³ (39.1 l)			
Annular Downcomer + Upper Head Bypass	0.54 ft. ³ (15.3 l)	0.54 ft. ³ (15.3 l)			
Core Bypass	0.44 ft. ³ (12.4 l)	0.44 ft. ³ (12.4 l)			
Lower Plenum	0.81 ft. ³ (22.8 l)	0.81 ft. ³ (22.8 l)			
Riser	1.64 ft. ³ (46.4 l)	1.64 ft. ³ (46.4 l)			
Upper Plenum	1.46 ft. ³ (41.3 l)	1.46 ft. ³ (41.3 l)			
Upper Head	1.90 ft. ³ (53.8 l)	1.90 ft. ³ (53.8 l)			
CMTs	10.1 ft. ³ (286.0 l)	10.1 ft. ³ (286.0 l)			
Accumulators	10.1 ft. ³ (286.0 l)	7.64 ft. ³ (216.2 l)			
IRWST Injection Line	0.18 ft. ³ (5.1 l)	0.18 ft. ³ (5.1 l)			
TOTAL INVENTORY					

TABLE 4.2.5-3

WATER INVENTORY AFTER TEST S00401 WAS COMPLETED

Water level as measured by DP-B16P (-0.45 psi) was 13.12 in. (328 mm) above hot leg

Component	Volume (ft. ³)/(l)	Net Vol (ft. ³)/(l)	Temp (°F)	Relative Density	Mass (lbm)
Loops	8.97 ft. ³ (254.0 l)	0.0 ft. ³ (0.0 l)			(a,b,c)
Pressurizer	3.37 ft. ³ (95.4 l)	0.0 ft. ³ (0.0 l)			
Surge Line	0.34 ft. ³ (9.6 l)	0.0 ft. ³ (0.0 l)			
Tubular Downcomer	1.38 ft. ³ (39.1 l)	1.38 ft. ³ (39.1 l)			
Annular Downcomer Upper Head Bypass	0.54 ft. ³ (15.3 l)	0.43 ft. ³ (12.1 l)			
Core Bypass	0.44 ft. ³ (12.4 l)	0.44 ft. ³ (12.4 l)			
Lower Plenum	0.81 ft. ³ (22.8 l)	0.81 ft. ³ (22.8 l)			
Riser	1.64 ft. ³ (46.4 l)	1.64 ft. ³ (46.4 l)			
Upper Plenum	1.46 ft. ³ (41.3 l)	0.12 ft. ³ (34.4 l)			
Upper Head	1.90 ft. ³ (53.8 l)	0.0 ft. ³ (0.0 l)			
CMTs	10.1 ft. ³ (286.0 l)	0.0 ft. ³ (0.0 l)			
Accumulator	10.1 ft. ³ (286.0 l)	0.0 ft. ³ (0.0 l)			
IRWST	0.18 ft. ³ (5.1 l)	0.0 ft. ³ (0.0 l)			
TOTAL INVENTORY					

WATER INJECTED FROM THE IRWST DURING EVENT

IRWST Injection	Del Elev (psi)	Area (in ²)	Temp (°F)	Rel Dens	Mass (lbm)
	i				j(a,b,c)

**TABLE 4.2.5-4
MASS BALANCE FOR TEST S00401**

	Starting Inventory (lbm)	Ending Inventory (lbm)
Total Primary System		(a,b,c)
IRWST Injection		
Break		
ADS-1, -2, -3		
ADS-4		
TOTAL		
Ending Inventory/Starting Inventory (lbm)		
Ending Inventory/Starting Inventory (%)		

The following figures have been intentionally deleted
from this document due to their proprietary nature.

**TEST DATA PLOT PACKAGE
CHANNEL LIST BY COMPONENT**

COMPONENT	CHANNEL	UNITS	PLOT	COMMENT
ACCA	F_A20E	lbm/sec.	39	
ACCA	L_A20E	ft.	34	
ACCB	F_B20E	lbm/sec.	39	
ACCB	L_B20E	ft.	34	
ADS 1, 2, & 3	IF30flw	lbm/sec.	44	Flow rate derived from IF030P
ADS 1, 2, & 3	IF030P	lbm	43	Catch tank
ADS 4 & SG	IF40flw	lbm/sec.	44	Flow rate derived from IF040P
ADS 4 & SG	IF040P	lbm	43	Catch tank
ANND C	DP-A021P	psi	24	To cold leg-A1
ANND C	DP-A022P	psi	25	To cold leg-A2
ANND C	DP-B021P	psi	26	To cold leg-B1
ANND C	DP-B022P	psi	27	To cold leg-B2
BREAK LINE	IF05flw	lbm/sec.	44	Flow rate derived from IF005P
BREAK LINE	IF005P	lbm	43	Catch tank
CLA	DP-A001P	psi	24	To cold leg-A1
CLA	DP-A002P	psi	25	To cold leg-A2
CLA	DP-A09P	psi	22	Pump suction
CLA	T-A10P	°F	11	Steam generator outlet
CLA1	F_A01P	lbm/sec.	36	
CLA1	T-A021PL	°F	13	Downcomer inlet
CLA1	T-A11P	°F	11	Pump outlet
CLA2	F_A02P	lbm/sec.	36	
CLA2	T-A022PL	°F	13	Downcomer inlet
CLB	DP-B001P	psi	26	To cold leg-B1

**TEST DATA PLOT PACKAGE
CHANNEL LIST BY COMPONENT (Cont.)**

COMPONENT	CHANNEL	UNITS	PLOT	COMMENT
CLB	DP-B002P	psi	27	To cold leg-B2
CLB	DP-B09P	psi	23	Pump suction
CLB	T-B10P	°F	12	Steam generator outlet
CLB1	F_B01P	lbm/sec.	36	
CLB1	T-B021PL	°F	14	Downcomer inlet
CLB1	T-B11P	°F	12	Pump outlet
CLB2	F_B02P	lbm/sec.	36	
CLB2	T_B022PL	°F	14	Downcomer inlet
CMTA	F_A40E	lbm/sec.	38	
CMTA	L_A40E	ft.	33	
CMTA	T-A401E	°F	15	Top (242.25 in.)
CMTA	T-A403E	°F	15	216.75 in.
CMTA	T-A405E	°F	15	191.25 in.
CMTA	T-A407E	°F	15	165.75 in.
CMTA	T-A409E	°F	15	140.25 in.
CMTA	T-A411E	°F	15	114.75 in.
CMTA	T-A413E	°F	15	89.25 in.
CMTA	T-A415E	°F	15	63.75 in.
CMTA	T-A417E	°F	15	38.25 in.
CMTA	T-A420E	°F	15	Bottom (0 in.)
CMTB	F_B40E	lbm/sec.	38	
CMTB	L_B40E	ft.	33	
CMTB	T-B401E	°F	16	Top (242.25 in.)
CMTB	T-B403E	°F	16	216.75 in.
CMTB	T-B405E	°F	16	191.25 in.
CMTB	T-B407E	°F	16	165.75 in.
CMTB	T-B409E	°F	16	140.25 in.
CMTB	T-B411E	°F	16	114.75 in.
CMTB	T-B413E	°F	16	89.25 in.

**TEST DATA PLOT PACKAGE
CHANNEL LIST BY COMPONENT (Cont.)**

COMPONENT	CHANNEL	UNITS	PLOT	COMMENT
CMTB	T-B415E	°F	16	63.75 in.
CMTB	T-B417E	°F	16	38.25 in.
CMTB	T-B420E	°F	16	Bottom (0 in.)
CVCS	F-001A	psi	42	
DVIA	T-A00E	°F	13	
DVIB	T-B00E	°F	14	
HLA	DP-A04P	psi	20	
HLA	T-A03PL	°F	5	Vertical, near power channel
HLA	T-A03PO	°F	5	Horizontal, near power channel
HLA	T-A04P	°F	5	Near steam generator inlet
HLB	DP-B04P	psi	21	
HLB	T-B03PL	°F	6	Vertical, near power channel
HLB	T-B03PO	°F	6	Horizontal, near power channel
HLB	T-B04P	°F	6	Near steam generator inlet
IRWST	F_A60E	lbm/sec.	40	
IRWST	F_B60E	lbm/sec.	40	
IRWST	L_060E	ft	32	
IRWST	T-061E	°F	17	Bottom
IRWST	T-062E	°F	17	Below middle
IRWST	T-063E	°F	17	Middle
IRWST	T-064E	°F	17	Above middle
IRWST	T-065E	°F	17	Top
PC	W_00P	kW	1	
PC-HB	L_000P	ft	30	Heater bundle
PC-HR	TW018P20	°F	3	Heater rod
PC-HR	TW018P48	°F	3	Heater rod
PC-HR	TW019P82	°F	3	Heater rod
PC-HR	TW020P24	°F	3	Heater rod
PC-HR	TW020P87	°F	3	Heater rod

**TEST DATA PLOT PACKAGE
CHANNEL LIST BY COMPONENT (Cont.)**

COMPONENT	CHANNEL	UNITS	PLOT	COMMENT
PC-UH	T-016P	°F	4	Upper head
PC-UP	L_A15P	ft.	30	Bottom of the upper plenum
PC-UP	L_A16P	ft.	31	Top of the upper plenum
PC-UP	T-015P	°F	4	Upper plenum
PC-UH	L_017P	ft.	31	Upper head
PC-UP	L_A14P	ft.	31	Above top of the active fuel
PRHR	DP-A81AE	psi	29	Supply line inverted U-tube
PRHR	DP-A81BE	psi	29	Supply line inverted U-tube
PRHR	DP-A81E	psi	28	Supply line
PRHR	DP-A82E	psi	28	Heat exchanger
PRHR	DP-A83E	psi	28	Return line
PRHR	F_A80E	lbm/sec.	37	Return line
PRHR	T-A82E	°F	19	Inlet
PRHR	T-A83E	°F	19	Exit
PRZ	L_010P	ft.	32	
PRZ	P-027P	psia	2	
PRZ	T-026P	°F	18	487 in.
SGA	DP-A05P	psi	20	Hot side
SGA	DP-A06P	psi	20	Hot side
SGA	DP-A07P	psi	22	Cold side
SGA	DP-A08P	psi	22	Cold side
SGA	F_A01S	lbm/sec.	41	Main SGA feed
SGA	F_A20A	lbm/sec.	41	Secondary SGA feed
SGA	L_A10S	ft.	35	Overall level
SGA	P-A04S	psia	2	Secondary system
SGA	T-A01S	°F	10	MFW-A
SGA	T-A05P	°F	7	Hot side
SGA	T-A05S	°F	9	Hot side - riser
SGA	T-A06P	°F	7	Hot side

TEST DATA PLOT PACKAGE
CHANNEL LIST BY COMPONENT (Cont.)

COMPONENT	CHANNEL	UNITS	PLOT	COMMENT
SGA	T-A08P	°F	11	Cold side
SGA	TW-A06S	°F	7	Hot side
SGB	DP-B05P	psi	21	Hot side
SGB	DP-B06P	psi	21	Hot side
SGB	DP-B07P	psi	23	Cold side
SGB	DP-B08P	psi	23	Cold side
SGB	F_B01S	lbm/sec.	41	Secondary SGA feed
SGB	F_B20A	lbm/sec.	41	Secondary SGB feed
SGB	L_B10S	ft.	35	Overall level
SGB	P-B04S	psia	2	Secondary system
SGB	T-B01S	°F	10	MFW-B
SGB	T-B05P	°F	8	Hot side
SGB	T-B05S	°F	9	Hot side - riser
SGB	T-B06P	°F	8	Hot side
SGB	T-B07P	°F	8	U-tube top
SGB	T-B08P	°F	12	Cold side
SGB	TW-B06S	°F	8	Hot side
SL	T-020P	°F	18	Surge line near pressurizer
TDC	DP-001P	psi	25,26	Top
TDC	DP-002P	psi	24,25,26,27	Bottom
TDC	T-001PL	°F	13,14	Top
TDC	T-003P	°F	13,14	Bottom
TSAT-PRZ		°F	18	Based on P-027P
UH-TSAT		°F	4	Based on P-017P

The data plots are found in the proprietary version of this document.

4.2.6 One-In. Cold-Leg Break with Three PRHR HX Tubes, without Nonsafety Systems (S01613)

This matrix test was performed to be identical to matrix test S00401 with the exception that the number of PRHR HX tubes in use was increased from 1 tube to 3 tubes. This test simulated a 1-in. break in the bottom of cold leg-B2. The test began with the initiation of the break in cold leg-B2, which was the cold leg with the CMT-B pressure balance line connection. The break location was just downstream from the cold leg to the core makeup tank (CMT) balance line connection. This test was performed without any nonsafety systems (chemical and volume control system [CVCS] makeup pumps, steam generator startup feedwater [SFW] pumps, and normal residual heat removal system [NRHR] pumps) operating.

Results are provided in the data plot package at the end of this section. The sequence of events for S01613 is listed in Table 4.2.6-1.

The AP600 SPES-2 tests were marked by distinctly different phases. These phases were characterized by the rate at which the primary system pressure decreased and the thermal-hydraulic phenomena occurring within the primary and safety systems. The different phases selected for the purpose of detailed evaluation of this LOCA are shown in Figure 4.2.6-1 and are as follows:

- Initial depressurization phase (IDP)—Point 1 to 2
- Pressure decay phase (PDP)—Point 2 to 3
- Automatic depressurization system (ADS) phase—Point 3 to 4
- Post-automatic depressurization system (post-ADS) phase—Point 4 to 5

Overall Test Observations

Figure 4.2.6-1 shows the plant primary system pressure during test S01613 (as measured at the top of the pressurizer), with selected component actuations and plant responses shown in relation to primary system pressure.

The IDP began with the initiation of the break, which resulted in a rapid reduction in pressure. The reactor trip (R) signal initiated at 1800 psia. The safety systems actuation (S) signal initiated at 1700 psia. The R and the S signals initiated the following actions:

- Decay power simulation (with heat loss compensation) initiated
- Main steamline isolation valves (MSLIVs) closed
- Main feedwater isolation valves (MFWIVs) closed
- CMT injection line isolation valves opened
- Passive residual heat removal (PRHR) return line isolation valve opened
- Reactor coolant pumps (RCPs) stopped running

Recirculation flow through the CMTs and flow through the PRHR heat exchanger (HX) began immediately after their isolation valves opened. Flashing/boiling occurred in the rod bundle and

upper-plenum regions of the power channel due to the rapid decrease in primary pressure to the fluid saturation pressure. The measured fluid level in the upper-upper plenum decreased to the hot-leg elevation. The flashing on the hot-leg side of the primary system stopped the rapid drop in primary system pressure. When the RCPs were shut off (at []^(a,b,c) seconds), the flow through the rod bundle began to oscillate (with a []^(a,b,c)-second period). This resulted in oscillations in the rod bundle and lower-upper plenum collapsed liquid level and fluid temperature, and system pressure.

During the initial stages of the PDP, the rod bundle collapsed liquid level decreased (fluid steam fraction increased). This caused an increasing steam fraction in the upper plenum and the hot legs. The hot leg-B fluid had a steam fraction close to that observed in the upper plenum. The steam fraction in hot leg-A was lower due to the selective removal of vapor from the hot leg into the PRHR HX inlet line.

Two-phase flow in the hot legs initiated draining of the steam generator U-tubes, as steam from the two-phase mixture collected in the top of the U-tubes. This stopped the primary system flow through the steam generators so that the power channel flow was composed predominantly of the flow through the PRHR HX. The steam fraction oscillations observed in the rod bundle and in the upper plenum ended when the steam generator U-tubes drained. Approximately []^(a,b,c) seconds into the test, the steam generator-B U-tubes began to drain. The steam generator-A U-tubes began to drain, approximately []^(a,b,c) seconds later due to the lower fluid steam fraction in hot leg-A.

Due to boiling in the rod bundle (data plots 30 and 31), two-phase flow entered the hot leg from the upper plenum and flowed through the PRHR HX. The flow into the PRHR HX consisted of intermittent periods of saturated water and steam which had an average steam fraction significantly greater than the fluid in the upper plenum. The average steam fraction at the PRHR HX inlet was as high as []^(a,b,c) percent, which enhanced the PRHR HX heat transfer from the primary system, as compared to its heat removal capability with single-phase saturated or subcooled water. When the primary system flow stabilized after the initial flow oscillations, a PRHR HX heat removal rate of []^(a,b,c) kW was calculated. This calculation was based on the steam fraction at the PRHR HX inlet (as calculated from the dP instrument readings in data plot 29), the averaged return flow rate, the HX inlet and outlet temperatures, and the pressure. This calculation, which assumes a slip coefficient of 1 between water and steam, may be lower than the actual heat transfer and should only be used for test-to-test comparison.

When the primary system pressure decreased to the saturation pressure for the fluid in the upper head, it began to drain (at approximately []^(a,b,c) seconds).

When the loop-B cold legs had partially emptied, the CMTs transitioned from their recirculation mode of operation to an intermittent draindown mode of operation at approximately []^(a,b,c) seconds.

During the first []^(a,b,c) seconds of this test (until ADS-1), []^(a,b,c) lbm of water were expelled through the break draining the: the pressurizer, the steam generator U-tubes, the power channel upper head, the power channel upper plenum above the hot leg, most of the cold legs, and approximately

[]^(a,b,c) percent of the CMTs. The heated rods that simulate the AP600 core decay heat reduced power to approximately 230 kW at 4800 seconds. This value consisted of 80-kW of decay heat and 150-kW of heat loss compensation. The mass flow rate out of the break was decreasing, indicating that cold leg-B2 was almost empty.

The ADS phase began with the actuation of ADS-1 (at approximately []^(a,b,c) seconds). ADS-2 and -3 occurred within the next []^(a,b,c) seconds. The heat loss compensation was removed from the rod bundle power decay simulation when ADS-1 occurred, reducing the rod bundle power to approximately 80 kW.

The ADS actuation increased the rate of primary system depressurization and resulted in high injection flow from the accumulators. The rapid injection of cold water from the accumulators (from []^(a,b,c) seconds) and the CMT injection flow refilled the power channel/upper plenum, the horizontal portion of the hot legs and the pressurizer. When the accumulator discharge ended the flow through the heater bundle decreased to the injection rate of the CMTs and the PRHR HX flow, and two-phase flow occurred again the heater bundle, hot leg-A, the PRHR HX, and into the pressurizer. The rod bundle steam fraction continued to increase (collapsed liquid level decreased) until after ADS-4 was actuated.

The mass flow rate through the break decreased sharply at approximately []^(a,b,c) seconds, indicating that cold leg-B2 emptied and that the break flow was steam. During the ADS phase, approximately []^(a,b,c) lbm of subcooled water were discharged from ADS-1, -2, and -3.

The post-ADS period began when ADS-4 actuated. ADS-4 occurred at []^(a,b,c) seconds, the fluid discharge through ADS-1, -2, and -3 stopped, and the pressurizer water drained back into hot leg-A. A small amount of CMT flow continued into the downcomer via the direct vessel injection (DVI) line. When the primary system pressure decreased below the pressure corresponding to the water elevation head of the IRWST, flow from the IRWST began. Shortly thereafter, the CMT flow ended. The flow from the IRWST gradually refilled and subcooled the power channel, restored single-phase water flow through the rod bundle, and partially refilled the upper-upper plenum. The PRHR HX supply line partially emptied at approximately []^(a,b,c) and the PRHR HX was no longer effective. A steady flow of subcooled water was established from the IRWST into the downcomer, through the power channel, and left the primary system through the ADS-4 flow paths.

This test demonstrated that the heater bundle was fully covered by a single- or two-phase fluid at all times during this test (data plots 30 and 31). There was no indication of heater rod temperature increase due to lack of cooling (data plot 3). Key parameters comparing the S01613 test with other tests are listed in Table 5-1 in Section 5.0.

Discussion of Test Transient Phases

- **Initial Depressurization Phase (0 to []^(a,b,c) Seconds)**

The initial depressurization phase (IDP) began with the initiation of the break (at time 0) and ended when the primary system pressure reached the saturation pressure of the fluid in the lower-upper plenum and the hot legs (Figure 4.2.6-1). This phase included the following events: R signal at 1800 psia (decay power simulation initiated and the MSIV closed), and S signal at 1700 psia (the MFWIV closed, the CMT injection line isolation valves opened, and the PRHR heat exchanger return line isolation valve opened—all with a 2-second delay; and RCP coastdown started after a 16.2-second delay). See Table 4.2.6-1.

Facility Response During the IDP:

From time 0 until the R signal occurred, the primary system pressure decreased due to the expansion of the pressurizer steam volume caused by fluid loss through the break. The pressurizer partially compensated for the loss of pressure by flashing; however, it was drained after []^(a,b,c) seconds (data plot 32). The R (at []^(a,b,c) seconds) and the S (at []^(a,b,c) seconds) signals were based on pressurizer pressure only. When the R signal occurred, the MSLIV closed and the power was reduced to 20 percent of full power after a 5.75-second delay and began to decay after a 14.5-second delay.

As a result of the power reduction without flow reduction, the rod bundle ΔT decreased due to the low power/flow ratio and the lower-upper plenum temperature dropped toward the cold-leg temperature. At the same time, the primary system pressure had decreased to []^(a,b,c) psia (the saturation pressure of the []^(a,b,c)°F water in the upper-upper plenum), and the upper-upper plenum began to flash and rapidly drain. System pressure decreased to approximately []^(a,b,c) psia at []^(a,b,c) seconds. At this time, the pressurizer was drained, but primary system pressure was still dictated by the temperature of the saturated vapor in the pressurizer (about []^(a,b,c)°F) and the fluid in the surge line. When the RCPs shut off (at []^(a,b,c) seconds), the rod bundle and upper-plenum fluid temperatures increased due to the increased power/flow ratio at the lower flow. System pressure increased temporarily until the decreasing rod bundle decay power and the decreasing lower-plenum temperature (due to the CMTs injecting cold water into the downcomer) began to reduce the lower-upper plenum fluid temperature. The decrease in primary system pressure resulted from the balance between the steam generation rate (from flashing primary fluid), the volumetric flow of liquid out of the break, and the steam condensation occurring in the PRHR HX. Steam was continually generated by boiling due to the heater power. As system pressure continued to decrease, more fluid reached its saturation pressure and flashed. The PRHR HX flow started before the RCPs were tripped and then continued by natural circulation (data plot 37). Primary system pressure stabilized at saturation pressure for the bulk hot fluid in the primary system (approximately 540°F), as shown in Figure 4.2.6-1. This ended the IDP.

- **Pressure Decay Phase ([]^(a,b,c) Seconds)**

The pressure decay phase (PDP) began when system pressure (Figure 4.2.6-1) reached saturation pressure for the bulk hot fluid in the primary system. This phase ended when ADS-1 opened on low CMT level (at approximately []^(a,b,c) seconds) and augmented the system depressurization. This phase was characterized by a slow decrease in overall system pressure and temperature. The rod bundle power (decay heat plus heat loss compensation) was reduced from 310 kW to 230 kW (data plot 1). At []^(a,b,c) seconds (rod bundle power was about 250 kW), the PRHR HX heat removal rate was approximately []^(a,b,c) kW. The recirculating CMTs provided approximately []^(a,b,c) kW effective heat removal from the primary system at this time. This heat removal plus energy lost through the break and the facility heat losses exceeded the rod bundle heat input to the primary system.

The initial CMT natural circulation operating mode was followed by draindown injection when the loop-B cold legs drained (data plot 38). The U-tubes of the steam generators had completely drained at this time (data plots 20 through 23) and had no effect the rest of the test. Accumulator injection was initiated when the primary system pressure dropped below 711 psia (at approximately []^(a,b,c) seconds) prior to ADS-1 actuation; however, the injection rate was low (less than []^(a,b,c) lbm/sec.) due to the small difference between system pressure and accumulator gas pressure (data plot 39).

Facility Response During the PDP:

The oscillating flow in the primary system that began after the RCPs were shutoff continued into the PDP. These flow oscillations resulted in wide variations in the steam fraction of the two-phase mixture exiting the rod bundle and flowing into the hot legs (data plots 30 and 31). These oscillations in steam fraction had a significant effect on the thermal buoyancy head that drove the flow in the primary system at this time, since it affected the two-phase flow density. These steam fraction oscillations were observed through the hot leg and the steam generators (data plots 20 and 21). However, the steam fraction oscillations were converted to flow oscillations in the cold legs since the two-phase mixture entering the steam generators left the steam generators as saturated water (data plots 24 through 27). Some of the steam was condensed in the steam generator U-tubes (the primary-side pressure was higher than the secondary-side pressure at this time, allowing some heat to be transferred to the secondary-side fluid). The remaining steam was separated from the two-phase mixture in the high point of the U-tubes (due to low velocity), eventually causing the U-tubes to begin to drain, and a free-water surface appeared at the top of the U-tubes (plots 20 and 22). At []^(a,b,c) seconds, all flow through steam generator-A stopped, since the free-water surface in the U-tubes had fallen too low to be overcome by the buoyancy head steam fraction oscillations. The oscillations were seen in temperatures and pressures throughout the primary system. When the steam generator U-tubes drained, these oscillations stopped. The steam generator-B U-tubes drained earlier than for steam generator-A due to the higher steam fraction in the fluid from hot leg-B.

The primary system pressure decay during the PDP began at a slow rate ($[]^{(a,b,c)}$ psi/sec.). At approximately $[]^{(a,b,c)}$ seconds, the primary system pressure decay rate increased to $[]^{(a,b,c)}$ psi/sec., (Figure 4.2.6-1). This happened when the CMTs transitioned from their recirculation mode to their draindown mode of operation. This transition occurred when the steam generator U-tubes on the cold-leg side drained and the B-loop cold legs partially drained, allowing the cold leg to CMT balance lines to drain. The increased rate of pressure decay was due to the increased injection rate of the cold liquid from the CMTs.

The CMTs began injecting cold fluid into the annular downcomer via the DVI lines when the S signal occurred. Initially, this injection from each CMT was driven by natural circulation (at approximately $[]^{(a,b,c)}$ lbm/sec.), with hot fluid flowing from the cold leg through the cold-leg balance line (CLBL) into the top of the CMT, replacing the cold fluid flowing from the bottom of the CMT. The CMT natural circulation flow rate slowed to $[]^{(a,b,c)}$ lbm/sec. at $[]^{(a,b,c)}$ seconds as the CMT filled with hot water and the cold-leg fluid temperature decreased, reducing the natural circulation driving head. When the loop-B cold legs were partially drained at about $[]^{(a,b,c)}$ seconds, the CLBLs of both CMTs drained, and the CMTs transitioned to their draindown mode. For this 1-inch LOCA, the break flow at this time was less than the nominal CMT draindown injection flow rate from the two CMTs. Therefore, when a free-water surface developed in the top of each CMT and the injection flow rate increased significantly the cold leg water level apparently increases. This blocks the path for steam to enter the balance lines and they refill with water. This caused the CMT injection to consist of intermittent short periods of draindown, alternating with short periods of refill with water from the cold legs (data plot 38). This resulted in a slow net drop of the CMT level. Complete transition to draindown occurred earlier in CMT-B than in CMT-A. The free-liquid surfaces in the CMTs were apparently established by both flashing of the water in the CLBLs and steam flowing to the CMTs from the cold legs.

The steam flow from the cold legs into the top of the CMTs heated/maintained the upper CMT surfaces and water surface at saturation temperature. However, flashing also occurred in the CMTs due to the high temperature of the fluid in the top of the CMTs (data plots 15 and 16) and the decreasing system pressure. The steam above the liquid surface in the CMTs and in the balance lines was superheated after ADS-1. Flashing kept the water temperature at saturation temperature while system pressure decayed.

The accumulators began to inject fluid when the primary system pressure dropped below 711 psia (at approximately $[]^{(a,b,c)}$ seconds); however, the injection rate was low prior to ADS-1 (data plot 39). However, this small accumulator flow contributed to maintaining sufficient water level in the loop-B cold legs to cause the observed intermittent CMT draindown/refill.

Throughout the PDP, the PRHR HX removed energy from the primary system. The combined effect of the PRHR HX heat removal and CMT heat removal and injection of cold water were sufficient to limit the steam fraction of the two-phase mixture exiting the rod bundle to approximately $[]^{(a,b,c)}$ percent during this phase (data plots 30 and 31).

- **Automatic Depressurization System Phase (4600 to 5650 Seconds)**

The automatic depressurization system (ADS) phase began with the actuation of ADS-1 and ended with the actuation of ADS-4 (Figure 4.2.5-1).

Facility Response During the ADS Phase:

With the actuation of ADS-1, followed by ADS-2 and ADS-3 within approximately []^(a,b,c) seconds, the rate of primary system depressurization increased from almost 0. (at the end of PDP) to []^(a,b,c) psi/sec. (at the start of the ADS phase). This rate gradually decreased as system pressure decreased.

The primary system depressurization after ADS actuation resulted in a high rate of water injection from accumulators-A and -B (data plot 39). The CMTs' injection flow increased to approximately []^(a,b,c) lbm/sec. after ADS-1 and gradually decreased as CMT level decreased (data plot 38). The accumulators injected cold water into the primary system for approximately []^(a,b,c) seconds (from []^(a,b,c) seconds) and then were empty. The accumulator and CMTs' injection refilled the power channel rod bundle region and upper plenum with subcooled water.

The pressurizer immediately began to refill when ADS-1 occurred (data plot 32). The pressurizer never filled completely with liquid, as two-phase fluid was discharged out of the primary system through the ADS-1, -2, and -3 flow paths. When ADS-4 occurred, the pressurizer drained and only a small amount of steam was vented through ADS-1, -2, and -3.

Prior to the ADS period, liquid left the primary system only through the break in the cold leg. With the actuation of the ADS, fluid left the system through the ADS from the top of the pressurizer. The mass flow through the cold-leg break decreased as break flow converted from liquid to predominately saturated steam as the cold leg voided and primary system pressure decreased (data plot 43).

The PRHR HX stopped flowing (at approximately []^(a,b,c) seconds) after the accumulators had emptied and the power channel/hot leg-A contained subcooled water. PRHR HX flow did not restart in spite of the subsequent increase in the steam fraction of fluid from the power channel.

- **Post-Automatic Depressurization System Phase (5650 Seconds to End of Test)**

The post-automatic depressurization system (post-ADS) phase began when ADS-4 occurred (Figure 4.2.5-1) and continued to the end of the test.

Facility Response During the Post-ADS Phase:

The primary system pressure rapidly decreased to near ambient after ADS-4 actuated. This caused the water level on the cold-leg side of the primary system to suddenly drop below the annular

downcomer into the tubular downcomer (data plot 25). This resulted in a significant increase in the steam fraction in the rod bundle and upper plenum; however, there was sufficient two-phase flow to keep the bundle fully cooled (data plots 30 and 31). Gravity flow from the IRV/ST began at approximately []^(a,b,c) seconds and quickly refilled the tubular and annular portions of the downcomer (data plot 40). The steam fraction of flow through the power channel immediately began to decrease and subcooled flow through the power channel and hot leg-A and out through ADS-4 was established by approximately []^(a,b,c) seconds. Also, the upper plenum became subcooled and partially refilled. This steady-state condition was the end of the test.

When ADS-4 occurred, liquid again left the system while only a small amount of steam left the system from ADS-1, -2 and -3.

Component Responses

• Power Channel

The power channel consisted of five volumes: the lower plenum, the riser with the heater rod bundle, the lower portion of the upper plenum below the hot leg, the upper portion of the upper plenum above the hot leg, and the upper head. When the break occurred, primary system pressure decreased to the R trip point (1800 psia) and the S trip point (1700 psia). However, since the water everywhere in the power channel was subcooled relative to system pressure, no boiling or flashing occurred up to this point. Nothing significant happened in the power channel until the rod bundle power was reduced to 20 percent, 5.75 seconds after the R signal. At this time, the temperature gradient across the rod bundle quickly decreased due to the reduced power/flow ratio (still full flow), and the power channel outlet temperature dropped toward the lower-plenum inlet temperature (Figure 4.6.5-2). However, the water in the upper portion of the upper plenum remained at []^(a,b,c)°F and it began to flash when system pressure dropped below saturation pressure of ([]^(a,b,c)). When the RCPs were turned off (16.2 seconds after the S signal), the power/flow ratio increased and the power channel outlet temperature increased resulting in boiling in the rod bundle and flashing in the upper plenum. This produced sufficient steam to control system pressure, and both temperature and pressure increased momentarily (data plots 30 and 31). The water temperature in the lower portion of the upper-plenum reached a peak and started to drop in response to increasing primary system natural circulation flow caused by the increasing steam fraction of fluid on the hot-leg side of the power channel, PRHR HX flow, and CMT flow. The upper-plenum and hot-leg temperatures stabilized at approximately []^(a,b,c)°F, and the primary pressure stabilized at the corresponding saturation pressure (approximately []^(a,b,c) psia) at the end of the IDP.

The temperature of the liquid in the upper plenum and hot legs controlled system pressure during the PDP (data plot 4). Flow oscillations were observed in the tubular downcomer and dP across the rod bundle (period []^(a,b,c) seconds) when the RCPs had coasted down, and these oscillations continued until about []^(a,b,c) seconds into the test. The flow oscillations led to oscillations in the rod bundle steam fraction as measured by the collapsed liquid levels in the heater bundle,

upper plenum, and hot leg (data plots 30 and 31). When the flow decreased, the steam fraction increased and resulted in an increase of the overall system pressure and the lower-upper plenum temperature (Figure 4.2.6-2). The overall system pressure oscillations were therefore out of phase with the tubular downcomer flow oscillations.

Data plots 30 and 31 show the collapsed liquid levels at various sections of the power channel during the S01613 test.

The liquid level in upper head started to decrease when system pressure decreased to the saturation pressure of the fluid temperature in the upper head (at about []^(a,b,c) seconds). Initially, the upper-head fluid temperature was only []^(a,b,c)°F and was therefore considerably cooler than the upper-plenum fluid temperature. Flashing of the fluid in the upper head began at []^(a,b,c) seconds, and the upper head was completely drained at approximately []^(a,b,c) seconds (data plot 4).

The upper-upper plenum began to flash when the primary system pressure decreased below []^(a,b,c) psia, and its level decreased reaching the hot-leg elevation at about []^(a,b,c) seconds. The top of the upper-upper plenum remained filled with steam until the end of the accumulator injection, when subcooled water in the lower portion of the upper plenum condensed the steam bubble in the upper-upper plenum (data plot 4). However, when accumulator injection ended, the upper-upper plenum again filled with steam. At []^(a,b,c) seconds, the upper-upper plenum again filled when water injected from the IRWST restored subcooled flow through the power channel.

The collapsed liquid level measurement in the lower-upper plenum provided a measurement of the steam fraction of flow exiting the rod bundle. During the PDP, this two-phase flow had a maximum steam fraction of []^(a,b,c) percent.

Data plot 30 shows the collapsed water level in the rod bundle oscillating following pump coastdown up until []^(a,b,c) seconds. This indicates apparent steam fractions in the rod bundle varying from []^(a,b,c) percent (with an approximately []^(a,b,c) second period). After the oscillations ended, the steam fraction of the rod bundle region increased from []^(a,b,c) percent to []^(a,b,c) percent, just before accumulator injection. The accumulator injection completely subcooled the rod bundle. However, when the injection ended, the two-phase flow was again produced, and the steam fraction of fluid in the rod bundle region reached a maximum ([]^(a,b,c) percent) just before IRWST injection during the post-ADS phase. The lower-upper plenum steam fraction increased to []^(a,b,c) percent at this time, but this high steam fraction was due to the fact that the level of the two-phase mixture temporarily dropped below the hot-leg elevation.

The collapsed level measured just above the heated portion of the rod bundle (data plot 31) provided steam fractions that correlated well with those measured for the rod bundle and provided evidence of the steam/water fraction of the two-phase flow exiting the top of the rod bundle.

- **Pressurizer**

The pressurizer began to drain when the break occurred and was completely drained in approximately []^(a,b,c) seconds (data plot 32). The water in the pressurizer flashed due to the loss of system pressure, and the temperature of the water dropped from []^(a,b,c)°F during this initial depressurization (data plot 18). The hot water flowing from the pressurizer surge line into hot leg-A caused a slight increase in the hot-leg temperature during this period, since it mixed with the flow from the power channel/upper plenum. The pressurizer remained drained until ADS-1 occurred, at approximately []^(a,b,c) seconds, when it refilled and reached a collapsed liquid level of approximately []^(a,b,c) feet and a two-phase mixture was discharged from the top of the pressurizer via the ADS-1, -2 and -3 flow paths. The collapsed liquid level decreased as the steam function of the two-phase flow through the rod bundle increased. A sharp temporary decrease in level occurred at approximately []^(a,b,c) seconds when the upper-upper plenum partially refilled with water. Level decrease continued after ADS-4, the pressurizer drained again at []^(a,b,c) seconds and its level then reached manometric agreement with the water level/pressure in the primary system.

- **Steam Generator**

The steam generators acted as the heat sink until the MSLIV closed and prevented further energy removal from the secondary side. This caused the temperature of the secondary side to increase toward the primary system hot-leg temperature, which at the same time was dropping due to the reduced power/flow ratio. When the RCPs coasted down, there was a temporary temperature increase due to the increased power/flow ratio with natural circulation flow in the primary system (Figure 4.2.5-2). The steam generator secondary-side water temperature then stabilized at approximately []^(a,b,c)°F at the end of the IDP.

For the first part of the PDP, the pressure on the primary side of the steam generator U-tubes was higher than the secondary side (data plot 2). This indicated that some heat transfer from the primary to secondary side occurred and caused some condensation of the steam in the two-phase fluid coming from the hot leg. Primary system pressure did not drop below the steam generator secondary-side pressure until approximately []^(a,b,c) seconds into the event, at which time the steam generator U-tubes were nearly drained.

At the end of the pump coastdown, flow oscillations began in the tubular downcomer and through the power channel. This caused significant oscillations in the collapsed liquid level in the rod bundle and, consequently, in the density of the two-phase flow from the rod bundle into the lower-upper plenum, the hot legs, and to the steam generators (data plots 20 and 21). Since the driving force for the natural circulation flow was the density difference between the single-phase fluid in the cold legs and downcomer entering the power channel and the two-phase mixture leaving the rod bundle in the lower-upper plenum and the hot legs; the flow oscillations were sustained as long as there was flow through the steam generators.

The flow oscillations in the hot legs reached the steam generators. In steam generator-A, the U-tubes were full until approximately []^(a,b,c) seconds into the transient. At this time, a free-water surface began to develop in the top of the U-tubes, primarily due to the separation of steam from the two-phase mixture from the hot leg at the low-flow velocities existing at natural circulation flow conditions. The fluid level on the hot-leg side of the U-tubes oscillated as it decreased. This condition continued until approximately []^(a,b,c) seconds into the transient, at which time the top of the U-tubes remained filled with saturated vapor and the U-tube water level decreased smoothly.

The fluid level on the cold-leg side of the steam generator-A U-tubes exhibited significant level oscillations from about []^(a,b,c) seconds and it appeared that intermittent flow over the top of the U-tubes occurred. At []^(a,b,c) seconds, the U-tube water level decreased smoothly and was drained at about []^(a,b,c) seconds.

Because of the higher steam fraction of the fluid in hot leg-B and steam generator-B, the time over which oscillations occurred was reduced and the U-tubes filled with saturated vapor sooner. As a result, the steam generator-B U-tubes began to drain at about []^(a,b,c) seconds.

The level in the steam generator-B hot-leg side U-tubes dropped to near zero at about []^(a,b,c) seconds. The cold-leg side U-tubes exhibited significant level oscillations from about []^(a,b,c) seconds which continued until the U-tubes were drained at []^(a,b,c) seconds (data plots 22 and 23).

- **Hot Legs**

Hot legs-A and -B were full of two-phase fluid until ADS-1 was actuated, when the measured level decreased (data plots 20 and 21). The hot legs were nearly drained at ADS-4 ([]^(a,b,c) seconds) and partially refilled after IRWST injection began. The principal difference between hot legs-A and -B was the influence of the PRHR HX on the void fraction in the hot legs during the PDP. Assuming that the fluid in the hot legs initially had the same steam fractions at the outlet of the power channel lower-upper plenum; the PRHR appears to have preferentially removed steam from hot leg-A (as seen in the very high steam fraction for the PRHR inlet flow), thereby reducing the steam fraction of the fluid in hot leg-A to less than the fluid steam fraction in hot leg-B. The apparent steam fraction in hot leg-A was []^(a,b,c) percent at []^(a,b,c) seconds; while in hot leg-B it was []^(a,b,c) percent. The hot-leg steam fraction affected the draining of the steam generators U-tubes, with steam generator-B draining earlier than steam generator-A.

- **Cold Legs**

Cold legs-A1 and -A2 remained full until []^(a,b,c) seconds (data plots 22 through 27), at which time the level decreased to the horizontal section of the pipes and drained at about []^(a,b,c) seconds. When ADS-4 occurred, the water level in the tubular downcomer temporarily dropped reaching []^(a,b,c) ft. below the hot-leg elevation at []^(a,b,c) seconds (data plot 24). The rod

bundle steam fraction fluid increased. After IRWST injection began at []^(a,b,c) seconds, the annular downcomer refilled and the cold and hot legs were partially refilled after []^(a,b,c) seconds to the level of []^(a,b,c) ft. above the hot leg.

Cold legs-B1 and -B2 remained full until []^(a,b,c) seconds into the event, at which time both cold legs-B1 and -B2 drained rapidly to the level of the horizontal section of the pipes. This reduced water level in cold leg-B1 and cold leg B-2 initiated the transition of the CMTs from their recirculation to draindown mode of operation. Cold legs-B1 and -B2 were refilled at []^(a,b,c) seconds to the level of []^(a,b,c) ft. above the hot leg. At this time, the cold leg to CMT balance lines were partially filled.

- **PRHR and IRWST**

At the initiation of the test, the PRHR HX was filled with subcooled liquid. When the S signal occurred, the PRHR HX isolation valve opened and flow started through the HX at a high flow rate due to the still operating RCPs. When the RCPs were shutoff and the power channel upper plenum and the hot legs filled with two-phase fluid, a large portion of the steam in hot leg-A flowed to the PRHR HX (data plot 29). The two-phase mixture, consisting of alternating slugs of steam and water, was condensed and subcooled in the PRHR HX (data plot 28) from []^(a,b,c)°F to below []^(a,b,c)°F. During the PDP (prior to ADS-1), there was a significant variation in the flow through the PRHR HX, caused by the variation in the steam fraction in hot leg-A. Steam condensation was apparently occurring in the PRHR HX as evidenced by the rapid and wide variations in dP measurements (data plots 28, 29, and 37).

When ADS-1 began, the power channel and the hot leg were refilled with subcooled water by accumulator injection. The driving head for the flow in the PRHR HX decreased (caused by the density difference between the fluid in the PRHR supply line and the return line) and the flow decreased and stopped. There was a short period of reverse flow at the end of the accumulator discharge. The subcooled fluid in the hot leg never filled the PRHR supply line, and hot fluid in this line flashed as system pressure decreased. Simultaneous flashing in the supply line and condensation in the PRHR HX resulted in a wide variations in the measured flow in the PRHR HX return line.

After the accumulator injection had ended, the rod bundle upper plenum again reached saturation temperature, and a two-phase mixture again occurred in the hot legs. Flow restarted in the PRHR HX, and the flow rate varied in response to the steam fraction in the hot leg. When ADS-4 fully depressurized the primary system and the IRWST flow began and refilled the power channel and the hot leg with subcooled water again, the flow through the PRHR HX stopped for the remainder of the transient. The subcooled fluid in the hot leg filled the PRHR supply line at []^(a,b,c) seconds.

The heatup of IRWST water resulting from the operation of the PRHR HX is shown in data plot 17. Following ADS-4, primary system pressure decreased to near ambient, and gravity flow

due to the water elevation head in the IRWST began injecting water into the annular downcomer via the DVI lines. The flow from the IRWST was sufficient to refill the power channel, downcomer, and loop piping and to establish subcooled fluid flow through the tube bundle and out through the ADS-4 flow paths (data plots 32 and 40).

- **Core Makeup Tanks**

The CMT injection was initiated two seconds after the S signal when the CMT injection line isolation valves were opened. Initially, the flow from the CMTs occurred by natural circulation; hot water from cold legs flowed to the top of the CMTs and cold water from the bottom of the CMTs flowed to the downcomer, via the DVI lines, into the power channel.

Initially, this recirculation rate was approximately []^(a,b,c) lbm/sec. from each CMT. The flow rate slowed down to []^(a,b,c) lbm/sec. at []^(a,b,c) seconds due to the decreased buoyant head driving force that occurred as the CMT water was replaced with hot water from the cold legs, and as the cold-leg water temperature decreased.

After cold legs-B1 and -B2 drained to the level of horizontal pipes at []^(a,b,c) seconds, flashing/drainage began in the cold-leg balance line. When the temperature at the top of the CMT reached the saturation temperature for primary system pressure, a free-water surface was established in the CMTs. This increased the driving head for the injection flow and resulted in a higher draindown flow rate. For the 1-inch LOCA, the break flow at this time was less than full CMT draindown flow rate. This caused the CMT injection to consist intermittent short periods of draindown which increased the cold leg water level and short periods of refill with water from the cold legs. This resulted in a slow decrease in CMT levels and the ADS-1 actuation was therefore delayed and occurred at a system pressure of approximately []^(a,b,c) psia, considerably below 711 psia accumulator gas pressure. Part of the accumulator coolant inventory was therefore injected into the primary system prior to ADS-1. This accumulator injection helped maintain the primary system coolant inventory at cold-leg elevation and thus contributed to intermittent CMT draindown/refill. For test S01613, the transition from recirculation to the draindown mode of operation occurred at []^(a,b,c) seconds for both CMT A and CMT B as shown in data plot 38. The CMT balance lines finally completely drained at []^(a,b,c) seconds (ADS-1), resulting in an increase in CMT injection flow rate. The steam in the CMT balance lines and at top of the CMTs was slightly superheated as the primary system pressure was rapidly reduced by ADS operation.

The CMTs were heated first by the hot liquid from the which replaced the cold water draining from the bottom of the CMTs. A stable, stratified thermal gradient was established in the CMTs (data plots 15 and 16). Later steam from the cold legs maintained the exposed metal and free-water surface temperatures at or near saturation temperature.

The CMT recirculation mode flow rate was initially approximately []^(a,b,c) lbm/sec. and steadily decreased to approximately []^(a,b,c) lbm/sec. when the transition to draindown began. The CMT average injection flow rate increased to approximately []^(a,b,c) lbm/sec. during the transition

period. After ADS-1 actuated, CMT injection increased again to []^(a,b,c) lbm/sec. and then gradually decreased with time. During the accumulator injection (ADS-1), the CMTs' draindown rate remained high. CMT-A was drained at about ADS-4 ([]^(a,b,c) seconds). The CMT-B injection flow rate decreased when the IRWST started at about []^(a,b,c) seconds, and CMT-B stopped flowing at []^(a,b,c) seconds and never completely drained (data plots 33 and 38).

- **Accumulators**

The accumulators provided water injection by a polytropic expansion of a compressed air volume stored within the accumulator. Accumulator injection started when the primary system pressure dropped below 711 psia at 2400 seconds. The accumulator injection flow rate was low until ADS-1 was actuated at approximately []^(a,b,c) seconds when the flow rate increased to approximately []^(a,b,c) lbm/sec. The accumulator injection after ADS actuation lasted approximately []^(a,b,c) seconds, and the accumulators were completely drained (data plot 34).

The effective polytropic coefficient of expansion was calculated for the accumulators (Figures 4.2.5-3 and 4.2.5-4) to be []^(a,b,c) for accumulator-A and -B. This was near the midpoint between isothermal expansion ($k = 1$) and adiabatic expansion ($k = 1.4$) and showed that some heat was picked up by the compressed air from the internal metal surfaces of the accumulator during the expansion.

Mass Discharge and Mass Balance

The catch tank weight measurements are shown in data plot 43 for the break flow, for the ADS-1, -2, and -3 flows, and for the ADS-4 flow. The break flow as shown in plot 44, which began when the test was initiated, was stable with a decreasing flow rate as system pressure dropped during the IDP and the PDP. When the ADS was actuated, the break location voided, and further discharge from the break was primarily saturated steam until IRWST injection refilled the cold leg after ADS-4.

The discharge from ADS-1, -2, and -3 was stable throughout the accumulator injection and increased temporarily when the injection ended. When ADS-4 occurred, the discharge of fluid from the top of the pressurizer essentially ended, and the fluid discharge from ADS-4 began. The ADS-4 fluid discharge rate was relatively stable and continued until the end of the test. The discharged masses are shown in Table 4.2.6-4.

The mass balance results for test S01613 were calculated based on water inventory before and after the test. Table 4.2.6-2 gives a detailed listing of the inventories of water in the various components before the test. Table 4.2.6-3 lists the inventories after the test and the amount of water injected into the vessel from the IRWST. The water level in the vessel was determined by the DP-B16P measurement to be []^(a,b,c) in. (577 mm) above the hot-leg centerline at the end of the test. Table 4.2.6-4 compares the mass balance for the system before and after the test and shows 102.6% agreement of the measurements.

**TABLE 4.2.6-1
SEQUENCE OF EVENTS FOR TEST S01613**

Event	Specified	Instrument Channel	Actual Time (sec.)
Break Opens	0	Z_001BC	(a,b,c)
R Signal	P = 1800 psia	P-027P	
MSL IV Closure	R signal + 2 sec.	Z_A04SO, F_A04S	
		Z_B04SO, F_B04S	
SCRAM	R signal + 5.7 sec.		
S Signal	P = 1700 psia	P-027P	
CMT IV Opening	S signal + 2 sec.	Z_A040EC, F-A40E	
		Z_B040EC, F-B40E	
PRHR Heat Exchanger Actuation	S signal + 2 sec.	Z_A81EC, F_A80E	
MFW IV Closure	S signal + 2 sec.	Z_B02S0, F_B01S	
		Z_A02S0, F_A01S	
Reactor Coolant Pumps Tripped	S signal + 16.2 sec.	DP-A00P	
		DP-B00P	
Accumulators	P-027P = 710 psia	F_A20E	
		F_B20E	
ADS-1	CMT level 67% +30 sec.	L_B40E	
		Z_001PC	
ADS-2	CMT level 67% +125 sec.	L_B40E	
		Z_002PC	
ADS-3	CMT level 67% +245 sec.	L_B40E	
		Z_003PC	
ADS-4 A/B	CMT level 20% +60 sec.	L_B40E	
		Z_004PC, F-040P	
IRWST Injection	P-027P = 26 psia	F_A60E	
		F_B60E	

**TABLE 4.2.6-2
WATER INVENTORY BEFORE TEST S01613**

PRIMARY SYSTEM					
Component	Volume (ft.³)/(l)	Net Vol (ft.³)/(l)	Temp (°F)	Relative Density	Mass (lbm)
Loops	8.97 ft. ³ (254.0 l)	8.97 ft. ³ (254.0 l)			
Pressurizer	3.37 ft. ³ (95.4 l)	1.82 ft. ³ (51.6 l)			
Surge Line	0.34 ft. ³ (9.6 l)	0.34 ft. ³ (9.6 l)			
Tubular Downcomer	1.38 ft. ³ (39.1 l)	1.38 ft. ³ (39.1 l)			
Annular Downcomer + High-Pressure Bypass	0.54 ft. ³ (15.3 l)	0.54 ft. ³ (15.3 l)			
Core Bypass	0.44 ft. ³ (12.4 l)	0.44 ft. ³ (12.4 l)			
Lower Plenum	0.81 ft. ³ (22.8 l)	0.81 ft. ³ (22.8 l)			
Riser	1.64 ft. ³ (46.4 l)	1.64 ft. ³ (46.4 l)			
Upper Plenum	1.46 ft. ³ (41.3 l)	1.46 ft. ³ (41.3 l)			
Upper Head	1.90 ft. ³ (53.8 l)	1.90 ft. ³ (53.8 l)			
CMT-A	5.05 ft. ³ (143.0 l)	5.05 ft. ³ (143.0 l)			
CMT-B	5.05 ft. ³ (143.0 l)	5.05 ft. ³ (143.0 l)			
ACC-A	5.05 ft. ³ (143.0 l)	3.90 ft. ³ (110.4 l)			
ACC-B	5.05 ft. ³ (143.0 l)	3.90 ft. ³ (110.4 l)			
IRWST Injection Line	0.18 ft. ³ (5.1 l)	0.18 ft. ³ (5.1 l)			
TOTAL PRIMARY INVENTORY					

(a,b,c)

TABLE 4.2.6-3
WATER INVENTORY AFTER TEST S01613
 Water level as measured by DP-B16P (-0.82 psi) was 23.08 in. (577 mm) above hot leg

Component	Volume (ft ³)/(l)	Net Vol (ft ³)/(l)	Temp (°F)	Relative Density	Mass (lbm)
Loops	8.97 ft. ³ (254.0 l)	8.97 ft. ³ (39.6 l)			
Pressurizer	3.37 ft. ³ (95.4 l)	0.04 ft. ³ (1.1 l)			
Surge Line	0.34 ft. ³ (9.6 l)	0.34 ft. ³ (9.6 l)			
Tubular Downcomer	1.38 ft. ³ (39.1 l)	1.38 ft. ³ (39.1 l)			
Annular Downcomer + High-Pressure Bypass	0.54 ft. ³ (15.3 l)	0.54 ft. ³ (15.3 l)			
Core Bypass	0.44 ft. ³ (12.4 l)	0.44 ft. ³ (12.4 l)			
Lower Plenum	0.81 ft. ³ (22.8 l)	0.81 ft. ³ (22.8 l)			
Riser	1.64 ft. ³ (46.4 l)	1.64 ft. ³ (46.4 l)			
Upper Plenum	1.46 ft. ³ (41.3 l)	1.41 ft. ³ (39.9 l)			
Upper Head	1.90 ft. ³ (53.8 l)	0.0 ft. ³ (0.0 l)			
CMT-A	5.05 ft. ³ (143 l)	0.0 ft. ³ (0.0 l)			
CMT-B	5.05 ft. ³ (143 l)	0.25 ft. ³ (7.0 l)			
ACC-A	5.05 ft. ³ (143 l)	0.0 ft. ³ (0.0 l)			
ACC-B	5.05 ft. ³ (143 l)	0.0 ft. ³ (0.0 l)			
IRWST Injection Line	0.18 ft. ³ (5.1 l)	0.18 ft. ³ (5.1 l)			
TOTAL PRIMARY INVENTORY					

(a,b,c)

WATER INJECTED FROM THE IRWST DURING EVENT			
IRWST Injection	dP (psi)	Area (in ²)	Mass (lbm)
Note 1	[] (a,b,c)

**TABLE 4.2.6-4
MASS BALANCE FOR TEST S01613**

	Starting Inventory (lbm)	Ending Inventory (lbm)
Total Primary System		
IRWST Injection During Transient		
Break Catch Tank		
ADS-1,-2,-3 Catch Tank		
ADS-4/Steam Generator Catch Tank		
TOTAL		
Ending Inventory/Starting Inventory (lbm)		
Ending Inventory/Starting Inventory (%)		

(a,b,c)

The following figures have been intentionally deleted
from this document due to their proprietary nature.

**TEST DATA PLOT PACKAGE
CHANNEL LIST BY COMPONENT**

COMPONENT	CHANNEL	UNITS	PLOT	COMMENT
ACCA	F_A20E	lbm/sec.	39	
ACCA	L_A20E	ft.	34	
ACCB	F_B20E	lbm/sec.	39	
ACCB	L_B20E	ft.	34	
ADS 1, 2, & 3	IF30flw	lbm/sec.	44	Flow rate derived from IF030P
ADS 1, 2, & 3	IF030P	lbm	43	Catch tank
ADS 4 & SG	IF40flw	lbm/sec.	44	Flow rate derived from IF040P
ADS 4 & SG	IF040P	lbm	43	Catch tank
ANND	DP-A021P	psi	24	To cold leg-A1
ANND	DP-A022P	psi	25	To cold leg-A2
ANND	DP-B021P	psi	26	To cold leg-B1
ANND	DP-B022P	psi	27	To cold leg-B2
BREAK LINE	IF05flw	lbm/sec.	44	Flow rate derived from IF005P
BREAK LINE	IF005P	lbm	43	Catch tank
CLA	DP-A001P	psi	24	To cold leg-A1
CLA	DP-A002P	psi	25	To cold leg-A2
CLA	DP-A09P	psi	22	Pump suction
CLA	T-A10P	°F	11	Steam generator outlet
CLA1	F_A01P	lbm/sec.	36	
CLA1	T-A021PL	°F	13	Downcomer inlet
CLA1	T-A11P	°F	11	Pump outlet
CLA2	F_A02P	lbm/sec.	36	
CLA2	T-A022PL	°F	13	Downcomer inlet
CLB	DP-B001P	psi	26	To cold leg-B1
CLB	DP-B002P	psi	27	To cold leg-B2
CLB	DP-B09P	psi	23	Pump suction
CLB	T-B10P	°F	12	Steam generator outlet
CLB1	F_B01P	lbm/sec.	36	
CLB1	T-B021PL	°F	14	Downcomer inlet
CLB1	T-B11P	°F	12	Pump outlet
CLB2	F-B02P	lbm/sec.	36	

**TEST S01613 PLOT PACKAGE
CHANNEL LIST BY COMPONENT (Cont.)**

COMPONENT	CHANNEL	UNITS	PLOT	COMMENT
CLB2	T_B022PL	°F	14	Downcomer inlet
CMTA	F_A40E	lbm/sec.	38	
CMTA	L_A40E	ft.	33	
CMTA	T-A401E	°F	15	Top 242.25 in.
CMTA	T-A403E	°F	15	216.75 in.
CMTA	T-A405E	°F	15	191.25 in.
CMTA	T-A407E	°F	15	165.75 in.
CMTA	T-A409E	°F	15	140.25 in.
CMTA	T-A411E	°F	15	114.75 in.
CMTA	T-A413E	°F	15	89.25 in.
CMTA	T-A415E	°F	15	63.75 in.
CMTA	T-A417E	°F	15	38.25 in.
CMTA	T-A420E	°F	15	Bottom 0 in.
CMTB	F_B40E	lbm/sec.	38	
CMTB	L_B40E	ft.	33	
CMTB	T-B401E	°F	16	Top 242.25 in.
CMTB	T-B403E	°F	16	216.75 in.
CMTB	T-B405E	°F	16	191.25 in.
CMTB	T-B407E	°F	16	165.75 in.
CMTB	T-B409E	°F	16	140.25 in.
CMTB	T-B411E	°F	16	114.75 in.
CMTB	T-B413E	°F	16	89.25 in.
CMTB	T-B415E	°F	16	63.75 in.
CMTB	T-B417E	°F	16	38.25 in.
CMTB	T-B420E	°F	16	Bottom 0 in.
CYCS	F-001A	psi	42	
DVIA	T-A00E	°F	13	
DVIB	T-B00E	°F	14	
HLA	DP-A04P	psi	20	

**TEST S01613 PLOT PACKAGE
CHANNEL LIST BY COMPONENT (Cont.)**

COMPONENT	CHANNEL	UNITS	PLOT	COMMENT
HLA	T-A03PL	°F	5	Vertical, near power channel
HLA	T-A03PO	°F	5	Horizontal, near power channel
HLA	T-A04P	°F	5	Near steam generator inlet
HLB	DP-B04P	psi	21	
HLB	T-B03PL	°F	6	Vertical, near power channel
HLB	T-B03PO	°F	6	Horizontal, near power channel
HLB	T-B04P	°F	6	Near steam generator inlet
IRWST	F_A60E	lbm/sec.	40	
IRWST	F_B60E	lbm/sec.	40	
IRWST	L_060E	ft	32	
IRWST	T_061E	°F	17	Bottom
IRWST	T-062E	°F	17	Below middle
IRWST	T-063E	°F	17	Middle
IRWST	T-064E	°F	17	Above middle
IRWST	T-065E	°F	17	Top
NRHRA	F-A00E	psi	42	
NRHRB	F-B00E	psi	42	
PC	W_00P	kW	1	
PC-HB	L_000P	ft	30	Heater bundle
PC-HR	TW018P20	°F	3	Heater rod
PC-HR	TW018P48	°F	3	Heater rod
PC-HR	TW020P87	°F	3	Heater rod
PC-UH	T-016P	°F	4	Upper head
PC-UP	L_A15P	ft.	30	Bottom of the upper plenum
PC-UP	L_A16P	ft.	31	Top of the upper plenum
PC-UP	T-015P	°F	4	Upper plenum
PC-UH	L_017P	ft.	31	Upper head
PC-UP	L_A14P	ft.	31	Above top of the active fuel
PRHR	DP-A81AE	psi	29	Supply line inverted U-tube

**TEST S01613 PLOT PACKAGE
CHANNEL LIST BY COMPONENT (Cont.)**

COMPONENT	CHANNEL	UNITS	PLOT	COMMENT
PRHR	DP-A81BE	psi	29	Supply line inverted U-tube
PRHR	DP-A81E	psi	28	Supply line
PRHR	DP-A82E	psi	28	Heat exchanger
PRHR	DP-A83E	psi	28	Return line
PRHR	F_A80E	lbm/sec.	37	Return line
PRHR	T-A82E	°F	19	Inlet
PRHR	T-A83E	°F	19	Exit
PRZ	L_010P	ft.	32	
PRZ	P-027P	psia	2	
PRZ	T-026P	°F	18	487 in.
SGA	DP-A05P	psi	20	Hot side
SGA	DP-A06P	psi	20	Hot side
SGA	DP-A07P	psi	22	Cold side
SGA	DP-A08P	psi	22	Cold side
SGA	F_A01S	lbm/sec.	41	
SGA	F_A20A	lbm/sec.	41	
SGA	L_A10S	ft.	35	Overall level
SGA	P-A04S	psia	2	Secondary system
SGA	T-A01S	°F	10	MFW-A
SGA	T-A05P	°F	7	Hot side
SGA	T-A05S	°F	9	Hot side - riser
SGA	T-A06P	°F	7	Hot side
SGA	T-A08P	°F	11	Cold side
SGA	TW-A06S	°F	7	Hot side
SGB	DP-B05P	psi	21	Hot side
SGB	DP-B06P	psi	21	Hot side
SGB	DP-B07P	psi	23	Cold side
SGB	DP-B08P	psi	23	Cold side
SGB	F_B01S	lbm/sec.	41	

**TEST S01613 PLOT PACKAGE
CHANNEL LIST BY COMPONENT (Cont.)**

COMPONENT	CHANNEL	UNITS	PLOT	COMMENT
SGB	F_B20A	lbm/sec.	41	
SGB	L_B10S	ft.	35	Overall level
SGB	P-B04S	psia	2	Secondary system
SGB	T-B01S	°F	10	MFW-B
SGB	T-B05P	°F	8	Hot side
SGB	T-B05S	°F	9	Hot side - riser
SGB	T-B06P	°F	8	Hot side
SGB	T-B07P	°F	8	U-tube top
SGB	T-B08P	°F	12	Cold side
SGB	TW-B06S	°F	8	Hot side
SL	T-020P	°F	18	Surge line near pressurizer
TDC	DP-001P	psi	25,26	Top
TDC	DP-002P	psi	24,25,26,27	Bottom
TDC	T-001PL	°F	13,14	Top
TDC	T-003P	°F	13,14	Bottom
TSAT-PRZ		°F	18	Based on P-027P
UH-TSAT		°F	4	Based on P-017P



The data plots are found in the proprietary version of this document.

4.2.7 Two-In. Direct Vessel Injection Line Break (S00605)

This matrix test simulated a 2-in. break in the direct vessel injection (DVI) line without any nonsafety systems operating. The test started with the initiation of the break, located on DVI line B just upstream of the DVI nozzle on the annular downcomer. This test was performed without any nonsafety systems operating (chemical and volume control system [CVCS] makeup pumps, steam generator startup feedwater (SFW) pumps and normal residual heat removal [NRHR] pumps).

Results are provided in the data plot package at the end of this section. The sequence of events for S00605 is listed in Table 4.2.7-1.

The tests in SPES-2 were marked by distinctly different phases. These phases were characterized by the primary system pressure decreased and the thermal-hydraulic phenomena occurring within the primary and safety systems. The different phases selected for purpose of detailed evaluation of this LOCA are shown in Figure 4.2.7-1 and are as follows:

- Initial depressurization phase (IDP)—Point 1 to 2
- Pressure decay phase (PDP)—Point 2 to 3
- Automatic depressurization system (ADS) phase—Point 3 to 4
- Post-automatic depressurization system (post ADS) phase—Point 4 to 5

Overall Test Observations

Figure 4.2.7-1 shows the plant primary system pressure during test S00605 (as measured at the top of the pressurizer), with selected component actuations and primary system responses shown in relation to the primary system pressure.

The IDP started with the initiation of the break, which resulted in a rapid reduction in pressure. The reactor trip (R) signal initiated at []^(a,b,c) psia, and the safety systems actuation (S) signal initiated at []^(a,b,c) psia. The R and the S signals initiated the following actions:

- Decay power simulation (with heat loss compensation) started
- Main steam line isolation valves (MSLIVs) closed
- Main feedwater isolation valves (MFWIVs) closed
- Core makeup tank (CMT) injection line isolation valves opened
- Passive residual heat removal (PRHR) return line isolation valve opened
- Reactor coolant pumps (RCPs) shut off

Recirculation flow through the CMTs and flow through the PRHR heat exchanger (HX) flow started immediately after their isolation valves were opened. Primary pressure rapidly decreased to the saturation pressure of the fluid in the rod bundle and upper plenum. Boiling was initiated in the rod bundle and the upper-upper plenum fluid flashed, causing its fluid level to decrease to the hot-leg elevation. This flashing stopped the rapid decrease in primary system pressure. When the RCPs were

shut off (at []^(a,b,c) seconds), the flow through the primary system started to oscillate (period approximately []^(a,b,c) seconds), resulting in oscillations in the rod bundle and lower-upper plenum fluid steam fractions, temperatures, and the system pressure.

During the PDP, the steam fraction of the fluid in the rod bundle increased. This resulted in an increasing steam fraction in the lower-upper plenum and the hot legs. Both hot legs contained two-phase fluid with the hot leg-B fluid steam fraction very close to that in the lower-upper plenum. The steam fraction in hot leg-A was much lower due to the removal of steam from the hot leg into the PRHR HX inlet line.

The two-phase flow in the hot legs initiated draining of the steam generator U-tubes, as steam from the two-phase mixture collected in the top of the U-tubes. The U-tubes in steam generator-B began to drain first due to the higher void fraction in hot leg-B, at approximately []^(a,b,c) seconds. Approximately []^(a,b,c) seconds later, steam generator-A U-tubes began to drain. When the U-tubes had drained, the primary system flow through the steam generators stopped so that the power channel flow consisted predominantly of the flow through the PRHR HX. The steam fraction/flow oscillations observed through the primary system stopped when flow through the steam generators ended.

Due to boiling in the rod bundle (data plots 30 and 31), two-phase flow entered the hot leg from the lower-upper plenum and flowed to the PRHR HX. The flow to the PRHR HX consisted of alternating slugs of steam and water, which had an average steam fraction significantly greater than the hot-leg fluid. The average steam fraction at the PRHR HX inlet was as high as []^(a,b,c) percent, which enhanced the PRHR HX heat removal from the primary system, as compared to its heat removal capability with single-phase saturated or subcooled water. When the primary system flow stabilized after the initial flow oscillations, a PRHR HX heat removal rate of []^(a,b,c) kW was calculated. This calculation was based on the average steam fraction of the flow in the PRHR HX supply line (as calculated from the differential pressure [dP] instrument readings in data plot 29), the average return flow, the inlet and outlet temperatures, and the pressure. This calculation assumes a slip coefficient of 1 between steam and water and may, therefore, give slightly lower values than the actual heat transfer. It should be used only for test-to-test comparison.

When the loop-B cold legs had partially emptied, the CMTs transitioned from the recirculation mode to a draindown mode of operation. This increased the CMT injection flow rate and the rate of primary system pressure decrease. This happened at approximately []^(a,b,c) seconds for both CMTs. When the primary system pressure decreased to the saturation pressure of the water in the upper head, the upper-head water began to flash and the upper head started to drain (at []^(a,b,c) seconds).

During the first []^(a,b,c) seconds (prior to ADS-1), []^(a,b,c) lbm of water were discharged through the break draining the pressurizer, the steam generator U-tubes, the power channel upper head, and the power channel upper plenum above the hot leg, and most of the cold legs, and []^(a,b,c) percent of the CMTs (which initiated the ADS actuation). The rod bundle decay heat simulation had reduced the power level to approximately 270 kW at []^(a,b,c) seconds, which consisted of 120 kW of decay heat

and 150 kW for facility heat loss compensation. The break flow was steady, indicating that the direct vessel injection (DVI) line was still full of water at this time.

The ADS actuation increased the rate of primary system depressurization and resulted in a high injection flow from the accumulators. The rapid injection of cold water from the accumulators (at []^(a,b,c) to []^(a,b,c) seconds into the event) temporarily reduced the steam fraction of the two-phase flow through the rod bundle and the upper plenum. The pressurizer level increased, reaching a collapsed liquid level of approximately []^(a,b,c) ft.

When the accumulator injection ended, the flow rate through the heater bundle was reduced to the injection flow from the CMTs and the PRHR HX flow, so the steam fraction of the two-phase flow through the rod bundle and upper plenum to the pressurizer and out the ADS-1, -2, and -3 increased; and the pressurizer collapsed liquid level decreased.

The fluid discharge through the break slowed when ADS-1 occurred at []^(a,b,c) seconds (due to the accompanying reduction in primary system pressure. The break flow further decreased significantly after the accumulator discharge ended at approximately []^(a,b,c) seconds. This reduction occurred because the water level in the annular downcomer decreased below the DVI line elevation, and the break fluid became steam. Prior to ADS-1, approximately []^(a,b,c) lbm of fluid were discharged through the break. During the ADS phase, approximately []^(a,b,c) lbm of fluid was discharged from the ADS-1, -2, and -3 and []^(a,b,c) lbm were discharged through the break. This water was supplied primarily by the accumulators. After accumulator injection ended, the rod bundle fluid steam fraction again increased since PRHR HX flow had sharply decreased and only the CMTs were providing injection into the primary system.

The post-ADS phase began when ADS-4 was actuated. ADS-4 was actuated manually (due to a fault of the facility control system) at []^(a,b,c) seconds. The fluid discharge through ADS-1, -2, and -3 decreased sharply, and almost all fluid was now discharged through ADS-4. A small amount of CMT flow was still being provided. When the primary system pressure had been reduced below the pressure corresponding to the water elevation head of the IRWST, flow from the IRWST to the downcomer began and CMT flow decreased and shortly thereafter ended. The flow from the IRWST gradually refilled the power channel rod bundle and lower-upper plenum with subcooled water and the upper-upper plenum partially refilled. A steady flow of subcooled water was then flowing from the IRWST into the downcomer, through the power channel, and left the primary system through ADS-4 flow paths and the DVI line break.

The PRHR HX flow decreased during accumulator injection, increased temporarily, and then decreased and stopped after ADS-4 actuation.

This test demonstrated that the heater bundle was fully covered by water or a two-phase mixture at all times during this event (data plots 30 and 31). There was no indication of heater rod temperatures increasing due to lack of cooling (see data plot 3). Key parameters describing the S00605 event are listed in Table 5.1-1, in Section 5.0.

Discussion of Test Transient Phases

- **Initial Depressurization Phase ([]^(a,b,c) to []^(a,b,c) Seconds)**

The initial depressurization phase (IDP) began with the initiation of the break (at time []^(a,b,c)) and lasted until the primary system pressure was dictated by the saturation pressure of the fluid in the upper plenum and the hot legs (Figure 4.2.7-1). This phase included the following events: initiation of the break, R signal to []^(a,b,c) psia (decay power simulation initiated and the MSLIV closed), and S signal at []^(a,b,c) psia (the MFWIV closed, the CMT injection line isolation valves opened, and the PRHR HX return line isolation valve opened—all with a []^(a,b,c)-second delay, and RCP coastdown initiated after a []^(a,b,c)-second delay). See Table 4.2.7-1.

Facility Response During the IDP:

The break was initiated at time []^(a,b,c). From time []^(a,b,c) until the R signal, the primary system pressure decreased as the pressurizer steam bubble expanded due to the fluid loss through the break. The pressurizer water partially compensated for the loss of pressure by flashing; however, the pressurizer was drained within the first []^(a,b,c) seconds of the event (data plot 32). The R (at []^(a,b,c) seconds) and the S (at []^(a,b,c) seconds) signals were based on pressurizer pressure only. When the R signal occurred, the MSLIV was closed, and the power was reduced to []^(a,b,c) percent of full power after a []^(a,b,c)-second delay and began to decay after a []^(a,b,c)-second delay. As a result of the power reduction without flow reduction, the rod bundle ΔT decreased due to the low power/flow ratio and the lower-upper plenum temperature decreased toward the cold-leg temperature ([]^(a,b,c)°F). The system pressure was dictated by the hot-leg/upper-plenum saturation pressure, and the pressure decreased to the saturation pressure at []^(a,b,c)°F (approximately []^(a,b,c) psia at approximately []^(a,b,c) seconds), see Figure 4.2.7-2. When the RCPs were shut off (at []^(a,b,c) seconds), the rod bundle and the lower-upper plenum temperatures increased due to the increased power/flow ratio at the lower flow. The system pressure increased temporarily until the decreasing decay power and the decreasing lower-plenum temperature (due to CMT injecting cold fluid into the downcomer) started reducing the upper-plenum temperature. The primary system pressure decrease resulted from the balance between the steam generation rate (from flashing primary fluid), the volumetric flow of liquid out the break, and the steam condensation rate of the PRHR HX. Steam was continually being generated by boiling due to the heater power. As the system pressure continued to decrease, more fluid reached its saturation pressure and started to flash. The PRHR HX flow started before the RCPs were shut off and continued by natural circulation after they were turned off (data plot 37). The primary system pressure stabilized at the saturation pressure for the bulk hot fluid in the system (approximately []^(a,b,c)°F. This ended the IDP.

- **Pressure Decay Phase ([]^(a,b,c) to []^(a,b,c) Seconds)**

The pressure decay phase (PDP) started when the primary system pressure (Figure 4.2.7-1) was dictated by the saturation pressure of the bulk hot fluid and ended when ADS-1 was opened on low CMT level and augmented the system depressurization. This phase was characterized by a slow decrease in overall system pressure and temperature. The rod bundle power (decay heat plus facility heat loss compensation) was reduced from 340 kW to 270 kW (data plot 1) while the PRHR HX removed heat at a rate of approximately []^(a,b,c) kW (calculated at []^(a,b,c) seconds). The recirculating CMTs provided additional heat removal replacing the hot primary water system that entered the CMTs through the balance lines with cold water. This heat removal plus energy lost through the break and the facility heat losses exceeded the rod bundle heat input into the primary system.

The initial CMT natural circulation operating mode was followed by draindown injection when the loop-B cold legs drained (data plot 38). The U-tubes of the steam generators had completely drained at this time and did not affect the rest of the transient (data plots 20 to 23). Accumulator injection was initiated when system pressure dropped below []^(a,b,c) psia following ADS-1 actuation (data plot 39).

Facility Response during the PDP:

The oscillating flow in the primary system that began after the RCPs were shut off continued into the PDP. These flow oscillations resulted in wide variations in the steam fraction of the two-phase mixture exiting the rod bundle and flowing into the hot legs (data plots 30 to 31). These oscillations in void fraction affected the two-phase fluid density and the thermal buoyancy head that drove the flow through the primary system. The steam fraction oscillations were noticeable through the hot leg and the steam generators (data plots 20 to 21). However, these steam fraction oscillations are observed as flow oscillations in the cold legs (data plots 24 to 27) since the two-phase mixture entering the steam generators left the steam generators as water. Some of the steam was condensed in the steam generator U-tubes (the primary-side pressure was higher than the secondary-side pressure at this time, allowing some heat to be transferred to the secondary-side fluid). The rest of the steam was separated from the two-phase mixture in the high point of the U-tubes (due to the low velocity), and eventually caused the U-tubes to begin to drain and free surface appeared at the top of the U-tubes. However, the buoyancy head in the hot leg was high enough to spill liquid over the top of the U-tubes at the peaks of the oscillations. At []^(a,b,c) seconds, the steam generator U-tubes began to drain, since the free surface had fallen too low to be overcome by the buoyancy head oscillations (plots 20 and 22). For steam generator-B, the U-tube drained earlier at []^(a,b,c) seconds, due to the higher void fraction in the fluid from hot leg-B. When the steam generator U-tubes were completely drained (about []^(a,b,c) to []^(a,b,c) seconds), the oscillations in the primary system stopped.

The primary system pressure decay during the PDP started at a slow rate of []^(a,b,c) psi/sec. At approximately []^(a,b,c) seconds into the event, the pressure decay rate increased to []^(a,b,c)

psi/sec. This happened when the CMTs transitioned from their recirculation mode to their draindown mode of operation. This transition occurred after the steam generator U-tubes drained and the loop-B cold legs partially drained, allowing the cold leg to CMT balance lines to drain. CMT recirculation to draindown transition occurred, the CMT injection flow rate increased. The increased rate of pressure decrease was due to the increased injection rate of the cold liquid from the CMTs (Figure 4.2.7-1).

CMTs started injecting cold fluid into the annular downcomer via the DVI lines when the S signal occurred. Initially, this injection was by natural circulation at approximately []^(a,b,c) lbm/sec. from each CMT. Hot water flowed from the cold leg through the CLBL into the top of each CMT, replacing the cold fluid flowing from the bottom of CMT. At approximately []^(a,b,c) seconds (data plot 38), the CMTs transitioned to their draindown injection mode and a free-water surface developed in the top of each CMT as the levels started to drop (data plot 33). The injection flow, once draindown started, was approximately []^(a,b,c) lbm/sec for CMT-A and []^(a,b,c) lbm/sec. for CMT-B. It gradually decreased as the CMT levels decreased, reducing the driving head (data plot 38).

The free liquid surfaces in the CMTs were established by the draining of the balance lines, allowing steam to flow from the cold legs to the CMTs. However, flashing in the CMTs seemed to occur after this time due to the high temperature (saturation temperature) of the fluid in the top of the CMTs (data plot 15) and the decreasing system pressure. Flashing kept the hot CMT water temperature at saturation while the pressure decayed.

The accumulator started to inject fluid into the downcomer when the primary system pressure dropped below []^(a,b,c) psia (at approximately []^(a,b,c) seconds), following ADS-1 (data plot 39).

Throughout the PDP, the PRHR removed energy from the primary system. The combined effect of the PRHR HX heat removal and the cold injection flow from the CMTs were sufficient to limit the steam fraction of the two-phase mixture exiting the rod bundle to approximately []^(a,b,c) percent (data plots 30 and 31).

- **Automatic Depressurization System Phase ([]^(a,b,c) Seconds to []^(a,b,c) Seconds)**

The automatic depressurization system (ADS) phase began with the actuation of ADS-1 and ended with the actuation of ADS-4 (Figure 4.2.7-1).

Facility Response During the ADS Phase:

With the actuation of ADS-1, followed by ADS-2 and ADS-3 within approximately []^(a,b,c) seconds, the rate of primary system depressurization increased from []^(a,b,c) psi/sec. at the end of the PDP to []^(a,b,c) psi/sec. at the start of the ADS period. This rate gradually decreased as the system pressure decreased.

The primary system depressurization after ADS actuation resulted in a high rate of water injection from accumulators-A and -B (data plots 33 and 39). The accumulators injected cold water into the primary system for approximately []^(a,b,c) seconds (from []^(a,b,c) seconds to []^(a,b,c) seconds) and were then drained. The accumulator and CMT injection reduced the steam fraction of the fluid flowing through the rod bundle and the lower-upper plenum. When the accumulator delivery was completed, the water level in the downcomer decreased significantly, dropping approximately []^(a,b,c) ft. below the annular portion of the downcomer. This was reflected in a significant increase in the steam fraction in the rod bundle and lower-upper plenum fluid; however, two-phase fluid flow was maintained through the rod bundle keeping it cooled (data plots 30 and 31).

The pressurizer immediately started to refill when ADS-1 occurred (data plot 32). The pressurizer never filled completely with liquid as two-phase fluid was discharged out of the primary system through the ADS. When ADS-4 occurred, the pressurizer drained and only a small amount of steam was vented through ADS-1, -2, and -3.

Prior to the ADS phase, liquid left the primary system through the break in the DVI line only. With the actuation of the ADS, liquid and steam left the system through the ADS from the top of the pressurizer. The mass flow through the break decreased as primary pressure decreased and as the break flow converted from liquid to predominantly steam when the annular downcomer water level fell below the break elevation (data plots 43 and 44).

- **Post-Automatic Depressurization System Phase ([]^(a,b,c) Seconds to End-of-Test)**

The post-automatic depressurization system (post-ADS) phase started when ADS-4 occurred and lasted to the end of the event (Figure 4.2.7-1).

Facility Response during the Post-ADS Phase:

When the accumulator delivery completed, the water level in the downcomer decreased to approximately []^(a,b,c) ft below the hot-leg elevation at []^(a,b,c) seconds (well into the tubular downcomer), and the steam fraction of flow through the core and upper plenum increased since the CMT injection flow was less than the ADS flow (data plot 25). However, there was sufficient two-phase fluid flow through the rod bundle to keep it cooled (data plots 30 and 31). The primary system pressure rapidly decreased to near ambient following ADS-4 actuation and gravity flow from the IRWST into the downcomer started (data plot 40). The cold flow from the IRWST gradually refilled the power channel and hot legs with subcooled water, and partially collapsed the steam bubble in the upper-upper plenum.

Prior to ADS-4 actuation, ADS-1, -2, -3 flow leaving the primary system was approximately []^(a,b,c) lbm/sec. after ADS-4 actuation, flow through ADS-1, -2, -3 decreased while ADS-4 flow increased to []^(a,b,c) lbm/sec. The flow rate through the break continued at a steady rate of []^(a,b,c) lbm/sec.

The PRHR HX flow, which had steadily decreased, stopped at about []^(a,b,c) seconds (data plot 37).

The test was terminated when there was subcooled flow from the IRWST, through the power channel and out through the ADS-4 flow paths.

Component Responses

• Power Channel (PC)

The power channel consists of five volumes: the lower plenum, the riser with the heater rod bundle, the lower-upper plenum below hot leg, the upper-upper plenum above hot leg, and the upper head. When the break occurred, the primary system pressure decreased to the R trip point ([]^(a,b,c) psia) and the S trip point ([]^(a,b,c) psia). However, since the water everywhere in the power channel was at a temperature below the saturation temperature for the system pressure, no boiling or flashing occurred up to this point. Nothing significant happened in the power channel until the rod bundle power was reduced to []^(a,b,c) percent []^(a,b,c) seconds after the R signal. At this time, the rod bundle ΔT decreased due to the reduced power/flow ratio (still full flow), and the power channel outlet temperature dropped toward the lower plenum inlet temperature (Figure 4.2.7-2). The upper-upper plenum still contained fluid at []^(a,b,c)°F and started to flash when the system pressure dropped below []^(a,b,c) psia. When the RCPs were stopped ([]^(a,b,c) seconds after the S signal), the power/flow ratio increased, and the power channel outlet temperature increased resulting in boiling/flashing in the rod bundle. This produced sufficient steam to control the system pressure, and both temperature and pressure increased momentarily until the upper-upper plenum was drained down to the hot leg elevation (data plots 30 and 31). The lower-upper plenum temperature reached a peak and started to drop, responding to increasing primary system natural circulation flow caused by the increasing steam fraction of fluid on the hot-leg side of the power channel. The upper-plenum and hot-leg temperatures stabilized at approximately []^(a,b,c)°F, and the primary pressure was stabilized at the hot-leg saturation pressure (approximately []^(a,b,c) psia) at the end of IDP.

The temperature of the fluid in the lower-upper plenum and hot legs controlled the system pressure during the PDP (data plot 4 and Figure 4.2.7-2). Oscillations in the steam fraction of the fluid exiting the rod bundle (period of []^(a,b,c) seconds) started when the RCPs had coasted down. These oscillations disappeared at about []^(a,b,c) seconds after the steam generator U-tubes had drained.

Data plots 30 and 31 show the collapsed liquid levels at various sections of the power channel during the S00605 test.

The upper head started to drain when the system pressure decreased to the saturation pressure for the fluid temperature in the upper head (at about []^(a,b,c) seconds). The upper-head fluid temperature was initially only []^(a,b,c)°F and was therefore considerably cooler than the upper-

upper plenum fluid temperature. Flashing of the fluid in the upper head started at []^(a,b,c) seconds, and the upper head drained completely when ADS-1 occurred at approximately []^(a,b,c) seconds (data plot 4).

The upper-upper plenum flashed when the primary system pressure decreased below []^(a,b,c) psia, and its level decreased to the hot-leg elevation. The upper-upper plenum remained filled with steam until IRWST injection refilled the power channel with subcooled water at []^(a,b,c) seconds. The upper-upper plenum steam bubble was partially condensed (data plot 4).

The collapsed liquid level in the lower-upper plenum indicates the steam fraction of the two-phase flow exiting the rod bundle steam. This measurement and the rod bundle collapsed liquid measurement indicated that the maximum steam fraction of the two-phase, cooling flow during the PDP was approximately []^(a,b,c) percent at []^(a,b,c) seconds.

Data plot 30 shows the oscillating collapsed levels in the rod bundle following the coastdown of the RCPs, indicating steam fractions varied from []^(a,b,c) percent to []^(a,b,c) percent in this phase, with a period of approximately []^(a,b,c) seconds. The accumulator injection reduced the steam fraction in the rod bundle; however, when the accumulator injection ended, the rod bundle steam fraction increased again and reached a maximum steam fraction ([]^(a,b,c) percent) just before the IRWST injection started. The lower-upper plenum showed a steam fraction of []^(a,b,c) percent during this period. This high steam fraction was due, in part, to the fact that the level of two-phase mixture in the lower-upper plenum temporarily dropped below the hot-leg elevation.

The collapsed level measured just above the heated portion of the rod bundle (data plot 31) provides fluid steam fractions that correlated well with those measured in the rod bundle.

- **Pressurizer**

The pressurizer started to drain when the break occurred and was completely drained in approximately []^(a,b,c) seconds (data plot 32). The water in the pressurizer flashed due to the loss of system pressure, and the temperature of the water dropped from []^(a,b,c)°F during this initial depressurization (data plot 18). The hot water exiting the pressurizer surge line into the hot leg-A caused a slight increase in the hot leg temperature during this period, since it mixed with the flow from the power channel/upper plenum. The pressurizer stayed drained until ADS occurred, at which time it refilled, reaching a collapsed liquid level of []^(a,b,c) ft. and discharged two-phase mixture. The pressurizer collapsed liquid level decreased after accumulator injection ended in response to the increasing steam fraction exiting the power channel. This continued until ADS-4, at which time the pressurizer again drained completely at []^(a,b,c) seconds and the level reached manometric agreement with the water level in the primary system.

- **Steam Generator**

The steam generators acted as the heat sink until the MSLIV closed and prevented further energy removal from the secondary side. This caused the temperature of the secondary side to increase toward the primary system hot-leg temperature, which at the same time was dropping due to the reduced power/flow ratio. When the RCPs had coasted down, a temporary temperature increase occurred due to the increased power/flow ratio with natural circulation flow in the primary system. The steam generator secondary-side water temperature stabilized at approximately []^(a,b,c)F at the end of the IDP.

For the first part of the PDP, the pressure on the primary side of the steam generators was higher than the secondary side, indicating that some heat transfer from the primary to secondary side was occurring, causing some condensing of the two-phase fluid coming from the hot leg. The primary system pressure did not drop below the steam generator secondary-side pressure until approximately []^(a,b,c) seconds into the event, at which time the cold-leg side of the U-tubes was completely drained, and the hot-leg side was partially drained.

At the end of the RCP coastdown, flow oscillations started to occur in the tubular downcomer and through the power channel. This caused significant oscillations in the collapsed liquid level measured in the rod bundle, caused by oscillations in the steam fraction of the two-phase liquid flowing through the rod bundle into the hot legs and to the steam generators. Since the driving force for the natural circulation flow was the density difference between the single-phase fluid in the cold legs and downcomer entering the power channel and the two-phase mixture leaving the power channel and in the hot legs, the flow oscillations were sustained as long as there was flow through the steam generators.

The fluid level on the hot-leg side of the steam generator U-tubes dropped below the top of the U-tubes in cycles, resulting in intermittent flow from the hot-leg side to the cold-leg side of the U-tubes. This condition continued until approximately []^(a,b,c) seconds into the transient for steam generator-A, at which time the oscillating two-phase fluid steam fraction did not have sufficient buoyancy to lift the free surface in the U-tube hot-leg side to the top of the U-tubes.

In steam generator-B, there were less defined flow oscillations, due to the higher void fraction in hot leg-B than hot leg-A. Intermittent flow over the top of the U-tubes ended approximately []^(a,b,c) seconds into the transient.

For both steam generators, the water in the hot-leg side of the U-tubes drained completely with ADS-1 actuation. The cold-leg side of the U-tubes exhibited significant level oscillations until they drained completely at about []^(a,b,c) seconds for steam generator-A, and []^(a,b,c) seconds for steam generator-B.

- **Hot Legs**

Hot legs-A and -B were filled with two-phase fluid to the steam generators before ADS-1 actuation (data plots 20 and 21). After ADS-1 and accumulator injection, the hot leg-B drained at approximately []^(a,b,c) seconds, while hot leg-A reflected the two-phase flow from the power channel into the pressurizer. Both hot-leg horizontal sections refilled after IRWST injection started. The principle difference between hot legs-A and -B was the influence of the PRHR on the steam fraction of the fluid in hot leg-A. The PRHR HX preferentially removed steam from hot leg-A, as seen in the very high steam fraction of the PRHR HX inlet flow, thereby reducing the steam fraction of the fluid in hot leg-A as compared with hot leg-B. The hot leg steam fraction affected the draining of the steam generator U-tubes, resulting in earlier draining in steam generator-B than in steam generator-A.

- **Cold Legs**

Cold legs-A1 and -A2 remained full until []^(a,b,c) seconds into the event (data plots 22 through 27). When ADS-1 occurred, the level decreased to the cold-leg downcomer nozzle elevation at about []^(a,b,c) seconds. Flashing occurred throughout this period as evidenced by the simultaneous decrease in the measured water levels in the annular downcomer. When accumulator injection ended, the water level in the downcomer and reached []^(a,b,c) ft. ([]^(a,b,c) ft. below the hot-leg elevation) at []^(a,b,c) seconds into the event and decreased.

When IRWST injection starts at []^(a,b,c) seconds into the event, the tubular and annular downcomer were gradually refilled (refilled at []^(a,b,c) seconds), and cold legs-A1 and -A2 were partially refilled beginning at []^(a,b,c) seconds.

Cold legs-B1 and -B2 remained full until []^(a,b,c) seconds into the event. At this time, both cold legs-B1 and B2 drained rapidly and the CMTs' transition to their draindown mode started at approximately []^(a,b,c) seconds. Cold legs-B1 and -B2 refilled after []^(a,b,c) seconds into the event.

- **PRHR and IRWST**

At the initiation of the test, the PRHR subsystem was filled with subcooled liquid. When the S signal occurred, the PRHR return line isolation valve opened, and flow started through the HX at high flow rate due to the still operating RCP. When the pumps were shut off and the upper plenum and the hot leg filled with two-phase fluid, a large portion of the steam in the hot leg-A flowed to the PRHR HX (average void fraction is []^(a,b,c) to []^(a,b,c) percent based on data plot 29). This two-phase mixture, consisting of alternating slugs of steam and water, was condensed and subcooled in the PRHR HX (data plot 28). When the primary system flow stabilized after the initial flow oscillations, the PRHR HX heat removal rate was calculated to be []^(a,b,c) kW. This calculation was based on the average void fraction of the flow in the PRHR supply line (as

calculated from the dP instrument readings in data plot 29), the average return flow, the HX inlet and outlet temperatures, and the pressure.

During the PDP (prior to ADS-1), there was a significant variation in the flow rate through the PRHR, caused by the variation in the steam fraction of the fluid in hot leg-A and the PRHR inlet line resulting in the wide range of the dP measurements in data plots 28, 29, and 37.

When the ADS initiated, the power channel and the hot-leg fluid steam fractions were reduced by the cold flow from the accumulators, reducing the driving head for the flow in the PRHR HX. The PRHR HX flow increased near the end of accumulator delivery (approximately []^(a,b,c) seconds) but oscillated widely apparently as alternating steam and water flow occurred in the supply line. Subsequently, the PRHR HX flow decreased and the supply line appeared to empty. PRHR HX flow stopped at approximately []^(a,b,c) seconds. The PRHR HX was submerged in the IRWST and the heatup of the water within the IRWST is shown in data plot 17.

When ADS-4 depressurized the system (starting at []^(a,b,c) seconds), IRWST flow began and provided sufficient water to refill the power channel with subcooled water.

- **Core Makeup Tanks**

The CMT injection was initiated []^(a,b,c) seconds after the S signal by opening the CMT injection line isolation valves. Initially, the flow from the CMT occurred by the natural circulation, hot water from the loop-B cold legs flowed through the CLBLs to the top of the CMTs, while cold water at the bottom of the CMTs flowed into the annular downcomer via the direct vessel line and into the power channel.

When the cold legs-B1 and -B2 drained to the level of the downcomer cold-leg nozzles, the balance lines drained and steam flowed to the top of the CMTs, resulting in a free-water surface in the CMTs. This increased the driving head for CMT injection flow to the gravity head of the CMT water and resulted in a higher draindown flow. For the 2-inch DVI line break simulation, cold legs-B1 and -B2 were drained at the same time, and the transition from the recirculation mode to the draindown mode of operation occurred simultaneously for the two CMTs (data plot 38).

The CMTs were heated first by the hot fluid from the cold legs, and later by steam from the cold legs. The hot, or heated, water in the CMTs remained thermally stratified (data plots 15 and 16), where the free-water surface temperature was at or near saturation temperature, while the water at lower levels in the CMT was cold.

The recirculation flow rate of the CMTs started at approximately []^(a,b,c) lbm/sec. for CMT-A and []^(a,b,c) lbm/sec. for CMT-B and decreased slightly before the transition to draindown injection started. The draindown mode flow rate was initially []^(a,b,c) lbm/sec. for CMT-A and []^(a,b,c) lbm/sec. for CMT-B, and gradually decreased with time as the CMT water level

decreased. During the accumulator injection (started at ADS-1), the draindown flow rates from the CMTs were temporarily reduced due to the increased backpressure in the DVI line caused by the accumulator injection. The CMT injection flow ended at approximately []^(a,b,c) seconds for CMT-A and []^(a,b,c) seconds for CMT-B, at which time they were completely drained (data plot 33).

- **Accumulators**

The accumulators provided water injection into the downcomer by a polytropic expansion of a compressed air volume stored within the accumulator. Water from the accumulators was injected when the primary system pressure dropped below []^(a,b,c) psia. The injection for both accumulators started after ADS-1 actuation (data plot 39). The accumulator injections for the S00605 test lasted approximately []^(a,b,c) seconds, and the accumulators were completely emptied when injection ended (data plot 34).

Mass Discharge and Mass Balance

The catch tanks weight measurements are shown in data plot 43 for the break flow and for the ADS-1, -2, -3 and -4 flows.

The break flow, which started when the event was initiated, was stable with a decreasing flow rate as the system pressure dropped during the IDP, the PDP, and after ADS was initiated. After ADS-3 actuation, flow through the break was greatly reduced but continued through the rest of the test.

The discharge from the pressurizer through ADS-1, -2, and -3 had an average flow rate of approximately []^(a,b,c) lbm/sec. After ADS-3 was actuated and the primary system pressure was low, ADS flow decreased rapidly in response to the reduction in injection flow that occurs when accumulator injection ended. ADS-1, -2, -3 flow ended when ADS-4 occurred.

When ADS-4 occurred, fluid discharge from ADS-4 was initially relatively stable and increased over the first []^(a,b,c) seconds of operation. Large oscillations in the flowrate are observed which apparently are caused by the alternate fill and drain of the upper-upper plenum (plots 44 and 31).

The discharged masses are shown in Table 4.2.7-4.

The mass balance results for test S00605 were calculated based on the water inventory before and after the test. Table 4.2.7-2 gives a detailed listing of the inventories of water in the various components before the test. Table 4.2.7-3 lists the inventories after the test and the amount of water injected from the IRWST. The water level in the power channel was determined by the DP-B16P measurement to be []^(a,b,c) in. (442 mm) above the hot-leg centerline at the end of the test. Table 4.2.7-4 compares the mass balance for the system before and after the test and shows []^(a,b,c) percent agreement of the measurements.

TABLE 4.2.7-1
SEQUENCE OF EVENTS FOR TEST S00605

Event	Specified	Instrument Channel	Actual Time
Break Opened	0		
R Signal	P = 1800 psia	P-027P	
MSLIV Closure	R + 2 sec.	Z_A04S0, F_A04S	
		Z_B04S0, F_B04S	
S Signal	P = 1700 psia	P-027P	
MFWIV Closure	S + 1 sec.	Z_B02S0, F_B01S	
		Z_A02S0, F_A01S	
CMT IV Opening	S + 2 sec.	Z_A040EC, F-A40E	
		Z_B040EC, F-B40E	
RCPs Tripped	S + 16.2 sec.	I-A1P, S-A1P	
		I-B1P, S-B1P	
PRHR HX Actuation	S + 2 sec.	Z_A81EC, F_A80E	
ADS-1	CMT level 67%	L_B40E	
	+30 sec.	Z_001PC	
Accumulators	P-027P = 710 psia	F_A20E	
		F_B20E	
ADS-2	CMT level 67%	L_B40E	
	+125 sec.	Z_002PC	
ADS-3	CMT level 67%	L_B40E	
	+245 sec.	Z_003PC	
ADS-4	CMT level 20%	L_B40E	
	+60 sec.	Z_004PC, F-040P	
IRWST Injection	P-027P = 26 psia	F_A60E	
		F_B60E	

(a,b,c)

*Manually opened with delay of about 90 seconds.

**TABLE 4.2.7-2
WATER INVENTORY BEFORE TEST S00605**

Component	Volume (ft.³)/(l)	Net Vol (ft.³)/(l)	Temp (°F)	Relative Density	Mass (lbm)
Loops	8.97 ft. ³ (254.0 l)	8.97 ft. ³ (254.0 l)			
Pressurizer	3.37 ft. ³ (95.4 l)	1.92 ft. ³ (54.3 l)			
Surge Line	0.34 ft. ³ (9.6 l)	0.34 ft. ³ (9.6 l)			
Tubular Downcomer	1.38 ft. ³ (39.1 l)	1.38 ft. ³ (39.1 l)			
Annular Downcomer+ High-Pressure Bypass	0.54 ft. ³ (15.3 l)	0.54 ft. ³ (15.3 l)			
Core Bypass	0.44 ft. ³ (12.4 l)	0.44 ft. ³ (12.4 l)			
Lower Plenum	0.81 ft. ³ (22.8 l)	0.81 ft. ³ (22.8 l)			
Riser	1.64 ft. ³ (46.4 l)	1.64 ft. ³ (46.4 l)			
Upper Plenum	1.46 ft. ³ (41.3 l)	1.46 ft. ³ (41.3 l)			
Upper Head	1.90 ft. ³ (53.8 l)	1.90 ft. ³ (53.8 l)			
CMTs	10.1 ft. ³ (286.0l)	10.1 ft. ³ (286.0l)			
Accumulator	10.1 ft. ³ (286.0l)	7.50 ft. ³ (215.2 l)			
IRWST Injection Line	0.18 ft. ³ (5.1 l)	0.18 ft. ³ (5.1 l)			
TOTAL INVENTORY					

(a,b,c)

TABLE 4.2.7-3
WATER INVENTORY AFTER TEST S00605 WAS COMPLETED
 Water level as measured by DP-B16P (-0.60 psi) was 442 mm above Hot Leg

Component	Volume (ft. ³)/(l)	Net Vol (ft. ³)/(l)	Temp (°F)	Relative Density	Mass (lbm)
Loops	8.97 ft. ³ (254.0 l)	1.62 ft. ³ (46 l)			
Pressurizer	3.37 ft. ³ (95.4 l)	0.0 ft. ³ (0 l)			
Surge Line	0.34 ft. ³ (9.6 l)	0.0 ft. ³ (0 l)			
Tubular Dowcomer	1.38 ft. ³ (39.1 l)	1.38 ft. ³ (39.1 l)			
Annular Dowcomer + High-Pressure Bypass	0.54 ft. ³ (15.3 l)	0.47 ft. ³ (13.2 l)			
Core Bypass	0.44 ft. ³ (12.4 l)	0.44 ft. ³ (12.4 l)			
Lower Plenum	0.81 ft. ³ (22.8 l)	0.81 ft. ³ (22.8 l)			
Riser	1.64 ft. ³ (46.4 l)	1.64 ft. ³ (46.4 l)			
Upper Plenum	1.46 ft. ³ (41.3 l)	1.26 ft. ³ (35.6 l)			
Upper Head	1.90 ft. ³ (53.8 l)	0.0 ft. ³ (0 l)			
CMTs	10.1 ft. ³ (286.0 l)	0.0 ft. ³ (0 l)			
Accumulator	10.1 ft. ³ (286.0 l)	0.0 ft. ³ (0 l)			
IRWST Injection Line	0.18 ft. ³ (5.1 l)	0.18 ft. ³ (5.1 l)			
TOTAL INVENTORY					
WATER INJECTED FROM THE IRWST DURING EVENT					
IRWST Injection	Del Elev (psi)	Area (in ²)		Mass (lbm)	
	1.21	1007.5		1219.1	

(a,b,c)

TABLE 4.2.7-4
MASS BALANCE FOR TEST S00605

	Starting Inventory (lbm)	Ending Inventory (lbm)
Total Primary System	[]
IRWST Injection		
BREAK		
ADS-1,-2,-3		
ADS-4		
TOTAL		
Ending Inventory/Starting Inventory (lbm)		
Ending Inventory/Starting Inventory (%)		101.7

(a,b,c)

The following figures have been intentionally deleted
from this document due to their proprietary nature.

**TEST S00605 PLOT PACKAGE
CHANNEL LIST BY COMPONENT**

COMPONENT	CHANNEL	UNITS	PLOT	COMMENT
ACCA	F_A20E	lbm/sec.	39	
ACCA	L_A20E	ft.	34	
ACCB	F_B20E	lbm/sec.	39	
ACCB	L_B20E	ft.	34	
ADS 1, 2, & 3	IF30FLW	lbm/sec.	44	Flow rate derived from IF030P
ADS 1, 2, & 3	IF030P	lbm	43	Catch tank
ADS 4 & SG	IF40FLW	lbm/sec.	44	Flow rate derived from IF040P
ADS 4 & SG	IF040P	lbm	43	Catch tank
ANNDC	DP-A021P	psi	24	To cold leg-A1
ANNDC	DP-A022P	psi	25	To cold leg-A2
ANNDC	DP-B021P	psi	26	To cold leg-B1
ANNDC	DP-B022P	psi	27	To cold leg-B2
BREAK LINE	IF05FLW	lbm/sec.	44	Flow rate derived from IF005P
BREAK LINE	IF005P	lbm	43	Catch tank
CLA	DP-A001P	psi	24	To cold leg-A1
CLA	DP-A002P	psi	25	To cold leg-A2
CLA	DP-A09P	psi	22	Pump suction
CLA	T-A10P	°F	11	Steam generator outlet
CLA1	F_A01P	lbm/sec.	36	
CLA1	T-A021PL	°F	13	Downcomer inlet
CLA1	T-A11P	°F	11	Pump outlet
CLA2	F_A02P	lbm/sec.	36	
CLA2	T-A022PL	°F	13	Downcomer inlet
CLB	DP-B001P	psi	26	To cold leg-B1

**TEST S00605 PLOT PACKAGE
CHANNEL LIST BY COMPONENT (Cont.)**

COMPONENT	CHANNEL	UNITS	PLOT	COMMENT
CLB	DP-B002P	psi	27	To cold leg-B2
CLB	DP-B09P	psi	23	Pump suction
CLB	T-B10P	°F	12	Steam generator outlet
CLB1	F_B01P	lbm/sec.	36	
CLB1	T-B021PL	°F	14	Downcomer inlet
CLB1	T-B11P	°F	12	Pump outlet
CLB2	F_B02P	lbm/sec.	36	
CLB2	T-B022PL	°F	14	Downcomer inlet
CMTA	F_A40E	lbm/sec.	38	
CMTA	L_A40E	ft.	33	
CMTA	T-A401E	°F	15	Top (242.25 in.)
CMTA	T-A403E	°F	15	216.75 in.
CMTA	T-A405E	°F	15	191.25 in.
CMTA	T-A407E	°F	15	165.75 in.
CMTA	T-A409E	°F	15	140.25 in.
CMTA	T-A411E	°F	15	114.75 in.
CMTA	T-A413E	°F	15	89.25 in.
CMTA	T-A415E	°F	15	63.75 in.
CMTA	T-A417E	°F	15	38.25 in.
CMTA	T-A420E	°F	15	Bottom (0 in.)
CMTB	F_B40E	lbm/sec.	38	
CMTB	L_B40E	ft.	33	
CMTB	T-B401E*	°F	16	Top (242.25 in.)
CMTB	T-B403E*	°F	16	216.75 in.
CMTB	T-B405E*	°F	16	191.25 in.
CMTB	T-B407E*	°F	16	165.75 in.
CMTB	T-B409E*	°F	16	140.25 in.
CMTB	T-B411E*	°F	16	114.75 in.
CMTB	T-B413E*	°F	16	89.25 in.

**TEST S00605 PLOT PACKAGE
CHANNEL LIST BY COMPONENT (Cont.)**

COMPONENT	CHANNEL	UNITS	PLOT	COMMENT
CMTB	T-B415E*	°F	16	63.75 in.
CMTB	T-B417E*	°F	16	38.25 in.
CMTB	T-B420E*	°F	16	Bottom (0 in.)
CVCS	F-001A	psi	42	
DVIA	T-A00E	°F	13	
DVIB	T-B00E	°F	14	
HLA	DP-A04P	psi	20	
HLA	T-A03PL	°F	5	Vertical, near power channel
HLA	T-A03PO	°F	5	Horizontal, near power channel
HLA	T-A04P	°F	5	Near steam generator inlet
HLB	DP-B04P	psi	21	
HLB	T-B03PL	°F	6	Vertical, near power channel
HLB	T-B03PO	°F	6	Horizontal, near power channel
HLB	T-B04P	°F	6	Near steam generator inlet
IRWST	F_A60E	lbm/sec.	40	
IRWST	F_B60E	lbm/sec.	40	
IRWST	L_060E	ft	32	
IRWST	T-061E	°F	17	Bottom
IRWST	T-062E	°F	17	Below middle
IRWST	T-063E	°F	17	Middle
IRWST	T-064E	°F	17	Above middle
IRWST	T-065E	°F	17	Top
PC	W_00P	kW	1	
PC-HB	L_000P	ft	30	Heater bundle
PC-HR	TW018P20	°F	3	Heater rod
PC-HR	TW018P48	°F	3	Heater rod
PC-HR	TW020P87	°F	3	Heater rod
PC-UH	T-016P	°F	4	Upper head
PC-UP	L_A15P	ft	30	Lower-upper plenum

TEST S00605 PLOT PACKAGE
CHANNEL LIST BY COMPONENT (Cont.)

COMPONENT	CHANNEL	UNITS	PLOT	COMMENT
PC-UP	L_A16P	ft.	31	Upper-upper plenum
PC-UP	T-015P	°F	4	Upper plenum
PC-UH	L_017P	ft.	31	Upper head
PC-UP	L_A14P	ft.	31	Above top of heater bundler
PRHR	DP-A81AE	psi	29	Supply line inverted U-tube
PRHR	DP-A81BE	psi	29	Supply line inverted U-tube
PRHR	DP-A81E	psi	28	Supply line
PRHR	DP-A82E	psi	28	Heat exchanger
PRHR	DP-A83E	psi	28	Return line
PRHR	F_A80E	lbm/sec.	37	Return line
PRHR	T-A82E	°F	19	Inlet
PRHR	T-A83E	°F	19	Exit
PRZ	L_010P	ft.	32	
PRZ	P-027P	psia	2	
PRZ	T-026P	°F	18	487 in.
SGA	DP-A05P	psi	20	Hot side
SGA	DP-A06P	psi	20	Hot side
SGA	DP-A07P	psi	22	Cold side
SGA	DP-A08P	psi	22	Cold side
SGA	F_A01S	lbm/sec.	41	Main feed
SGA	F_A20A	lbm/sec.	41	Secondary feed
SGA	L_A10S*	ft.	35	Overall level
SGA	P-A04S	psia	2	Secondary system
SGA	T-A01S	°F	10	MFW-A
SGA	T-A05P	°F	7	Hot side
SGA	T-A05S	°F	9	Hot side - riser
SGA	T-A06P	°F	7	Hot side
SGA	T-A08P	°F	11	Cold side
SGA	TW-A06S	°F	7	Hot side

**TEST S00605 PLOT PACKAGE
CHANNEL LIST BY COMPONENT (Cont.)**

COMPONENT	CHANNEL	UNITS	PLOT	COMMENT
SGB	DP-B05P	psi	21	Hot side
SGB	DP-B06P	psi	21	Hot side
SGB	DP-B07P	psi	23	Cold side
SGB	DP-B08P	psi	23	Cold side
SGB	F_B01S	lbm/sec.	41	Main feed
SGB	F_B20A	lbm/sec.	41	Secondary feed
SGB	L_B10S*	ft.	35	Overall level
SGB	P-B04S	psia	2	Secondary system
SGB	T-B01S	°F	10	MFW-B
SGB	T-B05P	°F	8	Hot side
SGB	T-B05S	°F	9	Hot side - riser
SGB	T-B06P	°F	8	Hot side
SGB	T-B07P	°F	8	U-tube top
SGB	T-B08P	°F	12	Cold side
SGE	TW-B06S	°F	8	Hot side
SL	T-020P	°F	18	Surge line near pressurizer
TDC	DP-001P	psi	25,26	Top
TDC	DP-002P	psi	24,25,26,27	Bottom
TDC	T-001PL	°F	13,14	Top
TDC	T-003P	°F	4,13,14	Bottom
TSAT-PRZ	n/a	°F	18,19	Based on P-027P
TSAT-UH	n/a	°F	4	Based on P-017P

*Failed channels

The data plots are found in the proprietary version of this document.

4.2.8 Double-Ended Guillotine DVI Line Break (S00706)

This matrix test simulated a double-ended guillotine (DEG) break of one of the two direct vessel injection-B(DVI-B) lines with only the passive safety-features used for mitigation. The test started with the initiation of the break located on the DVI-B line. For this break, the test facility was set up such that the break flows from the CMT-B side and the vessel side of the break were measured separately; the CMT-side break flow was measured by IF040P, and the vessel side was measured by IF005P.

This test was performed without any nonsafety systems operating (chemical and volume control system [CVCS] makeup pumps, steam generator startup feedwater pumps, and normal residual heat removal [NRHR] pumps). Results are provided in the data plot package at the end of this section. The sequence of events for S00706 is listed in Table 4.2.8-1.

The tests in SPES-2 were marked by distinctly different phases. These phases were characterized by the rate at which primary system pressure decreased and the thermal-hydraulic phenomena occurring within the primary and safety systems. The different phases selected for purpose of detailed test evaluation shown in Figure 4.2.8-1 and are as follows:

- Initial depressurization phase (IDP)—Point 1 to 2
- Pressure decay phase (PDP)—Point 2 to 3
- Automatic depressurization phase (ADP phase)—Point 3 to 4
- Post-automatic depressurization system phase (post-ADS phase)—Point 4 to 5

Overall Test Observations

Figure 4.2.8-2 shows the plant primary system pressure during test S00706 (as measured at the top of the pressurizer), with selected component actuations and plant responses shown in relation to the primary system pressure.

The test started with the initiation of the break in the DVI-B line by simultaneously opening the two break valves. During the first []^(a,b,c) seconds, subcooled water was discharged through the CMT side of the break, quickly draining CMT-B and accumulator-B (most of this occurred in the first []^(a,b,c) seconds) directly into the collection tank without entering the primary system. The rapid draining of CMT-B initiated the ADS-1 at []^(a,b,c) seconds.

The IDP started with the initiation of the break, which resulted in a rapid reduction in pressure. The reactor trip (R) signal initiated at 1800 psia and the safety systems actuation (S) signal initiated at 1700 psia. The R and S signals initiated the following actions:

- Decay power simulation (with heat loss compensation) initiated
- Main steamline isolation valves (MSLIVs) closed
- Main feedwater isolation valves (MFWIVs) shut off

-
- Core makeup tank (CMT) injection line isolation valves opened
 - Passive residual heat removal (PRHR) return flow isolation valve opened
 - Reactor coolant pumps (RCPs) shutoff

Recirculation flow through CMT-A and the PRHR flow started immediately after the isolation valves were opened. Due to the rapid loss of pressure down to saturation pressure for the fluid in the power channel, boiling was initiated in the rod bundle and the upper-upper plenum flashed. The fluid level upper-upper plenum dropped below the hot-leg elevation. This flashing slowed the rapid drop in primary system pressure. When the RCPs shutoff (at []^(a,b,c) seconds), the flow through the primary system started to oscillate. This resulted in oscillations in the rod bundle and upper-plenum fluid steam fractions, lower-upper plenum temperature, and system pressure. The oscillations ended approximately []^(a,b,c) seconds into the test, when the steam generator U-tubes drained.

During the PDP, the rod bundle steam fraction increased. This resulted in an increasing steam fraction in the upper plenum and the hot legs. The steam fraction in hot leg-A was slightly lower than hot leg-B due to the removal of vapor from hot leg-A by the PRHR HX. At approximately []^(a,b,c) seconds into the event, the steam generator-B U-tubes had drained due to the higher void fraction in hot leg-B. Approximately []^(a,b,c) seconds later, the steam generator-A U-tubes were drained.

The two-phase flow in the hot legs caused the steam generator U-tubes to drain since steam from the two-phase mixture collected in the top of the U-tubes. This stopped the flow through the primary system, and the power channel flow was reduced to the flow through the PRHR HX and the CMT-A injection flow.

For the first []^(a,b,c) seconds of test S00706, the fluid flow to the PRHR HX inlet consisted of a nearly uniform two-phase mixture of steam and water. This two-phase mixture was created by flashing in the power channel and hot leg that occurred as a result of the rapid depressurization of the primary system. The steam fraction increased as primary pressure decreased; and the PRHR HX measured^d return flow rate decreased apparently as the inlet fluid density decreased. From []^(a,b,c) seconds, slightly superheated steam flowed to the PRHR HX.

When ADS-4 occurred (at approximately []^(a,b,c) seconds), severe flashing in the upper plenum filled the hot leg with very high steam fraction mixture, which flowed to the PRHR HX for a period of approximately []^(a,b,c) seconds. When the flashing subsided (at approximately []^(a,b,c) seconds), the PRHR flow again converted to slightly superheated steam. The mass flow rate through the PRHR was very low from []^(a,b,c) until approximately []^(a,b,c) seconds, at which time the PRHR HX started to refill and alternating steam then water slug flow typical of the LOCA events began. At []^(a,b,c) seconds, the hot leg was refilled to the elevation of the PRHR nozzle and the slug flow through the PRHR was replaced by a more uniform two-phase flow, which lasted until the test was terminated.

After the initial primary system flow oscillations had stabilized, a PRHR HX heat removal rate of []^(a,b,c) kW was calculated. This calculation was based on the void fraction of the flow in the PRHR supply line (as calculated from the dP instrument readings in data plot 29), the average return flow, the HX inlet and outlet temperatures, and the pressure. It assumes a slip coefficient of 1 between the steam and water and may, therefore, give slightly lower values than the actual heat transfer. It should be used only for test-to-test comparison.

At []^(a,b,c) seconds, when the loop-B cold legs had partially emptied, CMT-A transitioned from the recirculation mode to the draindown mode of operation. This increased the cold injection flow and the rate of primary system pressure decay. The upper head started to drain when the primary system pressure dropped to the saturation pressure for the upper head (at []^(a,b,c) seconds) and was completely drained (at []^(a,b,c) seconds).

During the first []^(a,b,c) seconds (ADS-1), []^(a,b,c) lbm of fluid were discharged through the downcomer side of the break, and drained the cold-leg side of the primary system was drained down to the DVI nozzle elevation. A two-phase mixture existed in the hot leg up to the lower part of the steam generator U-tubes (hot side). The pressurizer and the power channel upper plenum above the hot-leg elevation were drained. CMT-B was partially drained, which initiated ADS actuation.

The break flow from the downcomer side of the break was steady for the first []^(a,b,c) seconds, indicating that the DVI line was full of water. The level on the cold-leg side of the primary system had decreased to the DVI nozzle elevation. The break flow sharply decreased at []^(a,b,c) seconds, indicating steam and water was now discharged and that the rod bundle decay heat simulation reduced the power level to approximately 545 kW before ADS-1 occurred at []^(a,b,c) seconds, consisting of 395 kW decay heat and 150 kW heat loss compensation. The power measured for the heater bundle was approximately twice that specified for this test for the first []^(a,b,c) seconds and did not match the specified power level until approximately []^(a,b,c) seconds (Appendix B, page B-45, plot 2).

The actuation of ADS-1 at []^(a,b,c) seconds had little effect on the already rapid rate of primary system depressurization. Accumulator-A began injecting water at about []^(a,b,c) seconds, and ADS-2 occurred at []^(a,b,c) seconds. The injection of cold fluid from accumulator-A ([]^(a,b,c) seconds) was insufficient to maintain the water level in the annular downcomer. The collapsed liquid levels in the tubular downcomer decreased rapidly at about []^(a,b,c) seconds, indicating that the downcomer fluid flashed. At this time, the steam fraction in the rod bundle and upper plenum increased. The maximum rod bundle steam fraction and minimum level in the tubular downcomer occurred at []^(a,b,c) seconds, near the end of the accumulator-A delivery. The pressurizer began to refill after ADS actuation and reached a collapsed liquid level of about []^(a,b,c) feet at []^(a,b,c) seconds. Pressurizer level (and ADS-1, -2, and -3 flow) decreased through []^(a,b,c) seconds. The pressurizer remained partially filled until approximately []^(a,b,c) seconds.

When the accumulator discharge ended (at []^(a,b,c) seconds), the CMT-A injection (suppressed by the accumulator-A injection) restarted and the IRWST-A injection started. The PRHR flow stopped at []^(a,b,c) seconds and the PRHR HX and supply line were drained. At this time, the combined

injection flow from CMT-A and IRWST-A started to raise the water level in the tubular downcomer and the steam fraction in the rod bundle gradually decreased (collapsed liquid level increased) and the lower-upper plenum gradually refilled to the hot-leg elevation (at approximately []^(a,b,c) seconds). At []^(a,b,c) seconds, the water level in the hot legs was sufficient to restart the flow through the PRHR. At about []^(a,b,c) seconds, rod bundle boiling had been suppressed and a steady-state condition existed for the rest of the test.

The fluid discharge from downcomer side of the break slowed when the water level in the annular downcomer decreased to the elevation of the DVI line and converted to steam. The CMT-A and IRWST injection flows gradually refilled the downcomer to the DVI nozzle elevation at []^(a,b,c) seconds.

Both CMT-B and accumulator-B drained through the CMT side of the break. Flow from the IRWST injection line-B to the break started at approximately []^(a,b,c) seconds.

The discharge flow rate through ADS-1, -2, and -3, was very small due to the rapid depressurization of the primary system, and the high steam fraction flow from the power channel prior to ADS-4 actuation.

This test demonstrated that the heater bundle was fully covered by water or cooled by a two-phase mixture at all times during this test (data plots 30 and 31), and there was no indication of heater rod temperatures increasing due to lack of cooling (data plot 3). Key parameters comparing the S00706 test with other tests are listed in Table 5.1-1, in Section 5.0.

Discussion of Test Transient Phases

- **Initial Depressurization Phase ([]^(a,b,c) Seconds)**

The initial depressurization phase (IDP) began with the initiation of the break (at time 0) and lasted until the primary system pressure was supported at the saturation pressure of the fluid in the upper plenum and the hot legs (see Figures 4.2.8-1 and 4.2.8-2). This phase included the following events: R signal at 1800 psia (decay power simulation initiated and the MSLIV closed), and S signal at 1700 psia (the MFWIV closed, the CMT injection line isolation valves opened, and the PRHR heat exchanger return line isolation valves opened—all with a 2-second delay, and RCP coastdown initiated after a 16.2-second delay). See Table 4.2.8-1.

Facility Response during the IDP:

From time 0 until the R signal occurred, the system lost pressure due to the expansion of the pressurizer steam bubble resulting from fluid loss through the break. The pressurizer partially compensated for the loss of pressure by flashing; however, it was drained within the first []^(a,b,c) seconds of the test (data plot 32). The R (at 14 seconds) and the S (at 17 seconds) signals were based on pressurizer pressure only. When the R signal occurred, the MSIV was

closed and the power was reduced to 20 percent of full power after a 5.75-second delay and began to decay after a 14.5-second delay.

As a result of the rod bundle power reduction without primary system flow reduction, the core ΔT decreased due to the low power/flow ratio and the lower-upper plenum temperature decreased toward the lower-plenum temperature []^(a,b,c). At []^(a,b,c) seconds, the primary system pressure reached the saturation pressure for the water in the upper-upper plenum []^(a,b,c) and the level in the upper upper-plenum decreased to the hot-leg elevation as this water flashed and its temperature decreased to []^(a,b,c). The primary system pressure continued to decrease to the saturation pressure corresponding to the hot-leg/upper-plenum fluid temperature []^(a,b,c) and reached []^(a,b,c) psia at approximately []^(a,b,c) seconds (Figure 4.2.8-2). When the RCPs were shutoff (at []^(a,b,c) seconds), the rod bundle outlet and the lower-upper plenum temperature increased to []^(a,b,c) due to the increased power/flow ratio. The system pressure increased temporarily until the loss of pressure (due to the break flow, the decreasing decay power, and the CMT injecting cold fluid into the downcomer) started reducing the lower upper plenum temperature. The system pressure decrease resulted from the balance between the steam generation rate (from flashing fluid), the volumetric flow of fluid out the break, and the steam condensation rate by the PRHR HX. Steam was continually being generated by core boiling due to the heater power. The PRHR flow began before the RCPs were shut off and then continued by natural circulation (data plot 37). This ended the IDP.

- **Pressure Decay Phase ([]^(a,b,c) Seconds)**

The pressure decay phase (PDP) started when the system pressure was supported by the saturation pressure of the fluid in the lower upper-plenum and hot legs (Figures 4.2.8-1 and 4.2.8-2). The phase ended when injection from accumulator-A started. ADS-1 was actuated at approximately []^(a,b,c) seconds; however, since the primary system pressure was rapidly decreasing at that time the only effect of ADS-1 was a small steam release from the pressurizer. This did not significantly affect the primary system pressure decay rate.

The PDP was characterized by decreasing the overall primary system pressure and temperature, which was much slower than during the IDP. The rod bundle power (decay heat plus heat loss compensation) was reduced from 1000 kW to 545 kW at ADS-1, and to 280 kW at the end of this phase (data plot 1 and Figure 4.2.8-2). The PRHR HX heat of approximately []^(a,b,c) (calculated at []^(a,b,c) seconds when the PRHR HX flow stabilized), and the CMT-A injection flow facility heat losses and energy out the break and ADS provided additional heat removal from the primary system.

The initial CMT-A injection by natural circulation transitioned to draindown injection at []^(a,b,c) seconds when the loop-B cold legs were emptying (data plot 38). The U-tubes of the steam generators began to drain at approximately []^(a,b,c) seconds; the cold-leg side of the U-tubes was completely drained at []^(a,b,c) seconds; and the hot-leg side of the U-tubes drained at []^(a,b,c) seconds (data plots 20 to 23). The steam generators did not affect the rest of the test

after the U-tubes were drained. The accumulator injection initiated when system pressure dropped below []^(a,b,c) psia just as ADS-2 actuated (data plot 39).

Facility Response during the PDP:

Following to coastdown of the RCPs pumps, flow oscillations occurred in the primary system which continued into PDP. These flow oscillations resulted in wide oscillations in the steam fraction of the two-phase mixture in the rod bundle (data plots 30 to 31), hot legs, and steam generators (data plots 20 to 21). These steam fraction oscillations became flow oscillation in the cold legs (data plots 24 to 27). Some of the steam in the two-phase mixture from the hot legs was condensed in the U-tubes (the primary-side pressure was higher than the secondary-side pressure at this time, allowing some heat to be transferred to the secondary-side fluid). The rest of the steam was separated from the two-phase fluid and collected in the high point of the U-tubes (due to the low velocity) and a free-water surface appeared at the top of the U-tubes. The cold-leg side of the U-tubes was completely drained at []^(a,b,c) seconds, and the hot-leg side was drained at []^(a,b,c) seconds (data plots 20 to 23). The water level on the cold-leg side of the primary system decreased to the DVI nozzle elevation (in the annular downcomer) at []^(a,b,c) seconds, due to the discharge of fluid out of the downcomer side of the break and the break mass flow decreased sharply since it now mostly consisted of steam.

The primary system depressurization rate during the PDP began at []^(a,b,c) psi/sec. When the break flow through the downcomer side of the break transitioned from water to steam, the primary system pressure depressurization rate increased to []^(a,b,c) psi/sec. Also at this time, CMT-A (Figure 4.2.8-4) transitioned from recirculation to draindown and its injection flow increased, contributing to the increase in the primary system pressurization.

CMT-A started to inject cold fluid into the downcomer via DVI line-A just after the S signal occurred. Initially, this injection was by natural circulation at approximately []^(a,b,c) lbm/sec., with hot water flowing from the cold leg through the cold-leg balance line (CLBL) into the top of the CMT, while cold water flowed from the bottom of CMT-A into the downcomer. At approximately []^(a,b,c) seconds (data plot 38), CMT-A transitioned to its draindown operating mode and a free-water surface developed in the top of the CMT as the levels started to drop (data plot 33). The injection flow, once draindown flow began, increased to []^(a,b,c) lbm/sec. CMT-A (data plot 38).

During CMT-A recirculation, the hot water from cold leg-B1 remained at the top of the CMT and did not mix with the cold CMT water. Later, steam from cold leg B1 flowed to CMT-A after the loop-B cold legs drained and condensed on the cold water and metal surfaces in the CMT-A, heating them to saturation temperature. The CMT water remained thermally stratified throughout CMT operation (data plot 15). Some of the hot water at the top of CMT-A may have flashed during the rapid decrease in primary system pressure.

CMT-B emptied quickly through the CMT side of the break. After it was drained, CMT-B was the path to the CMT side of the break for steam from cold leg-B2 for the rest of the test.

Throughout the PDP, the PRHR HX removed energy from the primary system. The PRHR HX cooling and the cold injection flow from CMT-A were insufficient to subcool the core during this period. The observed void fraction in the core oscillated from []^(a,b,c) percent (data plots 30 and 31).

- **Automatic Depressurization System Phase ([]^(a,b,c) Seconds)**

The automatic depressurization system (ADS) phase began approximately 65 seconds after the actuation of ADS-1 (when accumulator-A injection began) and ended with the actuation of ADS-4 (Figure 4.2.8-1).

Facility Response during the ADS Phase:

With the actuation of ADS-1, followed by ADS-2 and ADS-3 within 186 seconds, the rate of system depressurization increased from []^(a,b,c) psi/sec. at the end of the PDP to []^(a,b,c) psi/sec. during the early part of the ADS phase. This depressurization rate gradually decreased as the primary system pressure decreased. During the rapid depressurization from []^(a,b,c) seconds, flashing occurred in the annular and the tubular downcomers (data plot 25). This resulted in increased break flow through the downcomer side of the break as downcomer water was lifted to the break elevator.

A high rate of water injection was provided from accumulator-A (data plot 39) and draindown of the CMT-A continued (data plot 33). Accumulator-A injected cold water into the downcomer for approximately []^(a,b,c) seconds (from []^(a,b,c) seconds) and was then drained. The accumulator injection was insufficient to maintain/restore the water level in the downcomer. The water in the tubular downcomer flashed and level decreased during accumulator injection.

The pressurizer began to refill after ADS-1 actuation occurred and reached a collapsed liquid level of about []^(a,b,c) seconds. Pressurizer level (and ADS-1, -2, and -3 flow) decreased through []^(a,b,c) seconds. The pressurizer remained partially filled until about []^(a,b,c) seconds, and there was little or no steam flow through ADS-1, -2, and -3, after ADS-4 occurred (at []^(a,b,c) seconds).

During the ADS phase, the break flow from the downcomer side of the break consisted mostly of steam with some water from the flashing downcomer. The break flow from the CMT side of the break included steam from cold leg-B2 (via CMT-B), accumulator-B water, and a small amount of IRWST water.

- **Post-Automatic Depressurization System Phase ([]^(a,b,c) Seconds to End-of-Test)**

The post-automatic depressurization system (post-ADS) phase began when ADS-4 occurred (at []^(a,b,c) seconds) and continued to the end of the test (Figure 4.2.8-1).

System Response during the Post-ADS Phase:

The accumulator-A delivery continued into the post-ADS period and ended at approximately []^(a,b,c) seconds. Near the end of the accumulator delivery, the water level in the downcomer dropped to a level []^(a,b,c) ft. below the hot-leg elevation at []^(a,b,c) seconds ([]^(a,b,c) percent of tubular downcomer was drained, data plot 25), since the accumulator-A and CMT-A injection could not keep up with the ADS and break flows. During the accumulator-A injection, the CMT-A injection was partially suppressed, until the accumulator injection ended.

Concurrent with the decrease in water level in the downcomer, the steam fraction of the fluid in the rod bundle region increased to a maximum of []^(a,b,c) percent (data plots 30 and 31) and the lower-upper plenum steam fraction almost reached []^(a,b,c) percent; however, there was no indication of heater rod heat up due to lack of cooling. The maximum rod bundle steam fraction and minimum water level in the tubular downcomer occurred at []^(a,b,c) seconds.

After ADS-4 was actuated (at []^(a,b,c) seconds), only a small amount of saturated steam was vented through ADS-1, -2, and -3.

The primary system pressure was []^(a,b,c) psia when ADS-4 was actuated, and it was reduced to approximately []^(a,b,c) psia when the IRWST injection through the DVI-A nozzle into the downcomer started at []^(a,b,c) seconds (data plot 40). The combined effect of the IRWST-A and the CMT-A injection began to refill the downcomer and simultaneously reduced the steam fraction of flow through the rod bundle, through the upper plenum and into the hot legs.

The PRHR HX stopped flowing at approximately []^(a,b,c) seconds; however, as the IRWST flow decreased the steam fraction of fluid leaving the power channel, flow restarted at approximately []^(a,b,c) seconds. The cold flow from the IRWST and the PRHR gradually reduced boiling in the rod bundle and refilled the downcomer to the elevation of the broken DVI line. This steady-state condition was considered the end of the test.

Component Responses

- **Power Channel**

The power channel consists of 5 volumes: the lower plenum, the riser with the heater rod bundle, the lower upper-plenum below hot leg, the upper-upper plenum above hot leg, and the upper head. When the break occurred, the system pressure decreased to the R trip point (1800 psia) and the S

trip point of 1700 psia. However, since all the water in the primary system was below the saturation temperature for the system pressure, no boiling or flashing occurred up to this point.

Nothing significant happened in the power channel until the core power had been reduced to 20 percent (1000 kW) at []^(a,b,c) seconds. At this time, the ΔT across the rod bundle decreased due to the reduced power flow ratio (still full flow), and the lower upper-plenum temperature decreased toward the lower-plenum temperature (Figure 4.2.8-2). The upper-upper plenum water, which was at []^(a,b,c) fluid temperature, flashed when the primary system pressure dropped below []^(a,b,c) psia and decreased to []^(a,b,c) at []^(a,b,c) seconds. When the RCPs coasted down (from []^(a,b,c) seconds into the event), the power flow ratio increased and the power channel outlet temperature again increased. Boiling in the rod bundle and the flashing in the upper plenum produced sufficient amounts of steam to temporarily increase the system pressure; and the lower upper-plenum temperature increased momentarily until the upper-upper plenum was drained down to the hot leg elevation at []^(a,b,c) seconds (data plot 30 and 31). The primary system pressure reached []^(a,b,c) psia at []^(a,b,c) seconds.

At []^(a,b,c) seconds, the temperature of the fluid in the lower-upper plenum dictated the primary system pressure (data plot 4 and Figure 4.2.8-2). A short period of oscillations of the fluid in the rod bundle (period of []^(a,b,c) seconds) began when the RCPs had coasted down and disappeared at about []^(a,b,c) seconds into the test.

Data plots 30 and 31 show the collapsed liquid levels at various sections of the power channel during the S00706 test.

The upper head started to drain when the system pressure reached the saturation pressure of the fluid temperature in the upper head (at about []^(a,b,c) seconds). The upper head fluid temperature was initially only []^(a,b,c) and was, therefore, considerably cooler than the upper-upper plenum fluid temperature. Fluid flashing in the upper head caused its water level to decrease and it had drained completely by []^(a,b,c) seconds (data plot 4).

The upper-upper plenum started to flash at []^(a,b,c) seconds and continued to flash during the RCP coast down. The level dropped to the hot leg elevation by []^(a,b,c) seconds (Figure 4.2.8-3). The upper-upper plenum level never recovered during this test and it stayed at or below the hot-leg elevation until the end of this test (temperatures in data plot 4).

The steam fraction in the rod bundle increased from the time the RCPs coasted down to []^(a,b,c) seconds (data plots 30 and 31). At this time, the steam fraction reached []^(a,b,c) percent, and the collapsed liquid level in the lower-upper plenum decreased below the top of the unheated portion of the rod bundle. However, the top of the heated portion of the rod bundle was covered by two-phase mixture, and there was no indication of heater rod heat-up due to lack of cooling (data plot 3).

Concurrent with the increase in rod bundle steam fraction and decrease in fluid level in the lower-upper plenum, the water level in the downcomer decreased to []^(a,b,c) ft. (hot-leg elevation is 0) at []^(a,b,c) seconds.

Data plot 30 shows that the collapsed levels in the rod bundle exhibited a short period of oscillations following the RCP coastdown, with apparent steam fractions in the rod bundle ranging from []^(a,b,c) percent. The injection from accumulator-A ([]^(a,b,c) seconds) did not reduce the steam fraction in the rod bundle, and the maximum steam fraction (minimum collapsed liquid level) occurred near the end of the injection. When the IRWST-A injection started at []^(a,b,c) seconds, combined with the CMT-A injection, the water level in the downcomer started to recover. The tubular downcomer was refilled by approximately []^(a,b,c) seconds, and the level continued to rise into the annular downcomer. The steam fraction of flow through the rod bundle decreased steadily, and the two-phase mixture level in the lower-upper plenum increased to the hot-leg elevation. However, the flow through the rod bundle remained two-phase (steam fraction about []^(a,b,c) percent) for the rest of the test.

This test resulted in a []^(a,b,c) in the rod bundle; however, there was no indication of a temperature increase in the rod thermocouples. Also, this test was more severe than intended due to the higher than specified rod bundle power simulation.

- **Pressurizer**

The pressurizer started to drain when the break occurred and was completely drained in 18 seconds (data plot 32). The water in the pressurizer flashed due to the loss of system pressure, and the temperature of the water dropped from []^(a,b,c) during this initial depressurization (data plot 18). The hot water exiting the pressurizer surge line into the hot leg-A caused a slight increase in the hot leg temperature, since it mixed with the flow from the power channel/upper plenum. The pressurizer remained empty until ADS-1 occurred, at which time it partially refilled to a collapsed liquid level of about []^(a,b,c) seconds, and discharged some two-phase mixture from the top via the ADS. The pressurizer level decreased to approximately []^(a,b,c) seconds as ADS-1, -2, and -3 flow decreased to almost zero. At []^(a,b,c) seconds the pressurizer again drained completely.

- **Steam Generator**

The steam generators acted as the heat sink until the MSLIV closed and prevented further energy removal from the secondary side. This caused the temperature of the steam generator secondary-side fluid to increase toward the primary system hot leg temperature, which at the same time was dropping due to the reduced power/flow ratio.

For the first part of the PDP, the pressure on the primary side of the steam generators U-tubes was higher than the steam generator secondary-side, indicating that some heat transfer from the primary to secondary side occurred and causing some condensing of the two-phase fluid coming from the

hot leg. The primary system pressure dropped below the steam generator secondary-side pressure at approximately []^(a,b,c) seconds. At this time, the cold side of the U-tubes was completely drained, and the hot side was partially drained. Data plot A indicates that there was some heat transfer from the steam generators to the primary system fluid, which was rapidly reducing in temperature due to the rapid depressurization of the primary system.

At the end of the pump coastdown, flow oscillations started to occur in the tubular downcomer and through the power channel. This caused oscillations of the density of the two-phase flow through the rod bundle into the hot legs and to the steam generators. These flow oscillations were sustained as long as there was flow through the steam generators and ended at approximately []^(a,b,c) seconds.

Steam generator-B U-tubes began to drain at []^(a,b,c) seconds. The level on the hot-leg side of the U-tubes dropped to the []^(a,b,c) percent elevation in []^(a,b,c) seconds and were completely drained after []^(a,b,c) seconds. Steam generator-1 U-tubes began to drain at 105 seconds. The level on the hot-leg side and dropped to the []^(a,b,c) percent elevation after []^(a,b,c) seconds and were drained at []^(a,b,c) seconds. The cold-leg side of the U-tubes were drained for both steam generators at []^(a,b,c) seconds (data plots 20 through 23).

- **Hot Legs**

The hot legs were full of two-phase fluid until about []^(a,b,c) seconds (data plots 20 and 21). Hot leg-A and hot leg-B collapsed liquid levels decreased when the steam generator U-tubes drained on the hot-leg side. Hot leg-B was drained at []^(a,b,c) seconds, and hot leg-A completely drained at []^(a,b,c) seconds (after ADS-4 occurred). Both hot legs started to partially refill at []^(a,b,c) seconds, when IRWST-A and CMT-A injection was refilling the power channel.

There was a slight difference in the observed steam fraction in hot legs-A and -B before they drained, due to the fact that the PRHR HX preferentially removed steam from hot leg-A (as seen in the very high steam fraction in the fluid at the PRHR HX inlet). This reduced the steam fraction of the fluid in hot leg-A as compared with hot leg-B. The hot leg void fraction affected the steam generator U-tube draining, resulting in earlier draining in steam generator-B than in steam generator-A.

- **Cold Legs (Including Tubular Downcomer and Annular Downcomer)**

The cold legs remained full until []^(a,b,c) seconds and then quickly drained. The loop-B cold legs emptied at []^(a,b,c) seconds, and the loop-A cold leg-A were drained to the cold leg nozzle elevation at []^(a,b,c) seconds. All four cold legs remained completely drained for the duration of the event (data plots 22 through 27).

The annular downcomer started to drain (through the broken DVI-B nozzle) at []^(a,b,c) seconds, and its level decreased to the DVI nozzle elevation by []^(a,b,c) seconds. Flashing in the

downcomer started at []^(a,b,c) seconds and continued through []^(a,b,c) seconds, when the level began to be restored.

The tubular downcomer reached a collapsed level of []^(a,b,c) ft. ([]^(a,b,c) percent of tubular downcomer empty at []^(a,b,c) seconds) before the injection flow from the CMT-A and the IRWST started to refill the downcomer and power channel. The tubular downcomer was refilled at []^(a,b,c) seconds, and the annular downcomer was refilled to the DVI nozzle elevation at approximately []^(a,b,c) seconds.

- **PRHR and IRWST**

At the initiation of the break, the PRHR subsystem was filled with subcooled liquid. When the S signal occurred, the PRHR return line isolation valve opened, and a high flow rate started through the HX due to the still operating RCP. When the RCPs were shut off and the upper plenum and the hot leg filled with two-phase fluid, a large portion of the steam in hot leg-A flowed to the PRHR HX (average fluid steam fraction is []^(a,b,c) percent based on data plot 29). This high steam fraction enhanced the PRHR HX heat removal from the primary system. The two-phase mixture was condensed and subcooled in the PRHR HX (data plot 28). When the primary system flow stabilized after the initial flow oscillations a PRHR HX heat removal rate of []^(a,b,c) kW was calculated at []^(a,b,c) seconds. This calculation was based on the average steam fraction of the fluid in the PRHR supply line (as calculated from the dP instrument readings in data plot 29), the average steam flow rate, the HX inlet and outlet temperatures, and the pressure.

For the first []^(a,b,c) seconds of test S00706, the fluid flow to the PRHR HX inlet consisted of a nearly uniform two-phase mixture of steam and water. This two-phase mixture was created by flashing in the power channel and hot leg that occurred as a result of the rapid depressurization of the primary system. The steam fraction of the two-phase mixture increased as primary pressure decreased; and the PRHR HX measured return flow rate decreased, apparently as the inlet fluid density decreased. From []^(a,b,c) seconds slightly superheated steam flowed to the PRHR HX. When ADS-4 occurred (at approximately []^(a,b,c) seconds), severe flashing in the upper plenum filled the hot leg with very high steam fraction mixture, which flowed to the PRHR HX for a period of approximately []^(a,b,c) seconds. When the flashing subsided (approximately at []^(a,b,c) seconds), the PRHR flow again converted to slightly superheated steam. The mass flow rate through the PRHR was very low from []^(a,b,c) until approximately []^(a,b,c) seconds, at which time the PRHR HX started to refill and alternating steam then water slug flow, typical of the LOCA events began. At []^(a,b,c) seconds the hot leg was refilled to the elevation of the PRHR nozzle and the slug flow through the PRHR was replaced by a more uniform two-phase flow which lasted until the test was terminated.

The PRHR HX was submerged in the IRWST (heatup of the water within the IRWST is shown in data plot 17). Following ADS-4, the primary system pressure decreased to near ambient, and gravity flow due to the water elevation head in the IRWST started to inject water into the DVI-A

line. This flow was sufficient to help partially refill the primary system (data plots 30, 31, 32, and 40).

- **Core Makeup Tanks (CMTs)**

The CMT injection was initiated []^(a,b,c) seconds after the ζ signal by opening the CMT injection line isolation valves. CMT-B injection spilled to the CMT side of the double-ended DVI line break and was collected in a weigh tank.

Initially, the injection flow from the CMT-A was by natural circulation with hot water from the cold leg B1 flowing through the CLBL to the top of the CMT-A, and cold water from the bottom of CMT-A flowing into the downcomer via DVI-A line.

When cold legs-B1 and -B2 drained to the level of the cold leg downcomer nozzles, steam flowed through the CLBL to the top of CMT-A, resulting in a free-water surface. This increased the driving head for the injection flow and resulted in an increase in injection flow approximately []^(a,b,c) seconds. (Data plot 38).

CMT-A was heated first by the hot fluid from the CLBL, and later by steam from the cold leg condensing on the free-water and metal surfaces in the upper part of the CMT. A stable stratified thermal gradient was established in the CMT-A water (data plot 15), where the free-water surface temperature was at or near saturation temperature; and water at the bottom of the tank was cold. As the CMT drained the heated water moved lower in the tank.

The recirculation flow-through the CMT-A was approximately []^(a,b,c) lbm/sec. The draindown injection began at []^(a,b,c) lbm/sec. and gradually decreased with time. During the accumulator injection, the draindown rate from the CMT-A was temporarily reduced due to back pressure in the common DVI line A piping. The CMT-A injection flow steadily decreased until the end of the test, at which time CMT-A still had some water inventory (data plot 33).

- **Accumulators**

The accumulators provided water injection by a polytropic expansion of a compressed air volume at the top of the accumulator. Water flowed from accumulator-A when the primary system pressure decreased below []^(a,b,c) psia at about []^(a,b,c) seconds, and lasted until []^(a,b,c) seconds, (data plot 39). The accumulator-A injection for the S00706 test lasted approximately []^(a,b,c) seconds, and accumulator-A was completely drained when the injection ended (data plot 34). Accumulator-B flow spilled to the CMT side of the DVI line-B break and was collected in a weigh tank. Accumulator B flow to the break stopped from about []^(a,b,c) seconds.


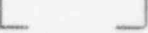
Mass Discharge and Mass Balance

The catch tank weight measurements are shown in data plot 43 for the break flows, and for the ADS-1, -2, -3, and -4 flows. IF040P collected the water from CMT-B and accumulator-B and the IRWST-B flow. Also, the steam from cold leg-B2 (flowing through CMT-B) was condensed and collected, and when ADS-4 occurred the additional flow from ADS-4 was also collected in this tank. The downcomer side DVI line break flow, which started when the test was initiated, was stable until the downcomer level decreased to the DVI nozzle elevation. Then the flow decreased as it changed to two-phase flow. Increases in the break flow during the time when the downcomer fluid was flashing indicated that some downcomer water was lifted to the break elevation. When the system refilled to the DVI nozzle elevation water again flowed from the break.

The discharge flow through ADS-1, -2, and -3 started out low because the primary pressure had already decreased and the steam fraction of fluid leaving the power channel was high. After ADS-4, the ADS-1, -2, and -3 flow decreased rapidly as it converted to pure steam. The discharged masses are shown in Table 4.2.8-4.

The mass balance results for test S00706 were calculated based on the water inventory before and after the test. Table 4.2.8-2 gives a detailed listing of the inventories of water in the various components before the test. Table 4.2.8-3 lists the inventories after the test and the amount of water injected into the downcomer from the IRWST. The water level in the power channel was determined by the DP-B15P measurement to be below the hot-leg centerline at the end of the test (at the DVI line nozzle elevation). Table 4.2.8-4 compares the mass balance for the system before and after the test and shows agreement (within 1.1 percent) of the measurements.

**TABLE 4.2.8-1
SEQUENCE OF EVENTS FOR TEST S00706**

Event	Specified	Instrument Channel	Actual Time
Break Opens	0		 (a,b,c)
R Signal	P = 1800 psia	P-027P	
MSL IV Closure	R + 2 sec.	Z_A04SO, F_A04S	
		Z_B04SO, F_B04S	
S Signal	P = 1700 psia	P-027P	
MFW IV Closure	S + 2 sec.	Z_B02SO, F_B01S	
		Z_A02SO, F_A01S	
CMT IV Opening	S + 2 sec.	Z_A040EC, F-A40E	
		Z_B040EC, F-B40E	
RCPs Tripped	S + 16.2 sec.	I-A1P, S-A1P	
		I-B1P, S-B1P	
PRHR HX Actuation	S + 2 sec.	Z_A81EC, F_A80E	
ADS-1	CMT level 67%	L_B40E	
	+30 sec.	Z_001PC	
Accumulators	P-027P = 710 psia	F_A20E	
		F_B20E	
ADS-2	CMT level 67%	L_B40E	
	+125 sec.	Z_002PC	
ADS-3	CMT level 67%	L_B40E	
	+245 sec.	Z_003PC	
ADS-4	CMT level 20%	L_B40E	
	+60 sec.	Z_004PC, F-040P	
IRWST Injection	P-027P = 26 psia	F_A60E	
		F_B60E	

**TABLE 4.2.8-2
WATER INVENTORY BEFORE TEST S00706**

Component	Volume (ft.³/(l))	Net Volume (l)	Temp (°F)	Relative Density	Mass (lb)
Loops	8.97 ft. ³ (254.0 l)	8.97 ft. ³ (254.0 l)			(a,b,c)
Pressurizer	3.37 ft. ³ (95.4 l)	1.89 ft. ³ (53.5 l)			
Surge Line	0.34 ft. ³ (9.6 l)	0.34 ft. ³ (9.6 l)			
Tubular Downcomer	1.38 ft. ³ (39.1 l)	1.38 ft. ³ (39.1 l)			
Annular Downcomer + High-Pressure Bypass	0.54 ft. ³ (15.3 l)	0.54 ft. ³ (15.3 l)			
Core Bypass	0.44 ft. ³ (12.4 l)	0.44 ft. ³ (12.4 l)			
Lower Plenum	0.81 ft. ³ (22.8 l)	0.81 ft. ³ (22.8 l)			
Riser	1.64 ft. ³ (46.4 l)	1.64 ft. ³ (46.4 l)			
Upper Plenum	1.46 ft. ³ (41.3 l)	1.46 ft. ³ (41.3 l)			
Upper Head	1.90 ft. ³ (53.8 l)	1.90 ft. ³ (53.8 l)			
CMTs	10.1 ft. ³ (286.0 l)	10.1 ft. ³ (286.0 l)			
Accumulator	10.1 ft. ³ (286.0 l)	7.84 ft. ³ (222.0 l)			
IRWST Injection Line	0.18 ft. ³ (5.1 l)	0.18 ft. ³ (5.1 l)			
TOTAL INVENTORY					

**TABLE 4.2.8-3
WATER INVENTORY AFTER TEST 500706 WAS COMPLETED**

Component	Volume (L)	Net Volume (L)	Temp (°F)	Relative Density	Mass (lb)
Loops	8.97 ft. ³ (254.0 l)	0.0 ft. ³ (0.0 l)			
Pressurizer	3.37 ft. ³ (95.4 l)	0.0 ft. ³ (0.0 l)			
Surge Line	0.34 ft. ³ (9.6 l)	0.0 ft. ³ (0.0 l)			
Tubular Downcomer	1.38 ft. ³ (39.1 l)	1.38 ft. ³ (39.1 l)			
Annular Downcomer + HPBP	0.54 ft. ³ (15.3 l)	0.15 ft. ³ (4.3 l)			
Core Bypass	0.44 ft. ³ (12.4 l)	0.44 ft. ³ (12.4 l)			
Lower Plenum	0.81 ft. ³ (22.8 l)	0.81 ft. ³ (22.8 l)			
Riser	1.64 ft. ³ (46.4 l)	1.64 ft. ³ (46.4 l)			
Upper Plenum	1.46 ft. ³ (41.3 l)	1.32 ft. ³ (37.3 l)			
Upper Head	1.90 ft. ³ (53.8 l)	0.0 ft. ³ (0.0 l)			
CMTs	10.1 ft. ³ (286.0 l)	0.74 ft. ³ (21.0 l)			
Accumulator	10.1 ft. ³ (286.0 l)	0.0 ft. ³ (0.0 l)			
IRWST Injection Line	0.18 ft. ³ (5.1 l)	0.18 ft. ³ (5.1 l)			
TOTAL INVENTORY					
WATER INJECTED FROM THE IRWST DURING EVENT					
IRWST Injection	dP (psi)	Area (in ²)	Temp (°F)	Relative Density	Mass (lb)

**TABLE 4.2.8-4
MASS BALANCE FOR TEST S00706**

	Starting Inventory (lb/m)	Ending Inventory (lb/m)	
Total Primary System			(a,b,c)
IRWST Injection			
Power Channel Side Break			
ADS-,1, -2, -3			
ADS-4 + CMT-Side Break			
TOTAL			
Ending Inventory/Starting Inventory (lbm)			
Ending Inventory/Starting Inventory (%)			

The following figures have been intentionally deleted
from this document due to their proprietary nature.

**TEST S00706 PLOT PACKAGE
CHANNEL LIST BY COMPONENT**

COMPONENT	CHANNEL	UNITS	PLOT	COMMENT
ACCA	F_A20E	lbm/sec.	39	
ACCA	L_A20E	ft.	34	
ACCB	F_B20E	lbm/sec.	39	
ACCB	L_B20E	ft.	34	
ADS 1, 2, & 3	IF30FLW	lbm/sec.	44	Flow rate derived from IF030P
ADS 1, 2, & 3	IF030P	lbm	43	Catch tank
ADS 4 & SG	IF40FLW	lbm/sec.	44	Flow rate derived from IF040P
ADS 4 & SG	IF040P	lbm	43	Catch tank
ANNDC	DP-A021P	psi	24	To cold leg-A1
ANNDC	DP-A022P	psi	25	To cold leg-A2
ANNDC	DP-B021P	psi	26	To cold leg-B1
ANNDC	DP-B022P	psi	27	To cold leg-B2
BREAK LINE	IF05FLW	lbm/sec.	44	Flow rate derived from IF005P
BREAK LINE	IF005P	lbm	43	Catch tank
CLA	DP-A001P	psi	24	To cold leg-A1
CLA	DP-A002P	psi	25	To cold leg-A2
CLA	DP-A09P	psi	22	Pump suction
CLA	T-A10P	°F	11	Steam generator outlet
CLA1	F_A01P	lbm/sec.	36	
CLA1	T-A021PL	°F	13	Downcomer inlet
CLA1	T-A11P	°F	11	Pump outlet
CLA2	F_A02P	lbm/sec.	36	
CLA2	T-A022PL	°F	13	Downcomer inlet
CLB	DP-B001P	psi	26	To cold leg-B1

**TEST DATA PLOT PACKAGE
CHANNEL LIST BY COMPONENT (Cont.)**

COMPONENT	CHANNEL	UNITS	PLOT	COMMENT
CLB	DP-B002P	psi	27	To cold leg-B2
CLB	DP-B09P	psi	23	Pump suction
CLB	T-B10P	°F	12	Steam generator outlet
CLB1	F_B01P	lbm/sec.	36	
CLB1	T-B021PL	°F	14	Downcomer inlet
CLB1	T-B11P	°F	12	Pump outlet
CLB2	F_B02P	lbm/sec.	36	
CLB2	T-B022PL	°F	14	Downcomer inlet
CMTA	F_A40E	lbm/sec.	38	
CMTA	L_A40E	ft.	33	
CMTA	T-A401E	°F	15	Top (242.25 in.)
CMTA	T-A403E	°F	15	216.75 in.
CMTA	T-A405E	°F	15	191.25 in.
CMTA	T-A407E	°F	15	165.75 in.
CMTA	T-A409E	°F	15	140.25 in.
CMTA	T-A411E	°F	15	114.75 in.
CMTA	T-A413E	°F	15	89.25 in.
CMTA	T-A415E	°F	15	63.75 in.
CMTA	T-A417E	°F	15	38.25 in.
CMTA	T-A420E	°F	15	Bottom (0 in.)
CMTB	F_B40E	lbm/sec.	38	
CMTB	L_B40E	ft.	33	
CMTB	T-B401E	°F	16	Top (242.25 in.)
CMTB	T-B403E	°F	16	216.75 in.
CMTB	T-B405E	°F	16	191.25 in.
CMTB	T-B407E	°F	16	165.75 in.
CMTB	T-B409E	°F	16	140.25 in.
CMTB	T-B411E	°F	16	114.75 in.
CMTB	T-B413E	°F	16	89.25 in.

**TEST DATA PLOT PACKAGE
CHANNEL LIST BY COMPONENT (Cont.)**

COMPONENT	CHANNEL	UNITS	PLOT	COMMENT
CMTB	T-B415E	°F	16	63.75 in.
CMTB	T-B417E	°F	16	38.25 in.
CMTB	T-B420E	°F	16	Bottom (0 in.)
CVCS	F-001A	psi	42	
DVIA	T-A00E	°F	13	
DVIB	T-B00E	°F	14	
HLA	DP-A04P	psi	20	
HLA	T-A03PL	°F	5	Vertical, near power channel
HLA	T-A03PO	°F	5	Horizontal, near power channel
HLA	T-A04P	°F	5	Near steam generator inlet
HLB	DP-B04P	psi	21	
HLB	T-B03PL	°F	6	Vertical, near power channel
HLB	T-B03PO	°F	6	Horizontal, near power channel
HLB	T-B04P	°F	6	Near steam generator inlet
IRWST	F_A60E	lbm/sec.	40	
IRWST	F_B60E	lbm/sec.	40	
IRWST	L_060E	ft	32	
IRWST	T-061E	°F	17	Bottom
IRWST	T-062E	°F	17	Below middle
IRWST	T-063E	°F	17	Middle
IRWST	T-064E	°F	17	Above middle
IRWST	T-065E	°F	17	Top
PC	W_00P	kW	1	
PC-HB	L_000P	ft	30	Heater bundle
PC-HR	TW018P20	°F	3	Heater rod
PC-HR	TW018P48	°F	3	Heater rod
PC-HR	TW020P87	°F	3	Heater rod
PC-UH	T-016P	°F	4	Upper head
PC-UP	L_A15P	ft.	30	Lower-upper plenum

TEST DATA PLOT PACKAGE
CHANNEL LIST BY COMPONENT (Cont.)

COMPONENT	CHANNEL	UNITS	PLOT	COMMENT
PC-UP	L_A16P	ft.	31	Upper-upper plenum
PC-UP	T-015P	°F	4	Upper plenum
PC-UH	L_017P	ft.	31	Upper head
PC-UP	L_A14P	ft.	31	Above top of the heated length
PRHR	DP-A81AE	psi	29	Supply line inverted U-tube
PRHR	DP-A81BE	psi	29	Supply line inverted U-tube
PRHR	DP-A81E	psi	28	Supply line
PRHR	DP-A82E	psi	28	Heat exchanger
PRHR	DP-A83E	psi	28	Return line
PRHR	F_A80E	lbm/sec.	37	Return line
PRHR	T-A82E	°F	19	Inlet
PRHR	T-A83E	°F	19	Exit
PRZ	L_010P	ft.	32	
PRZ	P-027P	psia	2	
PRZ	T-026P	°F	18	487 in.
SGA	DP-A05P	psi	20	Hot side
SGA	DP-A06P	psi	20	Hot side
SGA	DP-A07P	psi	22	Cold side
SGA	DP-A08P	psi	22	Cold side
SGA	F_A01S	lbm/sec.	41	Main feed
SGA	F_A20A	lbm/sec.	41	Secondary feed
SGA	L_A10S*	ft.	35	Overall level
SGA	P-A04S	psia	2	Secondary system
SGA	T-A01S	°F	10	MFW-A
SGA	T-A05P	°F	7	Hot side
SGA	T-A05S	°F	9	Hot side - riser
SGA	T-A06P	°F	7	Hot side
SGA	T-A08P	°F	11	Cold side
SGA	TW-A06S	°F	7	Hot side

TEST DATA PLOT PACKAGE
CHANNEL LIST BY COMPONENT (Cont.)

COMPONENT	CHANNEL	UNITS	PLOT	COMMENT
SGB	DP-B05P	psi	21	Hot side
SGB	DP-B06P	psi	21	Hot side
SGB	DP-B07P	psi	23	Cold side
SGB	DP-B08P	psi	23	Cold side
SGB	F_B01S	lbm/sec.	41	Main feed
SGB	F_B20A	lbm/sec.	41	Secondary feed
SGB	L_B10S*	ft.	35	Overall level
SGB	P-B04S	psia	2	Secondary system
SGB	T-B01S	°F	10	MFW-B
SGB	T-B05P	°F	8	Hot side
SGB	T-B05S	°F	9	Hot side - riser
SGB	T-B06P	°F	8	Hot side
SGB	T-B07P	°F	8	U-tube top
SGB	T-B08P	°F	12	Cold side
SGB	TW-B06S	°F	8	Hot side
SL	T-020P	°F	18	Surge line near pressurizer
TDC	DP-001P	psi	25,26	Top
TDC	DP-002P	psi	24,25,26,27	Bottom
TDC	T-001PL	°F	13,14	Top
TDC	T-003P	°F	4,13,14	Bottom
TSAT-PRZ	n/a	°F	18,19	Based on P-027P
TSAT-UH	n/a	°F	4	Based on P-017P

*Failed channels

4.2.9 Two-In. Cold-Leg/Core Makeup Tank Balance Line Break without Nonsafety Systems (S01007)

This matrix test simulated a 2-in. break in cold leg-B2/CMT-B balance line. The test began with the initiation of the break in the cold-leg/core makeup tank (CMT) balance line. This break was located between the balance line isolation valve and the CMT-B. This test was performed without any nonsafety systems (chemical and volume control system [CVCS] makeup pumps, steam generator startup feedwater [SFW] pumps, and normal residual heat removal system [NRHR] pumps) operating.

Results are provided in the data plot package at the end of this section. The sequence of events for S01007 is listed in Table 4.2.9-1.

The tests in SPES-2 were marked by distinctly different phases. These phases were characterized by the rate at which the primary system pressure decreased and the thermal-hydraulic phenomena occurring within the primary and safety systems. The phases selected for the purpose of detailed evaluation of this LOCA are shown in Figure 4.2.9-1 and are as follows:

- Initial depressurization phase (IDP)—Point 1 to 2
- Pressure decay phase (PDP)—Point 2 to 3
- Automatic depressurization system (ADS) phase—Point 3 to 4
- Post-automatic depressurization system (post-ADS) phase—Point 4 to 5

Overall Test Observations

Figure 4.2.9-1 shows plant primary system pressure during test S01007 (as measured at the top of the pressurizer), with selected component actuations and plant responses shown in relation to primary system pressure.

The IDP began with the initiation of the break, which resulted in a rapid reduction in pressure. The reactor trip (R) signal initiated at 1800 psia, and the safety systems actuation (S) signal initiated at 1700 psia. The R and the S signals initiated the following actions:

- Decay power simulation (with heat loss compensation).
- Main steamline isolation valves (MSLIVs) closed.
- Main feedwater isolation valves (MFWIVs) closed.
- CMT injection line isolation valves opened.
- Passive residual heat removal (PRHR) return flow isolation valve opened.
- Reactor coolant pumps (RCPs) shut off.

Recirculation flow through the CMT-A and PRHR heat exchanger (HX) flow started immediately after their isolation valves opened. Boiling occurred in the rod bundle and the upper-upper plenum fluid flashed due to the rapid decrease in primary pressure. The measured fluid level in the upper-upper

plenum dropped to the hot-leg elevation. The flashing on the hot-leg side of the primary system stopped the rapid drop in primary system pressure. When the RCPs were shut off (at []^(a,b,c) seconds), the flow through the primary system began to oscillate (with a period of approximately []^(a,b,c) seconds). This resulted in oscillations in the rod bundle and lower-upper plenum fluid steam fraction, the lower-upper plenum fluid temperature, and primary system pressure.

During the initial stages of the PDP, the rod bundle fluid steam fraction increased. This resulted in increasing steam fractions in the lower-upper plenum and the hot leg fluid. Both hot legs contained two-phase fluid. The hot leg-B fluid had a steam fraction close to that observed in the lower-upper plenum. However, the steam fraction in hot leg-A was much lower due to the selective removal of steam from the hot leg into the PRHR HX inlet line.

Two-phase flow in the hot legs initiated draining of the steam generator U-tubes, as steam from the two-phase mixture collected in the top of the U-tubes. This stopped the primary system flow through the steam generators so that the power channel flow was composed predominantly of the flow through the PRHR HX. The steam fraction oscillations observed in the rod bundle and in the upper-upper plenum stopped when the steam generator U-tubes drained. At approximately []^(a,b,c) seconds into the event, the steam generator-B U-tubes began to drain. This occurred earlier in steam generator-B than steam generator-A due to the higher steam fraction in hot leg-B fluid. Approximately []^(a,b,c) seconds later, the steam generator-A U-tubes drained.

The flow to the PRHR HX, consisting of alternating slugs of steam and water, had an average steam fraction significantly greater than the fluid in the lower-upper plenum. Due to boiling in the rod bundle (data plots 30 and 31), two-phase flow entered the hot leg from the lower-upper plenum and flowed to the PRHR HX. The average steam fraction at the PRHR inlet was as high as []^(a,b,c) to []^(a,b,c) percent, which enhanced the PRHR HX heat removal from the primary system, as compared to its heat removal capability with single-phase saturated or subcooled water. When the primary system flow stabilized after the initial flow oscillations, a PRHR HX heat removal rate of []^(a,b,c) kW was calculated. This calculation was based on the steam fraction of the flow in the PRHR supply line (as calculated from the dP instrument readings in data plot 29), the average return flow rate, the HX inlet and outlet temperatures, and the pressure. It assumes a slip coefficient of 1 between steam and water, and may therefore give slightly lower values than the actual heat transfer. It should be used only for test-to-test comparison.

When the loop-B cold leg had partially emptied, CMT-A transitioned from the recirculation mode to the drain-down mode of operation. This increased the CMT discharge flow and the rate of primary system pressure decay. This occurred at approximately []^(a,b,c) seconds for CMT-A and []^(a,b,c) seconds for CMT-B. When the primary system pressure dropped to the saturation pressure of the water in the upper head, the upper head began to drain (at []^(a,b,c) seconds).

During the first []^(a,b,c) seconds of this event, []^(a,b,c) lbm of steam/water were expelled through the break while draining the pressurizer, the steam generator U-tubes, the power channel upper head, the power channel upper-upper plenum, most of the cold legs, and approximately []^(a,b,c) percent of

the CMTs. The heated rods in the power channel that simulated the AP600 core decay heat reduced the power level to approximately 260 kW at 1070 seconds. This value consisted of 110-kW decay heat and 150-kW heat loss compensation. The break flow had decreased smoothly as primary pressure decreased, but had not sharply dropped in flow rate, indicating that cold leg-B2 was not yet empty.

The ADS phase began with the actuation of ADS-1 (at 1072 seconds). ADS-2 and -3 occurred within the next []^(a,b,c) seconds. The heat loss compensation was terminated from the decay heat simulation during ADS-1, and the rod bundle power level was reduced to approximately 110 kW.

The ADS actuation increased the rate of primary system depressurization and resulted in high injection flow from the accumulators. The rapid injection of cold fluid from the accumulators ([]^(a,b,c) seconds) temporarily refilled the power channel rod bundle and lower-upper plenum with subcooled water and partially filled the pressurizer. When the accumulator discharge ended, the flow through the heater bundle was reduced to the injection rate of the CMTs and the PRHR HX flow, and boiling occurred again in the heater bundle. Two-phase flow occurred again in hot leg-A, the PRHR HX, and to the ADS via the pressurizer.

The liquid discharge through the break was replaced by saturated steam at approximately []^(a,b,c) seconds. During the ADS phase, approximately []^(a,b,c) lbm of water were discharged from ADS-1, -2, and -3. This water was supplied primarily by the accumulators.

The post-ADS phase began when ADS-4 was actuated at []^(a,b,c) seconds. The fluid discharge through ADS-1, -2, and -3 ended, and pressurizer water level decreased as fluid was discharged through the ADS-4 flow paths. A small amount of CMT flow was still provided to the downcomer until approximately []^(a,b,c) seconds. When primary system pressure had been reduced below the pressure corresponding to the water elevation head of the IRWST, flow from the IRWST into the downcomer began and shortly thereafter the CMT flow ended. The flow from the IRWST refilled the primary system with subcooled water as boiling in the rod bundle slowly ended, and the upper plenum partially refilled. The PRHR HX flow stopped at approximately []^(a,b,c) seconds and was no longer effective. A steady flow of subcooled water then flowed from the IRWST into the downcomer, through the power channel, and left the primary system through the ADS-4 flow paths.

This test demonstrated that the heater bundle (active core) was fully covered by a single-phase water, or cooled by two-phase fluid at all times during this test (data plots 30 and 31). There was no indication of an increase in heater rod temperatures due to a lack of cooling (data plot 3). Key parameters describing the S01007 event are listed in Table 5-1 in Section 5.0.

Discussion of Test Transient Phases

- Initial Depressurization Phase ([]^(a,b,c) Seconds)

The initial depressurization phase (IDP) began with the initiation of the break (at time 0) and continued until primary system pressure reached saturation pressure of the fluid in the upper

plenum and the hot legs (Figure 4.2.9-1). This phase included the following events: initiation of the break, R signal at 1800 psia (decay power simulation initiated and the MSLIV closed), and S signal at 1700 psia (the MFWIV closed, the CMT injection line isolation valves opened, and the PRHR HX return line isolation valve opened—all with a 2-second delay, and RCP coastdown was initiated after a 16.2-second delay). See Table 4.2.9-1.

Facility Response during the IDP:

The break was initiated at time 0. From time 0 until the R signal occurred, the system lost pressure as a result of the expansion of the pressurizer steam volume due to the fluid loss through the break. The pressurizer partially compensated for the loss of pressure by flashing; however, it drained within the first []^(a,b,c) seconds of the test (data plot 32). The R (at []^(a,b,c) seconds) and the S (at []^(a,b,c) seconds) signals were based on pressurizer pressure only. When the R signal occurred the MSLIV was closed, and the rod bundle power was reduced to 20 percent of full power after a 5.75-second delay and began to decay after a 14.5-second delay.

As a result of the power reduction without flow reduction, the core ΔT decreased due to the low power/flow ratio, and the upper-plenum temperature decreased toward the lower-plenum temperature ([]^(a,b,c)°F). System pressure dropped down to a pressure of about []^(a,b,c) psia in []^(a,b,c) seconds and was dictated by the temperature ([]^(a,b,c)°F) of the saturated vapor in the pressurizer and the fluid in the surge line since the pressurizer at this time was drained. When the RCPs were shut off at []^(a,b,c) seconds, the rod bundle and the upper-plenum temperatures increased due to the increased power/flow ratio at the lower primary system flow (Figure 4.2.9-2). System pressure increased temporarily until decreasing rod bundle power and the decreasing lower-plenum temperature (due to CMT injection into the downcomer) started reducing the rod bundle exit and lower-upper plenum temperatures. System pressure resulted from the balance between the steam generation rate (from flashing primary fluid), the volumetric flow of fluid out the break, and the steam condensation in the PRHR HX. Steam was continually generated by rod bundle boiling due to the heater power. As system pressure continued to fall, more fluid reached its saturation pressure and began to flash. Primary system pressure stabilized at the saturation pressure for the fluid in the hot-leg side of the power channel (approximately []^(a,b,c)°F). This ended the IDP.

• Pressure Decay Phase ([]^(a,b,c) Seconds)

The pressure decay phase (PDP) began when the primary system pressure (Figure 4.2.9-1) reached saturation pressure for the fluid in the hot-leg side of the power channel. This phase ended when ADS-1 was opened on low CMT level and augmented the system depressurization. This phase was characterized by a slow decrease in overall primary system pressure and temperature. The rod bundle power (decay heat plus heat loss compensation) was reduced from 330 kW to 260 kW (data plot 1). At []^(a,b,c) seconds the rod bundle power was 280 kW. The PRHR HX heat removal rate was approximately []^(a,b,c) kW. Additional heat removal was provided by the CMT

recirculation/draining, the break flow, and facility heat losses resulting in the observed slow decrease in primary pressure.

The initial CMT-A natural circulation operating mode was followed by draindown injection when the U-tubes of the steam generators were completely drained and cold leg-B1 partially emptied (data plot 38). The drained steam generators did not affect the rest of the test. The accumulator injection was initiated when system pressure dropped below 711 psia at approximately []^(a,b,c) seconds just prior to ADS-1 actuation. However, the initial injection rate was low (less than []^(a,b,c) lbm/sec.) until after ADS was actuated (data plot 39).

Facility Response during the PDP:

The oscillating flow observed in the primary system, following RCP coastdown, continued into the PDP. The flow oscillations resulted in wide oscillations of the steam fraction of the two-phase mixture exiting the rod bundle and flowing into the hot legs (data plots 30 to 31). These oscillations in steam fraction had a significant effect on the buoyancy that drove natural circulation flow through the primary system at this time. The steam fraction oscillations were observed through the hot leg and the steam generators (data plots 20 and 21). However, since the two-phase mixture entering the steam generators left the steam generators as saturated water, the steam fraction oscillations on the hot-leg side of the power channel were observed as flow oscillations in the cold legs (data plots 24 through 27). Some of the steam was condensed in the U-tubes (the primary-side pressure was higher than the secondary-side pressure at this time, allowing some heat to be transferred to the secondary-side fluid), while the remaining steam was separated from the two-phase mixture in the high point of the U-tubes (due to the low velocity); eventually allowing the U-tubes to drain. For steam generator-A, continuous U-tube flow was maintained until []^(a,b,c) seconds into the transient. From []^(a,b,c) seconds, intermittent flow was observed through the steam generator-A (data plots 20 and 22), when a free-water surface appeared at the top of the U-tubes. However, the buoyancy head in the hot leg caused water to spill over the top of the U-tubes at the peaks of the oscillations. At []^(a,b,c) seconds, the U-tubes drained in steam generator-A, since the free-water surface had fallen too low to be overcome by the buoyancy oscillations. Oscillations were also seen in temperatures and pressures throughout the primary system. When the steam generator U-tubes were completely drained (about []^(a,b,c) seconds), the oscillations in the primary system stopped. The steam generator-B U-tubes were completely drained at approximately []^(a,b,c) seconds, which was earlier than steam generator-A, due to the higher steam fraction in the fluid from hot leg-B.

System pressure decrease during the PDP started at a slow rate of []^(a,b,c) psi/sec. At approximately []^(a,b,c) seconds, the pressure decay rate increased to []^(a,b,c) psi/sec. (Figure 4.2.9-1). The increased rate of pressure decrease was due to the increased injection rate of the cold liquid from CMT-A and because the break flow was transitioning from water to steam. This occurred after the steam generator-B U-tubes drained and cold leg-B1 partially emptied, allowing the CMT-A balance line to drain and resulting in CMT-A transition from its recirculation

mode to its draindown mode of operation. Since the break was located in the cold leg to CMT balance line for CMT-B, CMT-B performance was marked by different than CMT-A.

CMT-A began injecting cold fluid into the downcomer when the S signal occurred. Initially this injection was by natural circulation at approximately []^(a,b,c) lbm/sec., with hot water flowing from the cold leg through the cold leg balance line (CLBL) into the top of the CMT as cold water flowed from the bottom of the CMT. After cold leg-B1 was partly drained at about []^(a,b,c) seconds, the CMT-A CLBL flashed/draind and CMT-A transitioned to its draindown mode. This transition occurred from []^(a,b,c) seconds (data plot 38) when a free-water surface developed in the top of the CMT-A as the level began to drop (data plot 33). Between []^(a,b,c) seconds, the CMT-A transition to injection mode was interrupted, as cold-leg water apparently covered the balance line inlet. The injection flow, once draindown flow began, increased to []^(a,b,c) lbm/sec. and then decreased as the CMT-A level decreased (reducing the driving head). See data plot 38.

Natural circulation flow did not occur through CMT-B following the S signal because of the break was located in the cold leg-B2 balance line. A small amount of injection flow from CMT-B started at 400 seconds when two-phase conditions occurred in the CMT-B balance line. At []^(a,b,c) seconds CMT-B draindown began when the CLBL was voided due to depressurization after ADS-1, and the CMT-B injection flow rate increased to []^(a,b,c) lbm/sec. ADS depressurization also caused flashing in the CMTs due to the high temperature (saturation temperature) of the fluid in the top of the CMTs (data plots 15 and 16) and the decreasing system pressure. Flashing occurred to keep the water temperature at saturation while the system pressure decayed.

The accumulators began to inject fluid into the DVI lines when system pressure dropped below 711 psia (at approximately []^(a,b,c) seconds); however, the injection rate was very low prior to ADS-1 (data plot 39).

Throughout the PDP, the combined effect of the PRHR HX cooling the primary fluid and the cold injection flow from the CMTs was sufficient to limit the steam fraction of the two-phase fluid cooling the rod bundle to less than approximately []^(a,b,c) percent (data plots 30 and 31).

• **Automatic Depressurization System Phase ([]^(a,b,c) Seconds)**

The automatic depressurization system (ADS) phase began with the actuation of ADS-1 and ended with the actuation of AI 5-4 (Figure 4.2.9-1).

Facility Response during the ADS Phase:

The actuation of ADS-1, followed by ADS-2 and ADS-3 within approximately []^(a,b,c) seconds, increased the rate of primary system depressurization to []^(a,b,c) psi/sec. This depressurization rate gradually decreased as system pressure decreased.

The primary system depressurization after ADS actuation resulted in a high rate of water injection from accumulators-A and -B (data plot 39). The accumulators injected cold water into the primary system for approximately []^(a,b,c) seconds (from []^(a,b,c) seconds) and were completely emptied. The accumulator injection refilled the rod bundle region and the lower-upper plenum with subcooled water. The high accumulator injection flow rate partly suppressed the CMT-A injection, since a CMT and accumulator share a common DVI line.

The pressurizer immediately began to refill when ADS-1 occurred, and steam and water were vented from the pressurizer through the ADS (data plot 32). The pressurizer collapsed liquid level increased to approximately []^(a,b,c) ft. by the time accumulator injection ended. This level subsequently decreased to []^(a,b,c) ft. in apparent agreement with the increasing steam fraction of fluid flowing from the power channel to hot leg-A, into the pressurizer and out through the ADS-1, -2, and -3 flow paths.

Prior to the ADS phase, the break flow leaving the primary system through the break in the CMT balance line was water then a water/steam mixture. After the actuation of the ADS, the mass flow through the break decreased sharply since the break fluid converted from liquid to steam as the cold leg-B2 completely emptied (data plot 43).

- **Post-Automatic Depressurization System Phase (2090 Seconds to End of Test)**

The post-automatic depressurization system (post-ADS) phase began when ADS-4 occurred (Figure 4.2.9-1) and continued to the end of the event.

Facility Response during the Post-ADS Phase:

The system pressure rapidly decreased to near atmospheric pressure when ADS-4 was actuated. This resulted in a significant increase in the steam fraction in the rod bundle, and upper-plenum fluid and the water level in the downcomer decreased rapidly into the tubular downcomer. Gravity flow from the IRWST into the downcomer began at approximately []^(a,b,c) seconds. (data plot 40). The cold flow from the IRWST refilled the power channel with subcooled water including the downcomer, rod bundle, lower-upper plenum, and the hot legs. At approximately []^(a,b,c) seconds, the upper-upper plenum became subcooled and partially refilled. This steady-state condition was considered the end of the test.

When ADS-4 was actuated, flow through ADS-1, 2, and -3 stopped and the pressurizer water level decreased to approximately []^(a,b,c) ft. in apparent manometric agreement with the primary system.

The PRHR stopped flowing at approximately []^(a,b,c) seconds (data plot 37).

Component Responses

- **Power Channel**

The power channel consisted of five volumes: the lower plenum, the riser with the heated rod bundle, the lower-upper plenum below the hot leg, the upper-upper plenum above the hot leg, and the upper head. When the break occurred, system pressure decreased to the R trip point (1800 psia) and the S trip point (1700 psia). However, since the water in the power channel was subcooled relative to system pressure, no boiling or flashing occurred up to this point. When the rod bundle power was reduced to 20 percent (5.75 seconds after the R signal), the temperature gradient across the core rapidly decreased due to the reduced power/flow ratio (still full flow), and the power channel outlet temperature dropped toward the lower-plenum inlet temperature (Figure 4.2.9-2). The upper-upper plenum still contained []^(a,b,c)°F water and began to flash when the system pressure dropped below []^(a,b,c) psia. When the RCPs were shut off (16.2 seconds after the S signal), the power/flow ratio increased and the power channel outlet temperature increased, resulting in boiling in the rod bundle. This boiling together with the flashing in the upper-upper plenum produced sufficient steam to stop the system pressure decrease. Both temperature and pressure increased momentarily until the upper-upper plenum had drained down to the hot-leg elevation (data plots 30 and 31). The lower-upper plenum fluid temperature reached a peak and then began to decrease, responding to the increasing natural circulation flow through the primary system. The hot-leg side of the power channel stabilized at a temperature of approximately []^(a,b,c)°F and a pressure of approximately []^(a,b,c) psia (the hot-leg saturation pressure) at the end of the IDP.

The temperature of the fluid in the hot-leg side of the power channel controlled the system pressure during the PDP (data plot 4). Flow oscillations began in the primary system (with a []^(a,b,c)-second period) when the RCPs had coasted down, and continued until about []^(a,b,c) seconds. The flow oscillations led to oscillations in the rod bundle steam fraction and, therefore, in the collapsed liquid level measured in the heater bundle, lower-upper plenum, and hot leg (data plots 30 and 31). When the downcomer flow decreased, steam fractions increased, resulting in an increase of the overall system pressure and in the rod bundle exit temperature (Figure 4.2.9-2). The overall system pressure oscillations were therefore out of phase with the tubular downcomer flow oscillations.

Data plots 30 and 31 show the collapsed liquid levels at various sections of the power channel during the S01007 test.

The upper head began to drain when the system pressure decreased to the saturation pressure of the water in the upper head (at about []^(a,b,c) seconds). The upper-head fluid temperature initially was about []^(a,b,c)°F, and primary pressure was approximately []^(a,b,c) psia when

flashing started at []^(a,b,c) seconds. The upper head quickly emptied when ADS-1 occurred at approximately []^(a,b,c) seconds (data plot 31).

The upper-upper plenum water level, which had decreased to the elevation of the hot legs after the RCPs had coasted down, stayed at the hot-leg elevation until the end of the accumulator injection. When the rod bundle and lower-upper plenum were refilled with subcooled water, the steam bubble in the upper-upper plenum was partially condensed (see temperatures in data plot 4). However, when the accumulator injection ended, the level again decreased to the hot-leg elevation or below. At []^(a,b,c) seconds, the water injected from the IRWST again condensed the steam bubble in the upper-upper plenum and it refilled (plot 31).

The collapsed level measured just above the top of rod bundle (data plot 31) provides a good indication of the steam fraction of the two-phase fluid exiting the top of the rod bundle. This measurement indicates that the maximum steam fraction of this fluid was []^(a,b,c) percent prior to accumulator, and reached []^(a,b,c) percent prior to IRWST injection.

Data plot 30 shows the collapsed levels in the rod bundle oscillating following the coastdown of the RCPs. This indicated apparent steam fractions in the rod bundle ranging from []^(a,b,c) percent to []^(a,b,c) percent with a period of approximately []^(a,b,c) seconds. The oscillations ended at a maximum fluid steam fraction of []^(a,b,c) percent before the accumulator injection. The accumulator injection completely refilled and subcooled the rod bundle. However, when the injection ended, the boiling began again and reached a maximum ([]^(a,b,c) percent steam fraction) just before the IRWST injection started. The lower-upper plenum level indicates a steam fraction of []^(a,b,c) percent just prior to IRWST injection. This high steam fraction was due to the two-phase mixture level in the upper-upper plenum temporarily dropped below the hot-leg elevation.

• Pressurizer

The pressurizer began to drain when the break occurred and was completely drained in approximately []^(a,b,c) seconds (data plot 32). The water in the pressurizer flashed due to the loss of system pressure, and the temperature of the water dropped from []^(a,b,c)°F during this initial depressurization (data plot 18). The pressurizer remained drained until ADS-1 occurred. At this time, the collapsed liquid level increased to about []^(a,b,c) ft. during the time the accumulator was injecting. This level then decreased to []^(a,b,c) ft. by the time IRWST injection started, apparently in response to the increasing steam fraction of the fluid flowing from the power channel to hot leg-A; into the pressurizer; and out through the ADS-1, -2, and -3 flow paths. After ADS-4 actuation, the pressurizer level decreased to []^(a,b,c) ft. where it reached manometric agreement with the primary system.

- **Steam Generator**

The steam generators acted as the heat sink until the MSLIV closed and prevented further energy removal from the secondary side. This caused the temperature (and pressure) of the secondary side to increase toward the primary system hot-leg temperature. The steam generators stabilized at approximately []^(a,b,c)°F (and []^(a,b,c) psia) at the end of the IDP.

For the first part of the PDP, the primary system pressure was higher than the steam generator secondary-side pressure (data plot 2). This indicated that some heat transfer from the primary to secondary side occurred and caused some condensation of the steam in the two-phase fluid coming from the hot leg. The primary system pressure did not drop below the steam generator secondary-side pressure until approximately []^(a,b,c) seconds into the event, at which time the U-tubes had already nearly drained.

At the end of the RCP coastdown, flow oscillations began in the primary system. This caused wide variations in the collapsed liquid level (fluid steam fraction) in the core and, consequently, in the density of the two-phase flow from the rod bundle into the hot legs and to the steam generators (data plots 20 and 21).

These hot-leg steam fraction oscillations reached the steam generators. In steam generator-A, the U-tubes began to have a free-water surface at the top of the U-tubes, at approximately []^(a,b,c) seconds due primarily to the separation of steam from the two-phase mixture at the low-flow velocities existing at the natural circulation flow conditions. However, as the fluid level on the hot-leg side dropped below the top of the U-tubes the oscillation from the hot leg would refill the tube. At []^(a,b,c) seconds the top of the hot-leg side of the steam generator-A U-tubes remained filled with saturated vapor and primary system flow through the steam generator-A stopped. The cold-leg side of the steam generator-A U-tubes showed significant level oscillations from about []^(a,b,c) seconds until they were completely drained at about []^(a,b,c) seconds and affected the draindown of the steam generator U-tubes.

The steam fraction/flow oscillations in steam generator-B were reduced, due to the higher steam fraction of the fluid in the hot leg-B. Consequently, the steam generator-B U-tubes started draining earlier (at about []^(a,b,c) seconds) since it took less time to fill the top of steam generator-B U-tubes with steam.

The level in the hot-leg side of the steam generator-B U-tubes decreased to nearly zero in about []^(a,b,c) seconds. The cold-leg side of the steam generator-B U-tubes was nearly drained at []^(a,b,c) seconds (data plots 22 and 23).

- **Hot Legs**

Hot legs-A and -B were full of two-phase mixture until ADS-1 (data plots 20 and 21). Prior to ADS-1, the observed collapsed liquid levels in the hot legs indicated that the PRHR preferentially

removed steam from hot leg-A (as seen in the very high void fraction for the PRHR inlet flow), thereby reducing the steam fraction of the fluid in hot leg-A as compared with hot leg-B. The higher steam fraction in hot leg-B resulted in earlier U-tube draindown in steam generator-B than in steam generator-A. After ADS-1 was actuated, the levels in both hot legs decreased with hot leg-A remaining filled with two-phase mixture to the elevation of the surge line connection. The hot legs were nearly drained at ADS-4 ([]^(a,b,c) seconds) and were partially refilled after IRWST injection started.

- **Cold Legs**

Cold legs-A1 and -A2 remained full until ADS-1 (data plots 22 through 27). Then the level decreased until the horizontal pipes temporarily drained at about []^(a,b,c) seconds. Significant level oscillations were observed. When ADS-4 occurred, the fluid collapsed level in the tubular downcomer temporarily dropped []^(a,b,c) ft below the hot-leg elevation at []^(a,b,c) seconds (data plot 24). After IRWST injection began at []^(a,b,c) seconds into the event, the annular downcomer was refilled, and the cold legs were partially refilled to the level of []^(a,b,c) ft. above the hot leg.

After the steam generator-B U-tubes on the cold-leg side drained at []^(a,b,c) seconds, the RCP-B suction pipe drained and emptied at about []^(a,b,c) seconds. At []^(a,b,c) seconds, both cold legs-B1 and -B2 drained rapidly to the level of their horizontal pipe sections. At this time, CMT-A began to transition to its downcomer operating mode. Cold legs-B1 and -B2 remained empty until []^(a,b,c) seconds when they were refilled by IRWST injection to []^(a,b,c) ft. above the hot-leg elevation at the end of the test. After []^(a,b,c) seconds, the cold-leg-to-CMT balance lines were partially filled.

- **PRHR and IRWST**

At the initiation of the event, the PRHR HX was filled with subcooled liquid. When the S signal occurred, the PRHR return flow isolation valve opened, and a high flowrate began through the HX due to the still operating RCPs. When the RCPs were shut off and the upper plenum and the hot legs filled with two-phase fluid, a large portion of the steam in hot leg-A flowed to the PRHR HX (void fraction was []^(a,b,c) percent based on data plot 29). The two-phase mixture, consisting of slugs of steam and water, was condensed and subcooled in the PRHR HX (data plot 28). During the PDP (prior to ADS-1), a significant variation in the flow through the PRHR HX was caused by the variation in the void fraction of the fluid in hot leg-A.

Steam condensation in the PRHR HX resulted in a wide variations in the differential pressure (dP) in data shown in plots 28, 29, and 37. After the primary system flow/steam fraction oscillations ended the flow and level in the PRHR HX stabilized, and a well behaved condensation process was observed in the HX for the rest of the PDP with an average return flow rate of approximately []^(a,b,c) lbm/sec.

When the ADS initiated, the power channel and the hot legs were gradually refilled with subcooled water by the cold flow from the accumulators. The driving head for the flow in the PRHR decreased (provided by the density difference between the fluid in the PRHR supply line and the return line), and the flow decreased to approximately []^(a,b,c) lbm/sec. The subcooled fluid in the hot leg never filled the PRHR supply line, and hot fluid in this line flashed as system pressure decreased. The simultaneous flashing in the supply line and condensation in the HX resulted in a wide variations in the flow measured in the PRHR return line.

After the accumulator injection ended, the rod bundle, lower-upper plenum and hot legs again reached saturation contained two-phase fluid and PRHR HX flow increased to about []^(a,b,c) lbm/sec. The flow rate was observed to decrease until ADS-4 activation, and then increase. After ADS-4 depressurized the system and the IRWST flow commenced and refilled the core rod bundle and the hot leg with subcooled water, the flow in the PRHR HX stopped for the remainder of the test.

The heatup of the water within the IRWST due to PRHR HX operation is shown in data plot 17. Following ADS-4 at []^(a,b,c) seconds, the primary system pressure decreased to near ambient and gravity. Driven injection from the IRWST started at about []^(a,b,c) seconds. The IRWST flows gradually refilled the power channel and single-phase water flow was established through the power channel, into the hot legs and through the ADS-4 flow paths. The primary system began to cool below the saturation temperature for pressure inside the primary system (data plots 32 and 40).

• Core Makeup Tanks

The CMT injection was initiated []^(a,b,c) seconds after the S signal by opening the CMT injection line isolation valve. Initially, the injection flow from the CMT-A was by natural circulation, with hot water from cold leg-B1 flowing through the cold leg balance line to the top of CMT-A, and the cold the CMT water flowing into the downcomer and into the power channel. This recirculation rate was approximately []^(a,b,c) lbm/sec. from CMT-A.

After cold legs-B1 and -B2 drained to the level of the horizontal pipes (at []^(a,b,c) seconds), flashing began in the CLBLs. When the temperature at the top of the CMT reached the saturation temperature for primary system pressure, a free-water surface was established in CMT-A due to the separation of saturated vapor from two-phase fluid in the balance line. This increased the driving head for the injection flow and resulted in a higher draindown flow. For CMT-A, this occurred at []^(a,b,c) seconds when the flow increased to []^(a,b,c) lbm/sec.

For the S01007 test, the break was located in the cold leg-B2 balance line; and therefore, there was no recirculation through CMT-B. A small amount of flow started from CMT-B at []^(a,b,c) seconds as the break flow from cold leg-B2 transitioned from single-phase liquid to a two-phase mixture. Some steam reached the top of CMT-B initiating heatup of the CMT fluid (data plot 16). The CMT-B balance line voided and drained at []^(a,b,c) seconds (ADS-1). This

resulted in a transition to the CMT-B draindown injection of flow rate []^(a,b,c) lbm/sec. During the accumulator injection ([]^(a,b,c) seconds), the CMTs' injection was reduced to []^(a,b,c) lbm/sec. for CMT-A, and []^(a,b,c) lbm/sec. for CMT-B.

The CMTs were heated by the hot liquid from the loop-B cold legs. Later, the CMTs were heated by the condensation of steam from the cold leg on the free-water and metal surfaces in the upper part of the CMTs. A stratified temperature gradient was established in the CMTs (data plots 15 and 16), where the free-water surface water temperature was at (or near) saturation temperature, and the bottom temperature remained cold.

After ADS-4 (at []^(a,b,c) seconds), the CMTs injection decreased and stopped at approximately []^(a,b,c) seconds. CMTs were never drained completely.

- **Accumulators**

The accumulators provided water injection into the downcomer by a polytropic expansion of a compressed air volume stored within the accumulator. Water from the accumulators was injected when the primary system pressure dropped below 711 psia. The accumulator injection began shortly before ADS-1 at a very low flow rate. However, when ADS-1 occurred, the injection rate became high (data plot 39). The accumulator injection for the S01007 event lasted approximately []^(a,b,c) seconds. The accumulators were completely drained when the injection ended (data plot 34).

The effective polytropic coefficient of expansion was calculated for the accumulators (Figures 4.2.9-3 and 4.2.9-4) to be []^(a,b,c) for accumulator-A and []^(a,b,c) for accumulator-B. This was near the midpoint between isothermal expansion ($k = 1$) and adiabatic expansion ($k = 1.4$) and showed that some heat was picked up by the air from the internal metal surfaces of the accumulator during the expansion.

Mass Discharge and Mass Balance

The catch tank weight measurements are shown in data plot 43 for the break flow, for the ADS-1, -2, and -3 flows, and for the ADS-4 flow.

The break flow, which started when the test was initiated, was stable with a decreasing flow rate as the system pressure dropped during the IDP and the PDP. When ADS occurred, the break location voided and further discharge from the break was primarily saturated steam until the IRWST injection refilled the cold leg after ADS-4.

The discharge from ADS-1, -2, and -3 was stable throughout the accumulator injection and decreased temporarily when the accumulator injection ended. When ADS-4 occurred, the discharge of fluid from the top of the pressurizer ended, and the fluid discharge from ADS-4 started. The ADS-4 fluid discharge was relatively stable but was affected by filling/drainage of upper-upper plenum.

The discharged masses are shown in Table 4.2.9-3.

The mass balance results for test S01007 were calculated based on water inventory before and after the S01007 test. Table 4.2.9-1 gives a detailed listing of the inventories of water in the various components before the test. Table 4.2.9-2 lists the inventories after the test and the amount of water injected into the power channel from the IRWST. The water level in the power channel was determined by the DP-B16P measurement to be []^(a,b,c) in. ([]^(a,b,c) mm) above the hot-leg centerline at the end of the test. Table 4.2.9-3 compares the mass balance for the system before and after the test and shows that measured masses are within []^(a,b,c) percent.

**TABLE 4.2.9-1
SEQUENCE OF EVENTS FOR TEST S01007**

Event	Specified	Instrument Channel	Actual Time (sec.)
Break Opens	0		(a,b,c)
R Signal	P = 1800 psia	P-027P	
MSL IV Closure	R signal +2 sec.	Z_A04SO, F_A04S	
		Z_B04SO, F_B04S	
S Signal	P = 1700 psia	P-027P	
MFW IV Closure	S signal + 2 sec.	Z_B02SO, F_B01S	
		Z_A02SO, F_A01S	
CMT IV Opening	S signal + 2 sec.	Z_A040EC, F-A40E	
		Z_B040EC, F-B40E	
RCPs Tripped	S signal + 16.2 sec.	I-A1P, S-A1P	
		I-B1P, S-B1P	
PRHR Heat Exchanger Actuation	S signal + 2 sec.	Z_A81EC, F_A80E	
ADS-1	CMT level 67% +30 sec.	L_B40E	
		Z_001PC	
Accumulators	P-027P = 710 psia	F_A20E	
		F_B20E	
ADS-2	CMT level 67% +125 sec.	L_B40E	
		Z_002PC	
ADS-3	CMT level 67% +245 sec.	L_B40E	
		Z_003PC	
ADS-4	CMT level 20% +60 sec.	L_B40E	
		Z_004PC, F-040P	
IRWST Injection	P-027P = 26 psia	F_A60E	
		F_B60E	

**TABLE 4.2.9-2
WATER INVENTORY BEFORE TEST S01007**

Component	Volume (ft. ³)/(l)	Net Volume (ft. ³)/(l)	Temp (°F)	Relative Density	Mass (lbm)
Loops	8.97 ft. ³ (254.0 l)	8.97 ft. ³ (254.0 l)			(a,b,c)
Pressurizer	3.37 ft. ³ (95.4 l)	1.78 ft. ³ (50.5 l)			
Surge Line	0.34 ft. ³ (9.6 l)	0.34 ft. ³ (9.6 l)			
Tubular Downcomer	1.38 ft. ³ (39.1 l)	1.38 ft. ³ (39.1 l)			
Annular Downcomer + High-Pressure Bypass	0.54 ft. ³ (15.3 l)	0.54 ft. ³ (15.3 l)			
Core Bypass	0.44 ft. ³ (12.4 l)	0.44 ft. ³ (12.4 l)			
Lower Plenum	0.81 ft. ³ (22.8 l)	0.81 ft. ³ (22.8 l)			
Riser	1.64 ft. ³ (46.4 l)	1.64 ft. ³ (46.4 l)			
Upper Plenum	1.46 ft. ³ (41.3 l)	1.46 ft. ³ (41.3 l)			
Upper Head	1.90 ft. ³ (53.8 l)	1.90 ft. ³ (53.8 l)			
CMTs	10.1 ft. ³ (286.0 l)	10.1 ft. ³ (286.0 l)			
Accumulator	10.1 ft. ³ (286.0 l)	0.78 ft. ³ (220.9 l)			
IRWST Injection Line	0.18 ft. ³ (5.1 l)	0.18 ft. ³ (5.1 l)			
TOTAL INVENTORY					

TABLE 4.2.9-3
WATER INVENTORY AFTER TEST S01007 WAS COMPLETED
 Water level as measured by DP-B16P (-0.50 psi) was 19.72 in. (352 mm) above Hot Leg

Component	Volume (ft. ³)/(l)	Net Volume (ft. ³)/(l)	Temp (°F)	Relative Density	Mass (lbm)
Loops	8.97 ft. ³ (254.0 l)	1.24 ft. ³ (35.0 l)			[] ^(a,b,c)
Pressurizer	3.37 ft. ³ (95.4 l)	0.0 ft. ³ (0.0 l)			
Surge Line	0.34 ft. ³ (9.6 l)	0.0 ft. ³ (0.0 l)			
Tubular Downcomer	1.38 ft. ³ (39.1 l)	1.38 ft. ³ (39.1 l)			
Annular Downcomer + High-Pressure Bypass	0.54 ft. ³ (15.3 l)	0.48 ft. ³ (13.7 l)			
Core Bypass	0.44 ft. ³ (12.4 l)	0.44 ft. ³ (12.4 l)			
Lower Plenum	0.81 ft. ³ (22.8 l)	0.81 ft. ³ (22.8 l)			
Riser	1.64 ft. ³ (46.4 l)	1.64 ft. ³ (46.4 l)			
Upper Plenum	1.46 ft. ³ (41.3 l)	1.33 ft. ³ (37.6 l)			
Upper Head	1.90 ft. ³ (53.8 l)	0.0 ft. ³ (0.0 l)			
CMT-A	0.50 ft. ³ (143.0 l)	0.24 ft. ³ (6.9 l)			
CMT-B	0.50 ft. ³ (143.0 l)	1.10 ft. ³ (31.3 l)			
Accumulator	10.1 ft. ³ (286.0 l)	0.0 ft. ³ (0.0 l)			
IRWST Injection Line	0.18 ft. ³ (5.1 l)	0.18 ft. ³ (5.1 l)			
TOTAL INVENTORY					
WATER INJECTED FROM THE IRWST DURING EVENT					
IRWST Injection	dP (psi)	Area (in²)			Mass (lbm)
	1.26	1007.5			[] ^(a,b,c)

**TABLE 4.2.9-4
MASS BALANCE FOR TEST S01007**

	Starting Inventory (lb/m)	Ending Inventory (lb/m)	
Total Primary System			(a,b,c)
IRWST Injection			
Break*			
ADS -1,-2,-3			
ADS-4**			
TOTAL			
Ending Inventory/Starting Inventory (lb/m)			
Ending Inventory/Starting Inventory (%)			

* Includes only the break flow from the cold-leg side of the break.

** Includes the break flow from the CMT side of the break plus the ADS-4 flow.

The following figures have been intentionally deleted
from this document due to their proprietary nature.

**TEST S01007 PLOT PACKAGE
CHANNEL LIST BY COMPONENT**

COMPONENT	CHANNEL	UNITS	PLOT	COMMENT
ACCA	F_A20E	lbm/sec.	39	
ACCA	L_A20E	ft.	34	
ACCB	F_B20E	lbm/sec.	39	
ACCB	L_B20E	ft.	34	
ADS 1, 2, & 3	IF30flw	lbm/sec.	44	Flow rate derived from IF030P
ADS 1, 2, & 3	IF030P	lbm	43	Catch tank
ADS 4 & SG	IF40flw	lbm/sec.	44	Flow rate derived from IF040P
ADS 4 & SG	IF040P	lbm	43	Catch tank
ANND	DP-A021P	psi	24	To cold leg-A1
ANND	DP-A022P	psi	25	To cold leg-A2
ANND	DP-B021P	psi	26	To cold leg-B1
ANND	DP-B022P	psi	27	To cold leg-B2
BREAK LINE	IF05flw	lbm/sec.	44	Flow rate derived from IF005P
BREAK LINE	IF005P	lbm	43	Catch tank
CLA	DP-A001P	psi	24	To cold leg-A1
CLA	DP-A002P	psi	25	To cold leg-A2
CLA	DP-A09P	psi	22	Pump suction
CLA	T-A10P	°F	11	Steam generator outlet
CLA1	F-A01P	lbm/sec.	36	
CLA1	T-A021PL	°F	13	Downcomer inlet
CLA1	T-A11P	°F	11	Pump outlet
CLA2	F_A02P	lbm/sec.	36	
CLA2	T-A022PL	°F	13	Downcomer inlet
CLB	DP-B001P	psi	26	To cold leg-B1
CLB	DP-B002P	psi	27	To cold leg-B2
CLB	DP-B09P	psi	23	Pump suction
CLB	T-B10P	°F	12	Steam generator outlet
CLB1	F_B01P	lbm/sec.	36	

**TEST S01007 PLOT PACKAGE
CHANNEL LIST BY COMPONENT (Cont.)**

COMPONENT	CHANNEL	UNITS	PLOT	COMMENT
CLB1	T-B021PL	°F	14	Downcomer inlet
CLB1	T-B11P	°F	12	Pump outlet
CLB2	F_B02P	lbm/sec.	36	
CLB2	T-B022PL	°F	14	Downcomer inlet
CMTA	F_A40E	lbm/sec.	38	
CMTA	L_A40E	ft.	33	
CMTA	T-A401E	°F	15	Top (242.25 in.)
CMTA	T-A403E	°F	15	216.75 in.
CMTA	T-A405E	°F	15	191.25 in.
CMTA	T-A407E	°F	15	165.75 in.
CMTA	T-A409E	°F	15	140.25 in.
CMTA	T-A411E	°F	15	114.75 in.
CMTA	T-A413E	°F	15	89.25 in.
CMTA	T-A415E	°F	15	63.75 in.
CMTA	T-A417E	°F	15	38.25 in.
CMTA	T-A420E	°F	15	Bottom (0 in.)
CMTB	F_B40E	lbm/sec.	38	
CMTB	L_B40E	ft.	33	
CMTB	T-B401E	°F	16	Top (242.25 in.)
CMTB	T-B403E	°F	16	216.75 in.
CMTB	T-B405E	°F	16	191.25 in.
CMTB	T-B407E	°F	16	165.75 in.
CMTB	T-B409E	°F	16	140.25 in.
CMTB	T-B411E	°F	16	114.75 in.
CMTB	T-B413E	°F	16	89.25 in.
CMTB	T-B415E	°F	16	63.75 in.
CMTB	T-B417E	°F	16	38.25 in.
CMTB	T-B42E	°F	16	Bottom (0 in.)
DVIA	T-A00E	°F	13	

**TEST S01007 PLOT PACKAGE
CHANNEL LIST BY COMPONENT (Cont.)**

COMPONENT	CHANNEL	UNITS	PLOT	COMMENT
HLA	T-A03PL	°F	5	Vertical, near power channel
HLA	T-A03PO	°F	5	Horizontal, near power channel
HLA	T-A04P	°F	5	Near steam generator inlet
HLB	DP-B04P	psi	21	
HLB	T-B03PL	°F	6	Vertical, near power channel
HLB	T-B03PO	°F	6	Horizontal, near power channel
HLB	T-B04P	°F	6	Near steam generator inlet
IRWST	F_A60E	lbm/sec.	40	
IRWST	F_B60E	lbm/sec.	40	
IRWST	L_060E	ft.	32	
IRWST	T_061E	°F	17	Bottom
IRWST	T-062E	°F	17	Below middle
IRWST	T-063E	°F	17	Middle
IRWST	T-064E	°F	17	Above middle
IRWST	T-065E	°F	17	Top
NRHRA	F-A00E	psi	42	
NRHRB	F-B00E	psi	42	
PC	W_00P	kW	1	
PC-HB	L_000P	ft.	30	Heater bundle
PC-HR	TW018P20	°F	3	Heater rod
PC-HR	TW018P48	°F	3	Heater rod
PC-HR	TW020P87	°F	3	Heater rod
PC-UP	L_A15P	ft.	30	Lower-upper plenum
PC-UP	L_A16P	ft.	31	Upper-upper plenum
PC-UP	T-015P	°F	4	Upper plenum
PC_UH	L_017P	ft.	31	Upper head
PC_UP	L_A14P	ft.	31	Above top of the active fuel
PRHR	DP-A81AE	psi	29	Supply line inverted U-tube
PRHR	DP-A81BE	psi	29	Supply line inverted U-tube

**TEST S01007 PLOT PACKAGE
CHANNEL LIST BY COMPONENT (Cont.)**

COMPONENT	CHANNEL	UNITS	PLOT	COMMENT
PRHR	DP-A83E	psi	28	Return line
PRHR	F_A80E	lbm/sec.	37	Return line
PRHR	T-A82E	°F	19	Inlet
PRHR	T-A83E	°F	19	Exit
PRZ	L_010P	ft.	32	
PRZ	P-027P	psia	2	
PRZ	T-026P	°F	18	487 in.
SGA	DP-A05P	psi	20	Hot side
SGA	DP-A06P	psi	20	Hot side
SGA	DP-A07P	psi	22	Cold side
SGA	DP-A08P	psi	22	Cold side
SGA	F_A01S	lbm/sec.	41	
SGA	F_A20A	lbm/sec.	41	
SGA	L_A10S	ft.	35	Overall level
SGA	P-A04S	psia	2	Secondary system
SGA	T-A01S	°F	10	MFW-A
SGA	T-A05P	°F	7	Hot side
SGA	T-A05S	°F	9	Hot side - riser
SGA	TW-A06S	°F	7	Hot side
SGB	DP-B05P	psi	21	Hot side
SGB	DP-B06P	psi	21	Hot side
SGB	DP-B07P	psi	23	Cold side
SGB	DP-B08P	psi	23	Cold side
SGB	F_B01S	lbm/sec.	41	
SGB	F_B20A	lbm/sec.	41	
SGB	L_B10S	ft.	35	Overall level
SGB	P-B04S	psia	2	Secondary system
SGB	T-B01S	°F	10	MFW-B
SGB	T-B05P	°F	8	Hot side

TEST S01007 PLOT PACKAGE
CHANNEL LIST BY COMPONENT (Cont.)

COMPONENT	CHANNEL	UNITS	PLOT	COMMENT
SGB	T-B07P	°F	8	U-tube top
SGB	T-B08P	°F	12	Cold side
SGB	TW-B06S	°F	8	Hot side
SL	T-020P	°F	18	Surge line near pressurizer
TDC	DP-001P	psi	24,25,26,27	Top
TDC	DP-002P	psi	24,25,26,27	Bottom
TDC	T-001PL	°F	13,14	Top
TSAT-PRZ		°F	18	Based on P-027P
UH-TSAT		°F	4	Based on P-017P

4.2.10 Double-Ended Guillotine Cold Leg to CMT Balance Line Break without Nonsafety Systems (S00908)

This test S00908 was a blind test; therefore, this section has been intentionally left blank and will be provided later.

4.2.11 Steam Generator Tube Rupture with Nonsafety Systems Operational and Operator Action (S01309)

This matrix test simulated a steam generator tube rupture (SGTR) with both the passive and nonsafety systems operational and with operator action for mitigation. There were two operator actions simulated for this test: cooldown of the primary system by dumping steam through the intact steam generator power-operated relief valve (PORV) to obtain hot-leg subcooling (while limiting the overall cooldown rate of the primary system); and subsequent controlled depressurization of the primary system to terminate primary to secondary leakage using an ADS-1 valve.

There was no core makeup tank (CMT) draindown during this test. Therefore there was no actuation of the automatic depressurization system (ADS) primary system depressurization function, no in-containment refueling water storage tank (IRWST) injection, and no significant accumulator injection. The chemical and volume control system (CVCS) and startup feedwater system (SFWS) were automatically initiated and controlled throughout this test.

Operator actions were simulated using a logic programmed into the SPES-2 plant control computer. However, during the performance of the test, cold startup feedwater was added to the steam generators and cold water was injected into the primary system. This resulted in lower primary system temperatures than anticipated and satisfied the overall cooldown rate criteria. Therefore, the plant computer did not automatically perform all operations. Plant personnel manually performed the following actions:

- Beginning at approximately []^(a,b,c) seconds and re-occurring every []^(a,b,c) seconds, the steam generator-A PORV was opened for []^(a,b,c) seconds (Table 4.2.11-1) until it was left full open at []^(a,b,c) seconds.
- Beginning at []^(a,b,c) seconds and re-occurring every []^(a,b,c) seconds, the ADS-1 valve was opened for []^(a,b,c) seconds (Table 4.2.11-2) until the test was terminated.
- From []^(a,b,c) to []^(a,b,c) seconds at []^(a,b,c) second intervals, the ADS-3 valve was mistakenly opened for []^(a,b,c) seconds (Table 4.2.11-3) instead of the steam generator-A PORV.

As in test runs S01110 and S01211, the single SGTR was simulated via a line connected from the primary side (coolant pump B suction piping) to the secondary side of steam generator-B (approximately []^(a,b,c) ft. above the tube sheet), with a break orifice diameter scaled to simulate []^(a,b,c) times the area of a single AP600 steam generator tube diameter.

Results are provided in the data plot package at the end of this section. The sequence of events for S01309 is listed in Table 4.2.11-4.

Non-loss-of-coolant accident (non-LOCA) tests at SPES-2, including steam generator tube ruptures and main steam line break, did not result in ADS actuation and, therefore, include only the first two phases

observed in LOCA recovery. The phases identified for the purpose of detailed evaluation of the thermal-hydraulic phenomena occurring within the primary and safety systems for non-LOCA events are shown in Figure 4.2.11-1 and are as follows:

- Initial depressurization phase (IDP)— Points 1 to 2
- Pressure decay phase (PDP)— Points 2 to 3

Overall Test Observations

This test simulated a steam generator tube rupture (SGTR) with nonsafety systems operating with the operator performing manual actions. Therefore, specific actuation setpoints and anticipated operator actions were performed that impacted the facility response and made this test different from S01110 (an SGTR with nonsafety systems inoperable and no operator actions). These differences are outlined in Table 4.2.11-5.

Based on the setpoints and actuations in Table 4.2.11-5, the following overall test observations are made. Figure 4.2.11-1 shows the facility primary system pressure during matrix test S01309 (as measured at the top of the pressurizer) with selected component actuations shown in relation to the primary system pressure.

The IDP began with the opening of the SGTR break valve at time zero seconds and ended at approximately []^(a,b,c) seconds when the primary system pressure had stabilized and when operator actions to control the primary system heat removal and depressurization began. The pressurizer pressure did not begin to decrease upon initiation of the SGTR because the pressurizer internal heaters and pressure control remained on until []^(a,b,c) seconds. Pressurizer level (shown in data plot 32) began to decrease immediately upon break initiation. The reactor trip (R) signal and the safety systems actuation (S) signal were actuated at []^(a,b,c) seconds when the pressurizer level reached []^(a,b,c) ft. These actuations, combined with the []^(a,b,c)-second delay in the reactor coolant pump (RCP) trip, caused an expected sudden cooldown and shrinkage of the primary system inventory. This was evidenced by the rapid draining of the pressurizer from []^(a,b,c) ft. to []^(a,b,c) ft., and the rapid depressurization from approximately []^(a,b,c) psia to []^(a,b,c) psia. During the IDP, the water in the power channel and hot legs remained subcooled.

At []^(a,b,c) seconds, the pressurizer pressure rapidly decreased from approximately []^(a,b,c) psia to approximately []^(a,b,c) psia. This was caused by an inadvertent opening of the ADS-1 valve by the facility control computer. (The control computer was to begin depressurizing the steam generator-A to obtain and/or increase subcooling in hot leg-A based on T-A04P. The ADS was to actuate only if []^(a,b,c)°F subcooling was present.) After the ADS actuation, there was little or no subcooling present (shown in data plot 5). The time of this event corresponded to the S signal []^(a,b,c) minutes ([]^(a,b,c) seconds) specified for the automatic functions to start. The combined effect of both the steam generator-A PORV and the ADS-1 valve actuation was to rapidly reduce the hot leg-A temperature (as measured by T-A04P) from []^(a,b,c)°F to []^(a,b,c)°F, and reduce the primary system pressure to (or near) the hot-leg saturation pressure.

During the initial portion of the PDP (from []^(a,b,c) seconds to []^(a,b,c) seconds), the primary system depressurized from []^(a,b,c) psia to []^(a,b,c) psia and the hot-leg temperature decreased from []^(a,b,c)°F to []^(a,b,c)°F; that is, the pressure essentially equaled the hot-leg saturation pressure. The hot-leg temperature decrease closely matched the desired []^(a,b,c)°F/hr cooldown rate. Therefore, no actuations of the steam generator-A PORV were performed. After []^(a,b,c) seconds, the cooldown rate of hot leg-A became less than []^(a,b,c)°F/hr apparently due to the automatic isolation of the startup feedwater flow to the steam generator-A.

In order to restore the desired hot-leg cooldown rate, test personnel were instructed to manually open the steam generator-A PORV for []^(a,b,c) seconds at []^(a,b,c)-second intervals. The test personnel, however, cycled one of the two ADS-1 valves (orifice sized to simulate one of two ADS-1 valves at []^(a,b,c) percent open) at approximately []^(a,b,c) seconds. This caused a reduction in primary system pressure, a loss of hot-leg subcooling, and delayed the initiation of steam generator-A PORV operation until approximately []^(a,b,c) seconds. From the time the ADS-1 valve was opened until approximately []^(a,b,c) seconds, no hot-leg subcooling margin was established—although break flow was reduced and continued to decrease. After approximately []^(a,b,c) seconds, the CMTs were becoming fully heated. This resulted in hotter injection flow to the vessel and effectively reducing the primary system heat removal rate. Opening the steam generator-A PORV for []^(a,b,c) second intervals was not sufficient to maintain the desired []^(a,b,c)°F/hr cooldown rate. Therefore, at approximately []^(a,b,c) seconds, the steam generator-A PORV was opened and left in the open position. This resulted in a cooldown rate of approximately []^(a,b,c)°F/hr, which established a []^(a,b,c)°F hot-leg subcooling margin at approximately []^(a,b,c) seconds. The ADS-1 valve was then cycled opened and closed to reduce primary system pressure. This resulted in the termination of break flow from the primary to secondary side.

In conclusion, this test indicated that although the operator actions (which were performed to subcool the hot leg and reduce pressurizer pressure) were not performed at optimal time intervals, the nonsafety systems and manual actions did maintain the plant hot legs in a single-phase, nonvoided condition throughout the transient recovery. Also, from an overall standpoint, the SPES-2 recovery was very successful in that the break flow was rapidly reduced by the primary system depressurization during the IDP. However, it was evident that a cooldown rate of []^(a,b,c)°F/hr was required at SPES-2 to obtain hot-leg subcooling margin and allow the pressurizer to be depressurized more quickly during the PDP of the transient.

During the entire PDP of this event, the rod bundle and hot legs remained near or below saturation temperature, as evidenced by the rod bundle collapsed level and PRHR HX supply line differential pressure (dP) instruments which showed no voiding. The flow from the primary system to the steam generator-B secondary side via the SGTR is shown in Figure 4.2.11-2.

Discussion of Test Transient Phases

- **Initial Depressurization Phase ([]^(a,b,c) to []^(a,b,c) Seconds)**

The initial depressurization phase (IDP) began with the initiation of the break at time zero and continued until []^(a,b,c) seconds when the primary system depressurization was slowed (that is, when primary system pressure was supported by the saturation pressure of the upper plenum and hot legs). This period included the following major events: initiation of CVCS makeup flow to the primary system when pressurizer level decreased to the low level setpoint of []^(a,b,c) ft. at []^(a,b,c) seconds; shut-off of the one operating PZR internal heater when pressurizer level decreased to []^(a,b,c) ft. at []^(a,b,c) seconds; and simultaneous R and S signal initiation when pressurizer level decreased to the low-low level setpoint of []^(a,b,c) ft. at []^(a,b,c) seconds. The R and S signals initiated the following actions: the main steamline isolation valves (MSLIVs) and (MFWIVs) closed; the CMT injection line isolation valves and the PRHR HX return line isolation valve were opened— all with a []^(a,b,c)-second delay; decay power simulation was initiated after a []^(a,b,c)-second delay; RCP coastdown was initiated after a []^(a,b,c)-second delay; and the CVCS setpoints were reset to ON when pressurizer level was less than []^(a,b,c) percent ([]^(a,b,c) ft.) and to OFF when pressurizer level was greater than []^(a,b,c) percent ([]^(a,b,c) ft.). Also during the IDP, operator action to isolate startup feedwater flow from the faulted steam generator-B was simulated at []^(a,b,c) seconds (S signal []^(a,b,c) minutes), and operator action to initiate additional primary system cooling by opening the steam generator-A PORV was simulated beginning at S signal []^(a,b,c) minutes. As pointed out above, the ADS-1 valve was inadvertently opened with the steam generator-A PORV at approximately []^(a,b,c) seconds.

Facility Response during the IDP:

The overall response of the primary system following break initiation was as expected with no unusual occurrences until the ADS-1 valve was inadvertently opened at approximately []^(a,b,c) seconds at the end of the IDP.

Pressurizer level began to decrease when the break valve was opened and decreased at a steady rate until the R and S signal were actuated on low-low pressurizer level ([]^(a,b,c) ft.) at []^(a,b,c) seconds. Following the initiation of the rod bundle power decay and before the delayed trip of the RCPs, the low power/flow ratio caused a rapid reduction in the rod bundle outlet temperature from approximately []^(a,b,c)°F to approximately []^(a,b,c)°F. The resultant shrinkage in RCS fluid volume, combined with the break flow, rapidly emptied the pressurizer and level was not restored until approximately []^(a,b,c) seconds during the PDP. CVCS makeup flow to the primary system was initiated at []^(a,b,c) seconds. However, since CVCS injection rate was small at only []^(a,b,c) lbm/sec. ([]^(a,b,c) gpm in AP600) compared to the break flow, the CVCS injection had little effect on the pressurizer level decrease.

The primary system temperatures responded as expected during the IDP; for example, the hot-leg temperatures responded to the reduced power/flow ratio prior to RCP trip—dropping momentarily

and then recovering prior to establishing natural circulation flow. The cold leg-A temperatures dropped due to the PRHR heat exchanger operation, and the downcomer temperature decreased due to the addition of cold CMT water. However, cold leg-B temperatures (without the PRHR heat exchanger) momentarily increased at the time of the trip in response to steam generator MSLIV closure and remained relatively constant as dictated by steam generator-B pressure. The overall temperature decrease of the rod bundle inlet and outlet during the IDP was approximately []^(a,b,c)°F ([]^(a,b,c)°F to []^(a,b,c)°F).

From time zero until the pressurizer internal heater was shut off at []^(a,b,c) seconds, the primary system pressure was maintained at normal operating pressure. This was to be expected, since the single pressurizer internal heater was rated at []^(a,b,c) kW maximum, which is equivalent to approximately []^(a,b,c) kW in the AP600 plant and was controlled to maintain normal plant pressure. Once the pressurizer internal heater was shutoff, the primary pressure decreased slowly due to the continued expansion of the pressurizer steam bubble since there was still a net fluid loss through the break. The initiation of CVCS makeup flow into the primary system at []^(a,b,c) lbm/sec. beginning at []^(a,b,c) seconds was smaller than the initial break flow and had little effect on the pressurizer pressure (or level discussed above) which was approximately []^(a,b,c) psia just prior to the R and S signals. When the R and S signals were generated at []^(a,b,c) seconds (by pressurizer low-low level), the power decay was initiated and safety injection actuations occurred. As a result of the rod bundle power reduction without flow reduction, the primary pressure dropped suddenly to approximately []^(a,b,c) psia. Pressure decay was then smooth in response to the decreasing primary system temperature with the pressurizer pressure equaling the hot leg saturation pressure ([]^(a,b,c) psia) at []^(a,b,c) seconds. After the R and the S signals, the CVCS makeup flow and CMT net injection flow almost matched the average break flow.

- **Pressure Decay Phase ([]^(a,b,c) Seconds to End-of-Test)**

The pressure decay phase (PDP) began at approximately []^(a,b,c) seconds when the system pressure (Figure 4.2.11-1) was initially supported at the saturation pressure determined by the rod bundle outlet temperature. As discussed previously, the ADS-1 valve was opened by the facility control computer at approximately []^(a,b,c) seconds causing a drop in pressure from approximately []^(a,b,c) psia to []^(a,b,c) psia.

This phase of the test was characterized by a slow decrease in overall system pressure and temperature. As discussed previously, operator actions to obtain hot-leg subcooling margin and to reduce the primary system temperature and pressure were not effectively initiated until approximately []^(a,b,c) seconds and []^(a,b,c) seconds, respectively. As a result, throughout most of the PDP the hot-leg side of the primary system was close to or below saturation with primary pressure primarily dictated by the pressurizer steam bubble pressure.

Facility Response during the PDP:

The system responses during this phase were very predictable since level, temperature, and pressure responses were typically slow.

The pressurizer level versus time (data plot 32) shows that the pressurizer level began to recover at approximately []^(a,b,c) seconds and increased smoothly to approximately 1 ft. at []^(a,b,c) seconds. During this initial part of the PDP ([]^(a,b,c) to []^(a,b,c) seconds), break flow to the faulted steam generator-B was approximately []^(a,b,c) lbm/sec. and was more than offset by the CVCS makeup flow of []^(a,b,c) lbm/sec. and the CMT net injection of approximately []^(a,b,c) lbm/sec. during this same time period. Since the primary system temperature in the cold legs, power channel, and hot legs only decreased by approximately []^(a,b,c)°F, the shrinkage of the primary-side fluid was limited.

From approximately []^(a,b,c) to []^(a,b,c) seconds, the ADS-1 valve was cycled open and closed. Due to the decrease in primary pressure, the upper-head temperature reached saturation and began to drain, decreasing in level from []^(a,b,c) ft. to []^(a,b,c) ft., while the pressurizer level increased from approximately []^(a,b,c) ft. to []^(a,b,c) ft. This pressurizer level (approximately []^(a,b,c) percent) resulted in the shutoff of the CVCS makeup pump. Pressurizer level decreased very slowly throughout a []^(a,b,c)-second interval with the CMT net injection closely matching break flow and primary system shrinkage. When the steam generator-A PORV remained open at approximately []^(a,b,c) seconds (reducing primary fluid temperature) and the CMTs became fully heated (minimizing their net injection), pressurizer level decreased at a faster rate reaching approximately []^(a,b,c) ft. at []^(a,b,c) seconds (even though break flow was close to zero after []^(a,b,c) seconds). At approximately []^(a,b,c) seconds, the ADS-1 valve was opened intermittently to reduce primary system pressure since hot leg-A was []^(a,b,c)°F subcooled thereby terminating the break flow. This resulted in some accumulator flow causing an increase in pressurizer level.

The primary system temperatures responded predictably throughout the PDP. The primary system remained at or below saturation temperature. Increases in the cooldown rate can be attributed to when the steam generator-A PORV was opened or when steam generator-A startup feedwater flow was on. Decreases in the cooldown rate can be attributed to when steam generator-A startup feedwater was isolated or when the CMT outlet temperatures increased. Data plot 5 shows the hot leg-A temperature versus time.

Primary system pressure decreased smoothly throughout the PDP averaging approximately []^(a,b,c) psi/sec., with small rapid decreases in pressure caused by ADS-1 actuation. The secondary-side pressures also behaved predictably; for example, the isolated steam generator-B pressure closely followed the primary system pressure, and steam generator-A pressure decreases resulted from steam generator-A PORV actuations.

Component Responses

- **Power Channel**

The primary-side fluid flow path appears to remain single phase throughout this event (exceptions were the upper head upper-upper plenum). The lower-upper plenum, the heater rod bundle, and the bottom of the upper plenum to the hot leg show no evidence of voiding based on the dP instruments. Therefore, only key responses for selected parameters are discussed below.

The heater rod power versus time is shown in data plot 1. Because there was no ADS actuation on low CMT level, the heat loss compensation of []^(a,b,c) kW was maintained through the event. Review of the decay power curve showed that the actual heater rod power closely matched the decay heat versus time specified plus []^(a,b,c) kW.

The heater rod temperatures (data plot 3) closely followed the fluid temperatures throughout the event, and there were no unexpected increases in rod temperature.

The upper head level (plot 31) began to drain at approximately []^(a,b,c) seconds when the primary system pressure dropped to the upper-head saturation pressure ([]^(a,b,c) F/[]^(a,b,c) psia). This draindown corresponded to when one of the ADS-1 valves were cycled opened and closed from []^(a,b,c) seconds to approximately []^(a,b,c) seconds. This draindown also corresponded to the increase in pressurizer level observed at this time. This resulted in shutoff of the CVCS makeup to the primary system. After secondary-side cooling was established by opening the steam generator-A PORV at approximately []^(a,b,c) seconds, the upper-head level continued to decrease in response to the decreasing primary pressure. This resulted in nearly stable pressurizer levels until approximately []^(a,b,c) seconds. At []^(a,b,c) seconds, the ADS-1 valve was opened to reduce primary system pressure and terminate break flow. The resulting sudden decreases in primary system pressure were observed to cause further decreases in upper-head level. As evidenced by the upper-upper plenum level, the upper-head steam bubble expanded into the upper-upper plenum.

The fluid level in the upper-upper plenum of the power channel (data plot 31) appeared to be constant throughout the event until approximately []^(a,b,c) seconds. As discussed above, after []^(a,b,c) seconds the upper-upper plenum level showed oscillations and a decrease as a result of the continued expansion of the steam in the power channel upper head. No level decrease was observed in the lower-upper plenum level instrument, suggesting that the upper head steam bubble did not expand down to the hot legs (plot 30).

- **Pressurizer**

The pressurizer behavior was described earlier in this section.

• Steam Generator

The two steam generators showed very distinct and expected differences because of the nature of the steam generator tube rupture and the operator actions taken during the tube rupture recovery. Prior to and just after the R and S signals were initiated, both steam generators operated identically. Data plots 2 and 35 show the steam generator-A and steam generator-B pressures and levels. Two seconds after the R and S signals, the main steam line isolation valve for each steam generator was closed, and the rod bundle power was maintained for approximately []^(a,b,c) seconds longer. This resulted in a rapid increase in steam generator pressure from the normal operating pressure of []^(a,b,c) psia to []^(a,b,c) psia. Following the decrease in rod bundle power, the decrease and subsequent increase in hot-leg temperature that occurred due to the delayed RCP shutoff was reflected as a small pressure decrease and recovery in both steam generators. Steam generator pressures equilibrated until after the operator completed the isolation of the faulted steam generator-B. At approximately []^(a,b,c) seconds when the steam generator-A PORV was cycled opened and closed, steam generator-A pressure decreased as expected, and steam generator-B pressure remained equal to the saturation pressure corresponding to the primary fluid temperature. Steam generator-A pressure remained slightly below steam generator-B through []^(a,b,c) seconds since more cold startup feedwater was added to steam generator-A.

Steam generator-A and steam generator-B level responses were nearly identical until approximately []^(a,b,c) seconds after the steam generator tube rupture initiation. At the time of the reactor trip at []^(a,b,c) seconds, both steam generator levels oscillated rapidly from []^(a,b,c) ft. to []^(a,b,c) ft. due to the collapse of voids, and both quickly recovered to approximately []^(a,b,c) ft. at []^(a,b,c) seconds (as shown in data plot 35).

At []^(a,b,c) minutes after the S signal ([]^(a,b,c) seconds), the startup feedwater to the faulted steam generator-B was isolated. This isolation was to simulate quick and accurate operator identification of the faulted steam generator.

The observed level response of steam generator-B (the faulted steam generator) was affected by an incomplete isolation of startup feedwater. Operator action to isolate startup feedwater at approximately []^(a,b,c) seconds only reduced startup feedwater flow to steam generator-B from approximately []^(a,b,c) lbm/sec. to approximately []^(a,b,c) lbm/sec. (Figure 4.2.11-4). This startup feedwater flow was significant since break flow from []^(a,b,c) seconds through []^(a,b,c) seconds was only approximately []^(a,b,c) lbm/sec. Startup feedwater to steam generator-B was fully isolated at approximately []^(a,b,c) seconds when steam generator-A level reached approximately []^(a,b,c) ft. (high level control setpoint) terminating startup feedwater pump operation. Steam generator-B level was steady from []^(a,b,c) seconds until approximately []^(a,b,c) seconds even though break flow into steam generator-B averaged approximately []^(a,b,c) lbm/sec. (approximately []^(a,b,c) lbs total) during this time. Steam generator-B level increased again starting at []^(a,b,c) seconds, apparently responding to startup feedwater injection initiation to steam generator-A. After []^(a,b,c) seconds, the level is above []^(a,b,c) ft., which is the top of the level instrument range.

It was apparent that the startup feedwater isolation valve for steam generator-B was not fully closing and that complete startup feedwater isolation only occurred when no startup feedwater was required by either steam generator (that is, common startup feedwater supply was OFF). As a result, the steam generator-B level exceeded the instrumentation range in this test.

Steam generator-A level and pressure responses throughout the remainder of the event were as expected. After startup feedwater flow to steam generator-B was reduced at approximately []^(a,b,c) seconds, steam generator-A level was increased at a faster rate than steam generator-B, and therefore, steam generator-A level was higher than steam generator-B level from []^(a,b,c) seconds to []^(a,b,c) seconds. Startup feedwater addition refilled steam generator-A to approximately []^(a,b,c) ft. at approximately []^(a,b,c) seconds and startup feedwater was then isolated. Steam generator-A level was reduced from []^(a,b,c) ft. to []^(a,b,c) ft. by the cycling of the PORV beginning at []^(a,b,c) seconds. At []^(a,b,c) seconds, startup feedwater was resumed and steam generator-A level was restored to []^(a,b,c) ft. at approximately []^(a,b,c) seconds, and startup feedwater was terminated. Between []^(a,b,c) and approximately []^(a,b,c) seconds when the PORV was being cycled, each PORV actuation caused a level instrumentation oscillation. After approximately []^(a,b,c) seconds when the PORV was left open, steam generator-A level quickly decreased, causing startup feedwater injection, and then increased until startup feedwater isolation as dictated by the level control system. Steam generator-A pressure decreased whenever the PORV was opened.

- **Hot Legs**

Hot legs-A and -B were maintained full of liquid throughout the test. Data plots 5 and 6 illustrate the hot-leg temperatures versus time and were discussed in previous subsections.

- **Cold Legs**

Cold legs were filled with subcooled water throughout the test. Data plots 13 and 14 illustrate the cold-leg temperatures versus time. The effect of the PRHR heat exchanger heat removal and steam generator-A PORV operation on cold legs-A1 and A-2 can be observed and compared to cold legs-B1 and -B2. Since there was essentially no heat removal by the steam generator-B during the transient, the loop B cold-leg temperatures remained within approximately []^(a,b,c)°F of the hot-leg temperatures.

Data plot 36 illustrates the cold-leg flow versus time that occurs after RCPs have been tripped and the primary system flow was only by natural circulation. Cold legs-A1 and -A2 flows included the PRHR heat exchanger return flow. Also, although there was no heat removal (steaming) from the steam generators until the steam generator-A PORV was opened at approximately []^(a,b,c) seconds, significant natural circulation flows were indicated (approximately 1 lbm/sec. per cold leg at []^(a,b,c) seconds; []^(a,b,c) percent to []^(a,b,c) percent of full flow). After []^(a,b,c) seconds, cold legs-A1 and -A2 natural circulation flows increased in response to steam generator-A depressurization via the PORV, reaching approximately []^(a,b,c) lbm/sec. after []^(a,b,c) seconds when the PORV was left open. Flows

from cold legs-B1 and -B2 decreased during this time as steam generator-B became a heat source as primary system cooldown occurred.

- **Passive Residual Heat Removal Heat Exchanger**

At the initiation of the event, the PRHR subsystem was filled with subcooled liquid. When the S signal occurred, the PRHR return valve opened after a []^(a,b,c)-second delay, and a high level of flow through the heat exchanger occurred since the RCPs were still operating. When the pumps were shutoff, the PRHR flow rate decreased to the recirculation flow rate of about []^(a,b,c) lbm/sec. The PRHR flow decreased steadily during the event and ended at []^(a,b,c) lbm/sec. at []^(a,b,c) seconds. Single-phase water flow in the PRHR supply line was maintained throughout the event. The PRHR heat exchanger fluid return temperature was initially []^(a,b,c)°F and decreased only slightly to []^(a,b,c)°F at []^(a,b,c) seconds. The PRHR heat exchanger heat removal rate decreased steadily; []^(a,b,c) kW at []^(a,b,c) seconds, []^(a,b,c) kW at []^(a,b,c) seconds, []^(a,b,c) kW at []^(a,b,c) seconds, and []^(a,b,c) kW at []^(a,b,c) seconds. The IRWST temperature increased with time, resulting from PRHR operation (data plot 17). The IRWST water temperature at the top of the tank (T-065E) was only []^(a,b,c)°F at []^(a,b,c) seconds.

- **Core Makeup Tanks (CMTs)**

CMT recirculation started []^(a,b,c) seconds after the S signal occurred. The flow from the CMTs occurred due to natural circulation. Hot water from cold legs-B1 and -B2 flowed to the top of the CMT-A and CMT-B, respectively, via their balance lines. And cold water from the bottom of the CMTs flowed into the power channel. In this test, where the cold legs remained full and subcooled, no CMT draindown occurred and the CMTs continued to recirculate with the recirculation flow rate, decreasing with time. As shown in data plot 42, the initial CMT injection rate was []^(a,b,c) lbm/sec. and it decreased to approximately []^(a,b,c) lbm/sec. at []^(a,b,c) seconds. The net total mass increase to the primary system from the observed CMT recirculation rates and CMT temperatures were approximately []^(a,b,c) lbm/sec. from []^(a,b,c) seconds to []^(a,b,c) seconds, approximately []^(a,b,c) lbm/sec. at []^(a,b,c) seconds, approximately []^(a,b,c) lbm/sec. at []^(a,b,c) seconds, approximately []^(a,b,c) lbm/sec. at []^(a,b,c) seconds, approximately []^(a,b,c) lbm/sec. at []^(a,b,c) seconds, and approximately []^(a,b,c) lbm/sec. at []^(a,b,c) seconds. The effective heat removed from the primary system by the recirculating CMTs at time []^(a,b,c) seconds was approximately []^(a,b,c) kW.

The decrease in CMT recirculation flow rate versus time was due to decreasing buoyancy driving head caused by CMT heatup and, to a lesser extent, by decreasing cold-leg temperature. A stratified temperature gradient was established in the CMTs (data plots 15 and 16) where the water temperature at the top of the CMTs was near that of the cold leg temperature, and the water temperature at the bottom of the CMT remained cold. As the CMTs continued to recirculate, the heated water layer was observed to move downward (to get thicker) in the tank with time. The continuously decreasing temperature of the leading edge of the hot water layer, moving down the tank, was caused by the cooling effect of the cold CMT metal mass it encountered and due to heat

losses from the uninsulated tank walls. The heated layer of water reached the bottom of the CMT at approximately []^(a,b,c) seconds.

In this SGTR event, the CMTs recirculated for a long enough time to completely heat up, reaching an almost steady-state condition at approximately []^(a,b,c) seconds. The heat losses from each CMT at this time was approximately []^(a,b,c) kW.

Mass Discharge and Mass Balance

Due to the use of the steam generator-A PORV and ADS-1 and ADS-3 valves, there was some discharged mass in this test (as shown in data plot 44 and listed in Table 4.2.11-6). The discharged mass to the ADS-1, -2, and -3 catch tank through the ADS-1 and -3 valves was only []^(a,b,c) lbm. The discharged mass to the ADS-4 steam generator catch tank through the steam generator-A PORV was []^(a,b,c) lbm. The break mass flow (from primary side to secondary side) began when the break valve was opened at time zero (Figure 4.2.11-3). The flow rate rapidly decreased throughout the IDP ([]^(a,b,c) seconds). During the first []^(a,b,c) seconds until the MSLIV and MFWIV were closed, about []^(a,b,c) lbm of liquid were lost from the primary system (Figure 4.2.11-3) to the secondary system. A small amount of flow continued until the primary-side pressure was reduced to the steam generator-B secondary-side pressure at about []^(a,b,c) seconds. Additionally, there was mass added to the primary system from the CVCS and to the secondary system from the startup feedwater during the transient (data plot 42 and Figure 4.2.11-4, respectively).

The primary system mass balance results for test S01309 were calculated based on water inventory before and after the S01309 test. Table 4.2.11-6 gives a detailed listing of the inventories of water in the various components before the test. Table 4.2.11-7 lists the inventories after the test. The primary system remained water solid throughout the transient with the exception of voiding in the upper head and upper-upper plenum region of the power channel. Table 4.2.11-8 provides a mass balance for the system before and after the test, and shows excellent agreement of the measurements before and after testing. The mass inventory at the end of the test is within 1.8 percent of the starting inventory.

Note that the Quick Look Report (Reference 2, PXS-T2R-029), which incorporated a rough estimate of the steam generator secondary side mass, did not include the flow through the SGTR break line in the mass balance calculation. Therefore, a primary side only calculation, which includes the integrated SGTR break flow, lessens the amount of uncertainty in the mass balance and best assures the validity of pertinent test data.

TABLE 4.2.11-3

ADS-3 Valve (Z_003PO)			
Opened(s)	Closed(s)	Δt (s) Opened	Δt (s) Closed
			(a,b,c)

**TABLE 4.2.11-4
SEQUENCE OF EVENTS FOR TEST S01309**

Event	Specified	Instrument Channel	Actual Time (sec.)
Break Opens	0	Z-00280	(a,b,c)
CVCS On	PZR level = 10.0 ft.	L-010P	
Pressurizer Internal Heater Off	PZR level = 6.6 ft.		
Pressurizer Low Level (R, S Signals)	PZR low level = 0.676 m	L-010P	
MSLIV Closure	PZR LL + 2 sec.	Z_A04SO, F_A04S	
		Z_B04SO, F_B04S	
MFWIV Closure	PZR LL + 2 sec.	Z_B02SO, F_B01S	
		Z_A02SO, F_A01S	
CMT IV Opening	PZR LL + 2 sec.	Z_A040EC, F-A40E	
		Z_B040EC, F-B40E	
PRHR HX Actuation	PZR LL + 2 sec.	Z_A81EC, F_A80EG	
Scram	PZR LL + 5.7 sec.	—	
Startup feedwater	L-010P = 0.676 m	L-010P	
RCPs Tripped	PZR LL + 16.2 sec.	DP-A00P	
		DP-B00P	
SFW Isolation to Steam Generator-B	S + 5 min.		
ADS-1	CMT level 67% +30 sec.	L_B40E	Note 1
		Z_001PC	Note 1
Steam Generator-A PORV Open Permission	S + 7 min.		
Accumulators	P-027P = 710 psia	F_A20EG	Note 1
		F_B20EG	Note 1
ADS-2	CMT level 67% +125 sec.	L_B40E	Note 1
		Z_002PC	Note 1
ADS-3	CMT level 67% +245 sec.	L_B40E	Note 1
		Z_003PC	Note 1
ADS-4	CMT level 20% +60 sec.	L_B40E	Note 1
		Z_004PC, F-040P	Note 1
IRWST Injection	P-027P = 26 psia	F_A60EG	Note 1
		F_B60EG	Note 1

NOTE 1: []

**TABLE 4.2.11-5
ACTION/EFFECT DURING TEST S01309**

Setpoints/Actuations	Observed/Desired Effect
PZR internal heater remains on until PZR level = [] ^(a,b,c) ft	Pressurizer pressure remained at approximately [] ^(a,b,c) psia until pressurizer level dropped to [] ^(a,b,c) ft. High PZR pressure resulted in high break flow. Trips occurred at [] ^(a,b,c) psia rather than at [] ^(a,b,c) psia as in test S01110.
Two of six PZR external heaters remained on throughout the transient after S signal.	No apparent effect. Pressurizer level was maintained below heaters.
Prior to S signal, CVCS pump started when PZR level [] ^(a,b,c) ft and injects [] ^(a,b,c) lbs/sec.	CVCS flow small compared to break flow, but slowed rate of PZR level decrease.
The R and S signals were actuated on low PZR level ([] ^(a,b,c) ft) rather than low PZR pressure as in LOCA tests.	Similar to S01110.
The S signal resets CVCS pump setpoints to maintain PZR level between [] ^(a,b,c) and [] ^(a,b,c) ft.	CVCS pump ON/OFF based on PZR level.
Startup feedwater started on S signal.	Both steam generator levels increase after initial level collapse that occurs after trip.
ADS-1 orifice resized to represent one of two ADS-1 valves opened at [] ^(a,b,c) percent and programmed to automatically open if RCS hot leg-A is subcooled.	Represented one ADS valve opened to [] ^(a,b,c) percent ([] ^(a,b,c) percent open for [] ^(a,b,c) seconds out of every [] ^(a,b,c) second interval).
ADS-3 orifice resized to represent one of two ADS-1 valves opened at [] ^(a,b,c) percent. Controlled manually.	Provided the ability to manually perform the same function as ADS-1 valve above.
Steam generator-A PORV programmed to automatically open for [] ^(a,b,c) seconds every [] ^(a,b,c) second interval, as required, to cooldown and achieve a [] ^(a,b,c) °F hot leg temperature at [] ^(a,b,c) seconds. Steam generator-A PORV has manual over-ride capability.	Provides PORV capacity similar to AP600. Manual over-ride provides capability for operator to dump additional secondary-side steam.
Operator identifies faulted steam generator at 5 minutes after S signal ([] ^(a,b,c) seconds) and isolates startup feedwater to faulted steam generator.	At [] ^(a,b,c) minutes after S, the faulted steam generator level is higher than the intact steam generator level. Note: startup feedwater injection to intact steam generator causes its level to be higher from [] ^(a,b,c) to [] ^(a,b,c) seconds.

TABLE 4.2.11-5 (Continued)
ACTION/EFFECT DURING TEST S01309

Setpoints/Actuations	Observed/Desired Effect
At [] ^(a,b,c) minutes after S signal, the facility control computer was set to automatically open the steam generator-A PORV for [] ^(a,b,c) seconds to initiate/maintain a [] ^(a,b,c) F/hr cooldown rate. Cooldown rate checked every [] ^(a,b,c) seconds.	This was intended to mimic operator action to establish a subcooled condition in hot leg-A.
When hot leg-1 was subcooled by [] ^(a,b,c) F, the facility control computer was set to open the ADS-1 valve for [] ^(a,b,c) seconds (subcooling checked every [] ^(a,b,c) seconds).	This was intended to mimic operator action to minimize RCS pressure in order to equalize RCS and faulted steam generator-B pressure (terminate break flow).

**TABLE 4.2.11-6
WATER INVENTORY BEFORE TEST S61309**

Component	Volume (ft. ³)/(l)	Net Vol (ft. ³)/(l)	Temp (°F)	Relative Density	Mass (lbm)
Loops	8.97 ft. ³ (254.0 l)	8.97 ft. ³ (254.0 l)			(a,b,c)
Pressurizer	3.37 ft. ³ (95.4 l)	1.82 ft. ³ (51.6 l)			
Surge Line	0.34 ft. ³ (9.6 l)	0.34 ft. ³ (9.6 l)			
Tubular Downcomer	1.38 ft. ³ (39.1 l)	1.38 ft. ³ (39.1 l)			
Annular Downcomer + High Pressure Bypass	0.54 ft. ³ (15.3 l)	0.54 ft. ³ (15.3 l)			
Core Bypass	0.44 ft. ³ (12.4 l)	0.44 ft. ³ (12.4 l)			
Lower Plenum	0.81 ft. ³ (22.8 l)	0.81 ft. ³ (22.8 l)			
Riser	1.64 ft. ³ (46.4 l)	1.64 ft. ³ (46.4 l)			
Upper Plenum	1.46 ft. ³ (41.3 l)	1.46 ft. ³ (41.3 l)			
Upper Head	1.90 ft. ³ (53.8 l)	1.90 ft. ³ (53.8 l)			
CMT-A	5.05 ft. ³ (143.0 l)	5.05 ft. ³ (143.0 l)			
CMT-B	5.05 ft. ³ (143.0 l)	5.05 ft. ³ (143.0 l)			
Accumulator-A	5.05 ft. ³ (143.0 l)	3.97 ft. ³ (112.4 l)			
Accumulator-B	5.05 ft. ³ (143.0 l)	3.99 ft. ³ (112.9 l)			
IRWST Injection Line	0.18 ft. ³ (5.1 l)	0.18 ft. ³ (5.1 l)			
TOTAL INVENTORY					

TABLE 4.2.11-7
WATER INVENTORY AFTER TEST S01309
 Water level as measured by DP-B16P (-0.58 psi) is 16.28 in. (407 mm) above hot leg

Component	Volume (ft. ³)/(l)	Net Vol (ft. ³)/(l)	Temp (°F)	Relative Density	Mass (lbm)
Loops	8.97 ft. ³ (254.0 l)	8.97 ft. ³ (254.0 l)			^(a,b,c)
Pressurizer	3.37 ft. ³ (95.4 l)	0.81 ft. ³ (22.8 l)			
Surge Line	0.34 ft. ³ (9.6 l)	0.34 ft. ³ (9.6 l)			
Tubular Downcomer	1.38 ft. ³ (39.1 l)	1.38 ft. ³ (39.1 l)			
Annular Downcomer + High-Pressure Bypass	0.54 ft. ³ (15.3 l)	0.45 ft. ³ (12.8 l)			
Core Bypass	0.44 ft. ³ (12.4 l)	0.44 ft. ³ (12.4 l)			
Lower Plenum	0.81 ft. ³ (22.8 l)	0.81 ft. ³ (22.8 l)			
Riser	1.64 ft. ³ (46.4 l)	1.64 ft. ³ (46.4 l)			
Upper Plenum	1.46 ft. ³ (41.3 l)	1.27 ft. ³ (36.6 l)			
Upper Head	1.90 ft. ³ (53.8 l)	0.0 ft. ³ (0.0 l)			
CMT-A	5.05 ft. ³ (143.0 l)	5.05 ft. ³ (143.0 l)			
CMT-B	5.05 ft. ³ (143.0 l)	5.05 ft. ³ (143.0 l)			
Accumulator-A	5.05 ft. ³ (143.0 l)	3.47 ft. ³ (98.3 l)			
Accumulator-B	5.05 ft. ³ (143.0 l)	3.64 ft. ³ (103.1 l)			
IRWST Injection Line	0.18 ft. ³ (5.1 l)	0.18 ft. ³ (5.1 l)			
TOTAL INVENTORY					

WATER INJECTED FROM THE IRWST DURING EVENT			
IRWST Injection	dP (psi)	Area (in ²)	Mass (lb)
Note 1	0.0		0.0

Note 1: The IRWST did not inject for this transient.

**TABLE 4.2.11-8
MASS BALANCE FOR TEST S01309**

	Starting Inventory (lbm)	Ending Inventory (lbm)
Total Primary System		(a,b,c)
CVCS Make-up During Transient		
IRWST Injection During Transient		
Break Catch Tank		
ADS-1, -2, and -3 Catch Tank		
Break Flow to Secondary Side		
TOTAL		
Ending Inventory/Starting Inventory (lbm)		
Ending Inventory/Starting Inventory (percent)		98.2%

The following figures have been intentionally deleted
from this document due to their proprietary nature.

**TEST S01309 PLOT PACKAGE
CHANNEL LIST BY COMPONENT**

Component	Channel	Units	Plot	Comment
ACCA	F_A20E	lbm/sec.	39	
ACCA	L_A20E	ft.	34	
ACCB	F_B20E	lbm/sec.	39	
ACCB	L_B20E	ft.	34	
ADS 1, 2, & 3	F_030P	lbm/sec.	44	Flow rate derived
ADS 1, 2, & 3	IF030P	lbm	43	Catch tank
ADS 4 & SG	F_040P	lbm/sec.	44	Flow rate derived
ADS 4 & SG	IF040P	lbm	43	Catch tank
ANNDP	DP-A021P	psi	24	To cold leg-A1
ANNDP	DP-A022P	psi	25	To cold leg-A2
ANNDP	DP-B021P	psi	26	To cold leg-B1
ANNDP	DP-B022P	psi	27	To cold leg-B2
BREAKLINE	F_005P	lbm/sec.	44	Flow rate derived
BREAK LINE	IF005P	lbm	43	Catch tank
CLA	DP-A001P	psi	24	To cold leg-A1
CLA	DP-A002P	psi	25	To cold leg-A2
CLA	DP-A09P	psi	22	Pump suction
CLA	T-A10P	°F	11	Steam generator outlet
CLA1	F-A01P	lbm/sec.	36	
CLA1	T-A021PL	°F	13	Downcomer inlet
CLA1	T-A11P	°F	11	Pump outlet
CLA2	F_A02P	lbm/sec.	36	
CLA2	T-A022PL	°F	13	Downcomer inlet
CLB	DP-B001P	psi	26	To cold leg-B1
CLB	DP-B002P	psi	27	To cold leg-B2
CLB	DP-B09P	psi	23	Pump suction
CLB	T-B10P	°F	12	Steam generator outlet
CLB1	F_B01P	lbm/sec.	36	
CLB1	T-B021PL	°F	14	Downcomer inlet

**TEST S01309 PLOT PACKAGE
CHANNEL LIST BY COMPONENT (Continued)**

Component	Channel	Units	Plot	Comment
CLB1	T-B11P	°F	12	Pump outlet
CLB2	F-B02P	lbm/sec.	36	
CLB2	T-B022PL	°F	14	Downcomer inlet
CMTA	F_A40E	lbm/sec.	38	
CMTA	L_A40E	Ft	33	
CMTA	T-A401E	°F	15	Top 242.25 in.
CMTA	T-A403E	°F	15	216.75 in.
CMTA	T-A405E	°F	15	191.25 in.
CMTA	T-A407E	°F	15	165.75 in.
CMTA	T-A409E	°F	15	140.25 in.
CMTA	T-A411E	°F	15	114.75 in.
CMTA	T-A413E	°F	15	89.25 in.
CMTA	T-A415E	°F	15	63.75 in.
CMTA	T-A417E	°F	15	38.25 in.
CMTA	T-A420E	°F	15	Bottom 0 in.
CMTB	F_B40E	lbm/sec.	38	
CMTB	L_B40E	ft.	33	
CMTB	T-B401E	°F	16	Top 242.25 in.
CMTB	T-B403E	°F	16	216.75 in.
CMTB	T-B405E	°F	16	191.25 in.
CMTB	T-B407E	°F	16	165.75 in.
CMTB	T-B409E	°F	16	140.25 in.
CMTB	T-B411E	°F	16	114.75 in.
CMTB	T-B413E	°F	16	89.25 in.
CMTB	T-B415E	°F	16	63.75 in.
CMTB	T-B417E	°F	16	38.25 in.
CMTB	T-B420E	°F	16	Bottom 0 in.
CVCS	F-001A	psi	42	
DVIA	T-A00E	°F	13	
DVIB	T-B00E	°F	14	

TEST S01309 PLOT PACKAGE
CHANNEL LIST BY COMPONENT (Continued)

Component	Channel	Units	Plot	Comment
HLA	DP-A04P	psi	20	
HLA	T-A03PL	°F	5	Vertical, near power channel
HLA	T-A03PO	°F	5	Horizontal, near power channel
HLA	T-A04P	°F	5	Near steam generator inlet
HLB	DP-B04P	psi	21	
HLB	T-B03PL	°F	6	Vertical, near power channel
HLB	T-B03PO	°F	6	Horizontal, near power channel
HLB	T-B04P	°F	6	Near steam generator inlet
IRWST	F_A60E	lbm/sec.	40	F_A61E for S00303
IRWST	F_B60E	lbm/sec.	40	F_B61E for S00303
IRWST	L_060E	Ft.	32	
IRWST	T_061E	°F	17	Bottom
IRWST	T-062E	°F	17	Below mid
IRWST	T-063E	°F	17	Middle
IRWST	T-064E	°F	17	Above mid
IRWST	T-065E	°F	17	Top
NRHRA	F-A00E	psi	42	
NRHRB	F-B00E	psi	42	
PC	W_00P	kW	1	
PC-HB	L_000P	ft.	30	Heater bundle
PC-HR	TW018P20	°F	3	Heater rod
PC-HR	TW018P48	°F	3	Heater rod
PC-HR	TW019P82	°F	3	Heater rod
PC-HR	TW020P24	°F	3	Heater rod
PC-HR	TW020P61	°F	3	Heater rod
PC-HR	TW020P87	°F	3	Heater rod
PC-UH	T-016P	°F	4	Upper head
PC-UP	L_A15P	ft.	30	Lower upper plenum
PC-UP	L_A16P	ft.	31	Upper upper plenum
PC-UP	T-015P	°F	4	Upper plenum

**TEST S01309 PLOT PACKAGE
CHANNEL LIST BY COMPONENT (Continued)**

Component	Channel	Units	Pirot	Comment
PC_UH	L_017P	ft.	31	Upper head
PC_UP	L_A14P	ft.	31	Above top of the active fuel
PRHR	DP-A81AE	psi	29	Supply line inv U-tube
PRHR	DP-A81BE	psi	29	Supply line inv U-tube
PRHR	DP-A81E	psi	28	Supply line
PRHR	DP-A82E	psi	28	Heat exchanger
PRHR	DP-A83E	psi	28	Return line
PRHR	F_A80E	lbm/sec.	37	Return line
PRHR	T-A82E	°F	19	Inlet
PRHR	T-A83E	°F	19	Exit
PRZ	L_010P	ft.	32	
PRZ	P-027P	psia	2	
PRZ	T-026P	°F	18	487 in.
SGA	DP-A05P	psi	20	Hot side
SGA	DP-A06P	psi	20	Hot side
SGA	DP-A07P	psi	22	Cold side
SGA	DP-A08P	psi	22	Cold side
SGA	F_A01S	lbm/sec.	41	
SGA	F_A20S	lbm/sec.	41	
SGA	L_A10S	ft.	35	Overall level
SGA	P-A04S	psia	2	Secondary system
SGA	T-A01S	°F	10	MFW-A
SGA	T-A05P	°F	7	Hot side
SGA	T-A05S	°F	9	Hot side - riser
SGA	T-A06P	°F	7	Hot side
SGA	T-A08P	°F	11	Cold side
SGA	TW-A06S	°F	7	Hot side
SGB	DP-B05P	psi	21	Hot side
SGB	DP-B06P	psi	21	Hot side
SGB	DP-B07P	psi	23	Cold side

**TEST S01309 PLOT PACKAGE
CHANNEL LIST BY COMPONENT (Continued)**

Component	Channel	Units	Plot	Comment
SGB	DP-B08P	psi	23	Cold side
SGB	F_B01S	lbm/sec.	41	
SGB	F_B20S	lbm/sec.	41	
SGB	L_B10S	ft.	35	Overall level
SGB	P-B04S	psia	2	Secondary system
SGB	T-B01S	°F	10	MFW-B
SGB	T-B05P	°F	8	Hot side
SGB	T-B05S	°F	9	Hot side - riser
SGB	T-B06P	°F	8	Hot side
SGB	T-B07P	F	8	U-tube top
SGB	T-B08P	°F	12	Cold side
SGB	TW-B06S	°F	8	Hot side
SL	T-020P	°F	18	Surge line near pressurizer
TDC	DP-001P	psi	25	Top
TDC	DP-001P	psi	26	Top
TDC	DP-002P	psi	24	Bottom
TDC	DP-002P	psi	27	Bottom
TDC	DP-002P	psi	26	Bottom
TDC	DP-002P	psi	25	Bottom
TDC	T-001PL	°F	13	Top
TDC	T-001PL	°F	14	Top
TDC	T-003P	°F	13	Bottom
TDC	T-003P	°F	14	Bottom
TSAT-PRZ		°F	18	Based on P-027P
UH-TSAT		°F	4	Based on P-017P

The data plots are found in the proprietary version of this document.

4.2.12 Steam Generator Tube Rupture without Nonsafety Systems (S01110)

This matrix test simulated a steam generator tube rupture (SGTR) without any nonsafety systems operating or operator actions, and with only the automatic passive safety systems used for accident mitigation. The pressurizer internal heaters were shut-off at break initiation and the chemical and volume control system (CVCS), normal residual heat removal (NRHR) function, and startup feedwater system (SFWS) were shut-off for this test. The single SGTR is simulated via a line connected from the primary side (reactor coolant pump (RCP) B suction piping) to the secondary side of steam generator-A (approximately []^(a,b,c) ft. above the tube sheet), with a break orifice diameter scaled to simulate []^(a,b,c) times the area of a AP600 steam generator tube.

Results are provided in the data plot package at the end of this section. The sequence of events for S01110 is listed in Table 4.2.12-1. During mitigation of the SGTR, there was no core makeup tank (CMT) draindown, and no accumulator or in-containment refueling water storage tank (IRWST) injection throughout the transient.

Since this SGTR test did not result in automatic depressurization system (ADS) actuation only the first two event phases observed in loss-of-coolant accident (LOCA) recovery occurred. The event phases selected for purpose of detailed evaluation of the non-LOCA events are shown in Figure 4.2.12-1 and are as follows:

- Initial depressurization phase (IDP) – Point 1 to 2
- Pressure decay phase (PDP) – Point 2 to 3

Overall Test Observations

Figure 4.2.12-1 shows the facility primary system pressure during matrix test S01110 (as measured at the top of the pressurizer) in relation to selected component actuations and other facility responses.

The IDP began with the opening of the break valve between the primary and secondary side, causing the pressurizer to drain. Because the pressurizer heaters were not on after break initiation, there was a reduction in pressure due to pressurizer steam expansion.

When the pressurizer level dropped to []^(a,b,c) ft. at []^(a,b,c) seconds, the reactor trip (R) and safety system actuation (S) signals were actuated. []^(a,b,c) seconds later, the main steam line isolation valves (MSLIVs) and main feedwater isolation valves (MFWIVs) were closed, the CMT and passive residual heat removal (PRHR) heat exchanger (HX) return line isolation valves were opened, and the RCPs coasted down with a []^(a,b,c)-second delay (at []^(a,b,c) seconds into the event). Rod bundle power was reduced to []^(a,b,c) percent of full power after a []^(a,b,c)-second delay (at []^(a,b,c) seconds), and the simulated power decay began after a []^(a,b,c)-second delay. The bundle power was maintained 150 kW above the scaled decay power to compensate for facility heat losses.

The recirculation flow through the CMTs and the PRHR flow began immediately after the isolation valves were opened. The changing rod bundle power to flow ratio caused by the time delays between rod bundle power was reduced. When the RCPs were tripped and coasted down, this reduction caused a sharp decrease, then increase in the hot leg temperature. This reduction also caused a rapid decrease in pressurizer pressure from []^(a,b,c) to []^(a,b,c) psia followed by a slight increase in pressure. Primary pressure then decreased to the steam generator saturation pressure due to heat transfer to the steam generators. The IDP ended at []^(a,b,c) seconds, when hot leg/upper plenum temperature ([]^(a,b,c)°F) started to control the primary system pressure; and break flow stabilized at approximately []^(a,b,c) lb/sec. (Figure 4.2.12-5). Data plot 31 shows that the level of the upper-upper plenum above the hot legs began to decrease.

During the initial portion of the PDP (up to []^(a,b,c) seconds), the primary system, with the exception of the upper-upper plenum and upper head, remained water solid. Primary system cooling was provided by the PRHR HX, CMT recirculation, break flow, and facility heat losses. At []^(a,b,c) seconds, these were 83 kW, 84 kW, 7 kW and approximately 125 kW, respectively (approximately 300 kW total), as compared to the heated rod power of 245 kW at []^(a,b,c) seconds. Thus, the primary and secondary system temperature and pressure slowly decreased throughout the PDP. The above PRHR HX heat removal rate was based on the steam fraction of the flow in the PRHR supply line (calculated to be low at this time, as determined from the dP instrument readings in data plot 29) and the PRHR flow rate, HX inlet and outlet temperatures, and pressure.

As shown in data plot 31, at approximately []^(a,b,c) seconds the upper-upper plenum and the upper head began to drain at a significant rate. This resulted in an increasing pressurizer level (data plot 32). The upper-upper plenum drained rapidly from approximately []^(a,b,c) seconds and was completely drained to the hot leg elevation at approximately []^(a,b,c) seconds.

At this time, primary system and secondary system pressures were essentially equalized and several events occurred almost simultaneously:

- The break flow to steam generator-B decreased from approximately []^(a,b,c) lbm/sec. at []^(a,b,c) seconds to approximately []^(a,b,c) at []^(a,b,c) seconds (Figure 4.2.12-5). Total break flow mass from the primary system to secondary side of steam generator-B was approximately []^(a,b,c) lbm (Figure 4.2.12-3).
- The steam generator-B tubes began to drain at approximately []^(a,b,c) seconds.
- The loop-B cold leg flows decreased and loop-A flows increased momentarily.
- Steam voiding began in the rod bundle resulting in two-phase flow through the lower-upper plenum, hot legs, PRHR supply line, etc.
- The pressurizer level rapidly increased in response to the draining steam generator-B tubes, upper head, and primary system steam generation.

This resulted in oscillations of temperature, steam fraction, tubular downcomer flow, and system pressure, all of which continued throughout the test. The pressurizer was completely filled at []^(a,b,c) seconds and remained filled until the test was terminated. The CMT natural recirculation flow continued, but the flow rate was decreasing. The upper head was completely drained at []^(a,b,c) seconds, and the level never recovered. The primary system pressure oscillated about the secondary system pressure and there was a small alternating flow in the break line.

Due to periodic boiling in the heater rod bundle (data plots 30 and 31), two-phase mixture with wide variations in steam fraction entered the hot leg and flowed to the steam generators and PRHR HX. This resulted in alternating slugs of steam and water in the PRHR HX supply line, which resulted in oscillations in the PRHR heat removal rate and return flow rate. The oscillating return to flow into the cold legs and tubular downcomer caused small heater rod temperature oscillations.

Hot leg-B fluid had a steam fraction close to that in the lower-upper plenum. However, the steam fraction in hot leg-A was lower due to the selective removal of steam from the hot leg into the PRHR inlet line. The steam fraction at the PRHR HX inlet oscillated and reached high peaks, which enhanced the PRHR heat removal from the primary system as compared to the heat removal with single-phase saturated or subcooled water before []^(a,b,c) seconds.

As stated above, the steam generator-B U-tubes began draining at approximately []^(a,b,c) seconds into the event. At the end of the event, the steam generator-B U-tubes were drained, including part of the pump B suction line. The U-tubes steam generator-A never drained; however, there was an oscillating flow with wide variations in steam fraction in the upper section of the U-tubes.

This test demonstrated that the heater rod bundle was fully covered (single-phase or two-phase mixture) at all times during this test (data plots 30 and 31) and that there was no indication of heater rod temperatures increasing due to lack of cooling (data plot 3). Also, the passive safety system functions were shown to mitigate the consequences of a SGTR with no operator actions or use of nonsafety systems. Key parameters comparing the S01110 test with other tests are listed in Table 5-1 in Section 5.0.

Discussion of Test Transient Phases

- **Initial Depressurization Phase (0 to 1050 Seconds)**

The initial depressurization phase (IDP) began with the initiation of the break (at time 0) and lasted until the primary system pressure decreased to the saturation pressure for the upper plenum and the hot legs (Figure 4.2.12-1). This period included the following events: initiation of the break, the actuation of the R and S signals, closure of the MSLIV and MFWIV, opening of the CMT injection line isolation valves, and opening of the PRHR HX return line isolation valve; all with a []^(a,b,c)-second delay. Rod bundle power was reduced to []^(a,b,c) percent with a []^(a,b,c)-second delay, the rod bundle decay power was initiated with a []^(a,b,c) second delay, and RCP coastdown was initiated after a []^(a,b,c)-second delay.

System Response during the IDP:

The break was initiated at time 0. From time 0 until the R and S signals were activated (at []^(a,b,c) seconds), the system lost pressure due to the fluid loss through the break resulting in a decreased pressurizer level and an expansion of the pressurizer steam bubble. When the trip signals were activated, the power was reduced to []^(r,h,c) percent of full power after []^(a,b,c) seconds. At []^(a,b,c) seconds, the SPES-2 integrated power from the time of the R signal simulates the AP600 post-trip integrated power. The SPES-2 power was then decreased to simulate the AP600 decay heat plus 150 kW for facility heat loss compensation, which was maintained throughout this transient. The MSLIV was closed at []^(a,b,c) seconds. As a result of the power reduction without flow reduction, the rod bundle ΔT decreased, and lower-upper plenum temperature dropped temporarily to the lower plenum temperature of []^(a,b,c)°F. The system pressure decreased to []^(a,b,c) psia at []^(a,b,c) seconds (Figure 4.2.12-2). At this time, the pressurizer drained and the system pressure was controlled by the temperature of the saturated fluid ([]^(a,b,c)°F) in the surge line. When the RCPs were shut off (at []^(a,b,c) seconds), the rod bundle and the lower-upper plenum temperatures increased to []^(a,b,c)°F, a result of the increased power/flow ratio for the rod bundle at the lower flow. The system pressure increased temporarily to []^(a,b,c) psia until there was a drop in the decay power and there was a reduction in the plenum temperature. The lower plenum temperature was affected by the CMT cold fluid injection into the downcomer and the PRHR HX flow into cold leg. The pressure decreased at a rate of []^(a,b,c) psia/sec in this time period (at []^(a,b,c) seconds). The CMT recirculation flow and the PRHR flow, break flow, and facility heat losses were sufficient to keep the flow through the power channel subcooled.

The PRHR flow started before the RCPs were shut off and continued by natural circulation after RCP coastdown (data plot 37). The primary system pressure stabilized at the saturation pressure for the bulk temperature of fluid on the hot-leg side of the power channel (approximately 540°F) at []^(a,b,c) seconds. This ended the IDP.

- **Pressure Decay Phase (1050 Seconds to End-of-Test)**

The pressure decay phase (PDP) began when the primary system pressure (Figure 4.2.12-2) was dictated by the saturation pressure for the hot-leg fluid temperature, and continued until the end of the test. This phase was characterized by a slow decrease in the overall system pressure and temperature. The rod bundle power (decay power plus heat loss compensation) reduced from []^(a,b,c) kW to []^(a,b,c) kW (data plot 1).

At []^(a,b,c) seconds (bundle power []^(a,b,c) kW), the PRHR HX heat removal rate was approximately []^(a,b,c) kW, the CMTs provided approximately []^(a,b,c) kW effective heat removal due to the cold CMT water replacing the hot water entering the CMTs through the balance lines, the break flow removed approximately []^(a,b,c) kW, and facility heat losses were approximately []^(a,b,c) kW. Thus, the total heat removal exceeded heat input (299 kW versus 245 kW), there was no boiling in the rod bundle, and primary system pressure decreased slowly.

From []^(a,b,c) to approximately []^(a,b,c) seconds the upper-upper plenum and upper head drained and partially refilled the pressurizer.

At []^(a,b,c) seconds into the test, the primary- and secondary-side pressures equalized, the steam generator U-tubes began to drain, and the break flow and the heat transfer to the secondary side decreased. Periodic boiling in the rod bundle and related temperature, steam fraction flow, and pressure oscillations began and continued throughout the test.

The U-tubes of steam generator-B were drained and the RCP-B suction line was partly drained at about []^(a,b,c) seconds into the event (data plots 21 and 23). The test was terminated at about []^(a,b,c) seconds.

System Response during the PDP:

The system pressure decreased during this phase ([]^(a,b,c) to []^(a,b,c) seconds) at a rate of []^(a,b,c) psia/sec.

After []^(a,b,c) seconds when the primary- and secondary-side pressures equalized, and the CMT outlet water temperature increased and boiling began to occur in the rod bundle, the steam fraction of the two-phase fluid leaving the rod bundle and the single-phase flow in the rod bundle oscillated (data plots 30 and 31). These oscillations in the void fraction had a significant effect on the thermal buoyancy head that drove the flow through the primary system at this time, since there were also oscillations in the steam fraction of the fluid flowing through the hot legs and the steam generators (data plots 20 and 21). The two-phase mixture entering the steam generators left the steam generators as saturated water. Some of the steam condensed in the cold-leg side of the U-tubes, and the remaining steam was separated from the two-phase mixture in the high point of the steam generator U-tubes (due to the low velocity). The steam generator-B U-tubes began to drain at this time and the cold-leg side U-tubes were drained at []^(a,b,c) seconds, and the U-tubes on the hot-leg side drained at []^(a,b,c) seconds into the event. The primary system flow/steam fraction oscillations were seen as level fraction oscillations in pump suction B.

For steam generator-A, the flow continued until the end of the test; however, there was an oscillating steam fraction at the top of steam generator-A U-tubes (data plots 20 and 22).

The CMT recirculation flow rate decreased throughout the test due to decreasing buoyancy head as the CMT became heated and, to a lesser extent, as cold-leg temperatures decreased. The water flowing from the bottom of the CMTs began to increase in temperature at []^(a,b,c) seconds.

Component Responses

- Power Channel

The power channel consisted of five volumes: the lower plenum, the heater rod bundle, the lower-upper plenum (below the hot leg), the upper-upper plenum (above the hot leg), and the upper head. When the break occurred, the system pressure began to drop, and the pressurizer began to drain. Nothing significant occurred in the power channel until the power was reduced to []^(a,b,c) percent by the R signal, after a []^(a,b,c)-second delay. At this time, the ΔT across the rod bundle decreased due to the reduced power/flow ratio (still full flow), and the rod bundle outlet temperature decreased toward the lower plenum temperature of []^(a,b,c)°F (Figure 4.2.12-2). When the RCPs were shut off, the power/flow ratio increased and the power channel outlet temperature increased. The lower-upper plenum temperature reached a peak ([]^(a,b,c)°F) and began to decrease due to decreasing rod bundle power and lower plenum temperature. The primary system pressure decrease stopped at []^(a,b,c) psig, corresponding to the saturation pressure of the fluid in the hot-leg side of the power channel (approximately []^(a,b,c)°F). This marked the end of the IDP ([]^(a,b,c) seconds). Since the coolant everywhere in the power channel was at or below the saturation temperature for the system pressure, no boiling or flashing occurred in the power channel during the IDP (Figure 4.2.12-2).

The temperature of the fluid on the hot-leg side of the power channel dictated the system pressure during the PDP (data plot 4). The primary system was sufficiently cooled by steady PRHR flow, natural CMT recirculation, and facility heat losses, and no boiling occurred until []^(a,b,c) seconds into the event. The upper-upper plenum and upper head began to drain at about []^(a,b,c) seconds. The upper-upper plenum was drained to the hot leg elevation at about []^(a,b,c) seconds and the level never recovered (data plots 30 and 31).

The upper head began to drain when the system pressure reached the saturation pressure for the fluid temperature in the upper head (at []^(a,b,c) seconds) and it was completely drained at []^(a,b,c) seconds. The upper-head fluid temperature was initially only []^(a,b,c)°F. After this time, the upper-head temperature followed the saturation temperature for system pressure throughout the remainder of the test.

Flow oscillations with a []^(a,b,c)-second period were observed in the tubular downcomer. These oscillations began at about []^(a,b,c) seconds and continued until the test ended at about []^(a,b,c) seconds. The flow oscillations led to oscillations of the collapsed liquid levels in the rod bundle, upper plenum, hot leg, steam generators, and PRHR HX supply line. When the downcomer flow decreased, rod bundle steam fraction increased. The boiling resulted in an increase of the overall system pressure and temperature (Figure 4.2.12-2). The overall system pressure oscillations were therefore out of phase with the tubular downcomer flow oscillations.

Data plots 30 and 31 show the collapsed liquid levels at various sections of the power channel. Data plot 30 shows the collapsed level in the heater rod bundle oscillating after

[]^(a,b,c) seconds, indicating apparent void fractions in the bundle from []^(a,b,c) to []^(a,b,c) percent with a period of approximately []^(a,b,c) seconds. The collapsed level measured just above the heated portion of the rod bundle (above TAF, data plot 31), provided an indication of the steam fraction of the fluid leaving the rod bundle ([]^(a,b,c) to []^(a,b,c) percent). The steam fraction variations are temporarily reduced at approximately []^(a,b,c) seconds due to draining of the steam generator-B tubes.

- **Pressurizer**

The pressurizer began to drain when the break occurred and was completely drained in approximately []^(a,b,c) seconds (data plot 32). The water in the pressurizer flashed due to the loss of system pressure, and the temperature of the water dropped from []^(a,b,c)°F during this initial depressurization (data plot 18). The hot water leaving the pressurizer surge line into hot leg-A caused a slight increase in the hot-leg temperature during this period, since it mixed with the flow from the power channel upper plenum. The pressurizer remained drained until []^(a,b,c) seconds, at which time it began to refill in response to draining of the upper-upper plenum and upper head. The pressurizer was completely filled to []^(a,b,c) ft. at []^(a,b,c) seconds and remained filled for the rest of the test.

- **Steam Generator**

Because of the break, fluid was lost from the primary system to the secondary side of steam generator-B. The steam generators acted as the heat sink until the MSLIV closed and prevented further energy removal from the secondary side. This caused the temperature of the secondary side to increase until []^(a,b,c) seconds toward the primary system hot-leg temperature, which at the same time was dropping due to the reduced power/flow ratio. When the RCPs had coasted down, a temporary temperature increase occurred on the steam generator's primary side due to the increased power/flow ratio at the natural circulation flow condition. The temperature then stabilized at approximately []^(a,b,c)°F at the end of the IDP.

The secondary-side B temperature was lower than that on secondary-side A. Both secondary-side temperatures decreased after []^(a,b,c) seconds to approximately []^(a,b,c)°F at the end of the test. The water level in steam generator-A was almost unchanged, while on side B it had increased by []^(a,b,c) ft. at the end of test due to the break flow into steam generator-B (Figures 4.2.12-4 and 4.2.12-5). This level began to oscillate after []^(a,b,c) seconds following pressure oscillations on the primary side (data plot 35).

For the IDP and the first part of the PDP (until []^(a,b,c) seconds), the pressure in the primary system was higher than the steam generator secondary side pressure (data plot 2). This indicated that some heat transfer (in addition to break flow) was occurring from the primary to secondary side of the steam generators.

At approximately []^(a,b,c) seconds, flow oscillations began to occur in the tubular downcomer. As the same time, oscillations occurred in the collapsed liquid level measured in the bundle, which indicated there were oscillations of the steam fraction of the two-phase liquid flowing through the rod bundle into the hot legs and to the steam generators (data plots 20 and 21). Thus the driving forces for the natural circulation flow, the density difference between the single-phase fluid in the cold legs and downcomer to the power channel and the two-phase mixture leaving the rod bundle and filling the hot legs, were oscillating.

The two-phase mixture entering the steam generators left the steam generators as water. Some of the steam was condensed in the U-tubes, and the rest of the steam was separated from the two-phase mixture in the high point of the steam generator-B U-tubes (due to the low flow velocity). This resulted in oscillating steam fractions in the upper part of the U-tubes of both steam generators. Since the fluid steam fraction in the hot leg-B was higher (steam from two-phase mixture was selectively drawn into the PRHR supply line from hot leg-A) the steam generator-B U-tubes were filled with steam and drained.

From []^(a,b,c) seconds until []^(a,b,c) seconds, intermittent flow was observed through steam generator-B. At []^(a,b,c) seconds, the flow through steam generator-B stopped, and the U-tubes cold-leg side were drained at []^(a,b,c) seconds, and the U-tubes hot-leg side were drained at []^(a,b,c) seconds. After this time, water level oscillations occurred in the RCP-B suction piping (data plots 21 and 23).

Also at []^(a,b,c) seconds until the end of the test, significant temperature oscillations were observed in both cold legs-A and -B from the RCP suction piping into the annular downcomer.

- **Hot Legs**

Hot legs-A and -B contained single-phase water (data plots 20 and 21) until []^(a,b,c) seconds. Starting at []^(a,b,c) seconds, the steam fraction of the fluid in the hot legs began to oscillate with the same frequency as in the power channel. The PRHR preferentially removed steam from the two-phase mixture in the hot leg-A, which reduced the steam fraction of fluid in hot leg-A to []^(a,b,c) to []^(a,b,c) percent. The steam fraction in hot leg-B was similar to that in the lower-upper plenum and varied between []^(a,b,c) and []^(a,b,c) percent.

- **Cold Legs**

The cold legs contained subcooled water throughout the test (data plots 22 through 27). After []^(a,b,c) seconds, the flow in the cold legs oscillated (greater amplitude was seen in cold leg-A because of oscillating flow in the PRHR return line). In addition, the temperature in both cold legs also oscillated.

- **PRHR and IRWST**

At the initiation of the test, the PRHR HX and piping were filled with subcooled liquid. When the R and S signals were actuated, the PRHR HX return valve opened after a []^(a,b,c)-second delay, and a high flow started through the HX due to the still-operating RCP. When the RCPs had coasted down the PRHR HX flow rate decreased to the recirculation flow rate of about []^(a,b,c) lbm/sec. Single-phase water flowed in the PRHR HX supply line and was subcooled to about []^(a,b,c)°F at the PRHR HX exit. When pressure, flow, and steam fraction oscillations started in the power channel and the hot leg filled with two-phase mixture, a very large portion of the steam in hot leg-A flowed to the PRHR HX (data plot 29) and intermittent water and steam flowed from the hot leg-A to the PRHR HX. The two-phase mixture was condensed and subcooled in the PRHR HX heat exchanger (data plot 28). Oscillations in the primary system void fraction resulted in wide PRHR HX flow rate oscillations. The maximum flow rate was as high as []^(a,b,c) lbm/sec., and the average flow rate was about []^(a,b,c) lbm/sec. The PRHR HX exit temperature (oscillating) increased by about []^(a,b,c)°F after []^(a,b,c) seconds.

The high average steam fraction of the fluid in the PRHR HX supply line enhanced the PRHR HX heat removal from the primary system. After []^(a,b,c) seconds, the tubular downcomer temperature (oscillating) decreased by approximately []^(a,b,c)°F.

The PRHR HX was submerged in the IRWST (heatup of the water within the IRWST is shown in data plot 17).

- **Core Makeup Tanks (CMTs)**

CMTs started injecting cold fluid into the direct vessel injection line []^(a,b,c) seconds after the R and S signals occurred. The injection flow from the CMT was by natural circulation, with hot water from the loop-B cold legs flowing through the cold leg balance lines (CLBLs) to the top of the CMTs, and cold water from the bottom of the CMTs flowing to the downcomer and into the power channel.

The CMT flow rate (data plot 38) decreased throughout the test (from about []^(a,b,c) lbm/sec. to []^(a,b,c) lbm/sec.) due to decreasing buoyancy driving head as the cold CMT water was replaced with hot water from the cold legs. The hot water remained thermally stratified in the CMTs (data plots 15 and 16), where the water temperature at the top of the CMTs was near to the loop-B cold leg water temperature, while the water temperature at the bottom of the tank remained cold. Data plots 15 and 16 also show that the layer of heated water in CMT-A and -B increased in depth as recirculation continued, with the leading water being cooled as it came in contact with cold CMT surfaces at lower elevations. The water being discharged from CMT-A and -B began to increase in temperature at approximately []^(a,b,c) and []^(a,b,c) seconds, respectively. At the same time, the CMT recirculation flow rates (data plot 38) began to decrease at a faster rate. At []^(a,b,c) seconds, when the test was terminated, the CMT recirculation flow and temperatures were almost constant. These flows and CMT ΔT 's are most likely exaggerated in SPES-2 due to

the larger-than-scaled metal surface area of the SPES-2 CMT. The indicated steady state heat loss from the SPES-2 CMTs at this time was approximately 9 kW per CMT.

Mass Discharge and Mass Balance

The break mass flow (from primary side to secondary side) started when the break valve was opened at "0" time. The flow rate rapidly decreased throughout the IDP ([]^(a,b,c) seconds). A small amount of flow continued until the primary and secondary-side pressures equalized at about []^(a,b,c) seconds. After that time, alternating flow was seen in the break line responding to oscillating primary system pressure (data plot 45). The total mass discharged to the secondary side due to the break was about []^(a,b,c) lbm (Figure 4.2.12-3).

The mass balance results for test S01110 were calculated based on primary side water inventory before and after the S01110 event taking into account the SGTR break flow between the primary and secondary side. Table 4.2.12-1 gives a detailed listing of the inventories of water in the various components before the test. Table 4.2.12-2 lists the inventories after the event. The water level in the vessel was determined by the DP-B15P measurement to be []^(a,b,c) in. ([]^(a,b,c) mm) above the hot leg centerline at the end of the test. Table 4.2.12-3 provides a the mass balance of all the primary side components before and after the test and shows that these masses agreed to within []^(a,b,c) percent.

Note that the Quick Look Report (Reference 2, PXS-T2R-026), which incorporated a rough estimate of the steam generator secondary side mass, did not include the flow through the SGTR break line in the mass balance calculation. Therefore, a primary side only calculation, which includes the integrated SGTR break flow, lessens the amount of uncertainty in the mass balance and best assures the validity of pertinent test data.

**TABLE 4.2.12-1
SEQUENCE OF EVENTS FOR TEST S01110**

Event	Specified	Instrument Channel	Actual Time (Sec.)
Break Opens	0	P-027P	(a,b,c)
Pressurizer Low Level R	PZR low level = 0.38 m	L-010P	
MSLIV Closure	PZR LL + 2 sec.	Z_A04SO, F_A04S	
		Z_B04SO, F_B04S	
MFWIV Closure	PZR LL + 2 sec.	Z_B02SO, F_B01S	
		Z_A02SO, F_A01S	
CMT-IV Opening	PZR LL + 2 sec.	Z_A040EC, F-A40E	
		Z_B040EC, F-B40E	
PRHR Heat Exchanger Actuation	PZR LL + 2 sec.	Z_A81EC, F_A80EG	
Scram	PZR LL + 5.7 sec.	—	
RCPs Tripped	PZR LL + 16.2 sec.	I-A1P, S-A1P	
		I-B1P, S-B1P	
ADS-1	CMT level 67%	L_B40E	Note 1
	+30 sec.	Z_001PC	Note 1
Accumulators	P-027P = 710 psia	F_A20EG	Note 1
		F_B20EG	Note 1
ADS-2	CMT level 67%	L_B40E	Note 1
	+125 sec.	Z_002PC	Note 1
ADS-3	CMT level 67%	L_B40E	Note 1
	+245 sec.	Z_003PC	Note 1
ADS-4	CMT level 20%	L_B40E	Note 1
	+60 sec.	Z_004PC, F-040P	Note 1
IRWST Injection	P-027P = 26 psia	F_A60EG	Note 1
		F_B60EG	Note 1

NOTE 1: ADS, Accumulators, and IRWST did not actuate or inject throughout this transient.

**TABLE 4.2.12-2
WATER INVENTORY BEFORE TEST S01110**

Component	(ft.³) Volume/(l)	(ft.³) Net Vol/(l)	Temp (°F)	Relative Density	Mass (lbm/sec.)
Loops	8.97 ft. ³ (254.0 l)	8.97 ft. ³ (254.0 l)			(a,b,c)
Pressurizer	3.37 ft. ³ (95.4 l)	1.85 ft. ³ (51.4 l)			
Surge Line	0.34 ft. ³ (9.6 l)	0.34 ft. ³ (9.6 l)			
Tubular Downcomer	1.38 ft. ³ (39.1 l)	1.38 ft. ³ (39.1 l)			
Annular Downcomer + High-Pressure Bypass	0.54 ft. ³ (15.3 l)	0.54 ft. ³ (15.3 l)			
Core Bypass	0.44 ft. ³ (12.4 l)	0.44 ft. ³ (12.4 l)			
Lower Plenum	0.81 ft. ³ (22.8 l)	0.81 ft. ³ (22.8 l)			
Riser	1.64 ft. ³ (46.4 l)	1.64 ft. ³ (46.4 l)			
Upper Plenum	1.46 ft. ³ (41.3 l)	1.46 ft. ³ (41.3 l)			
Upper Head	1.90 ft. ³ (53.8 l)	1.90 ft. ³ (53.8 l)			
CMTs	10.1 ft. ³ (286.0 l)	10.1 ft. ³ (286.0 l)			
Accumulator	10.1 ft. ³ (286.0 l)	7.64 ft. ³ (222.7 l)			
IRWST Injection Line	0.18 ft. ³ (5.1 l)	0.18 ft. ³ (5.1 l)			
Total Inventory					[](a,b,c)

TABLE 4.2.12-3
WATER INVENTORY AFTER TEST S01110 IS COMPLETED
 Water Level as Measured by DP-B15P (0.90 psi) was 7.68 in. (192 mm) Below Hot Leg

Component	Volume (l)	Net Vol (l)	Temp (°F)	Relative Density	Mass (lbm/sec.)
Loops	8.97 ft. ³ (254.0 l)	7.10 ft. ³ (201.0 l)			(a,b,c)
Pressurizer	3.37 ft. ³ (95.4 l)	3.17 ft. ³ (89.8 l)			
Surge Line	0.34 ft. ³ (9.6 l)	0.34 ft. ³ (9.6 l)			
Tubular Downcomer	1.38 ft. ³ (39.1 l)	1.38 ft. ³ (39.1 l)			
Annular Downcomer + High-Pressure Bypass	0.54 ft. ³ (15.3 l)	0.24 ft. ³ (6.9 l)			
Core Bypass	0.44 ft. ³ (12.4 l)	0.44 ft. ³ (12.4 l)			
Lower Plenum	0.81 ft. ³ (22.8 l)	0.81 ft. ³ (22.8 l)			
Riser	1.64 ft. ³ (46.4 l)	1.64 ft. ³ (46.4 l)			
Upper Plenum	1.46 ft. ³ (41.3 l)	0.86 ft. ³ (24.4 l)			
Upper Head	1.90 ft. ³ (53.8 l)	0.0 ft. ³ (0.0 l)			
CMTs	10.1 ft. ³ (286.0 l)	10.1 ft. ³ (286.0 l)			
Accumulator	10.1 ft. ³ (286.0 l)	7.64 ft. ³ (222.7 l)			
IRWST Injection Line	0.18 ft. ³ (5.1 l)	0.18 ft. ³ (5.1 l)			
Total Inventory					(a,b,c)

**TABLE 4.2.12-4
MASS BALANCE FOR TEST S01110**

	Starting Inventory (lbm)	Ending Inventory (lbm)	
Total Primary System	[]	(a,b,c)
IRWST Injection			
Net Mass Through SGTR Break			
TOTAL			
MASS DIFFERENCE			
ACCURACY		99.6%	

The following figures have been intentionally deleted
from this document due to their proprietary nature.

**TEST DATA PLOT PACKAGE
CHANNEL LIST BY COMPONENT**

Component	Channel	Units	Plot	Comment
ACCA	F_A20E	lbm/sec.	39	
ACCA	L_A20E	ft.	34	
ACCB	F_B20E	lbm/sec.	39	
ACCB	L_B20E	ft.	34	
ADS 1, 2, & 3	IF30FLW	lbm/sec.	44	Flow rate derived
ADS 1, 2, & 3	IF030P	lbm	43	Catch tank
ADS 4 & SG	IF40FLW	lbm/sec.	44	Flow rate derived
ADS 4 & SG	IF040P	lbm	43	Catch tank
ANNDC	DP-A021P	psi	24	To cold leg-A1
ANNDC	DP-A022P	psi	25	To cold leg-A2
ANNDC	DP-B021P	psi	26	To cold leg-B1
ANNDC	DP-B022P	psi	27	To cold leg-B2
BREAK LINE	IF05FLW	lbm/sec.	44	Flow rate derived
BREAK LINE	IF005P	lbm	43	Catch tank
CLA	DP-A001P	psi	24	To cold leg-A1
CLA	DP-A002P	psi	25	To cold leg-A2
CLA	DP-A09P	psi	22	Pump suction
CLA	T-A10P	°F	11	Steam generator outlet
CLA1	F_A01P	lbm/sec.	36	
CLA1	T-A021PL	°F	13	Downcomer inlet
CLA1	T-A11P	°F	11	Pump outlet
CLA2	F_A02P	lbm/sec.	36	
CLA2	T-A022PL	°F	13	Downcomer inlet
CLB	DP-B001P	psi	26	To cold leg-B1
CLB	DP-B002P	psi	27	To cold leg-B2
CLB	DP-B09P	psi	23	Pump suction
CLB	T-B10P	°F	12	Steam generator outlet
CLB1	F_B01P	lbm/sec.	36	

**TEST DATA PLOT PACKAGE
CHANNEL LIST BY COMPONENT (Cont.)**

Component	Channel	Units	Plot	Comment
CLB1	T-B021PL	°F	14	Downcomer inlet
CLB1	T-B11P	°F	12	Pump outlet
CLB2	F_B02P	lbm/sec.	36	
CLB2	T-B022PL	°F	14	Downcomer inlet
CMTA	F_A40E	lbm/sec.	38	
CMTA	L_A40E	ft.	33	
CMTA	T-A401E	°F	15	Top (242.25 in.)
CMTA	T-A403E	°F	15	216.75 in.
CMTA	T-A405E	°F	15	191.25 in.
CMTA	T-A407E	°F	15	165.75 in.
CMTA	T-A409E	°F	15	140.25 in.
CMTA	T-A411E	°F	15	114.75 in.
CMTA	T-A413E	°F	15	89.25 in.
CMTA	T-A415E	°F	15	63.75 in.
CMTA	T-A417E	°F	15	38.25 in.
CMTA	T-A420E	°F	15	Bottom (0 in.)
CMTB	F_B40E	lbm/sec.	38	
CMTB	L_B40E	ft.	33	
CMTB	T-B401E	°F	16	Top (242.25 in.)
CMTB	T-B403E	°F	16	216.75 in.
CMTB	T-B405E	°F	16	191.25 in.
CMTB	T-B407E	°F	16	165.75 in.
CMTB	T-B409E	°F	16	140.25 in.
CMTB	T-B411E	°F	16	114.75 in.
CMTB	T-B413E	°F	16	89.25 in.
CMTB	T-B415E	°F	16	63.75 in.
CMTB	T-B417E	°F	16	38.25 in.
CMTB	T-B420E	°F	16	Bottom (0 in.)
CVCS	F-001A	psi	42	
DVIA	T-A00E	°F	13	

**TEST DATA PLOT PACKAGE
CHANNEL LIST BY COMPONENT (Cont.)**

Component	Channel	Units	Plot	Comment
DVIB	T-B00E	°F	14	
HLA	DP-A04P	psi	20	
HLA	T-A03PL	°F	5	Vertical, near power channel
HLA	T-A03PO	°F	5	Horizontal, near power channel
HLA	T-A04P	°F	5	Near steam generator inlet
HLB	DP-B04P	psi	21	
HLB	T-B03PL	°F	6	Vertical, near power channel
HLB	T-B03PO	°F	6	Horizontal, near power channel
HLB	T-B04P	°F	6	Near steam generator inlet
IRWST	F_A60E	lbm/sec.	40	F_A61E for S00303
IRWST	F_B60E	lbm/sec.	40	F_B61E for S00303
IRWST	L_060E	ft	32	
IRWST	T-061E	°F	17	Bottom
IRWST	T-062E	°F	17	Below middle
IRWST	T-063E	°F	17	Middle
IRWST	T-064E	°F	17	Above middle
IRWST	T-065E	°F	17	Top
PC	W_00P	kW	1	
PC-HB	L_000P	ft	30	Heater bundle
PC-HR	TW018P20	°F	3	Heater rod
PC-HR	TO018P48	°F	3	Heater rod
PC-HR	TW019P82	°F	3	Heater rod
PC-HR	TW020P24	°F	3	Heater rod
PC-HR	TW020P87	°F	3	Heater rod
PC-UH	T-016P	°F	4	Upper head
PC-UP	L_A15P	ft.	30	Lower-upper plenum
PC-UP	L_A16P	ft.	31	Upper-upper plenum
PC-UP	T-015P	°F	4	Upper plenum
PC-UH	L_017P	ft.	31	Upper head
PC-UP	L_A14P	ft.	31	Above top of the active fuel

**TEST DATA PLOT PACKAGE
CHANNEL LIST BY COMPONENT (Cont.)**

Component	Channel	Units	Plot	Comment
PRHR	DP-A81AE	psi	29	Supply line inverted U-tube
PRHR	DP-A81BE	psi	29	Supply line inverted U-tube
PRHR	DP-A81E	psi	28	Supply line
PRHR	DP-A82E	psi	28	Heat exchanger
PRHR	DP-A83E	psi	28	Return line
PRHR	F_A80E	lbm/sec.	37	Return line
PRHR	T-A82E	°F	19	Inlet
PRHR	T-A83E	°F	19	Exit
PRZ	L_010P	ft.	32	
PRZ	P-027P	psia	2	
PRZ	T-026P	°F	18	487 in.
SGA	DP-A05P	psi	20	Hot side
SGA	DP-A06P	psi	20	Hot side
SGA	DP-A07P	psi	22	Cold side
SGA	DP-A08P	psi	22	Cold side
SGA	F_A01S	lbm/sec.	41	Main feed
SGA	F_A20A	lbm/sec.	41	Secondary feed
SGA	L_A10S	ft.	35	Overall level
SGA	P-A04S	psia	2	Secondary system
SGA	T-A01S	°F	10	MFW-A
SGA	T-A05P	°F	7	Hot side
SGA	T-A05S	°F	9	Hot side - riser
SGA	T-A06P	°F	7	Hot side
SGA	T-A08P	°F	11	Cold side
SGA	TW-A06S	°F	7	Hot side
SGB	DP-B05P	psi	21	Hot side
SGB	DP-B06P	psi	21	Hot side
SGB	DP-B07P	psi	23	Cold side
SGB	DP-B08P	psi	23	Cold side
SGB	F_B01S	lbm/sec.	41	Main feed

**TEST DATA PLOT PACKAGE
CHANNEL LIST BY COMPONENT (Cont.)**

Component	Channel	Units	Plot	Comment
SGB	F_B20A	lbm/sec.	41	Secondary feed
SGB	L_B10S	ft.	35	Overall level
SGB	P-B04S	psia	2	Secondary system
SGB	T-B01S	°F	10	MFW-B
SGB	T-B05P	°F	8	Hot side
SGB	T-B05S	°F	9	Hot side - riser
SGB	T-B06P	°F	8	Hot side
SGB	T-B07P	°F	8	U-tube top
SGB	T-B08P	°F	12	Cold side
SGB	TW-B06S	°F	8	Hot side
SL	T-020P	°F	18	Surge line near pressurizer
TDC	DP-001P	psi	25,26	Top
TDC	DP-002P	psi	24,25,26,27	Bottom
TDC	T-001PL	°F	13,14	Top
TDC	T-003P	°F	4,13,14	Bottom
TSAT-PRZ	n/a	°F	18,19	Based on P-027P
TSAT-UH	n/a	°F	4	Based on P-017P

The data plots are found in the proprietary version of this document.

4.2.13 Steam Generators Tube Rupture without Nonsafety Systems, with Inadvertent ADS (S01211)

This test S01211 was a blind test; therefore, this section has been intentionally left blank and will be provided later.

4.2.14 Large Steam Line Break at Hot Standby Conditions without Nonsafety Systems (S01512)

This test S01512 was a blind test; therefore, this section has been intentionally left blank and will be provided later.

Blind Test Disclaimer

All blanks within the asterisks represent deleted text that relates to the blind tests, which will be provided at a later date.

5.0 TEST DATA COMPARISON

This section compares the results from the plant transients simulated in SPES-2 to highlight differences in the primary system conditions that occur and the resulting differences in the safety systems responses. The test matrix for SPES-2 consisted of nine primary system pipe breaks or loss of coolant accidents (LOCAs), three steam generator tube ruptures (SGTRs), and one steam line break (SLB).

The nine LOCA transients were performed at three different break locations: 1) cold leg-B2 between the cold leg-B2 to CMT-B balance line and the reactor vessel, 2) direct vessel injection (DVI) line B between the CMT, accumulator, in-containment refueling water storage tank (IRWST) discharge lines and the reactor vessel DVI nozzle, and 3) the cold leg-B2 to CMT-B pressure balance line near the balance line isolation valve. At each break location two break sizes were simulated; for the cold-leg location, two 1-in. and three 2-in. breaks were simulated; for the DVI line and the balance line locations; one 2-in. break and one double-ended guillotine (DEG) break were simulated.

The three SGTR transients were simulations of a complete break of one steam generator tube. One SGTR used only passive systems for mitigation, and one used passive systems combined with operator actions and active nonsafety systems. The third SGTR included ADS actuation shortly after the start of the event. The SGTR with subsequent ADS and the SLB transients will not be discussed in this section. These are standalone simulations which are fully discussed in Section 4.0, and they are not comparable to any other transients simulated.

5.1 Comparison Basis for LOCAs

The reference for comparison for all LOCA transients is test S00303, the 2-in. cold-leg break. Table 5.1-1 lists 33 parameters to compare/characterize the primary system and passive safety system response during each test.

The important conditions within the SPES-2 power channel for comparing the passive safety system responses for the various tests are heater rod temperatures, the steam fraction of fluid in the rod bundle region, and the water level in the downcomer. However, for all the events simulated in SPES-2, no uncovering of the active rod bundle or significant heater rod temperature increases due to lack of cooling were observed, even for the most severe test (S00706). Since no rod bundle dryout occurred, the parameters used for determining the severity of conditions inside the power channel were 1) the fluid steam fraction in the heater rod bundle region and 2) the downcomer minimum water level (fluid inventory).

Important comparisons outside the power channel include the times at which the core makeup tanks (CMTs) transition from their recirculation to draindown mode of operation, when the steam generator U-tubes drained, and the passive residual heat removal (PRHR) heat exchanger (HX) performance. Table 5.1-1 shows two periods of high fluid steam fraction for the rod bundle. The first is at the end of the pressure decay phase (PDP) (typically just before ADS-1 actuation and accumulator injection). The second is during the (post-ADS) phase (typically just before the IRWST injection starts). Figure 5.1-1 shows the rod bundle fluid steam fraction estimated from the collapsed levels near the end of the PDP plotted against the rate of primary system pressure decay (slope 2 in Table 5.1-1) for all the LOCA tests. The relationship between the steam fraction and the rate of depressurization indicates that flashing is a major contributor to the two-phase fluid steam fraction in the rod bundle at this time, in addition to boiling. Thus, the rod bundle fluid steam fraction seen prior to the accumulator injection is break-size dependent.

Figure 5.1-2 shows the general relationship between the steam fractions in and above the rod bundle with the minimum downcomer level just prior to the IRWST injection. The low water level in the downcomer is a consequence of reduced water inventory in the primary system at this time. More fluid has been lost from the system than injected by the accumulators and the CMTs leading up to the ADS-4 actuation. This results in downcomer water levels that are below the elevation of the top of the rod bundle for many events (see Table 5.1-1). Despite the low downcomer water level, the rod bundle remains fully covered with a two-phase mixture due to its much lower density. Figure 5.1-2 shows that the high rod bundle fluid steam fraction, which occurs just prior to IRWST injection, is largely dependent on the downcomer water level at that time. This water level is a result of the water inventory at the end of the accumulator delivery, and the net fluid losses during the subsequent time delay until ADS-4 actuation. This time delay is relatively fixed by the CMT draindown rate.

It should be noted that the two large breaks (DEG) behave differently than the small breaks (1 and 2 inch). These differences will be evaluated in a specified comparison of the results for the break sizes tested.

The PRHR HX performance is largely dependent on the conditions in hot leg-A. If the hot leg has two-phase flow, enhanced PRHR performance is observed as compared to when there is single-phase fluid in the hot leg. In general, the LOCA tests result in two-phase flow through hot legs and the PRHR HX, and accordingly the PRHR HX performance is enhanced. In the SGTR test (S01110) and the SLB test (S01412), single phase flow through the hot leg and PRHR HX resulted in lower PRHR heat removal rates at any given inlet temperature.

The following figures have been intentionally deleted
from this document due to their proprietary nature.

5.2 Comparison Basis for Non-LOCAs

Only two of the four non-LOCA transients simulated at SPES-2 are directly comparable. These two tests are test S01309 (a single tube SGTR with the passive safety systems, chemical and volume control system [CVCS], and startup feedwater system [SFWS] and operator actions for mitigation) and test S01110 (a single tube SGTR with only the passive safety systems operating and no operator actions).

The remaining two non-LOCA tests, test S01211 (a single SGTR with only passive safety systems operating and no operator actions, but with inadvertent ADS) and test S01512 (a large single-ended SLB with only safety systems operating) were each unique. These two tests were performed to demonstrate the response of the passive safety systems and overall plant to specific/limiting events. The results for test S01211 are discussed in Section 4.2.13 and, the results for the test S01512 are discussed in Section 4.2.14.

5.3 Comparison of Break Locations

The effect of break location can be examined by comparing the base test S00303 (2-in. LOCA in the bottom of cold leg-B2) with tests S00605 (2-in. break in the DVI nozzle B) and S01007 (2-in. LOCA in the cold leg-B2 to CMT-B balance line).

In evaluating the effect of break location, two important characteristics are the elevation of the break and the affected line. The break elevation primarily affects the amount of coolant lost through the break, while the line in which the break occurs affects the CMT performance, and as a consequence the ADS initiation timing.

These three break locations and their elevations are:

S00303	2-in. break located at the bottom of cold leg-B2, at elevation 1.46 ft. (hot-leg centerline is elevation 0 ft.)
S00605	2-in. break at DVI nozzle-B, at elevation -1.67 ft.
S01007	2-in. break located in the cold leg-B2 to CMT-B balance line, at elevation 19.4 ft. (from the top of cold leg-B2)

In all three tests, the draindown of the primary system starts with the pressurizer and the upper-upper plenum followed by the steam generator U-tubes (Table 5.1-1). The steam generator-B U-tube draindown occurs at comparable times for all three events, as expected, since the initial break flows are essentially equal for all three break locations (see Figure 5.3-1). The loop-B cold legs begin to drain after the steam generator-B U-tubes and this water level affects the break mass flow rate.

In general, the break flow continues at a high mass flow rate (subcooled water) until the primary system water level drains to the break elevation. The break flow converts to two-phase flow or steam with a lower mass flow rate. The DVI line break is at the lowest elevation in the primary system (at []^(a,b,c) ft), and the break flow continues to be subcooled water (see subsection 4.2.7, data plot 14) until the fluid level in the annular downcomer reaches the DVI nozzle elevation. As seen in Figure 5.3-1, more water is lost from the primary system before the break flow converts to two-phase fluid for the DVI line break than for the two other breaks. Similarly, more water is lost in test S00303 than in test S01007, since the break for S01007 is supplied from the top of the cold leg.

Figure 5.3-1 shows a decrease in the slope of the S01007 breakline catch tank curve at approximately []^(a,b,c) seconds, which is the time the cold leg-B water level has decreased to the top of the cold-leg nozzle elevation. This change in slope indicates the conversion of breakflow from subcooled water (from a full cold-leg pipe) to two-phase flow. There is a similar but less pronounced change in the

curve for test S00303 at []^(a,b,c) seconds and in test S00605 no change in break flow is indicated until after ADS actuation.

After ADS actuation the slope of the integrated break mass curve changes for all three tests. In tests S00303 and S01007, the slope of the curve becomes almost horizontal, approximately []^(a,b,c) seconds after ADS-1 indicating that mostly steam is being vented. Test S00605 however, finally transitions to two-phase flow after ADS.

Since the break flows for all three breaks are initially similar, the water level in the loop-B cold legs decreases to the top of the reactor vessel cold-leg nozzle elevation at similar times for the three tests (about []^(a,b,c) seconds). This is important for the CMT draindown initiation. The loop-A cold legs drain slower than the loop B cold legs for all tests due to the effect of the PRHR. The PRHR preferentially removes steam from hot leg-A, thereby delaying the draindown of steam generator-A U-tubes and the subsequent draindown of the loop-A cold legs.

The transition from CMT natural circulation to draindown mode of operation is a direct response to when the break flow begins to drain cold leg-B1 (for CMT-A) and -B2 (for CMT-B). The DVI line break (S00605) drains both cold legs at the same time (draining the two CMT pressure balance lines at []^(a,b,c) seconds, thereby initiating a simultaneous transition to draindown in both CMTs. For S00303, the break flow shows a conversion to two-phase flow at approximately []^(a,b,c) seconds (Figure 5.3-1). This indicates that cold leg-B2 is no longer full of water, allowing steam to enter the cold-leg balance line (CLBL) and initiating draindown mode of operation for CMT-B. However, the CMT-A transition to draindown lags CMT-B, indicating that cold leg-B1 drains after cold leg -B2 where the break is located.

In test S01007, the transition from natural circulation to draindown for CMT-A occurs at []^(a,b,c) seconds, when the cold leg-B1 drains. This is similar to the CMT transitions for tests S00303 and S00605. However, the CMT-B pressure balance line break location affects the CMT-B operation. The natural recirculation flow through the CMT-B is suppressed in test S01007 as long as the break flow consists of single-phase fluid (for about []^(a,b,c) seconds). Apparently, the 2-in. break flow is high enough to make the single-phase pressure drop from the cold leg greater than the buoyancy head for CMT recirculation and there is no flow from the break location to the top of the CMT. When two-phase break flow starts (after []^(a,b,c) seconds), some of the two-phase mixture flows to the top of the CMT-B, where the steam is condensed by the cold water in the CMT. This results in an unstable natural circulation flow (Subsection 4.2.9, data plot 38). Full transition to the draindown mode of operation from CMT-B is delayed until cold leg-B2 is completely drained and the break flow is pure steam at approximately []^(a,b,c) seconds. Figure 5.3-2 shows the differential pressure for the balance line to CMT-B for tests S00303 and S01007. Due to the breakflow in the balance line for S01007, the differential pressure (dP) increases approximately []^(a,b,c) psi, which is sufficient to overcome the buoyancy head from the cold water in CMT-B. When the two-phase flow starts in the balance line (see subsection 4.2.9 data plot 26), the differential pressure decreases sufficiently to allow unstable natural circulation flow until approximately []^(a,b,c) seconds. At this time, steam fills the balance line and CMT-B draindown is initiated.

The rod bundle steam fraction and the downcomer level are listed in Table 5.1-1 for these tests. The rod bundle steam fraction is estimated from the measured dP at three periods: 1) the flow oscillation period, which starts after the RCPs have coasted down, 2) the period just prior to the accumulator injection, and 3) the period just prior to IRWST injection.

The rod bundle steam fractions during the oscillation period are very similar for the three break locations. As discussed in Section 5.4, the void fraction range is primarily determined by the depressurization rate at this time and is, therefore, related to the break size.

The pre-accumulator injection period is characterized in Table 5.1-1 lists the steam fractions that occurred in the rod bundle, in the rod bundle exit (TAF) and in the lower-upper plenum, during the pre-accumulator injection period. The most notable difference between these events is that the rod bundle steam fraction for the DVI line break is higher ($[\quad]^{(a,b,c)}$ percent) than for the cold-leg and balance-line breaks ($[\quad]^{(a,b,c)}$ percent and $[\quad]^{(a,b,c)}$ percent). This indicates that the flow through the rod bundle and the fluid inventory is lowest for S00605 (DVI line), and highest for S01007 (balance line). Figure 5.1-1 shows that this is the reverse of the break flow rates and that the flow through breaks on the cold-leg side of the power channel directly reduce coolant flow to the rod bundle. Figure 5.3-3 shows that the downcomer level (measured as dP) for S00605 is rapidly decreasing to the DVI nozzle level before accumulator injection starts at approximately $[\quad]^{(a,b,c)}$ seconds. The annular downcomer is full for S00303 and S01007 prior to accumulator injection at $[\quad]^{(a,b,c)}$ seconds.

The high steam fractions that occur in the rod bundle, rod bundle outlet, and lower-upper plenum prior to IRWST injection are listed in Table 5.1-1 as is the minimum level in the downcomer. For these three tests the level in the lower-upper plenum drops below the hot-leg nozzle elevation (most for the DVI line break) and therefore do not reflect the actual fluid steam fraction. The rod bundle, and rod bundle outlet steam fractions for test S00303 (cold leg break) and test S01007 (balance line break) are very similar, as are the minimum downcomer levels. Test S00605 (DVI line break) shows nearly twice the rod bundle fluid steam fraction, higher rod bundle outlet steam fraction, and a much lower minimum level (measured as a dP) in the tubular downcomer, as shown in Figure 5.3-4. This low water inventory in test S00605 is due in part to the fact that there is less downcomer and power channel water inventory after accumulator injection, than in S00303 and S01007. During the accumulator injection for the cold leg and the balance line breaks, the rod bundle is subcooled and completely refilled, as seen in the increasing collapsed level for the rod bundle shown in Figure 5.3-5. However for the DVI line break, the collapsed level in the rod bundle indicates two-phase flow with approximately a $[\quad]^{(a,b,c)}$ percent void fraction ($[\quad]^{(a,b,c)}$ psi lower than S00303) still exists at the end of accumulator injection.

Table 5.3-1 shows the instantaneous fluid losses and injection flows from/to the primary system for S00303 and S00605 at three times: during accumulator injection, after accumulator injection, and during IRWST injection. The table shows that the changes in collapsed level in the rod bundle shown in Figure 5.3-5 are in direct response to the net change in the primary system water inventory. During the accumulator injection, more water is injected into the primary system than is ejected through the break and the ADS. The rod bundle collapsed level (measured as differential pressure) increases and

the void fraction for the rod bundle fluid decreases as the system water inventory increases. Conversely, after the accumulator injection ends []^(a,b,c) seconds for S00605, []^(a,b,c) seconds for S00303), the water inventory decreases, the rod bundle void fraction increases, and the downcomer level decreases into the tubular downcomer. When the IRWST flow begins ([]^(a,b,c) seconds for S00605, []^(a,b,c) seconds for S00303), there is a net gain in water inventory, and the rod bundle collapsed level again increases.

Figures 5.3-6 through 5.3-11 show the coolant inventory for the primary system (consisting of the power channel, hot legs and cold legs, and the steam generators) for the three 2-in. break events. The first figure for each event shows separately the coolant mass loss and the injected fluid mass from/to the primary system (Figure 5.3-6 for S00303). The second figure shows the change in coolant inventory (coolant deficit) during the test from the initiation of the break (Figure 5.3-7). It takes approximately []^(a,b,c) lbm of coolant deficit to completely empty the power channel. These figures show that the minimum coolant inventory occurs at the same time as the minimum level is observed in the downcomer and correlates well with the downcomer level and the rod bundle void fraction (Table 5.1-1).

The PRHR performance, as calculated after the oscillation period, is very similar for these three events. The PRHR heat removal rates are similar, despite the some differences in the average steam fraction.

In summary, the break location had a significant impact on the simulated 2-in. LOCAs. The break elevation affected the amount of reactor coolant loss through the break, which significantly influences the power channel coolant inventory prior to start of IRWST injection. Also, a 2-in. break in the cold leg to CMT balance line will initially prevent CMT recirculation and delay the transition to draindown of the affected CMTs. However, this did not greatly affect overall coolant inventory or the ADS-4 timing, since it is actuated by the level of the unaffected CMT.

**TABLE 5.3-1
COMPARISON OF S00605 AND S00303**

		S00605	S00605	S00605	S00303	S00303	S00303
		1200s	1900s	2000s	1000s	2000s	2200s
Break Flow	lbm/sec.	[]
ADS-1, -2, -3 Flow	lbm/sec.	[]
ADS-4 Flow	lbm/sec.	[]
Total Out	lbm/sec.	[]
Accumulators	lbm/sec.	[]
CMTs	lbm/sec.	[]
IRWST	lbm/sec.	[]
Total In	lbm/sec.	[]

(a,b,c)

(a,b,c)

The following figures have been intentionally deleted
from this document due to their proprietary nature.

5.4 Comparison of Break Sizes

The LOCA events listed in Table 5.1-1 include four break sizes: the 1-inch, the 2-inch, and two DEGs. The 2-in. and the DEG breaks were performed at two or more break locations.

The effect of break size will be examined by a direct comparison of the baseline test S00303 (2-in. LOCA in the bottom of CLB-2) with test S00401 (1-in. LOCA in the bottom of the CLB-2). This comparison will be extended to evaluate other break locations. A separate comparison will be made between tests S00706 (DEG break of the DVI nozzle B) and S00908 (DEG break of the cold leg-B2 to CMT-B balance line). These two tests are both DEG breaks, but they are very different in terms of effective break size, break location, and injection capability of the passive safety system components.

Figure 5.4-1 shows the coolant inventory for the primary system (except pressurizer) during S00303 and S00401. For the 2-in. break (S00303), the coolant inventory rapidly decreases to the []^(a,b,c) lbm level (corresponding to the elevation of cold-leg nozzles on the vessel) and the CMT draindown mode of operation is initiated. Since the CMT draindown flow rate (approximately []^(a,b,c) lbm/sec.) is less than the break flow rate (approximately []^(a,b,c) lbm/sec.), the CMT draindown is uninterrupted and ADS-1 actuates at []^(a,b,c) seconds. Although the primary system pressure has dropped to approximately []^(a,b,c) psia before ADS-1, there is very little discharge of coolant from the accumulators. When ADS-1 occurs, the coolant inventory is still near []^(a,b,c) lbm and essentially all of the accumulator water inventory is still available for refilling the power channel. The minimum coolant inventory is []^(a,b,c) lbm, and occurred at []^(a,b,c) seconds just prior to IRWST injection.

Test S00401, the 1-in. break, is four times smaller than the S00303 2-in. break, and therefore, the inventory decreases to the []^(a,b,c) lbm net coolant inventory level at a slower rate. As the inventory approaches []^(a,b,c) lbm, the cold legs begin to void, causing the CMT balance lines to drain. The CMTs then start a period of natural circulation combined with intermittent periods of draindown, which increases their overall injection rate sufficiently to keep the water level at the cold-leg nozzle elevation. At this time, the break flow is less than the overall injection from the CMTs and accumulator injection. (Because of the long time for draindown, the primary system pressure had dropped below []^(a,b,c) psia, and the accumulators provided a small amount of injection and delivered []^(a,b,c) percent of their water inventory). Following ADS-1 (about []^(a,b,c) seconds), the accumulators have less coolant inventory to inject. Therefore, the minimum coolant inventory prior to IRWST injection at []^(a,b,c) seconds is []^(a,b,c) lbm. This is []^(a,b,c) lbm less than the minimum inventory for S00303 and resulted from the expenditure of accumulator inventory prior to ADS-1; so less water was available for injection between ADS-1 and ADS-4. Therefore, a lower minimum coolant inventory occurs for the 1-in. break (S00401) compared to the 2-in. break (S00303). The lower minimum inventory is also reflected in the higher rod bundle steam fraction prior to IRWST injection, at the time of the minimum inventory for the 1-in. break.

Figure 5.4-2 shows the coolant inventory for S00908 (DEG of the CMT-B balance line) and S00706 (DEG of the DVI-B line). These two large-break events are very different from the small breaks and also from each other. S00908 is effectively a single-ended break, since the check valve in the CMT-B

discharge line prevented break flow from the CMT side of the break. The average total break flows for the first []^(a,b,c) sec. were []^(a,b,c) lbm/sec. for S00908 and []^(a,b,c) lbm/sec. for S00706. Additionally, the break elevations are different. In S00908, the break location is effectively on the top of cold-leg B2 at []^(a,b,c) ft.; and in S00706, it is at []^(a,b,c) ft., referenced to hot-leg centerline elevation. The discussion in Section 5.3 shows that the break elevation has an impact on the break flow and coolant inventory.

In S00706, there is a complete loss of injection from CMT-B, accumulator-B, and only one of two IRWST injection lines. This, in addition to the high break flow, resulted in the lowest minimum coolant inventory of all the tests performed at SPES-2. The coolant inventory in the power channel at []^(a,b,c) seconds is calculated to be approximately []^(a,b,c) lbm, which still provided cooling of the rod bundle with a high steam fraction ([]^(a,b,c) percent) two-phase fluid flow (see subsection 4.2.8, data plots 30 and 31). Figure 5.4-3 demonstrates that rod bundle cooling is adequate. This figure shows the difference between the temperature of heater rod no. 87 (at the highest elevation in the core (TW020P87) and the saturation temperature corresponding to primary system pressure for S00706 and S00303. In S00706, the rod temperature exceeded saturation temperature by approximately []^(a,b,c)°F when the highest void fraction occurred in the rod bundle and was about []^(a,b,c)°F above saturation when minimum coolant inventory occurred. This compares to test S00303, shown in Figure 5.4-5. The S00706 rod temperature was not much different from the reference test S00303, despite the much higher void fraction in the rod bundle.

*In test S00908 (the DEG balance line break), the break flow was greater than the injection flows until []^(a,b,c) seconds, and the inventory to decreased to []^(a,b,c) lbm (below the []^(a,b,c) lbm seen for the smaller breaks). The injection flow from CMT-A and from both accumulators was greater than the break flow from []^(a,b,c) seconds until []^(a,b,c) seconds, and the coolant inventory increased to []^(a,b,c) lbm by the end of the accumulator injection. The break location for S00908 in the CMT-B balance line eliminates normal injection from CMT-B. Comparison of coolant inventory of S00908 (Figure 5.4-2) with S00303 (Figure 5.3-7) shows that the S00908 inventory was only []^(a,b,c) lbm lower for S00908 after the accumulator injection. Also, the minimum inventory (occurring at []^(a,b,c) seconds for S00908) was only []^(a,b,c) lbm lower than S00303. Test S00908, in terms of severity (power channel inventory), was more similar to Test S00303 than Test S00706. This similarity is also reflected in the minimum downcomer level and steam fraction in the rod bundle shown in Table 5.1-1.

In summary, the 2-in. breaks at or above the cold-leg elevation, with only passive safety systems, resulted in minimum downcomer levels near []^(a,b,c) ft. The 1-in. break, at or above the cold-leg elevation, resulted in a downcomer levels near []^(a,b,c) ft. due to the delayed ADS-1 actuation, which resulted in the expenditure of accumulator inventory prior to ADS-1.*

Test S00706 (the DEG of the DVI-B), had a minimum downcomer level below []^(a,b,c) ft. This low level was the combined result of the high break flow, the complete loss of the B side passive safety systems injection, and the low elevation of the break location. Comparison of S00706 with S00605 (2-in. DVI break) indicates that the larger break size of S00706 results in a downcomer level that is []^(a,b,c) ft lower at the time of minimum inventory (prior to the IRWST injection).

The following figures have been intentionally deleted
from this document due to their proprietary nature.

5.5 Effects of Nonsafety Systems

The effect of nonsafety systems operation on the passive safety system response and overall plant response can be assessed by comparing the baseline test S00303 with test S00504. S00504 is a 2-in. break in the bottom of cold leg B-2, with the CVCS and NRHR pumped injection and SFWS addition to the steam generators simulated. The CVCS injection started on the safety systems actuation (S) signal, and the NRHR started to inject coolant after ADS-3 when the primary system pressure was reduced to less than the NRHR pump discharge pressure.

Table 5.1-1 shows that S00504 is very similar to S00303 had until ADS-1 was actuated. The reactor trip (R) and the S signals occurred at nearly identical times, and the pressure decay curves had similar slopes. The rod bundle stem fraction prior to ADS were very similar for the two tests. The CVCS injection did not seem to have significant impact on the initial part of the test although the maximum possible flow from two CVCS pumps was simulated. However, the water addition by the CVCS did impact the initiation of the CMT draindown mode of operation, which was delayed by approximately []^(a,b,c) seconds for CMT-B and []^(a,b,c) seconds for CMT-A relative to S00303. Therefore, ADS-1 occurred approximately []^(a,b,c) seconds later for S00504. The NRHR flows started at approximately []^(a,b,c) seconds when the primary pressure was approximately []^(a,b,c) psia and reached full flow at []^(a,b,c) seconds. As seen in subsection 4.2.4, data plot 33, the CMTs' draindown stopped when the NRHR flow started (at []^(a,b,c) seconds) due to the backpressure the NRHR flow imposes on the CMT discharge line. ADS-4 never occurs since the CMT draindown stopped before reaching the []^(a,b,c) percent trip level. The CMTs started to refill at approximately []^(a,b,c) seconds. Due to the injection provided by the CVCS and the NRHR, the level in the annular downcomer only dropped to []^(a,b,c) ft below the hot-leg centerline before refilling, compared with a minimum level of []^(a,b,c) ft for S00303.

Figure 5.5-1 shows the coolant inventory for S00504 and S00303. The CVCS injection affected the coolant inventory during the first part of the S00504 event, maintaining it close to []^(a,b,c) lbm until ADS-1 occurred. The accumulator injection then increased the coolant inventory to []^(a,b,c) lbm, approximately []^(a,b,c) lbm more than S00303. The inventory losses after the accumulator delivery are similar for the two events, until the NRHR injection matched the primary system inventory loss out the break (approximately []^(a,b,c) seconds), and then refill of the system started. The minimum inventory for the S00504 was []^(a,b,c) lbm and occurred when the minimum downcomer level of []^(a,b,c) ft occurs.

The nonsafety systems had a significant and ameliorating effect on the SPES-2 LOCA events. The additional coolant injection provided by the CVCS increased the coolant inventory prior to ADS-1, although the core steam fractions was not noticeably affected. The NRHR injection limited the minimum coolant inventory after the accumulator injection, and in fact refilled the primary system and subcooled the rod bundle. The high rod bundle steam fraction that occurred in test S00303, prior to IRWST injection did not occur in test S00504.

The following figures have been intentionally deleted
from this document due to their proprietary nature.

5.6 Other Key Test Results

This section discusses some of the special purpose LOCA tests that were performed in SPES, and the non-LOCA events (steam generator tube ruptures and SLB).

5.6.1 Comparison of PRHR Performance

The effect of additional PRHR capability on the LOCA mitigation can be assessed by comparing test S00401 (performed with one PRHR tube) with test S01613 (performed with 3 PRHR tubes). Both of these tests are 1-in. breaks in the bottom of cold leg-B2.

Table 5.1-1 indicates only a few differences between S01613 and S00401 that exceed expected normal test data scatter. The PRHR performance measured for S01613 is []^(a,b,c) percent higher than for S00401, which shows that the []^(a,b,c) percent increase in heat transfer area for the PRHR HX yielded some additional heat transfer. The PRHR flow is slightly higher for S01613; however, the biggest difference is that the PRHR HX exit temperature is []^(a,b,c)°F to []^(a,b,c)°F lower for S01613 than for S00401. ADS-1 occurred []^(a,b,c) seconds later for S01613, which showed that the CMTs drained at a slower rate during the time when alternating recirculation/draindown was occurring, than S00401. The minimum downcomer level was []^(a,b,c) ft. lower in S00401.

Figure 5.6-1 shows the primary system pressures for the two tests and clearly shows that S01613 pressure is decreasing more rapidly than S00401. This is a result of the higher PRHR heat removal for S01613. The faster pressure decrease resulted in more accumulator injection, which delayed the full transition to draindown injection from the CMTs and accordingly delayed the ADS-1 actuation.

Figure 5.6-2 shows the coolant inventory for tests S00401 and S01613. Both tests spend an extended time period at the []^(a,b,c) lbm inventory level. In S01613, however, the CMTs expended less inventory maintaining the coolant inventory at the []^(a,b,c) lbm level, due to the additional injection from the accumulators caused by the lower system pressure. ADS-1 was therefore delayed for S01613 relative to S00401. When ADS-1, 2, and 3 occur, approximately []^(a,b,c) lbm less fluid was discharged through ADS for S01613 due to the lower initial system pressure at the start of ADS. Therefore, S01613 had more coolant inventory than S00401 after the accumulator delivery, as shown in Figure 5.6-2. The net coolant losses from the end of accumulator delivery until the start of IRWST injection were very similar for the two events. However, since S01613 started this period with more coolant inventory, it also ended with more inventory than S00401, at the point of minimum coolant inventory in the vessel.

The greater PRHR heat removal in S01613 increased the primary system pressure decrease relative to S00401 prior to ADS-1. The overall effect of the lower system pressure mitigated the severity of the test.

5.6.2 Test Repeatability

The repeatability of the SPES-2 facility is demonstrated by a comparison of baseline test S00303, which was the first matrix test performed, with test S01703. Matrix test S01703 was the last matrix test and was performed at the conclusion of the SPES-2 test program. Test S01703 was performed at initial conditions as similar as possible to S00303.

Subsection 4.2.3 provides a detailed comparison of S01703 and S00303. There are very small differences shown in the comparison, and those that are shown can be explained as slight differences in initial conditions (Figure 5.6-3). Table 5.1-1 shows that there are no significant differences between the two tests, beyond what would be expected based on normal data scatter. The test facility repeatability demonstrated by tests S00303 and S01703 is clearly very good, and gives good confidence that the test to test differences observed in the matrix tests (as shown in Table 5.1-1), are real differences resulting from the differences in the transients being simulated.

5.6.3 Comparison of Steam Generator Tube Rupture

The steam generator tube rupture events S01110 (SGTR without nonsafety systems) and S01309 (SGTR with nonsafety systems and operator actions) are individually discussed in subsections 4.2.12 and 4.2.11 respectively. There were significant differences between the two tests and these are attributable to the effects of the nonsafety systems operating for S01309. Specifically the use of the SFW system and the steam generator-A PORV to maintain the primary system cooldown rate provided sufficient heat removal to maintain single-phase flow conditions in the primary system. Also, the pressurizer heater operation was maintained in S01309 until low pressurizer level occurred.

Figure 5.6-4 shows the primary system pressure for the two tests, depicting the S01309 pressure to be lower than S01110 due to the additional cooling provided by CVCS injection, SFWS addition, and steam generator-A PORV actuation. Figure 5.6-5 shows that the primary system pressure is higher than the steam generator-A pressure throughout the test for S01309. The steam generator-A provides sufficient heat removal from the primary system to maintain the primary system at single phase flow conditions. This, as seen in the dPs in the steam generator-A U-tubes, showing that primary system natural circulation flow was maintained through steam generator-A.

Figure 5.6-6 compares the rod bundle differential pressure for the two transients, showing that significant two-phase flow conditions started at approximately []^(a,b,c) seconds for S01110, while S01309 maintained single phase flow through the core until the test termination.

Figure 5.6-7 shows that the pressurizer levels differed greatly between the two tests. In S01110 the pressurizer refills completely by approximately []^(a,b,c) seconds, at which time the only steam volume in the primary system is in the upper head. In S01309, the pressurizer partially refilled at []^(a,b,c) seconds in response to venting through the ADS-1 flow path by operator action, and a low level was maintained for the rest of the test. The measured temperatures in the pressurizer in S01110 indicated that the pressurizer was subcooled at []^(a,b,c) seconds, at which time the pressurizer

completely filled. In S01309, the top of the pressurizer was superheated throughout the test, which is the reason it never fills completely. This occurred in part, because in S01309, the pressurizer heater was kept on and maintained full pressure/temperature until the pressurizer water level decreased to approximately []^(a,b,c) ft. at []^(a,b,c) seconds. In test S01110, the heater power was not sufficient to maintain pressurizer pressure and temperature. In addition since the pressure is significantly lower for S01309 (due to the additional heat removal), and the cooldown of the metal mass in the pressurizer lags the TSAT for the system.

In both of these tests the ADS was not actuated since the CMTs remained in their natural recirculation mode throughout the test.

The following figures have been intentionally deleted
from this document due to their proprietary nature.

BLIND TEST DISCLAIMER

All blanks within the asterisks represent deleted text that relates to the blind tests, which will be provided at a later date.

6.0 OBSERVATIONS AND CONCLUSIONS

The primary purpose of the test data discussed in this report is to provide a basis for validating computer codes developed for analysis of transients in the AP600 plant. The observations and conclusions made in this document are only applicable to the SPES-2 facility.

Key observations and conclusions are made from the SPES-2 testing in the following categories:

Overall Test Observations

1. * *
2. *

*

3. * *
4. * *
5. * *

Specific Observations for Small Break Loss-of-Coolant Accident Tests

6. Following a 2-in. LOCA, operation of the active, nonsafety chemical and volume control system (CVCS) and/or normal residual heat removal system (NRHR) had little effect prior to ADS-1 actuation; however, increased primary system inventory was observed after ADS-1, due to the active safety systems.
7. Following a 2-in. LOCA, operation of the active, nonsafety NRHR system prevented CMT draindown and ADS-4 actuation.
8. The 1-in. cold leg-B break resulted in higher void fraction/lower water inventory in the vessel than all 2-in. breaks simulated.
9. * *

10. *

*

11. Increasing the PRHR HX heat transfer area by 200 percent (from one tube to three tubes) resulted in only a []^(a,b,c) percent increase in heat transfer rate with two-phase flow inlet conditions.

Specific Observations for Steam Generator Tube Rupture Steam Line Break Tests

12. *

*

13. Nonsafety system operation and operator actions following the SGTR maintained the primary system in a subcooled condition and prevented hot leg voiding.

Test and Data Quality Conclusions

14. Thirteen of 17 tests performed in SPES-2 were determined to be acceptable for code validation purposes.
15. The repeatability of the facility and measured data was excellent, as evidenced by the comparison of S00303 with repeat test S01703 and by the consistency of test initial and boundary conditions.
16. The SPES-2 upper-head initial temperature was approximately []^(a,b,c) °F lower than the temperature originally specified in the test specification; however, consistent upper-head initial temperatures were maintained from test to test.
17. The gamma-densitometer and turbine flow meters did not provide useful data. The use of gamma-densitometers in small, heavy walled piping caused alignment and signal strength problems. Flow slugs/high flow velocity resulted in damage to the turbine flow meters. Electro-magnetic interference from the heater rods and power source caused problems with the signals from both the gamma-densitometer and the turbine meters.
18. The failure rate of the heated rod thermocouples was very high, but a sufficient number of thermocouples were operational to monitor the bundle temperature.

7.0 REFERENCES

1. *SPES-2 Facility Description*, WCAP-14073, Revision 0, May 1994.
2. Quick Look Reports:

PXS-T2R-011 SPES-2 Matrix Test S00303 Quick Look Report, June 1994
PXS-T2R-020 SPES-2 Matrix Test S00401 Quick Look Report, July 1994
PXS-T2R-021 SPES-2 Matrix Test S00504 Quick Look Report, July 1994
PXS-T2R-022 SPES-2 Matrix Test S00605 Quick Look Report, July 1994
PXS-T2R-023 SPES-2 Matrix Test S00706 Quick Look Report, July 1994
PXS-T2R-024 SPES-2 Matrix Test S00908 (Blind Test) Quick Look Report, July 1994
PXS-T2R-025 SPES-2 Matrix Test S01007 Quick Look Report, July 1994
PXS-T2R-026 SPES-2 Matrix Test S01110 Quick Look Report, July 1994
PXS-T2R-031 SPES-2 Matrix Test S01211 (Blind Test) Quick Look Report, October 1994
PXS-T2R-029 SPES-2 Matrix Test S01309 Quick Look Report, October 1994
PXS-T2R-032 SPES-2 Matrix Test S01512 (Blind Test) Quick Look Report, November 1994
PXS-T2R-033 SPES-2 Matrix Test S01613 Quick Look Report, December 1994
PXS-T2R-034 SPES-2 Matrix Test S01703 Quick Look Report, December 1994
3. *SPES-2 AP600 FHFP Integral Systems Test Specification*, PXS-T1P-002, Rev. 0, November 8, 1993.
4. *SPES-2, Scaling Update*, SIET Document No. 00185 RI92, Rev. 0, November 12, 1992.
5. *SPES-2 Cold Pre-Operational Test Results*, SIET Document No. 00238RP93, April 29, 1994.
6. *SPES-2 Hot Pre-Operational Test Results*, SIET Document No. 00311RP94, March 6, 1994.

APPENDIX A
DATA REDUCTION METHODS AND VALIDATION PROCESS

A-1 Introduction

The overall data reduction and data validation process is described in Section 3.0. This appendix describes the specific details of how the data was reduced and validated. It also provides examples of some data reduction and validation steps.

A-2 Day-of-Test Report

The first step in the data validation process, writing the Day-of-Test Report, was performed by the test site personnel immediately following the test. (A sample of the format for the report is shown in Figure A-1.) The Day-of-Test Report was issued with the electronic data files to the Westinghouse Energy Center within a couple of days of the test. Typically, the Day-of-Test Report was reviewed in parallel with processing the data files and plotting the data at Westinghouse.

Communications between the test site and Westinghouse Energy Center were not limited to the Day of-Test Report. Frequent telecommunications were held between the two sites. Additionally, there was always a Westinghouse test engineer at the site when a test was performed.

A-3 SPES_REDUCE Software

The electronic data file received from SIET contained test data in metric engineering units. Immediately following receipt of the data file, this data were converted at Westinghouse to English engineering units using the SPES_REDUCE program. The conversion factors used were as follows:

<u>Measurements</u>	<u>Units</u>	<u>Conversion Factors</u>
Differential pressure	kPa to psid	divide by 6.894
Mass flow	kg/sec. to lbm/sec.	divide by 0.454
Mass flow	g/sec. to lbm/sec.	divide by 454 (for those channels which end in g)
Mass	kg to lbm	divide by 0.454
Pressure	mPa to psia	divide by 0.00689
Temperature	°C to °F	multiply by (1.8°C) +32
Volumetric flow	dm ³ /sec. to ft. ³ /sec.	divide by 28.32
Fluid height	m to ft.	divide by 0.3048

Other units (such as amps, volts, kilowatts, or rpm) did not need to be converted.

SPES_REDUCE also assigned a 0 time to the data corresponding to the break initiation time. This was necessary since the data acquisition system (DAS) at the SPES-2 facility was started well in advance of the start of the test. Therefore, the recorded time was not relative to the test initiation. The break initiation time for each test was provided by SIET and input by Westinghouse to the

SPES_REDUCE software. The break initiation time was subtracted from each recorded time, which created some negative time data (about 5 minutes of pre-test data).

The output file from SPES_REDUCE was named SXXXYY.Master.Data, where XXX was the test sequence number and YY was the matrix number. This file was transmitted to the Nuclear Regulatory Commission (NRC) along with the Quick Look Report (QLR).

A-4 SPES_CORRECT Software

In several instances, it was necessary to modify the data received from SIET. The SPES_CORRECT software was used to modify the data by the following formula:

$$\text{NEW} = a * (\text{OLD} + b)^d + c$$

where:

NEW = newly created data
OLD = data to be modified or corrected
a, b, c, d = constants

The test data in Appendix A-4.1 and A-4.2 were modified using the above formula.

A-4.1 Test S00303

Since the in-containment refueling water storage tank (IRWST) flow differential pressure (dP) cells (F-A60E/F-B60E) were over-ranged, an alternate dP cell in the IRWST flow line could be used (DP-A61E/DP-B61E). The dP measurement was converted to flow using the calibration coefficients from the cold flow pre-operational tests.

For IRWST line A:

$$F_{A61E} = [\quad]^{(a,b,c)} * (DP-A61E + [\quad]^{(a,b,c)})$$

where:

$$\begin{matrix} a \\ b \\ c \\ d \end{matrix} = \left[\begin{matrix} \quad \\ \quad \\ \quad \\ \quad \end{matrix} \right]^{(a,b,c)}$$

For IRWST line B:

$$F_{B61E} = [\quad]^{(a,b,c)} * (DP-B61E + [\quad]^{(a,b,c)})$$

where:

$$\begin{aligned} a &= [\quad]^{(a,b,c)} \\ b &= [\quad] \\ c &= [\quad] \\ d &= [\quad] \end{aligned}$$

The respective data for IRWST line A are shown in Figure A-2; and the data for IRWST line B are shown in Figure A-3. F-A60E and F-B60E are the over-ranged dP cells; and F_A60E and F_B60E are the corresponding calculated flow rates. DP-A61E and DP-B61E are the measured dP measurements; and F_A61E and F_B61E are the respective calculated flow rates.

A-4.2 Test S01512

The startup feedwater flow (SFW) was not provided directly by SIET on the data tape; however, the calibration coefficients were provided. These coefficients were used in the SPES_CORRECT software to calculate the respective flow rates from the dP cells.

For SFW-A:

$$F_{A20A} = [\quad]^{(a,b,c)} * (F_{A20A})^{(a,b,c)}$$

where:

$$\begin{aligned} a &= [\quad]^{(a,b,c)} \\ b &= [\quad] \\ c &= [\quad] \\ d &= [\quad] \end{aligned}$$

The same equation applies to SFW-B.

A-4.3 Tests S00303, S00401, S00504, S00605, S00908, S01007, S01110

After these tests were run, SIET determined that the reference leg on DP-000P was incorrect in the calibration file. A value of []^(a,b,c) psi was subtracted from channel DP-000P for these seven tests, since the elevation between the pressure taps was []^(a,b,c) ft. ([]^(a,b,c) m) instead of []^(a,b,c) ft. ([]^(a,b,c) m), which was previously used. For tests completed after the S01110 test, the calibration file was corrected at the SPES-2 facility.

An example of the corrected and uncorrected data is shown in Figure A-4. The output file from SPES_REDUCE was modified by the SPES_CORRECT software.

A-4.4 Test S00504

The normal residual heat removal (NRHR) flows were not provided directly by SIET in the data tape; however, the calibration coefficients were provided in the SPES-2 Facility Description Report. These coefficients were used in the SPES_CORRECT software to calculate the respective flow rate from the dP cells.

For NRHR-A:

$$F_A00E = [\quad]^{(a,b,c)} * (F-A00E)^{l \quad (a,b,c)}$$

For NRHR-B:

$$F_B00E = [\quad]^{(a,b,c)} * (F-B00E)^{l \quad (a,b,c)}$$

After test S00504 was performed, it was determined that channel T-A021PL (cold leg-A1 to downcomer inlet temperature) was reading [$\quad]^{(a,b,c)}$ °C too high, therefore SPES_CORRECT was used to subtract [$\quad]^{(a,b,c)}$ °F from each recorded value.

A-4.5 Test S00706

In the detailed review of the data, it was determined that the calculation of the accumulator-B level (L_B20E) for test S00706 was incorrect for a portion of the test. This was attributed to a temperature used in the fluid level calculation measuring lower than [$\quad]^{(a,b,c)}$ °F for a short period of time. The SPES_CORRECT software was used to calculate the fluid level based upon the measured differential pressure and average accumulator temperature.

A-5 Initial Condition Validation Plots

To verify that the conditions prior to test initiation were properly established and within the acceptable tolerances, the NSA plot program was used to plot the actual data for the pre-test time period and the average of the respective data. The plot of the actual data with the average allowed the analyst to directly review the pre-test variations. The average of the data was also printed on these plots for tabulation in the QLRs. The following initial test conditions were assessed in this fashion:

- Rod power (W-00P)
- Pressurizer pressure (P-027P)
- Hot-leg temperatures (T-A03PL, T-A03PO, T-B03PL, T-B03PO)
- Vessel inlet temperature (T-003P)
- Vessel flow rate (F-003P)

- Cold-leg flow rate (F-A01P, F-A02P, F-B01P, F-B02P)
- Downcomer/upper-head bypass flow rate (F-014P)
- Pressurizer level (L_010P)
- Accumulator level (L_A20E, L_B20E)
- Accumulator water temperature (T-A22E, T-B22E)
- Accumulator pressure (P-A20E, P-B20E)
- IRWST level (L_060E)
- IRWST water temperature (T-063E)
- PRHR supply line temperature (T-A82E)
- Upper-head average temperature (T-015P/T-016P)
- Cold-leg balance line (CLBL) temperature (T-A142PL, T-B142PL)
- CMT level (L_A40E, L_B40E)
- CMT temperature (T-A411E, T-B411E)
- Steam generator level (L_A20S, L_B20S)
- Steam generator main feedwater (MFW) temperature (T-A01S, T-B01S)
- Steam generator pressure (P-A04S, P-B04S)

An example of this initial condition validation plot for test S00303 is shown in Figure A-5 for the pressurizer level.

A-6 Power Decay Curve Validation

To verify that the measured power decay curve was the same as the specified power decay curve, the NSA plot program was used to plot the specified normalized power against the corresponding measured normalized power. The measured power was normalized by calculating the ratio of the actual measured power by the average pre-test measured power as a function of time. An example of these specified and measured power decay curves for test S00303 are shown in Figure A-6.

The specified power decay curve is from Table 2.5-1 in Section 2.0.

A-7 NRC Notification

As a result of the ongoing SPES-2 data validation process, letters were issued to the NRC regarding any errors that were discovered in the previously published QLR. Two such letters were issued on the following subjects:

1. NTD-NRC-94-4310, "AP600 SPES-2 Test Quick Look Report Errata," October 10, 1994.

This letter documented that channel DP-000P was too high by a value of []^(a,b,c) psi in the Quick Look Report due to a calibration file error for eight tests (S00303, S00401, S00504, S00605, S00706, S00908, S01007, and S01110).

-
2. NTD-NRC-94-4334, "AP600 SPES-2 Test Quick Look Report Erratta No. 2,"
October 31, 1994.

This letter documented that eleven additional instruments were found to be failed due to an instrument card malfunction for three tests (S00605, S00706, and S00908 blind test).

DAY-OF-TEST REPORT

Test Facility: _____

Test No. _____ Date _____ Time _____

Initial Conditions:

Specified _____ Actual _____

Facility Configuration:

Specified _____ Actual _____

Any Observations, Unexpected Events During Test?

Any Failed Instruments Observed Prior to or During Test?

Any Deviation from Test Procedures?

Any Critical Instruments Functional? Plot Critical Instruments.

Any Facility Maintenance Performed Since Last Test?

Data Tape File Name(s):

Facility Engineer _____

Facility Manager _____

Figure A-1

SPES-2 TEST: S00303

Differential Pressure (psi)		Mass Flow Rate (lbm/s)				
A	—	F-A60E	108	0	0	IRWST inj. line A
B	- - -	DP-A61E	59	0	0	IRWST dischr. line A
Differential Pressure (psi)		Mass Flow Rate (lbm/s)				
C	- - - -	F_A60E	135	0	0	IRWST inj. line A
D	- - - -	F_A61E	481	0	0	IRWST Inj Line A

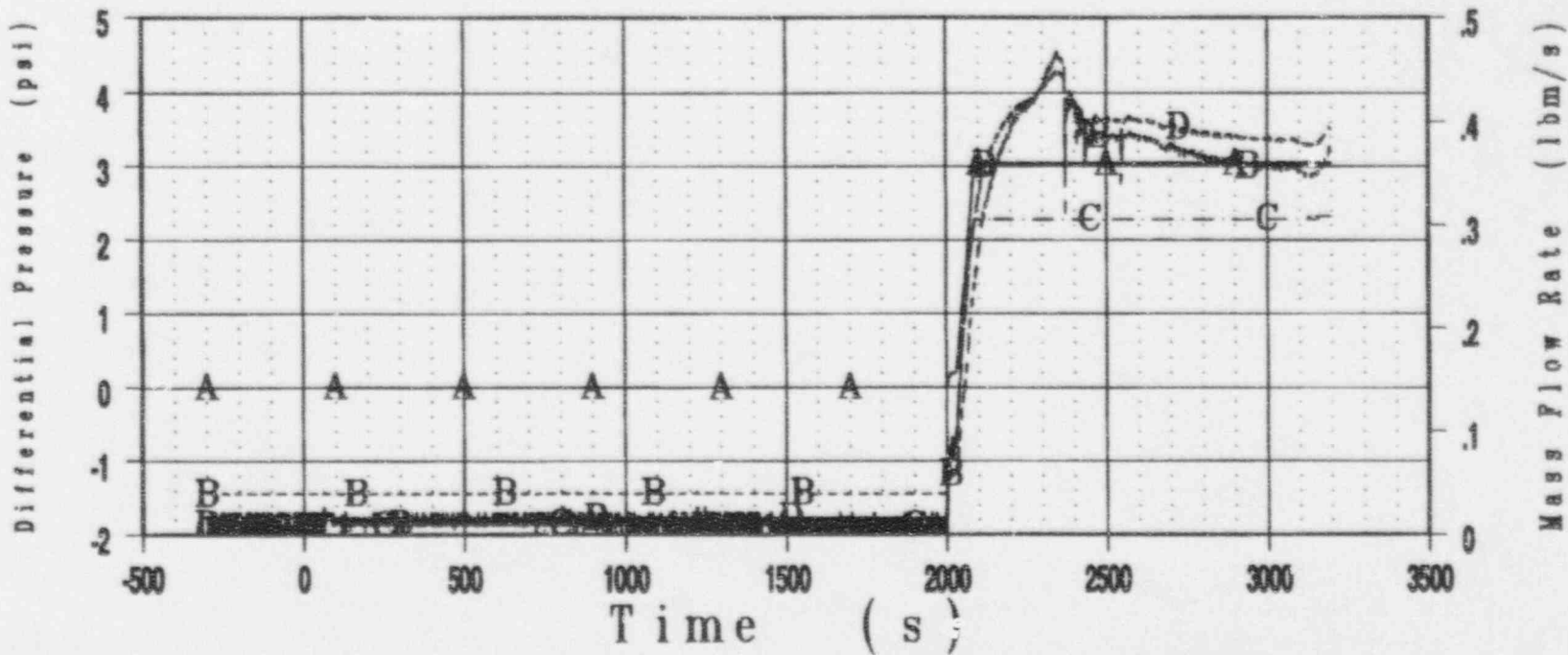


Figure A-2

SPES-2 TEST: S00303

Differential Pressure (psi)		Mass Flow Rate (lbm/s)			
A	—	F-B60E	120	0	IRWST inj. line B
B	- - -	DP-B61E	94	0	IRWST dischr. line B
Mass Flow Rate (lbm/s)					
G	- - - - -	F_B60E	143	0	IRWST inj. line B
D	- - -	F_B61E	482	0	IRWST Inj Line B

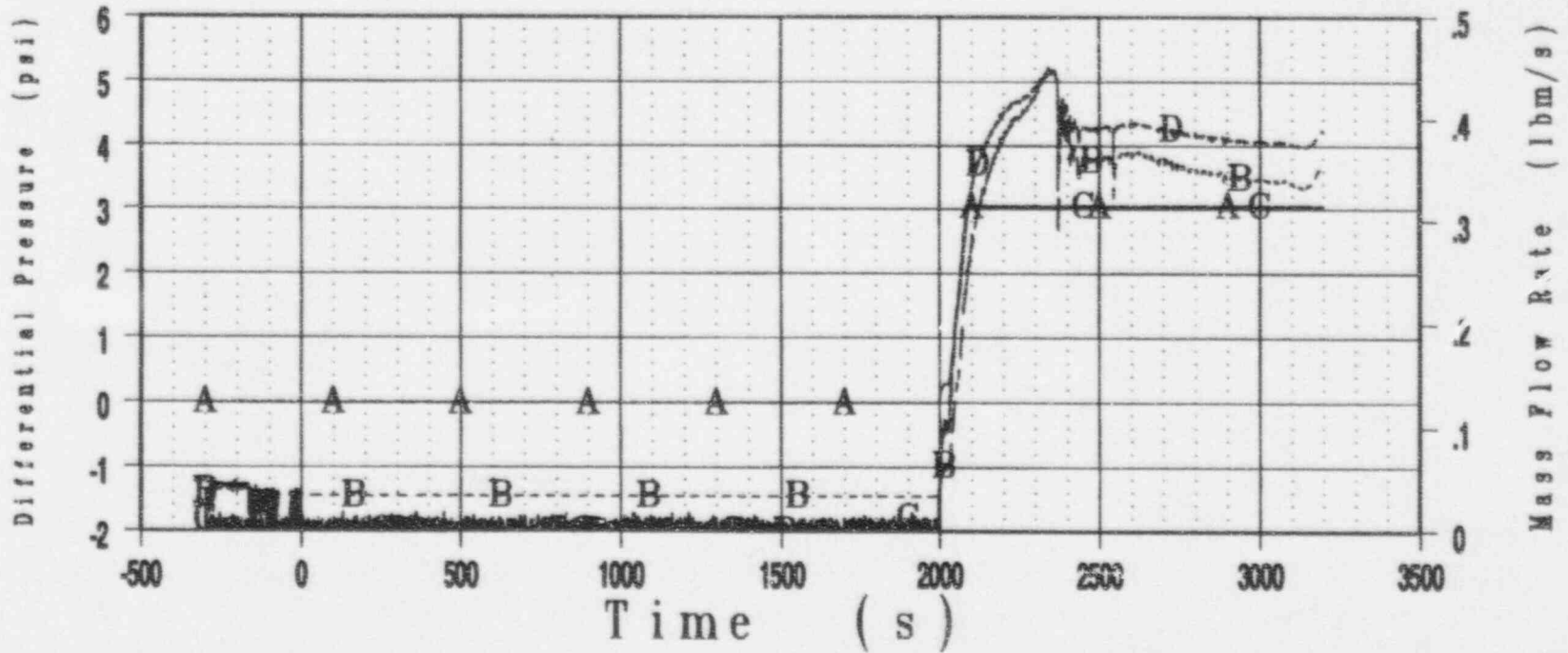


Figure A-3

ADS\$USER:S00303_SPES.DAT
Creation Date : Tue Sep 13 09:58:39 1994
SPES_REDUCE 1.2
30-APR-1994 12:08:58 AT
TP C1994/08/ 1 X1994/09/06 15:
----- DP-000P 3 0 0 PC DP -15" to 142"
----- DP-000P 483 0 0 PC DP -15" to 142"

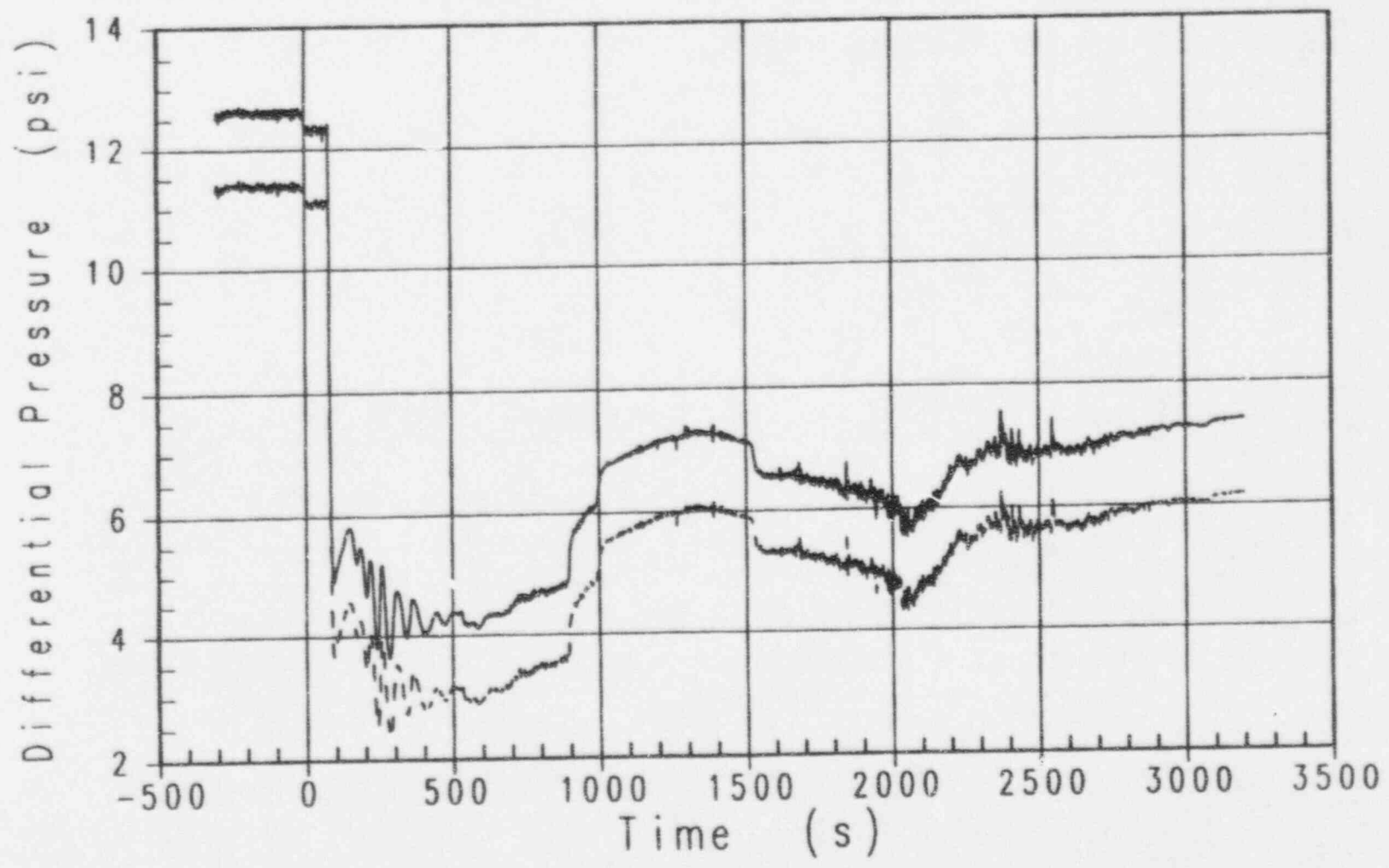


Figure A-4

ADS\$USER:S00303_SPES.DAT

———	L_010P	168	0	0 PRZ Level
----	12.3729	1	0	0 AVG of First 300 sec

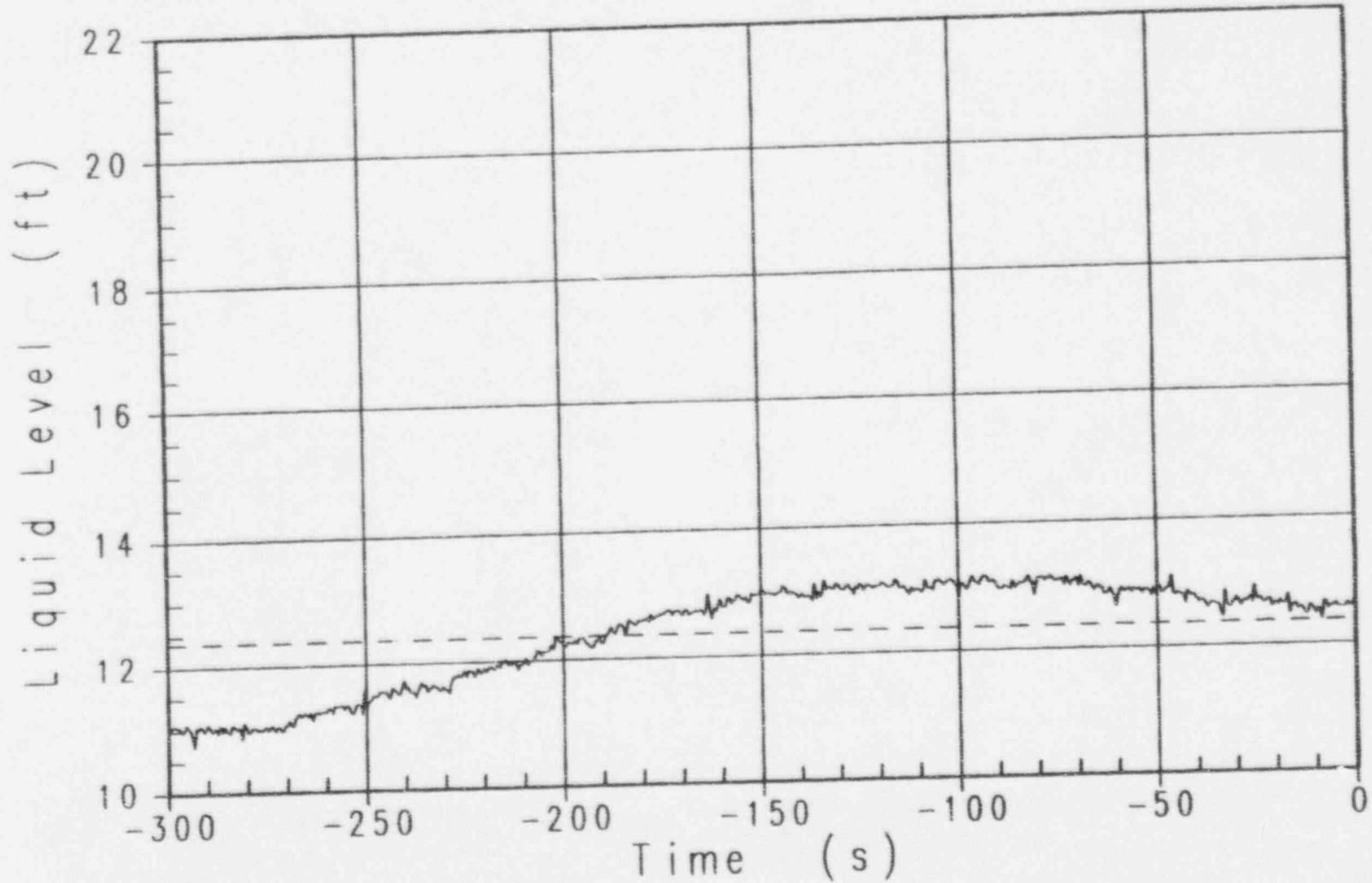


Figure A-5

ADS\$USER: S00303 SPES.DAT

465 0 Measured Power S003
1 0 Specified Power

— MPD
- - - SPD

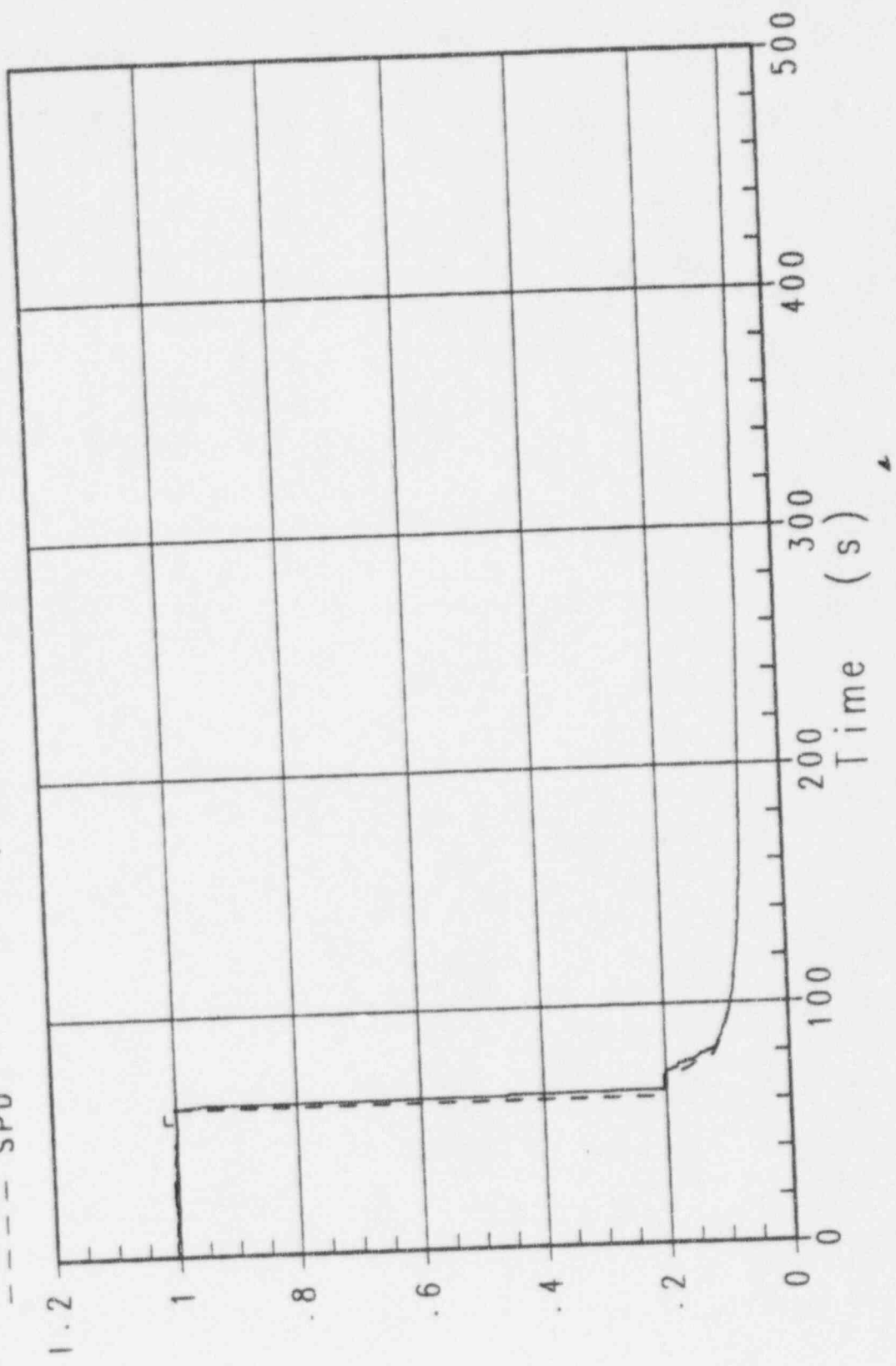


Figure A-6

**APPENDIX B
DATA VALIDATION**

APPENDIX B DATA VALIDATION

This appendix lists the results of the data validation review process described in Section 3.2. Table B-1 gives an overview of the results on a test-by-test basis. Table B-2 gives the mass balance results for for each test. Tables B-3 through B-15 give the results of the test initial conditions. At the end of the appendix, detailed plots of the measured power (W-00P) versus the specified power are given for each test.

**TABLE B-1
DATA VALIDATION PROCESS RESULTS**

Test Run Number	Test Date	Day of Test Report Review	Quick Look Report Review	Final Report Review	Comments
S00103	2/5/94	Accepted	Not Accepted	N/A	Not accepted due to setpoints change.
S00203	4/9/94	Accepted	Accepted	Not Accepted	Not accepted due to deletion of PZR to CMT balance line from AP600 design. QLR not issued.
S00303	4/30/94	Accepted	Accepted	Accepted	Data valid
S00401	5/6/94	Accepted	Accepted	Accepted	Data valid
S00504	5/18/94	Accepted	Accepted	Accepted	Data valid
S00605	5/27/94	Accepted	Accepted	Accepted	Data valid
S00706	6/10/94	Accepted	See comment	Accepted	QLR review revealed a deviation from specified power requirement. See subsection 4.2.8 for specifics.
S00807	6/15/94	Not Accepted	N/A	N/A	Data unacceptable. Day of test report revealed equipment failure nullified test results.
S00908 (blind)	6/23/94	Accepted	Accepted	Accepted	Data valid
S01007	7/7/94	Accepted	Accepted	Accepted	Data valid
S01110	7/14/94	Accepted	Accepted	Accepted	Data valid
S01211 (blind)	9/7/94	Accepted	Accepted	Accepted	Data valid
S01309	9/22/94	Accepted	Accepted	Accepted	Data valid
S01412	10/7/94	Not Accepted	N/A	N/A	Data unacceptable. Day of test report revealed equipment failure nullified test results.
S01512 (blind)	10/11/94	Accepted	Accepted	Accepted	Data valid
S01613	10/15/94	Accepted	Accepted	Accepted	Data valid
S01703	11/11/94	Accepted	Accepted	Accepted	Data valid

**TABLE B-2
MASS BALANCE RESULTS**

Test Run Number	Test Date	Final Mass/Initial Mass * 100 (%)	Acceptable within 10%
S00303	4/30/94	<input type="checkbox"/> (a,b,c)	Yes
S00401	5/6/94	<input type="checkbox"/>	Yes
S00504	5/18/94	<input type="checkbox"/>	Yes. Injection of water by non-safety systems contributes to discrepancy in mass balance.
S00605	5/27/94	<input type="checkbox"/>	Yes
S00700	6/10/94	<input type="checkbox"/>	Yes
S00908 (blind)	6/23/94	<input type="checkbox"/>	Yes
S01007	7/7/94	<input type="checkbox"/>	Yes
S01110	7/14/94	<input type="checkbox"/>	Yes
S01211 (blind)	9/7/94	<input type="checkbox"/>	Yes
S01309	9/22/94	<input type="checkbox"/>	Yes. Injection of water by non-safety systems contributes to discrepancy in mass balance.
S01512 (blind)10/11/94		<input type="checkbox"/>	No. The complex geometries of the steam generators may contribute to the discrepancy in the mass balance.
S01613	10/15/94	<input type="checkbox"/>	Yes
S01703	11/11/94	<input type="checkbox"/>	Yes

TABLE B-3
COMPARISON OF SPECIFIED AND ACTUAL TEST CONDITIONS FOR S00303

Condition (Instruments)	Specified	Actual	Comment
Rod Power (W-00P)	4991.6 ± 100 kW*	<input type="checkbox"/>	OK
Pressurizer Pressure (P-027P)	2250 ± 29 psia	<input type="checkbox"/>	OK
Average Hot-Leg Temperature (T-A03PO/T-A03PL/ T-B03PO/T-B03PL)	599.9 ± 9°F	<input type="checkbox"/>	OK
		<input type="checkbox"/>	OK
		<input type="checkbox"/>	OK
		<input type="checkbox"/>	OK
Reactor Vessel (Core) Inlet Temperature (T-003P)	529.5 ± 9°F	<input type="checkbox"/>	OK
Core Flow Rate (F-003P)	51.26 ± 0.55 lbm/sec.	<input type="checkbox"/>	OK
Cold-Leg Flow Rate (F-A01P/F-A02P/F-B01P/ F-B02P)	12.92 ± 0.22 lbm/sec.	<input type="checkbox"/>	OK
		<input type="checkbox"/>	Accepted (F-A02P), avg. loop A flow is 12.95 lbm/sec.
		<input type="checkbox"/>	OK
		<input type="checkbox"/>	OK
Downcomer Upper-Head Bypass Flow Rate (F-014P)	0.40 ± 0.11 lbm/sec.	<input type="checkbox"/>	OK
Pressurizer Level (L-010P)	12.4 ± 1.25 ft.	<input type="checkbox"/>	OK
Accumulator Level (L-A20E/L-B20E)	7.64 ± 0.36 ft.	<input type="checkbox"/>	OK
		<input type="checkbox"/>	OK
Accumulator Water Temperature (T-A22E/ T-B22E)	68 ± 9°F	<input type="checkbox"/>	OK
		<input type="checkbox"/>	OK
Accumulator Pressure (P-A20E/P-B20E)	711 ± 14.5 psia	<input type="checkbox"/>	OK
		<input type="checkbox"/>	OK
IRWST Level (L-060E)	27.9 ± 0.33 ft.	<input type="checkbox"/>	OK
IRWST Water Temperature (T-063E)	68 ± 9°F	<input type="checkbox"/>	OK

*4893.7 kW before 0 time

**TABLE B-3 (Cont.)
COMPARISON OF SPECIFIED AND ACTUAL TEST CONDITIONS FOR S00303**

Condition (Instruments)	Specified	Actual (g,b,c)	Comment
PRHR Supply Line Temperature (T-A82E)	347 ± 45°F		Accepted. Sufficient to ensure initiation of natural circulation flow.
Upper Head Average Temperature (T-015P/T-016P)	564.8 ± 9°F		Accepted. Facility design limits maximum temperature to ≤ cold-leg temperature.
PR to CMT Balance Line Temperature (T-A28P/T-B28P)	644 ± 45°F		N/A
Cold-Leg Balance Line Temperature (T-A142PL/T-B142PL)	509 ± 9°F		Accepted. Sufficient to ensure initiation of natural circulation flow.
			Accepted (T-B142PL). Sufficient to ensure initiation of natural circulation flow.
CMT Level (L-A40E/L-B40E)	full		OK
			OK
CMT Temperature (T-A411E/T-B411E)	68 ± 9°F		OK
			OK
Steam Generator Level (L-A20S/L-B20S) Narrow Range	4.86 ± 0.49 ft.		Accepted (L-A20S). Will not impact test results.
			OK
Steam Generator MFW Temperature (T-A01S/T-B01S)	439 ± 12.6°F		OK
			OK
Steam Generator Pressure (P-A04S/P-B04S)	711 ± 29 psia		OK
			OK

TABLE B-4
COMPARISON OF SPECIFIED AND ACTUAL TEST CONDITIONS FOR S00401

Condition (Instruments)	Specified	Actual <small>(a,b,c)</small>	Comment
Rod Power (W-00P)	4991.6 ± 100 kW*	<input type="checkbox"/>	OK
Pressurizer Pressure (P-027P)	2250 ± 29 psia	<input type="checkbox"/>	OK
Average Hot-Leg Temperature (T-A03PO/T-A03PL/ T-B03PO/T-B03PL)	599.9 ± 9°F	<input type="checkbox"/>	OK
		<input type="checkbox"/>	OK
		<input type="checkbox"/>	OK
		<input type="checkbox"/>	OK
Reactor Vessel (Core) Inlet Temperature (T-003P)	529.5 ± 9°F	<input type="checkbox"/>	OK
Core Flow Rate (F-003P)	51.26 ± 0.55 lbm/sec.	<input type="checkbox"/>	OK
Cold-Leg Flow Rate (F-A01P/F-A02P/F-B01P/ F-B02P)	12.92 ± 0.22 lbm/sec.	<input type="checkbox"/>	Accepted (F-A01P), avg. loop A flow is 12.88 lbm/sec.
		<input type="checkbox"/>	OK
		<input type="checkbox"/>	OK
		<input type="checkbox"/>	OK
Downcomer Upper-Head Bypass Flow Rate (F-014P)	0.40 ± 0.11 lbm/sec.	<input type="checkbox"/>	OK
Pressurizer Level (L-010P)	12.4 ± 1.25 ft.	<input type="checkbox"/>	OK
Accumulator Level (L-A20E/L-B20E)	7.64 ± 0.36 ft.	<input type="checkbox"/>	OK
		<input type="checkbox"/>	OK
Accumulator Water Temperature (T-A22E/ T-B22E)	68 ± 9°F	<input type="checkbox"/>	OK
		<input type="checkbox"/>	OK
Accumulator Pressure (P-A20E/P-B20E)	711 ± 14.5 psia	<input type="checkbox"/>	OK
		<input type="checkbox"/>	OK
IRWST Level (L-060E)	27.9 ± .33 ft.	<input type="checkbox"/>	OK
IRWST Water Temperature (T-063E)	68 ± 9°F	<input type="checkbox"/>	OK

*4893.7 kW before 0 time

**TABLE B-4 (Cont.)
COMPARISON OF SPECIFIED AND ACTUAL TEST CONDITIONS FOR S00401**

Condition (Instruments)	Specified	Actual <small>(a,b,c)</small>	Comment
PRHR Supply Line Temperature (T-A82E)	347 ± 45°F	☐	Accepted. Sufficient to ensure initiation of natural circulation flow.
Upper-Head Average Temperature (T-016P)	564.8 ± 9°F		Accepted. Facility design limits maximum temperature to ≤ cold leg temperature.
PR to CMT Balance Line Temperature (T-A28P/T-B28P)	644 ± 45°F		N/A
Cold-Leg Balance Line Temperature (T-A142PL/T-B142PL)	509 ± 9°F		Accepted. Sufficient to ensure initiation of natural circulation flow.
			Accepted (T-B142PL). Sufficient to ensure initiation of natural circulation flow.
CMT Level (L-A40E/L-B40E)	full		OK
			OK
CMT Temperature (T-A411E/T-B411E)	68 ± 9°F		OK
			OK
Steam Generator Level (L-A20S/L-B20S)	4.86 ± 0.49 ft.		OK
			OK
Steam Generator MFW Temperature (T-A01S/T-B01S)	439 ± 12.6°F		OK
			OK
Steam Generator Pressure (P-A04S/P-B04S)	711 ± 29 psia		OK
		☐	OK

TABLE B-5
COMPARISON OF SPECIFIED AND ACTUAL TEST CONDITIONS FOR S00504

Condition (Instruments)	Specified	Actual	(a,b,c) Comment
Rod Power (W-00P)	4991.6 ± 100 kW*	<input type="checkbox"/>	OK
Pressurizer Pressure (P-027P)	2250 ± 29 psia	<input type="checkbox"/>	OK
Average Hot-Leg Temperature (T-A03PO/T-A03PL/ T-B03PO/T-B03PL)	599.9 ± 9°F	<input type="checkbox"/>	OK
		<input type="checkbox"/>	OK
		<input type="checkbox"/>	OK
		<input type="checkbox"/>	OK
Reactor Vessel (Core) Inlet Temperature (T-003P)	529.5 ± 9°F	<input type="checkbox"/>	Accepted
Core Flow Rate (F-003P)	51.26 ± 0.55 lbm/sec.	<input type="checkbox"/>	OK
Cold-Leg Flow Rate (F-A01P/F-A02P/F-B01P/ F-B02P)	12.92 ± 0.22 lbm/sec.	<input type="checkbox"/>	OK
		<input type="checkbox"/>	Accepted (F-A02P), avg. loop A flow is 12.95 lbm/sec.
		<input type="checkbox"/>	OK
		<input type="checkbox"/>	OK
Downcomer-Upper Head Bypass Flow Rate (F-014P)	0.40 ± 0.11 lbm/sec.	<input type="checkbox"/>	OK
Pressurizer Level (L-010P)	12.4 ± 1.25 ft.	<input type="checkbox"/>	OK
Accumulator Level (L-A20E/L-B20E)	7.64 ± 0.36 ft.	<input type="checkbox"/>	OK
		<input type="checkbox"/>	OK
Accumulator Water Temperature (T-A22E/ T-B22E)	68 ± 9°F	<input type="checkbox"/>	OK
		<input type="checkbox"/>	OK
Accumulator Pressure (P-A20E/P-B20E)	711 ± 14.5 psia	<input type="checkbox"/>	OK
		<input type="checkbox"/>	OK
IRWST Level (L-060E)	27.9 ± .33 ft.	<input type="checkbox"/>	OK
IRWST Water Temperature (T-063E)	68 ± 9°F	<input type="checkbox"/>	OK

*4893.7 kW before time 0

**TABLE B-5 (Cont.)
COMPARISON OF SPECIFIED AND ACTUAL TEST CONDITIONS FOR S00504**

Condition (Instruments)	Specified	Actual <small>(g,b,c)</small>	Comment
PRHR Supply Line Temperature (T-A82E)	347 ± 45°F		Accepted. Sufficient to ensure initiation of natural circulation flow.
Upper-Head Average Temperature (T-016P)	564.8 ± 9°F		Accepted. Facility design limits maximum temperature to ≤ cold leg temperature.
PR to CMT Balance Line Temperature (T-A28P/T-B28P)	644 ± 45°F		N/A
Cold-Leg Balance Line Temperature (T-A142PL/T-B142PL)	509 ± 9°F		Accepted. Sufficient to ensure initiation of natural circulation flow. (T-A142PL)
			Accepted (T-B142PL). Sufficient to ensure initiation of natural circulation flow.
CMT Level (L-A40E/L-B40E)	full		OK
			OK
CMT Temperature (T-A411E/T-B411E)	68 ± 9°F		OK
			Accepted (T-B411E)
Steam Generator Level (L-A20S/L-B20S)	4.86 ± 0.49 ft.		OK
			OK
Steam Generator MFW Temperature (T-A01S/T-B01S)	439 ± 12.6°F		OK
			OK
Steam Generator Pressure (P-A04S/P-B04S)	711 ± 29 psia		OK
			OK

TABLE B-6
COMPARISON OF SPECIFIED AND ACTUAL TEST CONDITIONS FOR S00605

Condition (Instruments)	Specified	Actual (a,b,c)	Comment
Rod Power (W-00P)	4991.6 ± 100 kW*		OK
Pressurizer Pressure (P-027P)	2250 ± 29 psia		OK
Average Hot-Leg Temperature (T-A03PO/T-A03PL/ T-B03PO/T-B03PL)	599.9 ± 9°F		OK
			OK
			OK
			OK
Reactor Vessel (Core) Inlet Temperature (T-003P)	529.5 ± 9°F		OK
Core Flow Rate (F-003P)	51.26 ± 0.55 lbm/sec.		OK
Cold-Leg Flow Rate (F-A01P/F-A02P/F-B01P/ F-B02P)	12.92 ± 0.22 lbm/sec.		OK
			OK
			OK
			OK
Downcomer Upper-Head Bypass Flow Rate (F-014P)	0.40 ± 0.11 lbm/sec.		OK
Pressurizer Level (L-010P)	12.4 ± 1.25 ft.		OK
Accumulator Level (L-A20E/L-B20E)	7.64 ± 0.36 ft.		OK
			OK
Accumulator Water Temperature (T-A22E/ T-B22E)	68 ± 9°F		OK
			OK
Accumulator Pressure (P-A20E/P-B20E)	711 ± 14.5 psia		OK
			OK
IRWST Level (L-060E)	27.9 ± 0.33 ft.		OK
IRWST Water Temperature (T-063E)	68 ± 9°F		OK

*4893.7 kW before time 0

**TABLE B-6 (Cont.)
COMPARISON OF SPECIFIED AND ACTUAL TEST CONDITIONS FOR S00605**

Condition (Instruments)	Specified	Actual <small>(a,b,c)</small>	Comment
PRHR Supply Line Temperature (T-A82E)	347 ± 45°F	☐	Accepted. Sufficient to ensure initiation of natural circulation flow.
Upper-Head Average Temperature (T-015P/T-016P)	564.8 ± 9°F		Accepted. Facility design limits maximum temperature to ≤ cold leg temperature.
PR to CMT Balance Line Temperature (T-A28P/T-B28P)	644 + 45°F		N/A
Cold-Leg Balance Line Temperature (T-A142PL/T-B142PL)	509 ± 9°F		Accepted. Sufficient to ensure initiation of natural circulation flow.
			Accepted (T-B142PL). Sufficient to ensure initiation of natural circulation flow.
CMT Level (L-A40E/L-B40E)	full		OK
			OK
CMT Temperature (T-A411E/T-B411E)	68 ± 9°F		OK
			Accepted
Steam Generator Level (L-A20S/L-B20S)	4.86 ± 0.49 ft.		OK
			Accepted (L-B20S). Will not impact test results.
Steam Generator MFW Temperature (T-A01S/T-B01S)	439 ± 12.6°F		OK
			OK
Steam Generator Pressure (P-A04S/P-B04S)	711 ± 29 psia		OK
			OK

**TABLE B-7
COMPARISON OF SPECIFIED AND ACTUAL TEST CONDITIONS FOR S00706**

Condition (Instruments)	Specified	Actual	Comment
Rod Power (W-00P)	4991.6 ± 100 kW*		OK
Pressurizer Pressure (P-027P)	2250 ± 29 psia		OK
Average Hot-Leg Temperature (T-A03PO/T-A03PL/ T-B03PO/T-B03PL)	599.9 ± 9°F		OK
			OK
			OK
			OK
Reactor Vessel (Core) Inlet Temperature (T-003P)	529.5 ± 9°F		OK
Core Flow Rate (F-003P)	51.26 ± 0.55 lbm/sec.		OK
Cold Leg Flow Rate (F-A01P/F-A02P/F-B01P/ F-B02P)	12.92 ± 0.22 lbm/sec.		OK
			Accepted (F-A02P), avg. loop A flow is 12.95 lbm/sec.
			OK
			OK
Downcomer Upper-Head Bypass Flow Rate (F-014P)	0.40 ± 0.11 lbm/sec.		OK
Pressurizer Level (L-010P)	12.4 ± 1.25 ft.		OK
Accumulator Level (L-A20E/L-B20E)	7.64 ± 0.36 ft.		OK
			OK
Accumulator Water Temperature (T-A22E/ T-B22E)	68 ± 9°F		OK
			OK
Accumulator Pressure (P-A20E/P-B20E)	711 ± 14.5 psia		OK
			OK
IRWST Level (L-060E)	27.9 ± 0.33 ft.		OK
IRWST Water Temperature (T-063E)	68 ± 9°F		Accepted.

*4893.7 kW before time 0.

**TABLE B-7 (Cont.)
COMPARISON OF SPECIFIED AND ACTUAL TEST CONDITIONS FOR S00706**

Condition (Instruments)	Specified	Actual <small>(a,b,c)</small>	Comment
PRHR Supply Line Temperature (T-A82E)	> 212°F	<input type="checkbox"/>	OK
Upper-Head Average Temperature (T-015P/T-016P)	564.8 ± 9°F	<input type="checkbox"/>	Accepted. Facility design limits maximum temperature to ≤ cold leg temperature.
PR to CMT Balance Line Temperature (T-A28P/T-B28P)	644 ± 45°F	<input type="checkbox"/>	N/A
Cold-Leg Balance Line Temperature (T-A142PL/T-B142PL)	>329°F	<input type="checkbox"/>	OK
		<input type="checkbox"/>	OK
CMT Level (L-A40E/L-B40E)	full	<input type="checkbox"/>	OK
		<input type="checkbox"/>	OK
CMT Temperature (T-A411E/T-B411E)	68 ± 9°F	<input type="checkbox"/>	OK
		<input type="checkbox"/>	Accepted
Steam Generator Level (L-A20S/L-B20S)	4.86 ± 0.49 ft.	<input type="checkbox"/>	OK
		<input type="checkbox"/>	OK
Steam Generator MFW Temperature (T-A01S/T-B01S)	439 ± 12.6°F	<input type="checkbox"/>	OK
		<input type="checkbox"/>	OK
Steam Generator Pressure (P-A04S/P-B04S)	711 ± 29 psia	<input type="checkbox"/>	OK
		<input type="checkbox"/>	OK

**TABLE B-8
COMPARISON OF SPECIFIED AND ACTUAL TEST CONDITIONS FOR S00908**

Condition (Instruments)	Specified	Actual (a,b,c)	Comment
Rod Power (W-00P)	4991.6 ± 100 kW*		OK
Pressurizer Pressure (P-027P)	2250 ± 29 psia		OK
Average Hot-Leg Temperature (T-A03PO/T-A03PL/ T-B03PO/T-B03PL)	599.9 ± 9°F		OK
			OK
			OK
			OK
Reactor Vessel (Core) Inlet Temperature (T-003P)	529.5 ± 9°F		Accepted
Core Flow Rate (F-003P)	51.26 ± 0.55 lbm/sec.		OK
Cold-Leg Flow Rate (F-A01P/F-A02P/F-B01P/ F-B02P)	12.92 ± 0.22 lbm/sec.		OK
			OK
			OK
			OK
Downcomer Upper-Head Bypass Flow Rate (F-014P)	0.40 ± 0.11 lbm/sec.		OK
Pressurizer Level (L-010P)	12.4 ± 1.25 ft.		OK
Accumulator Level (L-A20E/L-B20E)	7.64 ± 0.36 ft.		OK
			OK
Accumulator Water Temperature (T-A22E/ T-B22E)	68 ± 9°F		OK
			OK
Accumulator Pressure (P-A20E/P-B20E)	711 ± 14.5 psia		OK
			OK
IRWST Level (L-060E)	27.9 ± 0.33 ft.		OK
IRWST Water Temperature (T-063E)	68 ± 9°F		Accepted

*4893.7 kW before time 0.

**TABLE B-8 (Cont.)
COMPARISON OF SPECIFIED AND ACTUAL TEST CONDITIONS FOR S00908**

Condition (Instruments)	Specified	Actual (a,b,c)	Comment
PRHR Supply Line Temperature (T-A82E)	> 212°F		OK
Upper-Head Average Temperature (T-016P)	564.8 ± 9°F		Accepted. Facility design limits maximum temperature to ≤ cold leg temperature.
PR to CMT Balance Line Temperature (T-A28P/T-B28P)	644 + 45°F		N/A
Cold-Leg Balance Line Temperature (T-A142PL/T-B142PL)	> 329°F		OK
			OK
CMT Level (L-A40E/L-B40E)	full		OK
			OK
CMT Temperature (T-A411E/T-B411E)	68 ± 9°F		Accepted (T-A411E)
			Accepted (T-B411E)
Steam Generator Level (L-A20S/L-B20S)	4.86 ± 0.49 ft.		Accepted (L-A20S). Will not impact test results.
			Accepted (L-B20S). Will not impact test results.
Steam Generator MFW Temperature (T-A01S/T-B01S)	439 ± 12.6°F		OK
			OK
Steam Generator Pressure (P-A04S/P-B04S)	711 ± 29 psia		OK
			OK

**TABLE B-9
COMPARISON OF SPECIFIED AND ACTUAL TEST CONDITIONS FOR S01007**

Condition (Instruments)	Specified	Actual	(a,b,c)	Comment
Rod Power (W-00P)	4991.6 ± 100 kW*			OK
Pressurizer Pressure (P-027P)	2250 ± 29 psia			OK
Average Hot-Leg Temperature (T-A03PO/T-A03PL/ T-B03PO/T-B03PL)	599.9 ± 9°F			OK
				OK
				OK
				OK
Reactor Vessel (Core) Inlet Temperature (T-003P)	529.5 ± 9°F			Accepted
Core Flow Rate (F-003P)	51.26 ± 0.55 lbm/sec.			OK
Cold-Leg Flow Rate (F-A01P/F-A02P/F-B01P/ F-B02P)	12.92 ± 0.22 lbm/sec.			Accepted (F-A01P), avg. loop A flow is 12.85 lbm/sec.
				OK
				OK
				OK
Downcomer-Upper Head Bypass Flow Rate (F-014P)	0.40 ± 0.11 lbm/sec.			OK
Pressurizer Level (L-010P)	12.4 ± 1.25 ft.			OK
Accumulator Level (L-A20E/L-B20E)	7.64 ± 0.36 ft.			OK
				OK
Accumulator Water Temperature (T-A22E/ T-B22E)	68 ± 9°F			Accepted
				Accepted
Accumulator Pressure (P-A20E/P-B20E)	711 ± 14.5 psia			OK
				OK
IRWST Level (L-060E)	27.9 ± 0.33 ft.			OK
IRWST Water Temperature (T-063E)	68 ± 9°F			Accepted

* 4893.7 kW before time 0.

**TABLE B-9 (Cont.)
COMPARISON OF SPECIFIED AND ACTUAL TEST CONDITIONS FOR S01007**

Condition (Instruments)	Specified	Actual	Comment
PRHR Supply Line Temperature (T-A82E)	> 212°F	[]	OK
Upper-Head Average Temperature (T-015P/T-016P)	564.8 ± 9°F	[]	Accepted. Facility design limits maximum temperature to ≤ cold leg temperature.
PR to CMT Balance Line Temperature (T-A28P/T-B28P)	644 ± 45°F	[]	N/A
Cold-Leg Balance Line Temperature (T-A142PL/T-B142PL)	> 329°F	[]	OK
CMT Level (L-A40E/L-B40E)	full	[]	OK
CMT Temperature (T-A411E/T-B411E)	68 ± 9°F	[]	Accepted (T-A411E)
Steam Generator Level (L-A20S/L-B20S)	4.86 ± 0.49 ft.	[]	Accepted (L-A20S). Will not impact test results.
Steam Generator MFW Temperature (T-A01S/T-B01S)	439 ± 12.6°F	[]	Accepted (T-A01S). Avg. temperature between A and B is 451.5°F.
Steam Generator Pressure (P-A04S/P-B04S)	711 ± 29 psia	[]	OK
		[]	OK

TABLE B-10
COMPARISON OF SPECIFIED AND ACTUAL TEST CONDITIONS FOR S01110

Condition (Instruments)	Specified	Actual (a,b,c)	Comment
Rod Power (W-00P)	4991.6 ± 100 kW*	—	OK
Pressurizer Pressure (P-027P)	2250 ± 29 psia	—	OK
Average Hot-Leg Temperature (T-A03PO/T-A03PL/ T-B03PO/T-B03PL)	599.9 ± 9°F	—	OK
		—	OK
		—	OK
		—	OK
Reactor Vessel (Core) Inlet Temperature (T-003P)	529.5 ± 9°F	—	Accepted
Core Flow Rate (F-003P)	51.26 ± 0.55 lbm/sec.	—	OK
Cold-Leg Flow Rate (F-A01P/F-A02P/F-B01P/ F-B02P)	12.92 ± 0.22 lbm/sec.	—	Accepted (F-A01P), avg. loop A flow is 12.92 lbm/sec.
		—	Accepted (F-A02P), avg. loop A flow is 12.92 lbm/sec.
		—	OK
		—	OK
Downcomer Upper-Head Bypass Flow Rate (F-014P)	0.40 ± 0.11 lbm/sec.	—	OK
Pressurizer Level (L-010P)	12.4 ± 1.25 ft.	—	OK
Accumulator Level (L-A20E/L-B20E)	7.64 ± 0.36 ft.	—	OK
		—	OK
Accumulator Water Temperature (T-A22E/ T-B22E)	68 ± 9°F	—	Accepted (T-A22E) Note 1
		—	Accepted (T-B22E) Note 1
Accumulator Pressure (P-A20E/P-B20E)	711 ± 14.5 psia	—	OK
		—	OK
IRWST Level (L-060E)	77.9 ± 0.32 ft.	—	OK

*4893.7 kW before time 0.

NOTE 1: Ambient air temperature in facility was unusually high due to plant heat-up and hot summer weather.

TABLE B-10 (Cont.)
COMPARISON OF SPECIFIED AND ACTUAL TEST CONDITIONS FOR S01110

Condition (Instruments)	Specified	Actual <small>(g,b,c)</small>	Comment
IRWST Water Temperature (T-063E)	68 ± 9°F		Accepted Note 1
PRHR Supply Line Temperature (T-A82E)	> 212°F		OK
Upper-Head Average Temperature (T-016P)	564.8 ± 9°F		Accepted
PR to CMT Balance Line Temperature (T-A28P/ T-B28P)	644 + 45°F		N/A
Cold-Leg Balance Line Temperature (T-A142PL/T-B142PL)	> 329°F		OK
			OK
CMT Level (L-A40E/ L-B40E)	20.5 ft.. (full)		OK
			OK
CMT Temperature (T-A411E/T-B411E)	68 ± 9°F		Accepted (T-A411E) Note 1
			Accepted (T-B411E) Note 1
Steam Generator Level (L-A20S/L-B20S)	4.86 ± 0.49 ft.		Accepted (L-A20S). Will not impact test results.
			OK
Steam Generator MFW Temperature (T-A01S/T-B01S)	439 ± 12.6°F		OK
			OK
Steam Generator Pressure (P-A04S/P-B04S)	711 ± 29 psia		OK
			OK

NOTE 1: Ambient air temperature in facility was unusually high due to plant heat-up and hot summer weather.

**TABLE B-11
COMPARISON OF SPECIFIED AND ACTUAL TEST CONDITIONS FOR S01211**

Condition (Instruments)	Specified	Actual (a,b,c)	Comment
Rod Power (W-00P)	4991.6 ± 100 kW*	<input type="checkbox"/>	OK
Pressurizer Pressure (P-027P)	2250 ± 29 psia	<input type="checkbox"/>	OK
Average Hot-Leg Temperature (T-A03PO/T-A03PL/ T-B03PO/T-B03PL)	599.9 ± 9°F	<input type="checkbox"/>	OK
		<input type="checkbox"/>	OK
		<input type="checkbox"/>	OK
		<input type="checkbox"/>	OK
Reactor Vessel (Core) Inlet Temperature (T-003P)	529.5 ± 9°F	<input type="checkbox"/>	Accepted
Core Flow Rate (F-003P)	51.26 ± 0.55 lbm/sec.	<input type="checkbox"/>	OK
Cold-Leg Flow Rate (F-A01P/F-A02P/F-B01P/ F-B02P)	12.92 ± 0.22 lbm/sec.	<input type="checkbox"/>	Accepted (F-A01P), avg. loop A flow is 12.87 lbm/sec.
		<input type="checkbox"/>	OK
		<input type="checkbox"/>	OK
		<input type="checkbox"/>	OK
Downcomer Upper-Head Bypass Flow Rate (F-014P)	0.40 ± 0.11 lbm/sec.	<input type="checkbox"/>	OK
Pressurizer Level (L-010P)	12.4 ± 1.25 ft.	<input type="checkbox"/>	OK
Accumulator Level (L-A20E/L-B20E)	7.64 ± 0.36 ft.	<input type="checkbox"/>	OK
		<input type="checkbox"/>	OK
Accumulator Water Temperature (T-A22E/ T-B22E)	68 ± 9°F	<input type="checkbox"/>	Accepted (T-A22E)
		<input type="checkbox"/>	Accepted (T-B22E)
Accumulator Pressure (P-A20E/P-B20E)	711 ± 14.5 psia	<input type="checkbox"/>	OK
		<input type="checkbox"/>	OK
IRWST Level (L-060E)	27.9 ± 0.33 ft.	<input type="checkbox"/>	OK

*4893.7 kW before time 0.

**TABLE B-11 (Cont.)
COMPARISON OF SPECIFIED AND ACTUAL TEST CONDITIONS FOR S01211**

Condition (Instruments)	Specified	Actual <small>(a,b,c)</small>	Comment
IRWST Water Temperature (T-063E)	68 ± 9°F	☐	Accepted
PRHR Supply Line Temperature (T-A82E)	>212°F		Accepted. Sufficient to ensure initiation of natural circulation flow.
Upper-Head Average Temperature (T-016P)	529.5 ± 9°F		Accepted. Facility design limits maximum temperature to ≤ cold leg temperature.
PR to CMT Balance Line Temperature (T-A28P/T-B28P)	644 + 45°F		N/A
			N/A
Cold-Leg Balance Line Temperature (T-A142PL/T-B142PL)	>329°F		OK
			OK
CMT Level (L-A40E/L-B40E)	20.5 ft. (full)		OK
			OK
CMT Temperature (T-A411E/T-B411E)	68 ± 9°F		Accepted (T-A411E)
			Accepted (T-B411E)
Steam Generator Level (L-A20S/L-B20S)	4.86 ± 0.49 ft.		Accepted (L-A20S). Will not impact test results.
			OK
Steam Generator MFW Temperature (T-A01S/T-B01S)	439 ± 12.6°F		OK
			OK
Steam Generator Pressure (P-A04S/P-B04S)	711 ± 29 psia		OK
		☐	OK

**TABLE B-12
COMPARISON OF SPECIFIED AND ACTUAL TEST CONDITIONS FOR S01309**

Condition (Instruments)	Specified	Actual (a,b,c)	Comment
Rod Power (W-00P)	4991.6 ± 100 kW*		OK
Pressurizer Pressure (P-027P)	2250 ± 29 psia		OK
Average Hot-Leg Temperature (T-A03PO/T-A03PL/ T-B03PO/T-B03PL)	599.9 ± 9°F		OK
			OK
			OK
			OK
Reactor Vessel (Core) Inlet Temperature (T-003P)	529.5 ± 9°F		OK
Core Flow Rate (F_003P)	51.26 ± 0.55 lbm/sec.		Accepted. Sum of cold-leg flow rates in conjunctions with core inlet/out temperatures were all within acceptable limits.
Cold-Leg Flow Rate (F_A01P/F_A02P/F_B01P/ F_B02P)	12.92 ± 0.22 lbm/sec.		OK
			OK
			Accepted (F_F01P), avg. loop B flow is 13.09 lbm/sec.
			OK
Downcomer Upper-Head Bypass Flow Rate (F_014P)	0.40 ± 0.11 lbm/sec.		OK
Pressurizer Level (L_010P)	12.4 ± 1.25 ft.		OK
Accumulator Level (L_A20E/L_B20E)	7.64 ± 0.36 ft.		OK
			OK
Accumulator Water Temperature (T-A22E/ T-B22E)	68 ± 9°F		OK
			OK
Accumulator Pressure (P-A20E/P-B20E)	711 ± 14.5 psia		OK
			OK
IRWST Level (L_060E)	27.9 ± 0.33 ft.		OK

*4893.7 kW before time 0.

NOTE 1: Ambient air temperature in facility was unusually high due to plant heat-up and hot summer weather.

**TABLE B-12 (Cont.)
COMPARISON OF SPECIFIED AND ACTUAL TEST CONDITIONS FOR S01309**

Condition (Instruments)	Specified	Actual (a,b,c)	Comment
IRWST Water Temperature (T-063E)	68 ± 9°F		OK
PRHR Supply Line Temperature (T-A82E)	> 212°F		OK
Upper Head Average Temperature (T-016P)	529.5 ± 9°F		OK
PR to CMT Balance Line Temperature (T-A28P/T-B28P)	644 + 45°F		N/A
			N/A
Cold-Leg Balance Line Temperature (T-A142PL/T-B142PL)	> 329°F		OK
			OK
CMT Level (L_A40E/L_B40E)	20.5 ft. ± 0.1 ft.		OK
			OK
CMT Temperature (T-A411E/T-B411E)	68 ± 9°F		OK
			OK
Steam Generator Level (L_A20S/L_B20S)	4.86 ± 0.49 ft.		OK
			OK
Steam Generator MFW Temperature (T-A01S/T-B01S)	439 ± 12.6°F		OK
			OK
Steam Generator Pressure (P-A04S/P-B04S)	711 ± 29 psia		OK
			OK

**TABLE B-13
COMPARISON OF SPECIFIED AND ACTUAL TEST CONDITIONS FOR S01512**

Condition (Instruments)	Specified	Actual (a,b,c)	Comment
Rod Power (W-00P)	-150	<input type="checkbox"/>	OK
Pressurizer Pressure (P-027P)	2250 ± 29 psia	<input type="checkbox"/>	OK
Average Hot-Leg Temperature (T-A03PO/T-A03PL/T-B03PO/T-B03PL)	545.0 ± 9°F*	<input type="checkbox"/>	Accepted, avg Hot-Leg is 554.3
		<input type="checkbox"/>	Accepted, avg Hot-Leg is 554.3
		<input type="checkbox"/>	OK
		<input type="checkbox"/>	Accepted, avg Hot-Leg is 554.3
Reactor Vessel (Core) Inlet Temperature (T-003P)	543.2 ± 9°F*	<input type="checkbox"/>	Accepted, avg core ΔT is -1°F as expected.
Core Flow Rate (F_003P)	51.26 ± 0.55 lbm/sec.	<input type="checkbox"/>	Accepted, cold-leg total flow is 51.6 lbm/sec.
Cold-Leg Flow Rate (F_A01P/F_A02P/F_B01P/F_B02P)	12.92 ± 0.22 lbm/sec.	<input type="checkbox"/>	OK
		<input type="checkbox"/>	OK
		<input type="checkbox"/>	Accepted, avg Loop B flow is 13.05 lbm/sec.
		<input type="checkbox"/>	OK
Downcomer Upper-Head Bypass Flow Rate (F_014P)	0.40 ± 0.11 lbm/sec.	<input type="checkbox"/>	OK
Pressurizer Level (L_010P)	6.56 ft. < PZR level* ≤ 8.2 ft.	<input type="checkbox"/>	OK
Accumulator Level (L_A20E/L_B20E)	7.64 ± 0.36 ft.	<input type="checkbox"/>	OK
		<input type="checkbox"/>	OK
Accumulator Water Temperature (T-A22E/T-B22E)	68 ± 9°F	<input type="checkbox"/>	OK
		<input type="checkbox"/>	OK
Accumulator Pressure (P-A20E/P-B20E)	711 ± 14.5 psia	<input type="checkbox"/>	OK
		<input type="checkbox"/>	OK
IRWST Level (L_060E)	27.9 ± .32 ft.	<input type="checkbox"/>	OK

*Specific to this test only; test simulated zero power, hot-standby conditions.

**TABLE B-13 (Cont.)
COMPARISON OF SPECIFIED AND ACTUAL TEST CONDITIONS FOR S01512**

Condition (Instruments)	Specified	Actual (a,b,c)	Comment
IRWST Water Temperature (T-063E)	68 ± 9°F		OK
PRHR Supply Line Temperature (T-A82E)	> 212°F		OK
Upper Head Average Temperature (T-016P)	543.2 ± 9°F*		Accepted. Facility design limits maximum temperature to ≤ cold leg temperature
PR to CMT Balance Line Temperature (T-A28P/T-B28P)	644 + 45°F		N/A
			N/A
Cold-Leg Balance Line Temperature (T-A142PL/f-B142PL)	> 329°F		OK
			OK
CMT Level (L_A40E/L_B40E)	20.5 ft. ± 0.1 ft.		OK
			OK
CMT Temperature (T-A411E/T-B411E)	68 ± 9°F		OK
			OK
Steam Generator Level (L_A20S/L_B20S)	4.86 ± 0.49 ft.		OK
			OK
Steam Generator MFW Temperature (T-A01S/T-B01S)			N/A for this test
			N/A for this test
Steam Generator Pressure (P-A04S/P-B04S)	1001 ± 29 psia*		OK
			OK

* Specific to this test only.

**TABLE B-14
COMPARISON OF SPECIFIED AND ACTUAL TEST CONDITIONS FOR S01613**

Condition (Instruments)	Specified	Actual (a,b,c)	Comment
Rod Power (W-00P)	4910 ± 100 kW*	□	OK
Pressurizer Pressure (P-027P)	2241 ± 29 psia		OK
Average Hot-Leg Temperature (T-A03PO/T-A03PL/ T-B03PO/T-B03PL)	602.2 ± 9°F		OK
			OK
			OK
			OK
Reactor Vessel (Core) Inlet Temperature (T-003P)	527.2 ± 9°F		OK
Core Flow Rate (F_003P)	51.54 ± 0.55 lbm/sec.		OK
Cold-Leg Flow Rate (F_A01P/F_A02P/F_B01P/ F_B02P)	12.85 ± 0.22 lbm/sec.		OK
			OK
			Accepted, avg. loop B flow is 13.01 lbm/sec.
			OK
Downcomer-Upper Head Bypass Flow Rate (F_014P)	0.40 ± 0.11 lbm/sec.		OK
Pressurizer Level (L_010P)	12.24 ± 1.25 ft.		OK
Accumulator Level (L_A20E/L_B20E)	7.55 ± 0.36 ft.		OK
			OK
Accumulator Water Temperature (T-A22E/ T-B22E)	68 ± 9°F		OK
			OK
Accumulator Pressure (P-A20E/P-B20E)	711 ± 14.5 psia		OK
			OK
IRWST Level (L_060E)	27.9 ± 0.32 ft.	□	OK

*4893.7 kW before time 0.

TABLE B-14 (Cont.)
COMPARISON OF SPECIFIED AND ACTUAL TEST CONDITIONS FOR S01613

Condition (Instruments)	Specified	Actual (a,b,c)	Comment
IRWST Water Temperature (T-063E)	68 ± 9°F	□	OK
PRHR Supply Line Temperature (T-A82E)	242.6 ± 45°F		OK
Upper Head Average Temperature (T-016P)	511 ± 9°F		Accepted. Facility design limits maximum temperature to ≤ cold leg temperature.
PR to CMT Balance Line Temperature (T-A28P/T-B28P)	644 ± 45°F		N/A
			N/A
Cold-Leg Balance Line Temperature (T-A142PL/T-B142PL)	453 ± 9°F		Accepted. Sufficient to ensure initiation of natural circulation flow.
			Accepted. Sufficient to ensure initiation of natural circulation flow.
CMT Level (L_A40E/L_B40E)	20.5 ft. ± 0.1 ft.		OK
			OK
CMT Temperature (T-A411E/T-B411E)	68 ± 9°F		OK
			OK
Steam Generator Level (L_A20S/L_B20S)	4.92 ± 0.49 ft.		OK
			OK
Steam Generator MFW Temperature (T-A01S/T-B01S)	432 ± 13°F		OK
			OK
Steam Generator Pressure (P-A04S/P-B04S)	711 ± 29 psia		OK
		□	OK

**TABLE B-15
COMPARISON OF SPECIFIED AND ACTUAL TEST CONDITIONS FOR S01703**

Condition (Instruments)	Specified	Actual (a,b,c)	Comment
Rod Power (W-00P)	4980 ± 100 kW*	—	OK
Pressurizer Pressure (P-027P)	2245 ± 29 psia	—	OK
Average Hot-Leg Temperature (T-A03PO/T-A03PL/ T-B03PO/T-B03PL)	603.3 ± 9°F	—	OK
		—	OK
		—	OK
		—	OK
Reactor Vessel (Core) Inlet Temperature (T-003P)	538.0 ± 9°F	—	OK
Core Flow Rate (F_003P)	51.59 ± 0.55 lbm/sec.	—	OK
Cold-Leg Flow Rate (F_A01P/F_A02P/F_B01P/ F_B02P)	12.90 ± 0.22 lbm/sec.	—	OK
		—	OK
		—	OK
		—	OK
Downcomer Upper-Head Bypass Flow Rate (F_014P)	0.40 ± 0.11 lbm/sec.	—	OK
Pressurizer Level (L_010P)	12.63 ± 1.25 ft.	—	OK
Accumulator Level (L_A20E/L_B20E)	7.55 ± 0.36 ft.	—	OK
		—	OK
Accumulator Water Temperature (T-A22E/ T-B22E)	69 ± 9°F	—	OK
		—	Accepted
Accumulator Pressure (P-A20E/P-B20E)	711 ± 14.5 psia	—	OK
		—	OK
IRWST Level (L_060E)	27.9 ± 0.33 ft.	—	OK

*4893.7 kW before time 0.

**TABLE B-15 (Cont.)
COMPARISON OF SPECIFIED AND ACTUAL TEST CONDITIONS FOR S01703**

Condition (Instruments)	Specified	Actual <small>(a,b,c)</small>	Comment
IRWST Water Temperature (T-063E)	74.7 ± 9°F		Accepted
PRHR Supply Line Temperature (T-A82E)	230.5 ± 22.5°F		OK
Upper-Head Average Temperature (T-016P)	519.8 ± 9°F		OK
PR to CMT Balance Line Temperature (T-A28P/T-B28P)	644 ± 45°F		N/A
			N/A
Cold-Leg Balance Line Temperature (T-A142PL/T-B142PL)	428 ± 9°F		Accepted. Sufficient to ensure initiation of natural circulation flow.
			Accepted. Sufficient to ensure initiation of natural circulation flow.
CMT Level (L_A40E/L_B40E)	20.5 ft. ± 0.1 ft.		OK
			OK
CMT Temperature (T-A411E/T-B411E)	69.8 ± 9°F		Accepted
			Accepted
Steam Generator Level (L_A20S/L_B20S)	4.1 ± 0.49 ft.		OK
			OK
Steam Generator MFW Temperature (T-A01S/T-B01S)	446 ± 12.6°F		OK
			OK
Steam Generator Pressure (P-A04S/P-B04S)	696 ± 29 psia		OK
			OK

The data plots are found in the proprietary version of this document.

APPENDIX C
SPES-2 INSTRUMENT LIST

C-1 Explanation of the Instrument Plant Code

Each instrument has been identified by means of a plant code (TAG) as:

X - WNYZ

The letters X, W, N, Y, Z have the following meaning:

X = Physical Parameter

DE = density
DP = differential pressure
F = flow rate
I = electrical current
IF = integral flow rate
L = level
P = absolute pressure
S = speed
T = fluid temperature
TW = wall temperature
V = voltage
W = electric power
Z = valve position

W = Loop Identifier

A = loop with pressurizer
B = loop without pressurizer
O = component/circuit belonging to both loops

N = Measurement Tag Number

Y = Plant System Identifier

P = primary system
S = secondary system
E = primary emergency system
A = auxiliary system

Z = Special Tag

E = external
EH = external high position
EL = external low position
EM = external medium position
H = from the top
I = internal
L = from the bottom
O = horizontal
O-C = open/close
V = vertical
NUMBER = power channel heated rod number
A.B.C. = gammadensitometer beam identifier

C-2 Instrument List Explanation

The main characteristics of the instruments are reported in Table C-1. The columns have the following meaning:

PLANT CODE	SPES-2 instrument identification code
INSTRUMENT TYPE	Type of instrument used for the measurement
LOCATION	Position of the instrument in the plant
MANUFACTURER	Instrument manufacturer
MODEL	Instrument model
SIET CODE	SIET instrument identification code
SPAN	Instrument span
M.U.	Engineering unit of the physical measurement
h	Height difference between pressure tap and instrument for absolute pressure measurement, pressure tap elevation difference for differential pressure (dP) measurement (m)
K(*)	Instrument hydraulic head = $\rho_{LC} * g * h$ (kPa)
M(*)	Instrument conversion constant (M.U. / mV) or (UNI7938, UNI7937) conversion matrix for thermocouples and thermoresistances
Q	Additional instrument constant (M.U.)
MANU. ACCURACY	Instrument accuracy given by manufacturer in percent or in engineering unit

(*) For differential pressure (dP) transmitters, the sign type (positive or negative) of these parameters depends on the instrument installation on the plant.

The main characteristics of the Venturi tubes and of the orifices used to measure the SPES-2 flow rates are reported in Table C-2. The columns have the following meaning:

TAG	SPES-2 instrument identification code
D	Pipe inside diameter (mm)
d	Nozzle throat diameter (mm)
α_c	Calibrated or calculated nozzle flux coefficient (m ²)
$\Delta\alpha_c$	Maximum error of the nozzle flux coefficient (\pm m ²)
$\sigma\alpha_c$	Standard deviation of the nozzle flux coefficient (\pm m ²)
TYPE	Type of the nozzle

**TABLE C-1
SPES-2 INSTRUMENT LIST**

PLANT CODE	INSTRUMENT	LOCATION	MANUFACTURER	MODEL	SIET CODE	SPAN	MLU	h (m)	K (kPa)	M (MLU/mV)	Q (MLU)	MANU. ACCURACY ±
DE-001PA	Venturi/DP-Transm.	Break line	GAMMATOM	AM	DE001	1 : 1000	kg/m ³	-	-	0.125	-123.68	5%
DE-001PB	Gammaden.	Break line	GAMMATOM	AM	DE001	1 : 1000	kg/m ³	-	-	0.125	-123.68	5%
DE-030PA	Gammaden.	ADS-1,-2,-3 header	GAMMATOM	CS	DE002	1 : 1000	kg/m ³	-	-	0.125	-123.68	5%
DE-030PB	Gammaden.	ADS-1,-2,-3 header	GAMMATOM	CS	DE002	1 : 1000	kg/m ³	-	-	0.125	-123.68	5%
DE-030PC	Gammaden.	ADS-1,-2,-3 header	GAMMATOM	CS	DE002	1 : 1000	kg/m ³	-	-	0.125	-123.68	5%
DE-040PA	Gammaden.	ADS-4 header	GAMMATOM	CS	DE003	1 : 1000	kg/m ³	-	-	0.125	-123.68	5%
DE-040PB	Gammaden.	ADS-4 header	GAMMATOM	CS	DE003	1 : 1000	kg/m ³	-	-	0.125	-123.68	5%
DE-040PC	Gammaden.	ADS-4 header	GAMMATOM	CS	DE003	1 : 1000	kg/m ³	-	-	0.125	-123.68	5%
DE-A01PA	Gammaden.	HL-A	GAMMATOM	CS	DE-004	1 : 1000	kg/m ³	-	-	0.125	-123.68	5%
DE-A01PB	Gammaden.	HL-A	GAMMATOM	CS	DE-004	1 : 1000	kg/m ³	-	-	0.125	-123.68	5%
DE-A01PC	Gammaden.	HL-A	GAMMATOM	CS	DE-004	1 : 1000	kg/m ³	-	-	0.125	-123.68	5%
DP-000E	DP - Transd.	DVI-A/DVI-B	SENSOTEC	Z/1901-12	TSD 038	-34 : 34	kPa	0	0	1.7647	0.21194	0.25%
DP-000P	DP - Transm.	PC riser	HONEYWELL	STD130	TMD 110	-60 : 60	kPa	4.441	43.551	0.03	-46.449	0.10%
DP-001P	DP - Transm.	PC tubular DC	HONEYWELL	STD120	TMD 057	0 : 100	kPa	2.555	-25.05	0.025	-50.05	0.10%
DP-002P	DP - Transm.	PC tubular DC	HONEYWELL	STD120	TMD 068	0 : 100	kPa	2.71	-26.576	0.025	-51.576	0.10%
DP-003P	DP - Transm.	DC Inlet/PC LP	HONEYWELL	STD120	TMD 053	0 : 70	kPa	0.242	-2.373	0.0175	-19.873	0.10%
DP-004P	DP - Transm.	PC LP	HONEYWELL	STD120	TMD 114	-30 : 30	kPa	0.932	9.14	-0.015	54.14	0.10%
DP-005P	DP - Transm.	PC riser	HONEYWELL	STD120	TMD 120	-20 : 20	kPa	0.741	7.27	-0.01	37.27	0.10%
DP-011P	DP - Transm.	PC riser	HONEYWELL	STD120	TMD 121	-15 : 35	kPa	1.48	14.514	0.0125	-12.986	0.10%
DP-012P	DP - Transm.	PC riser	HONEYWELL	STD120	TMD 118	-15 : 35	kPa	1.11	10.885	0.0125	-16.615	0.10%
DP-013P	DP - Transm.	PC riser	HONEYWELL	STD120	TMD 189	-15 : 35	kPa	1.11	10.885	0.0125	-16.615	0.10%
DP-014P	DP - Transm.	PC riser	HONEYWELL	STD120	TMD 127	-10 : 10	kPa	0.865	8.679	0.005	-6.321	0.10%
DP-017P	DP - Transm.	PC UH	HONEYWELL	STD120	TMD 122	0 : 50	kPa	1.889	-18.525	0.0125	-31.025	0.10%
DP-018P	DP - Transm.	HL-A/SL	HONEYWELL	STD120	TMD 129	-10 : 10	kPa	0.899	8.816	0.005	-6.184	0.10%
DP-019P	DP - Transm.	SL	HONEYWELL	STD120	TMD 140	-25 : 25	kPa	0.741	7.267	-0.0125	44.767	0.10%

**TABLE C-1
SPES-2 INSTRUMENT LIST (Cont.)**

PLANT CODE	INSTRUMENT	LOCATION	MANUFACTURER	MODEL	SIET CODE	SPAN	M.U.	h (m)	K (kPa)	M (M.U./mV)	Q (M.U.)	MANU. ACCURACY ±
DP-020P	DP - Transm.	SL	HONEYWELL	STD120	TMD 085	-50 : 50	kPa	3.426	33.598	-0.025	108.598	0.10%
DP-021P	DP - Transm.	PR	HONEYWELL	STD120	TMD 047	-20 : 20	kPa	1.444	14.161	-0.01	44.161	0.10%
DP-022P	DP - Transm.	PR	HONEYWELL	STD120	TMD 076	-20 : 20	kPa	1.444	14.161	-0.01	44.161	0.10%
DP-023P	DP - Transm.	PR	HONEYWELL	STD120	TMD 073	-20 : 20	kPa	1.444	14.161	-0.01	44.161	0.10%
DP-024P	DP - Transm.	PR	HONEYWELL	STD120	TMD 074	-20 : 20	kPa	1.444	14.161	-0.01	44.161	0.10%
DP-025P	DP - Transm.	PR	HONEYWELL	STD120	TMD 141	-10 : 10	kPa	0.43	4.217	-0.005	19.217	0.10%
DP-026P	DP - Transm.	PR	HONEYWELL	STD120	TMD 034	-10 : 10	kPa	0.32	3.138	-0.005	18.138	0.10%
DP-027P	DP - Transm.	PR	HONEYWELL	STD120	TMD 036	-10 : 10	kPa	0.235	2.305	-0.005	17.305	0.10%
DP-041P	DP - Transd.	CL-A1/B1	SENSOTEC	Z/1901-12	TSD 040	-34 : 34	kPa	0	0	1.7533	0.45007	0.25%
DP-042P	DP - Transd.	CL-A2/B2	SENSOTEC	Z/1901-12	TSD 041	-34 : 34	kPa	0	0	1.7371	1.45048	0.25%
DP-043P	DP - Transd.	CL-B1/B2	SENSOTEC	A-5/1901-12	TSD 042	-34 : 34	kPa	0	0	1.7975	-0.2567	0.25%
DP-044P	DP - Transd.	CL-A1/A2	SENSOTEC	Z/1901-12	TSD 039	-34 : 34	kPa	0	0	1.7599	0.13164	0.25%
DP-A001P	DP - Transm.	CL-A1	HONEYWELL	STD120	TMD 124	0 : 50	kPa	1.051	-10.297	0.0125	-22.797	0.10%
DP-A002P	DP - Transm.	CL-A2	HONEYWELL	STD120	TMD 126	0 : 50	kPa	1.051	-10.297	0.0125	-22.797	0.10%
DP-A00P	DP - Transm.	PCP-A	HONEYWELL	STD130	TMD 132	0 : 700	kPa	0.339	-3.325	-0.175	171.675	0.10%
DP-A00S	DP - Transm.	SG-A baffle	GOULD	PD3000-030	TMD 029	-2.5 : 2.5	kPa	0	0	0.00125	-3.75	0.25%
DP-A011P	DP - Transm.	CL-A1	HONEYWELL	STD120	TMD 046	-25 : 25	kPa	0	0	0.0125	-37.5	0.10%
DP-A012P	DP - Transm.	CL-A2	HONEYWELL	STD120	TMD 043	-25 : 25	kPa	0	0	0.0125	-37.5	0.10%
DP-A01S	DP - Transm.	SG-A riser	GOULD	PD3000-200	TMD 196	0 : 50	kPa	3.98	39.03	-0.0125	51.53	0.25%
DP-A021P	DP - Transm.	CL-A1/PC DC	HONEYWELL	STD120	TMD 138	0 : 70	kPa	1.245	-12.209	0.0175	-29.709	0.10%
DP-A022P	DP - Transm.	CL-A2/PC DC	HONEYWELL	STD120	TMD 039	0 : 70	kPa	1.245	-12.209	0.0175	-29.709	0.10%
DP-A02S	DP - Transm.	SG-A riser	HONEYWELL	STD120	TMD 054	0 : 70	kPa	6.5	63.743	-0.0175	81.243	0.10%
DP-A03P	DP - Transm.	SG-A in/out	HONEYWELL	STD130	TMD 055	-100 : 400	kPa	0	0	0.125	-225	0.10%
DP-A03S	DP - Transm.	SG-A separator	HONEYWELL	STD120	TMD 087	-50 : 50	kPa	3.2	31.381	-0.025	106.381	0.10%
DP-A04P	DP - Transm.	HL-A	HONEYWELL	STD120	TMD 115	-40 : 60	kPa	3.603	35.334	0.025	-29.666	0.10%

**TABLE C-1
SPES-2 INSTRUMENT LIST (Cont.)**

PLANT CODE	INSTRUMENT	LOCATION	MANUFACTURER	MODEL	SIET CODE	SPAN	MLU	h (m)	K (kPa)	M (MLU/mV)	Q (MLU)	MANU. ACCURACY ±
DP-A04S	DP - Transm.	SG-A separator	SCHLUMBERGER	BD5GA-3	TMD 013	-10 : 10	kPa	0.675	6.619	-0.005	21.619	0.25%
DP-A05P	DP - Transm.	U-tube SG-A	HONEYWELL	STD130	TMD 037	-60 : 120	kPa	5.125	50.2575	0.045	-54.741	0.10%
DP-A05S	DP - Transm.	SG-A dryers	HONEYWELL	STD120	TMD 056	0 : 10	kPa	0.69	6.766	-0.0025	9.266	0.10%
DP-A06P	DP - Transm.	U-tube SG-A	HONEYWELL	STD120	TMD 113	-40 : 60	kPa	3.75	36.775	0.025	-28.225	0.10%
DP-A06S	DP - Transm.	SG-A riser	GOULD	PD3006-400	TMD 199	0 : 30	kPa	2.15	21.084	-0.0075	28.584	0.25%
DP-A07P	DP - Transm.	U-tube SG-A	HONEYWELL	STD120	TMD 081	-30 : 70	kPa	3.75	-36.775	0.025	-91.775	0.10%
DP-A08P	DP - Transm.	U-tube SG-A	HONEYWELL	STD130	TMD 105	-60 : 100	kPa	5.125	-50.259	0.04	-150.26	0.10%
DP-A09P	DP - Transm.	PS-A	HONEYWELL	STD120	TMD 116	0 : 100	kPa	1.768	-17.338	0.025	-42.338	0.10%
DP-A15P	DP - Transm.	PC UP/HL-A	HONEYWELL	STD120	TMD 048	-15 : 15	kPa	1.014	9.944	0.0075	-12.556	0.10%
DP-A16P	DP - Transm.	HL-A/PC UP	HONEYWELL	STD120	TMD 049	0 : 20	kPa	0.666	-6.5	0.005	-11.531	0.10%
DP-A20E	DP - Transm.	ACC-A inj. line	HONEYWELL	STD130	TMD 104	-50 : 200	kPa	3.34	32.754	0.0625	-79.746	0.10%
DP-A28P	DP - Transm.	CMT-A PR bal. line	HONEYWELL	STD130	TMD 107	0 : 100	kPa	4.637	-45.47	0.025	-70.47	0.10%
DP-A40E	DP - Transm.	CMT-A inj. line	HONEYWELL	STD130	TMD 093	-25 : 105	kPa	2.615	-25.644	0.0325	-83.144	0.10%
DP-A41E	DP - Transm.	CMT-A	HONEYWELL	STD120	TMD 139	0 : 18	kPa	1.555	15.249	-0.0045	19.749	0.10%
DP-A42E	DP - Transm.	CMT-A	HONEYWELL	STD120	TMD 040	0 : 18	kPa	1.555	15.249	-0.0045	19.749	0.10%
DP-A43E	DP - Transm.	CMT-A	HONEYWELL	STD120	TMD 052	0 : 18	kPa	1.555	15.249	-0.0045	19.749	0.10%
DP-A44E	DP - Transm.	CMT-A	HONEYWELL	STD120	TMD 062	0 : 18	kPa	1.555	15.249	-0.0045	19.749	0.10%
DP-A45E	DP - Transm.	CMT-A CL-bal. line	HONEYWELL	STD120	TMD 063	-20 : 80	kPa	7.225	90.853	-0.025	115.853	0.10%
DP-A51E	DP - Transm.	IRWST inj. line A	HONEYWELL	STD120	TMD 117	0 : 100	kPa	1.015	-9.954	0.025	-34.954	0.10%
DP-A81AE	DP - Transm.	PRHR Supply Line	HONEYWELL	STD120	TMD 032	-50 : 50	kPa	2.629	25.782	0.025	-49.218	0.10%
DP-A81BE	DP - Transm.	PRHR Supply Line	HONEYWELL	STD130	TMD 099	-50 : 50	kPa	2.629	-25.782	0.025	-100.78	0.10%
DP-A81E	DP - Transm.	PRHR supply line	HONEYWELL	STD120	TMD 188	-20 : 80	kPa	8.006	78.512	-0.025	123.512	0.10%
DP-A82E	DP - Transm.	PRHR sup./ret.	HONEYWELL	STD120	TMD 066	-40 : 60	kPa	5.38	-52.76	0.025	-117.76	0.10%
DP-A83E	DP - Transm.	PRHR return line	HONEYWELL	STD120	TMD 041	0 : 50	kPa	1.13	-11.082	0.0125	-23.582	0.10%
DP-B001P	DP - Transm.	CL-B1	HONEYWELL	STD120	TMD 080	0 : 50	kPa	1.051	-10.297	0.0125	-22.797	0.10%

TABLE C-1
SPES-2 INSTRUMENT LIST (Cont.)

PLANT CODE	INSTRUMENT	LOCATION	MANUFACTURER	MODEL	SIET CODE	SPAN	M.U.	h (m)	K (kPa)	M (M.U./mV)	Q (M.U.)	MANU. ACCURACY ±
DP-B002P	DP - Transm.	CL-B2	HONEYWELL	STD120	TMD 069	0 : 50	kPa	1.051	-10.297	0.0125	-22.797	0.10%
DP-B00P	DP - Transm.	PCP-B	HONEYWELL	STD130	TMD 133	0 : 700	kPa	0.339	-3.325	-0.175	171.675	0.10%
DP-B00S	DP - Transm.	SG-B baffle	GOULD	PD3000 030-12	TMD 225	-2.5 : 2.5	kPa	0	0	0.00125	-3.75	0.25%
DP-B011P	DP - Transm.	CL-B1	HONEYWELL	STD120	TMD 071	-25 : 25	kPa	0	0	0.0125	-37.5	0.10%
DP-B012P	DP - Transm.	CL-B2	HONEYWELL	STD120	TMD 072	-25 : 25	kPa	0	0	0.0125	-37.5	0.10%
DP-B01S	DP - Transm.	SG-B riser	YOKOGAWA	EJ110	TMD 205	0 : 50	kPa	3.98	39.03	-0.0125	51.53	0.25%
DP-B021P	DP - Transm.	CL-B1/PC DC	HONEYWELL	STD120	TMD 051	0 : 70	kPa	1.245	-12.209	0.0175	-29.709	0.10%
DP-B022P	DP - Transm.	CL-B2/PC DC	HONEYWELL	STD120	TMD 061	0 : 70	kPa	1.245	-12.209	0.0175	-29.709	0.10%
DP-B02S	DP - Transm.	SG-B riser	HONEYWELL	STD120	TMD 060	0 : 70	kPa	6.5	63.743	-0.0175	81.243	0.10%
DP-B03P	DP - Transm.	SG-B in/out	HONEYWELL	STD130	TMD 109	-100 : 400	kPa	0	0	0.125	-225	0.10%
DP-B03S	DP - Transm.	SG-B separator	HONEYWELL	STD120	TMD 086	-50 : 50	kPa	3.2	41.381	-0.025	106.381	0.10%
DP-B04P	DP - Transm.	HL-A	HONEYWELL	STD120	TMD 050	-40 : 60	kPa	3.603	45.334	0.025	-29.666	0.10%
DP-B04S	DP - Transm.	SG-B separator	HONEYWELL	STD120	TMD 088	-10 : 10	kPa	0.675	9.9525	-0.005	21.619	0.10%
DP-P .5P	DP - Transm.	U-tube SG-B	HONEYWELL	STD130	TMD 131	-60 : 120	kPa	5.125	-9.741	0.045	-54.741	0.10%
DP-B05S	DP - Transm.	SG-B dryers	GOULD	PD3000-200	TMD 144	0 : 10	kPa	0.69	2.766	-0.0025	9.266	0.25%
DP-B06P	DP - Transm.	U-tube SG-B	HONEYWELL	STD120	TMD 089	-40 : 60	kPa	3.75	-3.225	0.025	-28.225	0.10%
DP-B06S	DP - Transm.	SG-B riser	GOULD	PD3000-200	TMD 154	0 : 30	kPa	2.15	21.084	-0.0075	28.584	0.25%
DP-B07P	DP - Transm.	U-tube SG-B	HONEYWELL	STD120	TMD 084	-30 : 70	kPa	3.75	-36.775	0.025	-91.775	0.10%
DP-B08P	DP - Transm.	U-tube SG-B	HONEYWELL	STD130	TMD 106	-60 : 100	kPa	5.125	-50.259	0.04	-150.26	0.10%
DP-B09P	DP - Transm.	PS-B	HONEYWELL	STD120	TMD 119	0 : 100	kPa	1.768	-17.338	0.025	-42.338	0.10%
DP-B15P	DP - Transm.	HL-B/PC UP	HONEYWELL	STD120	TMD 075	-15 : 15	kPa	1.014	9.944	0.0075	-12.556	0.10%
DP-B16P	DP - Transm.	HL-B/PC UP	HONEYWELL	STD120	TMD 137	0 : 20	kPa	0.666	-6.531	0.005	-11.531	0.10%
DP-B20E	DP - Transm.	ACC-B inj. line	HONEYWELL	STD130	TMD 097	-50 : 200	kPa	3.34	32.754	0.0625	-79.746	0.10%
DP-B28P	DP - Transm.	CMT-B PR bal. line	HONEYWELL	STD120	TMD 143	0 : 100	kPa	4.637	-45.47	0.025	-70.47	0.10%
DP-B40E	DP - Transm.	CMT-B inj. line	HONEYWELL	STD130	TMD 098	-25 : 105	kPa	2.615	-25.644	0.0325	-83.744	0.10%

**TABLE C-1
SPES-2 INSTRUMENT LIST (Cont.)**

PLANT CODE	INSTRUMENT	LOCATION	MANUFACTURER	MODEL	SIET CODE	SPAN	MU.	h (m)	K (kPa)	M (M.U./mV)	Q (M.U.)	MANU. ACCURACY ±
DP-B41E	DP - Transm.	CMT-B	HONEYWELL	STD120	TMD 090	0 : 18	kPa	1.555	15.249	-0.0045	19.749	0.10%
DP-B42E	DP - Transm.	CMT-B	HONEYWELL	STD120	TMD 130	0 : 18	kPa	1.555	15.249	-0.0045	19.749	0.10%
DP-B43E	DP - Transm.	CMT-B	HONEYWELL	STD120	TMD 091	0 : 18	kPa	1.555	15.249	-0.0045	19.749	0.10%
DP-B44E	DP - Transm.	CMT-B	HONEYWELL	STD120	TMD 038	0 : 18	kPa	1.555	15.249	-0.0045	19.749	0.10%
DP-B45E	DP - Transm.	CMT-B CL-bul. line	HONEYWELL	STD120	TMD 042	- 20 : 80	kPa	7.225	70.853	-0.025	115.853	0.10%
DP-B61E	DP - Transm.	BRWST inj. line B	SCHLUMBERGER	BTBF5GA3	TMD 016	0 : 100	kPa	1.015	-9.954	0.025	-34.954	0.25%
F-001BP	Venturi/DP-Transm.		HONEYWELL	STD120	TMD 142	0 : 40	kPa	0	0	0.01	-10	0.10%
F-001BS	Venturi/DP-Transm.		HONEYWELL	STD624	TMD 230	0 : 20	kPa	0	0	0.005	-5	0.10%
F-001A	DP-Transm.	CVS	BALEY	BC2521515	TMD 134	0 : 30	kPa	0	0	0.0075	-7.5	0.10%
F-002P	Turbine	PC tubular DC	CENG	4"	-	N/A	dm ³ /s	-	-	0.007	-0.00667	0.1%
F-003P	Venturi/DP-Transm.	PC tubular DC	HONEYWELL	STD120	TMD 082	0 : 80	kPa	0.161	-1.578	0.02	-21.574	0.10%
F-003P	Venturi/DP-Transm.	PC tubular DC	HONEYWELL	STD120	TMD 082	0 : 6	kPa	0.161	-1.578	0.0015	-3.103	0.10%
F-005P	Turbine	Break line	CENG	2"	-	N/A	dm ³ /s	-	-	0.0066	-0.0066	0.1%
F-014P	Venturi/DP-Transm.	DC-UH bypass	HONEYWELL	STD120	TMD 112	0 : 100	kPa	0.057	0.559	0.025	-24.441	0.10%
F-015P	Turbine	SL	CENG	1.5"	-	N/A	dm ³ /s	-	-	0.00038	-0.3725	0.1%
F-030P	Turbine	ADS-1,-2,-3 header	M.I.	3"	-	N/A	-	-	-	-	-	0.1%
F-040P	Turbine	ADS-4 header	CENG	3"	-	N/A	dm ³ /s	-	-	1	0	0.1%
F-A00E	Orifice/DP-Transm.	NRHR A	HONEYWELL	STD130	TMD 035	0 : 700	kPa	0	0	0.175	-175	0.10%
F-A01P	Venturi/DP-Transm.	CL-A1	HONEYWELL	STD120	TMD 077	0 : 60	kPa	0	0	0.015	-15	0.10%
F-A01P	Venturi/DP-Transm.	CL-A1	HONEYWELL	STD120	TMD 077	0 : 5	kPa	0	0	0.00125	-1.2588	0.10%
F-A01S	Orifice/DP-Transm.	MPW-A	HONEYWELL	STD130	TMD 095	0 : 250	kPa	0	0	0.0625	-62.5	0.10%
F-A02P	Venturi/DP-Transm.	CL-A2	HONEYWELL	STD120	TMD 078	0 : 5	kPa	0	0	0.00125	-1.2483	0.10%
F-A02P	Venturi/DP-Transm.	CL-A2	HONEYWELL	STD120	TMD 078	0 : 60	kPa	0	0	0.015	-15	0.10%
F-A02S	Venturi/DP-Transm.	SG-ADC	SCHLUMBERGER	BTBF5GA-3	TMD 202	0 : 100	kPa	0.085	-0.834	0.025	-25.834	0.25%
F-A03S	Venturi/DP-Transm.	SG-ADC	YOKOGAWA	EJ110	TMD 200	0 : 100	kPa	0.085	-0.834	0.025	-25.834	0.25%

TABLE C-1
SPES-2 INSTRUMENT LIST (Cont.)

PLANT CODE	INSTRUMENT	LOCATION	MANUFACTURER	MODEL	SIET CODE	SPAN	M.U.	h (m)	K (kPa)	M (M.U./mV)	Q (M.U.)	MANU. ACCURACY ±
F-A04S	Venturi/DP-Transm.	MSL-A	SCHLUMBERGER	BTDK5GA3	TMD 187	0 : 1000	kPa	0	0	0.25	-250	0.25%
F-A10P	Turbine	HL-A	CENG	3"		N/A	dm ³ /s	-	-	0.0039	-3.78	0.1%
F-A20A	Orifice/DP-Transm.	SFW-A	HONEYWELL	STD130	TMD 111	0 : 100	kPa	0.018	0.177	0.025	-24.823	0.10%
F-A20E	Venturi/DP-Transm.	ACC-A inj. line	HONEYWELL	STD120	TMD 123	0 : 50	kPa	0	0	0.0125	-12.5	0.10%
F-A40E	Venturi/DP-Transm.	CMT-A inj. line	HONEYWELL	STD120	TMD 135	0 : 20	kPa	0	0	0.005	-5	0.10%
F-A60E	Venturi/DP-Transm.	IRWST inj. line A	HONEYWELL	STD120	TMD 033	0 : 60	kPa	0	0	0.015	-15	0.10%
F-A80E	Venturi/DP-Transm.	PRHR return line	HONEYWELL	STD130	TMD 102	0 : 300	kPa	0	0	0.075	-75	0.10%
F-B00E	Orifice/DP-Transm.	NRHR B	HONEYWELL	STD130	TMD 094	0 : 700	kPa	0	0	0.175	-175	0.10%
F-B01P	Venturi/DP-Transm.	CL-B1	HONEYWELL	STD120	TMD 079	0 : 60	kPa	0	0	0.015	-15	0.10%
F-B01P	Venturi/DP-Transm.	CL-B1	HONEYWELL	STD120	TMD 079	0 : 5	kPa	0	0	0.00125	-1.2538	0.10%
F-B01S	Orifice/DP-Transm.	MPW-B	HONEYWELL	STD130	TMD 096	0 : 250	kPa	0	0	0.0625	-62.5	0.10%
F-B02P	Venturi/DP-Transm.	CL-B2	HONEYWELL	STD120	TMD 064	0 : 60	kPa	0	0	0.015	-15	0.10%
F-B02P	Venturi/DP-Transm.	CL-B2	HONEYWELL	STD120	TMD 064	0 : 5	kPa	0	0	0.00125	-1.2732	0.10%
F-B02S	Venturi/DP-Transm.	SG-B DC	HONEYWELL	STD130	TMD 231	0 : 100	kPa	0.085	-0.834	0.025	-25.834	0.10%
F-B03S	Venturi/DP-Transm.	SG-B DC	HONEYWELL	STD120	TMD 146	0 : 100	kPa	0.085	-0.834	0.025	-25.834	0.10%
F-B04S	Venturi/DP-Transm.	MSL-B	HONEYWELL	STD130	TMD 108	0 : 500	kPa	0	0	0.125	-125	0.10%
(*F-B04SM	Venturi/P-Transm.	MSL-B	HONEYWELL	STG180	TMR 60	0 : 6	MPa	10.28	-100.81	0.0015	-1.5	0.10%
(*F-B04SP	Venturi/P-Transm.	MSL-B	HONEYWELL	STG180	TMR 56	0 : 7	MPa	10.28	-100.81	0.00175	-1.75	0.10%
F-B20A	Orifice/DP-Transm.	SFW-B	HONEYWELL	STD130	TMD 108	0 : 100	kPa	0.018	0.177	0.025	-24.823	0.10%
F-B30E	Venturi/DP-Transm.	ACC-B inj. line	HONEYWELL	STD120	TMD 128	0 : 50	kPa	0	0	0.0125	-12.5	0.10%
F-B40E	Venturi/DP-Transm.	CMT-B inj. line	HONEYWELL	STD120	TMD 136	0 : 20	kPa	0	0	0.005	-5	0.10%
F-B60E	Venturi/DP-Transm.	IRWST inj. line B	HONEYWELL	STD130	TMD 145	0 : 60	kPa	0	0	0.015	-15	0.10%
I-01P	Shunt	Power busbar	CGE	A. 12000	DCP01	0 : 10000	A	-	-	122.42	0	0.20%
I-02P	Shunt	Power busbar	CGE	A. 12000	DCP02	0 : 10000	A	-	-	121	0	0.20%
I-03P	Shunt	Power busbar	CGE	A. 12000	DCP03	0 : 10000	A	-	-	120.98	0	0.20%

(*F-B04GVB = F-B04SP - F-B04SM (Derived measurement))

**TABLE C-1
SPES-2 INSTRUMENT LIST (Cont.)**

PLANT CODE	INSTRUMENT	LOCATION	MANUFACTURER	MODEL	SIET CODE	SPAN	MLU	h (m)	K (kPa)	M (MLU/mV)	Q (M.U.)	MANU. ACCURACY ±
I-04P	Shunt	Power busbar	CGE	A. 12000	DCP04	0 : 10000	A	-	-	120.43	0	0.20%
I-05P	Shunt	Power busbar	CGE	A. 12000	DCP05	0 : 10000	A	-	-	120.6	0	0.20%
I-06P	Shunt	Power busbar	TAMINI	A. 30000	DCP06	0 : 30000	A	-	-	310.824	0	0.20%
I-A1P	Ammeter	PCP-A	SCS	-	-	-140 : 140	A	-	-	0.028	0	-
I-B1P	Ammeter	PCP-B	SCS	-	-	-140 : 140	A	-	-	0.028	0	-
IF005P	Catch tank	Break line	BCS	Z1000	CHT02	0 : 1400	kg	-	-	153.152	-550	0.10%
IF030P	Catch tank	ADS-1,-2,-3 header	BCS	Z1000	CHT01	0 : 1400	kg	-	-	150.141	-550	0.10%
IF040P	Catch tank	ADS-4 header	BCS	Z1000	CHT03	0 : 1400	kg	-	-	152.924	-550	0.10%
L-010P	DP - Transm.	PR	HONEYWELL	STD130	TMD 092	0 : 66.3	kPa	6.206	60.8526	-0.01658	77.4326	0.10%
L-060E	DP - Transm.	IRWST	HONEYWELL	STD120	TMD 083	0 : 100	kPa	8.75	85.8	-0.025	110.8	0.10%
L-A10S	DP - Transm.	SG-A	HONEYWELL	STD130	TMD 100	0 : 134.16	kPa	13.68	134.155	-0.03354	167.695	0.10%
L-A20E	DP - Transm.	ACC-A	HONEYWELL	STD120	TMD 067	0 : 70	kPa	2.596	-22.143	0.0175	-39.643	0.10%
L-A20S	DP - Transm.	SG-A	HONEYWELL	STD120	TMD 058	0 : 26.09	kPa	2.66	26.088	-0.00652	32.608	0.10%
L-A40E	DP - Transm.	CMT-A	HONEYWELL	STD120	TMD 059	0 : 61	kPa	6.22	60.997	-0.01525	76.247	0.10%
L-B10S	DP - Transm.	SG-B	HONEYWELL	STD130	TMD 101	0 : 134.16	kPa	13.68	134.155	-0.03354	167.695	0.10%
L-B20E	DP - Transm.	ACC-B	HONEYWELL	STD120	TMD 044	0 : 70	kPa	2.596	-22.143	0.0175	-39.643	0.10%
L-B20S	DP - Transm.	SG-B	HONEYWELL	STD130	TMD 103	0 : 26.09	kPa	2.66	26.108	-0.0065	32.608	0.10%
L-B40E	DP - Transm.	CMT-B	HONEYWELL	STD120	TMD 070	0 : 61	kPa	6.22	60.997	-0.01525	76.247	0.10%
P-001P	P transmitter	PC tubular DC	HONEYWELL	STG180	TMR 065	0.1 : 20.1	MPa	1.755	-17.211	0.005	-4.9172	0.10%
P-003P	P transmitter	ADS-1,-2,-3 header	HONEYWELL	STG180	TMR 052	0.1 : 20.1	MPa	11.34	-111.178	0.005	-5.0112	0.10%
P-017P	P transmitter	PC UH	HONEYWELL	STG180	TMR 047	0.1 : 20.1	MPa	8.426	-82.631	0.005	-4.9826	0.10%
P-027P	P transmitter	PR	HONEYWELL	STG180	TMR 051	0.1 : 20.1	MPa	8.299	-81.385	0.005	-4.9814	0.10%
P-030P	P transmitter	ADS-1,-2,-3 header	ROSEMOUNT	1AP6E22MB	TMA 042	100 : 800	kPa	10.74	-105.294	0.175	-180.3	0.25%
P-040P	P transmitter	ADS-4 header	ROSEMOUNT	1AP6E22MB	TMA 043	100 : 800	kPa	8.64	-84.729	0.175	-159.73	0.25%
P-A01S	P transmitter	MFW-A	HONEYWELL	STG180	TMR 058	0.1 : 10.1	MPa	8.858	-86.867	0.0025	-2.4869	0.10%

TABLE C-1
SPES-2 INSTRUMENT LIST (Cont.)

PLANT CODE	INSTRUMENT	LOCATION	MANUFACTURER	MODEL	SIET CODE	SPAN	M.U.	h '(a)	K (kPa)	M (M.U./mV)	Q (M.U.)	MANU. ACCURACY ±
P-A04P	P transmitter	HL-A	HONEYWELL	STG180	TMR 049	0.1 : 20.1	MPa	8.674	-85.063	0.005	-4.9871	0.10%
P-A04S	P transmitter	MSL-A	HONEYWELL	STG180	TMR 055	0.1 : 10.1	MPa	9.783	-95.938	0.0025	-2.4959	0.10%
P-A20E	P transmitter	ACC-A	HONEYWELL	STG180	TMR 064	0.1 : 10.1	MPa	3.865	-37.903	0.0025	-2.4379	0.10%
P-A40A	P transmitter	CMT-A	SCHLUMBERGER	BTMP1GA2	TMR 076	0.1 : 10.1	MPa	0	0	0.0025	-2.4	0.10%
P-A40E	P transmitter	CMT-A	HONEYWELL	STG180	TMR 048	0.1 : 20.1	MPa	4.102	-40.227	0.005	-4.9402	0.10%
P-B01S	P transmitter	MPW-B	HONEYWELL	STG180	TMR 059	0.1 : 10.1	MPa	8.458	-82.945	0.0025	-2.4829	0.10%
P-B04P	P transmitter	HL-B	HONEYWELL	STG180	TMR 050	0.1 : 20.1	MPa	9.074	-88.986	0.005	-4.9879	0.10%
P-B04S	P transmitter	MSL-B	HONEYWELL	STG180	TMR 062	0.1 : 10.1	MPa	9.783	-95.938	0.0025	-2.4959	0.10%
P-B20E	P transmitter	ACC-B	HONEYWELL	STG180	TMR 054	0.1 : 10.1	MPa	4.265	-41.825	0.0025	-2.4418	0.10%
P-B40A	P transmitter	CMT-B	SCHLUMBERGER	BTMN1GA2	TMR 069	0.1 : 10.1	MPa	0	0	0.0025	-2.4	0.10%
P-B40E	P transmitter	CMT-B	HONEYWELL	STG180	TMR 057	0.1 : 20.1	MPa	3.302	-32.382	0.005	-4.9324	0.10%
S-A1P	Tachymeter	PCP-A	RADIOENERGIE	RE044N1	n.v.	-6000 : 6000	RPM	-	-	1.2075	8.18187	1.5%
S-B1P	Tachymeter	PCP-B	RADIOENERGIE	RE044N1	n.v.	-6000 : 6000	RPM	-	-	1.1749	9.60263	1.5%
T-001A	K thermocouple	CVCS	NUOVA TERMICS	ANSI MC96.1	TCK 405	50 : 400	°C	-	-	UNI 7938	-	ANSI SPECIAL
T-001B	K thermocouple	BREAK LINE	NUOVA TERMICS	ANSI MC96.1	TCK 411	50 : 400	°C	-	-	UNI 7938	-	ANSI SPECIAL
T-001P	K thermocouple	PC tubular DC	NUOVA TERMICS	ANSI MC96.1	TCK 320	50 : 400	°C	-	-	UNI 7938	-	ANSI SPECIAL
T-001PH	K thermocouple	PC tubular DC	NUOVA TERMICS	ANSI MC96.1	TCK 332	50 : 400	°C	-	-	UNI 7938	-	ANSI SPECIAL
T-001PL	K thermocouple	PC tubular DC	NUOVA TERMICS	ANSI MC96.1	TCK 331	50 : 400	°C	-	-	UNI 7938	-	ANSI SPECIAL
T-002P	K thermocouple	PC tubular DC	NUOVA TERMICS	ANSI MC96.1	TCK 369	50 : 400	°C	-	-	UNI 7938	-	ANSI SPECIAL
T-003P	K thermocouple	PC tubular DC	NUOVA TERMICS	ANSI MC96.1	TCK 361	50 : 400	°C	-	-	UNI 7938	-	ANSI SPECIAL
T-003PH	K thermocouple	PC tubular DC	NUOVA TERMICS	ANSI MC96.1	TCK 334	50 : 400	°C	-	-	UNI 7938	-	ANSI SPECIAL
T-003PL	K thermocouple	PC tubular DC	NUOVA TERMICS	ANSI MC96.1	TCK 333	50 : 400	°C	-	-	UNI 7938	-	ANSI SPECIAL
T-004P	K thermocouple	PC LP	NUOVA TERMICS	ANSI MC96.1	TCK 366	50 : 400	°C	-	-	UNI 7938	-	ANSI SPECIAL
T-014P	K thermocouple	PC DC-UH bypass	NUOVA TERMICS	ANSI MC96.1	TCK 367	50 : 400	°C	-	-	UNI 7938	-	ANSI SPECIAL
T-015P	K thermocouple	PC UP	NUOVA TERMICS	ANSI MC96.1	TCK 429	50 : 400	°C	-	-	UNI 7938	-	ANSI SPECIAL

**TABLE C-1
SPES-2 INSTRUMENT LIST (Cont.)**

PLANT CODE	INSTRUMENT	LOCATION	MANUFACTURER	MODEL	SIET CODE	SPAN	M.U.	h (m)	K (kPa)	M (M.U./mV)	Q (M.U.)	MANU. ACCURACY \pm
T-016P	K thermocouple	PC UH	NUOVA TERMICS	ANSI MC96.1	T016P	50 : 400	°C	-	-	UNI 7938	-	ANSI SPECIAL
T-018P	K thermocouple	SL	NUOVA TERMICS	ANSI MC96.1	TCK 430	50 : 400	°C	-	-	UNI 7938	-	ANSI SPECIAL
T-019PH	K thermocouple	SL	NUOVA TERMICS	ANSI MC96.1	TCK 322	50 : 400	°C	-	-	UNI 7938	-	ANSI SPECIAL
T-019PL	K thermocouple	SL	NUOVA TERMICS	ANSI MC96.1	TCK 335	50 : 400	°C	-	-	UNI 7938	-	ANSI SPECIAL
T-020P	K thermocouple	SL	NUOVA TERMICS	ANSI MC96.1	TCK 323	50 : 400	°C	-	-	UNI 7938	-	ANSI SPECIAL
T-021P	K thermocouple	PR	NUOVA TERMICS	ANSI MC96.1	TCK 451	50 : 400	°C	-	-	UNI 7938	-	ANSI SPECIAL
T-022P	K thermocouple	PR	NUOVA TERMICS	ANSI MC96.1	TCK 325	50 : 400	°C	-	-	UNI 7938	-	ANSI SPECIAL
T-023P	K thermocouple	PR	NUOVA TERMICS	ANSI MC96.1	TCK 326	50 : 400	°C	-	-	UNI 7938	-	ANSI SPECIAL
T-024P	K thermocouple	PR	NUOVA TERMICS	ANSI MC96.1	TCK 327	50 : 400	°C	-	-	UNI 7938	-	ANSI SPECIAL
T-025P	K thermocouple	PR	NUOVA TERMICS	ANSI MC96.1	TCK 328	50 : 400	°C	-	-	UNI 7938	-	ANSI SPECIAL
T-026P	K thermocouple	PR	NUOVA TERMICS	ANSI MC96.1	TCK 329	50 : 400	°C	-	-	UNI 7938	-	ANSI SPECIAL
T-030P	K thermocouple	ADS-1,-2,-3 header	NUOVA TERMICS	ANSI MC96.1	TCK 330	50 : 400	°C	-	-	UNI 7938	-	ANSI SPECIAL
T-031P	K thermocouple	PC DC	NUOVA TERMICS	ANSI MC96.1	TCK 363	50 : 400	°C	-	-	UNI 7938	-	ANSI SPECIAL
T-032P	K thermocouple	PC DC	NUOVA TERMICS	ANSI MC96.1	TCK 360	50 : 400	°C	-	-	UNI 7938	-	ANSI SPECIAL
T-033P	K thermocouple	PC DC	NUOVA TERMICS	ANSI MC96.1	TCK 365	50 : 400	°C	-	-	UNI 7938	-	ANSI SPECIAL
T-034P	K thermocouple	PC DC	NUOVA TERMICS	ANSI MC96.1	TCK 368	50 : 400	°C	-	-	UNI 7938	-	ANSI SPECIAL
T-035P	K thermocouple	PC DC	NUOVA TERMICS	ANSI MC96.1	TCK 370	50 : 400	°C	-	-	UNI 7938	-	ANSI SPECIAL
T-036P	K thermocouple	PC DC	NUOVA TERMICS	ANSI MC96.1	TCK 371	50 : 400	°C	-	-	UNI 7938	-	ANSI SPECIAL
T-040P	K thermocouple	ADS-4 header	NUOVA TERMICS	ANSI MC96.1	TCK 372	50 : 400	°C	-	-	UNI 7938	-	ANSI SPECIAL
T-041P	K thermocouple	PC DC	NUOVA TERMICS	ANSI MC96.1	TCK 373	50 : 400	°C	-	-	UNI 7938	-	ANSI SPECIAL
T-042P	K thermocouple	PC DC	NUOVA TERMICS	ANSI MC96.1	TCK 374	50 : 400	°C	-	-	UNI 7938	-	ANSI SPECIAL
T-043P	K thermocouple	PC DC	NUOVA TERMICS	ANSI MC96.1	TCK 375	50 : 400	°C	-	-	UNI 7938	-	ANSI SPECIAL
T-044P	K thermocouple	PC DC	NUOVA TERMICS	ANSI MC96.1	TCK 376	50 : 400	°C	-	-	UNI 7938	-	ANSI SPECIAL
T-045P	K thermocouple	PC DC	NUOVA TERMICS	ANSI MC96.1	TCK 377	50 : 400	°C	-	-	UNI 7938	-	ANSI SPECIAL
T-0465P	K thermocouple	PC DC	NUOVA TERMICS	ANSI MC96.1	TCK 378	50 : 400	°C	-	-	UNI 7938	-	ANSI SPECIAL

TABLE C-1
SPES-2 INSTRUMENT LIST (Cont.)

PLANT CODE	INSTRUMENT	LOCATION	MANUFACTURER	MODEL	SIET CODE	SPAN	M.U.	h (m)	K (kPa)	M (M.U./mV)	Q (M.U.)	MANU. ACCURACY \pm
T-A00E	K thermocouple	DVI A	NUOVA TERMICS	ANSI MC96.1	TCK 399	50 : 400	°C	-	-	UNI 7938	-	ANSI SPECIAL
T-A011P	K thermocouple	CL-A1	NUOVA TERMICS	ANSI MC96.1	TCK 380	50 : 400	°C	-	-	UNI 7938	-	ANSI SPECIAL
T-A012P	K thermocouple	CL-A2	NUOVA TERMICS	ANSI MC96.1	TCK 381	50 : 400	°C	-	-	UNI 7938	-	ANSI SPECIAL
T-A01P	K thermocouple	CL-A pump outlet	NUOVA TERMICS	ANSI MC96.1	TCK 382	50 : 400	°C	-	-	UNI 7938	-	ANSI SPECIAL
T-A01S	K thermocouple	MPW-A	NUOVA TERMICS	ANSI MC96.1	TCK 383	50 : 400	°C	-	-	UNI 7938	-	ANSI SPECIAL
T-A021PL	K thermocouple	CL-A1/DC inlet	NUOVA TERMICS	ANSI MC96.1	TCK 384	50 : 400	°C	-	-	UNI 7938	-	ANSI SPECIAL
T-A021PO	K thermocouple	CL-A1/DC inlet	NUOVA TERMICS	ANSI MC96.1	TCK 385	50 : 400	°C	-	-	UNI 7938	-	ANSI SPECIAL
T-A022PL	K thermocouple	CL-A2/ DC inlet	NUOVA TERMICS	ANSI MC96.1	TCK 386	50 : 400	°C	-	-	UNI 7938	-	ANSI SPECIAL
T-A022PO	K thermocouple	CL-A2/DC inlet	NUOVA TERMICS	ANSI MC96.1	TCK 387	50 : 400	°C	-	-	UNI 7938	-	ANSI SPECIAL
T-A02E	K thermocouple	NRHR A	NUOVA TERMICS	ANSI MC96.1	TCK 388	50 : 400	°C	-	-	UNI 7938	-	ANSI SPECIAL
T-A02S	K thermocouple	SG-A DC	NUOVA TERMICS	ANSI MC96.1	TCK 389	50 : 400	°C	-	-	UNI 7938	-	ANSI SPECIAL
T-A031PL	K thermocouple	CL-A1	NUOVA TERMICS	ANSI MC96.1	TCK 404	50 : 400	°C	-	-	UNI 7938	-	ANSI SPECIAL
T-A032PL	K thermocouple	CL-A2	NUOVA TERMICS	ANSI MC96.1	TCK 403	50 : 400	°C	-	-	UNI 7938	-	ANSI SPECIAL
T-A03PL	K thermocouple	HL-A	NUOVA TERMICS	ANSI MC96.1	TCK 390	50 : 400	°C	-	-	UNI 7938	-	ANSI SPECIAL
T-A03PO	K thermocouple	HL-A	NUOVA TERMICS	ANSI MC96.1	TCK 391	50 : 400	°C	-	-	UNI 7938	-	ANSI SPECIAL
T-A03S	K thermocouple	SG-A DC	NUOVA TERMICS	ANSI MC96.1	TCK 392	50 : 400	°C	-	-	UNI 7938	-	ANSI SPECIAL
T-A04P	K thermocouple	HL-A	NUOVA TERMICS	ANSI MC96.1	TCK 393	50 : 400	°C	-	-	UNI 7938	-	ANSI SPECIAL
T-A04S	K thermocouple	MSL-A	NUOVA TERMICS	ANSI MC96.1	TCK 394	50 : 400	°C	-	-	UNI 7938	-	ANSI SPECIAL
T-A05P	K thermocouple	SG-A U-tube	NUOVA TERMICS	ANSI MC96.1	T205P	50 : 400	°C	-	-	UNI 7938	-	ANSI SPECIAL
T-A05S	K thermocouple	SG-A riser	NUOVA TERMICS	ANSI MC96.1	T205S	50 : 400	°C	-	-	UNI 7938	-	ANSI SPECIAL
T-A06P	K thermocouple	SG-A U-tube	NUOVA TERMICS	ANSI MC96.1	T206P	50 : 400	°C	-	-	UNI 7938	-	ANSI SPECIAL
T-A06S	K thermocouple	SG-A riser	NUOVA TERMICS	ANSI MC96.1	T206S	50 : 400	°C	-	-	UNI 7938	-	ANSI SPECIAL
T-A07S	K thermocouple	SG-A riser	NUOVA TERMICS	ANSI MC96.1	TCK 397	50 : 400	°C	-	-	UNI 7938	-	ANSI SPECIAL
T-A08P	K thermocouple	SG-A U-tube	NUOVA TERMICS	ANSI MC96.1	T208P	50 : 400	°C	-	-	UNI 7938	-	ANSI SPECIAL
T-A08S	K thermocouple	SG-A riser	NUOVA TERMICS	ANSI MC96.1	T208S	50 : 400	°C	-	-	UNI 7938	-	ANSI SPECIAL

**TABLE C-1
SPES-2 INSTRUMENT LIST (Cont.)**

PLANT CODE	INSTRUMENT	LOCATION	MANUFACTURER	MODEL	SIET CODE	SPAN	M.U.	h (m)	K (kPa)	M (M.U./mV)	Q (M.U.)	MANU. ACCURACY \pm
T-A09P	K thermocouple	SG-A U-tube	NUOVA TERMICS	ANSI MC96.1	T209P	50 : 400	°C	-	-	UNI 7938	-	ANSI SPECIAL
T-A09S	K thermocouple	SG-A riser	NUOVA TERMICS	ANSI MC96.1	T209S	50 : 400	°C	-	-	UNI 7938	-	ANSI SPECIAL
T-A10P	K thermocouple	PS-A	NUOVA TERMICS	ANSI MC96.1	TCK 400	50 : 400	°C	-	-	UNI 7938	-	ANSI SPECIAL
T-A11P	K thermocouple	PS-A	NUOVA TERMICS	ANSI MC96.1	TCK 401	50 : 400	°C	-	-	UNI 7938	-	ANSI SPECIAL
T-A141P	K thermocouple	CMT-A CL-bal. line	NUOVA TERMICS	ANSI MC96.1	TCK 336	50 : 400	°C	-	-	UNI 7938	-	ANSI SPECIAL
T-A142PH	K thermocouple	CMT-A CL-bal. line	NUOVA TERMICS	ANSI MC96.1	TCK 337	50 : 400	°C	-	-	UNI 7938	-	ANSI SPECIAL
T-A142PL	K thermocouple	CMT-A CL-bal. line	NUOVA TERMICS	ANSI MC96.1	TCK 345	50 : 400	°C	-	-	UNI 7938	-	ANSI SPECIAL
T-A143P	K thermocouple	CMT-A CL-bal. line	NUOVA TERMICS	ANSI MC96.1	TCK 338	50 : 400	°C	-	-	UNI 7938	-	ANSI SPECIAL
T-A181E	K thermocouple	PRHR	NUOVA TERMICS	ANSI MC96.1	TCK 222	50 : 400	°C	-	-	UNI 7938	-	ANSI SPECIAL
T-A182E	K thermocouple	PRHR	NUOVA TERMICS	ANSI MC96.1	TCK 223	50 : 400	°C	-	-	UNI 7938	-	ANSI SPECIAL
T-A20A	K thermocouple	SFW	NUOVA TERMICS	ANSI MC96.1	TCK 402	50 : 400	°C	-	-	UNI 7938	-	ANSI SPECIAL
T-A21E	K thermocouple	ACC-A	NUOVA TERMICS	ANSI MC96.1	TCK 339	50 : 400	°C	-	-	UNI 7938	-	ANSI SPECIAL
T-A22E	K thermocouple	ACC-A inj. line	NUOVA TERMICS	ANSI MC96.1	TCK 340	50 : 400	°C	-	-	UNI 7938	-	ANSI SPECIAL
T-A23E	K thermocouple	ACC-A inj. line	NUOVA TERMICS	ANSI MC96.1	TCK 341	50 : 400	°C	-	-	UNI 7938	-	ANSI SPECIAL
T-A27P	K thermocouple	CMT-A PR bal. line	NUOVA TERMICS	ANSI MC96.1	TCK 342	50 : 400	°C	-	-	UNI 7938	-	ANSI SPECIAL
T-A281E	K thermocouple	PRHR	NUOVA TERMICS	ANSI MC96.1	TCK 224	50 : 400	°C	-	-	UNI 7938	-	ANSI SPECIAL
T-A28P	K thermocouple	CMT-A PR bal. line	NUOVA TERMICS	ANSI MC96.1	TCK 343	50 : 400	°C	-	-	UNI 7938	-	ANSI SPECIAL
T-A29P	K thermocouple	CMT-A PR bal. line	NUOVA TERMICS	ANSI MC96.1	TCK 344	50 : 400	°C	-	-	UNI 7938	-	ANSI SPECIAL
T-A401E	K thermocouple	CMT-A	NUOVA TERMICS	ANSI MC96.1	TCK 216	50 : 400	°C	-	-	UNI 7938	-	ANSI SPECIAL
T-A402E	K thermocouple	CMT-A	NUOVA TERMICS	ANSI MC96.1	TCK 215	50 : 400	°C	-	-	UNI 7938	-	ANSI SPECIAL
T-A403E	K thermocouple	CMT-A	NUOVA TERMICS	ANSI MC96.1	TCK 213	50 : 400	°C	-	-	UNI 7938	-	ANSI SPECIAL
T-A404E	K thermocouple	CMT-A	NUOVA TERMICS	ANSI MC96.1	TCK 212	50 : 400	°C	-	-	UNI 7938	-	ANSI SPECIAL
T-A405E	K thermocouple	CMT-A	NUOVA TERMICS	ANSI MC96.1	TCK 210	50 : 400	°C	-	-	UNI 7938	-	ANSI SPECIAL
T-A406E	K thermocouple	CMT-A	NUOVA TERMICS	ANSI MC96.1	TCK 209	50 : 400	°C	-	-	UNI 7938	-	ANSI SPECIAL
T-A407E	K thermocouple	CMT-A	NUOVA TERMICS	ANSI MC96.1	TCK 207	50 : 400	°C	-	-	UNI 7938	-	ANSI SPECIAL

TABLE C-1
SPES-2 INSTRUMENT LIST (Cont.)

PLANT CODE	INSTRUMENT	LOCATION	MANUFACTURER	MODEL	SIET CODE	SPAN	MLU	h (m)	K (kPa)	M (MLU/mV)	Q (MLU)	MANU. ACCURACY \pm
T-A408E	K thermocouple	CMT-A	NUOVA TERMICS	ANSI MC96.1	TCK 206	50 : 400	°C	-	-	UNI 7938	-	ANSI SPECIAL
T-A409E	K thermocouple	CMT-A	NUOVA TERMICS	ANSI MC96.1	TCK 204	50 : 400	°C	-	-	UNI 7938	-	ANSI SPECIAL
T-A410E	K thermocouple	CMT-A	NUOVA TERMICS	ANSI MC96.1	TCK 203	50 : 400	°C	-	-	UNI 7938	-	ANSI SPECIAL
T-A411E	K thermocouple	CMT-A	NUOVA TERMICS	ANSI MC96.1	TCK 201	50 : 400	°C	-	-	UNI 7938	-	ANSI SPECIAL
T-A412E	K thermocouple	CMT-A	NUOVA TERMICS	ANSI MC96.1	TCK 200	50 : 400	°C	-	-	UNI 7938	-	ANSI SPECIAL
T-A413E	K thermocouple	CMT-A	NUOVA TERMICS	ANSI MC96.1	TCK 198	50 : 400	°C	-	-	UNI 7938	-	ANSI SPECIAL
T-A414E	K thermocouple	CMT-A	NUOVA TERMICS	ANSI MC96.1	TCK 197	50 : 400	°C	-	-	UNI 7938	-	ANSI SPECIAL
T-A415E	K thermocouple	CMT-A	NUOVA TERMICS	ANSI MC96.1	TCK 195	50 : 400	°C	-	-	UNI 7938	-	ANSI SPECIAL
T-A416E	K thermocouple	CMT-A	NUOVA TERMICS	ANSI MC96.1	TCK 194	50 : 400	°C	-	-	UNI 7938	-	ANSI SPECIAL
T-A417E	K thermocouple	CMT-A	NUOVA TERMICS	ANSI MC96.1	TCK 192	50 : 400	°C	-	-	UNI 7938	-	ANSI SPECIAL
T-A418E	K thermocouple	CMT-A	NUOVA TERMICS	ANSI MC96.1	TCK 191	50 : 400	°C	-	-	UNI 7938	-	ANSI SPECIAL
T-A419E	K thermocouple	CMT-A	NUOVA TERMICS	ANSI MC96.1	TCK 190	50 : 400	°C	-	-	UNI 7938	-	ANSI SPECIAL
T-A41A	K thermocouple	CMT-A air	NUOVA TERMICS	ANSI MC96.1	TCK 172	50 : 400	°C	-	-	UNI 7938	-	ANSI SPECIAL
T-A420E	K thermocouple	CMT-A	NUOVA TERMICS	ANSI MC96.1	TCK 188	50 : 400	°C	-	-	UNI 7938	-	ANSI SPECIAL
T-A421E	K thermocouple	CMT-A inj. line	NUOVA TERMICS	ANSI MC96.1	TCK 346	50 : 400	°C	-	-	UNI 7938	-	ANSI SPECIAL
T-A422E	K thermocouple	CMT-A inj. line	NUOVA TERMICS	ANSI MC96.1	TCK 347	50 : 400	°C	-	-	UNI 7938	-	ANSI SPECIAL
T-A42A	K thermocouple	CMT-A air	NUOVA TERMICS	ANSI MC96.1	TCK 173	50 : 400	°C	-	-	UNI 7938	-	ANSI SPECIAL
T-A66E	K thermocouple	IRWST inj. line A	NUOVA TERMICS	ANSI MC96.1	TCK 406	50 : 400	°C	-	-	UNI 7938	-	ANSI SPECIAL
T-A81E	K thermocouple	PRHR supply line	NUOVA TERMICS	ANSI MC96.1	TCK 407	50 : 400	°C	-	-	UNI 7938	-	ANSI SPECIAL
T-A82E	K thermocouple	PRHR supply line	NUOVA TERMICS	ANSI MC96.1	TCK 533	50 : 400	°C	-	-	UNI 7938	-	ANSI SPECIAL
T-A83E	K thermocouple	PRHR return line	NUOVA TERMICS	ANSI MC96.1	TCK 409	50 : 400	°C	-	-	UNI 7938	-	ANSI SPECIAL
T-A84E	K thermocouple	PRHR return line	NUOVA TERMICS	ANSI MC96.1	TCK 457	50 : 400	°C	-	-	UNI 7938	-	ANSI SPECIAL
T-B00E	K thermocouple	DVI B	NUOVA TERMICS	ANSI MC96.1	TCK 463	50 : 400	°C	-	-	UNI 7938	-	ANSI SPECIAL
T-B011P	K thermocouple	CL-B1	NUOVA TERMICS	ANSI MC96.1	TCK 412	50 : 400	°C	-	-	UNI 7938	-	ANSI SPECIAL
T-B012P	K thermocouple	CL-B2	NUOVA TERMICS	ANSI MC96.1	TCK 413	50 : 400	°C	-	-	UNI 7938	-	ANSI SPECIAL

TABLE C-1
SPES-2 INSTRUMENT LIST (Cont.)

PLANT CODE	INSTRUMENT	LOCATION	MANUFACTURER	MODEL	SIET CODE	SPAN	U.L.	h (m)	K (kPa)	M (M.U./mV)	Q (M.U.)	MANU. ACCURACY ±
T-B01P	K thermocouple	CL-B pump outlet	NUOVA TERMICS	ANSI MC96.1	TCK 414	50 : 400	°C	-	-	UNI 7938	-	ANSI SPECIAL
T-B01S	K thermocouple	MPW-B	NUOVA TERMICS	ANSI MC96.1	TCK 415	50 : 400	°C	-	-	UNI 7938	-	ANSI SPECIAL
T-B021PL	K thermocouple	CL-B1/DC inlet	NUOVA TERMICS	ANSI MC96.1	TCK 416	50 : 400	°C	-	-	UNI 7938	-	ANSI SPECIAL
T-B021PO	K thermocouple	CL-B1/DC inlet	NUOVA TERMICS	ANSI MC96.1	TCK 417	50 : 400	°C	-	-	UNI 7938	-	ANSI SPECIAL
T-B022PL	K thermocouple	CL-B2/DC inlet	NUOVA TERMICS	ANSI MC96.1	TCK 418	50 : 400	°C	-	-	UNI 7938	-	ANSI SPECIAL
T-B022PO	K thermocouple	CL-B2/DC inlet	NUOVA TERMICS	ANSI MC96.1	TCK 419	50 : 400	°C	-	-	UNI 7938	-	ANSI SPECIAL
T-B02E	K thermocouple	NRHR B	NUOVA TERMICS	ANSI MC96.1	TCK 420	50 : 400	°C	-	-	UNI 7938	-	ANSI SPECIAL
T-B02S	K thermocouple	SG-B DC	NUOVA TERMICS	ANSI MC96.1	TCK 421	50 : 400	°C	-	-	UNI 7938	-	ANSI SPECIAL
T-B031PL	K thermocouple	CL-B1	NUOVA TERMICS	ANSI MC96.1	TCK 428	50 : 400	°C	-	-	UNI 7938	-	ANSI SPECIAL
T-B032PL	K thermocouple	CL-B2	NUOVA TERMICS	ANSI MC96.1	TCK 431	50 : 400	°C	-	-	UNI 7938	-	ANSI SPECIAL
T-B03PL	K thermocouple	HL-B	NUOVA TERMICS	ANSI MC96.1	TCK 422	50 : 400	°C	-	-	UNI 7938	-	ANSI SPECIAL
T-B03PO	K thermocouple	HL-B	NUOVA TERMICS	ANSI MC96.1	TCK 423	50 : 400	°C	-	-	UNI 7938	-	ANSI SPECIAL
T-B03S	K thermocouple	SG-B DC	NUOVA TERMICS	ANSI MC96.1	TCK 424	50 : 400	°C	-	-	UNI 7938	-	ANSI SPECIAL
T-B04P	K thermocouple	HL-B	NUOVA TERMICS	ANSI MC96.1	TCK 425	50 : 400	°C	-	-	UNI 7938	-	ANSI SPECIAL
T-B04S	K thermocouple	MSL-B	NUOVA TERMICS	ANSI MC96.1	TCK 426	50 : 400	°C	-	-	UNI 7938	-	ANSI SPECIAL
T-B05P	K thermocouple	SG-B U-tube	NUOVA TERMICS	ANSI MC96.1	T305P	50 : 400	°C	-	-	UNI 7938	-	ANSI SPECIAL
T-B05S	K thermocouple	SG-B riser	NUOVA TERMICS	ANSI MC96.1	T305S	50 : 400	°C	-	-	UNI 7938	-	ANSI SPECIAL
T-B06P	K thermocouple	SG-B U-tube	NUOVA TERMICS	ANSI MC96.1	T306P	50 : 400	°C	-	-	UNI 7938	-	ANSI SPECIAL
T-B06S	K thermocouple	SG-B riser	NUOVA TERMICS	ANSI MC96.1	T306S	50 : 400	°C	-	-	UNI 7938	-	ANSI SPECIAL
T-B07P	K thermocouple	SG-B U-tube	NUOVA TERMICS	ANSI MC96.1	T307P	50 : 400	°C	-	-	UNI 7938	-	ANSI SPECIAL
T-B07S	K thermocouple	SG-B riser	NUOVA TERMICS	ANSI MC96.1	T307S	50 : 400	°C	-	-	UNI 7938	-	ANSI SPECIAL
T-B08P	K thermocouple	SG-B U-tube	NUOVA TERMICS	ANSI MC96.1	T308P	50 : 400	°C	-	-	UNI 7938	-	ANSI SPECIAL
T-B08S	K thermocouple	SG-B riser	NUOVA TERMICS	ANSI MC96.1	T308S	50 : 400	°C	-	-	UNI 7938	-	ANSI SPECIAL
T-B09P	K thermocouple	SG-B U-tube	NUOVA TERMICS	ANSI MC96.1	T309P	50 : 400	°C	-	-	UNI 7938	-	ANSI SPECIAL
T-B09S	K thermocouple	SG-B riser	NUOVA TERMICS	ANSI MC96.1	T309S	50 : 400	°C	-	-	UNI 7938	-	ANSI SPECIAL

TABLE C-1
SPES-2 INSTRUMENT LIST (Cont.)

PLANT CODE	INSTRUMENT	LOCATION	MANUFACTURER	MODEL	SIET CODE	SPAN	MLU	h (m)	K (kPa)	M (MLU/mV)	Q (MLU)	MANU. ACCURACY \pm
T-B10P	K thermocouple	PS-B	NUOVA TERMICS	ANSI MC96.1	TCK 432	50 : 400	°C	-	-	UNI 7938	-	ANSI SPECIAL
T-B11P	K thermocouple	PS-B	NUOVA TERMICS	ANSI MC96.1	TCK 396	50 : 400	°C	-	-	UNI 7938	-	ANSI SPECIAL
T-B141P	K thermocouple	CMT-B CL-bal. line	NUOVA TERMICS	ANSI MC96.1	TCK 348	50 : 400	°C	-	-	UNI 7938	-	ANSI SPECIAL
T-B142PH	K thermocouple	CMT-B CL-bal. line	NUOVA TERMICS	ANSI MC96.1	TCK 349	50 : 400	°C	-	-	UNI 7938	-	ANSI SPECIAL
T-B142PL	K thermocouple	CMT-B CL-bal. line	NUOVA TERMICS	ANSI MC96.1	TCK 458	50 : 400	°C	-	-	UNI 7938	-	ANSI SPECIAL
T-B143P	K thermocouple	CMT-B CL-bal. line	NUOVA TERMICS	ANSI MC96.1	TCK 350	50 : 400	°C	-	-	UNI 7938	-	ANSI SPECIAL
T-B20A	K thermocouple	SFW	NUOVA TERMICS	ANSI MC96.1	TCK 427	50 : 400	°C	-	-	UNI 7938	-	ANSI SPECIAL
T-B21E	K thermocouple	ACC-B	NUOVA TERMICS	ANSI MC96.1	TCK 351	50 : 400	°C	-	-	UNI 7938	-	ANSI SPECIAL
T-B22E	K thermocouple	ACC-B inj. line	NUOVA TERMICS	ANSI MC96.1	TCK 353	50 : 400	°C	-	-	UNI 7938	-	ANSI SPECIAL
T-B23E	K thermocouple	ACC-B inj. line	NUOVA TERMICS	ANSI MC96.1	TCK 354	50 : 400	°C	-	-	UNI 7938	-	ANSI SPECIAL
T-B27P	K thermocouple	CMT-B PR bal. line	NUOVA TERMICS	ANSI MC96.1	TCK 355	50 : 400	°C	-	-	UNI 7938	-	ANSI SPECIAL
T-B28P	K thermocouple	CMT-B PR bal. line	NUOVA TERMICS	ANSI MC96.1	TCK 356	50 : 400	°C	-	-	UNI 7938	-	ANSI SPECIAL
T-B29P	K thermocouple	CMT-B PR bal. line	NUOVA TERMICS	ANSI MC96.1	TCK 357	50 : 400	°C	-	-	UNI 7938	-	ANSI SPECIAL
T-B401E	K thermocouple	CMT-B	NUOVA TERMICS	ANSI MC96.1	TCK 217	50 : 400	°C	-	-	UNI 7938	-	ANSI SPECIAL
T-B403E	K thermocouple	CMT-B	NUOVA TERMICS	ANSI MC96.1	TCK 214	50 : 400	°C	-	-	UNI 7938	-	ANSI SPECIAL
T-B405E	K thermocouple	CMT-B	NUOVA TERMICS	ANSI MC96.1	TCK 211	50 : 400	°C	-	-	UNI 7938	-	ANSI SPECIAL
T-B407E	K thermocouple	CMT-B	NUOVA TERMICS	ANSI MC96.1	TCK 208	50 : 400	°C	-	-	UNI 7938	-	ANSI SPECIAL
T-B409E	K thermocouple	CMT-B	NUOVA TERMICS	ANSI MC96.1	TCK 205	50 : 400	°C	-	-	UNI 7938	-	ANSI SPECIAL
T-B411E	K thermocouple	CMT-B	NUOVA TERMICS	ANSI MC96.1	TCK 202	50 : 400	°C	-	-	UNI 7938	-	ANSI SPECIAL
T-B413E	K thermocouple	CMT-B	NUOVA TERMICS	ANSI MC96.1	TCK 199	50 : 400	°C	-	-	UNI 7938	-	ANSI SPECIAL
T-B415E	K thermocouple	CMT-B	NUOVA TERMICS	ANSI MC96.1	TCK 196	50 : 400	°C	-	-	UNI 7938	-	ANSI SPECIAL
T-B417E	K thermocouple	CMT-B	NUOVA TERMICS	ANSI MC96.1	TCK 193	50 : 400	°C	-	-	UNI 7938	-	ANSI SPECIAL
T-B41A	K thermocouple	CMT-B air	NUOVA TERMICS	ANSI MC96.1	TCK 174	50 : 400	°C	-	-	UNI 7938	-	ANSI SPECIAL
T-B420E	K thermocouple	CMT-B	NUOVA TERMICS	ANSI MC96.1	TCK 189	50 : 400	°C	-	-	UNI 7938	-	ANSI SPECIAL
T-B421E	K thermocouple	CMT-B inj. line	NUOVA TERMICS	ANSI MC96.1	TCK 358	50 : 400	°C	-	-	UNI 7938	-	ANSI SPECIAL
T-B422E	K thermocouple	CMT-B inj. line	NUOVA TERMICS	ANSI MC96.1	TCK 359	50 : 400	°C	-	-	UNI 7938	-	ANSI SPECIAL

**TABLE C-1
SPES-2 INSTRUMENT LIST (Cont.)**

PLANT CODE	INSTRUMENT	LOCATION	MANUFACTURER	MODEL	SIET CODE	SPAN	MLU	h (m)	K (kPa)	M (M.U./mV)	Q (M.U.)	MANU. ACCURACY \pm
T-B42A	K thermocouple	CMT-B air	NUOVA TERMICS	ANSI MC96.1	TCK 175	50 : 400	°C	-	-	UNI 7938	-	ANSI SPECIAL
T-B66E	K thermocouple	IRWST inj. line B	NUOVA TERMICS	ANSI MC96.1	TCK 321	50 : 400	°C	-	-	UNI 7938	-	ANSI SPECIAL
TW-001P	K thermocouple	PC DC	NUOVA TERMICS	ANSI MC96.1	TCK 434	50 : 400	°C	-	-	UNI 7938	-	ANSI SPECIAL
TW-002P	K thermocouple	PC DC	NUOVA TERMICS	ANSI MC96.1	TCK 435	50 : 400	°C	-	-	UNI 7938	-	ANSI SPECIAL
TW-003P	K thermocouple	PC DC	NUOVA TERMICS	ANSI MC96.1	TCK 436	50 : 400	°C	-	-	UNI 7938	-	ANSI SPECIAL
TW-004P	K thermocouple	PC DC	NUOVA TERMICS	ANSI MC96.1	TCK 437	50 : 400	°C	-	-	UNI 7938	-	ANSI SPECIAL
TW-005P	K thermocouple	PC DC	NUOVA TERMICS	ANSI MC96.1	TCK 438	50 : 400	°C	-	-	UNI 7938	-	ANSI SPECIAL
TW-006P	K thermocouple	PC DC	NUOVA TERMICS	ANSI MC96.1	TCK 439	50 : 400	°C	-	-	UNI 7938	-	ANSI SPECIAL
TW-007P	K thermocouple	PC DC	NUOVA TERMICS	ANSI MC96.1	TCK 440	50 : 400	°C	-	-	UNI 7938	-	ANSI SPECIAL
TW-008P	K thermocouple	PC DC	NUOVA TERMICS	ANSI MC96.1	TCK 441	50 : 400	°C	-	-	UNI 7938	-	ANSI SPECIAL
TW-016P	K thermocouple	Upper head	NUOVA TERMICS	ANSI MC96.1	TCK 453	50 : 400	°C	-	-	UNI 7938	-	ANSI SPECIAL
TW-023P	K thermocouple	PR	NUOVA TERMICS	ANSI MC96.1	TCK 462	50 : 400	°C	-	-	UNI 7938	-	ANSI SPECIAL
TW-A03PL	K thermocouple	HL-A	NUOVA TERMICS	ANSI MC96.1	TCK 364	50 : 400	°C	-	-	UNI 7938	-	ANSI SPECIAL
TW-A05S	K thermocouple	SG-A U-tube	NUOVA TERMICS	ANSI MC96.1	TW205S	50 : 400	°C	-	-	UNI 7938	-	ANSI SPECIAL
TW-A06S	K thermocouple	SG-A U-tube	NUOVA TERMICS	ANSI MC96.1	TW206S	50 : 400	°C	-	-	UNI 7938	-	ANSI SPECIAL
TW-A08S	K thermocouple	SG-A U-tube	NUOVA TERMICS	ANSI MC96.1	TW208S	50 : 400	°C	-	-	UNI 7938	-	ANSI SPECIAL
TW-A10S	K thermocouple	SG-A DC	NUOVA TERMICS	ANSI MC96.1	TCK 442	50 : 400	°C	-	-	UNI 7938	-	ANSI SPECIAL
TW-A11S	K thermocouple	SG-A riser	NUOVA TERMICS	ANSI MC96.1	TCK 443	50 : 400	°C	-	-	UNI 7938	-	ANSI SPECIAL
TW-A12S	K thermocouple	SG-A	NUOVA TERMICS	ANSI MC96.1	TCK 455	50 : 400	°C	-	-	UNI 7938	-	ANSI SPECIAL
TW-A181E	K thermocouple	PRHR	NUOVA TERMICS	ANSI MC96.1	TCK 218	50 : 400	°C	-	-	UNI 7938	-	ANSI SPECIAL
TW-A182E	K thermocouple	PRHR	NUOVA TERMICS	ANSI MC96.1	TCK 220	50 : 400	°C	-	-	UNI 7938	-	ANSI SPECIAL
TW-A183E	K thermocouple	PRHR	NUOVA TERMICS	ANSI MC96.1	TCK 219	50 : 400	°C	-	-	UNI 7938	-	ANSI SPECIAL
TW-A281E	K thermocouple	PRHR	NUOVA TERMICS	ANSI MC96.1	TCK 221	50 : 400	°C	-	-	UNI 7938	-	ANSI SPECIAL
TW-A41AE	K thermocouple	CMT-A cont.	NUOVA TERMICS	ANSI MC96.1	TCK 164	50 : 400	°C	-	-	UNI 7938	-	ANSI SPECIAL
TW-A41AI	K thermocouple	CMT-A cont.	NUOVA TERMICS	ANSI MC96.1	TCK 168	50 : 400	°C	-	-	UNI 7938	-	ANSI SPECIAL

TABLE C-1
SPES-2 INSTRUMENT LIST (Cont.)

PLANT CODE	INSTRUMENT	LOCATION	MANUFACTURER	MODEL	SIET CODE	SPAN	M.U.	h (m)	K (kPa)	M (M.U./mV)	Q (M.U.)	MANU. ACCURACY \pm
TW-A41E	K thermocouple	CMT-A	NUOVA TERMICS	ANSI MC96.1	TCK 186	50 : 400	°C	-	-	UNI 7938	-	ANSI SPECIAL
TW-A42AE	K thermocouple	CMT-A cont.	NUOVA TERMICS	ANSI MC96.1	TCK 165	50 : 400	°C	-	-	UNI 7938	-	ANSI SPECIAL
TW-A42AI	K thermocouple	CMT-A cont.	NUOVA TERMICS	ANSI MC96.1	TCK 169	50 : 400	°C	-	-	UNI 7938	-	ANSI SPECIAL
TW-A42E	K thermocouple	CMT-A	NUOVA TERMICS	ANSI MC96.1	TCK 185	50 : 400	°C	-	-	UNI 7938	-	ANSI SPECIAL
TW-A43E	K thermocouple	CMT-A	NUOVA TERMICS	ANSI MC96.1	TCK 184	50 : 400	°C	-	-	UNI 7938	-	ANSI SPECIAL
TW-A44E	K thermocouple	CMT-A	NUOVA TERMICS	ANSI MC96.1	TCK 182	50 : 400	°C	-	-	UNI 7938	-	ANSI SPECIAL
TW-A45E	K thermocouple	CMT-A	NUOVA TERMICS	ANSI MC96.1	TCK 181	50 : 400	°C	-	-	UNI 7938	-	ANSI SPECIAL
TW-A46E	K thermocouple	CMT-A	NUOVA TERMICS	ANSI MC96.1	TCK 179	50 : 400	°C	-	-	UNI 7938	-	ANSI SPECIAL
TW-A47E	K thermocouple	CMT-A	NUOVA TERMICS	ANSI MC96.1	TCK 178	50 : 400	°C	-	-	UNI 7938	-	ANSI SPECIAL
TW-A48E	K thermocouple	CMT-A	NUOVA TERMICS	ANSI MC96.1	TCK 176	50 : 400	°C	-	-	UNI 7938	-	ANSI SPECIAL
TW-A81E	K thermocouple	PRHR supply line	NUOVA TERMICS	ANSI MC96.1	TWA81E	50 : 400	°C	-	-	UNI 7938	-	ANSI SPECIAL
TW-B05S	K thermocouple	SG-B U-tube	NUOVA TERMICS	ANSI MC96.1	TW305S	50 : 400	°C	-	-	UNI 7938	-	ANSI SPECIAL
TW-B06S	K thermocouple	SG-B U-tube	NUOVA TERMICS	ANSI MC96.1	TW306S	50 : 400	°C	-	-	UNI 7938	-	ANSI SPECIAL
TW-B08S	K thermocouple	SG-B U-tube	NUOVA TERMICS	ANSI MC96.1	TW308S	50 : 400	°C	-	-	UNI 7938	-	ANSI SPECIAL
TW-B09S	K thermocouple	SG-B U-tube	NUOVA TERMICS	ANSI MC96.1	TW309S	50 : 400	°C	-	-	UNI 7938	-	ANSI SPECIAL
TW-B10S	K thermocouple	SG-B DC	NUOVA TERMICS	ANSI MC96.1	TCK 444	50 : 400	°C	-	-	UNI 7938	-	ANSI SPECIAL
TW-B11S	K thermocouple	SG-B riser	NUOVA TERMICS	ANSI MC96.1	TCK 445	50 : 400	°C	-	-	UNI 7938	-	ANSI SPECIAL
TW-B41AE	K thermocouple	CMT-B cont.	NUOVA TERMICS	ANSI MC96.1	TCK 166	50 : 400	°C	-	-	UNI 7938	-	ANSI SPECIAL
TW-B41AI	K thermocouple	CMT-B cont.	NUOVA TERMICS	ANSI MC96.1	TCK 170	50 : 400	°C	-	-	UNI 7938	-	ANSI SPECIAL
TW-B41E	K thermocouple	CMT-B	NUOVA TERMICS	ANSI MC96.1	TCK 187	50 : 400	°C	-	-	UNI 7938	-	ANSI SPECIAL
TW-B42AE	K thermocouple	CMT-B cont.	NUOVA TERMICS	ANSI MC96.1	TCK 167	50 : 400	°C	-	-	UNI 7938	-	ANSI SPECIAL
TW-B42AI	K thermocouple	CMT-B cont.	NUOVA TERMICS	ANSI MC96.1	TCK 171	50 : 400	°C	-	-	UNI 7938	-	ANSI SPECIAL
TW-B44E	K thermocouple	CMT-B	NUOVA TERMICS	ANSI MC96.1	TCK 183	50 : 400	°C	-	-	UNI 7938	-	ANSI SPECIAL
TW-B46E	K thermocouple	CMT-B cont.	NUOVA TERMICS	ANSI MC96.1	TCK 180	50 : 400	°C	-	-	UNI 7938	-	ANSI SPECIAL
TW-B48E	K thermocouple	CMT-B	NUOVA TERMICS	ANSI MC96.1	TCK 177	50 : 400	°C	-	-	UNI 7938	-	ANSI SPECIAL

**TABLE C-1
SPES-2 INSTRUMENT LIST (Cont.)**

PLANT CODE	INSTRUMENT	LOCATION	MANUFACTURER	MODEL	SIET CODE	SPAN	M.U.	h (m)	K (kPa)	M (M.U./mV)	Q (M.U.)	MANU. ACCURACY \pm
TW011P07	K thermocouple	Rod bundle	NUOVA TERMICS	ANSI MC96.1	TW11P07	100 : 600	°C	-	-	UNI 7938	-	ANSI SPECIAL
TW011P11	K thermocouple	Rod bundle	NUOVA TERMICS	ANSI MC96.1	TW11P11	100 : 600	°C	-	-	UNI 7938	-	ANSI SPECIAL
TW011P53	K thermocouple	Rod bundle	NUOVA TERMICS	ANSI MC96.1	TW11P53	100 : 600	°C	-	-	UNI 7938	-	ANSI SPECIAL
TW011P82	K thermocouple	Rod bundle	NUOVA TERMICS	ANSI MC96.1	TW11P82	100 : 600	°C	-	-	UNI 7938	-	ANSI SPECIAL
TW011P83	K thermocouple	Rod bundle	NUOVA TERMICS	ANSI MC96.1	TW11P83	100 : 600	°C	-	-	UNI 7938	-	ANSI SPECIAL
TW011P91	K thermocouple	Rod bundle	NUOVA TERMICS	ANSI MC96.1	TW11P91	100 : 600	°C	-	-	UNI 7938	-	ANSI SPECIAL
TW012P47	K thermocouple	Rod bundle	NUOVA TERMICS	ANSI MC96.1	TW12P47	100 : 600	°C	-	-	UNI 7938	-	ANSI SPECIAL
TW012P71	K thermocouple	Rod bundle	NUOVA TERMICS	ANSI MC96.1	TW12P71	100 : 600	°C	-	-	UNI 7938	-	ANSI SPECIAL
TW013P61	K thermocouple	Rod bundle	NUOVA TERMICS	ANSI MC96.1	TW13P61	100 : 600	°C	-	-	UNI 7938	-	ANSI SPECIAL
TW013P68	K thermocouple	Rod bundle	NUOVA TERMICS	ANSI MC96.1	TW13P68	100 : 600	°C	-	-	UNI 7938	-	ANSI SPECIAL
TW014P41	K thermocouple	Rod bundle	NUOVA TERMICS	ANSI MC96.1	TW14P41	100 : 600	°C	-	-	UNI 7938	-	ANSI SPECIAL
TW014P44	K thermocouple	Rod bundle	NUOVA TERMICS	ANSI MC96.1	TW14P44	100 : 600	°C	-	-	UNI 7938	-	ANSI SPECIAL
TW014P49	K thermocouple	Rod bundle	NUOVA TERMICS	ANSI MC96.1	TW14P49	100 : 600	°C	-	-	UNI 7938	-	ANSI SPECIAL
TW014P68	K thermocouple	Rod bundle	NUOVA TERMICS	ANSI MC96.1	TW14P68	100 : 600	°C	-	-	UNI 7938	-	ANSI SPECIAL
TW015P07	K thermocouple	Rod bundle	NUOVA TERMICS	ANSI MC96.1	TW15P07	100 : 600	°C	-	-	UNI 7938	-	ANSI SPECIAL
TW015P11	K thermocouple	Rod bundle	NUOVA TERMICS	ANSI MC96.1	TW15P11	100 : 600	°C	-	-	UNI 7938	-	ANSI SPECIAL
TW015P23	K thermocouple	Rod bundle	NUOVA TERMICS	ANSI MC96.1	TW15P23	100 : 600	°C	-	-	UNI 7938	-	ANSI SPECIAL
TW015P39	K thermocouple	Rod bundle	NUOVA TERMICS	ANSI MC96.1	TW15P39	100 : 600	°C	-	-	UNI 7938	-	ANSI SPECIAL
TW015P53	K thermocouple	Rod bundle	NUOVA TERMICS	ANSI MC96.1	TW15P53	100 : 600	°C	-	-	UNI 7938	-	ANSI SPECIAL
TW015P83	K thermocouple	Rod bundle	NUOVA TERMICS	ANSI MC96.1	TW15P83	100 : 600	°C	-	-	UNI 7938	-	ANSI SPECIAL
TW015P91	K thermocouple	Rod bundle	NUOVA TERMICS	ANSI MC96.1	TW15P91	100 : 600	°C	-	-	UNI 7938	-	ANSI SPECIAL
TW016P14	K thermocouple	Rod bundle	NUOVA TERMICS	ANSI MC96.1	TW16P14	100 : 600	°C	-	-	UNI 7938	-	ANSI SPECIAL
TW016P37	K thermocouple	Rod bundle	NUOVA TERMICS	ANSI MC96.1	TW16P37	100 : 600	°C	-	-	UNI 7938	-	ANSI SPECIAL
TW016P41	K thermocouple	Rod bundle	NUOVA TERMICS	ANSI MC96.1	TW16P41	100 : 600	°C	-	-	UNI 7938	-	ANSI SPECIAL
TW016P44	K thermocouple	Rod bundle	NUOVA TERMICS	ANSI MC96.1	TW16P44	100 : 600	°C	-	-	UNI 7938	-	ANSI SPECIAL

**TABLE C-1
SPES-2 INSTRUMENT LIST (Cont.)**

PLANT CODE	INSTRUMENT	LOCATION	MANUFACTURER	MODEL	SIET CODE	SPAN	M.U.	h (m)	K (kPa)	M (M.U./mV)	Q (M.U.)	MANU. ACCURACY \pm
TW016P68	K thermocouple	Rod bundle	NUOVA TERMICS	ANSI MC96.1	TW16P68	100 : 600	°C	-	-	UNI 7938	-	ANSI SPECIAL
TW016P82	K thermocouple	Rod bundle	NUOVA TERMICS	ANSI MC96.1	TW16P82	100 : 600	°C	-	-	UNI 7938	-	ANSI SPECIAL
TW017P03	K thermocouple	Rod bundle	NUOVA TERMICS	ANSI MC96.1	TW17P03	100 : 600	°C	-	-	UNI 7938	-	ANSI SPECIAL
TW017P27	K thermocouple	Rod bundle	NUOVA TERMICS	ANSI MC96.1	TW17P27	100 : 600	°C	-	-	UNI 7938	-	ANSI SPECIAL
TW017P64	K thermocouple	Rod bundle	NUOVA TERMICS	ANSI MC96.1	TW17P64	100 : 600	°C	-	-	UNI 7938	-	ANSI SPECIAL
TW017P79	K thermocouple	Rod bundle	NUOVA TERMICS	ANSI MC96.1	TW17P79	100 : 600	°C	-	-	UNI 7938	-	ANSI SPECIAL
TW018P03	K thermocouple	Rod bundle	NUOVA TERMICS	ANSI MC96.1	TW18P03	100 : 600	°C	-	-	UNI 7938	-	ANSI SPECIAL
TW018P07	K thermocouple	Rod bundle	NUOVA TERMICS	ANSI MC96.1	TW18P07	100 : 600	°C	-	-	UNI 7938	-	ANSI SPECIAL
TW018P20	K thermocouple	Rod bundle	NUOVA TERMICS	ANSI MC96.1	TW18P20	100 : 600	°C	-	-	UNI 7938	-	ANSI SPECIAL
TW018P37	K thermocouple	Rod bundle	NUOVA TERMICS	ANSI MC96.1	TW18P37	100 : 600	°C	-	-	UNI 7938	-	ANSI SPECIAL
TW018P44	K thermocouple	Rod bundle	NUOVA TERMICS	ANSI MC96.1	TW18P44	100 : 600	°C	-	-	UNI 7938	-	ANSI SPECIAL
TW018P48	K thermocouple	Rod bundle	NUOVA TERMICS	ANSI MC96.1	TW18P48	100 : 600	°C	-	-	UNI 7938	-	ANSI SPECIAL
TW018P64	K thermocouple	Rod bundle	NUOVA TERMICS	ANSI MC96.1	TW18P64	100 : 600	°C	-	-	UNI 7938	-	ANSI SPECIAL
TW018P91	K thermocouple	Rod bundle	NUOVA TERMICS	ANSI MC96.1	TW18P91	100 : 600	°C	-	-	UNI 7938	-	ANSI SPECIAL
TW019P03	K thermocouple	Rod bundle	NUOVA TERMICS	ANSI MC96.1	TW19P03	100 : 600	°C	-	-	UNI 7938	-	ANSI SPECIAL
TW019P37	K thermocouple	Rod bundle	NUOVA TERMICS	ANSI MC96.1	TW19P37	100 : 600	°C	-	-	UNI 7938	-	ANSI SPECIAL
TW019P41	K thermocouple	Rod bundle	NUOVA TERMICS	ANSI MC96.1	TW19P41	100 : 600	°C	-	-	UNI 7938	-	ANSI SPECIAL
TW019P64	K thermocouple	Rod bundle	NUOVA TERMICS	ANSI MC96.1	TW19P64	100 : 600	°C	-	-	UNI 7938	-	ANSI SPECIAL
TW019P82	K thermocouple	Rod bundle	NUOVA TERMICS	ANSI MC96.1	TW19P82	100 : 600	°C	-	-	UNI 7938	-	ANSI SPECIAL
TW020P03	K thermocouple	Rod bundle	NUOVA TERMICS	ANSI MC96.1	TW20P03	100 : 600	°C	-	-	UNI 7938	-	ANSI SPECIAL
TW020P07	K thermocouple	Rod bundle	NUOVA TERMICS	ANSI MC96.1	TW20P07	100 : 600	°C	-	-	UNI 7938	-	ANSI SPECIAL
TW020P24	K thermocouple	Rod bundle	NUOVA TERMICS	ANSI MC96.1	TW20P24	100 : 600	°C	-	-	UNI 7938	-	ANSI SPECIAL
TW020P27	K thermocouple	Rod bundle	NUOVA TERMICS	ANSI MC96.1	TW20P27	100 : 600	°C	-	-	UNI 7938	-	ANSI SPECIAL
TW020P37	K thermocouple	Rod bundle	NUOVA TERMICS	ANSI MC96.1	TW20P37	100 : 600	°C	-	-	UNI 7938	-	ANSI SPECIAL
TW020P41	K thermocouple	Rod bundle	NUOVA TERMICS	ANSI MC96.1	TW20P41	100 : 600	°C	-	-	UNI 7938	-	ANSI SPECIAL

**TABLE C-1
SPES-2 INSTRUMENT LIST (Cont.)**

PLANT CODE	INSTRUMENT	LOCATION	MANUFACTURER	MODEL	SIET CODE	SPAN	M.U.	h (m)	K (kPa)	M (M.U./mV)	Q (M.U.)	MANU. ACCURACY \pm
TW020P44	K thermocouple	Rod bundle	NUOVA TERMICS	ANSI MC96.1	TW20P44	100 : 600	°C	-	-	UNI 7938	-	ANSI SPECIAL
TW020P49	K thermocouple	Rod bundle	NUOVA TERMICS	ANSI MC96.1	TW20P49	100 : 600	°C	-	-	UNI 7938	-	ANSI SPECIAL
TW020P53	K thermocouple	Rod bundle	NUOVA TERMICS	ANSI MC96.1	TW20P53	100 : 600	°C	-	-	UNI 7938	-	ANSI SPECIAL
TW020P64	K thermocouple	Rod bundle	NUOVA TERMICS	ANSI MC96.1	TW20P64	100 : 600	°C	-	-	UNI 7938	-	ANSI SPECIAL
TW020P68	K thermocouple	Rod bundle	NUOVA TERMICS	ANSI MC96.1	TW20P68	100 : 600	°C	-	-	UNI 7938	-	ANSI SPECIAL
TW020P79	K thermocouple	Rod bundle	NUOVA TERMICS	ANSI MC96.1	TW20P79	100 : 600	°C	-	-	UNI 7938	-	ANSI SPECIAL
TW020P82	K thermocouple	Rod bundle	NUOVA TERMICS	ANSI MC96.1	TW20P82	100 : 600	°C	-	-	UNI 7938	-	ANSI SPECIAL
TW020P87	K thermocouple	Rod bundle	NUOVA TERMICS	ANSI MC96.1	TW20P87	100 : 600	°C	-	-	UNI 7938	-	ANSI SPECIAL
TW020P91	K thermocouple	Rod bundle	NUOVA TERMICS	ANSI MC96.1	TW20P91	100 : 600	°C	-	-	UNI 7938	-	ANSI SPECIAL
TWA031PH	K thermocouple	CL-A1	NUOVA TERMICS	ANSI MC96.1	TCK 447	50 : 400	°C	-	-	UNI 7938	-	ANSI SPECIAL
TWA031PL	K thermocouple	CL-A1	NUOVA TERMICS	ANSI MC96.1	TCK 446	50 : 400	°C	-	-	UNI 7938	-	ANSI SPECIAL
TWA032PL	K thermocouple	CL-A2	NUOVA TERMICS	ANSI MC96.1	TCK 454	50 : 400	°C	-	-	UNI 7938	-	ANSI SPECIAL
TWA142P	K thermocouple	CMT-A CL-bal. line	NUOVA TERMICS	ANSI MC96.1	TCK 449	50 : 400	°C	-	-	UNI 7938	-	ANSI SPECIAL
TWA28P	K thermocouple	PR CMT-A bal. line	NUOVA TERMICS	ANSI MC96.1	TCK 467	50 : 400	°C	-	-	UNI 7938	-	ANSI SPECIAL
TWB142P	K thermocouple	CMT-B CL-bal. line	NUOVA TERMICS	ANSI MC96.1	TCK 450	50 : 400	°C	-	-	UNI 7938	-	ANSI SPECIAL
TWB28P	K thermocouple	PR CMT-B bal. line	NUOVA TERMICS	ANSI MC96.1	TCK 466	50 : 400	°C	-	-	UNI 7938	-	ANSI SPECIAL
T-062EA	RTD	IRWST	NUOVA TERMICS	PT100	TR 116	0 : 100	°C	-	-	UNI 7937	-	0.35
T-063EA	RTD	IRWST	NUOVA TERMICS	PT100	TR 119	0 : 100	°C	-	-	UNI 7937	-	0.35
T-064EA	RTD	IRWST	NUOVA TERMICS	PT100	TR 120	0 : 100	°C	-	-	UNI 7937	-	0.35
T-064EB	RTD	IRWST	NUOVA TERMICS	PT100	TR 121	0 : 100	°C	-	-	UNI 7937	-	0.35
T-064EC	RTD	IRWST	NUOVA TERMICS	PT100	TR 118	0 : 100	°C	-	-	UNI 7937	-	0.35
T-065EA	RTD	IRWST	NUOVA TERMICS	PT100	TR 122	0 : 100	°C	-	-	UNI 7937	-	0.35
T-065EB	RTD	IRWST	NUOVA TERMICS	PT100	TR 123	0 : 100	°C	-	-	UNI 7937	-	0.35
T-065EC	RTD	IRWST	NUOVA TERMICS	PT100	TR 117	0 : 100	°C	-	-	UNI 7937	-	0.35
T-PLANT	RTD	Environment	NUOVA TERMICS	PT100	TR124	0 : 50	°C	-	-	UNI 7937	-	0.25

TABLE C-1
SPES-2 INSTRUMENT LIST (Cont.)

PLANT CODE	INSTRUMENT	LOCATION	MANUFACTURER	MODEL	SIET CODE	SPAN	MLU	h (m)	K (kPa)	M (MLU/mV)	Q (MLU)	MANU. ACCURACY ±
T-061E	RTD	IRWST	NUOVA TERMICS	PT100	TR 01	0 : 100	°C	-	-	UNI 7937	-	0.35
T-062E	RTD	IRWST	NUOVA TERMICS	PT100	TR 02	0 : 100	°C	-	-	UNI 7937	-	0.35
T-063E	RTD	IRWST	NUOVA TERMICS	PT100	TR 03	0 : 100	°C	-	-	UNI 7937	-	0.35
T-064E	RTD	IRWST	NUOVA TERMICS	PT100	TR 04	0 : 100	°C	-	-	UNI 7937	-	0.35
T-065E	RTD	IRWST	NUOVA TERMICS	PT100	TR 05	0 : 100	°C	-	-	UNI 7937	-	0.35
V-01P	Voltmeter	Rod bundle	-	-	-	0 : 160	V	-	-	0.032	-	-
V-A1P	Voltmeter	PCP-A	-	-	-	-400 : 400	V	-	-	0.08	0	-
V-B1P	Voltmeter	PCP-B	-	-	-	-400 : 400	V	-	-	0.08	0	-
W-027PEH	Wattmeter	PR	IME	CW2	-	0 : 6000	W	-	-	-	-	1%
W-027PEL	Wattmeter	PR	IME	CW2	-	0 : 6000	W	-	-	-	-	1%
W-027PEM	Wattmeter	PR	IME	CW2	-	0 : 6000	W	-	-	-	-	1%
W-027PI	Wattmeter	PR	IME	CW2	-	0 : 32000	W	-	-	-	-	1%
Z-001PC	Limit switch	ADS-1	TELEMECANIQUE	-	Z-001PC	0 : 1	flag	-	-	-	-	-
Z-001PO	Limit switch	ADS-1	TELEMECANIQUE	-	Z-001PO	0 : 1	flag	-	-	-	-	-
Z-002PC	Limit switch	ADS-2	TELEMECANIQUE	-	Z-002PC	0 : 1	flag	-	-	-	-	-
Z-002PO	Limit switch	ADS-2	TELEMECANIQUE	-	Z-002PO	0 : 1	flag	-	-	-	-	-
Z-003PC	Limit switch	ADS-3	TELEMECANIQUE	-	Z-003PC	0 : 1	flag	-	-	-	-	-
Z-003PO	Limit switch	ADS-3	TELEMECANIQUE	-	Z-003PO	0 : 1	flag	-	-	-	-	-
Z-004BO	Limit switch	Steam dump	TELEMECANIQUE	-	Z-004BO	0 : 1	flag	-	-	-	-	-
Z-004BC	Limit switch	Steam dump	TELEMECANIQUE	-	Z-004BC	0 : 1	flag	-	-	-	-	-
Z-A02SC	Limit switch	MFW A isol.	TELEMECANIQUE	-	Z-A02SC	0 : 1	flag	-	-	-	-	-
Z-A02SO	Limit switch	MFW A isol.	TELEMECANIQUE	-	Z-A02SO	0 : 1	flag	-	-	-	-	-
Z-A04PC	Limit switch	ADS-4 A	TELEMECANIQUE	-	Z-A04PC	0 : 1	flag	-	-	-	-	-
Z-A04PO	Limit switch	ADS-4 A	TELEMECANIQUE	-	Z-A04PO	0 : 1	flag	-	-	-	-	-
Z-A04SC	Limit switch	MSL A isol.	TELEMECANIQUE	-	Z-A04SC	0 : 1	flag	-	-	-	-	-

**TABLE C-1
SPES-2 INSTRUMENT LIST (Cont.)**

PLANT CODE	INSTRUMENT	LOCATION	MANUFACTURER	MODEL	SIET CODE	SPAN	MU.	h (m)	K (kPa)	M (MU./mV)	Q (MU.)	MANU. ACCURACY \pm
Z-A04SO	Limit switch	M' A isol.	TELEMECANIQUE	-	Z-A04SO	0 : 1	flag	-	-	-	-	-
Z-A06SC	Limit switch	SG-A PORV	TELEMECANIQUE	-	Z-A06SC	0 : 1	flag	-	-	-	-	-
Z-A06SO	Limit switch	SG-A PORV	TELEMECANIQUE	-	Z-A06SO	0 : 1	flag	-	-	-	-	-
Z-A40EC	Limit switch	CMT-A inj. line	TELEMECANIQUE	-	Z-A40EC	0 : 1	flag	-	-	-	-	-
Z-A40EO	Limit switch	CMT-A inj. line	TELEMECANIQUE	-	Z-A40EO	0 : 1	flag	-	-	-	-	-
Z-A45PC	Limit switch	CMT-A CL bal. line	TELEMECANIQUE	-	Z-A45PC	0 : 1	flag	-	-	-	-	-
Z-A45PO	Limit switch	CMT-A CL bal. line	TELEMECANIQUE	-	Z-A45PO	0 : 1	flag	-	-	-	-	-
Z-A81EC	Limit switch	PRHR supply line	TELEMECANIQUE	-	Z-A81EC	0 : 1	flag	-	-	-	-	-
Z-A81EO	Limit switch	PRHR supply line	TELEMECANIQUE	-	Z-A81EO	0 : 1	flag	-	-	-	-	-
Z-B02SC	Limit switch	MPW-B isol.	TELEMECANIQUE	-	Z-B02SC	0 : 1	flag	-	-	-	-	-
Z-B02SO	Limit switch	MPW-B isol.	TELEMECANIQUE	-	Z-B02SO	0 : 1	flag	-	-	-	-	-
Z-B04PC	Limit switch	ADS-4 B	TELEMECANIQUE	-	Z-B04PC	0 : 1	flag	-	-	-	-	-
Z-B04PO	Limit switch	ADS-4 B	TELEMECANIQUE	-	Z-B04PO	0 : 1	flag	-	-	-	-	-
Z-B04SC	Limit switch	MSL-B isol.	TELEMECANIQUE	-	Z-B04SC	0 : 1	flag	-	-	-	-	-
Z-B04SO	Limit switch	MSL-B isol.	TELEMECANIQUE	-	Z-B04SO	0 : 1	flag	-	-	-	-	-
Z-B06SC	Limit switch	SG-B PORV	TELEMECANIQUE	-	Z-B06SC	0 : 1	flag	-	-	-	-	-
Z-B06SO	Limit switch	SG-B PORV	TELEMECANIQUE	-	Z-B06SO	0 : 1	flag	-	-	-	-	-
Z-B40EC	Limit switch	CMT-B inj. line	TELEMECANIQUE	-	Z-B40EC	0 : 1	flag	-	-	-	-	-
Z-B40EO	Limit switch	CMT-B inj. line	TELEMECANIQUE	-	Z-B40EO	0 : 1	flag	-	-	-	-	-
Z-B45PC	Limit switch	CMT-B CL bal. line	TELEMECANIQUE	-	Z-B45PC	0 : 1	flag	-	-	-	-	-
Z-B45PO	Limit switch	CMT-B CL bal. line	TELEMECANIQUE	-	Z-B45PO	0 : 1	flag	-	-	-	-	-

N/A = Not Applicable

**TABLE C-2
VENTURI TUBE AND ORIFICE CHARACTERISTICS**

TAG	LOCATION	D (mm)	d (mm)	αc (m ²)	$\Delta \alpha c$ (\pm m ²)	$\sigma \alpha c$ (\pm m ²)	TYPE
F-A01P (*)	CL-1/A	53.98	29.7	1.0236 E-3 (*)	1.02 E-5 (*)	1.02 E-5 (*)	VENTURI
F-A02P (*)	CL-2/A	53.98	29.7	1.0236 E-3 (*)	1.02 E-5 (*)	1.02 E-5 (*)	VENTURI
F-B01P (*)	CL-1/B	53.98	29.7	1.0236 E-3 (*)	1.02 E-5 (*)	1.02 E-5 (*)	VENTURI
F-B02P (*)	CL-2/B	53.98	29.7	1.0236 E-3 (*)	1.02 E-5 (*)	1.02 E-5 (*)	VENTURI
F-003P (*)	PC DOWNCOMER	87.32	53.8	3.46216 E-3(*)	3.46 E-5 (*)	3.46 E-5 (*)	VENTURI
F-014P	DC-UH BYPASS	24.3	9	8.89314 E-5	3.24 E-7	1.91 E-7	VENTURI
F-A20E	ACC-A INJECTION LINE	24.3	7.8	6.52794 E-5	3.1 E-7	1.46 E-7	VENTURI
F-B20E	ACC-B INJECTION LINE	24.3	7.8	6.61016 E-5	3.06 E-7	1.41 E-7	VENTURI
F-A40E	CMT-A INJECTION LINE	15.59	7.93	6.76155 E-5	2.75 E-7	1.8 E-7	VENTURI
F-B40E	CMT-B INJECTION LINE	15.59	7.93	6.5513 E-5	2.74E-07	1.74 E-7	VENTURI
F-A80E	PRHR LINE	15.59	5.35	3.14071 E-5	1.02 E-7	6.59 E-8	VENTURI
F-A60E	IRWST DISCHARGE A	11.84	5.3	3.0594 E-5	1.24 E-7	8.09 E-8	VENTURI
F-B60E	IRWST DISCHARGE B	11.84	5.3	3.14324 E-5	1.32 E-7	7.05 E-8	VENTURI
F-A02S	SG-A DOWNCOMER	42.8	21.4	5.07167 E-4	2.53 E-6	1.91 E-6	VENTURI
F-A03S	SG-A DOWNCOMER	42.8	21.4	5.08755 E-4	2.93 E-6	2.08 E-6	VENTURI
F-B02S	SG-B DOWNCOMER	42.8	21.4	5.06692 E-4	1.82 E-6	9.7 E-7	VENTURI
F-B03S	SG-B DOWNCOMER	42.8	21.4	5.08287 E-4	2.04 E-6	1.27 E-6	VENTURI
F-A04S (*)	SG-A MSL	73.7	19.7	4.30003 E-4(*)	4.3 E-6 (*)	4.3 E-6 (*)	VENTURI
F-B04S (*)	SG-B MSL	73.7	19.7	4.30003 E-4(*)	4.3 E-6 (*)	4.3 E-6 (*)	VENTURI
F-A00E	NRHR LOOP A	24.3	3.42	8.45843 E-6	3.18 E-8	2.17 E-8	ORIFICE
F-B00E	NRHR LOOP B	24.3	3.42	8.40930 E-6	3.39 E-8	2.18 E-8	ORIFICE
F-A01S	SG-A FWL	38.1	15	1.63445 E-4	1.1 E-6	5.83 E-7	ORIFICE
F-B01S	SG-B FWL	38.1	15	1.66985 E-4	5.39 E-7	2.57 E-7	ORIFICE
F-A20A	SG-A SFWL	13.9	4	1.1986 E-5	5.36 E-8	3.79 E-8	ORIFICE
F-B20A	SG-B SFWL	13.9	4	1.15846 E-5	6.16 E-8	4.21 E-8	ORIFICE
F-001A	CVCS	13.9	3	6.66312 E-6	3.19 E-8	1.63 E-8	ORIFICE
F-001BP	SGTR LINE	20.7	4	1.82204 E-5	1.46E-07	9.13 E-8	VENTURI
F-001BS	SGTR LINE	20.7	4	1.73298 E-5	1.54 E-7	1.0 E-7	VENTURI

(*) Not calibrated nozzles; flux coefficients and errors calculated in accordance with UNI-10023 specifications.

APPENDIX D
SPES-2 INOPERABLE AND MODIFIED INSTRUMENTS

Table D-1 summarizes the instruments that were failed or inoperable for the acceptable SPES-2 matrix tests. The gamma-densitometers were inoperable for the entire test program due to unstable electronics. The turbine meters were inoperable for the entire test program due to magnetic noise—except for F-030P, which failed mechanically. Most of these instrument channels were previously identified as failed in the quick look reports (QLR), or notification was provided to the NRC after issuance of the QLR. The data for the inoperable channels has not been included in the electronic data files for this final data report.

Table D-2 identifies the channels that were out of range for the acceptable tests and the time period that these channels were out of range. Those channels which were out of range for less than 2 seconds were not identified in this table since this short duration has minimal impact on the data. The instrument modifications for the acceptable tests are also shown in Table D-2. These modifications represent changes from the instrumentation list as shown in Appendix C. The instruments listed in Appendix C represent those instruments recorded at the end of the tests.

TABLE D-1
SPES-2 FAILED INSTRUMENTS

Chn#	0303	0401	0504	0605	0706	0908	1007	1110	1211	1309	1512	1613	1703
DE-001PA/B	F	F	F	F	F	F	F	F	F	F	F	F	F
DE-030PA/B/C	F	F	F	F	F	F	F	F	F	F	F	F	F
DE-040PA/B/C	F	F	F	F	F	F	F	F	F	F	F	F	F
DE-A01PA/B/C	F	F	F	F	F	F	F	F	F	F	F	F	F
DP-A00P				F	F	F							
DP-B00P				F	F	F							
DP-A81AE				F	F	F							
DP-A81BE				F	F	F							
F-A10P	F	F	F	F	F	F	F	F	F	F	F	F	F
F-A04S				F	F	F							
F-B04S				F	F	F							
F-002P	F	F	F	F	F	F	F	F	F	F	F	F	F
F-003P	F	F	F	F	F	F	F	F	F	F	F	F	F
F-015P	F	F	F	F	F	F	F	F	F	F	F	F	F
F-030P	F	F	F	F	F	F	F	F	F	F	F	F	F
F-040P	F	F	F	F	F	F	F	F	F	F	F	F	F
L-A1P/B1P		F	F	F	F	F	F	F	F	F	F	F	F
L-A10S*				F	F	F							
L-B10S*				F	F	F							
L-A20S				F	F	F							
L-B20S				F	F	F							
S-A1P/B1P	F		F	F	F	F	F	F	F	F	F	F	F
T-A07P	F	F	F	F	F	F	F	F	F	F	F	F	F
T-A031PL													
T-A142PH	F	F	F	F	F	F	F						F

TABLE D-1
SPES-2 FAILED INSTRUMENTS (Cont.)

Chn#	0303	0401	0504	0605	0706	0908	1007	1110	1211	1309	1512	1613	1703
T-B142PH	F	F	F	F	F	F	F						
T-B401E*			F	F									
T-B403E*			F	F									
T-B405E*			F	F									F
T-B407E*			F	F									
T-B409E*			F	F									
T-B411E*			F	F									
T-B413E*			F	F									
T-B415E*			F	F									
T-B417E*			F	F									
T-B420E*			F	F									
TW-A07S	F	F	F	F	F	F	F	F	F	F	F	F	F
TW-B07S	F	F	F	F	F	F	F	F	F	F	F	F	F
TWO16P14		F	F	F	F	F	F	F	F	F	F	F	F
TWO19P82			F	F	F	F	F	F	F	F	F	F	F
TWO20P24			F	F	F	F	F	F	F	F	F	F	F
V-A1P/B1P			F	F	F	F	F	F	F	F	F	F	F
W-027PEH*		F	F	F	F	F	F	F	F	F	F	F	F
W-027PEM*		F	F	F	F	F	F	F	F	F	F	F	F
W-027PEL*		F	F	F	F	F	F	F	F	F	F	F	F
W-027P1*				F	F	F	F	F	F	F	F	F	F
Z_B40EC				F	F	F	F	F	F	F	F	F	F

* Critical instruments

**TABLE D-2
OUT-OF-RANGE AND MODIFIED INSTRUMENTS BY TEST**

TIN	Out-of-Range Instrument	Comments	Instrument "Zero" Out of Specification	Modified Instrument	Reason for Modification	Corrective Action
S00303	F-A04S	Nozzle pressure drop too high.	DP-A00S (22.2 mV)	F-A00E	Measure the total ACC-A discharge line dP from ACC-A lower tap to DVI.	Moved from NRHR and located on ACC-A discharge line (kPa only).
	F-B04S	Nozzle pressure drop too high.	DP-A06S (-37.6 mV)	F-B00E	Measure the total ACC-B discharge line dP from ACC-B lower tap to DVI.	Moved from NRHR and located on ACC-B discharge line (kPa only).
	T-001A F-001A	Measurement not required.	DP-B05S (-300.8 mV)			
	T-A02E F-A00E	Measurement not required.	DP-B06S (-23.1 mV)			
	T-B02E F-B00E	Measurement not required.		DP-000P	Error in SAD database.	Subtract 8.48 kPa to the values.
	T-A20A F-A20A	Measurement not required.		T-061E	Error in drawing.	Must be read as T-065E.
	T-B20A F-B20A	Measurement not required.		T-062E	Error in drawing.	Must be read as T-064E.
	DP-001P	OOB-LL (2372s ± 2380s)		T-065E	Error in drawing.	Must be read as T-061E.
	DP-002P	OOB-LL (2372s ± 2432s)		T-064E	Error in drawing.	Must be read as T-062E.
	DP-003P	OOB-LL (83s ± EOT)		DP-011P	To avoid instrument limiting.	Permanently modified span from 0-30 kPa to -15+35 kPa.
	DP-018P	OOB-HL (63s ± 72s)				
		OOB-LL (993s ± 1000s)		DP-012P	To avoid instrument limiting.	Permanently modified span from 0-40 kPa to -15+35 kPa.
	DP-019P	OOB-LL (64s ± 69s)				
		OOB-HL (991s ± 1002s)		DP-013P	To avoid instrument limiting.	Permanently modified span from 0-35 kPa to -15+35 kPa.
	DP-A00P	OOB-HL (140s ± 218s)				
	DP-A05S	OOB-HL (-300s ± 53s)				
	DP-A20E	OOB-HL (996s ± 1392s)				
	DP-A28P	OOB-LL (-300s ± 83s)				
		OOB-HL (166s ± 188s)				
		OOB-HL (560s ± 588s)				
		OOB-LL (991s ± 2028s)				
	DP-A40E	OOB-LL (1383s ± 1386s)				
	DP-A41E	OOB-HL (63s ± 84s)				
	DP-A42E	OOB-HL (2s ± 150s)				
	DP-A44E	OOB-HL (63s ± 71s)				
	DP-A81E	OOB-LL (115s ± 1040s)				
		OOB-LL (1549s ± 1934s)				
		OOB-LL (2321s ± 2402s)				
	DP-A82E	OOB-HL (-300s ± 84s)				
	DP-A83E	OOB-HL (68s ± 86s)				
		OOB-LL (1074s ± 2005s)				
		OOB-LL (2261s ± EOT)				
	DP-B00P	OOB-HL (138s ± 148s)				
	OOB-HL (1737s ± 1760s)					
	OOB-HL (2502s ± 2548s)					
	OOB-HL (2969s ± 3050s)					

Note:

Out of range for instrument high limit (at least for 2s); OOB-LL = Out of range for instrument low limit (at least for 2s); EOT = End of test.

TABLE D-2
OUT-OF-RANGE AND MODIFIED INSTRUMENTS BY TEST (Cont.)

TIN	Out-of-Range Instrument	Comments	Instrument "Zero" Out of Specification	Modified Instrument	Reason for Modification	Corrective Action
S00303 (Cont.)	DP-B00S	OOR-HL (-300s ÷ 402s)				
		OOR-LL (404s ÷ EOT)				
	DP-B05S	OOR-HL (-300s ÷ 57s)				
	DP-B06P	OOR-LL (1293s ÷ 1297s)				
	DP-B08P	OOR-HL (1294s ÷ 1296s)				
	DP-B20E	OOR-HL (998s ÷ 1387s)				
	DP-B28P	OOR-LL (-300s ÷ 82s)				
		OOR-HL (168s ÷ 378s)				
		OOR-LL (991s ÷ 1467s)				
		OOR-LL (1683s ÷ 2028s)				
	DP-B40E	OOR-LL (1382s ÷ 1384s)				
	DP-B41E	OOR-HL (1s ÷ 85s)				
	DP-B42E	OOR-HL (40s ÷ 83s)				
	DP-B43E	OOR-HL (33s ÷ 84s)				
	DP-B44E	OOR-HL (64s ÷ 72s)				
	F-003P	OOR-LL (351s ÷ 371s)				
	F-014P	OOR-LL (64s ÷ EOT)				
	F-A60E	OOR-HL (2088s ÷ EOT)				
F-A80E	OOR-HL (67s ÷ 1134s)					
	OOR-HL (1439 ÷ 1442s)					
	OOR-HL (1601s ÷ 1602s)					
	OOR-HL (1823s ÷ 1940s)					
F-B60E	OOR-HL (2088s ÷ EOT)					

Note:

Out of range for instrument high limit (at least for 2s); OOR-LL = Out of range for instrument low limit (at least for 2s); EOT = End of test.

**TABLE D-2
OUT-OF-RANGE AND MODIFIED INSTRUMENTS BY TEST (Cont.)**

TIN	Out-of-Range Instrument	Comments	Instrument "Zero" Out of Specification	Modified Instrument	Reason for Modification	Corrective Action
S00401	T-001A	Measurement not required.	DP-A005 (25.2 mV)	F-A00E	Measure the total ACC-A discharge line dP from ACC-A lower tap to DYL.	Moved from NRHR and located on ACC-A discharge line (kPa only).
	T-A02E	Measurement not required.	DP-B055 (-21.3 mV)			
	T-B02E	Measurement not required.	DP-B065 (-38.9 mV)			
	T-A20A	Measurement not required.	DP-A065 (-44.5 mV)			
	T-B20A	Measurement not required.				
	F-A04S	Nozzle pressure drop too high.				
	F-B04S	Nozzle pressure drop too high.				
	DP-003P					
	DP-018P					
	DP-019P					
	DP-A00P					
	DP-A021P					
	DP-A05S					
	DP-A20E					
	DP-A28P					
	DP-A41E					
	DP-A42E					
	DP-A44E					
	DP-A45E					
	DP-A81E					
	DP-A82E					
	DP-A83E					
	DP-B00P					

Note:
Out of range for instrument high limit (at least for 2s); OOR-LL = Out of range for instrument low limit (at least for 2s); EOT = End of test.

**TABLE D-2
OUT-OF-RANGE AND MODIFIED INSTRUMENTS BY TEST (Cont.)**

TTN	Out-of-Range Instrument	Comments	Instrument "Zero" Out of Specification	Modified Instrument	Reason for Modification	Corrective Action
S00401 (Cont.)	DP-B00S	OOH (-300s + 894s) OOR-LL (1429s + EOT)				
	DP-B05S	OOH-LL (-300s + 245s)				
	DP-B06P	OOH-LL (5018s + 5021s)				
	DP-B20E	OOH-LL (4698s + 5065s)				
	DP-B28P	OOH-LL (-300s + 273s) OOH-LL (2908s + 4173s) OOH-LL (4609s + 5789s)				
	DP-B41E	OOH-LL (252s + 276s)				
	DP-B42E	OOH-LL (252s + 275s)				
	DP-B43E	OOH-LL (251s + 275s)				
	DP-B44E	OOH-LL (255s + 266s)				
	DP-B45E	OOH-LL (4702s + 5219s) OOH-LL (5681s + 5789s)				
	F-014P	OOH-LL (254s + EOT)				
	F-A80E	OOH-LL (258s + 276s)				
	L-A40E	OOH-LL (257s + 272s)				
	L-B40E	OOH-LL (255s + 262s)				

Note:
Out of range for instrument high limit (at least for 2s); OOR-LL = Out of range for instrument low limit (at least for 2s); EOT = End of test.

**TABLE D-2
OUT-OF-RANGE AND MODIFIED INSTRUMENTS BY TEST (Cont.)**

TIN	Out-of-Range Instrument	Comments	Instrument "Zero" Out of Specification	Modified Instrument	Reason for Modification	Corrective Action	
S00504	F-A04S	Nozzle pressure drop too high.	DP-A06S (-48.2 mV)	DP-000P	Error in SAD database.	Subtract 8.48 kPa to the values.	
	F-B04S	Nozzle pressure drop too high.	DP-B05S (-41.2 mV)	DP-A20E	To avoid the instrument limit and measure the total ACC-A discharge line dP from ACC-A lower tap to DVI.	Permanently modified span from -50+50 kPa to -50+200 kPa and permanently modified the hydraulic installation.	
	DP-003P	OOR-LL (84s + EOT)	DP-A00P (27.3 mV)				
	DP-018P	OOR-HL (64s + 74s)					
		OOR-LL (1055s + 1057s)					
		OOR-LL (1447s + 1483s)					
	DP-019P	OOR-LL (66s + 70s)			DP-B20E	To avoid the instrument limit and measure the total ACC-B discharge line DP from ACC-B lower tap to DVI.	Permanently modified span from -50+50 kPa to -50+200 kPa and permanently modified the hydraulic installation.
		OOR-HL (1053s + 1059s)					
		OOR-HL (1448s + 1483s)					
	DP-A021P	OOR-LL (1303s + 1386s)					
		OOR-LL (3788s + 3797s)					
	DP-A022P	OOR-LL (3788s + 3798s)					
	DP-A05S	OOR-HL (-300s + 53s)			DP-A81E	To avoid the instrument limit.	Permanently modified the hydraulic installation.
	DP-A06P	OOR-LL (1456s + 1457s)					
	DP-A20E	OOR-LL (-300s + 750s)					
		OOR-HL (1227s + 1236s)					
		OOR-LL (3732s + 4326s)					
	DP-A28P	OOR-LL (-300s + 84s)					
		OOR-HL (174s + 200s)					
		OOR-HL (635s + 674s)					
		OOR-LL (1052s + EOT)					
	DP-A40E	OOR-LL (1448s + 1457s)					
		OOR-LL (2560s + 2887s)			DP-A82E	To avoid the instrument limit.	Permanently modified span from -50+50 kPa to -20+80 kPa and permanently changed hydraulic installation of the instrument in the plant connecting the instrument positive side to the FRHR inlet and the negative to the HL-A.
	DP-A41E	OOR-HL (64s + 86s)					
	DP-A42E	OOR-HL (0s + 156s)					
	DP-A44E	OOR-HL (65s + 68s)			T-A021PL	DAS amplifier noise.	Permanently modified span from -50+50 kPa -40+60 kPa.
	DP-A45E	OOR-HL (2809s + 2869s)					
	DP-A82E	OOR-HL (-300s + EOT)			F-A00E	Measure NRHR flow rate.	Subtract 10°C to the values.
	DP-A83E	OOR-HL (69s + 88s)			F-B00E	Measure NRHR flow rate.	Relocated on NRHR.
		OOR-LL (1073s + 1730s)					
	OOR-LL (2308s + 2316s)						
	OOR-LL (3787s + 3813s)						
	OOR-LL (4300s + 4301s)						
DP-B00P	OOR-HL (1562s + 1567s)						
DP-B00S	OOR-HL (-300s + 452s)						
	OOR-LL (453s + EOT)						
DP-B021P	OOR-LL (3790s + 3798s)						
DP-B05S	OOR-HL (-300s + 59s)						

Note:

Out of range for instrument high limit (at least for 2s); OOR-LL = Out of range for instrument low limit (at least for 2s); EOT = End of test.

**TABLE D-2
OUT-OF-RANGE AND MODIFIED INSTRUMENTS BY TEST (Cont.)**

TTN	Out-of-Range Instrument	Comments	Instrument "Zero" Out of Specification	Modified Instrument	Reason for Modification	Corrective Action
S00504 (Cont.)	DP-B28E	OOB-LL (-300s + 84s) OOB-HL (179s + 431s)				
	DP-B40E	OOB-LL (1052s + 4290s)				
		OOB-LL (1440s + 1448s)				
	DP-B41E	OOB-LL (2473s + 2493s)				
		OOB-LL (2869s + 4159s)				
	DP-B42E	OOB-HL (1s + 155s)				
		OOB-HL (64s + 78s)				
	DP-B43E	OOB-HL (64s + 86s)				
		OOB-HL (66s + 74s)				
	DP-B44E	OOB-HL (3789s + 3793s)				
		OOB-LL (65s + EOT)				
	F-014P	OOB-HL (69s + 88s)				
		OOB-HL (78s + 99s)				
	F-A80E	OOB-LL (102s + 1413s)				
		OOB-LL (-300s + 750s)				
	F-B20A	OOB-HL (1227s + 1336s)				
		OOB-LL (3749s + 4318s)				
DP-B20E						

Note:
Out of range for instrument high limit (at least for 2s); OOB-LL = Out of range for instrument low limit (at least for 2s); EOT = End of test.

**TABLE D-2
OUT-OF-RANGE AND MODIFIED INSTRUMENTS BY TEST (Cont.)**

TIN	Out-of-Range Instrument	Comments	Instrument "Zero" Out of Specification	Modified Instrument	Reason for Modification	Corrective Action
S00605	F-A04S	Nozzle pressure drop too high.	DP-A06S (-46.8 mV)	DP-003P	Error in SAD database.	Subtract 8.48 kPa to the values. Acquired as T-A02E. Not installed on break line. Not installed on break line.
	F-B04S	Nozzle pressure drop too high.	DP-A00S (32.0 mV)			
	T-001A F-001A	Measurement not required.	DP-B05S (-39.3 mV)	T-A021PL	SAD amplifier damaged.	
	T-A02E F-A00E	Measurement not required.		DE-001PA	Instrument not available.	
	T-B02E F-B00E	Measurement not required.				
	T-A20A F-A20A	Measurement not required.				
	T-B20A F-B20A	Measurement not required.		DE-001PB	Instrument not available.	
	DP-002P	OOR-LL (2237s + 2281s)				
	DP-003P	OOR-LL (91s + EOT)				
	DP-018P	OOR-HL (70s + 80s)				
		OOR-HL (2236s + 2249s)				
	DP-019P	OOR-LL (72s + 77s)				
		OOR-HL (904s + 908s)				
		OOR-LL (2237s + 2244s)				
	DP-A05P	OOR-LL (1962s + 1965s)				
	DP-A05S	OOR-HL (-300s + 63s)				
	DP-A06P	OOR-LL (1855s + 1870s)				
	DP-A20E	OOR-LL (-300s + 807s)				
		OOR-HL (970s + 996s)				
	DP-A28P	OOR-LL (-300s + 90s)				
		OOR-HL (181s + 381s)				
		OOR-LL (903s + 1023s)				
		OOR-LL (1218s + 1222s)				
		OOR-LL (1316s + 1376s)				
		OOR-LL (1491s + 1747s)				
	DP-A41E	OOR-HL (70s + 92s)				
	DP-A42E	OOR-HL (0s + 155s)				
DP-A44E	OOR-HL (72s + 90s)					
DP-A82E	OOR-HL (-300s + 90s)					
DP-A83E	OOR-HL (75s + 93s)					
	OOR-LL (1193s + 2903s)					

Note:

Out of range for instrument high limit (at least for 2s); OOR-LL = Out of range for instrument low limit (at least for 2s); EOT = End of test.

**TABLE D-2
OUT-OF-RANGE AND MODIFIED INSTRUMENTS BY TEST (Cont.)**

TIN	Out-of-Range Instrument	Comments	Instrument "Zero" Out of Specification	Modified Instrument	Reason for Modification	Corrective Action
S00605 (Cont.)	DP-B00P	OOR-HL (129s + 156s) OOR-HL (990s + 1080s) OOR-HL (1205s + 3090s)				
	DP-B00S	OOR-HL (-300s + 404s) OOR-LL (405s + 432s) OOR-HL (439s + 452s) OOR-LL (456s + EOT)				
	DP-B05S	OOR-HL (-300s + 65s)				
	DP-B20E	OOR-LL (-300s + 800s) OOR-HL (995s + 1138s)				
	DP-B28P	OOR-LL (-300s + 90s) OOR-HL (183s + 419s) OOR-LL (903s + 1765s)				
	DP-B40E	OOR-HL (798s + 801s)				
	DP-B41E	OOR-HL (1s + 400s)				
	DP-B42E	OOR-HL (70s + 81s)				
	DP-B43E	OOR-HL (70s + 92s)				
	DP-B44E	OOR-HL (72s + 79s)				
	F-014P	OOR-LL (71s + EOT)				
	F-A02S	OOR-LL (114s + 2836s)				
	F-A80E	OOR-HL (75s + 94s)				
	F-B01S	OOR-HL (-300s + 57s)				
	L-B40E	OOR-HL (71s + 77s)				

Note:

Out of range for instrument high limit (at least for 2s); OOR-LL = Out of range for instrument low limit (at least for 2s); EOT = End of test.

**TABLE D-2
OUT-OF-RANGE AND MODIFIED INSTRUMENTS BY TEST (Cont.)**

TIN	Out-of-Range Instrument	Comments	Instrument "Zero" Out of Specification	Modified Instrument	Reason for Modification	Corrective Action
500706	F-A04S	Nozzle pressure drop too high.	DP-A06S (-46 mV)	DP-000P	Error in SAD database.	Subtract 8.48 kPa to the values. Acquired as T-A02E. Not installed on break line. Not installed on break line.
	F-B04S	Nozzle pressure drop too high.	DP-B05S (-21.6 mV)	T-A021PL	SAD amplifier damaged.	
	T-001A	Measurement not required.	DP-B06S (-23.3 mV)	DE-001PA	Instrument not available.	
	T-A02E	Measurement not required.		DE-001PB	Instrument not available.	
	T-B02E	Measurement not required.				
	T-A20A	Measurement not required.				
	T-B20A	Measurement not required.				
	DP-001P	Measurement not required.				
	DP-002P		OOB-LL (2050s + 2186s)			
	DP-003P		OOB-LL (2344s + 3022s)			
	DP-018P		OOB-LL (1113s + 1117s)			
	DP-019P		OOB-LL (1315s + 1802s)			
	DP-020P		OOB-LL (2050s + 3022s)			
	DP-A00P		OOB-LL (38s + EOT)			
	DP-A05P		OOB-HL (9s + 29s)			
	DP-A05S		OOB-LL (267s + 295s)			
	DP-A06P		OOB-LL (7s + 27s)			
	DP-A20E		OOB-HL (266s + 299s)			
	DP-A28P		OOB-LL (24s + 26s)			
	DP-A40E		OOB-HL (267s + 269s)			
	DP-A41E		OOB-HL (49s + 275s)			
	DP-A42E		OOB-HL (435s + 533s)			
	DP-A44E		OOB-LL (511s + 578s)			
	DP-A82E		OOB-HL (-300s + 16s)			
	DP-A83E		OOB-HL (506s + 507s)			
			OOB-LL (778s + 780s)			
		OOB-LL (-300s + 251s)				
		OOB-HL (333s + 608s)				
		OOB-LL (-300s + 37s)				
		OOB-HL (42s + 130s)				
		OOB-LL (265s + 319s)				
		OOB-LL (585s + 597s)				
		OOB-HL (1s + 31s)				
		OOB-HL (0s + 39s)				
		OOB-HL (266s + 268s)				
		OOB-HL (2s + 28s)				
		OOB-HL (-300s + 39s)				
		OOB-HL (21s + 42s)				
		OOB-LL (505s + 624s)				
		OOB-LL (963s + 3033s)				

Note:
Out of range for instrument high limit (at least for 2s); OOB-LL = Out of range for instrument low limit (at least for 2s); EOT = End of test.

**TABLE D-2
OUT-OF-RANGE AND MODIFIED INSTRUMENTS BY TEST (Cont.)**

TIN	Out-of-Range Instrument	Comments	Instrument "Zero" Out of Specification	Modified Instrument	Reason for Modification	Corrective Action
S00706 (Cont.)	DP-B00P	OOB-HL (41s + 173s) OOB-HL (2146s + 2204)				
	DP-B00S	OOB-HL (2932s + 2965s) OOB-HL (-300s + 149s)				
	DP-B05S	OOB-LL (150s + EOT)				
	DP-B20E	OOB-HL (-300s + 16s) OOB-LL (-300s + 709s)				
	DP-B28P	OOB-LL (-300s + 19s) OOB-HL (21s + 506s)				
	DP-B40E	OOB-HL (0s + 622s)				
	DP-B41E	OOB-HL (1s + 41s)				
	DP-B42E	OOB-HL (0s + 30s)				
	DP-B43E	OOB-HL (0s + 41s)				
	DP-B44E	OOB-HL (3s + 23s)				
	DP-B45E	OOB-HL (21s + 413s)				
	F-014P	OOB-LL (22s + EOT)				
	F-A02S	OOB-LL (47s + 1959s) OOB-LL (2338s + 2417s)				
	F-A20E	OOB-HL (531s + 581s)				
	F-A80E	OOB-HL (21 + 43s)				
	F-B01S	OOB-HL (-300 + 17s)				
	F-B20E	OOB-HL (1s + 113s) OOB-HL (325s + 383s)				

Note:
Out of range for instrument high limit (at least for 2s); OOB-LL = Out of range for instrument low limit (at least for 2s); EOT = End of test.

**TABLE D-2
OUT-OF-RANGE AND MODIFIED INSTRUMENTS BY TEST (Cont.)**

TIN	Out-of-Range Instrument	Comments	Instrument "Zero" Out of Specification	Modified Instrument	Reason for Modification	Corrective Action
S00908	F-A04S	Nozzle pressure drop too high.	DP-B00S (29.3 mV)	DP-000P	Error in SAD database.	Subtract 8.48 kPa to the values. Acquired as T-A02E. Not installed on break line. Not installed on break line.
	F-B04S	Nozzle pressure drop too high.	DP-B05S (-34.3 mV)			
	T-001A F-001A	Measurement not required.	DP-A06S (-54.4 mV)	T-A021PL	SAD amplifier damaged.	
	T-A02E F-A00E	Measurement not required.	DP-A00S (-63.2 mV)	DE-001PA	Instrument not available.	
	T-B02E F-B00E	Measurement not required.	DP-A04S (-26.5 mV)			
	T-A20A F-A20A	Measurement not required.		DE-001PB	Instrument not available.	
	T-B20A F-B20A	Measurement not required.				
	DP-001P	OOR-LL (965s + 900s)				
	DP-002P	OOR-LL (965s + 1076s)				
	DP-003P	OOR-LL (20s + EOT)				
	DP-018P	OOR-HL (0s + 19s)				
	DP-019P	OOR-LL (0s + 17s)				
	DP-020P	OOR-LL (0s + 9s)				
	DP-A00P	OOR-HL (35s + 45s)				
		OOR-HL (627s + 2628s)				
	DP-A05S	OOR-HL (-300s + 8s)				
	DP-A06P	OOR-LL (1785s + 1802s)				
	DP-A20E	OOR-LL (-300s + 180s)				
	DP-A28P	OOR-LL (-300s + 0s)				
		OOR-HL (1s + 8s)				
		OOR-LL (10s + 98s)				
		OOR-LL (722s + 1122)				
		OOR-LL (1425s + 1691s)				
	DP-A40E	OOR-LL (989s + 992s)				
	DP-A41E	OOR-HL (0s + 20s)				
	DP-A42E	OOR-HL (0s + 27s)				
		OOR-HL (117s + 119s)				
	DP-A44E	OOR-HL (1s + 22s)				
	DP-A82E	OOR-HL (-300s + 26s)				
	DP-A83E	OOR-HL (10s + 29s)				
		OOR-LL (675s + EOT)				
	DP-B00P	OOR-HL (29s + 2651s)				
	DP-B022P	OOR-LL (717s + 986s)				
DP-B05S	OOR-HL (-300s + 8s)					
DP-B20E	OOR-LL (-300s + 183s)					
DP-B28P	OOR-LL (-300s + 0s)					
	OOR-HL (1s + 1675s)					

Note:

Out of range for instrument high limit (at least for 2s); OOR-LL = Out of range for instrument low limit (at least for 2s); EOT = End of test.

**TABLE D-2
OUT-OF-RANGE AND MODIFIED INSTRUMENTS BY TEST (Cont.)**

TTN	Out-of-Range Instrument	Comments	Instrument "Zero" Out of Specification	Modified Instrument	Reason for Modification	Corrective Action	
S00998 (Cont.)	DP-B40E	OOB-LL (0s + 1682s)					
	DP-B41E	OOB-HL (-7s + 8s)					
	DP-B42E	OOB-HL (1727s + 1749s)					
	DP-B43E	OOB-HL (0s + 2s)					
	DP-B44E	OOB-HL (0s + 5s)					
	DP-B45E	OOB-HL (1568s + 1571s)					
	DP-B61E	OOB-HL (0s + 1695s)					
	F-014P	OOB-LL (1227s + 1321s)					
	F-A02S	OOB-LL (1618s + 1680s)					
	F-A80E	OOB-LL (93s + EOT)					
	L-B20S	OOB-LL (28s + 2586s)					
	L-B40E	OOB-HL (11s + 29s)					
			OOB-HL (1148s + 1205s)				
			OOB-LL (12s + EOT)				
		OOB-HL (1230s + 1232s)					

Note:
Out of range for instrument high limit (at least for 2s); OOB-LL = Out of range for instrument low limit (at least for 2s); EOT = End of test.

**TABLE D-2
OUT-OF-RANGE AND MODIFIED INSTRUMENTS BY TEST (Cont.)**

TIN	Out-of-Range Instrument	Comments	Instrument "Zero" Out of Specification	Modified Instrument	Reason for Modification	Corrective Action
S01007	F-A04S	Nozzle pressure drop too high.	DP-B05S (409.0 mV)	DP-000P	Error in SAD database.	Subtract 8.48 kPa to the values. Acquired as T-A02E. Not installed on break line. Not installed on break line. Span modified from 0-200 kPa to 0-500 kPa. Span modified from 0-200 kPa to 0-500 kPa. Span modified from 0-200 kPa to 0-1000 kPa. Instrument substitution difference between absolute transmitters F-B04SP (0-6000 kPa) and F-B04SM (0-6000 kPa).
	F-B04S	Nozzle pressure drop too high.		T-A021PL	SAD amplifier damaged.	
	T-001A F-001A	Measurement not required.		DE-001PA	Instrument not available.	
	T-A02E F-A00E	Measurement not required.				
	T-B02E F-B00E	Measurement not required.				
	T-A20A F-A20A	Measurement not required.		DE-001PB	Instrument not available.	
	T-B20A F-B20A	Measurement not required.				
	DP-001P	OOR-LL (2603s + 2605s)		F-A01S	To avoid the instrument limit.	
	DP-003P	OOR-LL (88s + EOT)				
	DP-018P	OOR-HL (68s + 76s)		F-B01S	To avoid the instrument limit.	
		OOR-LL (1168s + 1178s)				
	DP-019P	OOR-LL (68s + 74s)		F-A04S	To avoid the instrument limit.	
		OOR-HL (1168s + 1178s)				
	DP-A00P	OOR-HL (214s + 224s)				
		OOR-HL (1251s + 3628s)		F-B04S	To avoid the instrument limit.	
	DP-A20E	OOR-LL (-300s + 987s)				
	DP-A28P	OOR-LL (-300s + 87s)				
		OOR-HL (201s + 582s)				
		OOR-LL (1167s + 2163s)				
	DP-A41E	OOR-HL (68s + 90s)				
	DP-A42E	OOR-HL (68s + 81s)				
	DP-A44E	OOR-HL (68s + 76s)				
	DP-A82E	OOR-HL (-300s + 88s)				
	DP-A83E	OOR-HL (73s + 91s)				
		OOR-LL (1319s + 3851s)				
	DP-B00P	OOR-HL (105s + 3636s)				
	DP-B05S	OOR-LL (63s + EOT)				
	DP-B20E	OOR-LL (-300s + 984s)				
	DP-B28P	OOR-LL (-300s + 0s)				
		OOR-HL (89s + 1092s)				
	OOR-LL (1168s + 2163s)					
DP-B40E	OOR-LL (1s + 689s)					

Note:

Out of range for instrument high limit (at least for 2s); OOR-LL = Out of range for instrument low limit (at least for 2s); EOT = End of test.

**TABLE D-2
OUT-OF-RANGE AND MODIFIED INSTRUMENTS BY TEST (Cont.)**

TTN	Out-of-Range Instrument	Comments	Instrument "Zero" Out of Specification	Modified Instrument	Reason for Modification	Corrective Action
S01007 (Cont.)	DP-B41E DP-B42E DP-B43E DP-B44E F-014P F-A02S F-A80E L-B40E	OOR-HL (2s + 89s) OOR-HL (407s + 1160s) OOR-HL (67s + 78s) OOR-HL (67s + 89s) OOR-HL (519s + 541s) OOR-HL (610s + 1015s) OOR-HL (69s + 74s) OOR-HL (525s + 633s) OOR-LL (333s + EOT) OOR-LL (82s + EOT) OOR-HL (73s + 91s) OOR-HL (70s + 73s) OOR-HL (414s + 882s)				

Note:
Out of range for instrument high limit (at least for 2s); OOR-LL = Out of range for instrument low limit (at least for 2s); EOT = End of test.

**TABLE D-2
OUT-OF-RANGE AND MODIFIED INSTRUMENTS BY TEST (Cont.)**

TIN	Out-of-Range Instrument	Comments	Instrument "Zero" Out of Specification	Modified Instrument	Reason for Modification	Corrective Action	
S01110	F-A04S	Nozzle pressure drop too high.	DP-B06S (49.2 mV)	DP-000P	Error in SAD database.	Subtract 8.48 kPa to the values.	
	F-B04S	Nozzle pressure drop too high.	DP-A06S (22.9 mV)				
	T-001A F-001A	Measurement not required.	DP-B00S (-32.4 mV)	DE-001PA	Instrument not available.	Not installed on break line.	
	T-A02E F-A00E	Measurement not required.					
	T-B02E F-B00E	Measurement not required.		DE-001PB	Instrument not available.	Not installed on break line.	
	T-A20A F-A20A	Measurement not required.					
	T-B20A F-B20A	Measurement not required.		F-001BP	Measure the break flow from SG primary side to secondary side.	Installed on SGTR with span 0-40 kPa.	
	DP-003P	OOH-LL (512s + EOT)					
	DP-A00P	OOH-HL (555s + 598s)					
		OOH-HL (801s + 1112s)			F-001BS	Measure the break flow from SG secondary side to primary side.	Installed on SGTR with span 0-40 kPa.
	DP-A05S	OOH-HL (302s + 441s)					
	DP-A20E	OOH-LL (-300s + EOT)					
	DP-A28P	OOH-LL (-300s + 512s)		TW-016P	Westinghouse request.	Installed on UH.	
	DP-A41E	OOH-HL (498s + 503s)		TWA031PH	Westinghouse request.	Installed on CL-A1.	
	DP-A42E	OOH-HL (498s + 503s)		TWA031PL	Westinghouse request.	Installed on CL-A1.	
	DP-A82E	OOH-HL (-300s + 512s)		TWA032PL	Westinghouse request.	Installed on CL-A2.	
	DP-A83E	OOH-HL (495s + 515s)		TW-A12S	Westinghouse request.	Installed on steam dome.	
	DP-B00P	OOH-HL (550s + 1338s)		TW-A03PL	Westinghouse request.	Installed on HL-A.	
		OOH-HL (3309s + 3314s)		T-001B	Break flow measurement.	Installed on STGR break line.	
	DP-B05S	OOH-HL (-300s + 493s)					
	DP-B20E	OOH-LL (-300s + EOT)		TW-023P	Westinghouse request.	Installed on pressurizer.	
	DP-B28P	OOH-LL (-300s + 512s)					
	DP-B41E	OOH-HL (499s + 626s)					
	DP-B42E	OOH-HL (499s + 502s)					
	DP-B43E	OOH-HL (499s + 503s)					
	F-014P	OOH-LL (514s + EOT)					
	F-A02S	OOH-LL (512s + EOT)					

Note:

Out of range for instrument high limit (at least for 2s); OOH-LL = Out of range for instrument low limit (at least for 2s); EOT = End of test.

**TABLE D-2
OUT-OF-RANGE AND MODIFIED INSTRUMENTS BY TEST (Cont.)**

TIN	Out-of-Range Instrument	Comments	Instrument "Zero" Out of Specification	Modified Instrument	Reason for Modification	Corrective Action	
S01211	F-A04S	Nozzle pressure drop too high.	DP-B00S (28.9 mV) DP-A06S (22.6 mV)	DE-001PA	Instrument not available.	Not installed on break line.	
	F-B04S	Nozzle pressure drop too high.		DE-001PB	Instrument not available.		
	T-001A F-001A	Measurement not required.				Not installed on break line.	
	T-A02E F-A00E	Measurement not required.					
	T-B02E F-B00E	Measurement not required.					
	T-A20A F-A20A	Measurement not required.					
	T-B20A F-B20A	Measurement not required.					
	DP-003P	OOB-LL (496s + EOT)					
	DP-018P		OOB-LL (734s + 744s)				
			OOB-LL (844s + 849s)				
			OOB-HL (2700s + 2713s)				
	DP-019P	OOB-HL (724s + 987s)					
	DP-A00P		OOB-HL (1359s + 1361s)				
			OOB-HL (1670s + 1673s)				
			OOB-HL (3453s + 3693s)				
			OOB-HL (4033s + 5283s)				
			OOB-HL (5607s + 5632s)				
	DP-A20E		OOB-LL (-300s + 805s)				
			OOB-HL (887s + 982s)				
	DP-A28P		OOB-LL (-300s + 496s)				
			OOB-LL (723s + 1747s)				
	DP-A40E		OOB-LL (6900s + 6922s)				
			OOB-LL (7237s + EOT)				
	DP-A41E		OOB-HL (483s + 487s)				
			OOB-HL (627s + 645s)				
	DP-A42E		OOB-HL (483s + 487s)				
			OOB-HL (628s + 644s)				
DP-A82E	OOB-HL (-300s + 496s)						
DP-A83E		OOB-HL (480s + 499s)					
		OOB-LL (979s + 983s)					
		OOB-LL (1228s + 7576s)					
DP-B00P	OOB-HL (799s + 8895s)						
DP-B05S	OOB-HL (-300s + 478s)						
DP-B06P		OOB-LL (1139s + 1143s)					
		OOB-LL (2468s + 2476s)					
DP-B07P	OOB-HL (1139s + 1141s)						
DP-B20E		OOB-LL (-300s + 808s)					
		OOB-HL (887s + 982s)					

Note:

Out of range for instrument high limit (at least for 2s); OOB-LL = Out of range for instrument low limit (at least for 2s); EOT = End of test.

**TABLE D-2
OUT-OF-RANGE AND MODIFIED INSTRUMENTS BY TEST (Cont.)**

TTN	Out-of-Range Instrument	Comments	Instrument "Zero" Out of Specification	Modified Instrument	Reason for Modification	Corrective Action
S01211 (Cont.)	DP-B28P DP-B40E DP-B41E EP-B42E DP-B43E F-014P F-A80E	OOR-LL (-300s + 495s) OOR-LL (723s + 1820s) OOR-LL (6498s + EOT) OOR-HL (482s + 498s) OOR-HL (614s + 803s) OOR-HL (482s + 485s) OOR-HL (627s + 642s) OOR-HL (483s + 488s) OOR-HL (628s + 644s) OOR-LL (499s + EOT) OOR-HL (481s + 499s)				

Note:
Out of range for instrument high limit (at least for 2s); OOR-LL = Out of range for instrument low limit (at least for 2s); EOT = End of test.

TABLE D-2
OUT-OF-RANGE AND MODIFIED INSTRUMENTS BY TEST (Cont.)

TIN	Out-of-Range Instrument	Comments	Instrument "Zero" Out of Specification	Modified Instrument	Reason for Modification	Corrective Action
S01309	F-A04S	Nozzle pressure drop too high.	DP-B06S (22.8 mV)	DE-001PA	Instrument not available.	Not installed on break line.
	F-B04S	Nozzle pressure drop too high.	DP-A06S (11.4 mV)	DE-001PB	Instrument not available.	Not installed on break line.
	T-A02E F-A00E	Measurement not required.		F-001A	To avoid instrument limit.	Span modified from 0-180 kPa to 0-30 kPa
	T-B02E F-B00E	Measurement not required.		F-A80E	To avoid instrument limit.	Span modified from 0-180 kPa to 0-30 kPa.
	DP-003P	OOO-LL (489s ± EOT)				
	DP-A05S	OOO-HL (-300s ± 470s)				
	DP-A20E	OOO-LL (-300s ± 3847s)				
		OOO-LL (5662s ± 5997s)				
	DP-A28P	OOO-LL (-300s ± 488s)				
	DP-A41E	OOO-HL (476s ± 903s)				
		OOO-HL (2383s ± 2385s)				
	DP-A42E	OOO-HL (476s ± 480s)				
		OOO-HL (899s ± 903s)				
	DP-A82E	OOO-HL (-300s ± 488s)				
	DP-A83E	OOO-HL (472s ± 491s)				
	DP-B05S	OOO-HL (-300s ± 470s)				
	DP-B20E	OOO-LL (-300s ± 3791s)				
		OOO-LL (5662s ± 5997s)				
	DP-B28P	OOO-LL (-300s ± 489s)				
	DP-B41E	OOO-HL (476s ± 480s)				
		OOO-HL (623s ± 663s)				
		OOO-HL (899s ± 903s)				
	DP-B42E	OOO-HL (475s ± 480s)				
		OOO-HL (899s ± 901s)				
	DP-B43E	OOO-HL (475s ± 480s)				
		OOO-HL (899s ± 903s)				
	F-014P	OOO-LL (490s ± 4000s)				
	F-A20A	OOO-LL (-300s ± 846s)				
		OOO-LL (4343s ± 4650s)				
		OOO-LL (5463s ± 5632s)				
	OOO-LL (5953s ± EOT)					
F-A80E	OOO-HL (472s ± 491s)					
F-B20A	OOO-LL (471s ± 485s)					
	OOO-LL (2158s ± 2185s)					

Note:

Out of range for instrument high limit (at least for 2s); OOR-LL = Out of range for instrument low limit (at least for 2s); EOT = End of test.

**TABLE D-2
OUT-OF-RANGE AND MODIFIED INSTRUMENTS BY TEST (Cont.)**

TIN	Out-of-Range Instrument	Comments	Instrument "Zero" Out of Specification	Modified Instrument	Reason for Modification	Corrective Action
S01512	T-001A F-001A	Measurement not required.	DP-B00S (79.0 mV) DP-A00S (27.8 mV) DP-A06S (20.3 mV)	DE-001PA	Instrument not available.	Not installed on break line.
	T-A02E F-A00E	Measurement not required.		DE-001PB	Instrument not available.	Not installed on break line.
	T-B02E F-B00E	Measurement not required.		F-001A	To avoid instrument limit.	Span modified from 0-180 kPa to 0-30 kPa.
	T-A20A F-A20A	Measurement not required.		F-A80E	To avoid instrument limit.	Span modified from 0-80 kPa to 0-300 kPa.
	T-B20A F-B20A	Measurement not required.		T-A82E	Change of location.	Moved upstream of PRHR U-pipe.
	DP-003P	OOH-HL (21s ÷ EOT)		IF030P	Change of use.	Used in addition with IF040P to collect condensed steam from break.
	DP-A05S	OOH-HL (7s ÷ 47s)		F-A04S	Westinghouse request.	Venturi tube removed.
	DP-A20E	OOH-LL (-300s ÷ 2095s)		F-B04S		
	DP-A28P	OOH-LL (-300s ÷ 21s)				
	DP-A41E	OOH-HL (533s ÷ 1284s)				
	DP-A82E	OOH-HL (12s ÷ 22s)				
	DP-A83E	OOH-HL (-300s ÷ 6s)				
	DP-B00P	OOH-HL (6s ÷ 24s)				
	DP-B00P	OOH-HL (117s ÷ 154s)				
	DP-B05S	OOH-HL (7s ÷ 9s)				
	DP-B20E	OOH-LL (-300s ÷ 2144s)				
	DP-B28P	OOH-LL (-300s ÷ 21s)				
	DP-B41E	OOH-HL (607s ÷ 1319s)				
	F-014P	OOH-HL (5s ÷ 22s)				
	F-A80E	OOH-LL (22s ÷ EOT)				
F-A80E	OOH-HL (5s ÷ 23s)					

Note:

Out of range for instrument high limit (at least for 2s); OOH-LL = Out of range for instrument low limit (at least for 2s); EOT = End of test.

**TABLE D-2
OUT-OF-RANGE AND MODIFIED INSTRUMENTS BY TEST (Cont.)**

TIN	Out-of-Range Instrument	Comments	Instrument "Zero" Out of Specification	Modified Instrument	Reason for Modification	Corrective Action
S01613	T-001A F-001A	Measurement not required.	DP-A06S (23.2 mV)	DE-001PA	Instrument not available.	Not installed on break line.
	T-A02E F-A00E	Measurement not required.		DE-001PB	Instrument not available.	Not installed on break line.
	T-B02E F-B00E	Measurement not required.		T-A82E	Change of location.	Moved upstream of U-pipe.
	T-A20A F-A20A	Measurement not required.		T-001B	Change of location.	Moved upstream break valve.
	T-B20A F-B20A	Measurement not required.		T-B02E	Change of location.	Moved downstream break valve.
	DP-002P	OOR-LL (6153s + 6191s)				
	DP-003P	OOR-LL (270s + EOT)				
	DP-018P	OOR-HL (250s + 258s)				
		OOR-LL (4889s + 4891s)				
		OOR-HL (6147s + 6158s)				
	DP-019P	OOR-LL (251s + 254s)				
		OOR-LL (6148s + 6152s)				
	DP-A00P	OOR-HL (315s + 848s)				
		OOR-HL (4902s + 6768s)				
	DP-A021P	OOR-LL (4900s + 5069s)				
	DP-A04P	OOR-HL (-300s + 270s)				
	DP-A20E	OOR-LL (-300s + 2286s)				
	DP-A28P	OOR-LL (-300s + 269s)				
		OOR-HL (742s + 1211s)				
		OOR-HL (2423s + 4788s)				
		OOR-LL (4885s + 5764s)				
	DP-A41E	OOR-HL (249s + 272s)				
	DP-A42E	OOR-HL (249s + 271s)				
	DP-A44E	OOR-HL (250s + 273s)				
	DP-A45E	OOR-LL (4900s + 5344s)				
		OOR-LL (5708s + 5756s)				
	DP-A82E	OOR-HL (-300s + 255s)				
DP-A83E	OOR-HL (255s + 273s)					
	OOR-HL (599s + 601s)					
	OOR-HL (774s + 965s)					
	OOR-HL (1023s + 1182s)					
	OOR-LL (4548s + 6398s)					
DP-B00P	OOR-HL (295s + 6802s)					
DP-B05S	OOR-HL (-300s + 244s)					
DP-B20E	OOR-LL (-300s + 2297s)					

Note:

Out of range for instrument high limit (at least for 2s); OOR-LL = Out of range for instrument low limit (at least for 2s); EOT = End of test.

**TABLE D-2
OUT-OF-RANGE AND MODIFIED INSTRUMENTS BY TEST (Cont.)**

TIN	Out-of-Range Instrument	Comments	Instrument "Zero" Out of Specification	Modified Instrument	Reason for Modification	Corrective Action
S01613 (Cont.)	DP-B28P	OOR-LL (-300 ÷ 270s) OOR-HL (743s ÷ 889s) OOR-HL (1013s ÷ 1176s) OOR-HL (2423s ÷ 4788s) OOR-LL (4884s ÷ 5916s)				
	DP-B41E	OOR-HL (249s ÷ 273s)				
	DP-B42E	OOR-HL (249s ÷ 270s)				
	DP-B43E	OOR-HL (249s ÷ 271s)				
	DP-B44E	OOR-HL (251s ÷ 256s)				
	DP-B45E	OOR-LL (4896s ÷ 5366s) OOR-LL (5701s ÷ 5912s)				
	F-014P	OOR-LL (252s ÷ 983s)				
	F-A80E	OOR-HL (255s ÷ 273s)				
	L-B40C	OOR-HL (251s ÷ 255s)				
	F-001BP	OOR-LL (250s ÷ 256s)				
	DP-A05S	OOR-HL (-300s ÷ 243s)				

Note:

Out of range for instrument high limit (at least for 2s); OOR-LL = Out of range for instrument low limit (at least for 2s); EOT = End of test.

**TABLE D-2
OUT-OF-RANGE AND MODIFIED INSTRUMENTS BY TEST (Cont.)**

TIN	Out-of-Range Instrument	Comments	Instrument "Zero" Out of Specification	Modified Instrument	Reason for Modification	Corrective Action	
S01703	T-001A F-001A	Measurement not required.	DP-A04S (35.6 mV) DP-B04S (24.2 mV)	DE-001PA	Instrument not available.	Not installed on break line.	
	T-A02E F-A00E	Measurement not required.		DE-001PB	Instrument not available.	Not installed on break line.	
	T-B02E F-B00E	Measurement not required.		T-062EA	Westinghouse request.	Installed in IRWST.	
	T-A20A F-A20A	Measurement not required.		DP-001P	T-063EA	Westinghouse request.	Installed in IRWST.
	T-B20A F-B20A	Measurement not required.		DP-002P	T-064EA	Westinghouse request.	Installed in IRWST.
	DP-001P	OOR-LL (2389s ± 2391s)		DP-003P	T-064EB	Westinghouse request.	Installed in IRWST.
	DP-002P	OOR-LL (2389s ± 2391s)		DP-018P	T-064EC	Westinghouse request.	Installed in IRWST.
	DP-003P	OOR-LL (82s ± EOT)			T-065EA	Westinghouse request.	Installed in IRWST.
	DP-018P	OOR-HL (62s ± 70s)			T-065EB	Westinghouse request.	Installed in IRWST.
		OOR-LL (992s ± 1000s)			T-065EC	Westinghouse request.	Installed in IRWST.
	DP-019P	OOR-LL (63s ± 68s)					
		OOR-HL (991s ± 1001s)					
	DP-A00P	OOR-HL (211s ± 216s)					
		OOR-HL (1662s ± 3140s)					
	DP-A05S	OOR-HL (-300s ± 55s)					
	DP-A20E	OOR-LL (-300s ± 744s)					
		OOR-HL (1130s ± 1298s)					
		OOR-LL (2434s ± 2436s)					
	DP-A28P	OOR-LL (-300s ± 81s)					
		OOR-HL (164s ± 589s)					
		OOR-LL (911s ± 2052s)					
	DP-A40E	OOR-LL (1375s ± 1378s)					
	DP-A41E	OOR-HL (1s ± 84s)					
	DP-A42E	OOR-HL (52s ± 94s)					
	DP-A44E	OOR-HL (62s ± 76s)					
	DP-A82E	OOR-HL (-300s ± 82s)					
	DP-A83E	OOR-HL (67s ± 85s)					
		OOR-LL (1009s ± 1040s)					
		OOR-LL (1163s ± 2687s)					
	DP-B00P	OOR-HL (99s ± 147s)					
		OOR-HL (436s ± 3296s)					
	DP-B05S	OOR-HL (-300s ± 57s)					
	DP-B20E	OOR-LL (-300s ± 745s)					
	OOR-HL (1126s ± 1321)						
	OOR-LL (2433s ± 2437s)						
DP-B28P	OOR-LL (-300s ± 82s)						
	OOR-HL (164s ± 376s)						
	OOR-LL (991s ± 2053s)						
DP-B40E	OOR-LL (1350s ± 1354s)						

Note:

Out of range for instrument high limit (at least for 2s); OOR-LL = Out of range for instrument low limit (at least for 2s); EOT = End of test.

**TABLE D-2
OUT-OF-RANGE AND MODIFIED INSTRUMENTS BY TEST (Cont.)**

TIN	Out-of-Range Instrument	Comments	Instrument "Zero" Out of Specification	Modified Instrument	Reason for Modification	Corrective Action
S01703 (Coc.)	DP-B41E DP-B42E DP-B43E DP-B44E F-014P F-A80E L-B47E	OCOR-HL (1s + 84s) OCOR-HL (61s + 83s) OCOR-HL (0/s + 84s) OCOR-HL (62s + 71s) OCOR-LL (292s + EOT) OCOR-HL (67s + 85s) OCOR-HL (63s + 69s)				

Note:
Out of range for instrument high limit (at least for 2s); OCOR-LL = Out of range for instrument low limit (at least for 2s); EOT = End of test.

**APPENDIX E
ERROR ANALYSIS**

E-1 Objectives

The objectives of the error analysis are as follows:

- To describe the errors of the measurements performed during the SPES-2 test program.
- To give the results of the error analysis calculations.

The error analysis was performed in metric units; however, the final results are reported in English units.

E-2 Error Evaluation

During the test, all measured instrumentation data of the primary and secondary circuit were recorded at a sampling frequency of 1.0 Hz. The recorded data were converted to engineering units (SI) and then plotted versus time. The engineering values were also recorded on magnetic tape in order to transmit the data to Westinghouse Electric Corporation.

E-2.1 Direct Measured Quantities

The direct measured quantities (such as absolute pressures, pressure drops, fluid speed, voltages, current, etc.), acquired and recorded by data acquisition system (DAS), were converted into engineering (SI) units using linear formulas:

$$Y = \pm M * (mV - q) \pm K = \pm M * mV + Q$$

where:

- mV = signal coming from instrument
- M, q = calibration constants (q = instrument zero)
- K = instrument hydraulic head = $\rho_{LC} * g * h$
- Q = $\pm M * q \pm K$

and where:

- ρ_{LC} = water density assumed at ambient temperature = 1000 (kg/m³)
- h = pressure tap height difference (m)
- g = acceleration due to gravity = 9.80665 (m/sec.²)

To verify that the instrument will meet the required accuracy for test, the instruments were controlled and calibrated in the laboratory before installation in the facility. In the facility, the instrument was

checked just before the beginning of the experiment in order to control all the DAS recording channels. The instrument zero was verified daily before starting the test.

Temperatures

The temperature of the fluid, piping, components, and in-containment refueling water storage tank (IRWST) pool water were measured in degrees Celsius by using the following:

- Sheated thermocouples type K Chromel-Alumel, 0.5- to 1.5-mm OD
- Resistance thermal detector (RTD) thermoresistances type PT 100

A matrix E (mV), T (°C), for K-type thermocouples was generated by the following formula (UNI-7938 specifications):

$$E = \left(\sum_{(i=1)}^8 d_i T^i + 125 \exp [-1/2 * (T - 127/65)^2] \right) / 1000$$

where:

E = electrical signal (mV)

T = temperature (°C)

$d_0 = -1.853306 * 10^{-1}$

$d_1 = 3.891834 * 10^{-1}$

$d_2 = 1.664515 * 10^{-2}$

$d_3 = -7.870237 * 10^{-5}$

$d_4 = 2.283579 * 10^{-7}$

$d_5 = -3.570023 * 10^{-10}$

$d_6 = 2.993291 * 10^{-13}$

$d_7 = -1.284985 * 10^{-16}$

$d_8 = 2.223997 * 10^{-20}$

The value of temperature T (°C) was obtained from the signals coming from thermocouples E (mV), performing a linear interpolation of the matrix E, T. In the same way, the signals coming from thermoresistances (Ω) were converted to engineering units (°C) performing the linear interpolation of the PT100 type thermoresistance data characteristics generated by the following formula (UNI-7937 specifications):

$$R = 100 * (1 + 3.90802E-3 * T - 0.5802E-6 * T^2)$$

where:

T = temperature (°C)

R = measured RTD resistance (Ω)

Thermoresistances and thermocouples were calibrated in the laboratory to verify their accuracy. Before testing, a check to control the correspondence between the DAS recording channels and the instruments was also performed.

E-2.2 Derived Quantities

Flow Rates Measured by Nozzles (kg/sec.)

$$F = \alpha^* \cdot \epsilon \cdot (\Delta P_c \cdot \rho)^{0.5}$$

where:

$$\Delta P_c = \Delta P \pm \rho \cdot g \cdot h$$

For orifices, the following applies:

$$\epsilon = 1 - (0.41 + 0.35 \cdot \beta^4) \cdot \Delta P_c / (\sigma \cdot P_1)$$

For Venturi tubes, the following applies:

$$\epsilon = \left[\left(\frac{P_2}{P_1} \right)^{\frac{2}{\sigma}} \cdot \frac{\sigma}{\sigma-1} \cdot \frac{1 - \left(\frac{P_2}{P_1} \right)^{\frac{\sigma-1}{\sigma}}}{1 - \left(\frac{P_2}{P_1} \right)} \cdot \frac{1 - \beta^4}{1 - \beta^4 \cdot \left(\frac{P_2}{P_1} \right)^{\frac{2}{\sigma}}} \right]^{0.5}$$

where:

α = flux coefficient

α_c = calibrated or calculated flux coefficient (m^2) = $\alpha \cdot \frac{\pi d^2}{4} \cdot (2)^{0.5}$

ϵ = compressibility coefficient equal to one for liquid

ΔP_c = local pressure drop across the nozzle (Pa)

ρ = fluid density (kg/m^3)

- ΔP = measured pressure drop across the nozzle (Pa)
 P_1 = absolute pressure upstream the nozzle (Pa)
 g = gravity acceleration = 9.80665 (m/sec.²)
 h = pressure tap height difference (m)
 P_2/P_1 = ratio of outlet to inlet static pressure
 σ = 1.265 saturated steam isentropic exponent at 4.9 MPa
 β = d/D diameter ratio of the nozzle

The main characteristics of the nozzles are reported in Table C-2 of Appendix C.

The values of nozzle flux coefficients reported in the table were corrected, taking account of the fluid temperature measured upstream the nozzle using the following thermal expansion formula:

$$\alpha^* = \alpha_c * (1 + \lambda * (T - T_{cal}))^2$$

where:

- T = operating temperature
 T_{cal} = calibration temperature
 λ = linear thermal expansion coefficient = 1.2E-05 (1/°C)

Power Channel Electrical Power (kW)

$$W-000P = (I_1 + I_2 + I_3 + I_4 + I_5 + I_6) * V_{PC} * 10^{-3}$$

where:

- $I_1 + I_2 + I_3 + I_4 + I_5 + I_6$ = direct current feeding the rod bundle measured using six shunts (A)
 V_{PC} = voltage drop across the rod bundle (V)

Levels

The pressurizer, steam generator, and core makeup tank (CMT) collapsed levels were computed in meters using the following formula:

$$L = \frac{\Delta P - g * \rho_v * h}{g * (\rho_L - \rho_v)}$$

where:

- ρ_v = steam density in saturation condition (kg/m^3)
 ρ_L = liquid density (kg/m^3) computed at the following conditions:
- saturation conditions for steam generators and for pressurizer
 - average temperature for CMT
- ΔP = measured pressure drop between the taps (Pa)
 h = total pressure tap height difference (m)

NOTE: For IRWST level, $\rho_v = 0$ and $\rho_L = \text{IRWST water density}$.

The accumulator levels were calculated using the following formula:

$$L = \frac{\Delta P_{\text{inst}} - g * h1 * (\rho_{LC} - \rho_A)}{g * (\rho_L - \rho_A)}$$

where:

- ρ_A = $P/(R*T)$ = air density (kg/m^3)
 ρ_L = liquid density at operating conditions (kg/m^3)
 $h1$ = height difference between the accumulator lower tap and the instrument positive side (m)
 ΔP_{inst} = pressure drop (Pa) measured by instrument; the measurement has been performed with the negative hydraulic line full of air at the same pressure of the accumulator and the positive hydraulic line full of water
 ρ_{LC} = water density at ambient temperature assumed to equal 1000 (kg/m^3)

and where:

- R = gas constant of air = 287.037 (J/kg-K)
 T = air temperature (K)
 P = air pressure (Pa)

E-2.3 Measurement Errors

The absolute maximum error (Δ) and the standard deviation (σ) of the directly measured physical quantities (absolute and differential pressures, temperature, etc.) are defined as follows:

$$\Delta = \pm (\Delta_1 + \Delta K + \Delta_{BV} + \Delta_{RJ})$$

where:

- Δ_i = $\pm (\Delta_C + \Delta_{ps} + \Delta_{LCH})$ = SIET assigned instrument error
- Δ_C = maximum value between the manufacturer error and the maximum error of the performed calibrations for absolute and differential transmitters; maximum value between the ANSI special error and the maximum error of the performed calibrations for thermocouples; maximum value between the UNI-7937 error and the maximum error of the performed calibrations for thermoresistances
- Δ_{ps} = error of the reference primary standard (pressure gauge, reference thermocouple, reference thermoresistance) used in calibration
- Δ_{LCH} = error of the voltmeter used to acquire the instrument output signal during the calibration
- ΔK = maximum error of the instrument hydraulic head
- Δ_{BV} = acquisition card A/D converter bit value (acquisition card error)
- Δ_{RJ} = maximum error of the cold junction (only for thermocouples)

$$\sigma = \pm (\Delta_i^2 + \Delta^2 K + \Delta_{BV}^2 + \Delta_{RJ}^2)^{0.5}$$

The absolute maximum error and the standard deviation of the derived quantities (flow rate, levels, etc.) were calculated using the following error propagation formulas:

$$\Delta Y = \pm \sum_{i=1}^n \left| \frac{\delta Y}{\delta X_i} \right| * \Delta X_i$$

where,

$$Y = Y (X_i) \text{ with } i = 1 \dots n$$

$$\sigma Y = \pm \left[\sum_{i=1}^n \left(\frac{\delta Y}{\delta X_i} \right)^2 * \sigma^2 X_i \right]^{0.5}$$

where:

- Δ_{X_i} = maximum error of the quantities X_i
- σ_{X_i} = standard deviation of the quantities X_i

The error calculations were carried out using, in a conservative way, the upper value range of the instrument.

E-3 Absolute and Differential Pressure Transmitters

An absolute or differential pressure measurement was calculated as a derived parameter given by the following:

$$Y = \pm P_{inst} \pm K$$

where:

- Y = absolute pressure (P) or differential pressure (ΔP) to be measured
- P_{inst} = absolute pressure or differential pressure directly measured by the instrument
- K = $P_{LC} * g * h$ = instrument hydraulic head due to the presence of cold water inside the hydraulic connections between pressure taps and instrument
- P_{LC} = water density at ambient temperature assume to equal 1000 (kg/m^3)
- g = gravity acceleration = 9.80665 (m/sec^2)
- h = pressure taps elevation difference for ΔP measurements or height difference between pressure tap and instrument for P measurements (m)

In the case of absolute pressure measurement, the above equation becomes the following because the instrument is always installed below the facility pressure tap.

$$P = + P_{inst} - K$$

where:

$$P_{inst} = M * (mV - q) = \text{absolute pressure measured by instrument}$$

and where:

- mV = signal coming from instrument
- M,q = instrument calibration constants (q = instrument zero)

Therefore +M and -K were obtained using the DAS conversion constant data (see Table C-1 of Appendix C).

In the case of differential pressure measurement, the above equation assumes four different configurations—depending on the installation of the instrument (differential pressure cell) in the plant.

Configuration 1

If the normal direction of the flow is in the UP vertical direction and the negative (low-pressure) side of the instrument is the upper tap, then the equation becomes the following:

$$\Delta P = + P_{inst} + K$$

where:

P_{inst} = $M * (mV - q)$ = differential pressure measured by instrument equal to the (positive tap pressure) minus (negative tap pressure)

and where:

mV = signal coming from instrument

M, q = instrument calibration constants (q = instrument zero)

Therefore, $+M$ and $+K$ were obtained using the DAS conversion constant data sheet (see Table C-1 of Appendix C).

Configuration 2

If the normal direction of the flow is in the UP vertical direction (or when flow = 0 for water level measurements) and the positive (high-pressure) side of the instrument is connected to the upper tap, then the equation becomes the following:

$$\Delta P = - P_{inst} + K$$

where:

P_{inst} = $M * (mV - q)$ = differential pressure measured by instrument equal to the (positive tap pressure) minus (negative tap pressure)

and where:

mV = instrument calibration constant

M, q = instrument calibration constant (q = instrument zero)

Therefore, $-M$ and $+K$ were obtained using the DAS conversion constant data sheet (see Table C-1 of Appendix C).

Configuration 3

If the normal direction of the flow is in the DOWN vertical direction and the negative (low-pressure) side of the instrument is the bottom tap, then the equation becomes the following:

$$\Delta P = + P_{inst} - K$$

where:

$P_{inst} = M * (mV - q)$ = differential pressure measured by instrument equal to the (positive tap pressure) minus (negative tap pressure)

and where:

mV = signal coming from instrument

M, q = instrument calibration constants (q = instrument zero)

Therefore, +M and -K were obtained using the DAS conversion constant data sheet (see Table C-1 of Appendix C).

Configuration 4

If the normal direction of flow is in the DOWN vertical direction and the negative (low-pressure) side of the instrument is the upper tap, then the equation becomes the following:

$$\Delta P = - P_{inst} - K$$

where:

$P_{inst} = M * (mV - q)$ = differential pressure measured by instrument equal to the (positive tap pressure) minus (negative tap pressure)

and where:

mV = signal coming from instrument

M, q = instrument calibration constants (q = instrument zero)

Therefore, -M and -K were obtained using the DAS conversion constant data sheet (see Table C-1 of Appendix C).

E-3.1 Absolute or Differential Pressure Error Analysis

The absolute or differential pressure maximum error (ΔY) and the standard deviation (σY) are defined as follows:

$$\Delta Y = \pm (\Delta_I + \Delta K + \Delta_{BV})$$

where:

- Δ_I = $\pm (\Delta_C + \Delta_{PS} + \Delta_{LCH})$ = SIET assigned instrument error
- ΔK = maximum error of the instrument hydraulic head
- Δ_{BV} = acquisition card A/D converter bit value (acquisition card error)

and where:

- Δ_C = maximum value between the manufacturer error and the maximum error of the performed calibrations
- Δ_{PS} = maximum error of the reference primary standard (pressure gauge) used for the calibration
- Δ_{LCH} = maximum error of the voltmeter used to acquire the instrument output signal during the calibration

Neglecting the error contribution of the gravity acceleration and applying the error propagation formula ΔK results in the following:

$$\Delta K = \pm (g * h * \Delta \rho_{LC} + \rho_{LC} * g * \Delta h)$$

In data reduction, it is assumed that $\rho_{LC} = 1000 \text{ kg/m}^3$, but the density changes versus room temperature and the tests have been performed at different environment temperature (from 15°C to 30°C). For this reason, the following was assumed:

$$\Delta \rho_{LC} = \pm 4 \text{ kg/m}^3$$

The error contribution of the heights of the hydraulic lines (Δh) versus the h values had been assumed as follows:

$\Delta h = \pm 0.002$ m	for	0 m	$<h \leq 0.5$ m
$\Delta h = \pm 0.003$ m	for	0.5 m	$<h \leq 2$ m
$\Delta h = \pm 0.005$ m	for	2 m	$<h \leq 4$ m
$\Delta h = \pm 0.007$ m	for	4 m	$<h \leq 5$ m
$\Delta h = \pm 0.009$ m	for	5 m	$<h \leq 8$ m
$\Delta h = \pm 0.010$ m	for		$h > 8$ m

$$\sigma Y = \pm (\Delta_1^2 + \Delta^2 K + \Delta_{BV}^2)^{0.5}$$

E-3.2 Example of Absolute and Differential Pressure Error Calculation

The example of the error calculation is presented for the pressurizer absolute pressure P-027P and power channel pressure drop DP-000P measurements.

- Quantities and primary errors used in the error calculations of the absolute pressure P-027P (see Table E-3 and Section E-3)

$h = 8.299$ m (27.2 ft.)	$\Delta h = \pm 0.010$ m ($\pm .032$ ft.)	$g = 9.80665$ m/sec. ²
$\rho_{LC} = 1000$ kg/m ³	$\Delta \rho_{LC} = \pm 4$ kg/m ³	$\Delta_{BV} = \pm 12207$ Pa (± 1.77 psi)
$\Delta_c = \pm 20000$ Pa (± 2.90 psi)	$\Delta_{ps} = \pm 10050$ Pa (± 1.45 psi)	$\Delta_{LCH} = \pm 502$ Pa (± 0.072 psi)

Therefore,

$$\Delta_1 = \pm (\Delta_c + \Delta_{ps} + \Delta_{LCH}) = \pm 30552 \text{ Pa } (\pm 4.43 \text{ psi})$$

$$\begin{aligned} \Delta K &= \pm (g * h * \Delta \rho_{LC} * g * \Delta h) \\ &= \pm (9.80665 * 8.299 * 4 + 1000 * 9.80665 * 0.01) = \pm 424 \text{ Pa } (\pm 0.061 \text{ psi}) \end{aligned}$$

and:

$$\begin{aligned}\Delta(P-027P) &= \pm (\Delta_1 + \Delta K + \Delta_{BV}) = \pm (30552 + 424 + 12207) \\ &= \pm 43183 \text{ Pa} = \pm 0.043 \text{ MPa} (\pm 6.2 \text{ psi})\end{aligned}$$

$$\begin{aligned}\sigma(P-027P) &= \pm (\Delta_1^2 + \Delta^2 K + \Delta_{BV}^2)^{0.5} = \pm [(30552)^2 + (424)^2 + (12207)^2]^{0.5} \\ &= \pm 32903 \text{ Pa} = \pm 0.033 \text{ MPa} (\pm 4.7 \text{ psi})\end{aligned}$$

- Quantities and primary errors used in the error calculation of the differential pressure measurement DP-000P (see Table E-3)

$$\begin{aligned}h &= 4.441 \text{ m (14.57 ft.)} & \Delta h &= \pm 0.007 \text{ m} (\pm 0.023 \text{ ft.}) & g &= 9.80665 \text{ m/sec.}^2 \\ \rho_{LC} &= 1000 \text{ kg/m}^3 & \Delta \rho_{LC} &= \pm 4 \text{ kg/m}^3 & \Delta_{BV} &= \pm 73 \text{ Pa} (\pm .010 \text{ psi}) \\ \Delta_C &= \pm 240 \text{ Pa} (\pm .034 \text{ psi}) & \Delta_{PS} &= \pm 18 \text{ Pa} (\pm .003 \text{ psi}) & \Delta_{LCH} &= \pm 2 \text{ Pa} (\pm .0003 \text{ psi})\end{aligned}$$

Therefore,

$$\Delta_1 = \pm (\Delta_C + \Delta_{PS} + \Delta_{LCH}) = \pm (240 + 18 + 2) = \pm 260 \text{ Pa} (\pm 0.037 \text{ psi})$$

$$\begin{aligned}\Delta K &= \pm (g * h * \Delta \rho_{LC} + \rho_{LC} * g * \Delta h) \\ &= \pm (9.80665 * 4.441 * 4 + 1000 * 9.80665 * 0.007) = \pm 243 \text{ Pa} (\pm 0.035 \text{ psi})\end{aligned}$$

and:

$$\begin{aligned}\Delta (DP-000P) &= \pm (\Delta_1 + \Delta K + \Delta_{BV}) = \pm (260 + 243 + 73) = \pm 576 \text{ Pa} \\ &= \pm 0.576 \text{ kPa} (\pm 0.083 \text{ psi})\end{aligned}$$

$$\begin{aligned}\sigma (DP-000P) &= \pm (\Delta_1^2 + \Delta^2 K + \Delta_{BV}^2)^{0.5} = \pm [(260)^2 + (243)^2 + (73)^2]^{0.5} \\ &= \pm 363 \text{ Pa} = \pm 0.363 \text{ kPa} (\pm 0.053 \text{ psi})\end{aligned}$$

The results of the absolute and differential pressure error calculations are reported in Table E-3. The columns are defined as follows:

PLANT CODE	SPES-2 instrument identification code
h	Pressure tap elevation difference for differential pressure transmitters or height difference between pressure tap and instrument for absolute pressure transmitters (ft.)
Δh	Maximum error of the heights of the hydraulic lines (\pm ft.)
ΔK	Maximum error of the instrument hydraulic head (\pm psi) for absolute pressure transmitters, (\pm psi) for differential pressure transmitters
Δ_C	Maximum value between the manufacturer error and the maximum error of the calibrations performed (\pm psi) for absolute pressure transmitters, (\pm psi) for differential pressure transmitters
Δ_{PS}	Maximum error of the reference primary standard (pressure gauge) used for the calibrations (\pm psi) for absolute transmitters, (\pm psi) for differential pressure transmitters
Δ_{LCH}	maximum error of the voltmeter used to acquire the instrument output signal during the calibrations (\pm psi) for absolute pressure transmitters, (\pm psi) for differential pressure transmitters
Δ_{BV}	Acquisition card A/D converter bit value (acquisition card error) (\pm psi) for absolute pressure transmitters, (\pm psi) for differential pressure transmitters
$\Delta_I = \pm (\Delta_C + \Delta_{PS} + \Delta_{LCH})$	SIET assigned instrument error (\pm psi) for absolute pressure transmitters, (\pm psi) for differential pressure transmitters
Δ	Measurement maximum error (\pm psi) for absolute pressure transmitters, (\pm psi) for differential pressure transmitters
σ	Measurement standard deviation (\pm psi) for absolute pressure transmitters, (\pm psi) for differential pressure transmitters

E-4 Temperatures

The temperature of the fluid, piping, components, and IRWST pool water were measured by using:

- Sheated thermocouples type K Chromel-Alumel, 0.5- to 1.5-mm OD
- RTD thermoresistances type PT 100

A matrix E (mV), T (°C), for K-type thermocouples was generated by the following formula (UNI-7938 specifications):

$$E = \left(\sum_{i=0}^8 d_i T^i + 125 \exp \left[-1/2 * (T - 127/65)^2 \right] \right) / 1000$$

where:

E = electrical signal (mV)

T = temperature (°C)

$d_0 = -1.853306 * 10^1$

$d_1 = 3.891834 * 10^{-1}$

$d_2 = 1.664515 * 10^{-2}$

$d_3 = -7.870237 * 10^{-5}$

$d_4 = 2.283579 * 10^{-7}$

$d_5 = -3.570023 * 10^{-10}$

$d_6 = 2.993291 * 10^{-13}$

$d_7 = -1.284985 * 10^{-16}$

$d_8 = 2.223997 * 10^{-20}$

The value of temperature T (°C) was obtained from the signals coming from thermocouples E (mV), performing a linear interpolation of the matrix E, T. In the same way, the signals coming from thermoresistances (Ω) were converted in engineering units (°C) performing the linear interpolation of the PT100 type thermoresistance data characteristics generated by the following formula (UNI-7937 specifications):

$$R = 100 * (1 + 3.90802E-3 * T - 0.5802E-6 * T^2)$$

where:

T = temperature (°C)

R = measured RTD resistance (Ω)

Thermoresistances and thermocouples were calibrated in laboratory to verify accuracy. Before testing, a check to control the correspondence between the DAS recording channels and the instruments was also performed.

E-4.1 Temperature Error Analysis

The temperature maximum error (ΔT) and the standard deviation (σT) are defined as follows:

$$\Delta T = \pm (\Delta_i + \Delta_{BV} + \Delta_{RJ})$$

where:

Δ_i = ($\Delta_c + \Delta_{ps} + \Delta_{LCH}$) = SIET assigned error

Δ_{BV} = acquisition card A/D converter bit value (acquisition card error)

Δ_{RJ} = maximum error of the cold junction (only for thermocouples)

and where:

Δ_c = maximum value between the ANSI special error and the maximum error of the performed calibrations for thermocouples; maximum value between the UNI-7937 error and the maximum error of the performed calibrations for thermoresistances

Δ_{px} = error of the reference primary standard (reference thermocouple, reference thermoresistance) used in calibration

Δ_{LCH} = error of the voltmeter used to acquire the instrument output signal during the calibration

$$\sigma T = \pm (\Delta_i^2 + \Delta_{BV}^2 + \Delta_{RJ}^2)^{0.5}$$

NOTE: The ANSI special error for K-type thermocouples is defined as follows:

$$\pm 1.1 \text{ } ^\circ\text{C} \text{ or } 0.4\%, \text{ whichever is greater}$$

The UNI-7937 error for PT100 type thermoresistances is defined as follows:

$$\pm (0.15 + 0.002 * T_{\max}) \text{ } ^\circ\text{C}$$

where:

T_{max} = achievable maximum temperature ($^{\circ}\text{C}$)

E-4.2 Example of Error Calculations for Temperature Measurements

The example of the error calculation is presented for the temperature measurement T-03P (K-type thermocouple instrument) and the temperature measurement T-061E (PT100-type RTD instrument).

- Primary errors (see Table E-4) used in the error calculations of the temperature measurement T-003P (K-type thermocouple instrument):

$$\Delta_C = \pm 1.14^{\circ}\text{C} (\pm 2.05^{\circ}\text{F}) \quad \Delta_{PS} = \pm 0.12^{\circ}\text{C} (\pm .22^{\circ}\text{F}) \quad \Delta_{LCH} = \pm 0.01^{\circ}\text{C} (\pm .02^{\circ}\text{F})$$

$$\Delta_{BV} = \pm 0.1^{\circ}\text{C} (\pm .18^{\circ}\text{F}) \quad \Delta_{RJ} = \pm 0.1^{\circ}\text{C} (\pm .18^{\circ}\text{F})$$

Therefore,

$$\Delta_1 = \pm (\Delta_C + \Delta_{PS} + \Delta_{LCH}) = \pm (1.14 + 0.12 + 0.01) = \pm 1.27^{\circ}\text{C} (\pm 2.28^{\circ}\text{F})$$

$$\Delta (\text{T-003P}) = \pm (\Delta_1 + \Delta_{BV} + \Delta_{RJ}) = \pm (1.27 + 0.1 + 0.1) = \pm 1.47^{\circ}\text{C} (\pm 2.65^{\circ}\text{F})$$

$$\sigma (\text{T-003P}) = \pm (\Delta_1^2 + \Delta_{BV}^2 + \Delta_{RJ}^2)^{0.5} = \pm [(1.27)^2 + (0.1)^2 + (0.1)^2]^{0.5} = \pm 1.28^{\circ}\text{C} (\pm 2.30^{\circ}\text{F})$$

- Primary errors (see Table E-4) used in the error calculations of the temperature measurement T-061E (PT100-type RTD instrument):

$$\Delta_C = \pm 0.35^{\circ}\text{C} (\pm .63^{\circ}\text{F}) \quad \Delta_{PS} = \pm 0.12^{\circ}\text{C} (\pm .22^{\circ}\text{F}) \quad \Delta_{LCH} = \pm 0.01^{\circ}\text{C} (\pm .02^{\circ}\text{F})$$

$$\Delta_{BV} = \pm 0.05^{\circ}\text{C} (\pm .09^{\circ}\text{F})$$

Therefore,

$$\Delta_I = \pm (\Delta_C + \Delta_{PS} + \Delta_{LCH}) = \pm (0.35 + 0.12 + 0.01) = \pm 0.48^\circ\text{C} (\pm 0.86^\circ\text{F})$$

$$\Delta (T-061E) = \pm (\Delta_I + \Delta_{BV}) = \pm (0.48 + 0.05) = \pm 0.53^\circ\text{C} (\pm 0.95^\circ\text{F})$$

$$\sigma (T-061E) = \pm (\Delta_I^2 + \Delta_{BV}^2)^{0.5} = \pm [(0.48)^2 + (0.05)^2]^{0.5} = \pm 0.48^\circ\text{C} (\pm 0.86^\circ\text{F})$$

The results of the temperature error calculations are reported in Table E-4. The columns are defined as follows:

PLANT CODE	SPES-2 instrument identification code
Δ_C	Maximum value between the ANSI special error and the maximum error of the performed calibrations for thermocouples (\pm °F); maximum value between the UNI-7937 error and the maximum error of the performed calibrations for thermoresistances (\pm °F)
Δ_{PS}	Error of the reference primary standard (reference thermocouple, reference thermoresistance) used in calibration (\pm °F)
Δ_{LCH}	Error of the voltmeter used to acquire the instrument output signal during the calibration (\pm °F)
Δ_{BV}	Acquisition card A/D converter bit value (acquisition card error) (\pm °F)
Δ_{RJ}	Maximum error of the cold junction (only for thermocouples) (\pm °F)
$\Delta_I = \pm (\Delta_C + \Delta_{PS} + \Delta_{LCH})$	SIET assigned instrument error (\pm °F)
Δ	Measurement maximum error (\pm °F)
σ	Measurement standard deviation (\pm °F)

E-5 Load Cells

The masses discharged by break, ADS-1, -2, -3 and -4 valves, and steam generator's power-operated relief valve (PORV) were collected using three catch tanks and measured using a load cell system. Each catch tank was equipped with three load cells electrically connected in parallel mode (maximum load = 3000 kg; accuracy = $\pm 0.1\%$).

E-5.1 Load Cells Error Analysis

The maximum error (ΔIF) and the standard deviation (σIF) of the mass collected and weighed by catch tank were defined as follows:

$$\Delta IF = \pm (\Delta_1 + \Delta_{BV})$$

where:

$$\begin{aligned}\Delta_1 &= \pm (\Delta_C + \Delta_{PS} + \Delta_{LCH}) = \text{SIET assigned error} \\ \Delta_{BV} &= \text{acquisition card A/D converter bit value (acquisition card error)}\end{aligned}$$

and where:

$$\begin{aligned}\Delta_C &= \text{maximum value between the manufacturer error and the maximum error of the performed calibrations} \\ \Delta_{PS} &= \text{maximum error of the reference primary standard (set of weights and scale) used for the calibration} \\ \Delta_{LCH} &= \text{maximum error of the voltmeter used to acquire the output signal of the load cell system}\end{aligned}$$

$$\sigma IF = \pm (\Delta_1^2 + \Delta_{BV}^2)^{0.5}$$

E-5.2 Example of Load Cell Error Calculations

The example of the error calculations concerns the integral mass flow rate measurement IF005P.

Primary errors used in the error calculations (see Table E-5):

$$\begin{aligned}\Delta_C &= \pm 3 \text{ kg } (\pm 6.61 \text{ lb}) & \Delta_{PS} &= \pm 0.19 \text{ kg } (\pm 0.42 \text{ lb}) & \Delta_{LCH} &= \pm 0.34 \text{ kg } (\pm 0.74 \text{ lb}) \\ \Delta_{BV} &= \pm 2.24 \text{ kg } (\pm 4.94 \text{ lb})\end{aligned}$$

Therefore,

$$\Delta_1 = \pm (\Delta_C + \Delta_{PS} + \Delta_{LCH}) = \pm (3 + 0.19 + 0.34) = \pm 3.53 \text{ kg } (\pm 7.78 \text{ lb})$$

$$\Delta (\text{IF005P}) = \pm (\Delta_1 + \Delta_{BV}) = \pm (3.53 + 2.24) = \pm 5.77 \text{ kg } (\pm 12.72 \text{ lb})$$

$$\sigma (\text{IF005P}) = \pm (\Delta_1^2 + \Delta_{BV}^2)^{0.5} = \pm [(3.53)^2 + (2.24)^2]^{0.5} = \pm 4.18 \text{ kg } (\pm 9.22 \text{ lb})$$

The results of the load cell error calculations are reported in Table E-5 are defined as follows:

PLANT CODE	SPES-2 instrument identification code
Δ_C	Maximum value between the manufacturer error and the maximum error of the performed calibrations (\pm lb)
Δ_{PS}	Maximum error of the reference primary standard (set of weights and scale) used for the calibrations (\pm lb)
Δ_{LCH}	Maximum error of the voltmeter used to acquire the output signal of the load cell system during the calibration (\pm lb)
Δ_{BV}	Acquisition card A/D converter bit value (acquisition card error) (\pm lb)
$\Delta_1 = \pm (\Delta_C + \Delta_{PS} + \Delta_{LCH})$	SIET assigned instrument error (\pm lb)
Δ	Measurement maximum error (\pm lb)
σ	Measurement standard deviation (\pm lb)

E-6 Data Acquisition System (DAS)

This paragraph reports the accidental and systematic (recoverable) errors of the DAS. The accidental errors are as follows:

- Δ_{BV} = acquisition card A/D converter bit value (acquisition card error)
- Δ_{RJ} = maximum error of the cold junction (only for thermocouples)

There are eight types of cards used in the DAS:

- AMUX (analogical multiplexer) used to acquire absolute and differential pressure (32 channels/card)
- RTD (resistance thermal detector) used to acquire thermoresistances (8 channels/card)
- SG (strain gauge) used to acquire load cells, differential pressure transducers (8 channels/card)
- TC (thermocouple) used to acquire thermocouples (8 channels/card)
- TCX - 400 (thermocouple) used to acquire thermocouples (8 channels/card)
- TCS - 800 (thermocouple) used to acquire the rod bundle thermocouples (8 channels/card)
- TCX - 100 (low voltage signal) used to acquire the shunts (8 channels/card)
- TCX - 5000 (high voltage signal) used to acquire the voltage drop across the rod bundle (8 channels/card)

The error Δ_{BV} depends on the characteristics of the card and on the characteristics of the channel. It is defined as follows:

$$\Delta_{BV} = \pm \frac{A}{2^n * G} * M$$

where:

A = A/D converter full scale = 10000 (mV)

n = number of bits used by A/D converter = 12

G = channel amplifier gain having the following values:

G = 1 for AMUX card

G = 131.86 for RTD card

G = 166.67 for SG card

G = 609.9 for TC card

G = 304.9 for TCX-400 card

G = 150.25 for TCX-800 card

G = 50 for TCX-100 card

G = 1 for TCX-5000 card

M = Instrument conversion constant or conversion matrix for thermocouples and thermoresistances

The values of the errors Δ_{BV} for each measurement are reported in the tables of this appendix.

The maximum error of the cold junction Δ_{RJ} is given by manufacturer and is:

$$\Delta_{RJ} = \pm 0.1 \text{ (}^\circ\text{C)}$$

The systematic (recoverable) DAS errors are:

1. The thermocouples amplifier shifts. These values are reported in Table E-11.
2. The difference between the fluid density values calculated by DAS subroutines (ρ_{LDAS} , ρ_{VDAS}) and the values given by water-steam tables (ρ_{LTAB} , ρ_{VTAB}).

These differences ($\Delta\rho_L$, $\Delta\rho_V$) are shown in Tables E-1 and E-2.

E-7 Flow Venturi/Orifices

$$F = \alpha' * \epsilon * (\Delta P_c * \rho)^{0.5}$$

where:

$$\Delta P_c = \Delta P \pm \rho * g * h = \Delta P \pm K_i$$

and where:

- F = flow rate (kg/sec.)
 α' = $\alpha_c (1 + \lambda * (T - T_{ca}))^2$ = nozzle flux coefficient corrected by fluid temperature
 ϵ = compressibility coefficient equal to one for liquid
 ΔP_c = local pressure drop across the nozzle (Pa); if the nozzle is installed in an horizontal plane $\Delta P_c = \Delta P$
K_i = internal hydraulic head (only for nozzles installed in vertical plane)
 ΔP = P₁ - P₂ = measured pressure drop between the nozzle pressure taps (Pa)
 ρ = fluid density (kg/m³)
h = nozzle pressure tap height difference (m)
g = gravity acceleration = 9.80665 (m/sec.²)

and where:

- α_c = calibrated or calculated nozzle flux coefficient (m²) = $\alpha * \frac{\pi d^2}{4} * (2)^{0.5}$
 α = flux coefficient
T = operating fluid temperature (°C)

- λ = linear thermal expansion coefficient = 1.2E-05 (1/°C)
 T_{cal} = calibration fluid temperature \cong 20°C
 d = nozzle throat diameter (m)
 β = d/D = nozzle diameter ratio
 P_1 = absolute pressure upstream the nozzle (Pa)
 ϵ = $1 - (0.41 + 0.35 * \beta^4) * \Delta P_c / (\sigma * P_1)$ for orifices (UNI-10023 specifications)

For Venturi tubes, the following applies (UNI-10023 specifications):

$$\epsilon = \left[\left(\frac{P_2}{P_1} \right)^{\frac{2}{\sigma}} * \frac{\sigma}{\sigma-1} * \frac{1 - \left(\frac{P_2}{P_1} \right)^{\frac{\sigma-1}{\sigma}}}{1 - \left(\frac{P_2}{P_1} \right)} * \frac{1 - \beta^4}{1 - \beta^4 * \left(\frac{P_2}{P_1} \right)^{\frac{2}{\sigma}}} \right]^{0.5}$$

where:

- σ = steam isentropic exponent = 1.265 for saturated steam at 4.9 MPa

The main characteristics of the nozzles are reported in Table C-2 of Appendix C.

- $\Delta\alpha_c$ = maximum error of the nozzle flux coefficient (\pm m²)
 $\sigma\alpha_c$ = standard deviation of the nozzle flux coefficient (\pm m²)
 $\Delta\epsilon$ = compressibility factor error (only if $\epsilon \neq 1$) defined as suggested by UNI-10023 specifications as:

$$\Delta\epsilon = \pm 0.04 * \epsilon * \frac{\Delta P_c}{P_1} \text{ for orifices with } 0.23 \leq \beta \leq 0.75$$

$$\Delta\epsilon = \pm 0.08 * \epsilon * \frac{\Delta P_c}{P_1} \text{ for orifices with } 0.75 \leq \beta \leq 0.80$$

$$\Delta\epsilon = \pm 0.04 * \epsilon * \frac{\Delta P_c}{P_1} \text{ for Venturi tubes}$$

where:

$$\sigma\varepsilon = \Delta\varepsilon$$

$$\Delta\rho = \text{fluid density maximum error } (\pm \text{ kg/m}^3)$$

$$\sigma\rho = \text{fluid density standard deviation } (\pm \text{ kg/m}^3)$$

$$\Delta(\Delta P_c) = \text{maximum error of the nozzle local pressure drop } (\pm \text{ Pa})$$

$$\sigma(\Delta P_c) = \text{standard deviation of the nozzle local pressure drop } (\pm \text{ Pa})$$

$$\Delta K_i = \text{maximum error of the internal hydraulic head for nozzles installed in vertical plane } (\pm \text{ Pa})$$

$$\Delta(\Delta P) = \pm (\Delta_i + \Delta K + \Delta_{BV}) = \text{maximum error of the measured pressure drop of the nozzle}$$

$$\sigma(\Delta P) = \pm (\Delta_i^2 + \Delta^2 K + \Delta_{BV}^2)^{0.5} = \text{standard deviation of the measured pressure drop of the nozzle}$$

E-7.1 Flow Rate Error Analysis

The flow rate maximum error (ΔF) and the standard deviation (σF) were calculated applying the following error propagation formulas:

$$\Delta F = \pm \sum_{i=1}^n \left| \frac{\delta F}{\delta X_i} * \Delta X_i \right| \quad \text{with } i=1\dots n$$

$$\sigma F = \pm \left[\sum_{i=1}^n \left(\frac{\delta F}{\delta X_i} \right)^2 * \sigma^2 X_i \right]^{0.5}$$

where:

$$\Delta_{X_i} = \text{maximum error of the quantities } X_i$$

$$\sigma_{X_i} = \text{standard deviation of the quantities } X_i$$

In the calculation where the standard deviation (σ_{X_i}) of the variable X_i is not known, the standard deviation is assumed equal to the maximum error (Δ_{X_i}). The error calculations have been performed assuming the following hypotheses:

- The fluid density standard deviation was assumed to be equal to the correspondent maximum error. Therefore, $\sigma\rho = \Delta\rho$.
- The error contribution due to the thermal expansion correction of the nozzle flux coefficient was neglected. Therefore, in the error propagation, formulas were assumed to be:
 $\alpha' = \alpha_c$, $\Delta\alpha' = \Delta\alpha_c$, and $\sigma\alpha' = \sigma\alpha_c$.

- c. The error contribution (ΔK_i) due to the internal hydraulic head for the nozzles installed in vertical plane was neglected. Therefore, in the error propagation, formulas were assumed to be: $\Delta P_c = \Delta P$, $\Delta(\Delta P_c) = \Delta(\Delta P)$ and $\sigma(\Delta P_c) = \sigma(\Delta P)$.
- d. The error calculation was carried out using, in a conservative way, the span upper value of the instrument. Therefore, in the error propagation, the formula was assumed to be: $\Delta P_c = \text{maximum value of the instrument span}$.
- e. The recoverable error due to the difference between the fluid density value computed by the DAS subroutine and the value given by the water-steam tables was neglected.

Applying the error propagation formulas to the flow rate expression with the hypothesis reported, the following was obtained.

$$\Delta F = [\pm \epsilon * \Delta P_c^{0.5} * \rho^{0.5} * \Delta \alpha_c + \alpha_c * \Delta P_c^{0.5} * \rho^{0.5} * \Delta \epsilon + \alpha_c * \epsilon * 0.5 * \Delta P^{-0.5} * \rho^{0.5} * \Delta(\Delta P_c) + \alpha_c * \epsilon * \Delta P_c^{0.5} * 0.5 * \rho^{-0.5} * \Delta \rho]$$

Setting:

$$A = \epsilon * \Delta P_c^{0.5} * \rho^{0.5}; \quad B = \alpha_c * \Delta P_c^{0.5} * \rho^{0.5}$$

$$C = \alpha_c * \epsilon * 0.5 * \Delta P_c^{-0.5} * \rho^{0.5}; \quad D = \alpha_c * \epsilon * \Delta P_c^{0.5} * 0.5 * \rho^{-0.5}$$

The following can be written:

$$\Delta F = \pm [A * \Delta \alpha_c + B * \Delta \epsilon + C * \Delta(\Delta P_c) + D * \Delta \rho]$$

and:

$$\sigma F = \pm [A^2 * \sigma^2 \alpha_c + B^2 * \sigma^2 \epsilon + C^2 * \sigma^2(\Delta P_c) + D^2 * \sigma^2 \rho]^{0.5}$$

where:

$$\Delta\rho = \pm \left[\left| \frac{\rho(T_1 + \Delta T_1) - \rho(T_1 - \Delta T_1)}{2 * \Delta T_1} * \Delta T_1 \right|_{P_1} + \left| \frac{\rho(P_1 + \Delta P_1) - \rho(P_1 - \Delta P_1)}{2 * \Delta P_1} * \Delta P_1 \right|_{T_1} \right]$$

and where:

- P_1 = reference absolute pressure (MPa) upstream the nozzle
- T_1 = reference temperature (°C) upstream the nozzle
- ΔT_1 = maximum error of the temperature upstream the nozzle
- ΔP_1 = maximum error of the absolute pressure upstream the nozzle
- $\sigma\rho$ = $\Delta\rho$ = standard deviation of the fluid density

NOTE: As consequence of the excessive value of the pressure drop across the venturi tubes used to measure the steam flow generated by the steam generators, the measurements F-A04S and F-B04S are not valid; therefore, the error calculation of these measures has not been performed.

E-7.3 Example of Flow Rate Error Calculations

The example of the error calculations concerns the cold leg-A1 flow rate (F-A01P).

Reference conditions, measurements, and primary errors used in the calculation of the errors of F-A01P at initial steady-state conditions:

$$\begin{aligned} T_1 = T\text{-A011P} &= 280^\circ\text{C} & \Delta P_C = F\text{-A01P} &= 60000 \text{ Pa} \\ P_1 = P\text{-A04P} &= 15.6 \text{ MPa} & \rho &= 764.79 \text{ kg/m}^3 \\ \Delta\varepsilon = \sigma\varepsilon &= 0 & \varepsilon &= 1 \end{aligned}$$

From Tables E-3, E-4 and C-2, the following were obtained:

$$\begin{aligned} \Delta T_1 &= \pm 1.48^\circ\text{C} (\pm 2.66^\circ\text{F}) & \sigma T_1 &= \pm 1.29^\circ\text{C} (\pm 2.32^\circ\text{F}) \\ \Delta (\Delta P_C) &= \pm 116 \text{ Pa} (\pm .016 \text{ psi}) & \sigma (\Delta P_C) &= \pm 88 \text{ Pa} (\pm .012 \text{ psi}) \\ \Delta P_1 &= \pm 0.043 \text{ MPa} (\pm 6.26 \text{ psi}) & \sigma P_1 &= \pm 0.033 \text{ MPa} (\pm 4.77 \text{ psi}) \\ \alpha_c &= 1.0236\text{E-}3 \text{ m}^2 & \Delta\alpha_c &= \sigma\alpha_c = 1.02\text{E-}5 \text{ m}^2 \end{aligned}$$

Therefore using water-steam tables and assuming $\Delta\rho = \Delta\rho$, the following were obtained:

$$\Delta\rho = \pm \left[\left| \frac{762.06 - 767.24}{2 * 1.48} * 1.47 \right|_{P_i} + \left| \frac{764.83 - 764.74}{2 * 0.043} * 0.043 \right|_{T_i} \right]$$

Making calculations, the following were obtained:

$$\Delta\rho = \pm 2.66 \text{ kg/m}^3 (\pm .166 \text{ lb/ft.}^3)$$

$$\sigma\rho = \Delta\rho = \pm 2.66 \text{ kg/m}^3 (\pm .166 \text{ lb/ft.}^3)$$

$$A = \epsilon * \Delta P_c^{0.5} * \rho^{0.5} = 1 * (60000)^{0.5} * (764.79)^{0.5} = 6774.02$$

$$B = \alpha_c * \Delta P_c^{0.5} * \rho^{0.5} = 1.0236E-3 * (60000)^{0.5} * (764.79)^{0.5} = 6.93$$

$$\begin{aligned} C &= \alpha_c * \epsilon * 0.5 * \Delta P_c^{-0.5} * \rho^{0.5} \\ &= 1.0236E-3 * 1 * 0.5 * (60000)^{-0.5} * (764.79)^{0.5} = 5.78E-5 \end{aligned}$$

$$\begin{aligned} D &= \alpha_c * \epsilon * \Delta P_c^{0.5} * 0.5 * \rho^{-0.5} \\ &= 1.0236E-3 * 1 * (60000)^{0.5} * 0.5 * (764.79)^{-0.5} = 4.53E-3 \end{aligned}$$

$$\begin{aligned} \Delta (F-A01P) &= \pm [6774.02 * 1.02E-5 + 6.93 * 0 + 5.78E-5 * 116 + 4.53E-3 * 2.66] \\ &= \pm 0.088 \text{ kg/sec. } (\pm 0.194 \text{ lb/sec.}) \end{aligned}$$

$$\begin{aligned} \sigma (F-A01P) &= [(6774.02)^2 * (1.02E-5)^2 + (5.78E-5)^2 * (88)^2 + (4.53E-3)^2 * (2.66)^2]^{0.5} \\ &= \pm 0.070 \text{ kg/sec } (\pm 0.154 \text{ lb/sec.}) \end{aligned}$$

NOTE: The error calculation of the steam flow generated by steam generators were not performed because as consequence of the excessive value of the pressure drop across the venturi tubes used to measure the steam flow, the measurements F-A04S and F-B04S are not valid.

The results of the flow rate error calculation are reported in Table E-6. The columns are defined as follows:

PLANT CODE	SPES-2 instrument identification code
T_1	Fluid reference temperature upstream the nozzle ($^{\circ}\text{F}$)
ΔT_1	Maximum error of the fluid reference temperature upstream the nozzle (\pm $^{\circ}\text{F}$)
P_1	Reference absolute pressure upstream the nozzle (psi)
ΔP_1	Maximum error of the reference absolute pressure upstream the nozzle (\pm psi)
ρ	Fluid density (lb/ft^3)
$\Delta \rho$ *	Maximum error of the fluid density (\pm lb/ft^3)
ϵ	Compressibility coefficient
$\Delta \epsilon$	Compressibility coefficient maximum error
ΔP_c	Reference nozzle local pressure drop (psi) assumed equal to the span upper value of the instrument
$\Delta (\Delta P_c)$	Maximum error of the nozzle local pressure drop (\pm psi)
$\sigma (\Delta P_c)$	Standard deviation of the nozzle local pressure drop (\pm psi)
α_c	Nozzle flux coefficient (ft^2)
$\Delta \alpha_c$	Maximum error of the nozzle flux coefficient (\pm ft^2)
$\sigma \alpha_c$	Standard deviation of the nozzle flux coefficient (\pm ft^2)

* The fluid density standard deviation ($\sigma \rho$) was assumed to be equal to the correspondent maximum error. Therefore, $\sigma \rho = \Delta \rho$.

Δ	Measurement maximum error (\pm lb/sec.)
σ	Measurement standard deviation (\pm lb/sec.)

E-8 Power Channel Electrical Power

$$W-00P = (I_1 + I_2 + I_3 + I_4 + I_5 + I_6) * V_{PC} * 10^{-3}$$

where:

$W-00P$	= power channel power (kW)
$I_1+I_2+I_3+I_4+I_5$	= direct current feeding the rod bundle generated by the 8 MW group and measured by means of five shunts (A)
I_6	= direct current feeding the rod bundle generated by the 4 MW group and measured by means of one shunt (A)
V_{PC}	= voltage drop across the rod bundle (V)

E-8.1 Power Channel Electrical Power Error Analysis

The power channel electrical power maximum error Δ (W-00P) and the standard deviation σ (W-00P) were calculated applying the error propagation formulas as:

$$\Delta(W-00P) \pm (I_1 + I_2 + I_3 + I_4 + I_5 + I_6) * \Delta V_{PC} + V_{PC} * (\Delta I_1 + \Delta I_2 + \Delta I_3 + \Delta I_4 + \Delta I_5 + \Delta I_6) * 10^{-3}$$

Setting:

$$A = I_1 + I_2 + I_3 + I_4 + I_5 + I_6$$

The following can be written:

$$\sigma(W-00P) = \pm [A^2 * \sigma^2 V_{PC} + V_{PC}^2 * (\sigma^2 I_1 + \sigma^2 I_2 + \sigma^2 I_3 + \sigma^2 I_4 + \sigma^2 I_5 + \sigma^2 I_6)]^{0.5} * 10^{-3}$$

The voltage drop across the rod bundle is acquired by DAS through a voltage divider, so that:

$$V_{PC} = J * V_{DAS}$$

where:

$$J = \frac{R_1 + R_2}{R_1} = \text{voltage divider ratio} = 32$$
$$R_1 = 3125 \Omega = \text{voltage divider resistance}$$
$$R_2 = 96875 \Omega = \text{voltage divider resistance}$$
$$V_{DAS} = \text{voltage signal acquired by DAS}$$

The maximum error ΔV_{PC} was defined as follows:

$$\Delta V_{PC} = \pm (V_{DAS} * \Delta J + J * \Delta V_{DAS})$$

where:

$$\Delta V_{DAS} = \Delta_{BV} = \text{maximum error of the power channel voltage signal acquired by DAS}$$

$$\Delta J = \pm \left(\frac{R_2}{R_1^2} * \Delta R_1 + \frac{1}{R_1} * \Delta R_2 \right) = \pm 0.186$$

$$\sigma J = \Delta J; \sigma V_{DAS} = \Delta V_{DAS} = \Delta_{BV}$$

where:

$$\Delta R_1 = \pm 9.38 \Omega = \text{accuracy of the resistance } R_1$$

$$\Delta R_2 = \pm 290.6 \Omega = \text{accuracy of the resistance } R_2$$

The standard deviation σV_{PC} was calculated as follows:

$$\sigma V_{PC} = \pm (V_{DAS}^2 * \sigma^2 J + J^2 * \sigma^2 V_{DAS})^{0.5}$$

The generic maximum error (ΔI_i) of one of the six currents feeding the rod bundle is defined as follows:

$$\Delta I_i = \pm (\Delta_i + \Delta_{BV})$$

where:

- Δ_i = $\pm (\Delta_c + \Delta_{PS} + \Delta_{LCH})$ = SIET assigned instrument error
- Δ_c = maximum value between the manufacturer error and the maximum error of the performed calibration
- Δ_{PS} = maximum error of the reference primary standard (reference shunt) used for the calibration
- Δ_{LCH} = maximum error of the voltmeter (DAS) used to acquire the instrument output signal during the calibration

The generic standard deviation (σI_i) of one of the six currents feeding the rod bundle is defined as follows:

$$\sigma I_i = \pm (\Delta_i^2 + \Delta_{BV}^2)^{0.5}$$

E-8.2 Example of Power Channel Electrical Power Error Calculations

The example concerns the error calculations of the power channel power W-00P at initial steady-state conditions and at reduced power of 1000 kW during decay transient.

- Reference conditions, measurement and primary errors used in the calculations of the W-00P errors at initial steady-state conditions:

W-00P = 4991.6 kW	$V_{PC} = V-01P = 99.916$ V	$V_{DAS} = 3.122$ V
$I_1 = I-01P = 7112$ A	$I_2 = I-02P = 7112$ A	
$I_3 = I-03P = 7112$ A	$I_4 = I-04P = 7112$ A	
$I_5 = I-05P = 7112$ A	$I_6 = I-06P = 14400$ A	
$J = 32$	$\Delta J = \sigma J = \pm 0.186$	

From Table E-7, the following were obtained:

$\Delta I_1 = \Delta (I-01P) = \pm 40.76$ A	$\sigma I_1 = \sigma (I-01P) = \pm 35.37$ A
$\Delta I_2 = \Delta (I-02P) = \pm 40.76$ A	$\sigma I_2 = \sigma (I-02P) = \pm 35.37$ A
$\Delta I_3 = \Delta (I-03P) = \pm 40.82$ A	$\sigma I_3 = \sigma (I-03P) = \pm 35.41$ A
$\Delta I_4 = \Delta (I-04P) = \pm 40.82$ A	$\sigma I_4 = \sigma (I-04P) = \pm 35.41$ A

$$\begin{aligned} \Delta I_5 = \Delta (I-05P) &= \pm 40.72 \text{ A} & \sigma I_5 = \sigma (I-05P) &= \pm 35.35 \text{ A} \\ \Delta I_6 = \Delta (I-06P) &= \pm 127.22 \text{ A} & \sigma I_6 = \sigma (I-06P) &= \pm 133.34 \text{ A} \\ \Delta V_{DAS} = \Delta_{BV} &= \pm 2.44E-3 \text{ V} & \sigma V_{DAS} = \Delta_{BV} &= \pm 2.44E-3 \text{ V} \end{aligned}$$

Therefore,

$$\Delta V_{PC} = \Delta (V-01P) = \pm (3.122 * 0.186 + 32 * 2.44 E-3) = \pm 0.659 \text{ V}$$

$$\sigma V_{PC} = \sigma (V-01P) = \pm [(3.122)^2 * (0.186)^2 + (32)^2 * (2.44 E-3)^2]^{0.5} = \pm 0.586 \text{ V}$$

and:

$$\Delta (W-00P) = \pm [(7112 * 5 + 14400) * 0.659 + 99.916 * (40.76 + 40.76 + 40.82 + 40.82 + 40.72 + 127.22)] * 10^{-3} = \pm 66.01 \text{ kW}$$

$$\sigma (W-00P) = \pm \{ (7112 * 5 + 14400)^2 * (0.586)^2 + (99.916)^2 * [(35.37)^2 + (35.37)^2 + (35.41)^2 + (35.41)^2 + (35.35)^2 + (113.34)^2] \}^{0.5} * 10^{-3} = \pm 32.37 \text{ kW}$$

- Reference conditions, measurement, and primary errors used in the calculations of the W-00P errors during decay power transient at 1000 kW (only 4 MW group in operation):

$$\begin{aligned} W-00P &= 1000 \text{ kW} & V_{PC} = V-01P &= 44.721 \text{ V} & V_{DAS} &= 1.398 \text{ V} \\ I_1 = I_2 = I_3 = I_4 = I_5 &= 0 & I_6 = I - 06P &= 22360.5 \text{ A} \\ J &= 32 & \Delta J = \sigma J &= \pm 0.186 \end{aligned}$$

From Table E-7, the following were obtained:

$$\Delta I_6 = \Delta (I - 06P) = \pm 127.22 \text{ A}$$

$$\sigma I_6 = \sigma (I - 06P) = \pm 113.34 \text{ A}$$

Therefore,

$$\Delta V_{PC} = \Delta (V-01P) = \pm (1.398 * 0.186 + 32 * 2.44 E-3) = \pm 0.338 \text{ V}$$

$$\sigma V_{PC} = \sigma (V-01P) = \pm [(1.398)^2 * (0.186)^2 + (32)^2 * (2.44 E-3)^2]^{0.5} = \pm 0.271 \text{ V}$$

and:

$$\Delta (W-00P) = \pm (22360.5 * 0.338 + 44.721 * 127.22) * 10^{-3} = \pm 13.25 \text{ kW}$$

$$\sigma (W-00P) = \pm [(22360.5)^2 * (0.271)^2 + (44.721)^2 * (113.34)^2]^{0.5} * 10^{-3} = \pm 7.9 \text{ kW}$$

The results of the power channel electrical measurement error calculations are reported in Table E-7. The columns are defined as follows:

PLANT CODE	SPES-2 instrument identification code
$V_{PC} = V-01P$	Reference voltage drop value across the power channel (V)
V_{DAS}	Reference power channel voltage signal acquired by DAS (V)
$\Delta V_{DAS} = \Delta_{BV}$	Maximum error of the power channel voltage signal acquired by DAS (\pm V)
$\sigma V_{DAS} = \Delta_{BV}$	Standard deviation of the power channel voltage signal acquired by DAS (\pm V)
ΔR_1	Accuracy of the resistance R1 of the voltage divider used to acquire the power channel voltage (\pm Ω)
ΔR_2	Accuracy of the resistance R2 of the voltage divider used to acquire the power channel voltage (\pm Ω)
J	Voltage divider ratio

ΔJ	Maximum error of the voltage divider ratio
M.U.	Engineering unit of the measurement
Δ_C	Maximum value between the manufacturer error and the maximum error of the performed calibrations (\pm M.U.)
Δ_{ps}	Maximum error of the reference primary standard (reference shunt) used for the calibration (\pm M.U.)
Δ_{LCH}	Maximum error of the voltmeter used to acquire the instrument output signal during the calibration (\pm M.U.)
$\Delta_I = \pm (\Delta_C + \Delta_{ps} + \Delta_{LCH})$	SIET assigned instrument error (\pm M.U.)
Δ_{BV}	Acquisition card A/D converter bit value (acquisition card error) (\pm M.U.)
Δ	Measurement maximum error (\pm M.U.)
σ	Measurement standard deviation (\pm M.U.)

The power channel power errors have been calculated for three power values, at 4991.6 kW (nominal power), 1000 kW, and 200 kW. The results of the power channel power error calculations are reported in Table E-8. The columns are defined as follows:

PLANT CODE	SPES-2 instrument identification code
W = W-00P	Reference power channel power value (kW)
I₁ = I-01P**	Reference current measured by the shunt I-01P (A)
I₂ = I-02P**	Reference current measured by the shunt I-02P (A)
I₃ = I-03P**	Reference current measured by the shunt I-03P (A)

* The standard deviation of the voltage divider ratio (σJ) was assumed to be equal to the correspondent maximum error. Therefore, $\sigma J = \Delta J$.

** These currents are generated by the 8 MW power group. The maximum error and the standard deviation values are reported in Table E-7.

$I_4 = I-04P^*$	Reference current measured by the shunt I-04P (A)
$I_5 = I-05P^*$	Reference current measured by the shunt I-05P (A)
$I_6 = I-06P^{**}$	Reference current measured by the shunt I-06P (A)
V_{DAS}	Reference power channel voltage signal acquired by DAS (V)
ΔV_{DAS}	Maximum error of the power channel voltage signal acquired by DAS ($\pm V$)
$V_{PC} = V-01P$	Reference voltage drop across the power channel (V)
ΔV_{PC}	Maximum error of the reference voltage drop across the power channel ($\pm V$)
σV_{PC}	Standard deviation of the reference voltage drop across the power channel ($\pm V$)
Δ	Measurement maximum error ($\pm kW$)
σ	Measurement standard deviation ($\pm kW$)

E-9 Levels

The pressurizer, steam generator, and CMT collapsed levels were computed in meters using the following formula:

$$(I) \quad L = \frac{\Delta P - g * \rho_v * h}{g * (\rho_L - \rho_v)}$$

where:

- ρ_v = steam density in saturation condition (kg/m^3)
- ρ_L = liquid density (kg/m^3) computed at:
 - saturation conditions for steam generators and for pressurizer
 - average temperature for CMT
- Δp = measured pressure drop between the taps (Pa)
- h = total pressure tap height difference (m)

* These currents are generated by the 8 MW power group. The maximum error and the standard deviation values are reported in Table E-7.

** This current is generated by the 4 MW power group. The maximum error and the standard deviation values are reported in Table E-7.

NOTE: For IRWST level, $\rho_v = 0$ and $\rho_L =$ IRWST water density.

The accumulator levels were calculated in meters using the following formula:

$$(II) \quad L = \frac{\Delta P_{inst} - g * h_l * (\rho_{LC} - \rho_A)}{g * (\rho_L - \rho_A)}$$

where:

- ρ_A = $P/(R*T)$ = air density (kg/m^3)
 ρ_L = liquid density at operating conditions (kg/m^3)
 h_l = height difference between the accumulator lower tap and the instrument positive side (m)
 ΔP_{inst} = pressure drop (Pa) measured by instrument; the measurement has been performed with the negative hydraulic line full of air at the same pressure of the accumulator and the positive hydraulic line full of water
 ρ_{LC} = density of cold water filling the hydraulic line assumed = 1000 (kg/m^3)

and where:

- R = gas constant of air = 287.037 (J/kg-K)
 T = air temperature (K)
 P = air pressure (Pa)

E-9.1 Level Error Analysis

The level maximum error (ΔL) and the standard deviation (σL) were calculated applying the following error propagation formulas:

$$\Delta L = \pm \sum_{i=1}^n \left| \frac{\delta L}{\delta X_i} * \Delta X_i \right|$$

with $i = 1, \dots, n$

$$\sigma L = \pm \left[\sum_{i=1}^n \left(\frac{\delta L}{\delta X_i} \right)^2 * \sigma^2 X_i \right]^{0.5}$$

where:

- ΔX_i = maximum error of the quantities X_i
 σX_i = standard deviation of the quantities X_i

In the calculations where the standard deviation σX_i was not known, the standard deviation was assumed equal to the maximum error ΔX_i . The error calculations were performed assuming the following hypotheses:

- a. The standard deviation of the pressure tap height difference was assumed to be equal to the correspondent maximum error. Therefore, $\sigma h = \Delta h$.
- b. The error contribution due to the gravity acceleration was neglected, and the gravity acceleration value was assumed to be: $g = 9.80665 \text{ m/sec}^2$.
- c. The error calculation as carried out using, in a conservative way, the span upper value of the instrument; the measured pressure drop between the taps was assumed equal to the pressure drop measured by the instrument. Therefore, in the error propagation, the formula was assumed to be: $\Delta P = \Delta P_{\text{inst}} = \text{maximum value of the instrument span}$.
- d. The error contribution due to the gas constant of air was neglected, and the gas constant of air was assumed to be: $R = 287.037 \text{ (J/kg-K)}$.
- e. The recoverable error due to the difference between the fluid density values computed by DAS subroutines, and the values given by water-steam tables were neglected.
- f. The fluid density standard deviations were assumed equal to the correspondent maximum error. Therefore, $\sigma \rho = \Delta \rho$.

Applying the error propagation formulas to the level expression (I) used to calculate the level of the pressurizer, steam generators, and CMT collapsed level with the hypotheses reported, the following was obtained:

$$\Delta L = \pm \left[\left| \frac{\delta L}{\delta \Delta P} * \Delta (\Delta P) \right| + \left| \frac{\delta L}{\delta P_v} * \Delta P_v \right| + \left| \frac{\delta L}{\delta h} * \Delta h \right| + \left| \frac{\delta L}{\delta P_L} * \Delta P_L \right| \right]$$

Making calculations, the following were obtained:

$$\left| \frac{\delta L}{\delta \Delta P} * \Delta(\Delta P) \right| = \left| \frac{1}{g * (\rho_L - \rho_v)} \right| * \Delta(\Delta P) = A * \Delta(\Delta P)$$

$$\left| \frac{\delta L}{\delta P_v} * \Delta \rho_v \right| = \left| \frac{\Delta P - g * h * \rho_L}{g * (\rho_L - \rho_v)^2} \right| * \Delta P_v = B * \Delta \rho_v$$

$$\left| \frac{\delta L}{\delta h} * \Delta h \right| = \left| - \frac{\rho_v}{(\rho_L - \rho_v)} \right| * \Delta h = C * \Delta h$$

$$\left| \frac{\delta L}{\delta P_L} * \Delta \rho_L \right| = \left| \frac{g * h * \rho_v - \Delta P}{g * (\rho_L - \rho_v)^2} \right| * \Delta \rho_L = D * \Delta \rho_L$$

Therefore,

$$\Delta L = \pm [A * \Delta(\Delta P) + B * \Delta \rho_v + C * \Delta h + D * \Delta \rho_L]$$

$$\sigma L = \pm [A^2 * \sigma^2(\Delta P) + B^2 * \sigma^2 \rho_v + C^2 * \sigma^2 h + D^2 * \sigma^2 \rho_L]^{0.5}$$

The fluid density errors were calculated as:

$$\Delta \rho_v = \pm \left| \frac{\rho_v (P + \Delta(P)) - \rho_v (P - \Delta(P))}{2 * \Delta(P)} * \Delta(P) \right|$$

P = reference absolute pressure (saturation conditions)

$\Delta(P)$ = maximum error of the absolute pressure

$\Delta\rho_v$ = saturated steam density maximum error
 $\sigma\rho_v$ = $\Delta\rho_v$ = saturated steam density standard deviation

For pressurizer and steam generators (saturation conditions):

$$\Delta\rho_L = \pm \left| \frac{\rho_L (P + \Delta(P)) - \rho_L - (P - \Delta(P))}{2 * \Delta(P)} * \Delta(P) \right|$$

For CMT (subcooled conditions):

$$\Delta\rho_L = \pm \left[\left| \frac{\rho_L (P + \Delta(P)) - \rho_L - (P - \Delta(P))}{2 * \Delta(P)} * \Delta(P) \right|_T + \left| \frac{\rho_L (T + \Delta T) - \rho_L (T - \Delta T)}{2 * \Delta T} * \Delta T \right|_P \right]$$

$\Delta\rho_L$ = liquid density maximum error calculated in saturation conditions for pressurizer and steam generators and in subcooled conditions for CMT
 $\sigma\rho_L$ = $\Delta\rho_L$ = liquid density standard deviation
 T = average temperature of the CMT liquid temperature calculated using three temperatures—namely: T-A415E, T-417E, T-A420E and T-415E, T-B417E, T-B420E.
 $\Delta T = \pm \frac{\Delta T_1 + \Delta T_2 + \Delta T_3}{3}$ = maximum error of the average CMT liquid temperature
 $\Delta T_1, \Delta T_2, \Delta T_3$ = maximum errors of the three temperatures used to calculate the CMT liquid average temperature
 ΔP = reference pressure drop between the pressure taps assumed equal to the span upper value of the instrument
 $\Delta(\Delta P)$ = maximum error of the pressure drop between the pressure taps
 $\sigma(\Delta P)$ = standard deviation of the pressure drop between the pressure taps
 Δh = maximum error of the pressure tap height difference
 σh = Δh = standard deviation of the pressure tap height difference
 $\Delta\rho_L$ = CMT subcooled liquid density maximum error

Applying the error propagation formulas to the level expression (II) used to calculate the level of the accumulators with the hypotheses reported, the following was obtained:

$$\Delta L = \pm \left[\left| \frac{\delta L}{\delta \Delta P_{inst}} * \Delta(\Delta P_{inst}) \right| + \left| \frac{\delta L}{\delta P_{LC}} * \Delta P_{LC} \right| + \left| \frac{\delta L}{\delta h_1} * \Delta h_1 \right| + \left| \frac{\delta L}{\delta P_L} * \Delta P_L \right| + \left| \frac{\delta L}{\delta P_A} * \Delta P_A \right| \right]$$

Making the calculations, the following were obtained:

$$\left| \frac{\delta L}{\delta \Delta P_{inst}} * \Delta(\Delta P_{inst}) \right| = \left| \frac{1}{g * (\rho_L - \rho_A)} \right| * \Delta(\Delta P_{inst}) = A * \Delta(\Delta P_{inst})$$

$$\left| \frac{\delta L}{\delta h_1} * \Delta h_1 \right| = \left| - \frac{(\rho_{LC} - \rho_A)}{(\rho_L - \rho_A)} \right| * \Delta h_1 = B * \Delta h_1$$

$$\left| \frac{\delta L}{\delta \rho_{LC}} * \Delta \rho_{LC} \right| = \left| - \frac{h_1}{(\rho_L - \rho_A)} \right| * \Delta \rho_{LC} = C * \Delta \rho_{LC}$$

$$\left| \frac{\delta L}{\delta P_L} * \Delta P_L \right| = \left| \frac{g * h_1 * (\rho_{LC} - \rho_A) - \Delta P_{inst}}{g * (\rho_L - \rho_A)^2} \right| * \Delta P_L = D * \Delta P_L$$

$$\left| \frac{\delta L}{\delta \rho_A} * \Delta \rho_A \right| = \left| \frac{\Delta P_{inst} + g * h_1 * (\rho_L - \rho_{LC})}{g * (\rho_L - \rho_A)^2} \right| * \Delta \rho_A = E * \Delta \rho_A$$

Therefore,

$$\Delta L = \pm [A * \Delta(\Delta P_{inst}) + B * \Delta h_1 + C * \Delta \rho_{LC} + D * \Delta P_L + E * \Delta \rho_A]$$

$$\sigma L = \pm [A^2 * \sigma^2 (\Delta P_{inst}) + B^2 * \sigma^2 h_1 + C^2 * \sigma^2 \rho_{LC} + D^2 * \sigma^2 \rho_L + E^2 * \sigma^2 \rho_A]^{0.5}$$

where:

ΔP_{inst} = pressure drop measured by instrument assumed equal to the span upper value of the instrument

$\Delta(\Delta P_{inst})$ = $\pm (\Delta_1 + \Delta_{BV})$ = maximum error of the pressure drop measured by the instrument

$\sigma(\Delta P_{inst})$ = $\pm (\Delta_1^2 + \Delta_{BV}^2)^{0.5}$ = standard deviation of the pressure drop measured by the instrument

The meaning of the quantities Δ_1 and Δ_{BV} are defined in Section E-3.

Δh_1 = maximum error of the height difference between the accumulator lower tap and the instrument positive side

σh_1 = Δh_1 = standard deviation of the height difference between the accumulator lower tap and the instrument positive side

$\Delta \rho_{LC}$ = $\pm 4 \text{ kg/cm}^2$ = maximum error of the density of cold water filling the instrument hydraulic connections (see Section E-3)

$\sigma \rho_{LC}$ = $\Delta \rho_{LC}$ = standard deviation of the density of cold water filling the instrument hydraulic connections

$\Delta \rho_L$ = maximum error of the accumulator liquid density

$\sigma \rho_L$ = $\Delta \rho_L$ = standard deviation of the accumulator liquid density

$$\Delta \rho_L = \pm \left[\left| \frac{\rho_L (P + \Delta(P)) - \rho_L (P - \Delta(P))}{2 * \Delta(P)} * \Delta(P) \right|_T + \left| \frac{\rho_L (T + \Delta T) - \rho_L (T - \Delta T)}{2 * \Delta T} * \Delta T \right|_P \right]$$

P = reference accumulator absolute pressure = 4.9E6 (Pa)

T = reference accumulator liquid temperature = 20 (°C)

$\Delta(P)$ = maximum error of the accumulator absolute pressure

ΔT = maximum error of the accumulator liquid temperature

$\Delta \rho_A$ = maximum error of the accumulator air density

$\sigma \rho_A$ = $\Delta \rho_A$ = standard deviation of the accumulator air density

$$\Delta\rho_A = \pm \left[\frac{1}{R * T_A} * \Delta(P) + \frac{P}{R * T_A^2} * \Delta T_A \right]$$

where:

- T_A = 293.15 (K) = reference air temperature
 ΔT_A = maximum error of the accumulator air temperature \pm (K)
 P = reference accumulator absolute pressure (Pa)
 $\Delta(P)$ = maximum error of the accumulator absolute pressure (Pa)
 R = air gas constant = 287.037 (J/kg-K)

E-9.2 Example of Level Error Calculations

The example concerns the error calculations of the pressurizer level (L-010P).

Reference conditions, measurement, and primary errors used in the calculations of the errors of L-010P (see Table E-3)

$P = P-0.27P = 15.51 \text{ E6 (Pa)}$	$h = 6.206 \text{ (m)}$	$g = 9.80665 \text{ m/sec.}^2$
$\rho_L = 593.1 \text{ (kg/m}^3\text{)}$	$\rho_V = 102.06 \text{ (kg/m}^3\text{)}$	
$\Delta(P) = \Delta(P-0.27P) = \pm 43000 \text{ (Pa)}$		
$\Delta h = \pm 0.009 \text{ (m)}$	$\sigma h = \Delta h = \pm 0.009 \text{ (m)}$	
$\Delta P = L-010P = 66.3 \text{ E3 (Pa)}$		
$\Delta(\Delta P) = \Delta(L-010P) = \pm 545 \text{ (Pa)}$	$\sigma(\Delta P) = \sigma(L-010P) = \pm 376 \text{ (Pa)}$	

Therefore, using water-steam tables:

$$\Delta\rho_V = \pm \left| \frac{102.51 - 101.6}{2 * 43000} * 43000 \right| = \pm 0.46 \text{ kg/m}^3$$

$$\sigma\rho_V = \Delta\rho_V = \pm 0.46 \text{ kg/m}^3$$

$$\Delta\rho_L = \pm \left| \frac{593.06 - 594.64}{2 * 43000} * 43000 \right| = \pm 0.79 \text{ kg/m}^3$$

$$\sigma_{\rho_L} = \Delta\rho_L = \pm 0.79 \text{ kg/m}^3$$

$$A = \left| \frac{1}{g * (\rho_L - \rho_v)} \right| = \left| \frac{1}{9.80665 * (593.1 - 102.06)} \right| = 2.078E - 4$$

$$B = \left| \frac{\Delta P - g * h * \rho_L}{g * (\rho_L - \rho_v)^2} \right| = \left| \frac{66.3E3 - 9.80665 * 6.206 * 593.1}{9.80665 * (593.1 - 102.06)^2} \right| = 0.0128$$

$$C = \left| - \frac{\rho_v}{\rho_L - \rho_v} \right| = \left| - \frac{102.06}{(593.1 - 102.06)} \right| = 0.2078$$

$$D = \left| \frac{g * \rho_v * h - \Delta P}{g * (\rho_L - \rho_v)^2} \right| = \left| \frac{9.80665 * 102.06 * 6.206 - 66.3E3}{9.80665 * (593.1 - 102.06)^2} \right| = 0.0254$$

Therefore,

$$\Delta (L-010P) = \pm (2.078E-4 * 545 + 0.0128 * 0.46 + 0.2078 * 0.009 + 0.0254 * 0.79) = \pm 0.14 \text{ m } (\pm 0.46 \text{ ft.})$$

$$\sigma (L-010P) = \pm [(2.078E-4)^2 * (376)^2 + (0.0128)^2 * (0.46)^2 + (0.2078)^2 * (0.009)^2 + (0.0254)^2 * (0.79)^2]^{0.5} = \pm 0.08 \text{ m } (\pm 0.26 \text{ ft.})$$

The results of the pressurizer, steam generators, CMT, IRWST, level measurement error calculations are reported in Table E-9. The columns are defined as follows:

PLANT CODE	SPES-2 instrument identification code
P	Reference absolute pressure (psi)
$\Delta(P)$	Absolute pressure maximum error (\pm psi)

T	Reference CMT and IRWST liquid temperature (°F)
ΔT^*	Maximum error of the CMT and IRWST liquid temperature (\pm °F)
ρ_v	Saturated steam density (lb/ft. ³)
$\Delta \rho_v^{**}$	Saturated steam density maximum error (\pm lb/ft. ³)
ρ_L	Liquid density in saturation conditions for pressurizer and steam generators in subcooled conditions for CMT (lb/ft. ³)
$\Delta \rho_L^{**}$	Liquid density maximum error calculated in saturation condition for pressurizer and steam generators and in subcooled conditions for CMT (\pm lb/ft. ³)
ΔP^{***}	Reference pressure drop between the taps (psi)
$\Delta(\Delta P)$	Maximum error of the pressure drop between the taps (\pm psi)
$\sigma(\Delta P)$	Standard deviation of the pressure drop between the taps (\pm psi)
h	Pressure tap height difference (ft.)
Δh^{**}	Maximum error of the pressure tap height difference (\pm ft.)
Δ	Measurement maximum error (\pm ft.)
σ	Measurement standard deviation (\pm ft.)

* For CMT level error calculations $\Delta T = \pm \frac{\Delta T_1 + \Delta T_2 + \Delta T_3}{3}$

where:

ΔT_1 ; ΔT_2 ; ΔT_3 = maximum errors of the three temperatures (T-A415E, T-417E, T-420E or T-B415E, T-B417E, T-B420E) used to calculate the CMT liquid average temperature.

** The fluid density standard deviations (σP_L , σP_v) and the pressure tap height difference standard deviation (σh) were assumed to be equal to the correspondent maximum errors. Therefore, $\sigma P_L = \Delta P_L$; $\sigma P_v = \Delta P_v$; and $\sigma h = \Delta h$.

*** The calculations have been performed using the span upper value of the instrument.

The error calculations of the accumulator's level has been performed assuming the following reference conditions:

- P = reference accumulator absolute pressure = 4.9 E6 (Pa)
- T = reference accumulator liquid temperature = 20 (°C)
- T_A = reference accumulator air temperature = 293.15 (K)
- ρ_{LC} = density of the cold-water filling the instrument hydraulic line = 1000 kg/m³
- R = air gas constant = 287.037 (J/kg-K)

The results of the accumulator's level measurement error calculations are reported in the Table E-10. The columns are defined as follows:

PLANT CODE	SPES-2 instrument identification code
Δ(P)	Maximum error of the accumulator's absolute pressure (± psi)
ΔT	Maximum error of the accumulator's liquid temperature (± °F)
ΔT _(A)	Maximum error of the accumulator's air temperature (± °F)
ρ _L	Accumulator's liquid density (lb/ft. ³)
Δρ _L *	Maximum error of the accumulator's liquid density (± lb/ft. ³)
ρ _A	Accumulator's air density (lb/ft. ³)
Δρ _A *	Maximum error of the accumulator's air density (± lb/ft. ³)
Δρ _{LC} *	Density maximum error of the cold water filling the hydraulic line connecting the accumulator tap and the instrument positive side (± lb/ft. ³)
ΔP _{inst} **	Reference pressure drop measured by instrument (psi)
Δ(ΔP _{inst})	Maximum error of the pressure drop measured by instrument (± psi)

* The fluid density standard deviations (σ_{P_L}, σ_{P_A}, σ_{P_{LC}}) and the standard deviation of the height difference between the accumulator lower tap and the instrument positive side (σ_{h₁}) were assumed to be equal to the correspondent maximum errors. Therefore, σ_{P_L} = ΔP_L; σ_{P_A} = ΔP_A; σ_{P_{LC}} = ΔP_{LC}; and σ_{h₁} = Δh₁.

** The calculations have been performed using the span upper value of the instrument.

$\sigma(\Delta P_{inst})$	Standard deviation of the pressure drop measured by instrument (\pm psi)
h_1	Height different between the accumulator lower tap and the instrument positive side (ft.)
Δh_1^*	Maximum error of the height difference between the accumulator lower tap and the instrument positive side (\pm ft.)
Δ	Measurement maximum error (\pm ft.)
σ	Measurement standard deviation (\pm ft.)

E-10 Thermocouple Amplifier Shift

During the SPES-2 experiment a check of some thermocouple amplifier channels was performed in order to verify the amplifier shifts. The check was performed connecting the amplifier input channel to a reference standard K-type thermocouple and measuring the DAS amplifier output signal (SIET 00344P094 specification).

The results of the performed checks are reported in Table E-11. The columns are defined as follows:

PLANT CODE	SPES-2 instrument identification code
$T_{ref.}$	Reference temperature signal ($^{\circ}$ F) measured using a calibration voltmeter
$T_{meas.}$	Temperature measurement acquired by DAS ($^{\circ}$ F)
$SHIFT = T_{ref.} - T_{meas.}$	Channel amplifier shift ($^{\circ}$ F)
DATE	Date at which the check has been performed

* The fluid density standard deviations (σ_{P_L} , σ_{P_A} , $\sigma_{P_{LC}}$) and the standard deviation of the height difference between the accumulator lower tap and the instrument positive side (σ_{h_1}) were assumed to be equal to the correspondent maximum errors. Therefore, $\sigma_{P_L} = \Delta P_L$; $\sigma_{P_A} = \Delta P_A$; $\sigma_{P_{LC}} = \Delta P_{LC}$; and $\sigma_{h_1} = \Delta h_1$.

TABLE E-1
SUBCOOLED WATER DENSITY

P (MPa)	T (°C)	ρ_{LDAS} (kg/m³)	ρ_{LTAB} (kg/m³)	$\Delta\rho_L$ (kg/m³)
15.5	280	751.58	764.64	-13.06
12.5	280	751.58	760.23	-8.65
10.0	280	751.58	756.37	-4.79
10.0	260	783.16	790.64	-7.48
7.0	260	783.16	786.91	-3.75
5.0	260	783.16	784.31	-1.15
5.0	220	839.79	842.74	-2.95
4.0	220	839.79	841.89	-2.1
2.5	220	839.79	840.55	-0.76
2.5	170	897.07	898.39	-1.32
2.0	170	897.07	898.07	-1.0
1.0	170	897.07	897.42	-0.35
1.0	130	933.93	934.93	-1.0
0.5	130	933.93	934.67	-0.74
0.3	130	933.93	934.58	-0.65
0.1	80	971.96	971.63	+0.33

TABLE E-2
WATER AND STEAM DENSITIES AT SATURATION CONDITIONS

P (MPa)	ρ_{LDAS} (kg/m ³)	ρ_{LTAB} (kg/m ³)	$\Delta\rho_L$ (kg/m ³)	ρ_{VDAS} (kg/m ³)	ρ_{VTAB} (kg/m ³)	$\Delta\rho_v$ (kg/m ³)
15.6	592.53	592.21	+0.32	103.1	103.0	+0.1
12.4	648.84	648.26	+0.58	73.18	73.19	-0.01
11.6	662.56	661.68	+0.88	66.91	66.93	-0.02
10.0	689.45	688.42	+1.03	55.42	55.43	-0.01
7.5	730.23	731.15	-0.92	39.57	39.48	+0.09
4.9	780.35	779.73	+0.62	24.86	25.83	+0.03
2.5	832.2	835.28	-3.03	12.49	12.51	-0.02
1.0	887.3	887.0	+0.3	5.14	5.15	-0.01
0.5	916.82	915.08	+1.74	2.68	2.67	+0.01

**TABLE E-3
DIFFERENTIAL AND ABSOLUTE PRESSURE MEASUREMENT ERRORS**

Plant Code	h ±(ft.)	Δh ±(ft.)	ΔK ±(psi)	ΔC ±(psi)	ΔPS ±(psi)	ΔLCH ±(psi)	ΔBV ±(psi)	ΔI ±(psi)	Δ ±(psi)	σ ±(psi)
DP-000E	-	0	0	0.0247	0.0015	0.0001	0.0037	0.0262	0.0299	0.0265
DP-000P	14.57	0.023	0.0352	0.0348	0.0026	0.0003	0.0106	0.0377	0.0836	0.0527
DP-001P	8.38	0.0164	0.0217	0.1088	0.0044	0.0004	0.0089	0.1136	0.1441	0.116
DP-002P	8.89	0.0164	0.0225	0.0145	0.0044	0.0004	0.0089	0.0193	0.0507	0.031
DP-003P	0.79	0.0066	0.9042	0.0213	0.003	0.0002	0.0062	0.0246	0.035	0.0257
DP-004P	3.06	0.0098	0.0096	0.0152	0.0013	0.0001	0.0053	0.0166	0.0315	0.0199
DP-005P	2.43	0.0098	0.0085	0.0077	0.0009	0.0001	0.0035	0.0086	0.0207	0.0126
DP-011P	4.86	0.0098	0.0127	0.0181	0.0015	0.0001	0.0044	0.0198	0.0369	0.0239
DP-012P	3.64	0.0098	0.0106	0.0127	0.0015	0.0001	0.0044	0.0144	0.0294	0.0184
DP-013P	3.64	0.0098	0.0106	0.0127	0.0015	0.0001	0.0044	0.0144	0.0294	0.0184
DP-014P	2.84	0.0098	0.0092	0.0073	0.0004	0	0.0018	0.0077	0.0187	0.0121
DP-017P	6.2	0.0098	0.015	0.0073	0.0022	0.0002	0.0044	0.0097	0.0291	0.0184
DP-018P	2.95	0.0098	0.0094	0.0104	0.0004	0	0.0018	0.0109	0.022	0.0145
DP-019P	2.43	0.0098	0.0085	0.0181	0.0011	0.0001	0.0044	0.0193	0.0322	0.0215
DP-020P	11.24	0.0164	0.0266	0.0616	0.0022	0.0002	0.0089	0.064	0.0994	0.0699
DP-021P	4.74	0.0098	0.0125	0.0102	0.0009	0.0001	0.0035	0.0111	0.0271	0.0171
DP-022P	4.74	0.0098	0.0125	0.0102	0.0009	0.0001	0.0035	0.0111	0.0271	0.0171
DP-023P	4.74	0.0098	0.0125	0.0058	0.0009	0.0001	0.0035	0.0067	0.0228	0.0146
DP-024P	4.74	0.0098	0.0125	0.0174	0.0009	0.0001	0.0035	0.0183	0.0344	0.0225
DP-025P	1.41	0.0066	0.0053	0.0029	0.0004	0	0.0018	0.0034	0.0104	0.0065
DP-026P	1.05	0.0066	0.0047	0.0029	0.0004	0	0.0018	0.0034	0.0098	0.006
DP-027P	0.77	0.0066	0.0042	0.0029	0.0004	0	0.0018	0.0034	0.0093	0.0056
DP-041P	-	0	0	0.0247	0.0015	0.0001	0.0037	0.0262	0.03	0.0265
DP-042P	-	0	0	0.0247	0.0015	0.0001	0.0037	0.0262	0.0299	0.0265
DP-043P	-	0	0	0.0247	0.0015	0.0001	0.0038	0.0262	0.03	0.0265
DP-044P	-	0	0	0.0247	0.0015	0.0001	0.0037	0.0262	0.0299	0.0265
DP-A001P	3.45	0.0098	0.0102	0.008	0.0022	0.0002	0.0044	0.0104	0.025	0.0152
DP-A002P	3.45	0.0098	0.0102	0.0145	0.0022	0.0002	0.0044	0.0169	0.0316	0.0202
DP-A00P	1.11	0.0066	0.0048	0.1726	0.0305	0.0015	0.062	0.2046	0.2714	0.2138
DP-A00S	-	0	0	0.0018	0.0001	0	0.0004	0.0019	0.0024	0.002
DP-A011P	-	0	0	0.0174	0.0011	0.0002	0.0044	0.0187	0.0231	0.0192
DP-A012P	-	0	0	0.0288	0.0011	0.0002	0.0044	0.0301	0.0345	0.0305

**TABLE E-3
DIFFERENTIAL AND ABSOLUTE PRESSURE MEASUREMENT ERRORS (Cont.)**

Plant Code	h ±(ft.)	Δh ±(ft.)	ΔK ±(psi)	ΔC ±(psi)	ΔPS ±(psi)	ΔLCH ±(psi)	ΔBV ±(psi)	ΔI ±(psi)	Δ ±(psi)	σ ±(psi)
DP-A01S	13.06	0.0164	0.0298	0.0181	0.0022	0	0.0044	0.0203	0.0545	0.0363
DP-A021P	4.08	0.0098	0.0114	0.0102	0.003	0.0003	0.0062	0.0135	0.031	0.0187
DP-A022P	4.08	0.0098	0.0114	0.0102	0.003	0.0003	0.0062	0.0135	0.031	0.0187
DP-A02S	21.33	0.0295	0.0498	0.0102	0.003	0	0.0062	0.0132	0.0692	0.0519
DP-A03P	-	0	0	0.0725	0.0174	0.0018	0.0443	0.0917	0.136	0.1019
DP-A03S	10.5	0.0164	0.0253	0.0464	0.0022	0.0002	0.0089	0.0488	0.0829	0.0556
DP-A04P	11.82	0.0164	0.0276	0.0279	0.0026	0.0003	0.0089	0.0308	0.0673	0.0423
DP-A04S	2.21	0.0098	0.0081	0.0073	0.0004	0	0.0018	0.0077	0.0176	0.0113
DP-A05P	16.81	0.023	0.0391	0.0261	0.0052	0.0005	0.0159	0.0318	0.0869	0.0529
DP-A05S	2.26	0.0098	0.0082	0.0016	0.0004	0	0.0009	0.002	0.0111	0.0085
DP-A06P	12.3	0.0164	0.0284	0.029	0.0026	0.0003	0.0089	0.0319	0.0692	0.0436
DP-A06S	7.05	0.0164	0.0193	0.0109	0.0013	0	0.0027	0.0122	0.0342	0.023
DP-A07P	12.3	0.0164	0.0284	0.0363	0.003	0.0005	0.0089	0.0398	0.0771	0.0497
DP-A08P	16.81	0.023	0.0391	0.0232	0.0044	0.0007	0.0142	0.0283	0.0816	0.0503
DP-A09P	5.8	0.0098	0.0143	0.0145	0.0044	0.0004	0.0089	0.0193	0.0425	0.0256
DP-A15P	3.33	0.0098	0.01	0.0091	0.0007	0.0001	0.0027	0.0099	0.0226	0.0143
DP-A16P	2.19	0.0098	0.0081	0.0073	0.0009	0.0001	0.0018	0.0082	0.018	0.0116
DP-A20E	10.96	0.0164	0.0261	0.0834	0.0087	0.0008	0.0221	0.0929	0.1412	0.099
DP-A28P	15.21	0.023	0.0363	0.0163	0.0044	0.0005	0.0089	0.0212	0.0663	0.043
DP-A40E	8.58	0.0164	0.022	0.0236	0.0046	0.0005	0.0115	0.0287	0.0622	0.0379
DP-A41E	5.1	0.0098	0.0131	0.005	0.0008	0	0.0016	0.0058	0.0205	0.0144
DP-A42E	5.1	0.0098	0.0131	0.0065	0.0008	0	0.0016	0.0073	0.022	0.0151
DP-A43E	5.1	0.0098	0.0131	0.0065	0.0008	0	0.0016	0.0073	0.022	0.0151
DP-A44E	5.1	0.0098	0.0131	0.0026	0.0008	0	0.0016	0.0034	0.0181	0.0136
DP-A45E	23.7	0.0295	0.0539	0.0363	0.0035	0.0001	0.0089	0.0398	0.1026	0.0676
DP-A61E	3.33	0.0098	0.01	0.0145	0.0044	0.0004	0.0089	0.0192	0.0381	0.0234
DP-A81AE	8.63	0.0164	0.0221	0.0218	0.0035	0.0004	0.0089	0.0256	0.0565	0.035
DP-A81BE	8.63	0.0164	0.0221	0.0145	0.0022	0.0004	0.0089	0.0171	0.048	0.0293
DP-A81E	26.27	0.0328	0.0598	0.0254	0.0035	0.0002	0.0089	0.0291	0.0977	0.0671
DP-A82E	17.65	0.023	0.0406	0.0435	0.0035	0.0006	0.0089	0.0476	0.097	0.0631
DP-A83E	3.71	0.0098	0.0107	0.0091	0.0022	0.0002	0.0044	0.0115	0.0266	0.0163
DP-B001P	3.45	0.0098	0.0102	0.0127	0.0022	0.0002	0.0044	0.0151	0.0298	0.0188
DP-B002P	3.45	0.0098	0.0102	0.0091	0.0022	0.0002	0.0044	0.0115	0.0261	0.016
DP-B00P	1.11	0.0066	0.0048	0.1269	0.0305	0.0015	0.062	0.1589	0.2257	0.1706
DP-B00S	-	0	0	0.0056	0.0001	0	0.0004	0.0057	0.0062	0.0058
DP-B011P	-	0	0	0.0145	0.0011	0.0002	0.0044	0.0158	0.0202	0.0164
DP-B012P	-	0	0	0.019	0.0011	0.0002	0.0044	0.0203	0.0247	0.0208
DP-B01S	13.06	0.0164	0.0298	0.0181	0.0022	0	0.0044	0.0203	0.0545	0.0363

**TABLE E-3
DIFFERENTIAL AND ABSOLUTE PRESSURE MEASUREMENT ERRORS (Cont.)**

Plant Code	h ±(ft.)	Δh ±(ft.)	ΔK ±(psi)	ΔC ±(psi)	ΔPS ±(psi)	ΔLCH ±(psi)	ΔBV ±(psi)	ΔI ±(psi)	Δ ±(psi)	σ ±(psi)
DP-B021P	4.08	0.0098	0.0114	0.0102	0.003	0.0003	0.0062	0.0135	0.031	0.0187
DP-B022P	4.08	0.0098	0.0114	0.0102	0.003	0.0003	0.0062	0.0135	0.031	0.0187
DP-B02S	21.33	0.0295	0.0498	0.0102	0.003	0	0.0062	0.0132	0.0692	0.0519
DP-B03P	-	0	0	0.0725	0.0174	0.0018	0.0443	0.0917	0.136	0.1019
DP-B03S	10.5	0.0164	0.0253	0.0326	0.0022	0.0002	0.0089	0.035	0.0691	0.0441
DP-B04P	11.82	0.0164	0.0276	0.0145	0.0026	0.0003	0.0089	0.0174	0.0538	0.0338
DP-B04S	2.21	.098	0.0081	0.0194	0.0004	0	0.0018	0.0199	0.0297	0.0216
DP-B05P	16.81	0.023	0.0391	0.0313	0.0052	0.0005	0.0159	0.0371	0.0921	0.0562
DP-B05S	2.26	0.0098	0.0082	0.0019	0.0004	0	0.0009	0.0023	0.0114	0.0086
DP-B06P	12.3	0.0164	0.0284	0.029	0.0026	0.0003	0.0089	0.0319	0.0692	0.0436
DP-B06S	7.05	0.0164	0.0193	0.0109	0.0013	0	0.0027	0.0122	0.0342	0.023
DP-B07P	12.3	0.0164	0.0284	0.0283	0.003	0.0005	0.0089	0.0318	0.0691	0.0436
DP-B08P	16.81	0.023	0.0391	0.0232	0.0044	0.0007	0.0142	0.0283	0.0816	0.0503
DP-B09P	5	0.0098	0.0143	0.0145	0.0044	0.0004	0.0089	0.0193	0.0425	0.0256
DP-B15P	3	0.0098	0.01	0.0087	0.0007	0.0001	0.0027	0.0094	0.0221	0.014
DP-B16P	2.19	0.0098	0.0081	0.0029	0.0009	0.0001	0.0018	0.0039	0.0137	0.0091
DP-B20E	10.96	0.0164	0.0261	0.0363	0.0087	0.0008	0.0221	0.0458	0.094	0.0572
DP-B28P	15.21	0.023	0.0363	0.0145	0.0044	0.0005	0.0089	0.0194	0.0645	0.0421
DP-B40E	8.58	0.0164	0.022	0.0189	0.0046	0.0005	0.0115	0.024	0.0575	0.0345
DP-B41E	5.1	0.0098	0.0131	0.0026	0.0008	0	0.0016	0.0034	0.0187	0.0136
DP-B42E	5.1	0.0098	0.0131	0.0039	0.0008	0	0.0016	0.0047	0.0194	0.014
DP-B43E	5.1	0.0098	0.0131	0.0036	0.0008	0	0.0016	0.0043	0.019	0.0139
DP-B44E	5.1	0.0098	0.0131	0.0052	0.0008	0	0.0016	0.006	0.0207	0.0145
DP-B45E	23.7	0.0295	0.0539	0.0218	0.0035	0.0001	0.0089	0.0253	0.0881	0.0602
DP-B61E	3.33	0.0098	0.01	0.0363	0.0044	0.0004	0.0089	0.041	0.0599	0.0431
F-001BP	-	0	0	0.0099	0.0017	0.0001	0.0035	0.0117	0.0153	0.0123
F-001BS	-	0	0	0.0029	0.0009	0.0001	0.0018	0.0038	0.0056	0.0042
F-001A	-	0	0	0.0096	0.0013	0.0001	0.0027	0.011	0.0136	0.0113
F-003P	0.53	0.0066	0.0038	0.029	0.0035	0.0003	0.0071	0.0328	0.0436	0.0337
F-003P	0.53	0.0066	0.0038	0.0074	0.0003	0	0.0005	0.0077	0.012	0.0086
F-014P	0.19	0.0066	0.0032	0.0181	0.0044	0.0004	0.0089	0.0228	0.0349	0.0247
F-A00E	-	0	0	0.132	0.0305	0.0025	0.062	0.165	0.227	0.1763
F-A01P	-	0	0	0.0087	0.0026	0.0002	0.0053	0.0115	0.0168	0.0127
F-A01P	-	0	0	0.0023	0.0002	0	0.0004	0.0026	0.003	0.0026
F-A01S	-	0	0	0.0725	0.0109	0.0009	0.0221	0.0843	0.1065	0.0872
F-A02P	-	0	0	0.0007	0.0002	0	0.0004	0.001	0.0014	0.0011
F-A02P	-	0	0	0.0087	0.0026	0.0002	0.0053	0.0115	0.0168	0.0127
F-A02S	0.28	0.0066	0.0033	0.0363	0.0044	0.0004	0.0089	0.041	0.0531	0.0421
F-A03S	0.28	0.0066	0.0033	0.0363	0.0044	0.0004	0.0089	0.041	0.0531	0.0421
F-A04S	-	0	0	0.3626	0.0435	0.0033	0.0443	0.4095	0.4537	0.4118

**TABLE E-3
DIFFERENTIAL AND ABSOLUTE PRESSURE MEASUREMENT ERRORS (Cont.)**

Plant Code	h ±(ft.)	Δh ±(ft.)	ΔK ±(psi)	ΔC ±(psi)	ΔPS ±(psi)	ΔLCH ±(psi)	ΔBV ±(psi)	ΔI ±(psi)	Δ ±(psi)	σ ±(psi)
F-A20A	0.06	0.0066	0.0029	0.0218	0.0044	0.0004	0.0089	0.0265	0.0383	0.0281
F-A20E	-	0	0	0.0131	0.0022	0.0002	0.0044	0.0154	0.0198	0.016
F-A40E	-	0	0	0.0029	0.0009	0.0001	0.0018	0.0038	0.0056	0.0042
F-A60E	-	0	0	0.0087	0.0026	0.0002	0.0053	0.0115	0.0168	0.0127
F-A80E	-	0	0	0.1055	0.0131	0.0011	0.0266	0.1197	0.1462	0.1226
F-B00E	-	0	0	0.1015	0.0305	0.0025	0.062	0.1345	0.1965	0.1481
F-B01P	-	0	0	0.0152	0.0026	0.0002	0.0053	0.0181	0.0234	0.0188
F-B01P	-	0	0	0.0007	0.0002	0	0.0004	0.001	0.0014	0.0011
F-B01S	-	0	0	0.0725	0.0109	0.0009	0.0221	0.0843	0.1065	0.0872
F-B02P	-	0	0	0.0109	0.0026	0.0002	0.0053	0.0137	0.019	0.0147
F-B02P	-	0	0	0.0045	0.0002	0	0.0004	0.0048	0.0052	0.0048
F-B02S	0.28	0.0066	0.0033	0.0145	0.0044	0.0004	0.0089	0.0192	0.0314	0.0214
F-B03S	0.28	0.0066	0.0033	0.029	0.0044	0.0004	0.0089	0.0337	0.0459	0.035
F-B04S	-	0	0	0.1813	0.0218	0.0019	0.0443	0.205	0.2492	0.2096
F-B20A	0.06	0.0066	0.0029	0.0218	0.0044	0.0004	0.0089	0.0265	0.0383	0.0281
F-B20E	-	0	0	0.0073	0.0022	0.0002	0.0044	0.0096	0.014	0.0106
F-B40E	-	0	0	0.0032	0.0009	0.0001	0.0018	0.0041	0.0059	0.0045
F-B60E	-	0	0	0.0183	0.0026	0.0002	0.0053	0.0211	0.0264	0.0218
L-010P	20.36	0.0295	0.0481	0.0221	0.0029	0	0.0059	0.025	0.079	0.0546
L-060E	28.71	0.0328	0.064	0.0334	0.0044	0	0.0089	0.0377	0.1106	0.0748
L-A10S	44.88	0.0328	0.0921	0.0234	0.0058	0.0001	0.0119	0.0293	0.1332	0.0973
L-A20E (*)	8.52	0.0164	0.0219	0.0102	0.003	0.0003	0.0062	0.0135	0.0197	0.0149
L-A20S	8.73	0.0164	0.0222	0.011	0.0011	0	0.0023	0.0121	0.0367	0.0254
L-A40E	20.41	0.0295	0.0482	0.0204	0.0027	0	0.0054	0.0231	0.0767	0.0537
L-B10S	44.88	0.0328	0.0921	0.022	0.0058	0.0001	0.0119	0.028	0.1319	0.097
L-B20E (*)	8.52	0.0164	0.0219	0.0102	0.003	0.0003	0.0062	0.0135	0.0197	0.0149
L-B20S	8.73	0.0164	0.0222	0.0254	0.0011	0	0.0023	0.0265	0.0511	0.0347
L-B40E	20.41	0.0295	0.0482	0.0214	0.0027	0	0.0054	0.0241	0.0777	0.0541
F-B04SM	33.74	0.0328	0.074	2.5384	0.3046	0.0254	0.6197	2.8684	3.5608	2.9355
F-B04SP	33.74	0.0328	0.074	2.1758	0.2611	0.0218	0.5312	2.4587	3.0625	2.5164
P-001P	5.76	0.0098	0.0143	6.5274	1.4578	0.0726	1.7707	8.0578	9.8426	8.25
P-003P	37.19	0.0328	0.0787	2.9011	1.4578	0.0728	1.7707	4.4317	6.2811	4.773
P-017P	27.64	0.0328	0.0622	2.9011	1.4578	0.0728	1.7707	4.4316	6.2646	4.7727
P-027P	27.23	0.0328	0.0614	2.9011	1.4578	0.0728	1.7707	4.4316	6.2639	4.7727
P-A01S	29.06	0.0328	0.0675	1.4505	0.7325	0.0365	0.8853	2.2196	3.1697	2.3906
P-A04P	28.46	0.0328	0.0636	2.9011	1.4578	0.0728	1.7707	4.4316	6.2659	4.7727
P-A04S	32.1	0.0328	0.0699	1.4505	0.7325	0.0365	0.8853	2.2196	3.1749	2.3907
P-A20E	12.68	0.0164	0.0291	1.4505	0.7325	0.0364	0.8853	2.2194	3.134	2.3897
P-A40E	13.46	0.023	0.0333	2.9011	1.4578	0.0726	1.7707	4.4315	6.2356	4.7723
P-B01S	27.75	0.0328	0.0624	1.8132	0.7325	0.0365	0.8853	2.5822	3.53	2.7305

**TABLE E-3
DIFFERENTIAL AND ABSOLUTE PRESSURE MEASUREMENT ERRORS (Cont.)**

Plant Code	h ±(ft.)	Δh ±(ft.)	ΔK ±(psi)	ΔC ±(psi)	ΔPS ±(psi)	ΔLCH ±(psi)	ΔBV ±(psi)	ΔI ±(psi)	Δ ±(psi)	σ ±(psi)
P-B04P	29.77	0.0328	0.0659	2.9011	1.4578	0.0728	1.7707	4.4316	6.2682	4.7728
P-B04S	32.1	0.0328	0.0699	1.4505	0.7325	0.0365	0.8853	2.2196	3.1749	2.3907
P-B20E	13.99	0.023	0.0342	1.4505	0.7325	0.0364	0.8853	2.2194	3.1391	2.3898
P-B40E	10.83	0.0164	0.0259	2.9011	1.4578	0.0726	1.7707	4.4315	6.2282	4.7723
P-030P	35.23	0.0328	0.0753	0.2538	0.058	0.0028	0.062	0.3147	0.452	0.3296
P-040P	28.35	0.0328	0.0634	0.2538	0.058	0.0028	0.062	0.3146	0.4399	0.3268

**TABLE E-4
TEMPERATURE ERRORS**

Plant Code	ΔC $\pm(^{\circ}F)$	ΔPS $\pm(^{\circ}F)$	ΔLCH $\pm(^{\circ}F)$	ΔBV $\pm(^{\circ}F)$	ΔRJ $\pm(^{\circ}F)$	ΔI $\pm(^{\circ}F)$	Δ $\pm(^{\circ}F)$	σ $\pm(^{\circ}F)$
T-001A	1.98	0.22	0.02	0.17	0.18	2.21	2.57	2.23
T-001B	2.03	0.22	0.02	0.34	0.18	2.27	2.79	2.3
T-001P	2.04	0.22	0.02	0.17	0.18	2.27	2.63	2.28
T-001PH	2.05	0.22	0.02	0.17	0.18	2.28	2.65	2.3
T-001PL	2.05	0.22	0.02	0.17	0.18	2.29	2.65	2.3
T-002P	2.05	0.22	0.02	0.17	0.18	2.28	2.65	2.3
T-003P	2.04	0.22	0.02	0.17	0.18	2.28	2.65	2.3
T-003PH	2.02	0.22	0.02	0.34	0.18	2.25	2.77	2.28
T-003PL	2.02	0.22	0.02	0.34	0.18	2.25	2.77	2.28
T-004P	2.06	0.22	0.02	0.17	0.18	2.3	2.66	2.32
T-014P	2.05	0.22	0.02	0.17	0.18	2.29	2.65	2.3
T-015P	2.28	0.22	0.02	0.34	0.18	2.51	3.04	2.55
T-016P	2	0.22	0.02	0.17	0.18	2.23	2.59	2.25
T-018P	2.44	0.22	0.02	0.17	0.18	2.68	3.04	2.69
T-019PH	2.44	0.22	0.02	0.34	0.18	2.67	3.2	2.71
T-019PL	2.41	0.22	0.02	0.34	0.18	2.64	3.17	2.67
T-020P	2.5	0.22	0.02	0.17	0.18	2.74	3.1	2.75
T-021P	2.38	0.22	0.02	0.17	0.18	2.61	2.97	2.62
T-022P	2.52	0.22	0.02	0.17	0.18	2.76	3.11	2.77
T-023P	2.53	0.22	0.02	0.17	0.18	2.76	3.11	2.77
T-024P	2.52	0.22	0.02	0.17	0.18	2.76	3.11	2.77
T-025P	2.53	0.22	0.02	0.17	0.18	2.76	3.13	2.78
T-026P	2.52	0.22	0.02	0.17	0.18	2.75	3.11	2.77
T-030P	1.98	0.22	0.02	0.17	0.18	2.21	2.57	2.23
T-031P	2.05	0.22	0.02	0.17	0.18	2.29	2.65	2.3
T-032P	2.05	0.22	0.02	0.17	0.18	2.29	2.65	2.3
T-033P	2.06	0.22	0.02	0.17	0.18	2.3	2.66	2.32
T-034P	2.05	0.22	0.02	0.17	0.18	2.29	2.65	2.3
T-035P	2.05	0.22	0.02	0.17	0.18	2.28	2.65	2.3
T-036P	2.06	0.22	0.02	0.17	0.18	2.29	2.65	2.3
T-040P	1.98	0.22	0.02	0.17	0.18	2.21	2.57	2.23
T-041P	2.05	0.22	0.02	0.17	0.18	2.28	2.65	2.3

**TABLE E-4
TEMPERATURE ERRORS (Cont.)**

Plant Code	ΔC $\pm(^{\circ}F)$	ΔPS $\pm(^{\circ}F)$	ΔLCH $\pm(^{\circ}F)$	ΔBV $\pm(^{\circ}F)$	ΔRJ $\pm(^{\circ}F)$	ΔI $\pm(^{\circ}F)$	Δ $\pm(^{\circ}F)$	σ $\pm(^{\circ}F)$
T-042P	2.05	0.22	0.02	0.17	0.18	2.28	2.65	2.3
T-043P	2.06	0.22	0.02	0.17	0.18	2.3	2.66	2.32
T-044P	2.07	0.22	0.02	0.17	0.18	2.31	2.66	2.32
T-045P	2.07	0.22	0.02	0.17	0.18	2.3	2.66	2.32
T-046P	2.08	0.22	0.02	0.17	0.18	2.31	2.68	2.34
T-A00E	1.98	0.22	0.02	0.17	0.18	2.21	2.57	2.23
T-A011P	2.07	0.22	0.02	0.17	0.18	2.3	2.66	2.32
T-A012P	2.06	0.22	0.02	0.17	0.18	2.29	2.65	2.3
T-A01P	2.07	0.22	0.02	0.17	0.18	2.3	2.66	2.32
T-A01S	1.98	0.22	0.02	0.17	0.18	2.21	2.57	2.23
T-A021PL	2.06	0.22	0.02	0.17	0.18	2.29	2.65	2.3
T-A021PO	2.05	0.22	0.02	0.17	0.18	2.28	2.65	2.3
T-A022PL	2.07	0.22	0.02	0.17	0.18	2.3	2.66	2.32
T-A022PO	2.2	0.22	0.02	0.17	0.18	2.43	2.79	2.44
T-A02E	1.98	0.22	0.02	0.17	0.18	2.21	2.57	2.23
T-A02S	2.04	0.22	0.02	0.17	0.18	2.27	2.63	2.28
T-A031PL	1.98	0.22	0.02	0.17	0.18	2.21	2.57	2.23
T-A032PL	2.05	0.22	0.02	0.17	0.18	2.28	2.65	2.3
T-A03PL	2.29	0.22	0.02	0.17	0.18	2.53	2.88	2.53
T-A03PO	2.3	0.22	0.02	0.17	0.18	2.53	2.9	2.55
T-A03S	2.04	0.22	0.02	0.17	0.18	2.28	2.65	2.3
T-A04P	2.31	0.22	0.02	0.17	0.18	2.54	2.9	2.55
T-A04S	2.09	0.22	0.02	0.17	0.18	2.33	2.68	2.34
T-A05P	2.27	0.22	0.02	0.17	0.18	2.51	2.86	2.51
T-A05S	1.99	0.22	0.02	0.17	0.18	2.22	2.57	2.23
T-A06P	2.2	0.22	0.02	0.17	0.18	2.43	2.79	2.44
T-A06S	2.02	0.22	0.02	0.17	0.18	2.25	2.61	2.26
T-A07S	2.02	0.22	0.02	0.17	0.18	2.26	2.61	2.26
T-A08P	2.09	0.22	0.02	0.17	0.18	2.32	2.68	2.34
T-A08S	2.02	0.22	0.02	0.17	0.18	2.25	2.61	2.26
T-A09P	2.06	0.22	0.02	0.17	0.18	2.29	2.65	2.3
T-A09S	2.92	0.22	0.02	0.17	0.18	2.26	2.61	2.26

**TABLE E-4
TEMPERATURE ERRORS (Cont.)**

Plant Code	ΔC $\pm(^{\circ}F)$	ΔPS $\pm(^{\circ}F)$	ΔLCH $\pm(^{\circ}F)$	ΔBV $\pm(^{\circ}F)$	ΔRJ $\pm(^{\circ}F)$	ΔI $\pm(^{\circ}F)$	Δ $\pm(^{\circ}F)$	σ $\pm(^{\circ}F)$
T-A10P	2.1	0.22	0.02	0.17	0.18	2.33	2.7	2.35
T-A11P	2.07	0.22	0.02	0.17	0.18	2.3	2.66	2.32
T-A141P	2.05	0.22	0.02	0.17	0.18	2.29	2.65	2.3
T-A142PH	2.45	0.22	0.02	0.17	0.18	2.68	3.04	2.69
T-A142PL	2.08	0.22	0.02	0.17	0.18	2.25	2.61	2.26
T-A143P	2.02	0.22	0.02	0.17	0.18	2.25	2.61	2.26
T-A181E	2.74	0.54	0.02	0.34	0.18	3.3	3.82	3.32
T-A182E	2.82	0.54	0.02	0.34	0.18	3.39	3.91	3.41
T-A20A	1.98	0.22	0.02	0.17	0.18	2.21	2.57	2.23
T-A21E	1.98	0.22	0.02	0.17	0.18	2.21	2.57	2.23
T-A22E	1.98	0.22	0.02	0.17	0.18	2.21	2.57	2.23
T-A23E	1.98	0.22	0.02	0.17	0.18	2.21	2.57	2.23
T-A27P	1.98	0.22	0.02	0.34	0.18	2.21	2.74	2.25
T-A281E	2.83	0.54	0.02	0.34	0.18	3.39	3.91	3.41
T-A28P	1.98	0.22	0.02	0.34	0.18	2.21	2.74	2.25
T-A29P	2.01	0.22	0.02	0.34	0.18	2.24	2.75	2.27
T-A401E	1.98	0.54	0.02	0.34	0.18	2.54	3.06	2.57
T-A402E	1.98	0.54	0.02	0.34	0.18	2.54	3.06	2.57
T-A403E	1.98	0.54	0.02	0.34	0.18	2.54	3.06	2.57
T-A404E	1.98	0.54	0.02	0.34	0.18	2.54	3.06	2.57
T-A405E	1.98	0.54	0.02	0.34	0.18	2.54	3.06	2.57
T-A406E	1.98	0.54	0.02	0.34	0.18	2.54	3.06	2.57
T-A407E	1.98	0.54	0.02	0.34	0.18	2.54	3.06	2.57
T-A408E	1.98	0.54	0.02	0.34	0.18	2.54	3.06	2.57
T-A409E	1.98	0.22	0.02	0.34	0.18	2.21	2.74	2.25
T-A410E	1.98	0.54	0.02	0.34	0.18	2.54	3.06	2.57
T-A411E	1.98	0.54	0.02	0.34	0.18	2.54	3.06	2.57
T-A412E	1.98	0.54	0.02	0.34	0.18	2.54	3.06	2.57
T-A413E	1.98	0.54	0.02	0.34	0.18	2.54	3.06	2.57
T-A414E	1.98	0.54	0.02	0.34	0.18	2.54	3.06	2.57
T-A415E	1.98	0.54	0.02	0.34	0.18	2.54	3.06	2.57
T-A416E	1.98	0.54	0.02	0.34	0.18	2.54	3.06	2.57

**TABLE E-4
TEMPERATURE ERRORS (Cont.)**

Plant Code	ΔC $\pm(^{\circ}F)$	ΔPS $\pm(^{\circ}F)$	ΔLCH $\pm(^{\circ}F)$	ΔBV $\pm(^{\circ}F)$	ΔRJ $\pm(^{\circ}F)$	ΔI $\pm(^{\circ}F)$	Δ $\pm(^{\circ}F)$	σ $\pm(^{\circ}F)$
T-A417E	1.98	0.54	0.02	0.34	0.18	2.54	3.06	2.57
T-A418E	1.98	0.54	0.02	0.34	0.18	2.54	3.06	2.57
T-A419E	1.98	0.54	0.02	0.34	0.18	2.54	3.06	2.57
T-A41A	2.23	0.22	0.02	0.34	0.18	2.47	2.99	2.5
T-A420E	1.98	0.54	0.02	0.34	0.18	2.54	3.06	2.57
T-A421E	1.98	0.22	0.02	0.34	0.18	2.21	2.74	2.25
T-A422E	2.2	0.22	0.02	0.34	0.18	2.43	2.95	2.46
T-A42A	1.98	0.22	0.02	0.34	0.18	2.21	2.74	2.25
T-A66E	1.98	0.22	0.02	0.17	0.18	2.21	2.57	2.23
T-A81E	2.24	0.22	0.02	0.34	0.18	2.47	2.99	2.5
T-A82E	2.12	0.22	0.02	0.34	0.18	2.35	2.88	2.39
T-A83E	1.98	0.22	0.02	0.34	0.18	2.21	2.74	2.25
T-A84E	1.98	0.22	0.02	0.34	0.18	2.21	2.74	2.25
T-B00E	1.98	0.22	0.02	0.17	0.18	2.21	2.57	2.23
T-B011P	2.09	0.22	0.02	0.34	0.18	2.33	2.84	2.35
T-B012P	2.07	0.22	0.02	0.17	0.18	2.3	2.66	2.32
T-B01P	2.07	0.22	0.02	0.17	0.18	2.3	2.66	2.32
T-B01S	1.98	0.22	0.02	0.17	0.18	2.21	2.57	2.23
T-B021PL	2.05	0.22	0.02	0.17	0.18	2.28	2.65	2.3
T-B021PO	2.06	0.22	0.02	0.17	0.18	2.29	2.65	2.3
T-B022PL	2.05	0.22	0.02	0.17	0.18	2.29	2.65	2.3
T-B022PO	2.2	0.22	0.02	0.17	0.18	2.43	2.79	2.44
T-B02E	1.98	0.22	0.02	0.17	0.18	2.21	2.57	2.23
T-B02S	2.04	0.22	0.02	0.17	0.18	2.27	2.63	2.28
T-B031PL	2.07	0.22	0.02	0.17	0.18	2.31	2.66	2.32
T-B032PL	2.08	0.22	0.02	0.17	0.18	2.31	2.68	2.34
T-B03PL	2.3	0.22	0.02	0.17	0.18	2.54	2.9	2.55
T-B03PO	2.28	0.22	0.02	0.17	0.18	2.52	2.88	2.53
T-B03S	2.03	0.22	0.02	0.17	0.18	2.27	2.63	2.28
T-B04P	2.3	0.22	0.02	0.17	0.18	2.54	2.9	2.55
T-B04S	2.04	0.22	0.02	0.17	0.18	2.27	2.63	2.28
T-B05P	2.29	0.22	0.02	0.17	0.18	2.52	2.88	2.53

**TABLE E-4
TEMPERATURE ERRORS (Cont.)**

Plant Code	ΔC $\pm(^{\circ}F)$	ΔPS $\pm(^{\circ}F)$	ΔLCH $\pm(^{\circ}F)$	ΔBV $\pm(^{\circ}F)$	ΔRJ $\pm(^{\circ}F)$	ΔI $\pm(^{\circ}F)$	Δ $\pm(^{\circ}F)$	σ $\pm(^{\circ}F)$
T-B05S	2.02	0.22	0.02	0.17	0.18	2.25	2.61	2.26
T-B06P	2.2	0.22	0.02	0.17	0.18	2.44	2.79	2.44
T-B06S	2.02	0.22	0.02	0.17	0.18	2.26	2.61	2.26
T-B07P	2.14	0.22	0.02	0.17	0.18	2.38	2.74	2.39
T-B07S	2.03	0.22	0.02	0.17	0.18	2.27	2.63	2.28
T-B08P	2.11	0.22	0.02	0.17	0.18	2.34	2.7	2.35
T-B08S	2.03	0.22	0.02	0.17	0.18	2.27	2.63	2.28
T-B09P	2.07	0.22	0.02	0.17	0.18	2.31	2.66	2.32
T-B09S	2.02	0.22	0.02	0.17	0.18	2.25	2.61	2.26
T-B10P	2.08	0.22	0.02	0.17	0.18	2.32	2.68	2.34
T-B11P	2.08	0.22	0.02	0.17	0.18	2.31	2.68	2.34
T-B141P	2.05	0.22	0.02	0.34	0.18	2.28	2.81	2.32
T-B142PH	2.02	0.22	0.02	0.34	0.18	2.26	2.77	2.28
T-B142PL	2.01	0.22	0.02	0.17	0.18	2.24	2.61	2.26
T-B143P	2.03	0.22	0.02	0.34	0.18	2.26	2.79	2.3
T-B20A	1.98	0.22	0.02	0.17	0.18	2.21	2.57	2.23
T-B21E	1.98	0.22	0.02	0.17	0.18	2.21	2.57	2.23
T-B22E	1.98	0.22	0.02	0.17	0.18	2.21	2.57	2.23
T-B23E	1.98	0.22	0.02	0.34	0.18	2.21	2.74	2.25
T-B27P	1.98	0.22	0.02	0.34	0.18	2.21	2.74	2.25
T-B28P	1.98	0.22	0.02	0.34	0.18	2.21	2.74	2.25
T-B29P	2.02	0.22	0.02	0.34	0.18	2.25	2.77	2.28
T-B401E	1.98	0.54	0.02	0.34	0.18	2.54	3.06	2.57
T-B403E	1.98	0.54	0.02	0.34	0.18	2.54	3.06	2.57
T-B405E	1.98	0.54	0.02	0.34	0.18	2.54	3.06	2.57
T-B407E	1.98	0.54	0.02	0.34	0.18	2.54	3.06	2.57
T-B409E	1.98	0.54	0.02	0.34	0.18	2.54	3.06	2.57
T-B411E	1.98	0.54	0.02	0.34	0.18	2.54	3.06	2.57
T-B413E	1.98	0.54	0.02	0.34	0.18	2.54	3.06	2.57
T-B415E	1.98	0.54	0.02	0.34	0.18	2.54	3.06	2.57
T-B417E	1.98	0.54	0.02	0.34	0.18	2.54	3.06	2.57
T-B41A	1.98	0.22	0.02	0.34	0.18	2.21	2.74	2.25

**TABLE E-4
TEMPERATURE ERRORS (Cont.)**

Plant Code	ΔC $\pm(^{\circ}F)$	ΔPS $\pm(^{\circ}F)$	ΔLCH $\pm(^{\circ}F)$	ΔBV $\pm(^{\circ}F)$	ΔRJ $\pm(^{\circ}F)$	ΔI $\pm(^{\circ}F)$	Δ $\pm(^{\circ}F)$	σ $\pm(^{\circ}F)$
T-B420E	1.98	0.54	0.02	0.34	0.18	2.54	3.06	2.57
T-B421E	1.98	0.22	0.02	0.34	0.18	2.21	2.74	2.25
T-B422E	1.98	0.22	0.02	0.34	0.18	2.21	2.74	2.25
T-B42A	1.98	0.22	0.02	0.34	0.18	2.21	2.74	2.25
T-B66E	1.98	0.22	0.02	0.34	0.18	2.21	2.74	2.25
TW-001P	1.99	0.22	0.02	0.34	0.18	2.22	2.74	2.25
TW-002P	2.01	0.22	0.02	0.34	0.18	2.24	2.77	2.28
TW-003P	1.99	0.22	0.02	0.34	0.18	2.22	2.74	2.25
TW-004P	1.98	0.22	0.02	0.34	0.18	2.22	2.74	2.25
TW-005P	2.14	0.22	0.02	0.7	0.18	2.38	3.26	2.48
TW-006P	1.99	0.22	0.02	0.7	0.18	2.23	3.11	2.35
TW-007P	2	0.22	0.02	0.7	0.18	2.24	3.11	2.35
TW-008P	1.98	0.22	0.02	0.7	0.18	2.22	3.1	2.33
TW-016P	1.98	0.22	0.02	0.34	0.18	2.21	2.74	2.25
TW-023P	2.44	0.22	0.02	0.34	0.18	2.67	3.19	2.69
TW-A03PL	2.25	0.22	0.02	0.34	0.18	2.48	3.01	2.51
TW-A05S	2.07	0.22	0.02	0.34	0.18	2.3	2.83	2.34
TW-A06S	2.07	0.22	0.02	0.34	0.18	2.3	2.83	2.34
TW-A08S	2.05	0.22	0.02	0.17	0.18	2.29	2.65	2.3
TW-A10S	1.98	0.22	0.02	0.17	0.18	2.21	2.57	2.23
TW-A11S	2.01	0.22	0.02	0.17	0.18	2.24	2.61	2.26
TW-A12S	1.98	0.22	0.02	0.34	0.18	2.21	2.74	2.25
TW-A181E	1.98	0.54	0.02	0.34	0.18	2.54	3.06	2.57
TW-A182E	1.98	0.54	0.02	0.34	0.18	2.54	3.06	2.57
TW-A183E	1.98	0.54	0.02	0.34	0.18	2.54	3.06	2.57
TW-A281E	1.98	0.54	0.02	0.34	0.18	2.54	3.06	2.57
TW-A41AE	1.98	0.54	0.02	0.17	0.18	2.54	2.9	2.55
TW-A41AI	1.98	0.54	0.02	0.17	0.18	2.54	2.9	2.55
TW-A41E	1.98	0.54	0.02	0.17	0.18	2.54	2.9	2.55
TW-A42AE	1.98	0.54	0.02	0.34	0.18	2.54	3.06	2.57
TW-A42AI	1.98	0.22	0.02	0.34	0.18	2.21	2.74	2.25
TW-A42E	1.98	0.54	0.02	0.34	0.18	2.54	3.06	2.57

**TABLE E-4
TEMPERATURE ERRORS (Cont.)**

Plant Code	ΔC $\pm(^{\circ}F)$	ΔPS $\pm(^{\circ}F)$	ΔLCH $\pm(^{\circ}F)$	ΔBV $\pm(^{\circ}F)$	ΔRJ $\pm(^{\circ}F)$	ΔI $\pm(^{\circ}F)$	Δ $\pm(^{\circ}F)$	σ $\pm(^{\circ}F)$
TW-A43E	1.98	0.54	0.02	0.34	0.18	2.54	3.06	2.57
TW-A44E	1.98	0.54	0.02	0.34	0.18	2.54	3.06	2.57
TW-A45E	1.98	0.54	0.02	0.34	0.18	2.54	3.06	2.57
TW-A46E	1.98	0.54	0.02	0.34	0.18	2.54	3.06	2.57
TW-A47E	1.98	0.54	0.02	0.34	0.18	2.54	3.06	2.57
TW-A48E	1.98	0.54	0.02	0.34	0.18	2.54	3.06	2.57
TW-A81E	2.11	0.22	0.02	0.17	0.18	2.34	2.7	2.35
TW-B05S	2.09	0.22	0.02	0.34	0.18	2.32	2.84	2.35
TW-B06S	2.09	0.22	0.02	0.17	0.18	2.32	2.68	2.34
TW-B08S	2.06	0.22	0.02	0.17	0.18	2.29	2.65	2.3
TW-B09S	2.02	0.22	0.02	0.17	0.18	2.25	2.61	2.26
TW-B10S	1.98	0.22	0.02	0.17	0.18	2.21	2.57	2.23
TW-B11S	2.01	0.22	0.02	0.17	0.18	2.24	2.61	2.26
TW-B41AE	1.98	0.54	0.02	0.17	0.18	2.54	2.9	2.55
TW-B41AI	1.98	0.54	0.02	0.17	0.18	2.54	2.9	2.55
TW-B41E	1.98	0.54	0.02	0.34	0.18	2.54	3.06	2.57
TW-B42AE	1.98	0.54	0.02	0.34	0.18	2.54	3.06	2.57
TW-B42AI	1.98	0.54	0.02	0.34	0.18	2.54	3.06	2.57
TW-B44E	1.98	0.54	0.02	0.34	0.18	2.54	3.06	2.57
TW-B46E	1.98	0.54	0.02	0.34	0.18	2.54	3.06	2.57
TW-B48E	1.98	0.54	0.02	0.34	0.18	2.54	3.06	2.57
TW011P07	2.47	0.22	0.02	0.7	0.18	2.7	3.58	2.8
TW011P11	2.47	0.22	0.02	0.7	0.18	2.7	3.58	2.8
TW011P53	2.47	0.22	0.02	0.7	0.18	2.7	3.58	2.8
TW011P82	2.47	0.22	0.02	0.7	0.18	2.7	3.58	2.8
TW011P83	2.47	0.22	0.02	0.7	0.18	2.7	3.58	2.8
TW011P91	2.47	0.22	0.02	0.7	0.18	2.7	3.58	2.8
TW012P50	2.47	0.22	0.02	0.7	0.18	2.7	3.58	2.8
TW012P71	2.47	0.22	0.02	0.7	0.18	2.7	3.58	2.8
TW013P61	2.47	0.22	0.02	0.7	0.18	2.7	3.58	2.8
TW013P68	2.47	0.22	0.02	0.7	0.18	2.7	3.58	2.8
TW014P41	2.47	0.22	0.02	0.7	0.18	2.7	3.58	2.8

**TABLE E-4
TEMPERATURE ERRORS (Cont.)**

Plant Code	ΔC $\pm(^{\circ}F)$	ΔPS $\pm(^{\circ}F)$	ΔLCH $\pm(^{\circ}F)$	ΔBV $\pm(^{\circ}F)$	ΔRJ $\pm(^{\circ}F)$	ΔI $\pm(^{\circ}F)$	Δ $\pm(^{\circ}F)$	σ $\pm(^{\circ}F)$
TW014P44	2.47	0.22	0.02	0.7	0.18	2.7	3.58	2.8
TW014P49	2.47	0.22	0.02	0.7	0.18	2.7	3.58	2.8
TW014P68	2.47	0.22	0.02	0.7	0.18	2.7	3.58	2.8
TW015P07	2.47	0.22	0.02	0.7	0.18	2.7	3.58	2.8
TW015P11	2.47	0.22	0.02	0.7	0.18	2.7	3.58	2.8
TW015P23	2.47	0.22	0.02	0.7	0.18	2.7	3.58	2.8
TW015P39	2.47	0.22	0.02	0.7	0.18	2.7	3.58	2.8
TW015P53	2.47	0.22	0.02	0.7	0.18	2.7	3.58	2.8
TW015P83	2.47	0.22	0.02	0.7	0.18	2.7	3.58	2.8
TW015P91	2.47	0.22	0.02	0.7	0.18	2.7	3.58	2.8
TW016P14	2.47	0.22	0.02	0.7	0.18	2.7	3.58	2.8
TW016P37	2.47	0.22	0.02	0.7	0.18	2.7	3.58	2.8
TW016P37	2.47	0.22	0.02	0.7	0.18	2.7	3.58	2.8
TW016P41	2.47	0.22	0.02	0.7	0.18	2.7	3.58	2.8
TW016P68	2.47	0.22	0.02	0.7	0.18	2.7	3.58	2.8
TW016P82	2.47	0.22	0.02	0.7	0.18	2.7	3.58	2.8
TW017P03	2.47	0.22	0.02	0.7	0.18	2.7	3.58	2.8
TW017P27	2.47	0.22	0.02	0.7	0.18	2.7	3.58	2.8
TW017P64	2.47	0.22	0.02	0.7	0.18	2.7	3.58	2.8
TW017P79	2.47	0.22	0.02	0.7	0.18	2.7	3.58	2.8
TW018P03	2.47	0.22	0.02	0.7	0.18	2.7	3.58	2.8
TW018P07	2.47	0.22	0.02	0.7	0.18	2.7	3.58	2.8
TW018P20	2.51	0.22	0.02	0.7	0.18	2.75	3.64	2.85
TW018P37	2.47	0.22	0.02	0.7	0.18	2.7	3.58	2.8
TW018P44	2.47	0.22	0.02	0.7	0.18	2.7		2.8
TW018P48	2.47	0.22	0.02	0.7	0.18	2.7	3.58	2.8
TW018P64	2.47	0.22	0.02	0.7	0.18	2.7	3.58	2.8
TW018P91	2.47	0.22	0.02	0.7	0.18	2.7	3.58	2.8
TW019P03	2.47	0.22	0.02	0.7	0.18	2.7	3.58	2.8
TW019P37	2.47	0.22	0.02	0.7	0.18	2.7	3.58	2.8
TW019P41	2.47	0.22	0.02	0.7	0.18	2.7	3.58	2.8
TW019P82	2.47	0.22	0.02	0.7	0.18	2.7	3.58	2.8

**TABLE E-4
TEMPERATURE ERRORS (Cont.)**

Plant Code	ΔC $\pm(^{\circ}F)$	ΔPS $\pm(^{\circ}F)$	ΔLCH $\pm(^{\circ}F)$	ΔBV $\pm(^{\circ}F)$	ΔRJ $\pm(^{\circ}F)$	ΔI $\pm(^{\circ}F)$	Δ $\pm(^{\circ}F)$	σ $\pm(^{\circ}F)$
TW020P03	2.47	0.22	0.02	0.7	0.18	2.7	3.58	2.8
TW020P07	2.47	0.22	0.02	0.7	0.18	2.7	3.58	2.8
TW020P24	2.47	0.22	0.02	0.7	0.18	2.7	3.58	2.8
TW020P27	2.47	0.22	0.02	0.7	0.18	2.7	3.58	2.8
TW020P37	2.47	0.22	0.02	0.7	0.18	2.7	3.58	2.8
TW020P41	2.47	0.22	0.02	0.7	0.18	2.7	3.58	2.8
TW020P44	2.47	0.22	0.02	0.7	0.18	2.7	3.58	2.8
TW020P49	2.47	0.22	0.02	0.7	0.18	2.7	3.58	2.8
TW020P53	2.47	0.22	0.02	0.7	0.18	2.7	3.58	2.8
TW020P61	2.47	0.22	0.02	0.7	0.18	2.7	3.58	2.8
TW020P64	2.47	0.22	0.02	0.7	0.18	2.7	3.58	2.8
TW020P68	2.47	0.22	0.02	0.7	0.18	2.7	3.58	2.8
TW020P79	2.47	0.22	0.02	0.7	0.18	2.7	3.58	2.8
TW020P82	2.47	0.22	0.02	0.7	0.18	2.7	3.58	2.8
TW020P87	2.47	0.22	0.02	0.7	0.18	2.7	3.58	2.8
TW020P91	2.47	0.22	0.02	0.7	0.18	2.7	3.58	2.8
TWA031PH	1.98	0.22	0.02	0.34	0.18	2.22	2.74	2.25
TWA031PL	1.98	0.22	0.02	0.34	0.18	2.21	2.74	2.25
TWA032PL	1.98	0.22	0.02	0.34	0.18	2.21	2.74	2.25
TWA142P	1.98	0.22	0.02	0.17	0.18	2.21	2.57	2.23
TWA28P	1.98	0.22	0.02	0.34	0.18	2.21	2.74	2.25
TWB142P	1.98	0.22	0.02	0.34	0.18	2.21	2.74	2.25
TWB28P	1.98	0.22	0.02	0.17	0.18	2.21	2.57	2.23
T-061E	0.63	0.22	0.02	0.09	-	0.86	0.95	0.87
T-062E	0.63	0.22	0.02	0.09	-	0.86	0.95	0.87
T-063E	0.63	0.22	0.02	0.09	-	0.86	0.95	0.87
T-064E	0.63	0.22	0.02	0.09	-	0.86	0.95	0.87
T-065E	0.63	0.22	0.02	0.09	-	0.86	0.95	0.87
T-062EA	0.63	0.22	0.02	0.09	-	0.86	0.95	0.87
T-063EA	0.63	0.22	0.02	0.09	-	0.86	0.95	0.87
T-064EA	0.63	0.22	0.02	0.09	-	0.86	0.95	0.87
T-064EB	0.63	0.22	0.02	0.09	-	0.86	0.95	0.87

TABLE E-4
TEMPERATURE ERRORS (Cont.)

Plant Code	ΔC $\pm(^{\circ}F)$	ΔPS $\pm(^{\circ}F)$	ΔLCH $\pm(^{\circ}F)$	ΔBV $\pm(^{\circ}F)$	ΔRJ $\pm(^{\circ}F)$	ΔI $\pm(^{\circ}F)$	Δ $\pm(^{\circ}F)$	σ $\pm(^{\circ}F)$
T-064EC	0.63	0.22	0.02	0.09	-	0.86	0.95	0.87
T-065EA	0.63	0.22	0.02	0.09	-	0.86	0.95	0.87
T-065EB	0.63	0.22	0.02	0.09	-	0.86	0.95	0.87
T-065EC	0.63	0.22	0.02	0.09	-	0.86	0.95	0.87
T-PLANT	0.45	0.22	0.02	0.09	-	0.68	0.77	0.68

TABLE E-5
LOAD CELL ERRORS

Plant Code	ΔC $\pm(\text{lb})$	ΔPS $\pm(\text{lb})$	ΔLCH $\pm(\text{lb})$	ΔBV $\pm(\text{lb})$	ΔI $\pm(\text{lb})$	Δ $\pm(\text{lb})$	σ $\pm(\text{lb})$
IF005P	6.61	0.42	0.74	4.94	7.78	12.71	9.22
IF030P	6.61	0.33	0.73	4.84	7.67	12.51	9.08
IF040P	6.61	0.33	0.74	4.93	7.69	12.61	9.13

TABLE E-6
FLOW RATE (VENTURI/ORIFICES) ERRORS

Plant Code	T1 (°F)	ΔT1 ±(°F)	P1 (psi)	ΔP1 ±(psi)	ρ (lb./ft. ³)	Δρ ±(lb./ft. ³)	E	ΔE	ΔPC ±(psi)	Δ(ΔPC) ±(psi)	σ(ΔPC) ±(psi)	σc (ft. ²)	Δσc ±(ft. ²)	ρσc ±(ft. ²)	Δ ±(lb./sec.)	σ ±(lb./sec.)
F-001BP	536	2.79	2248.332	6.237308	47.45983	0.18212	1	0	5.802147	0.015231	0.01233	0.000196	1.57E-06	9.83E-07	0.00249	0.001211
F-001BS	536	2.79	928.3435	3.191181	46.83488	0.025572	1	0	2.901073	0.005657	0.004207	0.000187	1.66E-06	1.08E-07	0.001777	0.00105
F-001A	77	2.574	2248.332	6.237308	62.61075	0.025572	1	0	4.35161	0.013635	0.011329	7.17E-05	3.43E-07	1.75E-07	0.000528	0.000224
F-003P	536	2.646	2248.332	6.237308	47.69995	0.165281	1	0	11.60429	0.043661	0.033755	0.037268	0.000372	0.000372	0.805888	0.605408
F-003P	536	2.646	2248.332	6.237308	47.69995	0.165281	1	0	0.870322	0.012039	0.008583	0.037268	0.000372	0.000372	0.295984	0.170238
F-014P	536	2.646	2248.332	6.237308	47.69995	0.165281	1	0	14.50537	0.034813	0.024639	0.000957	3.49E-06	2.06E-06	0.011285	0.004957
F-A00E	68	2.574	145.0537	6.237308	62.28892	0.021206	1	0	101.5376	0.227009	0.176309	9.10E-05	3.42E-07	2.34E-07	0.002487	0.001337
F-A01P	536	2.664	2262.837	6.237308	47.69995	0.165904	1	0	8.70322	0.016826	0.012785	0.011018	0.00011	0.00011	0.193516	0.154899
F-A01P	536	2.664	2262.837	6.237308	47.69995	0.165904	1	0	0.725268	0.003046	0.002647	0.011018	0.00011	0.00011	0.065953	0.050359
F-A01S	446	2.574	710.763	3.191181	51.72905	0.124116	1	0	36.26342	0.106469	0.087177	0.001759	1.18E-05	6.28E-06	0.047577	0.020264
F-A02P	536	2.646	2248.332	6.237308	47.69995	0.165281	1	0	0.725268	0.001451	0.001015	0.011018	0.00011	0.00011	0.061582	0.049913
F-A02P	536	2.646	2248.332	6.237308	47.69995	0.165281	1	0	8.70322	0.016826	0.012785	0.011018	0.00011	0.00011	0.193416	0.154882
F-A02S	500	2.628	710.763	3.191181	48.90993	0.150935	1	0	14.50537	0.05309	0.042125	0.005459	2.72E-05	2.06E-05	0.082522	0.042609
F-A03S	500	2.628	710.763	3.191181	48.90993	0.150935	1	0	14.50537	0.05309	0.042125	0.005476	3.15E-05	2.24E-05	0.090396	0.045543
F-A20A	86	2.574	1015.376	3.191181	62.29516	0.028067	1	0	14.50537	0.038294	0.027994	0.000129	5.77E-07	4.08E-07	0.001588	0.000875
F-A20E	68	2.574	710.763	3.191181	62.40119	0.019335	1	0	7.252683	0.019872	0.016101	0.000703	3.34E-06	1.57E-06	0.00638	0.002544
F-A40E	122	2.736	1160.429	6.237308	61.83798	0.044283	1	0	2.901073	0.005657	0.004207	0.000728	2.96E-06	1.94E-06	0.003581	0.001845
F-A60E	104	0.954	23.20859	N.A.	61.89349	0.013098	1	0	8.70322	0.016826	0.012785	0.000329	1.33E-06	8.71E-07	0.002665	0.001428
F-A80E	500	2.736	159.559	6.237308	49.39018	0.15343	1	0	43.5161	0.146214	0.122578	0.000338	1.10E-06	7.09E-07	0.00691	0.003163
F-B00E	68	2.574	145.0537	6.237308	62.28892	0.021206	1	0	101.5376	0.196548	0.1481	9.05E-05	3.65E-07	2.35E-07	0.002532	0.001322
F-B01P	536	2.844	2248.332	6.237308	47.6906	0.177131	1	0	8.70322	0.023354	0.018909	0.011018	0.00011	0.00011	0.201026	0.155683
F-B01P	536	2.844	2248.332	6.237308	47.6906	0.177131	1	0	0.725268	0.001451	0.001015	0.011018	0.00011	0.00011	0.062189	0.050017

N.A. = Not allowable

TABLE E-6
FLOW RATE (VENTURI/ORIFICES) ERROR: (Cont.)

Plant Code	T1 (°F)	ΔT1 ±(°F)	P1 (psi)	ΔP1 ±(psi)	ρ (lb./ft. ³)	Δρ ±(lb./ft. ³)	E	ΔE	ΔPC ±(psi)	Δ(ΔPC) ±(psi)	σ(ΔPC) ±(psi)	σc (ft. ²)	Δσc ±(ft. ²)	ρσc ±(ft. ²)	Δ ±(lb./sec.)	σ ±(lb./sec.)
F-B02P	536	2.664	2248.332	6.237308	47.69995	0.165904	1	0	8.70322	0.019002	0.01465	0.011018	0.00011	0.00011	0.195425	0.155026
F-B02P	536	2.664	2248.332	6.237308	47.69995	0.165904	1	0	0.725268	0.005222	0.004807	0.011018	0.00011	0.00011	0.071871	0.051528
F-B02S	500	2.628	710.763	3.191181	48.90993	0.150935	1	0	14.50537	0.031332	0.021485	0.005454	1.96E-05	1.04E-05	0.061256	0.025291
F-B03S	500	2.628	710.763	3.191181	48.90993	0.150935	1	0	14.50537	0.045837	0.034958	0.005471	2.20E-05	1.37E-05	0.070589	0.031377
F-B20A	86	2.574	1015.376	3.191181	62.29516	0.028067	1	0	14.50537	0.038294	0.027994	0.000125	6.63E-07	4.53E-07	0.001751	0.000961
F-B20E	68	2.574	710.763	3.191181	62.40119	0.019335	1	0	7.252683	0.01407	0.010577	0.000712	3.29E-06	1.52E-06	0.005926	0.002327
F-B40E	122	2.736	1160.429	6.237308	61.83798	0.044283	1	0	2.901073	0.005947	0.004497	0.000705	2.95E-06	1.87E-06	0.003576	0.001793
F-B60E	104	0.954	23.20859	N.A.	61.89349	0.013098	1	0	8.70322	0.0264	0.021758	0.000338	1.42E-06	7.59E-07	0.003084	0.001322
F-A04S	504.5	2.682	710.763	3.191181	1.548647	0.025572	N.C.	N.C.	N.V.	0.498259	0.419205	0.004629	4.63E-05	4.63E-05	N.C.	N.C.
F-B04S	504.5	2.628	710.763	3.191181	1.548647	0.025572	N.C.	N.C.	N.V.	0.498259	0.419205	0.004629	4.63E-05	4.63E-05	N.C.	N.C.

N.V. = Not valid

N.C. = Not calculated

N.A. = Not allowable

TABLE E-7
POWER CHANNEL ELECTRICAL MEASUREMENT ERRORS

Plant Code	VPC (V)	VDAS (V)	Δ VDAS \pm (V)	σ VDAS \pm (V)	Δ R1 \pm (W)	Δ R2 \pm (W)	J	Δ J	M.U.	Δ C \pm (M.U.)	Δ PS \pm (M.U.)	Δ LCH \pm (M.U.)	Δ I \pm (M.U.)	Δ BV \pm (M.U.)	Δ \pm (M.U.)	σ \pm (M.U.)
V-01P	99.916	3.122	0.00244	0.00244	9.38	290.6	32	0.186	V	-	-	-	-	0.00244	0.6594	0.586
V-01P	44.721	1.397	0.00244	0.00244	9.38	290.6	32	0.186	V	-	-	-	-	0.00244	0.338	0.271
V-01P	20.000	0.625	0.00244	0.00244	9.38	290.6	32	0.186	V	-	-	-	-	0.00244	0.194	1.140
I-01P	-	-	-	-	-	-	-	-	A	24	5	5.88	34.88	5.88	40.76	35.37
I-02P	-	-	-	-	-	-	-	-	A	24	5	5.88	34.88	5.88	40.76	35.37
I-03P	-	-	-	-	-	-	-	-	A	24	5	5.91	34.91	5.91	40.82	35.41
I-04P	-	-	-	-	-	-	-	-	A	24	5	5.91	34.91	5.91	40.82	35.41
I-05P	-	-	-	-	-	-	-	-	A	24	5	5.86	34.86	5.86	40.72	35.35
I-06P	-	-	-	-	-	-	-	-	A	62.3	35.2	14.86	112.36	14.86	127.22	113.34

TABLE E-8
PC POWER ERRORS

Plant Code	W (KW)	I1 (A)	I2 (A)	I3 (A)	I4 (A)	I5 (A)	I6 (A)	VDAS (V)	Δ VDAS \pm (V)	VPC (V)	Δ VPC \pm (V)	σ VPC \pm (V)	Δ \pm (KW)	σ \pm (KW)
W-00P	4991.6	7112	7112	7112	7112	7112	14400	3.122	0.00244	99.916	0.659	0.586	66.01	32.37
W-00P	1000	0	0	0	0	0	22360.5	1.398	0.00244	44.721	0.338	0.271	13.25	7.91
W-00P	200	0	0	0	0	0	10000	0.625	0.00244	20	0.194	0.140	4.48	2.66

TABLE E-9
PRESSURIZER, SG's, CMT's, IRWST LEVEL MEASUREMENT ERRORS

Plant Code	P (psi)	$\Delta(P)$ \pm (psi)	T (°F)	ΔT (°F)	ρ_v (lb/ft. ³)	$\Delta\rho_v$ \pm (lb/ft. ³)	ρ_L \pm (lb/ft. ³)	$\Delta\rho_L$ \pm (lb/ft. ³)	ΔP (psi)	$\Delta(\Delta P)$ \pm (psi)	$\sigma(\Delta P)$ \pm (psi)	h (ft.)	Δh \pm (ft.)	Δ \pm (ft.)	σ \pm (ft.)
L-010P	2248.33	6.24	652.57	-	6.365	0.029	36.992	0.049	9.617	0.079	0.055	20.361	0.03	0.463	0.265
L-060E	14.51	-	68	0.95	0	0	62.264	0.007	14.505	0.111	0.075	28.707	0.033	0.26	0.173
L-A10S	710.76	3.19	504.77	-	1.549	0.007	48.632	0.027	19.46	0.133	0.097	44.882	0.033	0.444	0.299
L-A20S	710.76	3.19	504.77	-	1.549	0.007	48.632	0.027	3.784	0.037	0.025	8.727	0.016	0.12	0.078
L-A40E	1160.43	6.24	122	3.06	2.651	0.016	61.838	0.049	8.848	0.077	0.054	20.407	0.03	0.205	0.132
L-B10S	710.76	3.19	504.77	-	1.549	0.007	48.632	0.027	19.46	0.132	0.097	44.882	0.033	0.44	0.298
L-B20S	710.76	3.19	504.77	-	1.549	0.007	48.632	0.027	3.784	0.051	0.035	8.727	0.016	0.164	0.098
L-B40E	1160.43	6.24	122	3.06	2.651	0.016	61.838	0.049	8.848	0.078	0.054	20.407	0.03	0.207	0.133

TABLE E-10
ACCUMULATOR'S LEVEL MEASUREMENT ERRORS

Plant Code	$\Delta(P)$ $\pm(\text{psf})$	$\Delta(T)$ $\pm(^{\circ}\text{F})$	$\Delta(TA)$ $\pm(\text{F})$	ρ_L $(\text{lb}/\text{ft.}^3)$	$\Delta\rho_L$ $\pm(\text{lb}/\text{ft.}^3)$	ρ_A $(\text{lb}/\text{ft.}^3)$	$\Delta\rho_A$ $\pm(\text{lb}/\text{ft.}^3)$	$\Delta\rho_{LC}$ $\pm(\text{lb}/\text{ft.}^3)$	ΔP_{inst} $\pm(\text{psf})$	$\Delta(\Delta P_{inst})$ $\pm(\text{psf})$	$\sigma(\Delta P_{inst})$ $\pm(\text{psf})$	h1 (ft.)	$\Delta h1$ $\pm(\text{ft.})$	Δ $\pm(\text{ft.})$	σ $\pm(\text{ft.})$
L-A20E	3.134	2.574	2.574	62.401	0.019	3.632	0.034	0.249	10.154	0.02	0.015	0.791	0.002	0.01	0.005
L-B20E	3.139	2.574	2.574	62.401	0.019	3.632	0.034	0.249	10.154	0.02	0.015	0.791	0.002	0.01	0.005

TABLE E-11
THERMOCOUPLE AMPLIFIER SHIFTS

Plant Code	TREF. (°F)	TMEAS. (°F)	SHIFT (°F)	TREF. (°F)	TMEAS. (°F)	SHIFT (°F)	TREF. (°F)	TMEAS. (°F)	SHIFT (°F)	TREF. (°F)	TMEAS. (°F)	SHIFT (°F)	TREF. (°F)	TMEAS. (°F)	SHIFT (°F)	TREF. (°F)	TMEAS. (°F)	SHIFT (°F)	DATE
T-A05P	121.5	116.9	4.5	282	279.9	2.1	390.6	388.8	1.8	515.7	513.9	1.8	622.8	621.6	1.2	748.4	748.3	0.1	09/14/94
T-A05S	121.5	117	4.4	282	276.6	5.4	390.6	386.5	4.1	515.7	510.7	4.9	622.8	617.5	5.3	748.4	742.9	5.5	09/14/94
T-A06P	121.5	116.1	5.7	282	277.4	4.6	390.6	387.3	3.3	515.7	512.6	3.1	622.8	620.3	2.5	748.4	746.7	1.7	09/14/94
T-A06S	121.5	116.5	4.9	282	279.1	3	390.6	387.9	2.6	515.7	513.4	2.2	622.8	621.1	1.7	748.4	747.6	0.8	09/14/94
T-A07S	121.5	118.2	3.2	282	279.5	2.5	390.6	389.4	1.2	515.7	514.7	1	622.8	622.3	0.4	748.4	748.9	-0.5	09/14/94
T-A08P	121.5	118.4	3	282	279.5	2.5	390.6	392.5	1	515.7	515.2	0.5	622.8	622.7	0.1	748.4	749.3	-0.9	09/14/94
T-A08S	121.5	117.9	3.6	282	278.5	3.5	390.6	388.4	2.2	515.7	513.9	1.8	622.8	621.5	1.3	748.4	747.4	1.0	09/14/94
T-A09P	121.5	118.5	3	282	278.6	3.4	390.6	388.4	2.2	515.7	513.7	2	622.8	621.2	1.5	748.4	747.1	1.3	09/14/94
T-022P	122	121.6	0.4	302	304.8	-2.8	392	396.3	-4.3	518	522.7	-4.7	626	630	-4	752	757.1	-5.1	09/30/94
T-023P	122	121.4	0.6	302	304.8	-2.8	392	395.8	-3.8	518	522.5	-4.5	626	630.9	-4.9	752	757.5	-5.5	09/30/94
T-024P	122	122	0	302	305.1	-3.1	392	395.9	-3.9	518	522.6	-4.6	626	631	-5	752	756.9	-4.9	09/30/94
T-025P	122	122.3	-0.3	302	305.6	-3.6	392	396.5	-4.5	518	523.6	-5.6	626	632	-6	752	757.6	-5.6	09/30/94
T-026P	122	120.8	1.2	302	303.7	1.7	392	394.6	2.6	518	521.6	-3.6	626	629.6	3.6	752	756.6	4.6	09/30/94
T-030P	122	122	0	302	304.8	-2.8	392	395.9	-3.9	518	522.8	-4.8	626	631.4	-5.4	752	757.5	-5.5	09/30/94
T-031P	122	121.3	0.7	302	303.9	-1.9	392	395	-3	518	521.9	-3.9	626	630.3	-4.3	752	757.3	-5.3	09/30/94
T-032P	122	121.2	0.8	302	303.8	-1.8	392	394.6	-2.6	518	521.2	-3.2	626	629.6	3.6	752	756.2	4.2	09/30/94
T-033P	122	119.3	2.7	302	300.9	1.1	392	392.6	-0.6	518	518.7	-0.7	626	627.1	-1.1	752	753.9	1.9	09/30/94
T-034P	122	119.9	2.1	302	302.4	-0.4	392	393.7	-1.7	518	520.2	-2.2	626	628.9	-2.9	752	756	49	09/14/94
T-035P	122	119.7	2.3	302	301.9	0.1	392	392.9	-0.9	518	519.7	-1.7	626	628	-2	752	754.5	-2.5	09/30/94
T-036P	122	119.4	2.6	302	301.9	0.1	392	392.7	-0.7	518	519.8	-1.8	626	628.1	-2.1	752	754.9	-2.9	09/30/94
T-040P	122	119.4	2.6	302	301.9	0.1	392	392.3	-0.3	518	519.7	-1.7	626	627.6	-1.6	752	754.3	-2.3	09/30/94
T-041P	122	118.7	3.3	302	301.3	0.9	392	391.7	0.3	518	518.9	-0.9	626	626.9	0.9	752	753.7	1.7	09/30/94
T-042P	122	119.4	2.6	302	301.7	0.3	392	391.8	0.2	518	518.9	-0.9	626	626.6	-0.6	752	753.4	1.4	09/30/94

TABLE E-11
THERMOCOUPLE AMPLIFIER SHIFTS (°C/°F)

Plant Code	TREF. (°F)	TMEAS. (°F)	SHIFT (°F)	TREF. (°F)	TMEAS. (°F)	SHIFT (°F)	TREF. (°F)	TMEAS. (°F)	SHIFT (°F)	TREF. (°F)	TMEAS. (°F)	SHIFT (°F)	TREF. (°F)	TMEAS. (°F)	SHIFT (°F)	TREF. (°F)	TMEAS. (°F)	SHIFT (°F)	TREF. (°F)	TMEAS. (°F)	SHIFT (°F)	DATE
T-040P	122	119.5	2.5	302	303.8	0.2	392	392.1	-0.1	518	519	-1	626	626.9	-0.9	752	753.4	-1.4	880	880.904		09/14/04
T-040S	121.5	121.7	-0.2	282	283.4	-1.4	390.6	393.7	-3.2	515.7	518.9	-3.2	622.8	626.6	-3.8	748.4	754.6	-6.2	876	881.404		09/14/04
T-040S	121.5	122.1	-0.6	282	283.8	-1.8	390.6	393.6	-3.1	515.7	519.4	-3.8	622.8	627.7	-4.9	748.4	754.1	-5.7	876	881.404		09/14/04
T-040P	121.5	122.6	-1.2	282	284.4	-2.4	390.6	394.3	-3.7	515.7	519.7	-4.1	622.8	628.2	-5.5	748.4	754.5	-6.1	876	881.404		09/14/04
T-040S	121.5	122.5	-0.8	282	284.3	-2.3	390.6	394.2	-3.6	515.7	520	-4.3	622.8	629.5	-6.8	748.4	754.5	-6.1	876	881.404		09/14/04
T-040P	121.5	122.4	-1	282	284.3	-2.3	390.6	393.9	-3.3	515.7	519.7	-4.1	622.8	627.7	-5	748.4	753.8	-5.4	876	881.404		09/14/04
T-040S	121.5	122.6	-1.2	282	284.2	-2.2	390.6	394	-3.4	515.7	520	-4.3	622.8	627.9	-5.2	748.4	754.2	-5.8	876	881.404		09/14/04
T-040S	121.5	122.5	-1.1	282	284.8	-2.8	390.6	394.4	-3.8	515.7	520.4	-4.7	622.8	628.5	-5.8	748.4	754.8	-6.4	876	881.404		09/14/04
T-040S	121.5	122.7	-1.4	282	284.8	-2.8	390.6	394.5	-3.9	515.7	520.1	-4.4	622.8	628.3	-5.6	748.4	754.4	-6	876	881.404		09/14/04
T-A01FV0	121.5	119.2	2.3	282	281.4	0.6	385.9	386.2	-0.4	515.7	516.2	-0.5	622.8	623.4	-0.7	748.4	750.7	-2.3	876	881.404		09/14/04
T-A02BPL	121.5	120.1	1.3	282	282	0	385.9	386.8	-1	515.7	517.3	-1.6	622.8	625	-2.2	748.4	751.8	-3.4	876	881.404		09/14/04
T-A02BFO	121.5	120	1.5	282	282.4	-0.4	385.9	387.2	-1.3	515.7	518.1	-2.4	622.8	625.1	-2.4	748.4	752.8	-4.4	876	881.404		09/14/04
T-040P	121.5	119.3	2.1	282	281.6	0.5	385.9	386.3	-0.4	515.7	516.9	-1.2	622.8	624.5	-1.7	748.4	751.5	-3.1	876	881.404		09/14/04
T-A02S	121.5	120.2	1.3	282	282.2	-0.2	385.9	387	-1.1	515.7	517.3	-1.7	622.8	624.9	-2.2	748.4	751.7	-3.3	876	881.404		09/14/04
T-A00S	121.5	121	0.4	282	283.3	-1.3	385.9	388.1	-2.2	515.7	518.7	-3	622.8	626.3	-3.5	748.4	753	-4.6	876	881.404		09/14/04
T-A00P	121.5	120.9	0.6	282	282.8	-0.8	385.9	387.2	-1.3	515.7	517.8	-2.1	622.8	625.6	-2.8	748.4	752.1	-3.7	876	881.404		09/14/04
T-A00S	121.5	121	0.5	282	283	-1	385.9	387.2	-1.4	515.7	517.8	-2.1	622.8	625.7	-3	748.4	752.1	-3.7	876	881.404		09/14/04
T-A00S	121.5	121.5	-0.1	282	283.2	-1.2	390.6	392.8	-2.2	515.7	517.7	-2.1	622.8	625.4	-2.6	748.4	752.2	-3.8	876	881.404		09/14/04
T-A10P	121.5	120.2	1.2	282	282.1	-0.1	390.6	391.7	-1.1	515.7	517.2	-1.5	622.8	624.9	-2.2	748.4	751.6	-3.2	876	881.404		09/14/04
T-A11P	121.5	119.5	1.9	282	281.5	0.5	390.6	390.9	-0.3	515.7	516.5	-0.8	622.8	624.4	-1.6	748.4	750.8	-2.4	876	881.404		09/14/04
T-A141P	121.5	121.5	-0.1	282	283.3	-1.3	390.6	393.1	-2.5	515.7	518.8	-3.1	622.8	626.8	-4	748.4	753.5	-5.1	876	881.404		09/14/04
T-A142PH	121.5	118.5	2.9	282	280.1	1.9	390.6	389.7	0.9	515.7	515.2	0.5	622.8	622.9	-0.2	748.4	749.4	-1	876	881.404		09/14/04
T-A143P	121.5	121.2	0.3	282	283.1	-1.1	390.6	392.8	-2.2	515.7	518.4	-2.8	622.8	626.1	-3.3	748.4	752.7	-4.3	876	881.404		09/14/04
T-A020A	121.5	120.2	1.3	282	282.2	-0.2	390.6	392	-1.5	515.7	517.7	-2	622.8	625.3	-2.5	748.4	751.9	-3.5	876	881.404		09/14/04
T-020P	121.5	121.2	0.2	282	283.3	-1.3	390.6	393.1	-2.6	515.7	518.7	-3.1	622.8	626.7	-3.9	748.4	752.9	-4.5	876	881.404		09/14/04

TABLE E-11
THERMOCOUPLE AMPLIFIER SHIFTS (CONT.)

Plant Code	TREF. (°F)	TMEAS. (°F)	SHIFT (°F)	TREF. (°F)	TMEAS. (°F)	SHIFT (°F)	TREF. (°F)	TMEAS. (°F)	SHIFT (°F)	TREF. (°F)	TMEAS. (°F)	SHIFT (°F)	TREF. (°F)	TMEAS. (°F)	SHIFT (°F)	TREF. (°F)	TMEAS. (°F)	SHIFT (°F)	DATE
T-040P	121.5	122	-0.6	282	284.2	-2.2	385.9	393.1	-3.2	515.7	519.3	-3.7	622.8	627.5	-4.7	748.4	753.5	-5.1	9/16/94
T-045P	121.5	121.1	0.3	282	283.2	-1.2	385.9	388	2.1	515.7	518.7	-3	622.8	626.2	-3.5	748.4	752.8	-4.4	9/16/94
T-060P	121.5	121.2	0.2	282	283.5	-1.5	385.9	388.6	2.7	515.7	519.7	-4	622.8	627.2	-4.5	748.4	754	-5.6	9/16/94
T-A011P	121.5	120.9	0.5	282	283.3	-1.3	385.9	388.3	2.4	515.7	519.2	-3.5	622.8	626.8	-4	748.4	751.6	-3.2	9/16/94
T-A012P	121.5	120.3	1.2	282	282.4	0.4	385.9	387.2	1.3	515.7	517.7	-2	622.8	625.2	-2.5	748.4	751.7	-5.3	9/16/94
T-A01P	121.5	120.8	0.7	282	283	-1	385.9	387.8	1.9	515.7	518.4	-2.8	622.8	626	-3.3	748.4	752.5	-4.1	9/16/94
T-A015	121.5	120.9	0.5	282	283.2	-1.2	385.9	387.8	1.9	515.7	518.3	-2.6	622.8	626	-3.2	748.4	751.4	-4	9/16/94
T-A02E	121.5	90.8	30.6	282	251	31	385.9	353.3	32.6	515.7	482.5	33.2	622.8	590.3	32.7	748.4	715.5	32.9	9/16/94
T-B012P	121.5	121.7	-0.2	282	282.3	-0.3	390.6	392	-1.4	515.7	516.8	-1.1	622.8	624.3	-1.5	748.4	750.4	-2	9/16/94
T-B01P	121.5	122.3	-0.9	282	283.1	-1.1	390.6	392.3	-1.8	515.7	517.6	-1.9	622.8	625.2	-2.4	748.4	750.4	-2	9/16/94
T-B015	121.5	122.2	-0.7	282	283.1	-1.1	390.6	392.3	-1.7	515.7	517.4	-1.7	622.8	624.9	-2.1	748.4	750.6	-2.2	9/16/94
T-B021PL	121.5	120.5	0.9	282	280.8	1.2	390.6	393.5	-1.1	515.7	514.3	1.4	622.8	621.6	1.2	748.4	746.8	1.6	9/16/94
T-B021PO	121.5	121.6	-0.1	282	282.7	-0.7	390.6	391.9	1.3	515.7	517.3	-1.6	622.8	624.8	-2	748.4	750.8	-2.4	9/16/94
T-B022PL	121.5	121.7	-0.2	282	282.5	-0.5	390.6	391.9	-1.3	515.7	517.1	-1.5	622.8	624.5	-1.7	748.4	750.5	-2.1	9/16/94
T-B022PO	121.5	121.8	-0.3	282	282.7	-0.7	390.6	391.9	-1.4	515.7	517	-1.4	622.8	624.6	-1.9	748.4	750.7	-2.3	9/16/94
T-B03PO	121.5	121.4	0	282	282.2	-0.2	390.6	391.2	-0.6	515.7	516.3	-0.6	622.8	623.6	-0.8	748.4	751.3	-2.9	9/16/94
T-022P	122	119.4	2.6	302	303	-1	392	393.7	1.7	518	520.8	-2.8	626	629.3	-3.3	752	757.2	-5.2	9/30/94
T-003P	122	118.9	3.2	302	302.3	-0.3	392	393.1	-1.1	518	520.2	-2.2	626	628.7	-2.7	752	756.1	-4.1	9/30/94
T-004P	122	119.1	2.9	302	302.2	-0.2	392	393	-1	518	519.9	-1.9	626	628.6	-2.6	752	755.9	-3.9	9/30/94
T-001P	122	119.4	2.6	302	302.5	-0.5	392	393.7	-1.7	518	520.5	-2.5	626	629	-3	752	756.1	-4.1	9/30/94
T-B22E	122	120.8	1.2	302	303.5	-1.5	392	394.4	2.4	518	521.3	-3.3	626	629.9	-3.9	752	756.8	-4.8	9/30/94
T-A22E	122	120.2	1.8	302	303.3	-1.3	392	394.1	-2.1	518	521	-3	626	629.6	-3.6	752	756.7	-4.7	9/30/94
T-A00E	122	120.5	1.5	302	304.1	-2.1	392	395.3	-3.1	518	522.2	-4.2	626	631.1	-5.1	752	756.1	-4.1	9/30/94
T-001PH	122	121.1	0.9	302	304.1	-2.1	392	395	-3	518	522.1	-4.1	626	630.5	-4.5	752	757.6	-5.6	9/30/94
T-A031PL	121.5	121	0.4	282	283.4	-1.4	390.6	393.4	-2.9	515.7	519.3	-3.4	622.8	626.8	-4.1	748.4	753.1	-4.7	9/16/94

TABLE E-11
THERMOCOUPLE AMPLIFIER SHIFTS (Cont.)

Plant Code	TREF. (°F)	TMEAS. (°F)	SHIFT (°F)	TREF. (°F)	TMEAS. (°F)	SHIFT (°F)	TREF. (°F)	TMEAS. (°F)	SHIFT (°F)	TREF. (°F)	TMEAS. (°F)	SHIFT (°F)	TREF. (°F)	TMEAS. (°F)	SHIFT (°F)	TREF. (°F)	TMEAS. (°F)	SHIFT (°F)	DATE
T-A039A	121.5	122.5	1	282	284.2	2.2	390.6	393.5	3	515.7	519.4	3.7	622.8	627.2	4.4	748.4	752.6	4.2	9/14/94
T-B039L	121.5	121.9	-0.5	282	283.7	1.7	390.6	393.3	2.7	515.7	519.3	3.7	622.8	626.8	4.1	748.4	752.8	4.4	9/14/94
T-B039R	121.5	123	1.5	282	285.2	3.2	390.6	394.9	4.4	515.7	520.7	5	622.8	628.8	6	748.4	752.2	3.8	9/14/94
T-A142P	121.5	124.3	2.8	282	284.7	2.7	390.6	394.1	3.5	515.7	519.6	4	622.8	627.7	4.9	748.4	753.3	4.9	9/14/94
T-B142P	121.4	122.1	0.6	282	284.6	2.6	390.6	394.3	3.7	515.7	519.7	4.1	622.8	627.5	4.8	748.4	753.3	4.9	9/14/94
T-A039O	121.4	122.1	0.6	282	284.3	2.3	390.6	393.7	3.2	515.7	519.5	3.8	622.8	627.4	4.6	748.4	753.6	5.2	9/14/94
T-A039L	121.5	122.4	1	282	284.5	2.5	390.6	394	3.5	515.7	520	4.3	622.8	627.6	4.8	748.4	753.8	5.4	9/14/94
T-0001P	121.5	120.4	1.1	282	282.7	0.7	385.9	387.7	1.8	515.7	518.4	2.7	622.8	625.9	3.2	748.4	753.1	4.7	9/14/94
T-A21E	121.5	121.2	0.3	282	283.4	1.4	385.9	388.1	2.2	515.7	519.1	3.4	622.8	626.4	3.6	748.4	753.5	5.1	9/14/94
T-A23E	121.5	121.8	0.4	282	284.2	2.2	385.9	388.9	3	515.7	519.9	4.2	622.8	627	4.3	748.4	754.4	6	9/14/94
T-A55E	121.5	120.7	0.7	282	282.9	0.9	385.9	388	2.2	515.7	519	3.4	622.8	626	3.2	748.4	753.4	5	9/14/94
T-B09E	121.5	121.2	0.3	282	283.4	1.4	385.9	388.6	2.8	515.7	518.5	3.8	622.8	626.6	3.8	748.4	753.9	5.5	9/14/94
T-B02E	121.5	121.1	0.4	282	282.1	0.1	385.9	386.8	0.9	515.7	517.6	1.9	622.8	624.5	1.8	748.4	751.5	3.1	9/14/94
T-B21E	121.5	121.6	0.1	282	283.5	1.5	385.9	388.2	2.3	515.7	519	3.4	622.8	626.2	3.4	748.4	753.1	4.7	9/14/94
T-B07P	121.5	122.8	1.3	282	284.4	2.4	390.6	394.3	3.8	515.7	520	4.4	622.8	628.2	5.4	748.4	754	5.6	9/14/94
T-B07S	121.5	121.9	0.5	282	283.9	1.9	390.6	393.5	3	515.7	519.4	3.7	622.8	627.5	4.8	748.4	753.3	4.9	9/14/94
T-B08P	121.5	122.9	1.4	282	284.2	2.2	390.6	393.8	3.2	515.7	519.5	3.9	622.8	627.6	4.8	748.4	753.1	4.7	9/14/94
T-B08S	121.5	126	4.5	282	285.4	4.4	390.6	396.6	6	515.7	522.3	6.6	622.8	630.5	7.7	748.4	753.1	4.7	9/14/94
T-B09P	121.5	122.8	1.4	282	285	3	390.6	394.8	4.2	515.7	520.0	4.2	622.8	628.8	6	748.4	753.5	7.1	9/14/94
T-B09S	121.5	123.6	2.1	282	285.1	3.1	390.6	395.1	4.5	515.7	520.6	4.9	622.8	628.5	5.7	748.4	754.5	6.1	9/14/94
T-B10P	121.5	124.2	2.7	282	287.1	5.1	390.6	397.4	6.8	515.7	523.6	7.9	622.8	631.5	8.8	748.4	757.9	9.5	9/14/94
T-B11P	121.5	123.5	2	282	286.1	4.1	390.6	395.9	5.3	515.7	521.7	6	622.8	629.8	7	748.4	756.1	7.7	9/14/94
T-B21E	121.5	127.8	6.4	282	301.3	19.3	385.9	411.9	26	515.7	552.1	36.4	622.8	666.5	43.8	748.4	800.7	52.3	9/14/94
T-B06E	121.5	121	0.4	282	280.9	1.1	385.9	382.7	3.2	515.7	513	2.6	622.8	619.6	3.1	748.4	744.1	4.3	9/14/94
TW-064P	120.3	120.3	1.2	282	279.9	2.1	385.9	382.6	3.3	515.7	512.7	2.9	622.8	619.5	3.3	748.4	744.1	4.3	9/14/94

TABLE E-11
THERMOCOUPLE AMPLIFIER SHIFTS (Cont.)

Plant Code	TREF. (°F)	TMEAS. (°F)	SHIFT (°F)	TREF. (°F)	TREF. (°F)	SHIFT (°F)	TREF. (°F)	TREF. (°F)	SHIFT (°F)	TMEAS. (°F)	TREF. (°F)	SHIFT (°F)	TMEAS. (°F)	TREF. (°F)	SHIFT (°F)	TMEAS. (°F)	TREF. (°F)	SHIFT (°F)	DATE
TW-001P	121.5	123.8	2.4	282	284.1	2.1	385.9	386.3	-0.5	515.7	516.2	-0.5	622.8	623.1	-0.3	748.4	747.8	0.6	9/14/94
T-003PL	121.5	120.5	1	282	280	2	385.9	381.8	4.1	515.7	511.8	3.9	622.8	618.4	4.4	748.4	742.8	5.6	9/14/94
T-005PH	121.5	121.1	0.3	282	280.5	1.5	385.9	382.3	3.6	515.7	512.5	3.2	622.8	619.4	3.4	748.4	744.7	3.7	9/14/94
T-015P	121.5	120.3	1.2	282	279.1	2.9	385.9	380.3	5.6	515.7	510	5.6	622.8	616.1	6.6	748.4	740.4	8	9/14/94
TWB142PL	121.5	120.1	1.4	282	279.4	2.6	385.9	381.7	4.2	515.7	511.4	4.2	622.8	618.5	4.3	748.4	742.7	5.7	9/14/94
TW-002P	122	121.1	0.9	302	301.5	0.5	392	391.4	0.6	518	516.9	1.1	626	623.9	2.1	752	749.7	2.3	9/30/94
TW-003P	122	119.4	2.6	302	298.6	3.4	392	387.3	4.7	518	512.4	5.6	626	617.6	8.4	752	742.2	9.8	9/30/94
TW-005P	122	120.3	1.7	302	302.6	-0.6	392	392.3	-0.3	518	518.5	-0.5	626	624.8	1.2	752	750.6	1.4	9/30/94
TW-006P	122	121.6	0.4	302	303.6	-1.6	392	393.2	-1.2	518	518.5	-0.5	626	625.4	0.6	752	751	1	9/30/94
TW-007P	122	120.5	1.5	302	303.7	-1.7	392	393.2	-1.2	518	520	2	626	627.5	-1.5	752	757.2	1.2	9/30/94
TW-008P	122	119.6	2.4	302	301.8	0.2	392	391.5	0.5	518	517.7	0.3	626	624	2	752	749.8	2.2	9/30/94
T-B401E	77	51.8	25.2	482	374.3	107.7	(*)												
T-B402E	77	51.8	25.2	482	374.3	107.7	(*)												
T-B403E	77	51.8	25.2	482	374.3	107.7	(*)												
T-B404E	77	51.8	25.2	482	374.3	107.7	(*)												
T-B405E	77	51.8	25.2	482	374.3	107.7	(*)												
T-B406E	77	51.8	25.2	482	374.3	107.7	(*)												
T-B407E	77	51.8	25.2	482	374.3	107.7	(*)												
T-B408E	77	51.8	25.2	482	374.3	107.7	(*)												
T-B409E	77	51.8	25.2	482	374.3	107.7	(*)												
T-B410E	77	51.8	25.2	482	374.3	107.7	(*)												
T-B411E	77	51.8	25.2	482	374.3	107.7	(*)												
T-B412E	77	51.8	25.2	482	374.3	107.7	(*)												
T-B413E	77	51.8	25.2	482	374.3	107.7	(*)												
T-B414E	77	51.8	25.2	482	374.3	107.7	(*)												
T-B415E	77	51.8	25.2	482	374.3	107.7	(*)												
T-B416E	77	51.8	25.2	482	374.3	107.7	(*)												
T-B417E	77	51.8	25.2	482	374.3	107.7	(*)												
T-B418E	77	51.8	25.2	482	374.3	107.7	(*)												
T-B419E	77	51.8	25.2	482	374.3	107.7	(*)												
T-B420E	77	51.8	25.2	482	374.3	107.7	(*)												

(*) Test S00504 and S00605 only

**APPENDIX F
FULL-HEIGHT FULL-POWER
INTEGRAL SYSTEMS TEST
DELTA-P INSTRUMENTATION DATA REDUCTION**

F-1 Abstract

The differential pressure (dP) instrumentation in the SPES-2 test facility, in many cases, is used to determine component water levels and to measure dPs due to flow loss. This document is a guide for using the SPES-2 dP instrumentation data in order to separately determine both flow loss dP and fluid level portions of total measured dP, and to determine the void fraction of a two-phase fluid when boiling and flashing occur in the components during testing.

F-2 Introduction

In order to use the data from the SPES dP instrumentation, it is necessary to understand the arrangement of the dP cells, to account for the tap-to-tap elevation differences, and to compensate for fluid densities. With this understanding, the dP cell data can be used to obtain the dP due to friction losses and to measure level at low or no-flow conditions when the component friction loss due to flow is approximately 0.

The following sections provide a description of each type of dP cell installation used at SIET, a description of how the raw data should be processed, a list of the dP instruments, and the appropriate temperature instrument(s) that should be used in determining the density of fluid(s).

See Appendix F-7 for a summary of results.

F-3 Type 1 dP Cells

F-3.1 Installation and Offsets

The installation/characteristics of type 1 dP cells are as follows:

- The normal direction of flow is in the UP vertical direction, and the negative (low-pressure) side of the dP cell is the upper tap.

This causes flow losses to increase the measured dP since flow is from the positive (lower) tap to the negative (upper) tap.

- The data acquisition system (DAS) adds the tap-to-tap elevation difference to the dP at the instrument taps, converting this height to force (psi) using the following equation:

$$\rho_{wc}gh/144g_c$$

where:

- ρ_{wc} = density of cold water at ambient conditions (62.2 lbs_m/ft.³)
- g = acceleration due to gravity (32.2 ft./sec.²)
- h = tap-to-tap elevation difference (ft.)
- g_c = mass to force conversion (32.2 ft. - lb_m/sec.² - lb_f)

F-3.2 Friction Loss Determination

The friction loss portion of the measured dP when the component is full of water is calculated as follows:

$$\text{Recorded dP data (psid)} = \text{dP at instrument} + \rho_{wc}gh/144 g_c$$

where the dP at the instrument equals the (positive tap pressure) minus (negative tap pressure). That is,

$$\text{dP at instrument} = (\text{friction loss} + \rho_{wh}gh/144 g_c) - (\rho_{wc}gh/144 g_c)$$

where:

ρ_{wh} is the density of the hot process water in the component which must be determined based on the existing system pressure and the temperature of the water.

Since the DAS adds $\rho_{wc}gh/144 g_c$, then

$$\text{Recorded dP data (psid)} = \text{friction loss (psid)} + \rho_{wh}gh/144 g_c$$

and:

$$\text{Friction loss (psid)} = \text{recorded dP data (psid)} - \rho_{wh}gh/144 \text{ g}_c$$

F-3.3 Component Water Level Determination

The water level that exists between the dP cell taps can be calculated from the recorded dP data when the friction loss is negligible or when the flow is 0. This is done as follows:

$$\text{Recorded dP data (psid)} = \rho_{wh}Lg/144 \text{ g}_c + \rho_s (h - L) g/144 \text{ g}_c$$

where:

L = water level of water (ft.)

ρ_s = density of steam

This numerically reduces to the following:

$$L = [(144) (\text{dP data}) - (\rho_s h)] / (\rho_{wh} - \rho_s)$$

This level can be converted to percent level using the following:

$$\% \text{ level} = (L/h) * 100\%$$

The density of steam (ρ_s) can be ignored (assumed 0) in the above equation, with less than 1% error introduced, when system pressure is less than 500 psia.

Table F-1, provides a listing of dP instruments that operate as described above. Also listed are the pressure and temperature instrument(s) that should be used to determine ρ_{wh} and ρ_s in the above equations.

F-4 Type 2 dP Cells

F-4.1 Installation and Offsets

The installation/characteristics of type 2 cells are as follows:

- The normal direction of flow is in the DOWN vertical direction, and the negative (low-pressure) side of the dP cell is the bottom tap.

This causes flow losses to increase the measured dP since flow is from the positive (upper) tap to the negative (lower) tap.

- The DAS subtracts the tap-to-tap elevation difference from the dP at the instrument taps, converting this height to force (psi) using the following equation

$$\rho_{wc}gh/144 g_c$$

F-4.2 Friction Loss Determination

The friction loss portion of the measured dP when the component is full of water is calculated as follows:

$$\text{Recorded dP data (psid)} = \text{dP at instrument} - \rho_{wh}gh/144 g_c$$

where the dP at instrument equals (positive tap pressure) minus (negative tap pressure). That is,

$$\text{dP at instrument} = (\text{Friction loss} + \rho_{wc}gh/144 g_c) - (\rho_{wh}gh/144 g_c)$$

Since the DAS subtracts $\rho_{wc}gh/144 g_c$, then

$$\text{Recorded dP data (psid)} = \text{friction loss (psid)} - \rho_{wh}gh/144 g_c$$

and:

$$\text{Friction loss (psid)} = \text{recorded dP data (psid)} + \rho_{wh}gh/144 g_c$$

F-4.3 Component Water Level Determination

The water level that exists between the dP cell taps can be calculated from the recorded dP cell data when flow is approximately 0 (friction losses are 0 or negligible). This is done as follows:

$$\text{Recorded dP data (psid)} = \rho_{wc}gh/144 g_c - (\rho_{wh}gL/144 g_c + \rho_w g (h - L)/144 g_c) - \rho_{wc}gh/144 g_c$$

This numerically reduces to the following:

$$L = [(144) (\text{dP data}) + (\rho_s h)] / (\rho_s - \rho_{wh})$$

As stated above, ρ_s can be assumed to be 0 when system pressure is less than 500 psia.

This level can be converted to percent level using the following:

$$\% \text{ level} = (L/h) * 100\%$$

Table F-2 lists the dP instruments that operate as described above. Also listed are the pressure and temperature instrument(s) that should be used to determine ρ_{wh} and ρ_s in solving above equations.

F-5 Type 3 dP Cells

F-5.1 Installation and Offsets

The instrumentation/characteristics of type 3 dP cells are as follows:

- The positive (high-pressure) side of the dP cell is connected to the upper tap.
- The DAS adds the tap to tap elevation difference converting this height of water to force (psi) using the following equation:

$$\rho_{wc}gh/144 g_c$$

F-5.2 Friction Loss Determination

The friction loss portion of the measured dP when the component is full of water is calculated as follows:

$$\text{Recorded dP data (psid)} = \text{dP at instrument} + \rho_{wc}gh/144 g_c$$

Where the dP at the instrument equals the positive tap pressure minus the negative tap pressure. That is,

$$\text{dP at instrument} = (\text{Friction loss} + \rho_{wc}gh/144 g_c) - \rho_{wh}gh/144 g_c$$

Since the DAS adds $\rho_{wc}gh/144 g_c$, then

$$\text{Recorded dP data (psid)} = \text{friction loss (psid)} - \rho_{wh}gh/144 g_c + 2\rho_{wc}gh/144 g_c$$

and:

$$\text{Friction loss (psid)} = \text{recorded dP data (psid)} - 2\rho_{wc}gh/144 g_c + \rho_{wh}gh/144 g_c$$

F-5.3 Component Water Level Determination

The water level that exists between the dP cell taps can be calculated from the recorded dP data when the friction loss is negligible (when flow is approximately 0). This is done as follows:

$$\text{Recorded dP data} = \rho_{wc}gh/144 g_c - (\rho_{wh}gL/144 g_c + \rho_s (h - L) g/144 g_c) + \rho_{wc}gh/144 g_c$$

This numerically reduces to the following:

$$L = [(144) (\text{dP data}) + h(\rho_s - 2\rho_{wc})] / (\rho_s - \rho_{wh})$$

As stated above, ρ_s can be assumed to be 0 when system pressure is less than 500 psia. Also, this level can be converted to percent level using the following:

$$\% \text{ level} = (L/h) * 100\%$$

Table F-3, lists dP instruments that operate as described above. Also listed are the pressure and temperature instruments that should be used to determine ρ_{wh} and ρ_s used in the above equations.

F-6 Type 4 dP Cells

F-6.1 Installation and Offsets

The installation/characteristics of the type 4 dP cells are as follows:

- The positive (high-pressure) side of the dP cell is connected to the upper tap.
- No tap to tap elevation difference is added by the DAS.
- No significant flow or flow losses through the component are expected.

F-6.2 Friction Loss Determination

No friction losses are expected.

F-6.3 Component Water Level Determination

The water level that exists between the dP cell taps can be calculated from the measured dP data when the friction loss is negligible (for example, in large components such as tanks where level changes are relatively slow). Since the DAS does not add any compensation for tap elevations, then

$$\text{Recorded dP data} = \rho_{wc}gh/144g_c - (\rho_{wh}gL/144g_c + \rho_s(h - L)g/144g_c)$$

This numerically reduces to the following:

$$L = [(144) (\text{dP data}) + h(\rho_s - \rho_{wc})] / (\rho_s - \rho_{wh})$$

As stated above, ρ_s can be assumed to be 0 when system pressure is less than 500 psia. Also, level can be converted to percent level using

$$\% \text{ level} = (L/h) * 100\%$$

Table F-4 lists the dP instruments that operate as described above. Also listed are the pressure and temperature instruments that should be used to determine ρ_{wh} and ρ_s used in the above equations.

F-7 Conclusion/Summary

The following equations have been derived for calculating the friction loss (in psi) from the dP data measured for the SPES-2 tests. These equations (numerically reduced) are as follows:

- Type 1 dP cells : friction loss = dP data - $\rho_{wh}h/144$
- Type 2 dP cells : friction loss = dP data + $\rho_{wh}h/144$
- Type 3 dP cells : friction loss = dP data + $h(\rho_{wh} - 2\rho_{wc})/144$
- Type 4 dP cells : no friction loss is expected

The following equations have been derived for calculating the water level (in ft. H₂O) from the dP data (in psi) measured for the SPES-2 tests.

These equations (numerically reduced) are as follows:

- Type 1 dP cells : water level = $[(144) (\text{dP data}) - (\rho_s h)] / (\rho_{wh} - \rho_s)$
- Type 2 dP cells : water level = $[(144) (\text{dP data}) + (\rho_s h)] / (\rho_s - \rho_{wh})$
- Type 3 dP cells : water level = $[(144) (\text{dP data}) + h(\rho_s - 2\rho_{wc})] / (\rho_s - \rho_{wh})$
- Type 4 dP cells : water level = $[(144) (\text{dP data}) + h(\rho_s - \rho_{wc})] / (\rho_s - \rho_{wh})$

TABLE F-1
SPES-2, AP600 FULL-HEIGHT FULL-POWER INTEGRAL SYSTEMS TEST
SPES-2 TYPE 1 DP-TRANSMITTERS

Tag No.	Location	Upper Tap (+/-)	Tap Elev. Differ. (ft.)	Instrument Range (psi)	dP Meas. Range (psi)	Level Meas. Range (ft.)	Reference Temp. Instrument(s)	Reference Pressure (Note 1)
DP-000P	Power channel riser (overall)	-	17.41	-8.70 to +8.70	-1.16 to +16.24	0 to 17.41	$\frac{T003P + T015P}{2}$	
DP-011P	Power channel riser (bottom)	-	4.86	0 to +4.35	+2.10 to +6.45	0 to 4.86	T003P	
DP-012P	Power channel riser (bottom middle)	-	3.64	0 to 5.80	+1.58 to +7.38	0 to 3.64	$\frac{T003P + T015P}{2}$	
DP-013P	Power channel riser (top middle)	-	3.64	0 to 5.08	+1.58 to +6.65	0 to 3.64	$\frac{T003 + T015P}{2}$	
DP-014P	Power channel riser (top)	-	2.84	-1.45 to +1.45	-0.19 to +2.71	0 to 2.84	T015P	
DP-018P	Hot leg-A/surge line	-	2.95	-1.45 to +1.45	-0.17 to +2.73	0 to 2.95	T018P	
DP-A04P	Hot leg-A	-	11.82	-5.80 to +8.70	-0.68 to +13.82	0 to 11.82	TA03P0	
DP-B04P	Hot leg-B	-	11.82	-5.80 to +8.70	-0.68 to +13.82	0 to 11.82	TB03P0	
DP-A05P	U-tube steam generator-A (hot-leg side)	-	16.82	-8.70 to +17.40	-1.41 to +24.69	0 to 16.82	$\frac{TA06P + TA05P}{2}$	PA04P
DP-B05P	U-tube steam generator-B (hot-leg side)	-	16.82	-8.70 to +17.40	-1.41 to +24.69	0 to 16.82	$\frac{TB05P + TB06P}{2}$	PB04P
DP-A06P	U-Tube steam generator-A (Hot-leg side to top)	-	12.30	-5.80 to +8.70	-0.47 to +14.03	0 to 12.30	$\frac{TA06P + TA08P}{2}$	PA04P
DP-B06P	U-tube steam generator-B (HL Side to top)	-	12.30	-5.80 to +8.70	-0.47 to +14.03	0 to 12.30	$\frac{B06P + TB08P}{2}$	PB04P
DP-A15P	Power channel upper plenum/hot leg-A	-	3.33	-2.18 to +2.18	-0.73 to +3.62	0 to 3.33	T015P	
DP-B15P	Power channel upper plenum/hot leg-B	-	3.33	-2.18 to +2.18	-0.73 to +3.62	0 to 3.33	T015P	
DP-A20E	Accumulator-A Injection line	-	12.85	-7.25 to +7.25	-1.68 to +12.82	0 to 12.85	TA23P	PA20E
DP-B20E	Accumulator-B Injection line	-	12.85	-7.25 to +7.25	-1.68 to 12.82	0 to 12.85	TB23P	PB20E
DP-A81E	PRHR supply line	-	26.27	-7.25 to +7.25	±4.13 to +18.63	0 to 26.27	$\frac{TA82E + TA81E}{2}$	

1. Pressure channel P027A (pressurizer pressure) shall be used as the reference pressure instrument, unless otherwise noted.

**TABLE F-2
SPES-2, AP600 FULL-HEIGHT FULL POWER INTEGRAL SYSTEMS TEST
SPES-2 TYPE 2 DP-TRANSMITTERS**

Tag No.	Location	Upper Tap (+/-)	Tap Elev. Differ. (ft.)	Instrument Range (psi)	dP Meas. Range (psi)	Level Meas. Range (ft.)	Reference Temperature Instrument(s)	Reference Pressure (Note 1)
DP-001P	Power channel tubular downcomer (top)	+	-8.34	0 to +14.50	-3.63 to +10.87	0 to 8.34	T001P	
DP-002P	Power channel tubular downcomer (bottom)	+	-8.89	0 to +14.50	-3.85 to +10.65	0 to 8.89	T003P	
DP-017P	Power channel upper head	+	-6.20	0 to +7.25	-2.69 to +4.56	0 to 6.20	T016P	
DP-A001P	Cold leg-A1	+	-3.45	0 to +7.25	-1.49 to +5.76	0 to 3.45	TA31PL	
DP-B001P	Cold leg-B1	+	-3.45	0 to +7.25	-1.49 to +5.76	0 to 3.45	TB31PL	
DP-A002P	Cold leg-A2	+	-3.45	0 to +7.25	-1.49 to +5.76	0 to 3.45	TA32PL	
DP-B002P	Cold leg-B2	+	-3.45	0 to +7.25	-1.49 to +5.76	0 to 3.45	TB32PL	
DP-A021P	Cold leg-A1/power channel downcomer	+	-4.08	0 to +10.15	-1.77 to +8.38	0 to 4.08	<u>TA021PO + T001P</u> 2	
DP-B021P	Cold leg-B1/power channel downcomer	+	-4.08	0 to +10.15	-1.77 to +8.38	0 to 4.08	<u>TB021PO + T001P</u> 2	
DP-A022P	Cold leg-A2/power channel downcomer	+	-4.08	0 to +10.15	-1.77 to +8.38	0 to 4.08	<u>TA022PO + T001P</u> 2	
DP-B222P	Cold leg-B2/power channel downcomer	+	-4.08	0 to +10.15	-1.77 to +8.38	0 to 4.08	<u>TB022PO + T001P</u> 2	P017P
DP-A07P	U-tube steam generator-A (top to cold-leg side)	+	-12.30	-4.35 to +10.15	-9.68 to +4.82	0 to 12.30	<u>TA06P + TA08P</u> 2	
DP-B07P	U-tube steam generator-B (top to cold-leg side)	+	-12.30	-4.35 to +10.15	-9.68 to +4.82	0 to 12.30	<u>TB06P + TB08P</u> 2	
DP-A08P	U-tube steam generator-A (cold-leg side)	+	-16.82	-8.70 to +14.5	-15.99 to +7.21	0 to 16.82	TA09P	
DP-B08P	U-tube steam generator-B (cold-leg side)	+	-16.82	-8.70 to +14.5	-15.99 to +7.21	0 to 16.82	TB09P	
DP-A09P	Steam generator-A to RCP A	+	-5.80	0 to +14.5	-2.51 to +11.99	0 to 5.80	TA10P	
DP-B09P	Steam generator-B to RCP B	+	-5.80	0 to +14.5	-2.51 to +11.99	0 to 5.80	TB10P	
DP-A16P	Hot leg-A/power channel upper head	+	-2.19	0 to +2.9	-0.95 to +1.95	0 to 2.19	T015P	
DP-B16P	Hot leg-B/power channel upper head	+	-2.19	0 to +2.9	-0.95 to +1.95	0 to 2.19	T015P	
DP-A28P	CMT-A pressurizer balance line	+	-15.21	0 to +14.5	-6.59 to +7.91	0 to 15.21	TA28P	

1. Pressure channel P027A (Pressurizer Pressure) shall be used as the reference pressure instrument, unless otherwise noted.

TABLE F-2
SPES-2, AP600 FULL-HEIGHT FULL-POWER INTEGRAL SYSTEMS TEST
SPES-2 TYPE 2 DP-TRANSMITTERS (Cont.)

Tag No.	Location	Upper Tap (+/-)	Tap Elev. Differ. (ft.)	Instrument Range (psi)	dP Meas. Range (psi)	Level Meas. Range (ft.)	Reference Temperature Instruments	Reference Pressure (Note 1)
DP-B28P	CMT-B pressurizer balance line	+	-15.21	0 to 14.5	-6.59 to +7.91	0 to 15.21	TB28P	
DP-A40E	CMT injection line	+	-8.58	-3.63 to 15.25	-7.34 to +11.51	0 to 8.58	TA421E	PA40E
DP-B40E	CMT injection line	+	-8.58	-3.63 to +15.25	-7.34 to +11.51	0 to 8.58	TB421E	PB40E
DP-A61E	IRWST injection line A	+	-3.33	0 to +14.5	-1.44 to +13.06	0 to 3.33	T06SE	12.5 psig
DP-B61E	IRWST injection line B	+	-3.33	0 to +14.5	-1.44 to +13.06	0 to 3.33	T06SE	12.5 psig
DP-A82E	PRHR heat exchanger	+	-17.65	-7.25 to +7.25	-14.90 to +0.40	0 to 17.65	<u>TA82E + TA83E</u> 2	
DP-A83E	PRHR return line	+	-3.71	0 to +7.5	-1.61 to +5.64	0 to 3.71	TA83E	

1. Pressure channel P027A (pressurizer pressure) shall be used as the reference pressure instrument, unless otherwise noted.

TABLE F-3
SPES-2, AP600 FULL-HEIGHT FULL-POWER INTEGRAL SYSTEMS TEST
SPES-2 TYPE 3 DP-TRANSMITTERS

Tag No.	Location	Upper Tap (+/-)	Tap Elev. Differ. (ft.)	Instrument Range (psi)	dP Meas. Range (psi)	Level Meas. Range (ft.)	Reference Temperature	Reference Pressure (Note 1)
DP-003P	Downcomer to power channel lower plenum	+	+0.79	0 to 10.15	+0.34 to 10.49	0 to 0.79	T003P	
DP-004P	Power channel lower plenum	+	+3.06	-4.35 to 4.35	-3.02 to 1.33	0 to 3.06	T004P	
DP-005P	Power channel riser	+	+2.43	-2.90 to 2.90	-1.85 to 1.05	0 to 2.43	T003P	
DP-019P	Surge line	+	+2.43	-3.63 to 3.63	-2.57 to 4.68	0 to 2.43	T018P	
DP-020P	Surge line	+	+11.24	-7.25 to 7.25	-2.38 to 12.12	0 to 11.24	T020P	
DP-021P	Pressurizer	+	+4.74	-2.90 to 2.90	-0.85 to 4.95	0 to 4.74	T021P	
DP-022P	Pressurizer	+	+4.74	-2.90 to 2.90	-0.85 to 4.95	0 to 4.74	T022P	
DP-023P	Pressurizer	+	+4.74	-2.90 to 2.90	-0.85 to 4.95	0 to 4.74	T023P	
DP-024P	Pressurizer	+	+4.74	-2.90 to 2.90	-0.85 to 4.95	0 to 4.74	T024P	
DP-025P	Pressurizer	+	+1.41	-1.45 to 1.45	-0.84 to 2.06	0 to 1.41	T025P	
DP-026P	Pressurizer	+	+1.05	-1.45 to 1.45	-0.99 to 1.91	0 to 1.05	T026P	
DP-027P	Pressurizer	+	+0.77	-1.45 to 1.45	-1.12 to 1.78	0 to 0.77	T026P	
DP-A03S	Steam generator-A separator	+	+10.50	-7.25 to 7.25	-2.70 to 11.80	0 to 10.50	TA03S	PA04S
DP-B03S	Steam generator-B separator	+	+10.50	-7.25 to 7.25	-2.70 to 11.80	0 to 10.50	TB03S	PB04S
DP-A04S	Steam generator-A separator	+	+2.21	-1.45 to 1.45	-0.49 to 2.41	0 to 2.21	TA03S	PA04S
DP-B04S	Steam generator-B separator	+	+2.21	-1.45 to 1.45	-0.49 to 2.41	0 to 2.21	TB03S	PB04S
DP-A81AE	PRHR supply line	+	+8.63	-7.25 to 7.25	-3.51 to 10.99	0 to 8.62	TA82E	

1. Pressure channel P027A (pressurizer pressure) shall be used as the reference pressure instrument, unless otherwise noted.

TABLE F-4
SPES-2, AP600 FULL-HEIGHT FULL-POWER INTEGRAL SYSTEMS TEST
SPES-2 TYPE 4 DP-TRANSMITTERS

Tag No.	Location	Upper Tap (+/-)	Tap Elev. Differ. (ft.)	Instrument Range (psi)	dP Meas. Range (psi)	Level Meas. Range (ft.)	Reference Temperature Instrument(s)	Reference Pressure (Note 1)
DP-A01S	Steam generator-A riser	+	+13.06	0 to 7.25	-1.59 to 5.66	0 to 13.06	TA05S	PA04S
DP-B01S	Steam generator-B riser	+	+13.06	0 to 7.25	-1.59 to 5.66	0 to 13.06	TB05S	PB04S
DP-A02S	Steam generator-A riser	+	+21.33	0 to 10.15	-0.91 to 9.24	0 to 21.33	TA08S	PA04S
DP-B02S	Steam generator-A riser	+	+21.33	0 to 10.15	-0.91 to 9.24	0 to 21.33	TB08S	PB04S
DP-A05S	Steam generator-A dryer	+	+2.26	0 to 1.45	-0.47 to 0.98	0 to 2.26	N/A	N/A
DP-B05S	Steam generator-B dryer	+	+2.26	0 to 1.45	-0.47 to 0.98	0 to 2.26	N/A	N/A
DP-A06S	Steam generator-A riser	+	+7.05	0 to 4.35	-1.29 to 3.06	0 to 7.05	TA07S	PA04S
DP-B06S	Steam generator-B riser	+	+7.05	0 to 4.35	-1.29 to 3.06	0 to 7.05	TB07S	PB04S
DP-A41E	CMT-A (bottom)	+	+5.10	0 to 2.61	-0.40 to 2.21	0 to 5.10	<u>TA415E to TA420E</u> 6	PA40E
DP-A42E	CMT-A (low middle)	+	+5.10	0 to 2.61	-0.40 to 2.21	0 to 5.10	<u>TA411E to TA415E</u> 5	PA40E
DP-A43E	CMT-A (high middle)	+	+5.10	0 to 2.61	-0.40 to 2.21	0 to 5.10	<u>TA407E to TA411E</u> 5	PA40E
DP-A44E	CMT-A (top)	+	+5.10	0 to 2.61	-0.40 to 2.21	0 to 5.10	<u>TA401E to TA407E</u> 7	PA40E
DP-B41E	CMT-B (bottom)	+	+5.10	0 to 2.61	-0.40 to 2.21	0 to 5.10	<u>TB415E, 417E, 420E</u> 3	PB40E
DP-B42E	CMT-B (low middle)	+	+5.10	0 to 2.61	-0.40 to 2.21	0 to 5.10	<u>TB411E + TB413E</u> 2	PB40E

1. Pressure channel P027A (pressurizer pressure) shall be used as the reference pressure instrument, unless otherwise noted.

TABLE F-4
SPES-2, AP600 FULL-HEIGHT FULL-POWER INTEGRAL SYSTEMS TEST
SPES-2 TYPE 4 DP-TRANSMITTERS (Cont.)

Tag No.	Location	Upper Tap (+/-)	Tap Elev. Differ. (ft.)	Instrument Range (psi)	dP Meas. Range (psi)	Level Meas. Range (ft.)	Reference Temperature Instrument(s)	Reference Pressure (Note 1)
DP-B43E	CMT-B (high middle)	+	+5.10	0 to 2.61	-0.40 to 2.21	0 to 5.10	<u>TB1407E + TB409E</u> 2	PB40E
DP-B44E	CMT-B (top)	+	+5.10	0 to 2.61	-0.40 to 2.21	0 to 5.10	<u>TB401E, 403E, 405E</u> 3	PB40E
DP-A45E	CMT-A cold-leg balance line	+	+23.71	-2.90 to 11.60	-1.33 to 13.17	0 to 23.71	<u>TA141P + TA143P</u> 2	PA40E
DP-B45E	CMT-B cold-leg balance line	+	+23.71	-2.90 to 11.60	-1.33 to 13.17	0 to 23.71	<u>TB141P + TA143P</u> 2	PB40E

1. Pressure channel P027A (pressurizer pressure) shall be used as the reference pressure instrument, unless otherwise noted.

**APPENDIX G
FULL-HEIGHT FULL-POWER
INTEGRAL SYSTEMS TEST
DELTA-P INSTRUMENTATION DATA REDUCTION**

G-1 Abstract

The differential pressure (dP) instrumentation in the SPES-2 test facility, in many cases, is used to determine component water levels and to measure dPs due to flow loss. This document is a guide for using the SPES-2 dP instrumentation data in order to separately determine both flow loss dP and fluid level portions of total measured dP, and to determine the void fraction of a two-phase fluid when boiling and flashing occur in the components during testing.

G-2 Introduction

In order to use the data from the SPES dP instrumentation, it is necessary to understand the arrangement of the dP cells, to account for the tap-to-tap elevation differences, and to compensate for fluid densities. With this understanding, the dP cell data can be used to obtain the dP due to friction losses and to measure level at low or no-flow conditions when the component friction loss due to flow is approximately 0.

The following sections provide a description of each type of dP cell installation used at SIET, a description of how the raw data should be processed, a list of the dP instruments, and the appropriate temperature instrument(s) that should be used in determining the density of fluid(s).

See Appendix G-7 for a summary of results.

G-3 Type 1 dP Cells

G-3.1 Installation and Offsets

The installation/characteristics of type 1 dP cells are as follows:

- The normal direction of flow is in the UP vertical direction, and the negative (low-pressure) side of the dP cell is the upper tap.

This causes flow losses to increase the measured dP since flow is from the positive (lower) tap to the negative (upper) tap.

- The data acquisition system (DAS) adds the tap-to-tap elevation difference to the dP at the instrument taps, converting this height to force (psi) using the following equation:

$$\rho_{wc}gh/144g_c$$

Where:

ρ_{wc} = density of cold water at ambient conditions (62.2 lbs_m/ft.³)

g = acceleration due to gravity (32.2 ft./sec.²)

h = tap-to-tap elevation difference, (ft.)

g_c = mass to force conversion, (32.2 ft.-lb_m/sec.² - lb_f)

G-3.2 Friction Loss Determination

The friction loss portion of the measured dP when the component is full of water is calculated as follows:

$$\text{Recorded dP data (psid)} = \text{dP at instrument} + \rho_{wc}gh/144 g_c$$

Where the dP at the instrument equals the (positive tap pressure) minus (negative tap pressure).

That is,

$$(\text{Friction loss} + \rho_{wh}gh/144 g_c) - (\rho_{wc}gh/144 g_c)$$

Where ρ_{wh} is the density of the hot process water in the component which must be determined based on the existing system pressure and the temperature of the water.

Since the DAS adds $\rho_{wc}gh/144 g_c$, then

$$\text{Recorded dP data (psid)} = \text{friction loss (psid)} + \rho_{wh}gh/144 g_c$$

and:

$$\text{Friction loss} = \text{recorded dP data} - \rho_{wh}gh/144 g_c$$

G-3.3 Component Water Level Determination

The water level that exists between the dP cell taps can be calculated from the recorded dP data when the friction loss is negligible or when the flow is 0. This is done as follows:

$$\text{Recorded dP data (psid)} = \rho_{wh}Lg/144 g_c + \rho_s (h - L) g/144 g_c$$

Where:

L = water level of water (ft.)

ρ_s = density of steam

This numerically reduces to the following:

$$L = (144) (\text{dP data}) - (\rho_s h) / (\rho_{wh} - \rho_s)$$

This level can be converted to percent level using the following:

$$\% \text{ level} = L/h * 100\%$$

The density of steam (ρ_s) can be ignored (assumed 0) in the above equation, with less than 1% error introduced, when system pressure is less than 500 psia.

Table G-1, provides a listing of dP instruments that operate as described above. Also listed are the pressure and temperature instrument(s) that should be used to determine ρ_{wh} and ρ_s in the above equations.

G-4 Type 2 dP Cells

G-4.1 Installation and Offsets

The installation/characteristics of type 2 cells are as follows:

- The normal direction of flow is in the DOWN vertical direction, and the negative (low pressure) side of the dP cell is the bottom tap.

This causes flow losses to increase the measured dP since flow is from the positive (upper) tap to the negative (lower) tap.

- The DAS subtracts the tap-to-tap elevation difference from the dP at the instrument taps, converting this height to force (psi) using the following equation

$$\rho_{wc}gh/144 g_c$$

G-4.2 Friction Loss Determination

The friction loss portion of the measured dP when the component is full of water is calculated as follows:

$$\text{Recorded dP data (psid)} = \text{dP at instrument} - \rho_{wh}gh/144 g_c$$

Where the dP at instrument equals (positive tap pressure) minus (negative tap pressure). That is,

$$(\text{Friction loss} + \rho_{wc}gh/144 g_c) - (\rho_{wh}gh/144 g_c)$$

Since the DAS subtracts $\rho_{wc}gh/144 g_c$, then

$$\text{Recorded dP data} = \text{friction loss} - \rho_{wh}gh/144 g_c$$

and:

$$\text{Friction loss} = \text{recorded dP data} + \rho_{wh}gh/144 g_c$$

G-4.3 Component Water Level Determination

The water level that exists between the dP cell taps can be calculated from the recorded dP cell data when flow is approximately 0 (friction losses are 0 or negligible). This is done as follows:

$$\text{Recorded dP data (psid)} = \rho_{wc}gh/144 g_c - (\rho_{wh}gL/144 g_c + \rho_s g (h - L)/144 g_c) - \rho_{wc}gh/144 g_c$$

This numerically reduces to the following:

$$L = (144) (\text{dP data}) + (\rho_s h) / (\rho_s - \rho_{wh})$$

As stated above, ρ_s can be assumed to be 0 when system pressure is less than 500 psia.

This level can be converted to percent level using the following:

$$\% \text{ level} = L/h * 100\%$$

Table G-2 lists the dP instruments that operate as described above. Also listed are the pressure and temperature instrument(s) that should be used to determine ρ_{wh} and ρ_s in solving above equations.

G-5 Type 3 dP Cells

G-5.1 Installation and Offsets

The instrumentation/characteristics of type 3 dP cells are as follows:

- The positive (high-pressure) side of the dP cell is connected to the upper tap.
- The DAS adds the tap to tap elevation difference converting this height of water to force (psi) using the following equation:

$$\rho_{wc}gh/144 g_c$$

G-5.2 Friction Loss Determination

The friction loss portion of the measured dP when the component is full of water is calculated as follows:

$$\text{Recorded dP data (psid)} = \text{dP at instrument} + \rho_{wc}gh/144 g_c$$

Where the dP at the instrument equals the positive tap pressure minus the negative tap pressure. That is,

$$(\text{Friction losses} + \rho_{wc}gh/144 g_c) - \rho_{wh}gh/144 g_c$$

Since the DAS adds $\rho_{wc}gh/144 g_c$, then

$$\text{Recorded dP data} = \text{friction losses} \rho_{wh}gh/144 g_c + 2\rho_{wc}gh/144 g_c$$

and:

$$\text{Friction loss} = \text{recorded dP data} - 2\rho_{wc}gh/144 g_c + \rho_{wh}gh/144 g_c$$

G-5.3 Component Water Level Determination

The water level that exists between the dP cell taps can be calculated from the recorded dP data when the friction loss is negligible (when flow is approximately 0). This is done as follows:

$$\text{Recorded dP data} = \rho_{wc}gh/144 g_c - (\rho_{wh}gL/144 g_c + \rho_s (h - L) g/144 g_c) + \rho_{wc}gh/144 g_c$$

This numerically reduces to the following:

$$L = 144 (\text{dP Data}) + \rho_s h - 2\rho_{wc}h / \rho_s - \rho_{wh}$$

As stated above, p_s can be assumed to be 0 when system pressure is less than 500 psia. Also, this level can be converted to percent level using the following:

$$\% \text{ level} = L/h \times 100\%$$

Table G-3, lists dP instruments that operate as described above. Also listed are the pressure and temperature instruments that should be used to determine ρ_{wb} and ρ_s used in the above equations.

G-6 Type 4 dP Cells

G-6.1 Installation and Offsets

The installation/characteristics of the type 4 dP cells are as follows:

- The positive (high-pressure) side of the dP cell is connected to the upper tap.
- No tap to tap elevation difference is added by the DAS.
- No significant flow or flow losses through the component are expected.

G-6.2 Friction Loss Determination

No friction losses are expected.

G-6.3 Component Water Level Determination

The water level that exists between the dP cell taps can be calculated from the measured dP data when the friction loss is negligible (for example, in large components such as tanks where level changes are relatively slow). Since the DAS does not add any compensation for tap elevations, then

$$\text{Recorded dP data} = (\rho_{wc}gh/144g_c - (\rho_{wh}gL/144g_c + \rho_s(h - L)g/144g_c))$$

This numerically reduces to the following:

$$L = 144 (\text{dP data}) + h(\rho_s - \rho_{wc}) / \rho_s - \rho_{wh}$$

As stated above, ρ_s can be assumed to be 0 when system pressure is less than 500 psia. Also, level can be converted to percent level using

$$\% \text{ level} = L/h * 100\%$$

Table G-4 lists the dP instruments that operate as described above. Also listed are the pressure and temperature instruments that should be used to determine ρ_{wh} and ρ_s used in the above equations.

G-7 Conclusion/Summary

The following equations have been derived for calculating the friction loss (in psi) from the dP data measured for the SPES-2 tests. These equations (numerically reduced) are as follows:

- Type 1 dP Cells : Friction loss = dP data - $\rho_{wh}h/144$
- Type 2 dP Cells : Friction loss = dP data - $\rho_{wh}h/144$
- Type 3 dP Cells : Friction loss = dP data + $h(\rho_{wh} - 2\rho_{wc})/144$
- Type 4 dP Cells : No friction loss is expected

The following equations have been derived for calculating the water level (in ft. H₂O) from the dP data (in psi) measured for the SPES-2 tests.

These equations (numerically reduced) are as follows:

- Type 1 dP Cells : Water level = $144(\text{dP data}) - (\rho_s h) / (\rho_{wh} - \rho_s)$
- Type 2 dP Cells : Water level = $144(\text{dP data}) - (\rho_s h) / (\rho_s - \rho_{wh})$
- Type 3 dP Cells : Water level = $144(\text{dP data}) + H(\rho_s - 2\rho_{wc}) / (\rho_s - \rho_{wh})$
- Type 4 dP Cells : Water level = $144(\text{dP data}) + h(\rho_s - \rho_{wc}) / (\rho_s - \rho_{wh})$

TABLE G-1
SPES-2, AP600 FULL-HEIGHT FULL-POWER INTEGRAL SYSTEMS TEST
SPES-2 TYPE 1 DP-TRANSMITTERS

Tag No.	Location	Upper Tap (+/-)	Tap Elev. Differ. (ft.)	Instrument Range (psl)	dP Meas. Range (psl)	Level Meas. Range (ft.)	Reference Temp. Instrument(s)	Reference Pressure (Note 1)
DP-000P	Power channel riser (overall)	-	17.41	-8.70 to +8.70	-1.16 to +16.24	0 to 17.41	$\frac{T003P + T015P}{2}$	
DP-011P	Power channel riser (bottom)	-	4.86	0 to +4.35	+2.10 to +6.45	0 to 4.86	T003P	
DP-012P	Power channel riser (bottom middle)	-	3.64	0 to 5.80	+1.58 to +7.38	0 to 3.64	$\frac{T003P + T015P}{2}$	
DP-013P	Power channel riser (top middle)	-	3.64	0 to 5.08	+1.58 to +6.65	0 to 3.64	$\frac{T003 + T015P}{2}$	
DP-014P	Power channel riser (top)	-	2.84	-1.45 to +1.45	-0.19 to +2.71	0 to 2.84	T015P	
DP-018P	Hot leg-A/surge line	-	2.95	-1.45 to +1.45	-0.17 to +2.73	0 to 2.95	T018P	
DP-A04P	Hot leg-A	-	11.82	-5.80 to +8.70	-0.68 to +13.82	0 to 11.82	TA03P0	
DP-B04P	Hot leg-B	-	11.82	-5.80 to +8.70	-0.68 to +13.82	0 to 11.82	TB03P0	
DP-A05P	U-tube steam generator-A (hot-leg side)	-	16.82	-8.70 to +17.40	-1.41 to +24.69	0 to 16.82	$\frac{TA06P + TA05P}{2}$	PA04P
DP-B05P	U-tube steam generator-B (hot-leg side)	-	16.82	-8.70 to +17.40	-1.41 to +24.69	0 to 16.82	$\frac{TB05P + TB06P}{2}$	PB04P
DP-A06P	U-Tube steam generator-A (Hot-leg side to top)	-	12.30	-5.80 to +8.70	-0.47 to +14.03	0 to 12.30	$\frac{TA06P + TA08P}{2}$	PA04P
DP-B06P	U-tube steam generator-B (HL Side to top)	-	12.30	-5.80 to +8.70	-0.47 to +14.03	0 to 12.30	$\frac{B06P + TB08P}{2}$	PB04P
DP-A15P	PC upper plenum/hot leg-A	-	3.33	-2.18 to +2.18	-0.73 to +3.62	0 to 3.33	T015P	
DP-B15P	PC upper plenum/hot leg-B	-	3.33	-2.18 to +2.18	-0.73 to +3.62	0 to 3.33	T015P	
DP-A20E	Accumulator-A Injection line	-	12.85	-7.25 to +7.25	-1.68 to +12.82	0 to 12.85	TA23P	PA20E
DP-B20E	Accumulator-B Injection line	-	12.85	-7.25 to +7.25	-1.68 to 12.82	0 to 12.85	TB23P	PB20E
DP-A81E	PRHR supply line	-	26.27	-7.25 to +7.25	±4.13 to +18.63	0 to 26.27	$\frac{TA82E + TA81E}{2}$	

1. Pressure channel P027A (pressurizer pressure) shall be used as the reference pressure instrument, unless otherwise noted.

TABLE G-2
SPES-2, AP600 FULL-HEIGHT FULL POWER INTEGRAL SYSTEMS TEST
SPES-2 TYPE 2 DP-TRANSMITTERS

Tag No.	Location	Upper Tap (+/-)	Tap Elev. Differ. (ft.)	Instrument Range (psi)	dP Meas. Range (psi)	Level Meas. Range (ft.)	Reference Temperature Instrument(s)	Reference Pressure (Note 1)
DP-001P	Power channel tubular downcomer (top)	+	-8.34	0 to +14.50	-3.63 to +10.87	0 to 8.34	T001P	
DP-002P	Power channel tubular downcomer (bottom)	+	-8.89	0 to +14.50	-3.85 to +10.65	0 to 8.89	T003P	
DP-G17P	Power channel upper head	+	-6.20	0 to +7.25	-2.69 to +4.56	0 to 6.20	T016P	
DP-A001P	Cold leg-A1	+	-3.45	0 to +7.25	-1.49 to +5.76	0 to 3.45	TA31PL	
DP-B001P	Cold leg-B1	+	-3.45	0 to +7.25	-1.49 to +5.76	0 to 3.45	TB31PL	
DP-A002P	Cold leg-A2	+	-3.45	0 to +7.25	-1.49 to +5.76	0 to 3.45	TA32PL	
DP-B002P	Cold leg-B2	+	-3.45	0 to +7.25	-1.49 to +5.76	0 to 3.45	TB32PL	
DP-A021P	Cold leg-A1/power channel downcomer	+	-4.08	0 to +10.15	-1.77 to +8.38	0 to 4.08	<u>TA021PO + T001P</u> 2	
DP-B021P	Cold leg-B1/power channel downcomer	+	-4.08	0 to +10.15	-1.77 to +8.38	0 to 4.08	<u>TB021PO + T001P</u> 2	
DP-A022P	Cold leg-A2/power channel downcomer	+	-4.08	0 to +10.15	-1.77 to +8.38	0 to 4.08	<u>TA022PO + T001P</u> 2	
DP-B022P	Cold leg-B2/power channel downcomer	+	-4.08	0 to +10.15	-1.77 to +8.38	0 to 4.08	<u>TB022PO + T001P</u> 2	P017P
DP-A07P	U-tube steam generator-A (top to CL side)	+	-12.30	-4.35 to +10.15	-9.68 to +4.82	0 to 12.30	<u>TA06P + TA08P</u> 2	
DP-B07P	U-tube steam generator-B (top to CL side)	+	-12.30	-4.35 to +10.15	-9.68 to +4.82	0 to 12.30	<u>TB06P + TB08P</u> 2	
DP-A08P	U-tube steam generator-A (CL Side)	+	-16.82	-8.70 to +14.5	-15.99 to +7.21	0 to 16.82	TA09P	
DP-B08P	U-tube steam generator-B (CL Side)	+	-16.82	-8.70 to +14.5	-15.99 to +7.21	0 to 16.82	TB09P	
DP-A09P	Steam generator-A to RCP A	+	-5.80	0 to +14.5	-2.51 to +11.99	0 to 5.80	TA10P	
DP-B09P	Steam generator-B to RCP B	+	-5.80	0 to +14.5	-2.51 to +11.99	0 to 5.80	TB10P	
DP-A16P	Hot leg-A/power channel UH	+	-2.19	0 to +2.9	-0.95 to +1.95	0 to 2.19	T015P	
DP-B16P	Hot leg-B/power channel UH	+	-2.19	0 to +2.9	-0.95 to +1.95	0 to 2.19	T015P	
DP-A28P	CMT-A pressurizer balance line	+	-15.21	0 to +14.5	-6.59 to +7.91	0 to 15.21	TA28P	

1. Pressure Channel P027A (Pressurizer Pressure) shall be used as the reference pressure instrument unless otherwise noted.

TABLE G-2 (Continued)
SPES-2, AP600 FULL-HEIGHT FULL-POWER INTEGRAL SYSTEMS TEST
SPES-2 TYPE 2 DP-TRANSMITTERS

Tag No.	Location	Upper Tap (+/-)	Tap Elev. Differ. (ft.)	Instrument Range (psi)	dP Meas. Range (psi)	Level Meas. Range (ft.)	Reference Temperature Instruments	Reference Pressure (Note 1)
DP-B28P	CMT-B PZR balance line	+	-15.21	0 to 14.5	-6.59 to +7.91	0 to 15.21	TB28P	
DP-A40E	CMT-A injection line	+	-8.58	-3.63 to 15.25	-7.34 to +11.51	0 to 8.58	TA421E	PA40E
DP-B40E	CMT-B injection line	+	-8.58	-3.63 to +15.25	-7.34 to +11.51	0 to 8.58	TB421E	PB40E
DP-A61E	IRWST injection line A	+	-3.33	0 to +14.5	-1.44 to +13.06	0 to 3.33	T065E	12.5 psig
DP-B61E	IRWST injection line B	+	-3.33	0 to +14.5	-1.44 to +13.06	0 to 3.33	T065E	12.5 psig
DP-A82E	PRHR heat exchanger	+	-17.65	-7.25 to +7.25	-14.90 to +0.40	0 to 17.65	<u>TA82E + TA83E</u> 2	
DP-A83E	PRHR return line	+	-3.71	0 to +7.5	-1.61 to +5.64	0 to 3.71	TA83E	

1. Pressure channel P027A (pressurizer pressure) shall be used as the reference pressure instrument, unless otherwise noted.

TABLE G-3
SPES-2, AP600 FULL-HEIGHT FULL-POWER INTEGRAL SYSTEMS TEST
SPES-2 TYPE 3 DP-TRANSMITTERS

Tag No.	Location	Upper Tap (+/-)	Tap Elev. Differ. (ft.)	Instrument Range (psi)	dP Meas. Range (psi)	Level Meas. Range (ft.)	Reference Temperature	Reference Pressure (Note 1)
DP-003P	Downcomer to power channel lower plenum	+	+0.79	0 to 10.15	+0.34 to 10.49	0 to 0.79	T003P	
DP-004P	Power channel lower plenum	+	+3.06	-4.35 to 4.35	-3.02 to 1.33	0 to 3.06	T004P	
DP-005P	Power channel riser	+	+2.43	-2.90 to 2.90	-1.85 to 1.05	0 to 2.43	T003P	
DP-019P	Surge line	+	+2.43	-3.63 to 3.63	-2.57 to 4.68	0 to 2.43	T018P	
DP-020P	Surge line	+	+11.24	-7.25 to 7.25	-2.38 to 12.12	0 to 11.24	T020P	
DP-021P	Pressurizer	+	+4.74	-2.90 to 2.90	-0.85 to 4.95	0 to 4.74	T021P	
DP-022P	Pressurizer	+	+4.74	-2.90 to 2.90	-0.85 to 4.95	0 to 4.74	T022P	
DP-023P	Pressurizer	+	+4.74	-2.90 to 2.90	-0.85 to 4.95	0 to 4.74	T023P	
DP-024P	Pressurizer	+	+4.74	-2.90 to 2.90	-0.85 to 4.95	0 to 4.74	T024P	
DP-025P	Pressurizer	+	+1.41	-1.45 to 1.45	-0.84 to 2.06	0 to 1.41	T025P	
DP-026P	Pressurizer	+	+1.05	-1.45 to 1.45	-0.99 to 1.05	0 to 1.05	T026P	
DP-027P	Pressurizer	+	+0.77	-1.45 to 1.45	-1.12 to 1.78	0 to 0.77	T026P	
DP-A03S	Steam generator-A separator	+	+10.50	-7.25 to 7.25	-2.70 to 11.80	0 to 10.50	TA03S	PA04S
DP-B03S	Steam generator-B separator	+	+10.50	-7.25 to 7.25	-2.70 to 11.80	0 to 10.50	TB03S	PB04S
DP-A04S	Steam generator-A separator	+	+2.21	-1.45 to 1.45	-0.49 to 2.41	0 to 2.21	TA03S	PA04S
DP-B04S	Steam generator-B separator	+	+2.21	-1.45 to 1.45	-0.49 to 2.41	0 to 2.21	TB03S	PB04S
DP-A81AE	PRHR supply line	+	+8.63	-7.25 to 7.25	-3.51 to 10.99	0 to 8.62	TA82E	

1. Pressure channel P027A (pressurizer pressure) shall be used as the reference pressure instrument, unless otherwise noted.

TABLE G-4
SPES-2, AP600 FULL-HEIGHT FULL-POWER INTEGRAL SYSTEMS TEST
SPES-2 TYPE 4 DP-TRANSMITTERS

Tag No.	Location	Upper Tap (+/-)	Tap Elev. Differ. (ft.)	Instrument Range (psi)	dP Meas. Range (psi)	Level Meas. Range (ft.)	Reference Temperature Instrument(s)	Reference Pressure (Note 1)
DP-A01S	Steam generator-A riser	+	+13.06	0 to 7.25	-1.59 to 5.66	0 to 13.06	TA05S	PA04S
DP-B01S	Steam generator-B riser	+	+13.06	0 to 7.25	-1.59 to 5.66	0 to 13.06	TB05S	PB04S
DP-A02S	Steam generator-A riser	+	+21.33	0 to 10.15	-0.91 to 9.24	0 to 21.33	TA08S	PA04S
DP-B02S	Steam generator-A riser	+	+21.33	0 to 10.15	-0.91 to 9.24	0 to 21.33	TB08S	PB04S
DP-A05S	Steam generator-A dryer	+	+2.26	0 to 1.45	-0.47 to 0.98	0 to 2.26	N/A	N/A
DP-B05S	Steam generator-B dryer	+	+2.26	0 to 1.45	-0.47 to 0.98	0 to 2.26	N/A	N/A
DP-A06S	Steam generator-A riser	+	+7.05	0 to 4.35	-1.29 to 3.06	0 to 7.05	TA07S	PA04S
DP-B06S	Steam generator-B riser	+	+7.05	0 to 4.35	-1.29 to 3.06	0 to 7.05	TB07S	PB04S
DP-A41E	CMT-A (bottom)	+	+5.10	0 to 2.61	-0.40 to 2.21	0 to 5.10	<u>TA415E to TA420E</u> 6	PA40E
DP-A42E	CMT-A (low middle)	+	+5.10	0 to 2.61	-0.40 to 2.21	0 to 5.10	<u>TA411E to TA415E</u> 5	PA40E
DP-A43E	CMT-A (high middle)	+	+5.10	0 to 2.61	-0.40 to 2.21	0 to 5.10	<u>TA407E to TA411E</u> 5	PA40E
DP-A44E	CMT-A (top)	+	+5.10	0 to 2.61	-0.40 to 2.21	0 to 5.10	<u>TA401E to TA407E</u> 7	PA40E
DP-B41E	CMT-B (bottom)	+	+5.10	0 to 2.61	-0.40 to 2.21	0 to 5.10	<u>TB415E, 417E, 420E</u> 3	PB40E
DP-B42E	CMT-B (low middle)	+	+5.10	0 to 2.61	-0.40 to 2.21	0 to 5.10	<u>TB411E + TB413E</u> 2	PB40E

1. Pressure channel P027A (pressurizer pressure) shall be used as the reference pressure instrument, unless otherwise noted.

TABLE G-4 (Continued)
 SPES-2, AP600 FULL-HEIGHT FULL-POWER INTEGRAL SYSTEMS TEST
 SPES-2 TYPE 4 DP-TRANSMITTERS

Tag No.	Location	Upper Tap (+/-)	Tap Elev. Differ. (ft.)	Instrument Range (psi)	dP Meas. Range (psi)	Level Meas. Range (ft.)	Reference Temperature Instrument(s)	Reference Pressure (Note 1)
DP-B43E	CMT-B (high middle)	+	+5.10	0 to 2.61	-0.40 to 2.21	0 to 5.10	$\frac{TB1407E + TB409E}{2}$	PB40E
DP-B44E	CMT-B (top)	+	+5.10	0 to 2.61	-0.40 to 2.21	0 to 5.10	$\frac{TB401E, 403E, 405E}{3}$	PB40E
DP-A45E	CMT-A cold-leg balance line	+	+23.71	-2.90 to 11.60	-1.33 to 13.17	0 to 23.71	$\frac{TA141P + TA143P}{2}$	PA40E
DP-B45E	CMT-B cold-leg balance line	+	+23.71	-2.90 to 11.60	-1.33 to 13.17	0 to 23.71	$\frac{TB141P + TA143P}{2}$	PB40E

1. Pressure channel P027A (pressurizer pressure) shall be used as the reference pressure instrument, unless otherwise noted.